

ARCHITECTURE AND DEPOSITIONAL HISTORY  
OF THE LOWER CLORIDORME FORMATION,  
GASPÉ PENINSULA, QUÉBEC, CANADA

CENTRE FOR NEWFOUNDLAND STUDIES

---

**TOTAL OF 10 PAGES ONLY  
MAY BE XEROXED**

(Without Author's Permission)

SHERIF ABDEL MONEM AWADALLAH





**ARCHITECTURE AND DEPOSITIONAL HISTORY OF THE  
LOWER CLORIDORME FORMATION,  
GASPÉ PENINSULA, QUÉBEC, CANADA**

By

**Sherif Abdel Monem Awadallah**

**A thesis submitted to the School of Graduate Studies  
in partial fulfilment of the requirements  
for the degree of  
Doctor of Philosophy**

**Department of Earth Sciences  
Memorial University of Newfoundland  
May 2002**

**St. John's**

**Newfoundland**



**National Library  
of Canada**

**Acquisitions and  
Bibliographic Services**

**395 Wellington Street  
Ottawa ON K1A 0N4  
Canada**

**Bibliothèque nationale  
du Canada**

**Acquisitions et  
services bibliographiques**

**395, rue Wellington  
Ottawa ON K1A 0N4  
Canada**

*Your file Votre référence*

*Our file Notre référence*

**The author has granted a non-exclusive licence allowing the National Library of Canada to reproduce, loan, distribute or sell copies of this thesis in microform, paper or electronic formats.**

**The author retains ownership of the copyright in this thesis. Neither the thesis nor substantial extracts from it may be printed or otherwise reproduced without the author's permission.**

**L'auteur a accordé une licence non exclusive permettant à la Bibliothèque nationale du Canada de reproduire, prêter, distribuer ou vendre des copies de cette thèse sous la forme de microfiche/film, de reproduction sur papier ou sur format électronique.**

**L'auteur conserve la propriété du droit d'auteur qui protège cette thèse. Ni la thèse ni des extraits substantiels de celle-ci ne doivent être imprimés ou autrement reproduits sans son autorisation.**

**0-612-84077-8**

**Canada**



# **ODE TO THE CLORIDORME**

**K.T. PICKERING**

**JULY 1984**

**When I was in the Cloridorme**

**I "saw" some sediment deform**

**Way back in the Middle Ordovician**

**Before the present seas alteration**

**To reveal a foreland basin floor**

**The key to the past - an open door**

**Beds correlate over many kilometres**

**Sensitive geological chronometres**

**Showing reflected flows had once occurred**

**With thick mud caps, one highly stirred**

**Lie quiet now out on the shore**

**Turbidity currents they are no more**

## ABSTRACT

The lower Cloridorme Formation (Middle Ordovician) is superbly exposed along the southern shore of the St. Lawrence River. It is dominated by shale and is characterised by four turbidite architectural elements: megaturbidites, lobes, sandstone sheets and siltstone lenses. The lower Cloridorme Formation was deposited in a deep-marine setting akin to modern basin plains and distal submarine fan systems. The deep-marine setting was a foreland basin that developed in front of advancing thrust sheets during the Taconic Orogeny. The depositional environment evolved from a basin-plain setting to a submarine-fan setting, probably due to progradation of the turbidite system from the east.

The detailed correlation of more than seventy basin-wide megaturbidites and nine K-bentonite horizons permits the division of the lower part of the Cloridorme Formation into seven time-equivalent intervals, called “time-slices”, that vary spatially and temporally in their thickness, constituent facies and architectural elements. The main contribution of this thesis is the precise mapping and correlation of architectural elements in the lower Cloridorme Formation using the key beds and ash horizons, leading a better understanding of the depositional history of the lower Cloridorme Formation.

Megaturbidites are the most common architectural element. Megaturbidites were deposited from large flows initiated by major sediment failures that evolved into turbidity currents. Some of these megaturbidites were deflected and reflected against the basin margins and bathymetric highs. Megaturbidite geometries were controlled by bottom



topography and range from tabular to wedge shaped to gently lensing. The megaturbidites were deposited in basin-plain and the lower-fan environments. Megaturbidites are bounded by single event boundaries.

Lobe elements consist of structureless, mostly amalgamated sandstone beds that form 10-20 m-thick packets surrounded by shale. The sandstone beds were deposited from concentrated flows that did not travel long distances and were strongly controlled by bottom topography. The lobes formed mounds that controlled the flow of subsequent turbidity currents. The lobes have a tabular or a gently lensing geometry over distances of 1-3 km, but taper over longer distances. These lobes were deposited in a lower fan environment during periods of increased supply of coarse sediment to the area. The packets of beds that represent these lobes consist mostly of structureless sand in amalgamated units. These packets are bounded by erosional surfaces in most cases.

Sandstone sheets are not common. They were deposited on a basin plain as a variety of sandstone facies that range from structureless to well laminated. The sheets also contain laminated siltstone beds. The sheets become more muddy in a downcurrent direction. They have a tabular geometry and probably developed during periods of increased sand and silt supply reaching the area. Many of the beds in these sheets do not form amalgamated units. These sheets are bounded by erosional or non-erosional surfaces.

Siltstone lenses consist of laminated siltstone beds. They become more muddy and less distinct in a downcurrent direction. Over distances of 1-3 km, these deposits are

tabular or have a subdued lens shape. These lenses occur in both the basin plain and lower fan and are bounded by erosional or non-erosional surfaces.

A suggested depositional history of the lower Cloridorme Formation is provided which shows the influence of bottom topography on the distribution of the different facies and the geometry of beds and architectural elements. Seafloor irregularities were the result of the combined effects of tectonic, depositional and compactional factors. Deposition was influenced or controlled by local (autocyclic) factors such as channel switching and more regional (allocyclic) factors such as tectonics and sea-level changes.

The bed-thickness distributions of the turbidite beds of the lower Cloridorme Formation vary from mainly lognormal for the sandstone beds to exponential for the siltstone beds. The observed type of distribution is in many cases the summation of a mixture of subpopulations. Some of the bed-thickness populations approximate power-law distributions with a scaling parameter ranging from 1-2, but this fit to a power-law only applies to a subset of beds that represent a small part of the population. Thinner beds that form a greater part of the population might also follow a power-law distribution but have a much smaller power-law scaling parameter than the associated thicker beds. A comprehensive understanding of the depositional conditions and the factors that control the thicknesses of beds is required before attempting to infer submarine-fan subenvironments and triggering mechanisms for turbidity currents from the bed-thickness distribution.



## ACKNOWLEDGMENTS

First and foremost, I would like to thank almighty Allah for giving me strength and patience to successfully complete this thesis. I would also like to thank my family for their ongoing support and encouragement. In particular I would like to thank my late father and also my sisters, Juliet and Hanan , for financial assistance that covered all travel expenses during my first field season.

Other people provided help and support during the course of this study. I would like to extend my appreciation to my thesis supervisor, Professor R. N. Hiscott, for suggesting this project, providing advice, editing text, and providing partial financial support. I would like to thank Dr. Tom Calon, member of supervisory committee, for his advice and criticism.

I would like to express my gratitude to Professor Ali E. Aksu. Professor Aksu was a constant source of help, support and encouragement for the duration of my studies.

Members of my thesis examination committee, Professor K.T. Pickering (University College, London), Professor A.F. King and Dr. Andy Pulham (Department of Earth Sciences, Memorial University), provided many insightful comments and raised many questions. In particular I would like to thank Professor Pickering for many useful suggestions and his fairness.

Financial support for this study and for myself were provided partly by research grants to my supervisor. I would like to thank the School of Graduate Studies for the

numerous bursaries awarded to me over the years. In particular I would like to thank Dean Christopher Sharp and Dean Gregory Kealey and Mr. Paul Penny. I would like also to thank Professor Jim Wright, Head of the Department of Earth Sciences, for providing some financial support. I would like to thank office of the Dean of Science, particularly Professor Frederick Smith and Mr. Bruce Strong for offering me employment for many years. Also I would like to thank Mrs. Elizabeth Churchill (formerly of the Department of Earth Sciences) for teaching assistantships over the years. The Geological Society of America awarded me with a grant through their Grant-in-Aid program that covered expenses for part of my second field season expenses and geochemical analyses.

I would like to express my gratitude to the School of Graduate Studies for granting me a leave of absence for one year to attend to extenuating family matters. I would also like to thank Dean Chet Jablonski for his support and understanding.

Mr. Darren Smith, our department computer analyst, provided help on numerous occasions and solved many of my computer problems. I would also like to thank Dr. Joyce Macpherson and Miss Venessa Bennett for editing parts of my thesis, and Dr. Usama Ebead for his help with some computer programs.

I am grateful for the friendship, support and hospitality of the late Professor Susan McCorquodale, Ms. Frances-Oakley Power and Mr. Everett Day. I would like to thank my friends Amgad Hussein, A. Abdel Razek and Usama Ebead for their support and help.

Finally, I would like dedicate this thesis to the memory of my late father.





## TABLE OF CONTENTS

	Page
TITLE PAGE.....	i
ABSTRACT.....	iv
ACKNOWLEDGMENTS.....	vii
TABLE OF CONTENTS.....	ix
LIST OF FIGURES.....	xiv
LIST OF TABLES.....	xvii
LIST OF PLATES.....	xx
CHAPTER 1: INTRODUCTION	
1.1. Nature of the problem.....	1
1.2. Objectives of this study.....	4
1.3. Advantages of studying the Cloridorme Formation.....	6
1.4. Regional setting and structure.....	8
1.5. Stratigraphy of the Cloridorme Formation.....	11
1.6. Age and correlative units.....	15
1.7. Previous sedimentological work.....	17
1.8. Thesis outline.....	23
CHAPTER 2: THE STUDY AREA, FIELD AND LABORATORY METHODS	
2.1. The study area and the studied sequence.....	24
2.2. Areas of measured sections.....	28
2.2.1. Area A: Pointe-à-la-Renommée.....	28
2.2.2. Area B: Grand-Étang to Cloridorme.....	31
2.2.3. Area C: Pointe-à-la-Frégate.....	36

## TABLE OF CONTENTS (continued)

	Page
2.3. Inconsistencies in previous mapping.....	38
2.4. Structural framework of the measured sections .....	40
2.5. Field methods for section measurements.....	41
2.6. Laboratory analytical methods.....	44
<b>CHAPTER 3: FACIES DESCRIPTION AND INTERPRETATION</b>	
3.1. Database: geography, stratigraphy and terminology.....	47
3.2. Facies classification.....	54
3.3. Facies classes.....	57
3.4. Facies Class E (shale).....	62
3.4.1. Shale facies description.....	62
3.4.2. Shale facies interpretation.....	67
3.5. Facies Class D (siltstones, silty mudstones and siltstone-mudstone couplets).....	69
3.5.1. Description of facies D2.1.....	73
3.5.2. Interpretation of facies D2.1.....	81
3.5.3. Description of facies D2.2.....	85
3.5.4. Interpretation of facies D2.2.....	87
3.5.5. Description of facies D2.3.....	87
3.5.6. Interpretation of facies D2.3.....	87
3.6. Facies Class C (sandstone-mudstone couplets and muddy sandstones) .....	88
3.6.1. Disorganised sandstone facies group.....	88
3.6.1.1. Description of facies C1.1.....	89
3.6.1.2. Interpretation of facies C1.1.....	89
3.6.2. Organised sandstone facies group.....	91
3.6.2.1. Description of facies C2.1.....	92

## TABLE OF CONTENTS (continued)

	Page
3.6.2.2. Interpretation of facies C2.1 .....	97
3.6.2.3. Description of facies C2.2 .....	100
3.6.2.4. Interpretation of facies C2.2 .....	104
3.6.2.5. Description of facies C2.3 .....	105
3.6.2.6. Interpretation of facies C2.3 .....	108
3.6.2.7. Description of facies C2.4 .....	109
3.6.2.8. Interpretation of facies C2.4 .....	114
3.6.2.9. Description of facies C2.5 .....	123
3.6.2.10. Interpretation of facies C2.5 .....	124
3.7. Facies Class B (sandstones) .....	126
3.7.1. Disorganised sandstone beds of Class B .....	126
3.7.1.1. Description of Facies B1.1 .....	126
3.7.1.2. Interpretation of facies B1.1 .....	127
3.7.2. Organised sandstone beds of Class B .....	128
3.7.2.1. Description of facies B2.1 .....	129
3.7.2.2. Interpretation of facies B2.1 .....	131
3.7.2.3. Description of facies B2.2 .....	134
3.7.2.4. Interpretation of facies B2.2 .....	138
3.8. Other lithologies .....	142
3.9. Summary .....	143

## CHAPTER 4: CORRELATIONS OF MEGATURBIDITES AND

### K-BENTONITES

4.1. Introduction .....	146
4.2. Correlation of megaturbidites .....	147

## TABLE OF CONTENTS (Continued)

	Page
4.2.1. Correlation based on megaturbidite thicknesses and stratigraphic position.....	149
4.3. K-bentonite correlations.....	153
4.3.1. Correlation of K-bentonite horizons based on chemical fingerprinting.....	157
4.4. Conclusions.....	163

## CHAPTER 5: DEPOSITIONAL ENVIRONMENT, ARCHITECTURAL ELEMENTS AND DEPOSITIONAL HISTORY

5.1. Introduction.....	166
5.2. Architecture of turbidite bodies.....	173
5.3. Database, interpretation procedure and assumptions.....	175
5.4. Time-slices.....	178
5.4.1. Description of time-slice 1.....	178
5.4.2. Interpretation of time-slice 1.....	188
5.4.3. Description of time-slice 2.....	194
5.4.4. Interpretation of time-slice 2.....	202
5.4.5. Description of time-slice 3.....	206
5.4.6. Interpretation of time-slice 3.....	210
5.4.7. Description of time-slice 4.....	216
5.4.7.1. Description of sub-slice 4-1.....	216
5.4.7.2. Interpretation of sub-slice 4-1.....	225
5.4.7.3. Description of sub-slice 4-2.....	234
5.4.7.4. Interpretation of sub-facies 4-2.....	240
5.4.8. Description of time-slice 5.....	245

## TABLE OF CONTENTS (Continued)

	Page
5.4.9. Interpretation of time-slice 5.....	251
5.4.10. Description of time-slice 6.....	254
5.4.10.1. Description of sub-slice 6-1.....	254
5.4.10.2. Interpretation of sub-slice 6-1.....	263
5.4.10.3. Description of sub-slice 6-2.....	270
5.4.10.4. Interpretation of sub-slice 6-2.....	277
5.4.11. Description of time-slice 7.....	280
5.4.12. Interpretation of time-slice 7.....	288
5.5. Synthesis of depositional environments and depositional history.....	293
5.5.1. Time-slice 1 to time-slice 3.....	295
5.5.2. Time-slice 4.....	299
5.5.3. Time-slice 5.....	302
5.5.4. Time-slices 6 and 7.....	302
5.5.5. Post time-slice 7.....	303
5.6. Conclusions.....	303

## CHAPTER 6: BED THICKNESS DISTRIBUTIONS

6.1. Introduction.....	305
6.2. Class E bed thickness distribution.....	312
6.3. Class D bed thickness distribution.....	319
6.4. Class C bed thickness distribution.....	326
6.5. Class B bed thickness distribution.....	331
6.6. Comparison between facies classes and facies.....	332
6.7. Lateral and vertical trends in bed thickness distribution.....	339
6.8. Conclusions.....	345

## TABLE OF CONTENTS (Continued)

	Page
CHAPTER 7: CONCLUSIONS AND RECOMMENDATIONS	
7.1. Summary and conclusions.....	348
7.2. Recommendations and future work.....	352
REFERENCES.....	357
APPENDICES	
Appendix A:	
Appendix A1: Location of the rocks presented in the plates.....	A2
Appendix A2: Description of the areas of the measured sections.....	A5
Appendix A3: Logs of the measured section.....	A11
Appendix A4: Statistical methods used for K-bentonite correlations.....	A25
Appendix A5: Effects of folding on the sections thicknesses.....	A39
Appendix A6: Palinspastic map construction.....	A61
Appendix A5: Tables for thesis chapters.....	A72
Appendix B: Bed thickness distribution ( for Chapter 6).....	B1
Appendix C: CD-ROM disk in back pocket with the time-slices data	



## LIST OF FIGURES

	Page
1.1. Geographic location map.....	5
1.2. Geologic map of the area.....	10
1.3. Stratigraphic nomenclature of the Cloridorme and Deslandes formations .....	12
2.1. Location of the three detailed study areas .....	25
2.2. Map of detailed area A.....	30
2.3. Map of detailed area B (east) .....	32
2.4. Map of detailed area B (west) .....	33
2.5. Map of detailed area C.....	37
3.1. Stratigraphic overlap of the measured sections.....	48
3.2. Classification scheme adopted in this study.....	56
3.3. Facies classes relative abundances.....	61
3.4. Relative proportions of bed thickness categories for shale.....	65
3.5. Relative proportions of the facies of Class D.....	72
3.6. Percent of the number of beds and thicknesses for D2.1 subfacies.....	76
3.7. Relative proportion of bed thickness categories for D2.1 subfacies.....	77
3.8. Relative proportions of sandstone facies of group C2.....	93
3.9. Relative proportions of the bed thickness categories of the sandstone facies.....	93
3.10. Transition diagram for group A beds of facies C2.4.....	117
3.11. Transition diagram for group B beds of facies C2.4.....	119
3.12. Transition diagram for group C beds of facies C2.4 .....	122
4.1. Correlation of sections based on megaturbidite thicknesses.....	151
4.2. Photograph of K-bentonite horizon KB-1 in section FP1.....	155
4.3. Photograph of K-bentonite horizon KB-8 in section SYW.....	155
4.4. Territorial maps for the control group samples and the unknown samples.....	159
4.5. Scatter plots used to distinguish KB-6, KB-7 and KB-9.....	162

## LIST OF FIGURES (Continued)

	Page
4.6. Division of the studies sequence into time-slice.....	164
5.1. Architectural elements and bounding surfaces hierarchy .....	171
5.2. Long distance correlation of time-slice .....	181
5.3. Comparison of facies in time-slice 1 between areas A and C .....	183
5.4. Comparison of facies in time-slice 1 between areas A, B and C .....	184
5.5. Comparison of the number of beds in the mini-slices of time-slice 1.....	185
5.6. Short distance correlation of time-slice 1. ....	187
5.7. Long distance correlation panel for time- slice 2 .....	195
5.8. Comparison of facies in time-slice 2 between areas A, B and C .....	197
5.9. Comparison of the number of beds in the mini-slices of time-slice 2.....	199
5.10. Short distance correlation of time-slice 2. ....	201
5.11. Long distance correlation panel for time- slice 3 .....	207
5.12. Comparison of facies in time-slice 3 between areas A, B and C .....	208
5.13. Comparison of the number of beds in the mini-slices of time-slice 3.....	211
5.14. Short distance correlation of time-slice 3. ....	212
5.15. Comparison of the facies in time-slice 4 between areas A, B and C .....	217
5.16. Long distance correlation panel for sub-slice 4-1 .....	218
5.17. Number of beds in the mini-slices of sub-slice 4-1 in areas A, B and C.....	221
5.18. Short distance correlation of sub-slice 4-1. ....	223
5.19. Number of beds in the mini-slices of sub-slice 4-1 in area A .....	226
5.20. Long distance correlation for sub-slice 4-2 .....	235
5.21. Number of beds in the mini-slices of sub-slice 4-2 in areas A, B and C.....	237
5.22. Short distance correlation of sub-slice 4-2.....	239
5.23. Number of beds in the mini-slices of sub-slice 4-2 in area A .....	241
5.24. Long distance correlation for time-slice 5 .....	247

## LIST OF FIGURES (Continued)

	Page
5.25. Number of beds in the mini-slices of time-slice 5 in areas A, B and C.....	248
5.26. Short distance correlation of time-slice 5 .....	250
5.27. Number of beds in the mini-slices of time-slice 5 in area B .....	252
5.28. Comparison of the facies in sub-slice 6-1 .....	256
5.29. Long distance correlation panel for sub-slice 6-1 .....	257
5.30. Number of beds in the mini-slices of sub-slice 6-1 in areas A, B and C.....	259
5.31. Short distance correlation of sub-slice 6-1. ....	261
5.32. Number of beds in the mini-slices of sub-slice 6-1 in area A .....	262
5.33. Comparison of the facies in sub-slice 6-2 .....	272
5.34. Long distance correlation panel for sub-slice 6-2 .....	273
5.35. Number of beds in the mini-slices of sub-slice 6-2.....	275
5.36. Short distance correlation of sub-slice 6-2. ....	276
5.37. Long distance correlation panel for time-slice 7 .....	282
5.38. Comparison of the facies in time-slice 7 between areas B and C .....	283
5.39. Number of beds in the mini-slices of time-slice 7.....	284
5.40. Short distance correlation of time-slice 7. ....	287
5.41. Schematic of the depositional history.....	297
6.1. The lognormal, exponential and gamma distributions.....	309
6.2. Bed thickness distribution of beds of Class E.....	314
6.3. Comparison between the portability-log plot and the log-log plot.....	318
6.4. Bed thickness distribution of beds of Class D.....	321
6.5. Bed thickness distribution of facies D2.1.....	323
6.6. Comparison of the siltstone facies of Class D.....	324
6.7. Bed thickness distribution of bed of Class C.....	327
6.8. Bed thickness distribution of facies B2.2.....	333

## LIST OF FIGURES (Continued)

6.9. Comparison between the four facies classes.....	335
6.10. Comparison of the bed thickness data between facies and subfacies.....	338
6.11. Comparison between the bed thickness between time-slices in different areas.....	342

## LIST OF TABLES

	Pages
2.1. List of the measured sections and their location.....	26
2.2. Summary of the thicknesses, lithologies and palaeocurrents of the sections.....	27
3.1. Facies recognised in this study.....	55
3.2. Statistics for all the facies classes and component facies.....	58
3.3. Bed characteristics of facies C2.1.....	94
3.4. Bed characteristics of facies C2.2.....	102
3.5. Bed characteristics of facies C2.3.....	107
3.5. Comparison of the characteristics of the parts of facies B2.2.....	135
4.1. Field characteristics of K-bentonite horizons.....	156
5.1. Architectural elements characteristics.....	172
5.2. Percent of facies classes in the time-slices in different parts of the area.....	179
5.3. Summary of the characteristics of time-slices and mini-slices.....	296

## LIST OF PLATES

	Page
1. Facies Class E.....	64
2. Facies Class D occurring in packets that are laterally continuous.....	70
3. Subfacies D2.1A and D2.1B .....	74
4. Subfacies D2.1C, D2.1D, D2.1F and D2.1G.....	75
5. Subfacies D2.1E.....	86
6. Facies D2.2 and D2.3.....	86
7. Facies C1.1 and C2.1 .....	90
8. Facies C2.2 and facies C2.3.....	101
9. Facies C2.4.....	110
10. Facies B2.1 and B2.2 .....	130

## **CHAPTER 1**

### **INTRODUCTION**

#### **1.1. NATURE OF THE PROBLEM**

The study of deep marine turbidite systems, including submarine fans, has progressed considerably in the last half century. Depositional models have been proposed for modern and ancient submarine-fan deposits (Normark, 1970; Mutti and Ricci Lucchi, 1972; Heller and Dickinson, 1985; Shanmugam and Moiola, 1988; Reading and Richards, 1994, Stow *et al.*, 1996; Mutti *et al.*, 1999; Stelting *et al.*, 2000), but universal models for submarine fans and turbidite systems are still lacking (Mutti and Normark, 1991).

Attempts to construct a universal model (e.g., Walker, 1978) by combining information from both modern and ancient examples have not gained general acceptance (Nilsen, 1980). This is mainly because of the different scales of observations, and variable investigation methods and techniques used in the study of modern and ancient systems (Normark *et al.*, 1993; Shanmugam, 2000). It is now appreciated that there is a wide variety of modern submarine fans and turbidite systems and there are variations within individual fans or systems. Such variation should also be expected in ancient turbidite systems. Matching ancient systems with analogous modern systems is difficult and should be done using a common set of parameters and variables such as size, morphology and facies (Mutti and Normark, 1987, 1991; Shanmugam and Moiola, 1988; Pickering *et al.*, 1989; Reading and Orton, 1991; Reading and Richards, 1994; Stow *et al.*, 1996; Piper



and Normark, 2001).

Outcrop studies of ancient turbidite systems, carried out mainly in fold and thrust orogenic belts, provide a wealth of information on the physical characteristics of beds and groups of beds that permit the vertical analysis of the facies and facies associations of turbidite systems (Mutti *et al.*, 1999). The main disadvantage of outcrop studies is the lack (mainly due to structural complexities) of thick exposures that can be correlated over large areas. Such correlations permit detailed evaluation of the spatial distribution of different turbidite beds and bodies (Mutti and Normark, 1987; Normark *et al.*, 1993). Studies cited in the literature where turbidite systems were studied over long distances are limited to the more sandy exposures that form prominent outcrops, or to special facies (Hesse, 1974, 1995a; Ricci Lucchi and Valmori, 1980). These studies have emphasised the continuity of individual turbidite beds over tens of kilometres.

Outcrops of turbidite bodies span a critical gap in scale between seismic data and borehole data. Despite this, large scale features (e.g. levees) are difficult to recognise and identify; instead, they are deduced from local observations of facies and facies associations. Even in areas where biostratigraphic or chronostratigraphic data are available, it is usually of insufficient temporal resolution (mainly due to high sedimentation rates) to allow the establishment of detailed correlations necessary for the detailed study of the architecture of turbidite sand bodies (Normark *et al.*, 1993).

In contrast, near-surface studies of modern systems provide a wealth of information on depositional morphologies and the distribution of the surficial deposits

(Mutti and Normark, 1987, 1991; Pickering *et al.*, 1995; Piper *et al.*, 1999; Piper and Normark; 2001). Data obtained using different techniques (shallow seismic, coring and side-scan sonar) allow the identification of near-surface features that cannot be observed in most outcrops, but provide very limited information about facies successions, especially when compared with outcrop studies. The lack of suitable technology to core thick sandy intervals even in the Ocean Drilling Program (e.g., Ocean Drilling Program Leg 155, Amazon Fan) relegates the interpretation of facies characteristics to indirect techniques such as geophysical wireline logs (e.g., Schlumberger's Formation MicroScanner and Formation MicroImager). These techniques provide a wealth of new information but rarely supply the detail obtained from outcrop studies of facies.

In recent years, with extension of petroleum exploration into deeper water and the development of seismic stratigraphy and sequence stratigraphy, there has been renewed interest in deep marine turbidite deposits and their architecture, particularly from the petroleum industry. Sheet sandstones of turbidite origin may extend laterally for hundreds or thousands of metres and amalgamation of these sheet sandstone turbidite beds can form significant reservoirs (Hurst *et al.*, 2000). Some turbidites may be characterised by coarse grain size and/or good sorting (e.g., some channel deposits) making them potential targets for oil exploration. Despite the large volumes of oil in some of these reservoirs (Richards *et al.*, 1998), production may be hampered by the complex architecture of turbidite reservoirs. A better understanding of the factors that control the internal architecture and lateral continuity of these turbidite bodies and individual beds and deposits is critical to

improve and maximise oil recovery from turbidite reservoirs.

The importance of the three-dimensional organization of turbidite bodies has been emphasised in recent years with the introduction of new approaches focussed on the systematic study of deposit architecture. These studies define turbidite bodies by the presence of (i) specific facies types and (ii) distinctive bounding surfaces (Mutti and Normark, 1987, 1991; Normark *et al.*, 1993; Pickering *et al.*, 1995). This approach is similar to approaches used in studies of eolian and fluvial deposits (Brookfield, 1977; Allen, 1983; Miall, 1985). Only in recent years has this approach been applied to turbidite deposits (Mutti and Normark, 1987; Pickering *et al.*, 1995). Areas where turbidite deposits are well exposed and can be mapped over long distances are the best candidates for architectural analysis (Mutti *et al.*, 1999), but studies are limited. The Cloridorme Formation is considered in this thesis because of its excellent exposures over ~25 km of coastline in the Québec Appalachian.

## **1.2. OBJECTIVES OF THIS STUDY**

The primary goal of this thesis is to investigate and understand the depositional history of the turbidites of the Middle Ordovician Cloridorme Formation exposed in the coastal outcrops between Pointe-à-la-Frégate and Pointe-à-la-Renommée (Figure 1.1).

Three main objectives have been defined:

(1) To delineate the shape and geometry of turbidite bodies, i.e. the “architectural elements” that define this part of the Cloridorme Formation.

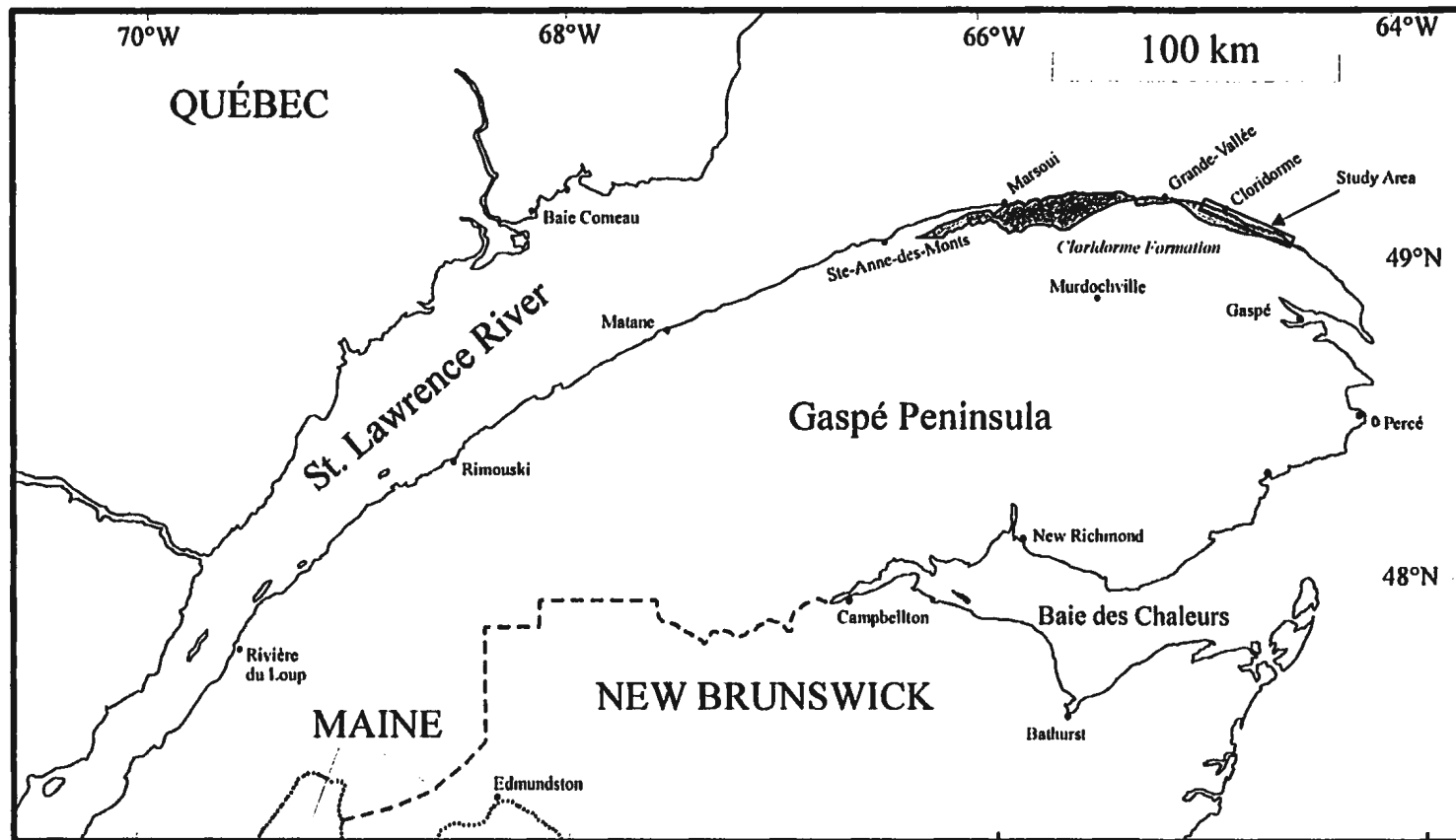


Figure 1.1. Geographical location map. The outcrops of the Cloridorme Formation are shown in a stippled pattern. The study area is also shown. Modified from Brisebois *et al.* (1991).

(2) To evaluate the parameters that controlled the development of these architectural elements.

(3) To investigate the bed-thickness distribution of the different facies of the Cloridorme Formation in order to determine the sedimentological factors that might control bed thickness distributions (i) vertically in individual sections and (ii) laterally within time-slices.

### **1.3. ADVANTAGES OF STUDYING THE CLORIDORME FORMATION**

The Middle Ordovician Cloridorme Formation of the Gaspé Peninsula, Québec, Canada, provides a unique opportunity to study the depositional architecture of deep-marine turbidite bodies. The Cloridorme Formation consists thick sequences (hundreds of metres) of deep-marine strata superbly exposed in several sections in a 25 km wide area. There are numerous marker beds that allow precise correlation between several measured sections. An additional advantage is that structural deformation is not intense.

The Cloridorme Formation was deposited in the Taconic foreland basin, and is exposed today on the south shore of the St. Lawrence River, Gaspé, Québec (Figure 1.1). These rocks have attracted many sedimentological studies over the years aimed at the description and interpretation of facies and facies associations in order to deduce depositional processes and sedimentary environments in different parts of the formation. Lateral continuity and correlation of beds over kilometres to tens of kilometres have attracted the interest of both academe and industry (e.g., Hiscott *et al.*, 1986; Cossey,

1994; Pickering *et al.*, 1995, Ma, 1996). Despite the numerous studies carried out in the Cloridorme Formation, the depositional environment and the influence of tectonics on deposition is not well understood (Hesse, 1982).

The main focus of this study is a 400-650 m-thick sequence, represented by the Pointe-à-la-Frégate Member and the upper part of the Manche-d'Épée Member (*sensu* Slivitzky *et al.*, 1991) of the Cloridorme Formation that is restricted geographically to the area between Pointe-à-la-Renommée (~ 4 km west of Anse-à-Valleau) and Pointe-à-la-Frégate, extending along strike for a distance of approximately 25 km (Chapter 2). This sequence is exposed at several closely spaced coastal outcrops. Several isochronous marker beds consisting of K-bentonite horizons or basin-scale megaturbidites are used for the first time in this thesis to correlate the sequence over the entire study area. Earlier correlations published by Pickering and Hiscott (1985,1995) contain errors because of miscorrelation of some megaturbidites.

The marker beds used in this thesis divide the 400-650 m-thick turbidite sequence into smaller chronostratigraphic units (time-slices). Within these time-slices, a variety of sandstone, siltstone and shale facies and associations can be placed in a well-constrained spatial context so as to evaluate the two-dimensional architecture of the turbidite bodies and the factors that control the evolution of individual facies and associations in time and space in this part of the Taconic foreland basin. The time-slice approach has not been previously applied in the Cloridorme Formation and very few examples from either ancient turbidite sequences or modern settings exist where sequences that are several hundreds of

metres thick were correlated in detail over distances of tens of kilometres. The results of this thesis, when combined with the results of other studies carried out in other parts of the Cloridorme Formation, lead to a better understanding of the depositional history of this area.

#### **1.4. REGIONAL SETTING AND STRUCTURE**

The Cambro-Ordovician rocks of northern Gaspé Peninsula form a 30 km-wide belt bounded to the north by the Gulf of St. Lawrence and to the south by an angular unconformity that separates them from the Silurian-Devonian rocks of the Connecticut Valley Synclinorium (St-Julien and Hubert, 1975; Slivitzky *et al.*, 1991). They are part of the Humber tectonostratigraphic zone of Williams (1979). Their lithologies and structures suggest that they were deposited and deformed during the formation and destruction of an Atlantic-type continental margin (St-Julien and Hubert, 1975). The rocks were affected by the Taconic and Acadian orogenies that are responsible for northward thrusting and oblique-slip faults, respectfully (Slivitzky *et al.*, 1991).

In the Québec Appalachians, the Humber zone is divided into four domains: the autochthonous domain; the foreland fold and thrust belt; the external nappes domain; and the internal nappes domain (St-Julien and Hubert, 1975). In the Gaspé Peninsula, the foreland fold and thrust belt is restricted to the Caradoc Ordovician Cloridorme Formation while the external domain consists of the Marsoui River Nappe (Llandeilo-Caradoc Deslandes Formation) and Ste-Anne River Nappe (Llanvirn-Llandeilo Cap Chat Mélange,



Llanvirn Tourelle Formation, Lower Cambrian Lake Matapédia facies of the Shickshock Group, Middle Cambrian l'Orignal Formation, Arenig Romieu Formation and Rivière Ouelle Formation) (Figure 1.2). Slivitzky *et al.* (1991) indicate that for the Cloridorme Formation, Deslandes Formation and Cap Chat Mélange, only the mélange does not respect the normal stacking order in which older units overthrust younger units. Instead, the Cloridorme Formation and the Marsoui River Nappe (Deslandes Formation) overthrust the older Cap Chat Mélange. Slivitzky *et al.* (1991) attribute this out-of-sequence thrusting to late movement, probably during the Acadian Orogeny.

Geological investigations relevant to the northern Gaspé Peninsula started in the middle eighteen hundreds with the work of William Logan (1863), who placed a structural discontinuity (Logan's Line) between the more strongly deformed allochthonous sedimentary rocks south of the St. Lawrence River and autochthonous Cambro-Ordovician platform rocks to the north. The position of this line has been debated, varying from an offshore position somewhere under the St. Lawrence River to on land somewhere in the Gaspé area. St-Julien and Hubert (1975) considered the Cloridorme Formation to be parautochthonous, and thus placed Logan's Line at its southern boundary. Ells (1883), McGerrigle (1954), Biron (1973) and, more recently, Lachambre and Brisebois (1990), Brisebois *et al.* (1991), and Slivitzky *et al.* (1991) carried out detailed mapping in the northern Gaspé.

Enos (1965) divided the Cloridorme Formation into three structural blocks. The sequence studied in this thesis is located in his central block, and is restricted

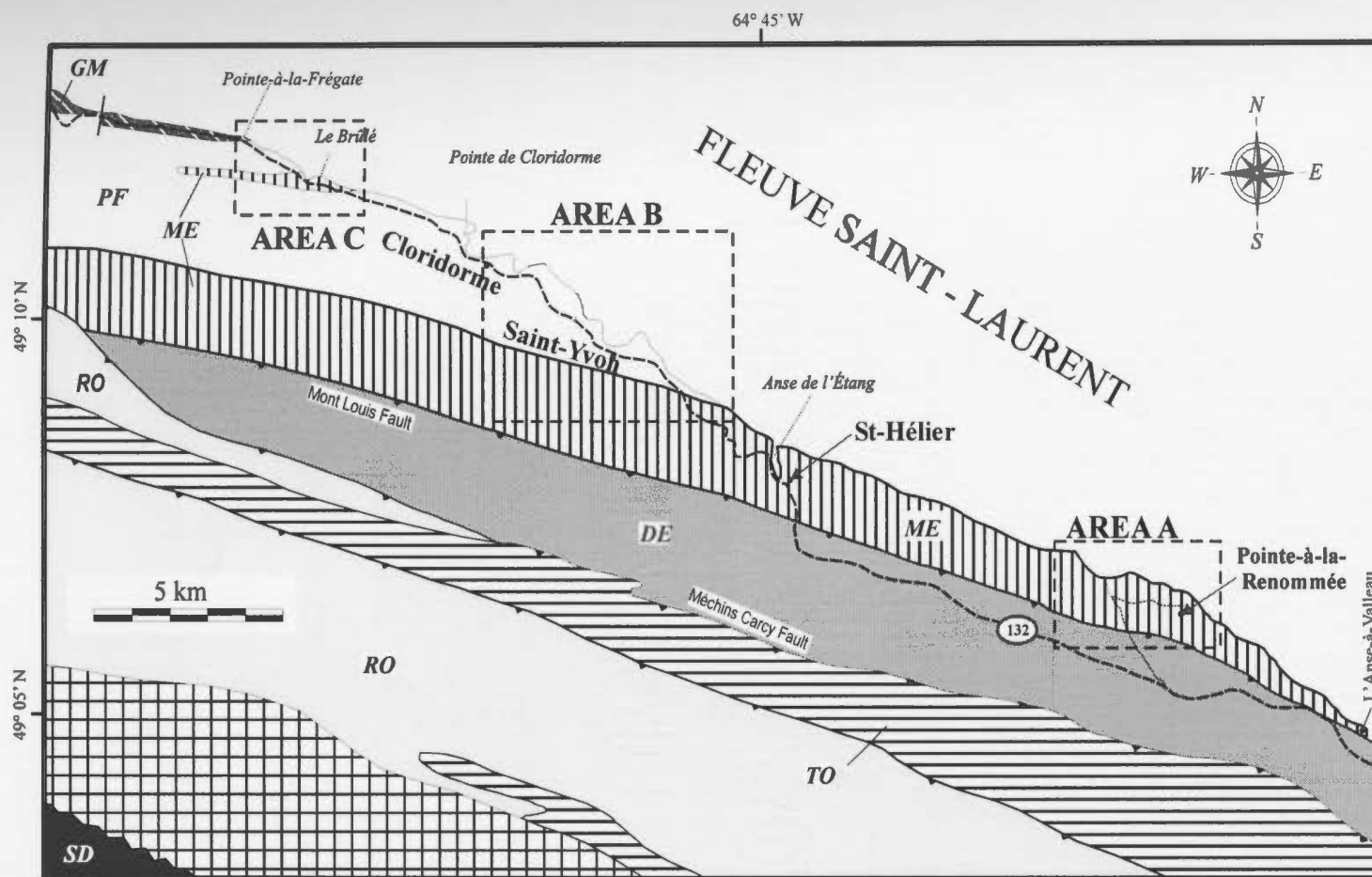


Figure 1.2. Geological map of the area showing main townships and the areas where the detailed sections were Measured (Chapter 2). The outcrops of the members of the Cloridorme Formation are shown (GM= Gros-Morne Member, PF= Pointe-à-la-Frégate Member, ME= Manche-d'Épée Member). Also shown are the outcrops of the Deslandes Formation (DE), Tourelle Formation (TO), Rivière Ouelle Formation (RO), Romieu Formation (RM) and the undifferentiated Silurian-Devonian (SD) sedimentary rocks. Geology from Slivitzky *et al.* (1991).

stratigraphically to the Pointe-à-la-Frégate (PF) and Manche-d'Épée (ME) members of Slivitzky *et al.* (1991), approximately equivalent to the  $\beta_2$ ,  $\beta_3$ ,  $\beta_4$  and  $\beta_5$  members of Enos (1965). The Slivitzky *et al.* (1991) division of the Cloridorme Formation will be followed in this thesis although correlations presented later raise questions about boundaries of some of their members (Chapter 2).

## 1.5. STRATIGRAPHY OF THE CLORIDORME FORMATION

Division of the Cloridorme Formation (Figure 1.3) is mainly based on lithostratigraphy, with members defined by the appearance or disappearance of certain facies or groups of facies (Enos, 1965, 1969a,b; Biron, 1973; Hiscott *et al.*, 1986; Slivitzky *et al.*, 1991; Kessler *et al.*, 1995; Prave *et al.*, 2000).

Enos (1965) named the rocks exposed between Jersey Cove and Marsoui (over a distance of 145 km) the Cloridorme Formation. He informally divided the formation into 14 members grouped into 3 sequences, with each sequence restricted to a specific structural block. The stratigraphic relationships between members in different blocks were unknown at that time. Enos (1965) designated these members with Greek letters and Arabic numbers. In this thesis, usage of this mixed Greek - Arabic code refer to the members of Cloridorme Formation as defined by Enos. The eastern block contains the alpha sequence and is divided into three members,  $\alpha_1$  to  $\alpha_3$ . This block is highly deformed and poorly exposed in certain areas. The central block, studied in detail by Enos (1965), is the least deformed, and consists of the beta sequence and its seven members,

N. American Series	Graptolite Zones of Eastern N. America	Graptolite Zones of Texas (Berry, 1960)	Biron (1973)	Hiscott <i>et al.</i> (1986)	Enos (1965) members	Slivitzky <i>et al.</i> (1991)	Kessler <i>et al.</i> (1995)	Prave <i>et al.</i> (2000)				
MIDDLE ORDOVICIAN	<i>Climacograptus spiniferus</i>	<i>Orthograptus 'intermedius'</i>	Cloridorme Group	Cloridorme Formation	Marsoui member	$\gamma$ 4	Rochers-Penchés Member	Up. Cloridorme Fm ( $\gamma$ of Enos ?)	Cloridorme Formation			
					Mont-Saint-Pierre member		$\gamma$ 3	Mont-Saint-Pierre Member				
	Petite-Vallée member	$\gamma$ 2				$\beta$ 7		L'Anse-Pleureuse Member		Lower Cloridorme Fm ( $\beta$ of Enos ?)		
	Manche-d'Épée member				$\gamma$ 1		$\beta$ 6 $\beta$ 5 $\beta$ 4 $\beta$ 3	Pointe-à-la-Frégate member			Pointe-à-la-Frégate Member	
		St-Héliér member				$\beta$ 2 $\beta$ 1		Manche-d'Épée Member				
	<i>Diplograptus multidentis</i>	No fauna										
	<i>Nemagraptus gracilis</i>	<i>Climacograptus bicornis</i> and <i>Nemagraptus gracilis</i>			Deslandes Fm	Deslandes Formation		$\alpha$ 3		Deslandes Formation	Deslandes Fm	Deslandes Fm
								$\alpha$ 2				

Figure 1.3. Comparison of the different stratigraphic nomenclature of Cloridorme and Deslandes formations. The boundaries of the informal members of Hiscott *et al.* (1986) are based on correlations with members the Enos (1969a). The boundaries of the formal member defined by Slivitzky *et al.* (1991) are based on the correlation of their maps with Enos (1969b) map. The base of the *C. Spiniferus* graptolite zone is placed in in the middle of the  $\gamma$  2 member of Enos (1969b) according to Riva and Malo (1988). The remaining graptolite zones boundaries are placed based on personal communications of the author with G. Riva in 2000. Major thrust faults are marked by the irregular lines. The sequence of interest to this study is shaded. Areas with a diagonal lines pattern represent gaps.

$\beta_1$  to  $\beta_7$ . The western block contains the gamma sequence; it is divided into four members,  $\gamma_1$  to  $\gamma_4$ . Enos (1965) defined the boundaries of each member by the appearance and disappearance of certain facies or groups of thick greywacke beds. For example, the base of the  $\beta_3$  member is defined by the appearance of a group of thick greywacke beds. Enos (1965) estimated the thickness of the Cloridorme Formation to be 7700 m, but stated that this estimate could have a 50% error.

Biron (1973) elevated the Cloridorme Formation to the rank of a group because he considered the gamma members to be mappable units that he elevated to four formations. He also reassigned the alpha sequence to the Deslandes Formation that is recognised elsewhere in the Gaspé region. This reassignment limited the Cloridorme Group to the beta and gamma sequences of Enos (1965) that are exposed between l'Anse-à-Valleau and Marsoui. All subsequent studies have limited the Cloridorme Formation (or Group) to the beta and gamma sequences of Enos (1965).

Hiscott *et al.* (1986) informally divided the Cloridorme Formation into five members, listed here from oldest to youngest: St-Hélér member, Pointe-à-la-Frégate member, Petite-Vallée member, Mont-St-Pierre member; and Marsoui member (Figure 1.3). Their division is based on lithofacies and widespread marker beds (megaturbidites).

Hiscott *et al.* (1986) suggested that: (1) the St-Hélér member is equivalent to  $\beta_1$  and the lower part of  $\beta_2$ ; (2) the Pointe-à-la-Frégate member is equivalent to  $\gamma_1$  in the west and, in the east, to the upper part of  $\beta_2$  through  $\beta_6$ ; (3) the Petite-Vallée member is equivalent to  $\gamma_2$  and  $\beta_7$ ; (4) the Mont-St-Pierre member is equivalent to  $\gamma_3$ ; and (5) the

Marsoui member is equivalent to  $\gamma_4$ . Hiscott *et al.* (1986) estimated the thickness of the Cloridorme Formation to be about 4000 m.

Slivitzky *et al.* (1991), like Enos (1965) and Hiscott *et al.* (1986), divided the Cloridorme Formation based on facies or key beds. They divided the Cloridorme Formation into six formal members, listed here from oldest to youngest: Manche-d'Épée Member (ME), Pointe-à-la-Frégate Member (PF), Gros-Morne Member (GM), L'Anse-Pleureuse Member (AP), Mont-St-Pierre Member (SP), and Rochers Penchés Member (RP). Slivitzky *et al.* (1991) made no reference to the Hiscott *et al.* (1986) division of the Cloridorme Formation, and members with the same name have quite different boundaries.

Kessler *et al.* (1995) divided the Cloridorme Formation into two parts, a lower Cloridorme Formation (equivalent to the beta sequence) and an upper Cloridorme Formation (equivalent to the gamma sequence). In their view, the lower Cloridorme Formation is separated from the upper Cloridorme Formation by an unconformity that spans an interval equivalent to the duration of the *Orthograptus ruedemanni* graptolite zone. Based on information credited to J. Riva and G. Kessler (1996 personal communications to Bloechl), Bloechl (1996) suggested that the Deslandes Formation is partly time equivalent to the Pointe-a-la-Frégate (PF) and Manche-d'Épée members of Slivitzky *et al.* (1991). Prave *et al.* (2000) suggested that the lower part of the Cloridorme Formation is even older and spans part of the *Nemagraptus gracilis* graptolite zone.

The previous summary clearly highlights the lack of an agreed stratigraphy for the Cloridorme Formation. Different studies use different divisions, due partly to the limited

palaeontological data collected from the area to constrain ages, but also due to erroneous mapping and correlations of researchers who have attempted to map and correlate this part of the Cloridorme Formation (Enos, 1965; Pickering and Hiscott, 1985; Hiscott *et al.*, 1986; Slivitzky *et al.*, 1991; Prave *et al.*, 2000).

## 1.6. AGE AND CORRELATIVE UNITS

The Cloridorme Formation is one of a number of Ordovician foreland-basin turbidite successions that form a discontinuous belt extending from Newfoundland to Tennessee (Enos, 1969a,b; Hiscott, 1984). In Québec, the Cloridorme Formation is time-equivalent to part of the Trenton Group, Utica Formation and the lower part of the Lorraine Group in the Montreal-Québec City area (St-Julien and Hubert, 1975; Barnes *et al.*, 1981); the Lorraine and St-Rosalie groups exposed in the St. Lawrence Lowlands (Globensky, 1987); and the Macasty Formation of Anticosti Island (Barnes *et al.*, 1981). Riva and Malo (1988) suggested that the Cloridorme Formation is also equivalent to the Garin Formation in the southern Gaspé Peninsula.

Parts of the Cloridorme Formation may be time-equivalent to the Long Point Formation in Newfoundland (Williams, 1979); the upper part of the Tetagouche Group of New Brunswick (Riva and Malo, 1988); the Blind Brook Formation of northern Maine (Riva and Malo, 1988); the Normanskill, Canajoharie, and Utica Shale formations exposed in the Hudson Valley area of New York (Berry, 1962, 1970; Enos, 1969a; Riva and Malo, 1988); and, perhaps, the Viola Group of Oklahoma (Riva and Malo, 1988).

The age of the Cloridorme Formation is based upon graptolite fossils collected during several studies carried out in the area since the nineteen fifties (McGerrigle, 1954; Berry, 1962, 1970; Enos, 1965; Riva, 1968; Riva and Malo, 1988). Extensive collections made by Enos (1965) and identified by Berry from different parts of the Cloridorme Formation contain only a small number of species. Based on these collections, Enos (1965) assigned the entire Cloridorme Formation (alpha, beta and gamma sequences) to the *Orthograptus truncatus* var. *intermedius* zone (zone 13 of west Texas of Berry, 1960).

Riva (1968,1974) suggested that the graptolite zones of west Texas are not applicable to eastern North America. Instead, Riva (1968) suggested that the Cloridorme Formation ranges in age from the *Nemagraptus gracilis* to the *Climacograptus spiniferous* zone (Figure 1.3). Slivitzky *et al.* (1991), suggested that the Cloridorme Formation ranges in age from the *Diplograptus multidentis* zone to the *C. spiniferous* zone. This age assignment was based upon many samples collected from different parts of the northern Gaspé Peninsula and identified by John Riva.

Age constraints for the studied sequence are based on a limited number of graptolite collections and information gleaned from other studies. During this study, graptolites were collected from time-slices 6 and 7 (upper part of Pointe-à-la-Frégate Member of Slivitzky *et al.*, 1991) and identified by J. Riva. His determinations suggest that the whole studied sequence is of *D. multidentis* zone age, now to be renamed the *Climacograptus bicornis* zone (J. Riva, personal communications, 1997, 2000). He



suggested that the top of the *D. multidentis* zone may be placed somewhere near the top of the section measured in the area of Pointe Séche (section SYE, see Chapter 2). Older beds of the Cloridorme Formation and Deslandes Formation were deposited during the *Nemagraptus gracilis* graptolite zone (Riva, 1968). Barnes and Williams (1991) indicate that the *D. multidentis* graptolite zone is equivalent to the lower part of the Mohawkian North American Series. According to Ross and Ross (1995) the lower part of the Mohawkian Series consists of the Blackriveran and Rockland stages that span a period of about 5-10 million years around ~460 Ma.

## 1.7. PREVIOUS SEDIMENTOLOGICAL WORK

A comprehensive sedimentological study of the Cloridorme Formation was carried out by Enos (1969a,b). Enos's work is referred to in several parts of this thesis so it will not be described in detail here. Briefly, he described turbidite facies, their petrography (Appendix A7) bed continuity, and erected a stratigraphy for each of three structural blocks.

An important conclusion of Enos's work is the lack of good lateral continuity of individual turbidite beds in the middle part of the Cloridorme Formation (β7 member). Subsequent work in the same area by Ma (1996) supported Enos (1969a,b) original conclusions. Cossey (1994) and Ma (1996) attributed the lack of lateral continuity of beds to seabed irregularity, shingling effects, syn-depositional faulting, slumping, sliding and sand redistribution following liquefaction. In contrast, turbidite beds in the lower members

of the Cloridorme Formation show lateral continuity for tens of kilometres (Enos, 1969b p. 706).

Walker (1969) studied the geometry of ripple-drift cross laminations and sole marks in the Petite-Vallée area and suggested that variation in flow parameters and the rate of sediment supply from suspension controlled the formation of different types of ripple-drift cross lamination. He also developed an ABC index ( $\text{ABC index (\%)} = A + 0.5B$ ) in order to interpret the proximal to distal character of turbidites. A and B represent the percentage of beds in a succession that begin with Bouma (1962) divisions A or B. If all the beds begin with division A, then the index=100% and the beds are considered proximal while if all the beds begin with division C, then the index=0% and the beds are considered distal. Walker (1970) studied the lateral changes in the ABC index in the area between Petite-Vallée and Grande-Vallée. He found that this index shows an initial increase followed by a more uniform decrease (e.g., 88→100→96→92 and 80→88→78→78). Walker (1970) attributed this change in the index to pinch and swell of the beds. Pett and Walker (1971) studied the morphology of flute casts and their relationship to the different Bouma divisions in the turbidites of the Cloridorme Formation exposed at Grande-Vallée, Petite-Vallée and St-Hélier. They discovered that flutes on the soles of beds that start with the Bouma (1962) A division tend to be filled with coarser sands and are associated with lateral ridges and grooves, while flutes on the soles of beds that start with division B or C are filled with fine and medium sand and are associated with other tool marks.

Parkash (1969) and Parkash and Middleton (1970) evaluated downcurrent changes

in palaeoflow and the evolution of sedimentary structures and sole marks of certain turbidite beds in the area between Grande-Vallée and Petite-Vallée. They discovered that sole marks change from tool marks and flutes in proximal areas to longitudinal ridges and grooves, or the absence of sole marks, in distal areas. They also noted that sole marks orientation becomes more variable from proximal to distal areas and they attributed this to the greater influence of bottom topography as a current decreases in speed. An important conclusion from the work of Parkash (1969) and Parkash and Middleton (1970) is that before the onset of deposition from turbidity currents, the lower part of the flow develops higher concentration and deposition takes place in two phases. In the first phase, a “quick bed” forms and is characterised by high sediment concentration in which the sediment particles are supported by dispersive pressure. Consolidation of this quick bed forms the lower part of a bed. In the second phase, the upper part of the bed is deposited from a more dilute suspension. Between the upper and lower part of the bed there is a distinct break in grain size that is marked by a joint.

Skipper (1971), Skipper and Middleton (1975), and Skipper and Bhattacharjee (1978) studied thick, laterally continuous turbidite beds in the lower part of the Cloridorme Formation in the area between Pointe-à-la-Renommée and St-Hélier. These studies recognised upcurrent dipping cross-stratification in some of these turbidites. The formation of these structures was attributed to antidune migration during deposition from turbidity currents. Many other features were observed in these beds such as the presence of intervals of pseudonodules. These were interpreted to have formed due to syn-

depositional deformation of rapidly deposited sediments. Other thick, more muddy, and laterally continuous beds (type 3 greywacke of Enos 1965) consist entirely of pseudonodules of different size in their lower parts. These beds were used by Skipper and co-workers to correlate the sections between Pointe-à-la-Renommée and St-Hélier.

Pickering and Hiscott (1985) studied thick turbidites including some of those interpreted by Skipper and co-workers. They concluded that putative upcurrent dips of cross-stratification instead formed as a result of flow reversals following reflections and deflections of large turbidity currents in a confined elongate basin. Pickering and Hiscott (1985) named these flows “contained flows”. This term has not been widely adopted by others. Instead, beds of this type with their characteristic thick mud caps are commonly called “megaturbidites”. Pantin and Leeder (1987), Edwards (1993), and Edwards *et al.* (1994) studied some of the same thick beds and suggested that different types of structural divisions, separated by mud drapes observed in these beds, are formed by reflected flows characterised by different types of bores. Kessler *et al.* (1990, 1995) interpreted the thick beds as the products of deposition from high velocity, pulsating supercritical turbidity currents. Pickering and Hiscott (1985,1995) used the mud-capped megaturbidites as distinctive marker beds to correlate the section exposed at Pointe-à-la-Renommée with those exposed at St-Hélier and Pointe-à-la-Frégate. A similar correlation was proposed by Hiscott *et al.* (1986) with the inclusion of two other sections exposed in the St-Yvon and Cap Barré areas. Hiscott *et al.* (1986) and Pickering (1987) suggested that during Llandeilo to mid-Caradoc time, the lower part of the Cloridorme Formation (composed

mostly of megaturbidites and shale) was deposited in a flat basin-plain or basin-floor setting associated with a foreland basin that developed in front of an advancing pile of thrust sheets (Pickering, 1987). The foreland basin was bounded outboard by an emergent orogenic belt consisting of a thick stack of thrust sheets. This foreland basin extended from Newfoundland to Alabama (Williams 1979). Hiscott *et al.* (1986) suggested that the foreland basin was segmented into approximately 100 km-long segments by structural highs. The basin was confined along its sides by steep margins that caused the reflection and deflection of the flows that deposited the megaturbidites. During the mid-Caradoc, more sand was deposited, forming sand packets that Hiscott *et al.* (1986) interpreted as lobes fed by slope channels. These lobes formed positive relief on the flat basin floor and controlled the spread of the currents that deposited subsequent megaturbidites. Data presented later in this thesis demonstrate that several of the correlations of Hiscott *et al.* (1986) are incorrect.

Slivitzky *et al.* (1991) identified 25 turbidite facies in the entire Cloridorme Formation: nine in the Pointe-à-la-Frégate Member and ten in the Manche-d'Épée Member. Some of their "facies" are actually internal divisions of single sediment-gravity-flow deposits. For example, a single graded bed has been divided by Slivitzky *et al.* (1991) into five facies (their figure C-10, p.50). This methodology is counter to normal sedimentological practice for the facies description of turbidites and related deposits, thus weakening their contribution. Other parts of the Cloridorme Formation were also studied. Beeden (1983) focussed on detailed analysis of facies and facies associations in order to

interpret depositional environments. Beeden (1983) studied the  $\gamma 4$  member of Enos (1965) in the Rivière-à-Claude area which he interpreted to represent an alternation of lobe and lobe-fringe environments.

Enos (1969a) indicated that the bed-thickness distributions of sandstone and siltstone beds exposed in the area between Petite-Vallée and Grande-Vallée are approximately lognormal. Drummond and Wilkinson (1996) and Drummond (1999) suggested that bed-thickness data collected from the Rochers Penchés Member and Mont-Saint-Pierre Member of the Cloridorme Formation are best fitted by the exponential distribution. Carlson (1998) and Carlson and Grotzinger (2001) studied the bed-thickness distribution in different parts of the Cloridorme Formation. These studies claim that different submarine-fan subenvironments can be inferred from the shape of the cumulative power-law distribution curve because processes such as amalgamation and erosion are more common in certain subenvironments and this is reflected in the shape and curvature of a log-log plot of  $N$  (the number of beds thicker than the  $T$ ), versus  $T$ , where  $T$  is the bed thickness. Carlson and Grotzinger (2001) suggested that beds exposed in the St-Hélier and Pointe-à-la-Frégate areas are best fitted by a power law distribution, marked by a linear trend in  $N > T$  versus  $T$  plots. This linear trend suggests little or no erosion or amalgamation and thus suggests a ponded basin-plain, lower fan-lobe or lobe-fringe environment. In the Petite-Vallée area, Carlson and Grotzinger (2001) indicate that bed thickness trends of the  $N > T$  versus  $T$  plots show both linear and curved trends suggesting an increase in the effect of amalgamation and erosion. This result was unexpected because

they considered rocks in the Petite-Vallée area as basin-plain deposits, and the distal equivalents to rocks exposed in the east. According to them, the bed thickness trends should show a better developed linear trend suggesting less erosion and amalgamation, and not a curved trend.

### **1.8. THESIS OUTLINE**

The thesis consists of seven chapters intended to elucidate the sedimentology of the lower Cloridorme Formation.

(i) Chapter 2 which describes the study area and how each locality fits into the structural framework of the area. Field techniques are also described in this chapter.

(ii) Chapter 3 describes sedimentary facies and interprets depositional processes.

(iii) Chapter 4 is concerned with correlation of each section measured in the area. Basin-wide turbidites and K-bentonites are used for the correlation. Using a selection of these beds, the studied sequence is divided into seven smaller units (time-slices).

(iv) Chapter 5 is concerned with reconstructing the depositional history of the studied sequence. This is achieved through detailed investigation of facies and the architectural elements within each of the seven time-slices. The depositional history of the area is discussed in a sequential manner (i.e. from older slices to younger slices).

(v) Chapter 6 discusses the thickness distribution of the different facies.

(vi) The final chapter outlines the conclusions of this study and suggests avenues for further research that will build on the contributions made by this thesis.

## **CHAPTER 2**

### **THE STUDY AREA, FIELD AND LABORATORY METHODS**

#### **2.1. THE STUDY AREA AND THE STUDIED SEQUENCE**

In the study area, located between L'Anse-à-Valleau and Pointe-à-la-Frégate, thirteen sections were described in detail (Figure 2.1, Table 2.1). These were chosen because of the excellent exposure and correlative stratigraphy, critical for the study of the geometry and architecture of these turbidite deposits. Sequences that could not be correlated through more than two measured sections are not included in the study. The upper 550 m of the Pointe-à-la-Frégate Member of Slivitzky *et al.* (1991), located west of Grand-Étang (detailed areas B and C), and equivalent strata in the Pointe-à-la-Renommée area (detailed area A), from the sequence that is the main focus of this study. In the Pointe-à-la-Renommée area, this sequence has been mapped as part of the Manche-d'Épée Member by Slivitzky *et al.* (1991); however, bed-by-bed correlations carried out during this study prove this assignment to be incorrect.

The rocks exposed in these sections are dominated by shale (~67%) and subequal amounts of siltstone (~18%) and sandstone (~16%) (Table 2.2). Carbonate beds and K-bentonites form less than 1%. Palaeocurrents measured from flutes and ripple lamination range between 280° - 320° (Table 2.2). Measurements collected from ripple lamination show a greater dispersion than those collected from flutes (§2.4).



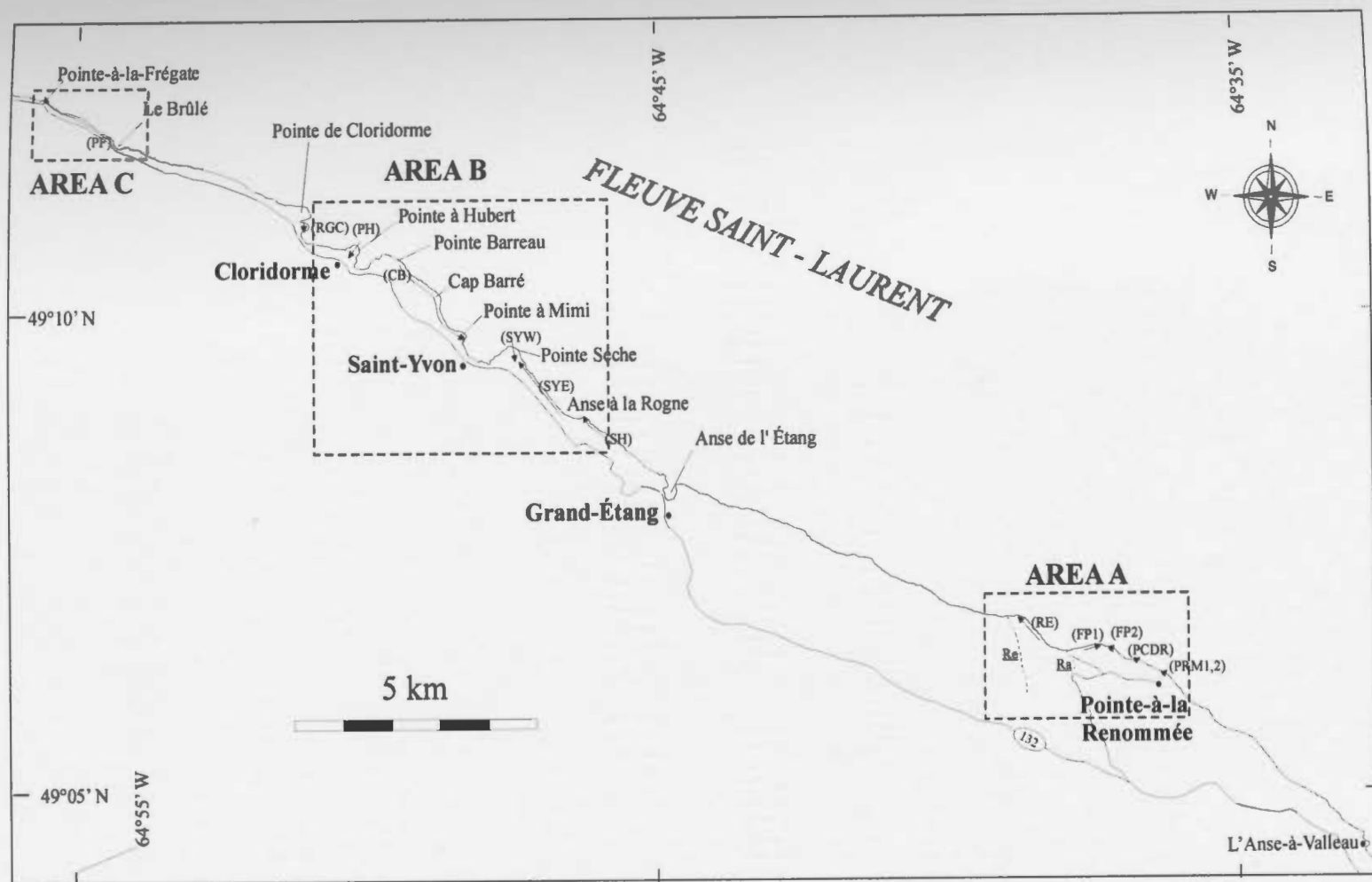


Figure 2.1. Location map with the three detailed study areas (A,B, and C). Also shown are the location of the measured sections (arrows, each arrow points to the top of a section). Note that Ruisseau à l'Échalote and Ruisseau à l'Ail in the Pointe-à-la-Renommée area are marked as Re and Ra, respectively.

Table 2.1. List of the measured sections, their location with reference to the National Military Grid, aerial photograph reference numbers, and the name of the geographic locality where each section is located.

Section	Grid Reference	Aerial Photograph	Geographic Name
PRM1	831406	Q-75335-2	Pointe-à-la-Renommée
PRM2	827407	Q-75335-2	Pointe-à-la-Renommée
PCDR	826409	Q-75335-2	Pointe des Canes de Roches
FP1	817412	Q-75335-3	Ruisseau à l'Ail
FP2	819411	Q-75335-3	Ruisseau à l'Ail
RE	802417	Q-75335-3	Ruisseau à l'Échalote
SH	710456	Q-75335-4	Anse à la Rogne
SYE	700464	Q-75343-70	Pointe Séche, St-Yvon (southern limb)
SYW	696468	Q-75343-70	Pointe Séche, St-Yvon (northern limb)
CB	680480	Q-75342-152	Cap Barré
PH	663490	Q-75342-153	Pointe à Hubert
RGC	652495	Q-75342-154	Rivière du Grand-Cloridorme
PF	597517	Q-75338.123	Pointe-à-la-Frégate

Table 2.2. Summary of the measured thicknesses, lithologies and directional data for each section in each of the detailed study areas. Note that the total thickness includes covered intervals. SD= standard deviation; # = number of.

	MAP AREA	C		B (WEST)		B (EAST)			A					
	SECTIONS	PF	RGC	PH	CB	SYW	SYE	SH	RE	FP1	FP2	PCDR	PRM1	PRM2
Thickness	Total Thickness (m)	774	65.4	106.6	290.2	140.8	450.5	240.6	275.7	230.8	107.3	220.1	33.5	51.8
	Number of Beds	6112	564	964	2664	1626	4241	1904	2473	2001	1085	2481	319	703
	Covered Intervals (m)	0	0.8	0	0	0.3	4.1	7.3	0	4.5	0	6.3	0	2.4
Lithologies	Sandstone %	16.5	5.1	4.8	14.5	19.6	17.3	12.3	12.1	12.4	17.4	21.2	32.7	23.3
	Siltstone %	14.6	23.4	19.6	15.8	25.1	18.1	13.1	15	13.3	16.9	17.7	13.2	25.9
	Shale %	67.9	71.5	74.5	69.3	55.0	64.0	73.1	71.9	73.3	65.5	61.0	53.4	50.6
	Carbonate %	0.8	0	0.6	0.2	0.1	0.4	1.4	1.0	0.9	0.2	0.01	0.6	0.2
	K-bentonite %	0.2	0.05	0.5	0.2	0.2	0.2	0.1	0.1	0.1	0.1	0.1	0.1	0.0
Directional Data	Bedding Dip	72	47	39	31	32	84	87	85	88	86	84	85	87
	Dip Direction	183	182	196	193	178	16	13	13	12	12	12	12	12
	Cleavage Dip	63	63	88	83	65	81	87	89	85	84	88	87	86
	Cleavage Dip Dir.	182	193	193	193	189	194	192	192	191	191	191	191	191
	Mean Current	280	233	312	321	299	294	274	280	280	279	281	286	285
	Current S.D.	±39	±21	±9	±19	±26	±33	±45	±26	±26	±19	±40	±37	±21
	Mean Flutes	269	246	ND	299	291	292	270	248	281	283	294	279	274
	Flutes S.D.	±30	--	ND	±7	±24	±21	±45	±20	±19	±17	±12	±34	±34
	# Flutes Measured	110	1	ND	20	22	15	49	42	17	13	35	5	5
	Mean Ripples	283	231	312	322	300	294	291	278	279	275	269	305	312
	Ripples S.D.	±41	±22	±9	±19	±26	±33	±42	±29	±30	±22	±51	±50	±18
	# Ripples Measured	337	7	28	280	98	203	13	53	30	12	38	2	2

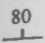
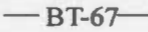
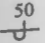
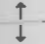

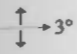

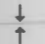

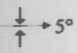


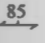
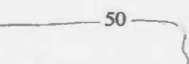
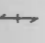


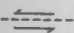


## **2.2. AREAS OF MEASURED SECTIONS**

The thirteen sections fall naturally into three geographic areas (Figure 2.1): Area A= Pointe-à-la-Renommée (sections RE, FP1, FP2, PCDR, PRM1, PRM2); Area B= Grand-Étang to Cloridorme (sections, SH, SYE, SYW, CB, PH, RGC); and Area C= Pointe-à-la-Frégate (section PF). The main characteristics of each section are summarized in Table 2.2.

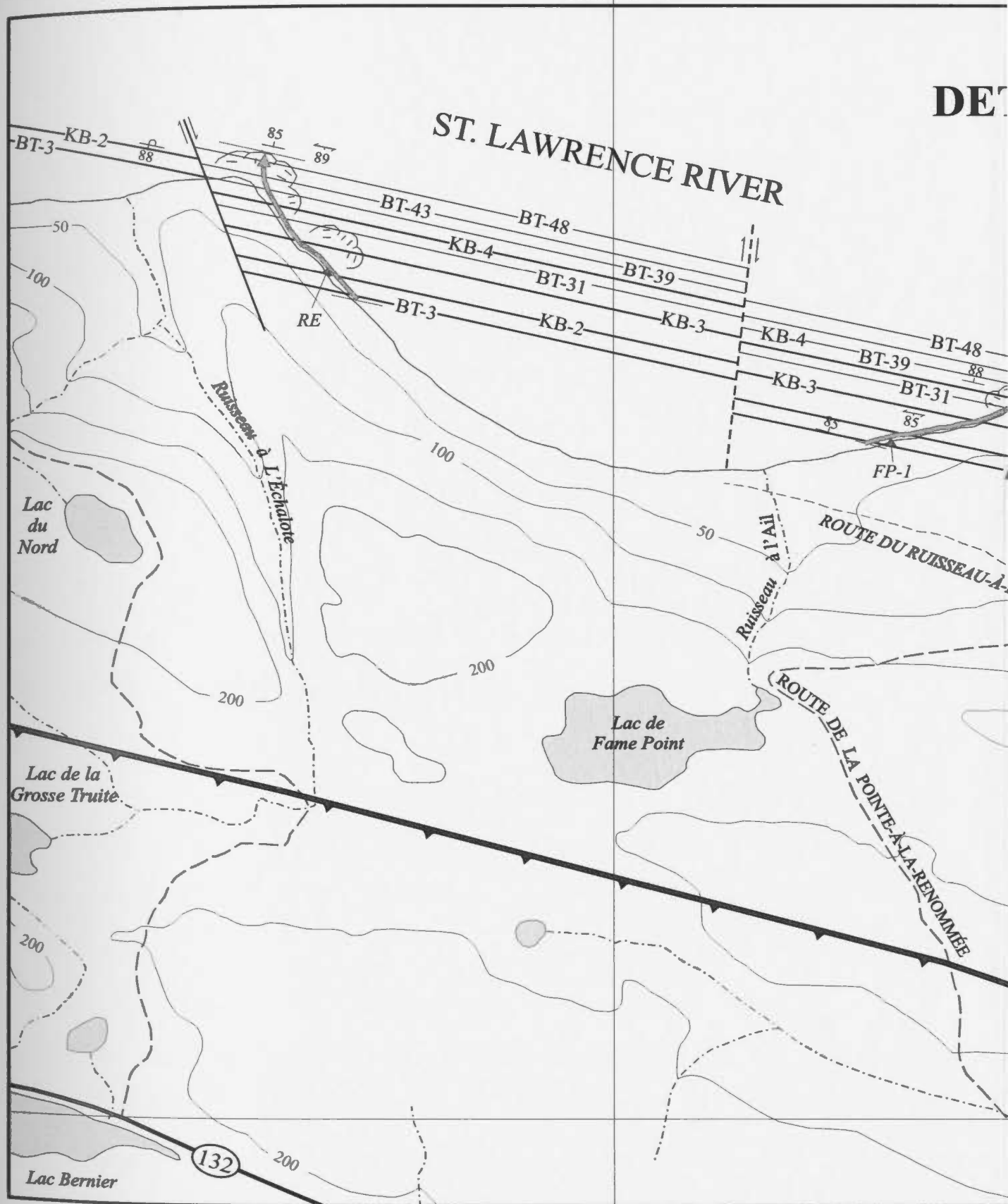
### **2.2.1. Area A: Pointe-à-la-Renommée (Figure 2.2)**

Access to the sections in this area is by the gravel road that intersects Route 132 about 3.5 km west of L'Anse-à-Valleau (National Military Grid 823386), called Route de la Pointe-à-la-Renommée. This gravel road terminates at the Tourist Information Centre, located at the old light house at Pointe-à-la-Renommée (830406). Access to sections RE, FP1 and FP2 is by the first dirt road to Ruisseau à l'Ail (812408) that branches off the gravel road (827406). Access to PCDR, PRM1 and PRM2 is by a second dirt road that branches off the same gravel road about 50 m before the Tourist Information Centre. This dirt road terminates at the beach near Pointe des Canes de Roches (825409). The base of the sequence examined in this thesis coincides with the base of the highest occurrence of a thick muddy graded bed (type 3 greywacke of Enos, 1965,1969a,1969b). This bed is exposed in section RE and FP1 and is labelled BT-3 on Figure 2.2. At section RE, this bed occurs about 900 m west of the mouth of Ruisseau à l'Ail, and at FP1 it occurs about 250 east of the mouth of Ruisseau à l'Ail. Parts of the sequence that are the main focus in

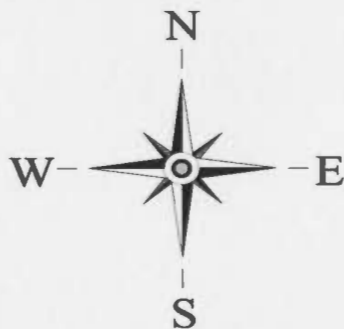
Key for abbreviations, symbols and patterns used in the maps of the detailed areas. This key applies to the maps for areas A, B and C. The marker beds were observed in the wave platform and are inferred to continue between sections.

	Strike and dip (amount indicated) of upright beds		Marker horizon (BT= megaturbidite, KB= K-bentonite)
	Strike and dip (amount indicated) of overturned beds		
	Non-plunging anticline		Line of section (arrow points to top).
	Plunging anticline (amount of plunge indicated)		Streams and rivers
	Non-plunging syncline		Lakes and ponds
	Plunging syncline (amount of plunge indicated)		
	Overturned anticline		Rocky shoreline (wave platform)
	Inclined cleavage (amount of dip indicated)		Elevation contours in metres
	Vertical cleavage		Paved highways
	Fault with apparent movement (observed)		
	Fault with apparent movement (inferred)		Gravel roads
	Thrust fault		

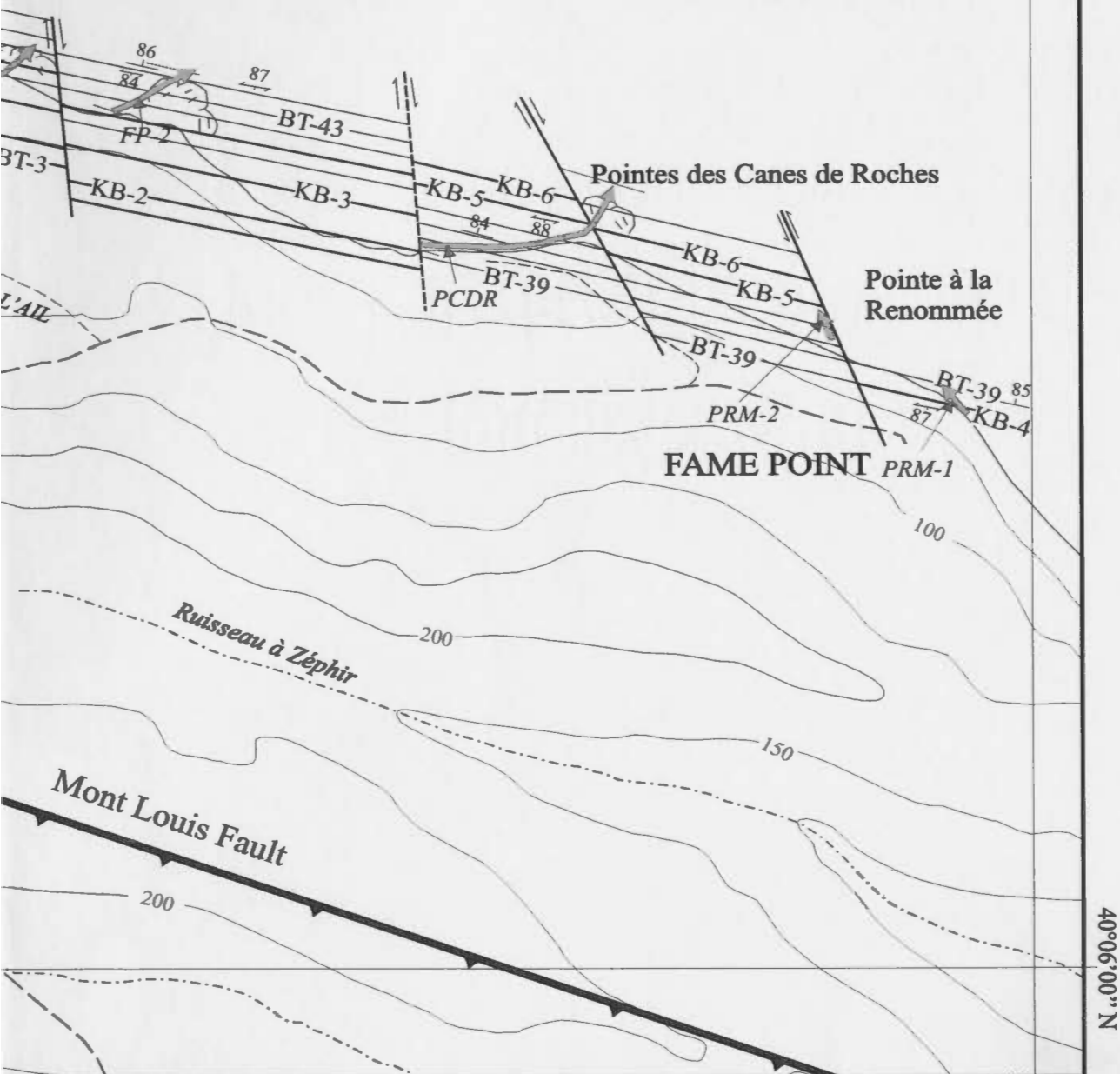
DET



## TAILED AREA (A)



1 km



this study are exposed elsewhere in the area, but the top of the sequence is not present in area A. The youngest beds in section PCDR form the top of the succession in this area, but are approximately 180 m below the top of the overall sequence considered in the thesis. The top is only exposed in areas B and C.

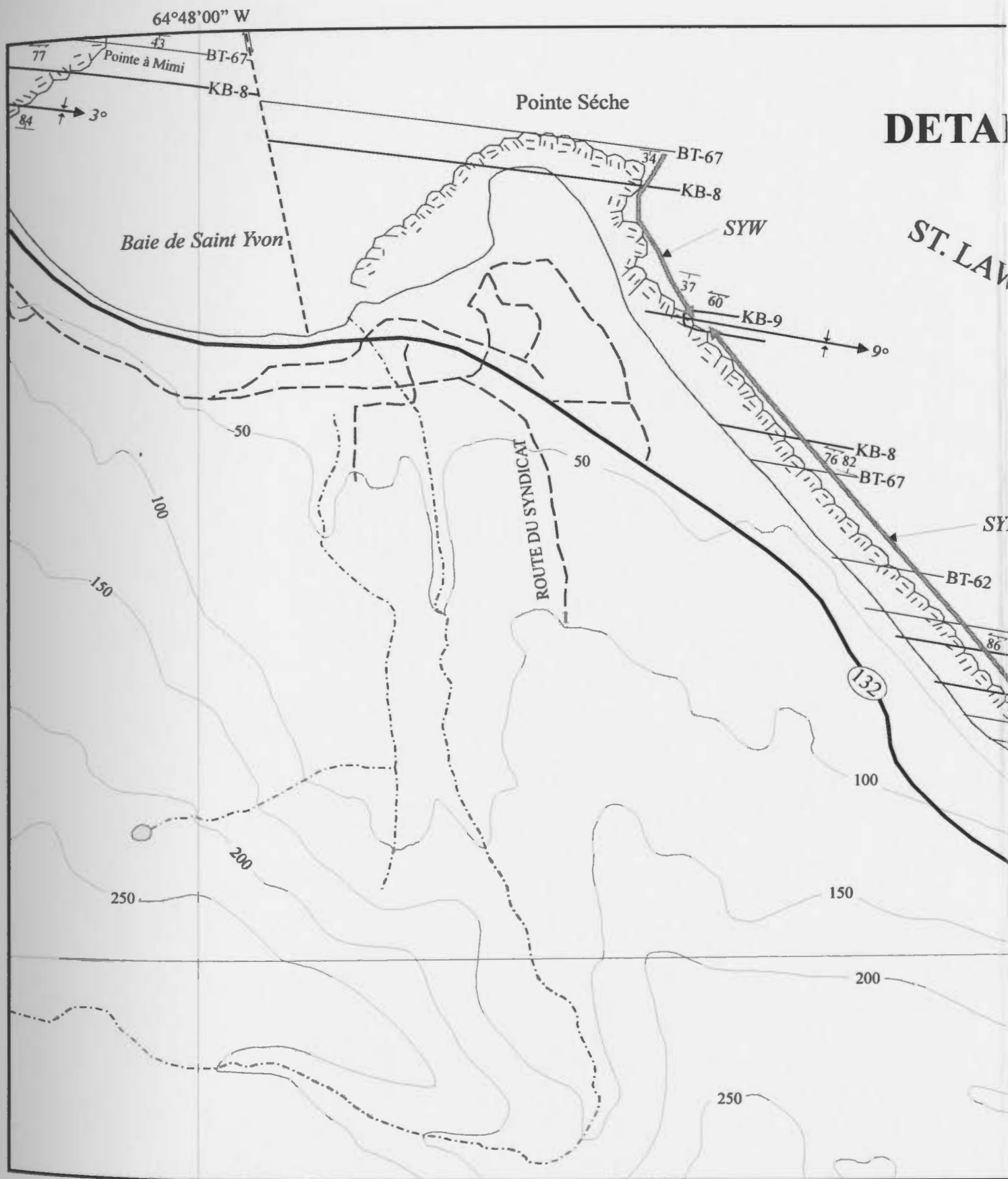
The rocks exposed in the Pointe-à-la-Renommée area were mapped as part of the  $\beta_1$  member by Enos (1965, 1969a, 1969b). Detailed correlations presented by Pickering and Hiscott (1985) between sections in the Pointe-à-la-Renommée area and Grand-Étang area show that both sections include strata of the  $\beta_2$  member of Enos (1965, 1969a, 1969b). The top of the approximately 7 m-thick turbidite bed that Enos (1965, 1969a, 1969b) used to mark the base of his  $\beta_2$  member is exposed in both areas. The PCDR, FP2 and PRM1 sections which overlie and partly overlap with the RE, FP1 and PRM2 sections are equivalent to the  $\beta_2$ - $\beta_5$  members of Enos (1965, 1969a, 1969b).

#### **2.2.2. Area B: Grand-Étang to Cloridorme (Figures 2.3 and 2.4)**

Six sections (SH, SYE, SYW, CB, PH, RGC) were measured in this area. The base of the SH section (715452) is located about 1.8 km west of the parking area at Grand-Étang (728440), which is the nearest point of access. Access to sections SYE and SYW is by the asphalt road and then the gravel roads (697465) that lead from Route 132 to Pointe Séche. Alternatively, SYE may be reached by the dirt road leading from the rear of the motel on the cliff top.

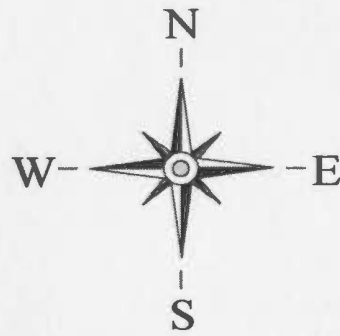
Access to the CB section is by the old asphalt road that branches from Route 132





64°46'00" W

# MAILED AREA (B EAST)

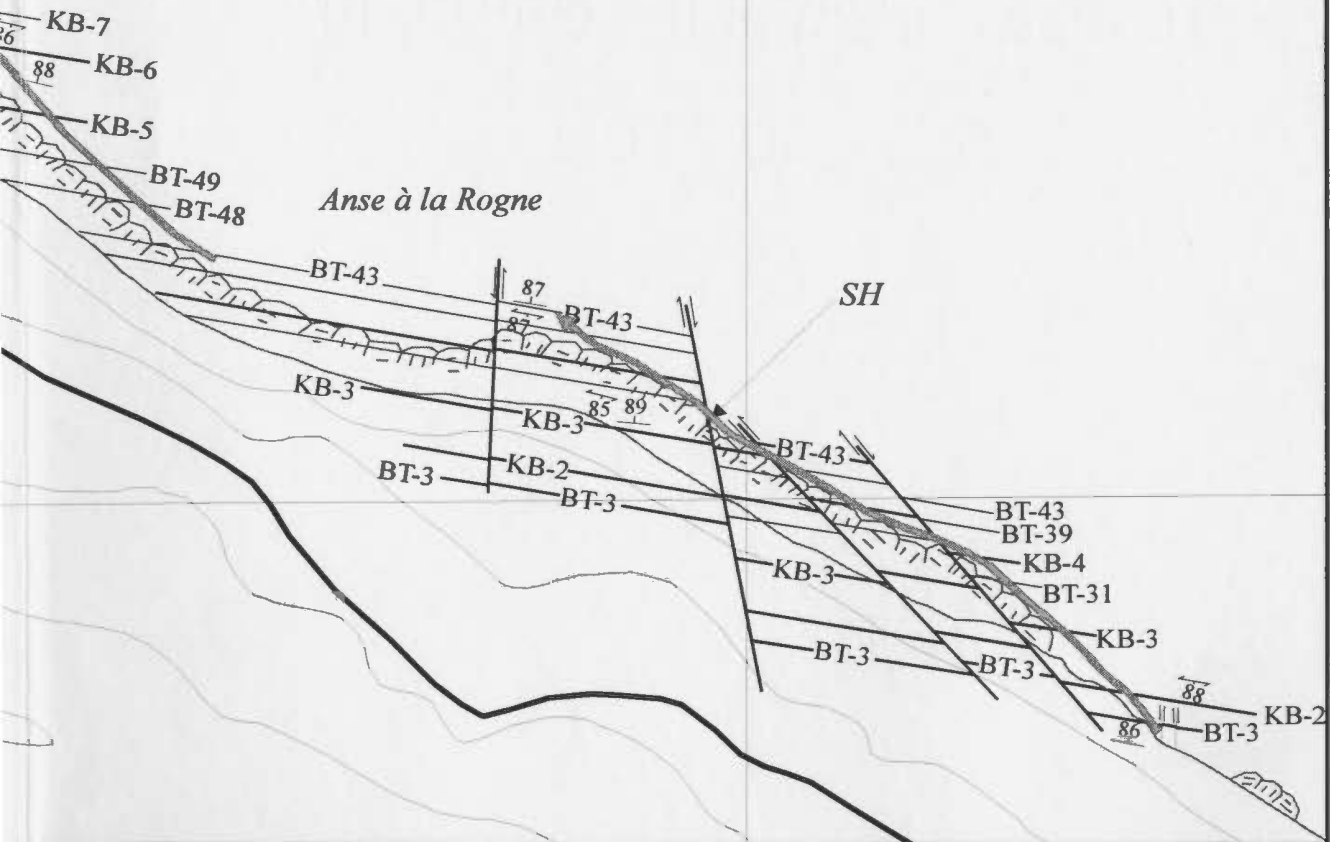


WRENCE RIVER

1 km

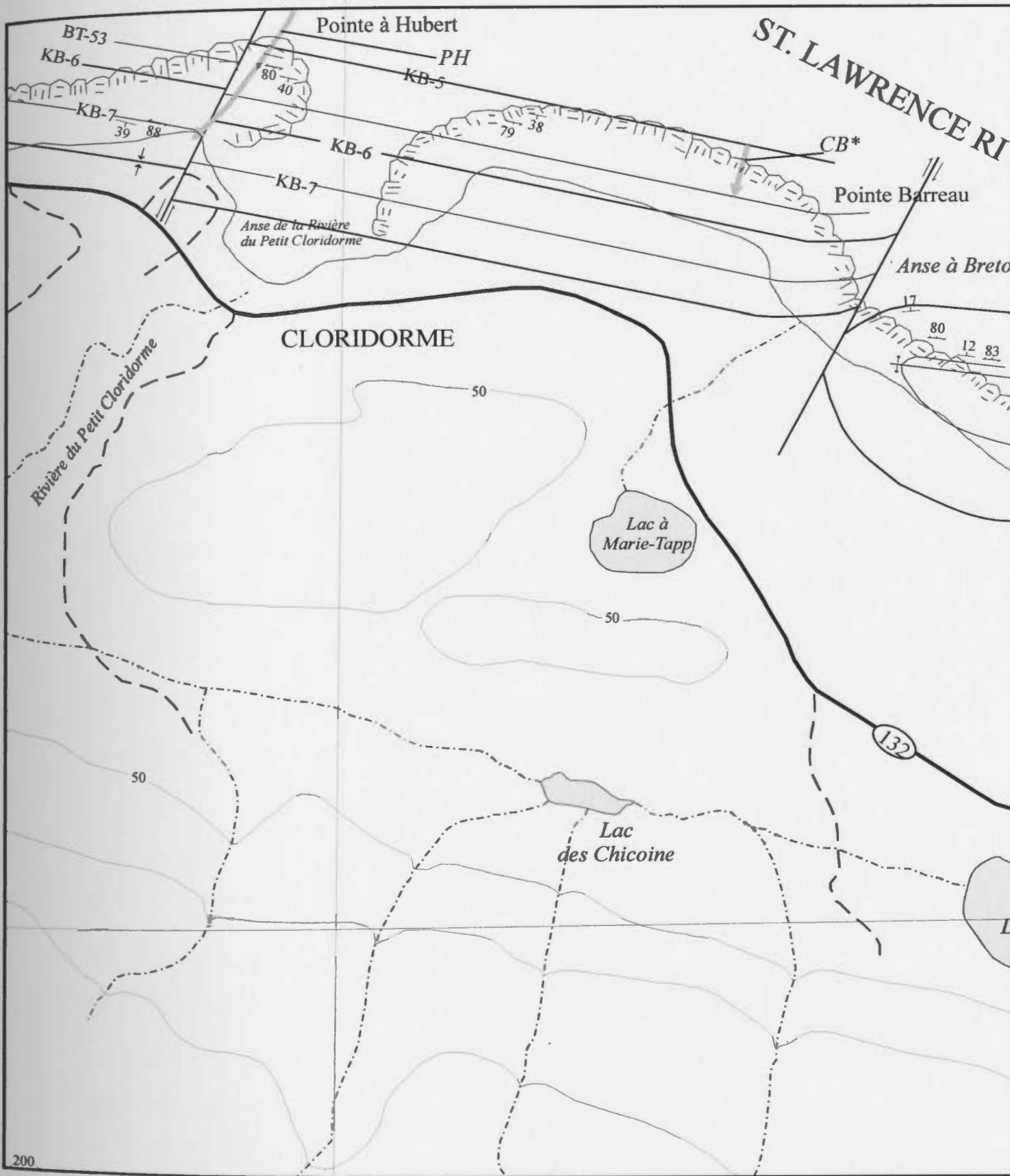


SYE

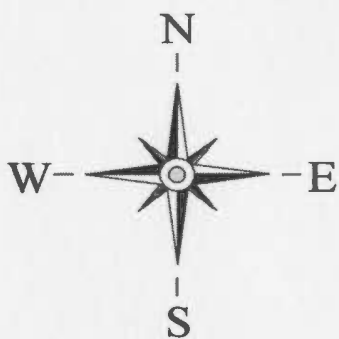


49°09'00" N

64°50'00" W

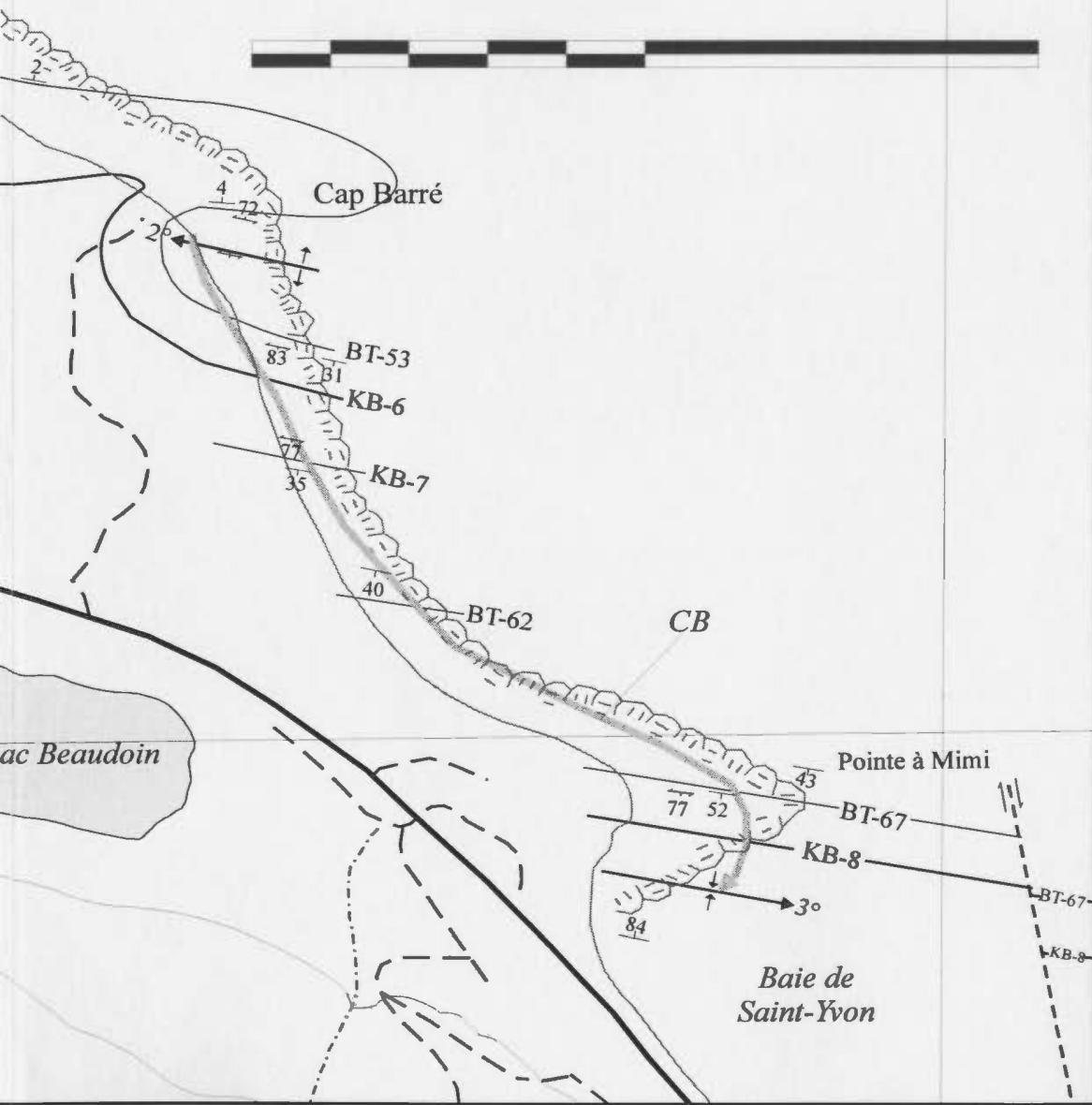


64°48'00" W



## DETAILED AREA (B WEST)

1 km



at the southern end of Baie de Saint-Yvon (687466) and terminates at the beach area on the west side of the bay. The top of the section is located at Pointe à Mimi. Good exposure of most of the section is available along the beach from Pointe à Mimi to Cap Barré (680480). The base of the CB section is only exposed at Pointe Barreau (673487) seaward of the fish plant near the eastern limit of the town of Cloridorme. Pointe Barreau is accessible by the gravel road that leads from Route 132 to the town cemetery.

Alternatively, the section may be reached by crossing the bridge located at Anse de la Rivière du Petit Cloridorme. The section is exposed on the east side of this cove. Section PH is exposed on the western side of the same cove and can be reached by crossing the bridge and walking to the west. Section RGC forms a small hill west of Baie de Cloridorme. It is easily accessible from the beach area east of Baie de Cloridorme wharf.

In area B, the base of the sequence examined in this thesis is placed at the base of the highest occurrence of a thick muddy graded bed (type 3 greywacke of Enos, 1965, 1969a, 1969b) located about 1km east of Anse à la Rogne (bed BT-3 in Figure 2.3). The top of this bed marks the base of the  $\beta_2$  member of Enos (1965, 1969a, 1969b) which is drawn on his map east of Anse à la Rogne. The section, for the most part, is continuous, albeit with some faults. The top of the sequence considered in the thesis is in the hinge area of the Point Séche syncline. The full sequence is equivalent to the topmost part of  $\beta_1$ , and  $\beta_2$  to  $\beta_5$  members of Enos (1965, 1969a, 1969b), who suggested that the base of  $\beta_5$  is represented by the beds in the hinge of the syncline. The sequence is equivalent to the upper 550 m of the Pointe-à-la-Frégate Member as defined by Slivitzky *et al.* (1991). If

the base of the overlying Gros-Morne Member of Slivitzky *et al.* (1991) is equivalent to the base of  $\beta 5$  of Enos (1965, 1969a, 1969b) in the Pointe-à-la-Frégate area, then the base of the Gros-Morne Member also should be located in the hinge of the Point Séche syncline. Parts of the full sequence are exposed at various sites from Pointe à Mimi to the area east of Baie de Cloridorme (Figure 2.4).

The rocks exposed east and west of Grand-Étang and in hinge area of the anticline at Le Brûlé were not studied because of their limited exposure (only a thin sequence is exposed at Le Brûlé) or poor exposure (sections east and west of Grand-Étang).

The shoreline between area A and area B has been studied in detail by Keith Skipper (Skipper, 1971; Skipper and Middleton, 1975; Skipper and Bhattacharjee, 1978) who indicated, based on detailed correlations of individual beds, that the strata exposed in this area are older than the sequence considered in this thesis.

The area between section RGC and section PF contains the most structurally deformed sequence of the entire thesis area. This area was examined in detail in order to investigate whether the exposed beds could be correlated to parts of other sections. No marker beds were found to tie this section to other sections. It is believed that the beds exposed in this area are older than the sequence considered in this thesis. Other studies support this conclusion (Enos, 1965, 1969a, 1969b). Only a small area, extending laterally just a few tens of metres and located west of the Cloridorme wharf, is equivalent to part of the base of the studied sequence. This area is bounded by faults to the east and west.

### 2.2.3. Area C: Pointe-à-la-Frégate (Figure 2.5)

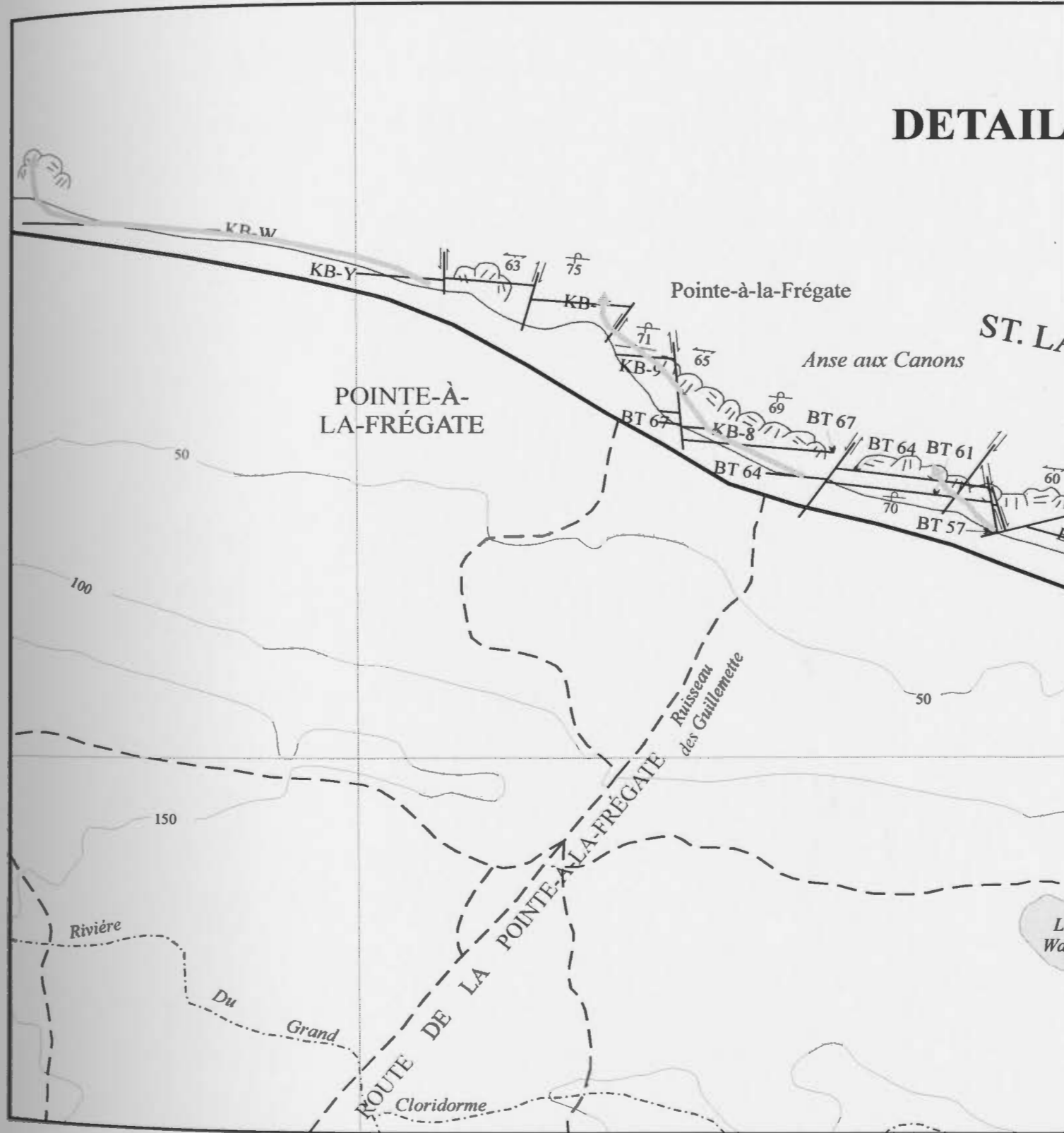
This is the longest section measured in the entire thesis area (Table 2.2). The section is very accessible because it is located close to Route 132 (Figure 2.5). The beach area can be accessed by any of the numerous dirt roads leading to the coast from Route 132. The base of the section is located tens of metres west of Le Brûlé and can be reached by walking along the beach. The top of the section is located close to the headland at Pointe-à-la-Frégate.

The complete sequence investigated in this thesis is exposed in area C. The exposure is continuous, albeit with some faults, from west of the hinge of the anticline at Le Brûlé to about 300 m west of the western headland at Pointe-à-la-Frégate (Figure 2.5). The base of the section is placed at the occurrence of a thick muddy graded turbidite bed (type 3 greywacke of Enos, 1965) that is prominently exposed on the west side of the cove west of Le Brûlé. This sequence is equivalent to the topmost part of the  $\beta_1$ ,  $\beta_2$ ,  $\beta_3$ ,  $\beta_4$  members and the lower part of the  $\beta_5$  member of Enos (1965, 1969a, 1969b). This corresponds to the upper 550 metres of the Pointe-à-la-Frégate Member of Slivitzky *et al.* (1991).

No rocks equivalent to the sequence exposed at, and to the west of, the headlands of Pointe-à-la-Frégate could be found in areas A and B, or elsewhere in area C. During the course of field work, the area between Pointe-à-la-Frégate and Petite-Vallée was visited and walked out several times in an attempt to relate the PF section with the rocks exposed to the east and west of the Anse de Petite-Vallée. These attempts were unsuccessful

64°56'00" W

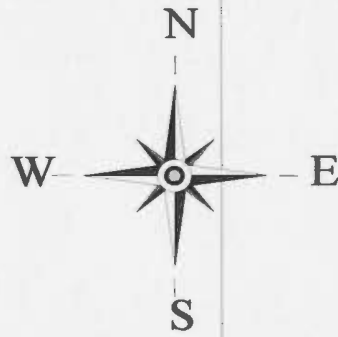
# DETAIL





# ED AREA C

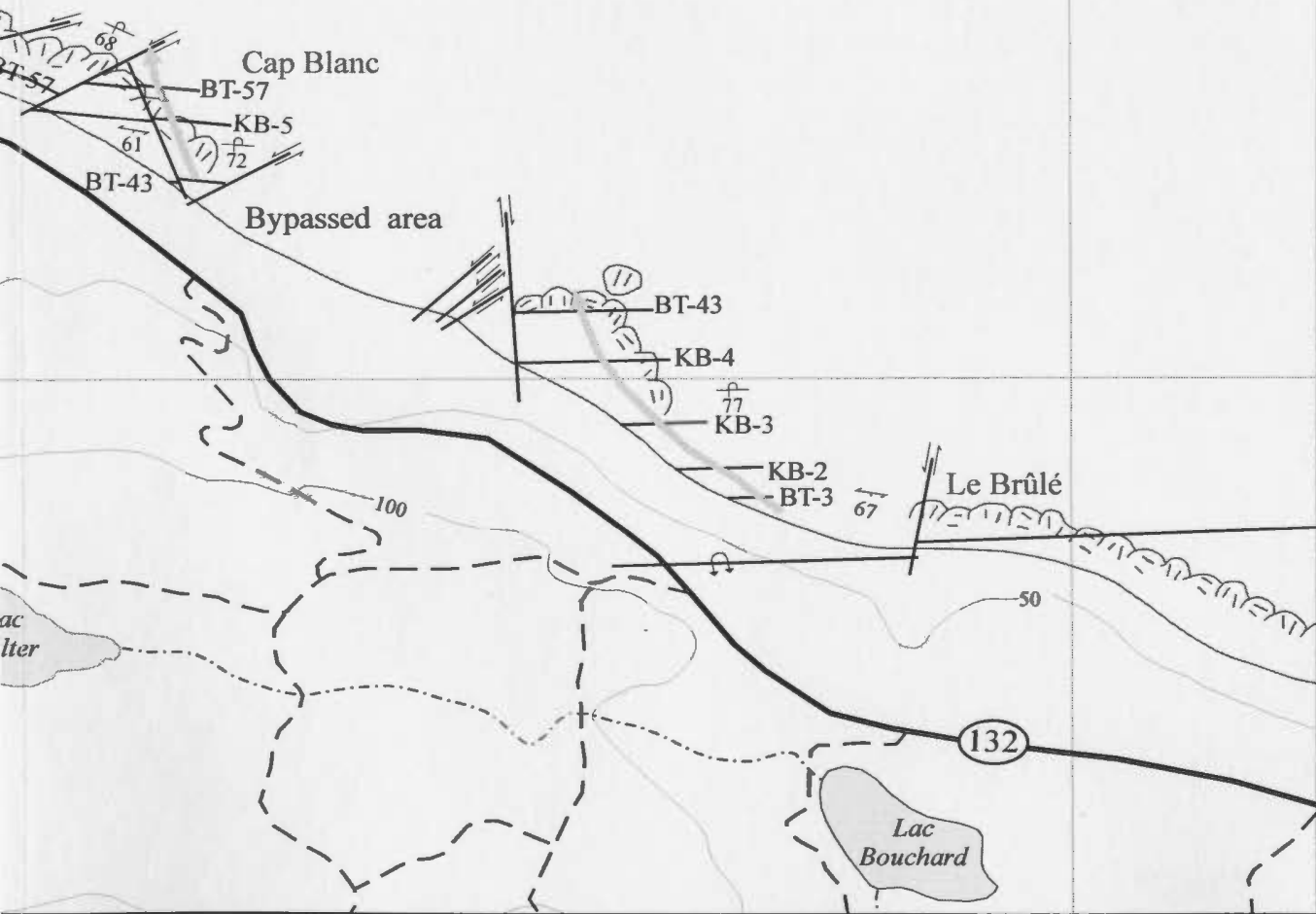
64°54'00" W



1 km



LAWRENCE RIVER



49°12'00" N

because of the poor exposures in parts of this area and the presence of several faults with undetermined stratigraphic displacements. Nevertheless, other studies have suggested that the beds exposed in the area west of Pointe-à-la-Frégate are younger than the sequence considered in this thesis (Enos, 1965, 1969a, 1969b; Slivitzky *et al.*, 1991).

### 2.3. INCONSISTENCIES IN PREVIOUS MAPPING

In the thesis area, difficulty was encountered when comparing boundaries of the Manche-d'Épée Member and the Pointe-à-la-Frégate Member, as mapped and defined by Slivitzky *et al.* (1991), with the beta members of Enos (1965, 1969a, 1969b). Slivitzky *et al.* (1991; Figure ET 88-14 carte n° 2093-1) show the Pointe-à-la-Frégate Member to be 635 m thick and equivalent to the  $\beta_2$  member of Enos (1965, 1969a, 1969b). Slivitzky *et al.* (1991) draw the base of the Pointe-à-la-Frégate Member inland, west of Le Brûlé while they draw the top of the member east of the eastern-most headland at Pointe-à-la-Frégate. Enos (1965, 1969a, 1969b) used the top of a ~7 m-thick muddy turbidite bed (a thick type 3 greywacke) as the base of his  $\beta_2$  member. This contact, is on the wave-cut platform west of Le Brûlé, well above the contact mapped by Slivitzky *et al.* (1991). Slivitzky *et al.* (1991; Figure ET 88-14 carte n° 2093-1) plot the top of this bed 190 m above the base of their member, consistent with their mapping but incompatible with their claim that the Pointe-à-la-Frégate Member shares a common base with the  $\beta_2$  member of Enos (1965, 1969a, 1969b). Furthermore, according to Enos (1965, 1969a, 1969b), the headlands of Pointe-à-la-Frégate are the type locality for the  $\beta_5$  member. This area also marks the base

of the Gros-Morne Member of Slivitzky *et al.* (1991), so that their Pointe-à-la-Frégate Member must include part if not all of the  $\beta 3$  and  $\beta 4$  members of Enos (1965, 1969a, 1969b) and not just the  $\beta 2$  member of Enos (1965, 1969a, 1969b) as they claim.

In the area east of Anse à la Rogne, Slivitzky *et al.* (1991) draw the base of their Pointe-à-la-Frégate Member at exactly the same location where Enos (1965, 1969a, 1969b) places the boundary between the  $\beta 1$  and  $\beta 2$  members; i.e., at the top of a distinctive, thick muddy turbidite bed (type 3 greywacke). Elsewhere in their report, Slivitzky *et al.* (1991) plot the top of this same bed 190 m above the base of the Pointe-à-la-Frégate Member. At the very least, Slivitzky *et al.* (1991) incorrectly equate their formal stratigraphy with the beta succession of Enos (1965, 1969a, 1969b), and inconsistently map the base of their Pointe-à-la-Frégate Member at significantly different stratigraphic levels (e.g., mapping west of Le Brûlé as compared to mapping east of Anse à la Rogne).

It is also unclear on what basis Slivitzky *et al.* (1991) equate their Manche-d'Épée Member to the  $\gamma 1$  member of Enos (1965, 1969a, 1969b). Enos (1965, 1969a, 1969b) declined to propose correlation between the western block that includes the  $\gamma 1$  to  $\gamma 4$  members and the central block that includes the  $\beta 1$  to  $\beta 7$  members. Hiscott *et al.* (1986) were the first to suggest that their informal Pointe-à-la-Frégate member is equivalent to the  $\gamma 1$  member of Enos (1965, 1969a, 1969b), which they renamed the Manche-d'Épée member [note that the Pointe-à-la-Frégate and Manche-d'Épée members of Hiscott *et al.* (1986) do not have the same stratigraphic position as formal members bearing the same names in the report of Slivitzky *et al.* (1991)]. If Slivitzky *et al.* (1991) equated their

formal Manche-d'Épée Member to the  $\gamma 1$  member of Enos (1965, 1969a, 1969b) based on the work of Hiscott *et al.* (1986), then it is unclear why Slivitzky *et al.* (1991) suggest that their Manche-d'Épée Member is equivalent to the  $\beta 1$  and  $\beta 2$  members of Enos (1965, 1969a), given that Hiscott *et al.* (1986) indicate that their Manche-d'Épée member is equivalent to the upper part of the  $\beta 3$  and all of the  $\beta 4$ ,  $\beta 5$ , and  $\beta 6$  members of Enos (1965, 1969a). This confusion may have arisen due to incorrect mapping by Enos (1965, 1969a) in the area east of Ruisseau à l'Échalote which was designated entirely as the  $\beta 1$  member.

## 2.4. STRUCTURAL FRAMEWORK OF THE MEASURED SECTIONS

The main structural features in the thesis area are a number of folds and faults (Figure A4.1). Two large folds are present. An overturned anticline with an east-west trending axis is located at Le Brûlé (Figure A4.1). Enos (1965, 1969b) traced this anticline from Le Brûlé to Le Grand-Ruisseau situated about 12 km to the west, and indicated that it plunges  $2^\circ$  towards the east. Lachambre and Brisebois (1990) and Slivitzky *et al.* (1991) indicated that the hinge area of this anticline at Le Brûlé is cut by two faults on either side of the headland at Le Brûlé. The displacement across the fault east of the headland was noted to be 45 m while the displacement across the fault west of the headland was 30 m. These displacements could not be verified during the course of this study. Section PF was measured in the northern overturned limb of this anticline away from the faults reported by these other workers.

The second major fold structure in the thesis area is an asymmetric syncline with a steeply-dipping southern limb extends from Pointe Séche to Pointe à Mimi (Figures 2.3 and 2.4). Enos (1965, 1969a, 1969b) suggested that this syncline extends westward to at least Rivière du Petit Cloridorme. Sections SH and SYE were measured in the southern limb of this syncline. Section SYW was measured in the more gently dipping northern limb (Figure 2.3), whereas sections in Area A (RE, FP1, FP2, PCDR, PRM1, PRM2) were measured in the steeply dipping southern limb of this syncline (Figure 2.2).

Two smaller open folds are superimposed on the southern limb of the Le Brûlé anticline. These minor folds are: (1) a syncline with an east-west trending axis located at Pointe à Hubert and Pointe Barreau (Figure 2.4); and (2) an anticline with an east-west axis located at Cap Barré (Figure 2.4). Section PH and the lowermost part of section CB were measured on the northern limb of this minor syncline. The remaining part of section CB was measured from the hinge area of the anticline at Cap Barré to the hinge area of the syncline exposed at Pointe à Mimi. Faults observed in the area are shown on detailed maps (Figures 2.2, 2.3, and 2.4).

## **2.5. FIELD METHODS FOR SECTION MEASUREMENTS**

A total of 211 days were spent in the field. Approximately two weeks were spent in reconnaissance and approximately 2958 m of section representing about 28,000 beds were measured and described in detail (bed-by-bed). The main lithologies observed in the thesis area are shale, siltstone and sandstone. Shale comprises about 67% of the measured

sections. Sandstone and siltstone are less common and comprise about 16% and about 18%, respectively. Diagenetic carbonate layers (limestone and dolomite) and volcanic ash layers are minor, constituting about 1% of the studied sections.

Field methods involved measurement of stratigraphic sections, mapping of the areas where sections are exposed, palaeocurrent measurements, and sampling of K-bentonite layers.

The detailed sections were generated by measuring bed thicknesses using a metric measuring tape. The tape was held normal to bedding planes. Beds were measured to the nearest 0.5 cm. Because of the large number of measurements in each section and the variable dips of beds in different sections, the accuracy of the measured thicknesses was confirmed with a 50 m tape. Each section was divided into segments ranging in thickness from 15 - 50 m. For each segment, dip and strike of the beds at the base and top of the segment were recorded. The true stratigraphic thickness of the section was then calculated using the following formula:

$$\text{Stratigraphic thickness} = (\text{horizontal distance}) \times \sin \text{dip angle}.$$

The lithology, sedimentary structures, palaeocurrents, nature of the bedding surfaces, grain size at the base and top of each bed and the mean grain size were recorded on a standardized field description sheet. Grain size was estimated using a comparison scale of mounted sieved sand fractions. This method has been shown to provide estimates of the coarsest 5-10 % of the sediment (Talling, 2001).

Based on the colour variations or the shape of the modern weathering surface

(suggesting variable hardness or resistance to erosion) it was possible to recognise that some shale units consisted of thinner beds. This was only observed in a few instances where the outcrop quality is good and could not be applied to the shale units in other outcrops. Thus, all shale horizons bounded at the top and bottom by other facies were counted and measured as single beds during field description.

Because fold plunges are less than  $10^\circ$ , no correction for plunge was applied to palaeocurrent measurements (Ramsay, 1961). Sole marks, mostly flutes and grooves, and ripples and ripple lamination were used to determine palaeocurrents directions. When measuring the palaeocurrent from a sole mark, the strike of the bed was determined with a compass and the strike line was marked on the bottom of the bed. A protractor was then used to measure the pitch of the linear feature on the bedding plane, and the pitch angle was noted. In the case of palaeocurrents measured from ripple marks, a similar technique was used employing a line perpendicular to ripple crests. In the case where the ripple form was not preserved on the upper bedding surface or it was not exposed, good three dimensional outcrops were located and the pitch of the palaeocurrent was estimated. The palaeocurrent direction was determined from the field data using the computer program GeoCalculator v.4.0 © developed by R. Holcombe of the University of Queensland, Australia. This program adds or subtracts the value of the pitch angle from the strike azimuth to determine the pre-folding orientation of the sole marks or ripple marks.

As a base for field work, 1:15000 aerial photographs were enlarged to a scale of approximately 1:8000. Folds, faults and many of the thick marker beds were drawn on

these photo enlargements.

## **2.6. LABORATORY ANALYTICAL METHODS**

Chemical analyses of the K-bentonite horizons were performed in order to determine whether chemistry could be used to discriminate between these horizons. A successful chemical distinction would allow a precise correlation of the studied sections (Chapter 4).

Chemical data were acquired from the analysis of several K-bentonite samples. The analyses were performed by Mr. Michael N. Tubrett, X-ray fluorescence (XRF) specialist at Memorial University of Newfoundland (MUN). Inductively coupled plasma-mass spectrometer (ICP-MS) analyses were carried out by Dr. Eric Hoffman of Activation Laboratories of Ancaster Ontario. K-bentonite horizons were identified based on criteria outlined in Chapter 3. Chips of each bentonite were extracted from the outcrop with a chisel and hammer, and bagged. These chips were mostly less than 1 cm<sup>3</sup> in size. Larger chips were broken by hand before splitting. Sample preparation consisted of splitting the original 1-2 kg sample of chips into two parts using a sample splitter. One part was kept as a reference sample. Approximately 50 grams of fresh rock chips were picked from the remaining part of the sample. Clean and fresh material was selected based mostly on the sample colour, which is much lighter green and grey (5GY6/1 - 5GY4/1) than any darker shale (5GY2/1 to N1) which might have been inadvertently collected with the K-bentonite chips during field sampling.



The 50g samples were crushed and pulverized in a SPEX mixer mill for approximately 20 minutes and dried at 60°C for 12 hours. The mill container and steel balls were thoroughly cleaned between samples. Each sample was then sieved through a 400 mesh (38 micron) stainless steel sieve. Five grams powder were used to prepare sample pellets for XRF analysis. Four grams powder were placed in a glass container and shipped to Activation Laboratories for ICP-MS analysis.

The preparation of the XRF pellets consisted of mixing each 5g sample power with 0.7g BRP-5933 Bakelite phenolic resin (Bakelite Thermosets Ltd, Brampton, Ontario, Canada). The sample powder and resin were homogenized for 15 minutes in a Norton roller mixer. The resulting mixed power was pressed for 5 seconds in a Herzog (model HTP40) pellet press (29 mm diameter mould) at a pressure of 20 tons. The pellets were baked in a Gallen Kamp hot box oven for 15 minutes at 200°C.

The XRF instrument at MUN is a Fison/ARL (Mississauga, Ontario, Canada) 8420+ sequential wavelength-dispersive X-ray spectrometer. This spectrometer is equipped with one goniometer which has five analysing crystals including a LiF200-H crystal which is treated for heavy element sensitivity. The instrument employs an argon flow-proportional detector (FPC) or a scintillation (SC) detector with an X-ray tube operated at 3 kW. Precision and detection limits for XRF analyses carried out at MUN are presented in Table A5-1.1, based on five analyses of five reference materials (DTS-1, BHVO-1, SY 2, SY-3, PACS-1) in each run. Standards AGV-1, DNC-1, JG-2 and BCR-1 were analysed once during each run. Details of the analytical procedures used with this instrument, calibration,

matrix corrections, precision and accuracy have been described in detail in Longerich (1995).

The ICP-MS instrument at Activation Laboratories is a Perkin-Elmer ELAN 6000 ICP-MS which uses a proprietary sample introductory methodology. Each sample or standard was mixed with a flux of lithium metaborate and lithium tetraborate and fused in an induction furnace. The melt was dissolved in a solution of 5% nitric acid ( $\text{HNO}_3$ ) containing an internal standard. The mixture was agitated continuously for about 30 minutes until complete dissolution. Reagent blanks with and without lithium borate flux were analysed as well as the method reagent blank. Calibration was performed using prepared USGS and Canmet certified reference materials (MAG-1, SY-3, MRG-1, DNC-1, BIR-1, W-2, GXR-1, STM-1) (Table A5-1.2). The samples were analysed in batches, each batch consisting of unknown samples, reference materials, a method reagent blank, and 17% replicates (Eric Hoffmann, Activation Laboratories, personal communications, 1997).

## **CHAPTER 3**

### **FACIES DESCRIPTION AND INTERPRETATION**

#### **3.1. DATABASE: GEOGRAPHY, STRATIGRAPHY AND TERMINOLOGY**

During field study, about 3,000 m of stratigraphic section were measured and described in detail from eleven locations. Generally, one continuous section was measured at each location. Most of the sections overlap (Figure 3.1), so that only about 770 m of the ~3,000 m are viewed as unique stratigraphy. A continuous section, albeit with some minor faults, exposes about 770 m of this unique stratigraphy in the PF section. The upper 200 m of the full 770 m section are only exposed west of and in the headlands of Pointe-à-la-Frégate and no where else in the thesis area. Thus, only parts of the remaining 570 m of unique stratigraphy are exposed in each of the other ten locations. A continuous section equivalent to this 570 m interval, albeit with some faults and duplications, is exposed in the SH-SYE section.

Some aspects of the sedimentology of the Cloridorme Formation were previously studied and a variety of facies have been identified (Chapter 2). However, a detailed description and a greater number of facies are presented here for the following reasons: (a) the detailed nature and scope of this study differs from those of regional studies (Enos, 1965; Hiscott *et al.*, 1986) or studies emphasising specific sedimentological aspects or facies of the Cloridorme Formation (Parkash, 1969; Walker, 1970; Skipper, 1971; Skipper and Middleton, 1975, Skipper and Bhattacharjee, 1978; Beeden, 1983; Slivitzky *et al.*,

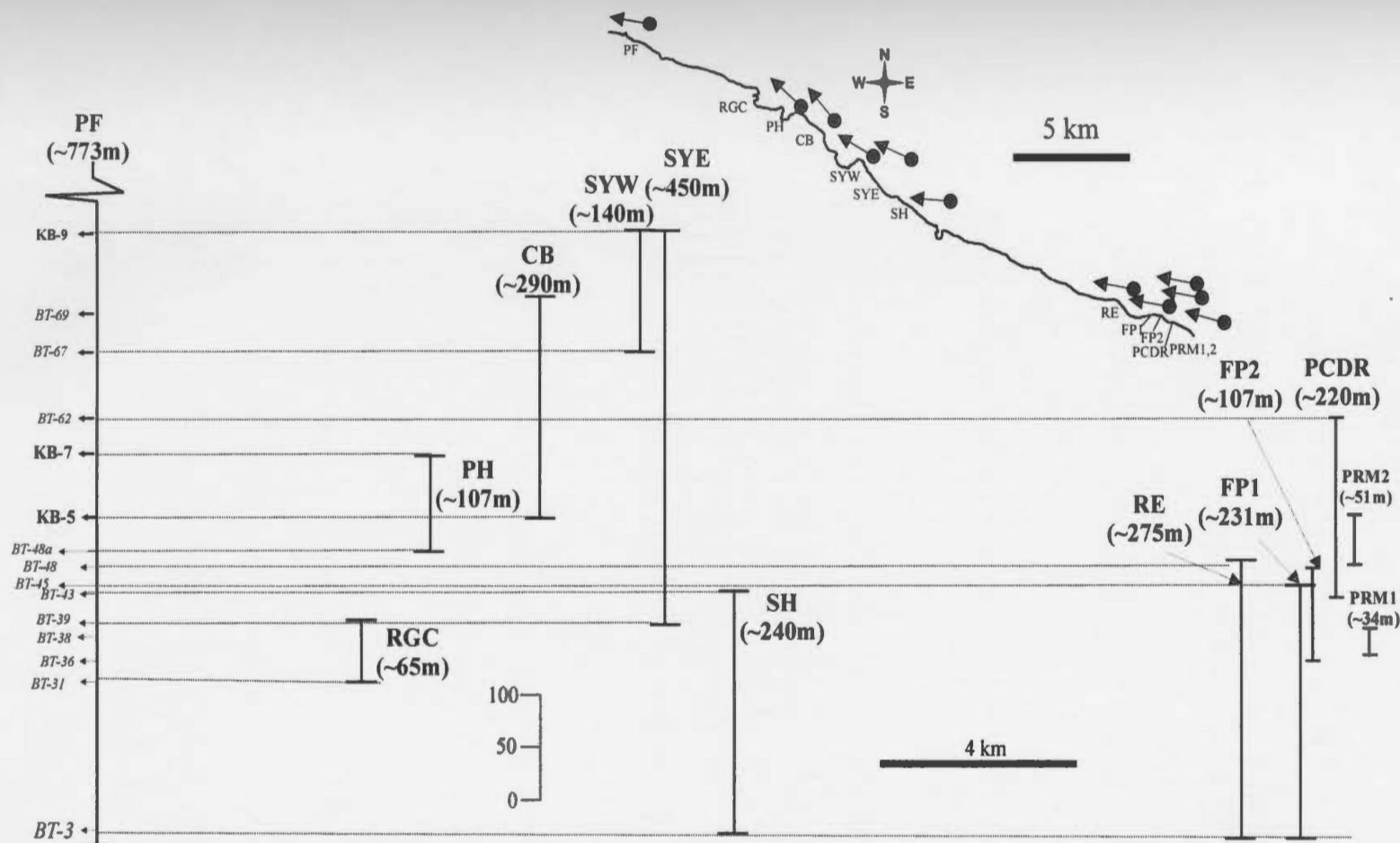


Figure 3.1. Correlation of the sections studied in this thesis. The vertical scale only applies to the PF section. All labelled marker beds in the PF section are present in the other sections, but only those marked by dotted lines are extended between the columns. The other sections are tied to the PF section and the total thickness for each section is shown (e.g., SH=240m). Stratigraphic overlap is based on the correlation of markers between sections (Figure 4.1). Markers are shown on section PF (BT=basin-wide megaturbidites, KB= K-bentonite horizons, Chapter 4). Distance between sections is approximate; the upper and lower parts of a section may not be equidistant from equivalent parts in other sections. For example, the upper parts of SYW and SYE are less than 50m apart where they form the upper part of the syncline at Pointe Séche, but the base of section SYW (top of BT-67) is ~0.5km away from the same bed in SYE, after projecting the bed at SYE along its strike. The position of the sections in the field is shown in Chapter 2 and Appendix A2, while the relative position of the sections at the time of deposition is discussed in Chapter 5. The average palaeocurrent trend (based on measurements carried out in this study) in each of the sections is shown on the inset map, top right of the figure.

1991; Ma, 1996); (b) a better understanding of the processes that formed different facies is now available compared to decades ago when some of the studies on the Cloridorme Formation were carried out; these new ideas necessitate a more detailed classification of facies.

Before a detailed description of the facies is presented, it is necessary to present definitions for some terms that are frequently used in this thesis to avoid confusion. These definitions are adapted from different sources.

*Turbidity currents*: “flows in which the sediment is supported mainly by the upward component of fluid turbulence” (Middleton and Hampton, 1976, p. 198).

*Debris flows*: “flows in which the larger grains are supported by a “matrix”, a mixture of interstitial fluid and fine sediment that has a finite yield strength” (Middleton and Hampton, 1976, p. 198).

*Slurry flows*: “muddy sand-rich sediment flows that exhibit both turbulent and cohesive sediment support and are transitional between end-member turbidity currents and cohesive debris flows” (Lowe and Guy, 2000, p. 33).

*Suspension*: “a mode of sediment transport in which the upward currents in eddies of turbulent flow are capable of supporting the weight of sediment particles and keeping them indefinitely held in the surrounding fluid” (Bates and Jackson, 1987, p.665).

*Traction*: “a mode of sediment transport in which the particles are swept along (on, near, or immediately above) and parallel to the bottom surface by rolling, sliding, dragging,

pushing, or saltation” (Bates and Jackson, 1987, p.694).

*Bed*: a sedimentary unit having a homogeneous lithology or with minor lithological variation (Stanley and Bouma, 1964). A bed may contain a variety of sedimentary structures. A bed is a lithologic unit forming part of a layer (Ricci Lucchi, 1981).

*Layer*: a sedimentary unit representing deposition from a single sedimentary event, not broken by recognisable erosional or non-depositional discontinuities (Hiscott, 1980, Ricci Lucchi, 1981). A layer may consist of several *divisions* each with different sedimentary structures but with gradational contacts between the divisions (Bouma, 1962). In this thesis, many layers consist of a lower sandstone or siltstone part and an overlying mudstone or shale part, both inferred to have been deposited by a single flow. These are referred to in the thesis as sandstone-mudstone or siltstone-mudstone couplets. In this thesis, the lower sandy or silty part of a couplet is considered as one bed and the overlying mudstone or shale part of a couplet is considered to be another bed. Thus, a sandstone-mudstone couplet or a siltstone-mudstone couplet is a single layer consisting of a lower sandstone/siltstone bed and an overlying mudstone/shale bed.

*Rock facies*: “a body of sedimentary rock with specific characteristics. It may be a single bed, or a group of multiple beds. Ideally, it should be a distinctive rock that formed under certain conditions of sedimentation, reflecting a particular process, set of conditions, or environment” (Reading and Levell, 1996, p. 19). Facies are distinguished mainly based on the bed lithology while subfacies are distinguished on the basis of a combination of the lithology and the internal structures (Ghibaudo, 1992).

*Megaturbidites*: large turbidite that can exceed 10 m in thickness and usually extend across most of the basin of deposition (Normark *et al.*, 1993).

*Amalgamated units*: two or more sandstone or siltstone beds that are superimposed with no shale in between. Amalgamated units are characterised by one or both of the following features that aid in their identification: (1) presence of an erosional (scour) surface (amalgamation surface) between beds — this scour surface may be planar or irregular, and (2) a marked grain size difference across the amalgamation surface. Amalgamated units are a common occurrence in deep-water deposits (Stow and Johansson, 2000).

*Packet*: several (more than 2) sandstone beds that occur together (with little or no shale between individual beds) and which are separated from other groups or packets by shale that may contain thin siltstone beds or laminae (Ojakangas, 1968). In this thesis, the term packet is not restricted to sandstone but may be applied to siltstone beds that otherwise fit the definition.

*Division*: part of a bed that is structurally homogeneous. In this thesis, division does not refer only to the turbidite divisions ( $T_a - T_e$ ) as defined by Bouma (1962) and Walker (1965) but also includes divisions exhibiting different sedimentary structures that cannot be described as one of the Bouma divisions or that do not follow the predicted vertical turbidite sequence (Bouma, 1962; Walker, 1965). In this thesis, the most common divisions observed are:

- (i) Massive, lacking sedimentary structures or grading.
- (ii) Structureless, lacking sedimentary structures but may exhibit grading.

(iii) Parallel lamination, a type of stratification where a part of a sedimentary layer is made of stratified units (laminae) thinner than 0.5 cm (Bouma, 1962). If the laminae are straight and parallel they are termed planar lamination.

(iv) Cross bedding, an arrangement of strata that are thicker than 1 cm and that are inclined at an angle to the main bedding (Bates and Jackson, 1987).

(v) Ripple cross-lamination, “small scale cross lamination formed by migrating current ripples developed during deposition, characterised by individual laminae whose thicknesses range between 0.08 cm and 0.3 cm” (Bates and Jackson, 1987, p.571).

(vi) Climbing-ripple lamination, cross stratified deposits where ripple crests ascend upward in the bed when traced in the downflow direction due to the climb of one ripple up the stoss side of the ripple immediately downstream (Jopling and Walker, 1968).

(vii) Convolute lamination, consisting of “wavy, extremely disorganised, and markedly and intricately crumpled, twisted, or folded laminae that are confined within a single, relatively thin, well defined, undeformed layer, that die out both upward and downward, and that are overlain and underlain by parallel undisturbed layers. It is characteristic of some coarse-silt or fine-sand beds and involves only the internal laminae of the bed (and not the bed itself, which remains undeformed). The structure appears to result from deformation during deposition of sediments that become partially liquified but still retain some cohesion” (Bates and Jackson, 1987, p. 145).

(viii) Pseudonodules, “a primary sedimentary structure consisting of a ball-like mass of sandstone enclosed in shale or mudstone, characterised by rounded base with upturned or



inrolling edges, and resulting from the settling of sand into underlying clay or mud which welled up between isolated sand masses” (Bates and Jackson, 1987, p. 536).

(ix) Wavy lamination, a kind of stratification in which the upper and lower limits of the laminae are undulatory and not straight (Bouma, 1962).

(x) Muddy lamination, deposits formed of laminae composed mostly of mud but containing minor amounts of silt-size and sand-size particles.

(xi) Near-horizontal stratification, stratified beds where individual stratification bands, each ~1 - 10 cm thick, rest on an essentially horizontal erosional surface and are inverse graded in the lower part. In beds characterised by this structure, the maximum grain size decreases from the lower to the upper stratification bands while thickness of individual bands decreases upward (Hiscott, 1994).

The main lithologies observed in the thesis area are shale, siltstone and sandstone. Shale is the most common lithology forming more than 67% of all measured sections. Siltstone and sandstone are less common forming about 18 % and 16 %, respectively. Carbonate layers (limestone and dolomite) and volcanic ash layers are minor forming less than 1 % of the measured sections.

Because rock texture as observed in the field is the main criterion used to classify facies in this study, and because limited or no mineralogical or compositional parameters were studied, terms such as calcilutites and calcareous wackes are not used. Other terms such as argillite and greywacke are also not used. Instead, sandstone, siltstone and shale

are used to designate the main lithotype names. Only the names limestone, dolomite and K-bentonite (altered volcanic ash) depend on composition.

The facies interpretations presented in this chapter are only based on field characteristics in single sections. The lateral relationships between facies, and the relationship of facies to architectural elements and facies tracts are discussed elsewhere in this thesis. Thirteen facies were observed in the thesis area (Table 3.1). A different, less detailed classification of the same rocks was presented by Enos (1965, 1969a,b; Table 3.1).

### 3.2. FACIES CLASSIFICATION

In this study, facies are classified according to the scheme of Pickering *et al.* (1989, 1995) but different facies codes are used (Figure 3.2). This classification scheme is hierarchical with facies classes divided into facies groups, which are further divided into constituent facies. Facies classes are defined largely on the texture of the gravelly, sandy or silty lower part of the layer and the relative thickness of the mud interbeds or caps (Pickering *et al.*, 1989). Facies classes are labelled in a similar way to Pickering *et al.* (1989). Facies classes are divided into a disorganised facies group (denoted by 1 following the facies class label, e.g. D1 for disorganised siltstone group) and an organised facies group (denoted by 2 following the facies class label, e.g. D2 for organised siltstone). Facies in an organised facies group show clearly defined tractional sedimentary structures while in a disorganised facies group they lack clear stratification or grading.

Table 3.1. Facies recognised in this study. For grain size, MD=mud, SL=silt, VF=very fine sand, F=fine sand, M=medium bedded, TK=thick bedded. Ta, Tb, Tc, Td, Te and combinations refer to Bouma (1962) divisions. For the K-bentonites) are not included.

Facies	% of section	Grain size (mean)	Bed thk. (mean)	Short description
B1.1	0.1	F-M	TK	Sharp contacts, poorly developed normal grading. Fluid pipes and shale clasts
B2.1	0.7	F-M	M	Sharp contacts, normally graded with spaced stratification. Fluid pipes and shale clasts common in the upper part.
B2.2	1.2	F	M	Sharp contacts, normal grading in the lower part, bedding joint, shale clasts in the upper part, planar lamination (rare)
C1.1	0.21	VF	M	Sharp-faint contacts, ungraded, muddy with common shale clasts
C2.1	5.9	F	M	Sharp contacts, normally graded. Tae, Tac, Tab, Tabc, sl clasts more common in Tae beds
C2.2	0.6	VF-F	M	Sharp contacts, normally graded. Tb, Tbc, Tbcd(?)
C2.3	2.1	VF-F	M	Sharp contacts, normally graded. Tc, Tcd
C2.4	4.3	F-M	TK	Sharp contacts, normally graded, laminated and pseudonodules
C2.5	0.5	M-CS	TK	Sharp contacts, ungraded with pseudonodules
D2.1	15.6	SL	TN	Sharp contacts, ungraded, laminated
D2.2	0.4	SL	TN	Sharp contacts, ungraded silt lenses in shale
D2.3	0.6	SL	LM	Sharp contacts, ungraded, laminated
E	67.3	MD	M	Sharp contacts, ungraded. Rare burrows and lamination

Fine sand, F=fine sand, M=medium sand, C=coarse sand. For bed thickness (Bed thk.), LM=laminae, TN=thin bedded, Uma (1962) divisions. For the origin, HD= high density, LD= low density. Other lithologies (carbonate layers and

t description	Origin	Enos (1965, 1969a,b) names
developed normal grading. Fluid escape	HD turbidity currents/ sandy debris flows	Type 1 greywacke (?)
bedded with spaced stratification. is common in the upper part.	HD turbidity currents	Type 1 greywacke (?)
grading in the lower part, bedding parallel upper part, planar lamination (rare, faint).	Muddy HD turbidity currents	Type 1/type 2 greywacke
bedded, muddy with common shale clasts.	Debris flows	Type 2 greywacke
bedded. Tae, Tac, Tab, Tabc, shale beds	LD and HD turbidity currents	Type 1 greywacke
bedded. Tb, Tbc, Tbcd(?)	LD turbidity currents, pulsating (?) currents	Type 1 greywacke
bedded. Tc, Tcd	LD turbidity currents	Type 1 greywacke
bedded, laminated and pseudonodules	Large turbidity currents	Calcareous wacke
with pseudonodules	Large turbidity currents	Type 3 greywacke
laminated	LD turbidity currents	Calcilutite 1,2
t lenses in shale	LD turbidity currents	Calcilutite 1
laminated	LD turbidity currents	Calcilutite 1
are burrows and lamination	Muddy turbidity currents	Argillite

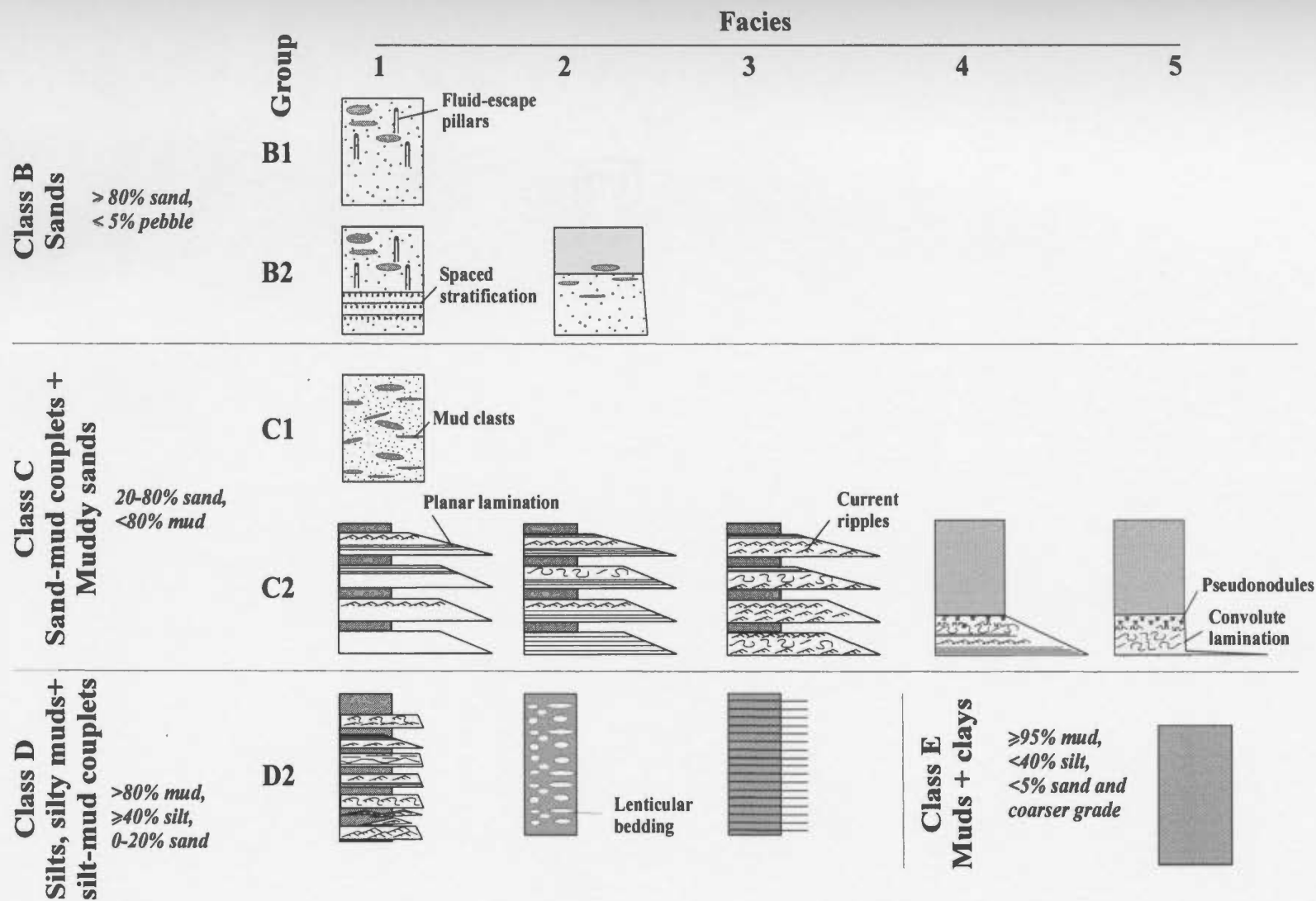


Figure 3.2. Modified classification scheme of Pickering *et al.* (1989). Only the facies present in the thesis area are presented. Note that the facies codes for the study area are different from those of Pickering *et al.* (1989), although the class and group characteristics are identical. Facies characteristics are summarised in Table 3.1.

Facies are labelled by numbers that follow the facies class and facies group label. Subfacies are labelled by a letter that follows the number that designates the facies. For example, subfacies D2.1C is a subfacies of facies D2.1 while facies D2.1 is a facies of the organised facies group (D2) of class D.

All the facies except one can be described using the Pickering *et al.* (1989) classification scheme. The facies that could not be classified, facies B2.2, may represent an uncommon type of deposit that is not widely known outside the Cloridorme Formation. Bed thickness is defined according to Ingram (1954): very thick beds, thicker than 100 cm; thick beds, 30-100 cm; medium beds, 10-30 cm; thin beds, 3-10 cm; very thin beds; 1-3 cm; thick laminae; 0.3 - 1 cm, and thin laminae, less than 0.3 cm.

### 3.3. FACIES CLASSES

Facies belonging to four facies classes have been recognised from the studied sections. According to Pickering *et al.* (1989), facies classes are differentiated mainly on the basis of texture into: (1) Class B, consisting of  $\geq 80\%$  sand and  $< 5\%$  gravel; (2) Class C, consisting of sand-mud couplets and muddy sand with 20-80% sand and  $< 80\%$  mud; (3) Class D, consisting of siltstone, silty mudstone and siltstone-mudstone couplets with  $> 80\%$  mud,  $\geq 40\%$  silt and  $< 20\%$  sand; and, (4) Class E, consisting of  $\geq 95\%$  mud,  $< 40\%$  silt grade,  $< 5\%$  sand and coarser grade,  $\leq 25\%$  biogenics. The main characteristics of the beds of each class are summarised in Table 3.2. Note that thicknesses for beds of Class C and Class D refer to the lower coarse part of the couplets only (sandstone or siltstone).

Table 3.2. Statistics for of all the facies classes and component facies observed in the thesis area. For grain size, ST=silt, VFS=very fine sand, FS=fine sand, MS=medium sand, CS= coarse sand, VCS=very coarse sand, and GN=granule. AVG=average, S.D.= standard deviation, AMAL= amalgamated. Subfacies of facies D2.1 are shown in *italics font* (e.g., *D2.1A*).

FACIES	THICKNESS				NUMBER OF BEDS				BED THICKNESS (cm)			BASAL GRAIN SIZE		
	TOTAL (m)	% OF CLASS	% OF ALL	% AMAL.	TOTAL	% OF CLASS	% OF ALL	% AMAL.	AVG.	S.D.	MIN/ MAX	AVG.	MIN	MAX
<b>Class B</b>	58.66	100	2.0	28.25	270	100	1	18.15	22	20	2/166	F	VF	VC
Gp.B1*	2.46	4.2	0.1	38.6	6	2.22	0.02	33.3	41	29	10.5/85	F-M	VF	C-VC
Gp.B2	56.2	95.8	1.9	27.8	264	97.8	0.95	17.8	21.3	19	2/166	F	VF	VC
B2.1	21.39	36.5	0.7	66	56	20.7	0.20	64.3	38.2	33	2/166	F-M	ST-VF	VC
B2.2	34.81	59.3	1.2	4.44	208	77	0.8	5.29	16.7	9	3.5/102.5	F	ST-VF	C-VC
<b>Class C</b>	400.6	100	13.63	21.5	1842	100	6.9	23.43	22	22	0.5/270	F	ST-VF	GR
Gp. C1*	6.17	1.5	0.21	12.5	42	2.3	0.2	11.90	14.7	8	3.5/38	VF	SL-VF	F
Gp. C2	394.5	98.5	13.4	21.64	1800	97.7	6.7	23.7	22	22	0.5/270	F	SL-VF	GR
C2.1	173.8	44.1	5.9	43	939	51	3.5	41	18.5	17	0.5/160	F	SL-VF	VCS-GR
C2.2	18.09	4.5	0.6	4.8	78	4.2	0.3	8.79	23.2	15	4/77	VF-F	VF	C-VC
C2.3	61.33	15.3	2.1	8.9	386	21.0	1.4	8.81	16.0	12	1/78.5	VF-F	SL-VF	VC
C2.4	125.6	31.8	4.3	0	379	20.6	1.4	0	33.2	27	2.5/151	F-M	SL-VF	VC-GR
C2.5	14.04	3.5	0.5	0	18	1.0	0.07	0	78	96	4.5/270	M-CS	SL-VF	GR

\* One facies B1.1 in group B1 and facies C1.1 in group C1

Table 3.2. Continued

FACIES	THICKNESS				NUMBER OF BEDS				BED THICKNESS (cm)		
	TOTAL (m)	% OF CLASS	% OF ALL	% AMAL.	TOTAL	% OF CLASS	% OF ALL	% AMAL.	AVG.	S.D.	MIN/ MAX
<b>Class D</b>	487.63	100	16.6	0.63	11249	100	41.9	0.14	4.1	5.2	<0.5/95.0
D2.1	457.07	93.8	15.6	0.63	9013	80.1	33.6	0.19	5.0	5.4	<0.5/95.0
D2.2	11.33	2.3	0.4	0	211	1.9	0.8	0	5.6	4.8	<0.5/25.0
D2.3	18.55	3.9	0.6	0	2026	18.0	7.5	0	0.7	0.5	<0.5/3.0
D2.1A	243.66	49.9	8.3	1.27	3971	35.3	14.8	0.43	6.1	5.3	0.5/95.0
D2.1B	49.24	10.1	1.7	0	2369	21.1	8.8	0	2.1	1.2	<0.5/10.0
D2.1C	51.63	10.6	1.8	0	557	4.95	2.1	0	9.3	5.5	1.0/35.0
D2.1D	26.64	5.5	0.9	0	302	2.7	1.1	0	8.8	8	1.0/53.0
D2.1E	33.61	7.0	1.1	0	1395	12.4	5.2	0	2.4	2.5	<0.5/24.5
D2.1F	12.47	2.6	0.42	0	161	1.4	0.6	0	7.7	4.9	1.5/25.0
D2.1G	39.82	8.2	1.4	0	257	2.3	1.0	0	15.5	9.6	3.5/60.0
<b>Class E*</b>	1992.16	100	67.30	0	13479	100	48.93	0	14.6	25.4	<0.5/510

\* In this thesis, Class E includes the shale parts of sand-mud and silt-mud couplets, a departure from the Pickering *et al.* (1989) classification scheme.



The upper shale parts of the couplets are included in Class E.

Shale is the only facies recognised in facies Class E. It is the most common facies forming about 67.3% of the total thickness of all measured sections (Figure 3.3). Mud caps overlying sandstone and siltstone beds of Class C and Class D are included in this facies class because it is difficult to differentiate between different shale beds that overlie each other without intervening sand or silt and because non turbidite mud cannot be distinguished from the turbidite mud that forms the mud caps of these couplets. A total of 13,479 shale beds were measured in all the section; these represent approximately 50% of the total number of beds measured in the studied sections.

Siltstones of Class D are the second most common facies in the area. These siltstones form the lower parts of siltstone-mudstone couplets and about 16.5% of the total measured sections. Several facies were observed in this class. Ripple lamination, some of which is convoluted, is the most common sedimentary structure. No disorganised siltstone facies were recognised. A total of 11,249 siltstone beds were measured in all the sections. These represent approximately 43% of all beds measured. Less than 20 of these beds occur in amalgamated units.

Sandstones of Class C are the third most common facies in the area and form about 13.5% of the thickness of all the measured sections. Sandstones representing the lower parts of organised sand-mud couplets are by far the most common occurrence. They form about 98.5% of all the facies in this class while disorganised muddy sandstone forms the remaining 1.5 %. A total of 1,842 sandstone beds, 42 of which are disorganised muddy

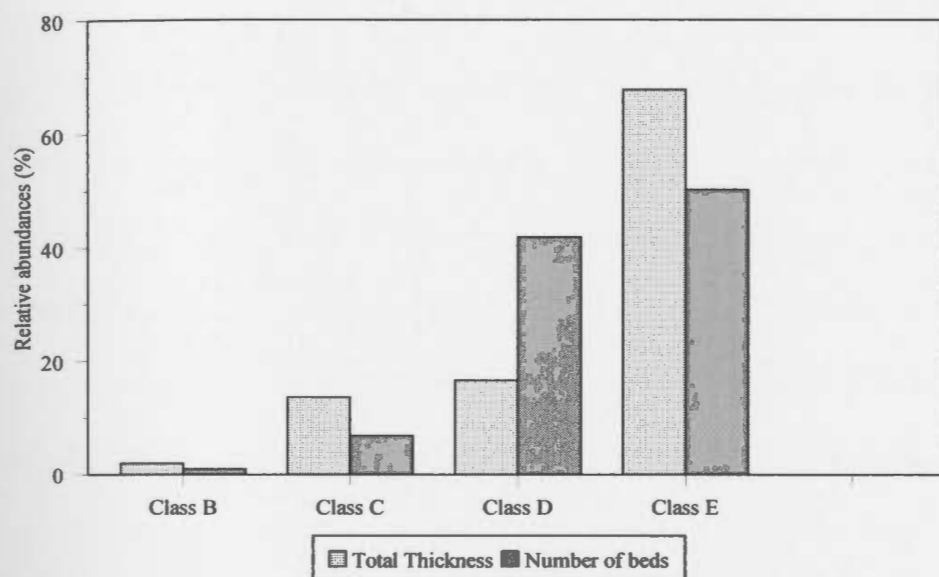


Figure 3.3 Relative facies class abundances (in percent) from all measured sections. Proportions are for the number of beds (dark grey pattern) and total thickness (dotted).

sandstone, were measured in all sections. Sandstone beds of Class C represent about 7% of the total number of beds measured. Many sandstone beds of this class occur in amalgamated units, especially facies C2.1.

Sandstone of Class B, the least common facies class, represents less than 2% of the measured sections. Only 270 sandstone beds, six of which are disorganised, were measured in all sections. Sandstone beds of Class B represent less than 1% of all the beds measured in the thesis area. About 18% of the sandstone beds of Class B occur in amalgamated units.

Carbonate and ash beds are the least common types of beds. In the thesis area, 102 carbonate beds and 72 ash beds were recognised. These beds combine for less than 1% of the total thickness and total number of beds in all sections. In the following section, facies Class E will be described first because it is most abundant, followed by Class D and Class C. Facies Class B, the least abundant, is described last.

### **3.4. FACIES CLASS E (SHALE)**

#### **3.4.1. Shale Facies: Description**

This facies comprises all shales that alternate with coarser beds of other facies. All mudstone, silty mudstone and claystone are grouped under a single facies, shale, because of: (1) the similar appearance of all occurrences of this facies in the field; (2) the strong slaty cleavage which obscures original structures or subtle features that might otherwise aid in the differentiation of different types of shale; and, (3) a lack of chemical data to

enable the recognition of different shale types. The Shale facies is equivalent to the argillite facies described by others from the area (Enos, 1965; Beeden, 1983).

Shale beds and laminae range in thickness from less than 0.5 cm to about 510 cm with an average bed thickness of 14.6 cm (Table 3.2). Colour on fresh and weathered surfaces is dark grey to black. Rarely, some lighter coloured or darker coloured bands of shale are also present. These bands vary in thickness from a few centimetres to tens of centimetres and colour changes coincide with an irregularly-shaped weathering profile. In the field, shale beds are separated from the underlying and overlying facies by sharp contacts; rarely, grading from the underlying beds into shale was observed (Plates 1).

Most of the shale beds (75%) are thin and medium bedded while very thin beds or laminae and thicker beds are less common forming the remaining 25%. Thin and medium bedded shale beds account for about 54% of the total thicknesses of shale while thick and very thick bedded shale beds account for 44% of the total thickness of the shale, although they represent less than 10% of the total number of beds (Figure 3.4). Shale is the least resistant facies to weathering (except for ash beds); shale beds weather into rough surfaces on the wave-cut platform.

Sedimentary structures are rare in the shale beds: only small scale loading between siltstone and sandstone and shale beds is present. These small loads may reach 0.5 cm x 2.0 cm in size and have a saucer shape. The loads form internally laminated silt lenses that may be isolated or connected by a thin silt lamina (facies D2.2). Burrows were rarely observed in shale beds. Only 2-3 burrows (*Zoophycus* ?) were observed in the shale in

P1.1



P1.2



Plate 1. Facies Class E. P1.1. Shows a thick shale interval that has an irregular weathering profile and suggests it consists of several shale beds. P1.2. Thick to very thick shale bed that is interpreted as a deposit of a large turbidity current that carried a silt and mud load (mud turbidite). Scale divisions =10cm.

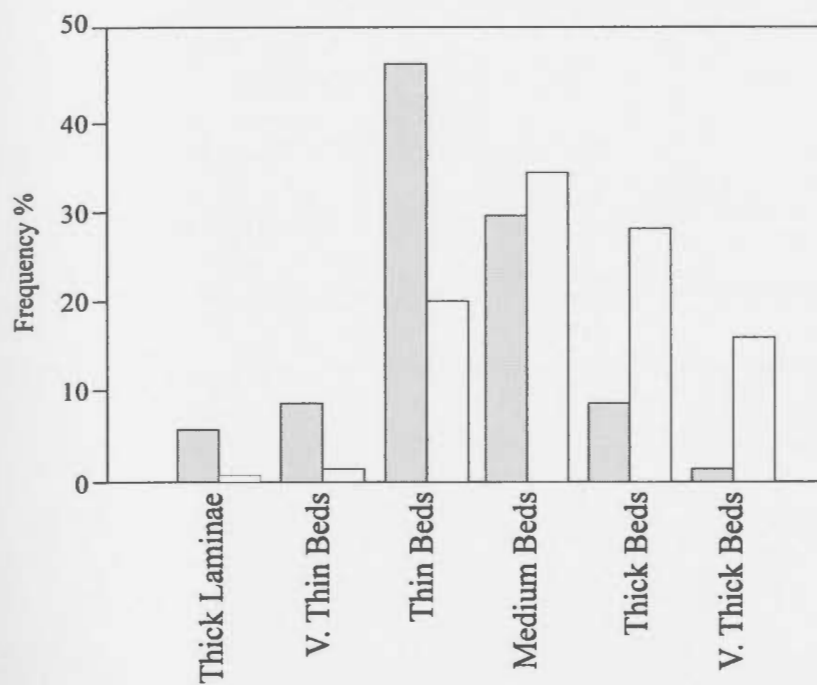


Figure 3.4. Relative proportions of the bed thickness categories of shale beds (in percent) from all measured sections. Proportions are for the number of beds (grey pattern) and the total thickness (no pattern).

the upper part of the RE section. However, burrowing activity is suggested by small protrusions found on the lower bedding planes of many siltstone and sandstone beds that overlie shale beds. A few graptolites were found in shale.

Enos (1965) indicated that the dominant clay minerals in these shales are chlorite and illite, based on data for shale clasts in turbidite sandstone beds. The dark colour of the shale is attributed to the presence of disseminated organic matter and fine grained pyrite (Enos, 1969). Recently, Garver *et al.* (1996) analysed nine shale samples from different parts of the Cloridorme Formation, one of which is from a section exposed at the town of Cloridorme (Royce, 1992). These samples were analysed using Inductively Coupled Plasma Mass Spectrometry (ICP-MS). The average trace-element abundances (mean of the nine samples) in parts per million (ppm) is: Ti = 0.81, V = 135.3, Cr = 167.5, Mn = 0.06, Co = 21.3, Ni = 111.5, and Cu = 45.8.

Based on petrography, Slivitzky *et al.* (1991) recognised four different mudstone and claystone facies in the Cloridorme Formation: (1) silty calcareous claystone, representing about 1% of the formation; (2) dolomitic mudstone-silty claystone-clay shale, representing 57% of the formation; (3) sandy conglomeratic mudstone and dolomitic conglomeratic mudstone, representing less than 1% of the formation; and, (4) Calcareous claystone and/or argillaceous calcilutite, representing about 5% of the formation. The petrology of these four facies is presented in Appendix A7.

### 3.4.2. Shale Facies Interpretation

Interpreting the processes that were responsible for the transport and deposition of mud that forms shale is difficult because of the structureless appearance of the shale and its cleaved nature. Several hypotheses have been suggested for the origin of shale; these centre on whether the mud was deposited by turbidity currents, bottom currents or by hemipelagic settling. Interpreting the origin of shales and mud is difficult even in modern sediments and requires many analyses that were not done in this study. These analyses are of limited value for lithified lower Paleozoic rocks such as those in the thesis area (Hesse, 1975).

Based on field observation, all the processes listed above may have contributed to deposition. The rare occurrence of trace fossils may suggest that most of the shale was deposited rapidly from turbidity currents, but the low number of trace fossils may only reflect unfavourable living conditions for organisms. Part of the shale overlying sandstone and siltstone beds was probably deposited by the same current that deposited the underlying coarser sediments. It is unknown what percentage of this shale was deposited by turbidity currents and what may have been deposited by other processes. The sharp lower contacts of the shale beds is mainly due to a difference in grain size and not to a break in deposition (*cf.* Piper, 1978). Shale units which show an irregular weathering profile probably consist of several thinner beds of different grain size or mineralogy (Plate 1.1). Based on this observation, it is suggested that some of the shale beds may have been deposited from multiple turbidity currents. These turbidity currents may have carried loads



consisting entirely of mud at their time of initiation or may have been the distal tails of flows that deposited their sand and silt loads elsewhere (Plate 1.2).

Enos (1965), based on lateral correlation and regression analysis of the thicknesses of shale, sandstone and siltstone facies against distance, suggested that 58% of the shale is of turbidite origin while Slivitzky *et al.* (1991) suggested that all the shale beds overlying sandstone and siltstone facies in the Manche-d'Épée and Pointe-à-la-Frégate members are mud caps deposited by the same current that deposited the underlying sandstone and siltstone beds.

Garver *et al.* (1996) suggested that the source of the shale of the Cloridorme Formation was the erosion of sedimentary rocks rich in Ni and Cr present in the uplifted thrust sheets in front of an arc colliding with the continental margin of Laurentia. The ultimate source of the Ni and Cr was ultramafic rocks of an ophiolite.

Most of the shale beds overlying other coarser facies described in this thesis were probably deposited by the same turbidity currents that deposited the underlying sandstone and siltstone. Some shale beds may have been deposited by a mud-load turbidity currents that deposited no sand or silt in the area of the measured sections. Some shale beds may have been deposited by other processes such as hemipelagic deposition or deposition from bottom currents. It is suggested here based on the rates of hemipelagic deposition that much of the shale is deposited from turbidity currents. Stow and Tabrez (1998) suggests that rates of hemipelagic deposition ranges from low (<5 cm/1000 yrs) to high (>20/1000years). The age of the entire Cloridorme Formation based on graptolite zones

(Chapter 1) is about six million years (Barnes *et al.*, 1981). Using these suggested ages and sedimentation rates, hemipelagic sediments may account for 300-1200 m of the Cloridorme Formation. These thicknesses represent a small percent of the thickness of the Cloridorme Formations that is approximately 6 km (Slivitzky *et al.*, 1991). Additional constraints on the origin of the shale beds, based on lateral correlation, are presented in Chapter 5.

### **3.5. FACIES CLASS D (SILTSTONES, SILTY MUDSTONES AND SILTSTONE-MUDSTONE COUPLETS)**

The siltstone facies in this class were classified by Enos (1965) into calcilutite 1 and calcilutite 2. Siltstone beds in the thesis area mostly belong to his calcilutite 1 category. Siltstone beds and laminae range in colour from bluish grey to brownish yellow. Most of the beds show strong reaction with dilute HCl. In some sections, siltstone beds appear continuous for tens to hundreds of metres (Plate 2.1). Some siltstone beds cluster into packets consisting mostly of siltstone beds with little or no intercalated shale (Plate 2.2).

The tops and bases of the siltstone beds are sharp. Siltstone beds are mainly ungraded, or subtle grading may have gone unnoticed in thin beds because of the fine grain size. Rarely, the tops grade into the overlying shale. Shale clasts are rare. Flutes, grooves and a variety of tool marks are common on the soles of these beds, especially in cliff outcrops where the soles of beds are better exposed. These features have been

P 2.1



P2.2

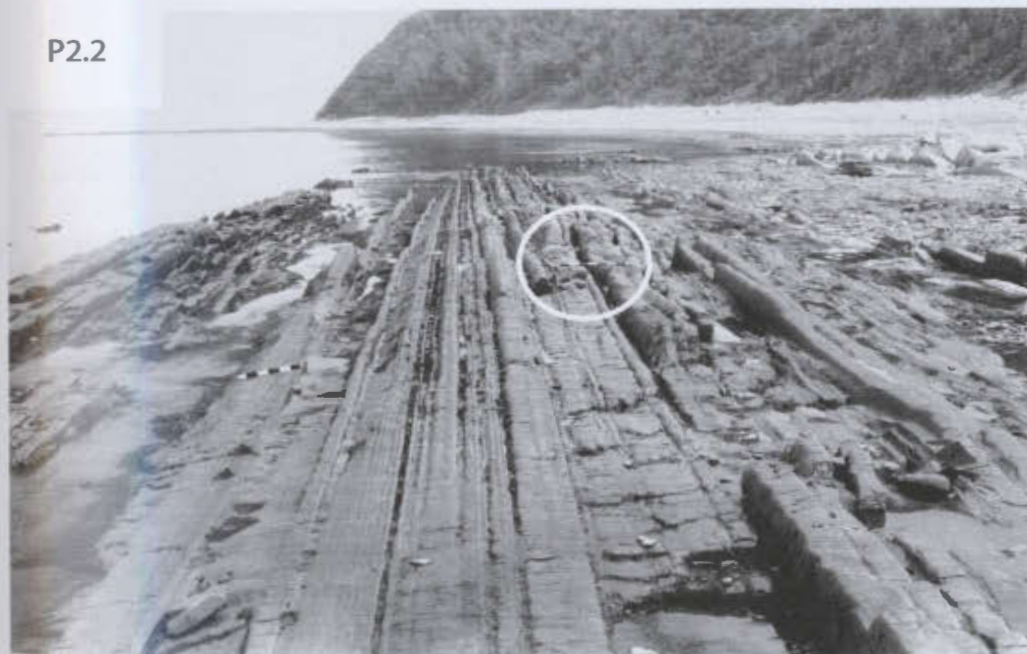


Plate 2.1. Siltstone beds of facies Class D in the lower part of section SYW showing lateral continuity for tens to hundreds of metres. Top is to the right.  
 Plate 2.2. Siltstone beds of facies Class D forming packets in the middle part of section PCDR. Some sandstone beds are also present (below circled scale).  
 Scale divisions = 10 cm. Top is to the left of the photograph.

described in detail by Enos (1965). The soles of many siltstone beds have <1 cm diameter hemispheric protrusions. The tops of many siltstone beds are wavy, due to the preservation of ripple forms, especially in the CB section where the upper bedding planes of many beds are exposed. The petrology of the siltstone facies is presented in Appendix A7.

Slivitzky *et al.* (1991) observed three main siltstone facies: silty carbonates (forming 11% of the Cloridorme Formation), calcareous argillaceous siltstone (<1% of the formation), and silty calcilutite (<10% of the formation). The facies of Slivitzky *et al.* (1991) correspond in many cases to particular divisions of turbidites, and are not compatible with the facies in this thesis which have not been defined in a way that splits individual turbidites into their constituent parts.

Based on the type of sedimentary structure or the sequence of sedimentary structures, the siltstone beds were classified into several facies and subfacies. In some cases, assignment of some beds to a certain facies or subfacies was somewhat difficult because gradation from one type to the other is common, especially for ripple-laminated siltstones, convoluted ripple-laminated siltstones, and convolute laminated siltstones. All the other physical characteristics of the siltstone facies and subfacies fit the descriptions given above. Graded stratified siltstone beds (facies D2.1) are the lower parts of siltstone-mudstone couplets and are the most common facies in this class (Figure 3.5). Siltstone lenses in shale (facies D2.2) and structureless siltstone beds (facies D2.3) are the other two facies in this group.

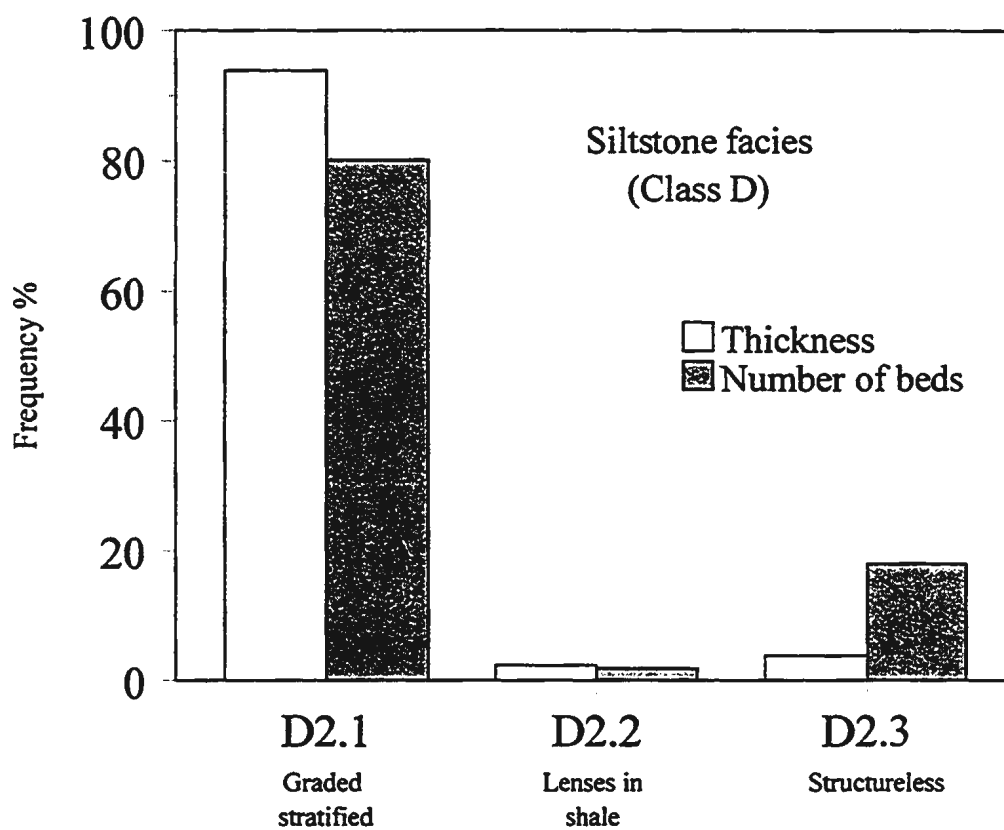


Figure 3.5. Relative proportions of the three facies of facies Class D (in percent) from all measured sections. Proportions are for the number of beds (grey pattern) and the total thickness (no pattern).

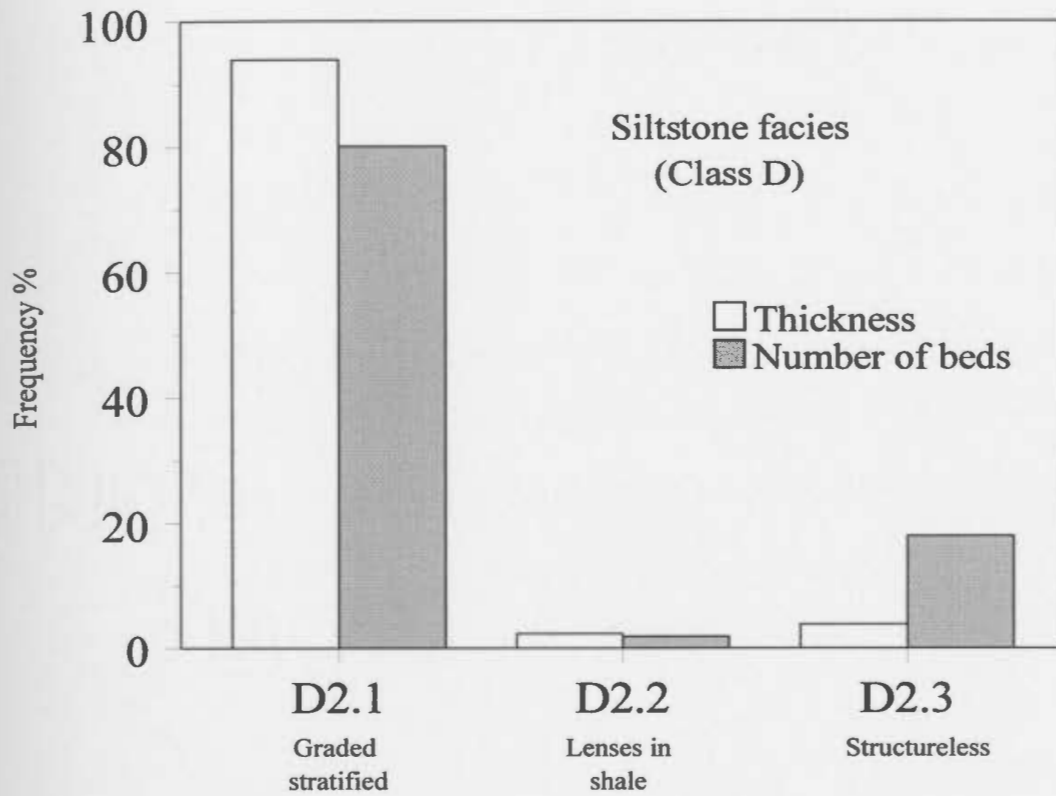
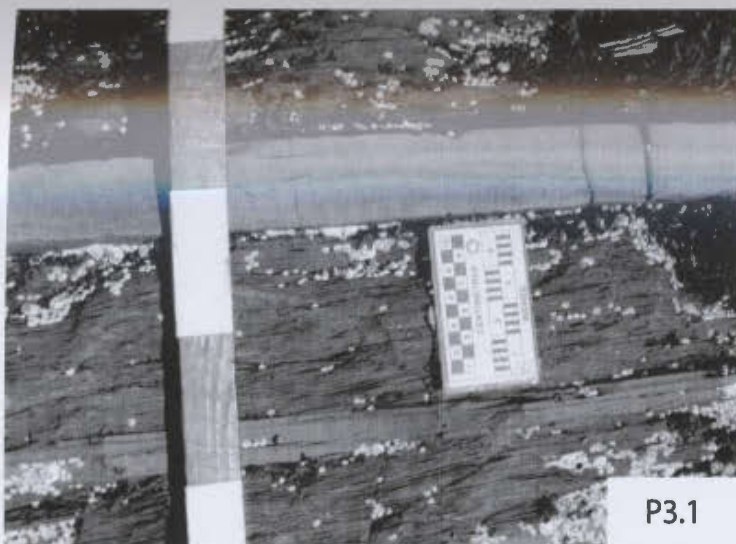


Figure 3.5. Relative proportions of the three facies of facies Class D (in percent) from all measured sections. Proportions are for the number of beds (grey pattern) and the total thickness (no pattern).

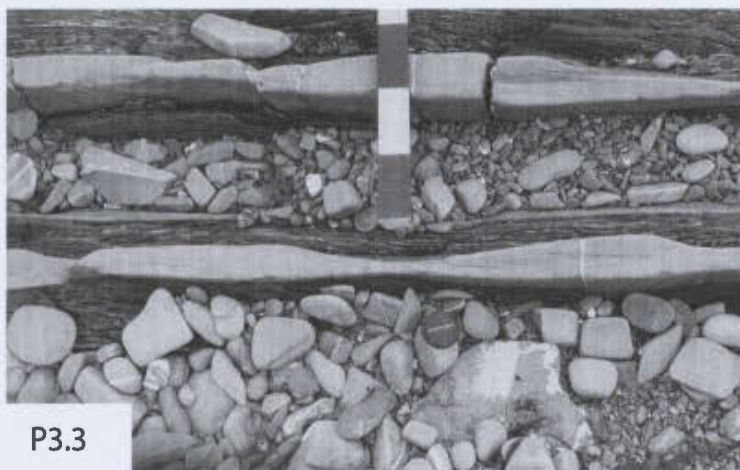




P3.1



P3.2



P3.3



P3.4

Plate 3. Subfacies of facies D2.1. P3.1 Subfacies D2.1A showing type A ripple-drift-cross-lamination (Jopling and Walker, 1968). P3.2. Subfacies D2.1A showing type B ripple-drift-cross-lamination. P3.2 and P3.4 are examples of subfacies D2.1B showing isolated "starved" ripples. Jacob Staff scale divisions = 10cm. Small rectangular scale has both centimetre and inch divisions.

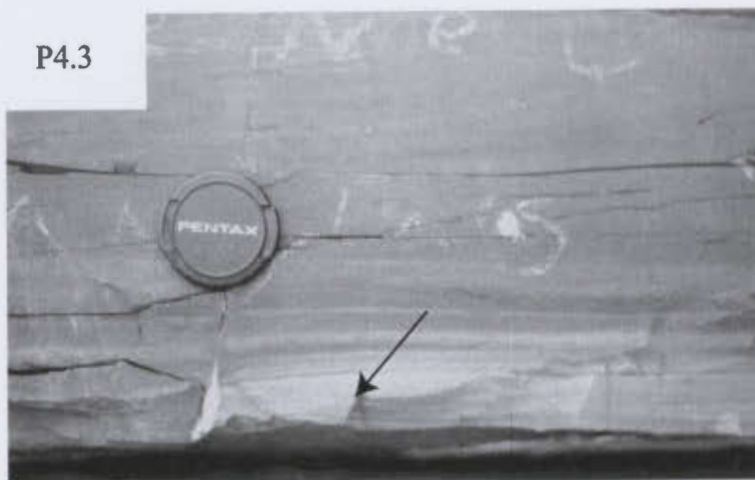


Plate 4. Subfacies of facies D2.1. P4.1 is subfacies D2.1C showing convoluted ripple lamination. P4.2 is subfacies D2.1D showing planar lamination followed by ripple/climbing ripple lamination. P4.3 is subfacies D2.1F showing ripple (arrow) lamination overlain by parallel lamination. P4.4 is subfacies D2.1G showing ripple lamination overlain by convolute lamination. Rectangular scale has both centimeter and inch divisions. Lens cap (5 diameter) is used for scale in P4.3.



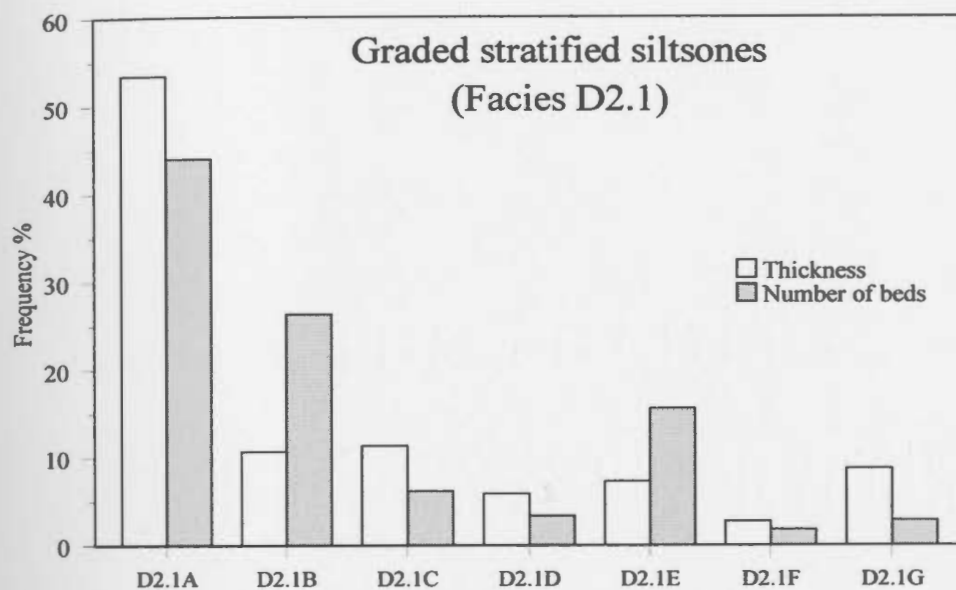


Figure 3.6. Relative proportions (in percent) of the number of beds and thickness of the subfacies of the graded stratified siltstone facies (D2.1).

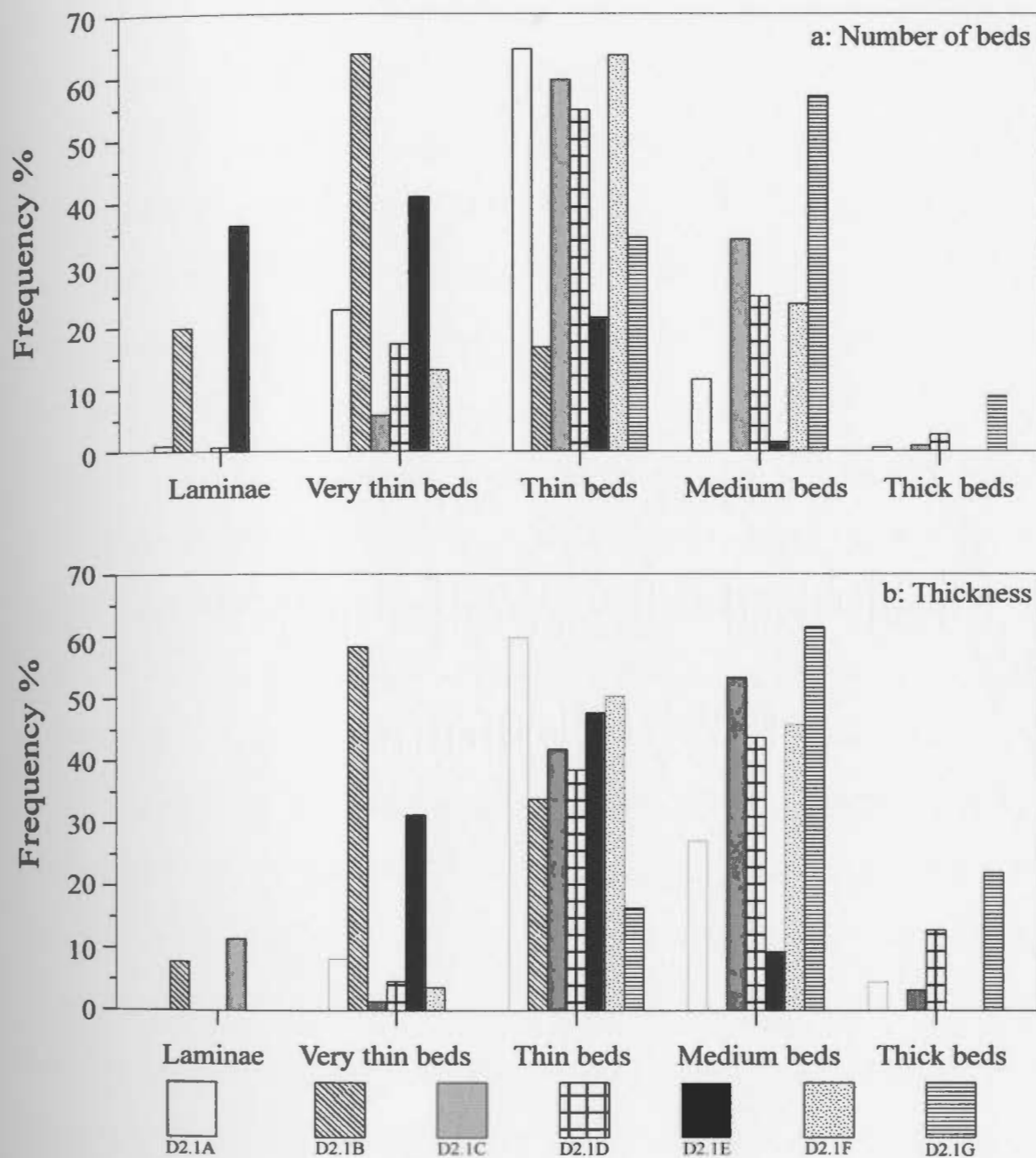


Figure 3.7. Relative proportions of the bed thickness categories of Ingram (1954) for the siltstone subfacies of facies D2.1 (graded stratified siltstone). Proportions are for the number of beds (a) and the total thickness (b). The reader will find this figure easiest to digest by focusing on a single pattern (e.g., single subfacies) and then noting how the beds (or cumulative thickness) are distributed over the different thickness categories.

The number of sets of cross lamination in a single bed varies from two to six. Beds consisting of two or three sets are the most common forming about 80% of all beds of subfacies D2.1A, while beds consisting of five or more sets are rare and form less than 3% of all the beds. Beds with a greater number of sets are usually thicker compared to beds with a smaller number of sets. Thick siltstone beds of subfacies D2.1A usually occur in packets of sandstone or siltstone. In some of these thick beds, when a single set of cross-lamination can be traced from the base to the top of the bed, the angle of climb may increase in a downflow direction, with the highest angles being at the top of the bed.

Generally, the angle of climb of the ripples varies from a few degrees to less than 20°, but for the thicker beds the angle of climb may exceed 20°. Climbing-ripple lamination similar to type A ripple-drift-cross-lamination of Jopling and Walker (1968), characterised by the lack of preservation of stoss side laminae, is the most common type of climbing-ripple lamination. Climbing ripple lamination similar to type B ripple-drift-cross-lamination of Jopling and Walker (1968), with preserved stoss side lamination, is present but less common and usually characterises only the thick siltstone beds. The alternation of light coloured laminae with dark coloured, more clayey laminae defines the lamination. When the upper bedding plane of some of the siltstone beds is exposed, the ripple crests are sinuous rather than straight.

Siltstone beds and laminae of subfacies D2.1B consist of a single set of ripples. This subfacies accounts for about 25% of the beds and laminae of facies D2.1 but because of their thin nature, the beds and laminae form only about 10% of the total thickness of

facies D2.1 (Plate 3). The ripple forms are fully preserved. The ripple wavelength or ripple spacing - defined by Harms (1969) as “the distance between crests measured parallel to the direction of the current or wave propagation” - is variable and ranges from 5 - 200 cm. The ripple amplitude or height - defined by Harms (1969) as “the elevation of the ripple crest above the adjacent trough” - ranges from 0.5 - 7 cm. Very thin beds form about 60% of the total thickness and number of beds in the subfacies; thick laminae and thin beds are less common (Figure 3.7).

Subfacies D2.1C consists of siltstone beds that exhibit convolute lamination, where the original structure cannot be recognised (Plate 4). This subfacies forms about 10% of the total thickness of facies D2.1 but the number of beds is small. Many of the beds have laminae that are contorted and consist of narrow anticlines separated by broader synclines while other beds have lamination with a variety of irregular shapes. Most beds of subfacies D2.1C are thin and medium bedded while very thin bed and thick beds form less than 10% of this subfacies (Figure 3.7).

Subfacies D2.1D consists of siltstone beds with a lower planar laminated division overlain by a ripple laminated division (Plate 4). The planar laminated part is usually thinner than the overlying ripple laminated part. The upper ripple lamination may consist of one ripple set or more than one set of climbing-ripple lamination. No variation in the grain size between the lower and upper part of the bed was recognised but the variation may have been small and thus not detected. Subfacies D2.1D forms <10% of the total thickness and total number of beds of facies D2.1 (Figure 3.6). Most of the beds are thin

and medium bedded while very thin and thick beds are less common (Figure 3.7).

Siltstone beds that consist of planar, parallel or wavy laminations (subfacies D2.1E) form more than 15% of the number of beds of facies D2.1 but less than 10% of the total thickness (Plate 5). Individual laminae are mostly less than 1 mm thick. Very thin beds form a large percentage of the total thickness of this subfacies (Figure 3.7).

Siltstone beds that consist of a ripple laminated division overlain by parallel lamination (subfacies D2.1F; Plate 4) are the least common subfacies; they form less than 5% of the number of the beds and the total thickness of facies D2.1. The lower part of the bed may consist of a single set or several sets of climbing-ripple lamination. The upper parallel laminated division may be wavy, mimicking the form of the underlying ripples, or planar. The thickness of the upper parallel laminated division may be thinner or thicker than the underlying ripple laminated division. Thin beds form more than 60% of the beds of subfacies D2.1F and more than 50% of its total thickness. Medium beds are less common, ~ 25% of beds, but form up to 45% of the total thickness of this subfacies.

Siltstone beds that consist of convolute lamination and ripple lamination form subfacies D2.1G (Plate 4). The ripple lamination may consist of a single set or several sets of climbing-ripple lamination. In most of the beds of this subfacies, the lower part of the bed consists of ripple/climbing-ripple lamination while the upper part of the bed consists of convolute lamination and is thicker. Siltstone beds consisting of a lower division of convolute lamination overlain by ripple lamination are also present but less common. Most of the beds are medium bedded while thin and thick beds are less common (Figure 3.7).

### **3.5.2. Interpretation of Facies D2.1**

This facies is interpreted as turbidity current deposits. The presence of flutes and grooves on the soles of some beds suggests that the currents that deposited these beds eroded part of the underlying mud while the round protrusions at the base of the siltstone beds are interpreted as silt fill of burrow entrances; these suggest limited erosion beneath some of the beds. The dominance of thin beds and laminae (85%) may suggest a low sediment concentration in the flows, or flows of small size. Alternatively, the thin character of the beds may be due to limited deposition from a bypassing turbidity current. Other studies have also shown that sandstone and siltstone beds exhibiting climbing-ripple lamination and ripple lamination, like many of the siltstone beds in this study, are usually characterised by thin and very thin beds (Bouma, 1962; Walker, 1967; Van Hoon 1970). The different subfacies formed as a result of variation of the sediment load, flow velocity or syn-depositional and post-depositional deformation of the deposited silt.

Recently, Shanmugam (1997) has suggested that ripple lamination and other tractional sedimentary structures observed in rocks interpreted as deep water deposits may be a product of deposition from bottom currents rather than turbidity currents. Siltstone beds observed in the thesis area do not show characteristics suggesting deposition from bottom currents (Stow and Piper, 1984). Climbing ripples, in particular, require high suspension fallout rates that are not characteristic of bottom currents. In addition, the narrow foreland basin suggested to have existed during the deposition of the Cloridorme Formation is an unlikely location for strong, persistent bottom currents.

Siltstone beds that are characterised by climbing-ripple laminations (subfacies D2.1A) suggest the importance suspension fallout during deposition (Jopling and Walker, 1968; Middleton and Hampton, 1976). The greater number of beds with no stoss side laminae points to conditions with a relatively low ratio of suspended load to traction load. Siltstone beds that are characterised by preservation of stoss side lamination, similar to type B ripple-drift-cross-lamination of Jopling and Walker (1968), suggest a higher ratio of suspended-load to traction-load deposition. These beds are relatively thick compared to the other siltstone beds and their occurrence within sandstone and siltstone packets suggests a relationship to conditions that favour formation of packets. These thick beds may have been deposited during periods of increased sediment concentration in decelerating turbidity currents, or during periods of flow expansion as the turbidity currents exited confining channels. The packets may have formed topographic highs on the sea floor at the time of deposition, causing a sudden reduction in the velocity of the current as it passed over a mound-shaped obstacle, as suggested Kneller (1995). The gradual upward increase in the angle of climb in some of these thick beds suggests an increase in the amount of sediment fallout from suspension (Walker, 1969). Thus, thick beds exhibiting climbing ripple lamination, similar to type B ripple-drift-cross-lamination of Jopling and Walker (1968), some of which shows an upward increase in the angle of climb, may have formed as a result of flows exiting confining channels and moving over obstacles. These obstacles may have been formed as a result of enhanced deposition at the channel terminations, forming so-called lobes (Normark, 1970; Mutti and Ricci Lucchi,

1972; Mutti and Normark, 1987; 1991).

The presence of thick beds of climbing ripples may have been partly a function of grain size. Small ripples are common bedforms in fine sediments such as fine sand and silt (Middleton and Southard, 1984), and the dominance of ripple lamination and climbing-ripple lamination in the siltstone beds suggests that the fine grain size may have been an important factor that controlled the type of facies deposited. Divisions of climbing-ripple lamination are far less common in coarser sandstone beds.

Siltstone beds and laminae (subfacies D2.1B) that consist of a single ripple set are interpreted to have been formed by the reworking of thin silt layers (Walker, 1965). These isolated ripples have been called “starved ripples” by many authors to reflect limited sediment supply. Wavelengths of up to 2 metres observed in some of these beds suggest that flows may have had a high viscosity due to a high concentration of suspended sediment in the turbidity current (Southard and Mackintosh, 1981).

Siltstone beds that show convolute lamination (subfacies D2.1C) are interpreted to form as a result of gravitational instability of rapidly deposited sediments (Middleton, 1993). Many ideas have been suggested for the origin of convolute lamination (Allen, 1982) but most research suggests that the structure forms due to the deformation of rapidly deposited sediments. Siltstone beds displaying convolute lamination have a mean bed thickness greater than other siltstone beds. These beds may have been deposited more rapidly from turbidity currents that carried relatively higher sediment concentration compared to other siltstone beds.



Siltstone beds that have a lower parallel laminated division and upper ripple/climbing-ripple laminated division (subfacies D2.1D) are interpreted as deposits from waning flows (Kneller, 1995). The lower planar laminated division was probably deposited under upper flow regime plane bed conditions while the overlying ripple laminated part was probably deposited under lower flow regime conditions (Middleton and Southard, 1984). The relative thinness of the lower planar laminated division compared to the overlying ripple laminated division might suggest that parallel laminae are not favoured in silt, or that during higher velocity flow conditions little sediment accumulated on the bed. The mean bed thickness of subfacies D2.1D is large compared to other siltstone subfacies, suggesting that these beds were perhaps formed beneath larger (thicker and/or longer) flows.

Siltstone beds that show parallel and wavy laminations (subfacies D2.1E) are interpreted to have been deposited under upper flow regime plane bed conditions (Allen, 1982; Middleton and Southard, 1984). The wavy nature of some of the lamination might indicate slight deformation after deposition.

Siltstone beds that show a ripple laminated division followed by a parallel laminated division (subfacies D2.1F) are rare and form only a small percent of the number and total thickness of the beds of facies D2.1. This may be due to the difficulty in recognising the upper parallel laminated  $T_d$  division of Bouma (1962), a problem encountered in weathered or tectonised exposures (Bouma, 1962; Walker, 1965). Siltstone beds showing a lower ripple laminated division and an overlying parallel

laminated division are interpreted as deposits from waning low concentration turbidity currents (Pickering *et al.*, 1989). The ripple laminations formed under lower flow regime conditions (Middleton and Southard, 1984). Many ideas and theories have been suggested for the formation of the upper parallel laminated division. These range from shear sorting (Stow and Bowen, 1980) to burst and sweep cycles (Hesse and Chough 1980). The origin of these laminations is beyond the scope of this study.

Siltstone beds that show a combination of ripple lamination and convolute lamination (subfacies D2.1G) formed when deformation affected only part of a bed. The lack of deformation of the lower part of a bed suggests that the underlying strata were probably firm and did not permit the sinking and deformation of the lower ripple sets. The upper deformed part may have consisted of sediments that were deposited more rapidly or with a higher percentage of fines.

### **3.5.3. Siltstone Lenses in Shale (Facies D2.2): Description**

This is the least common facies in this class (Figure 3.6). It consist of siltstone lenses encased in shale (Pate 6). These lenses vary considerably in shape and size. Some of the lenses are internally laminated. These laminae are mainly convoluted. Other lenses are structureless. The bedding-parallel length of individual lenses varies from a few centimetres to tens of centimetres while their thickness may reach several centimetres. Some lenses are arranged in a more-or-less continuous train that in some cases is connected by a layer of silt that ranges in thickness from a few millimetres to centimetres.

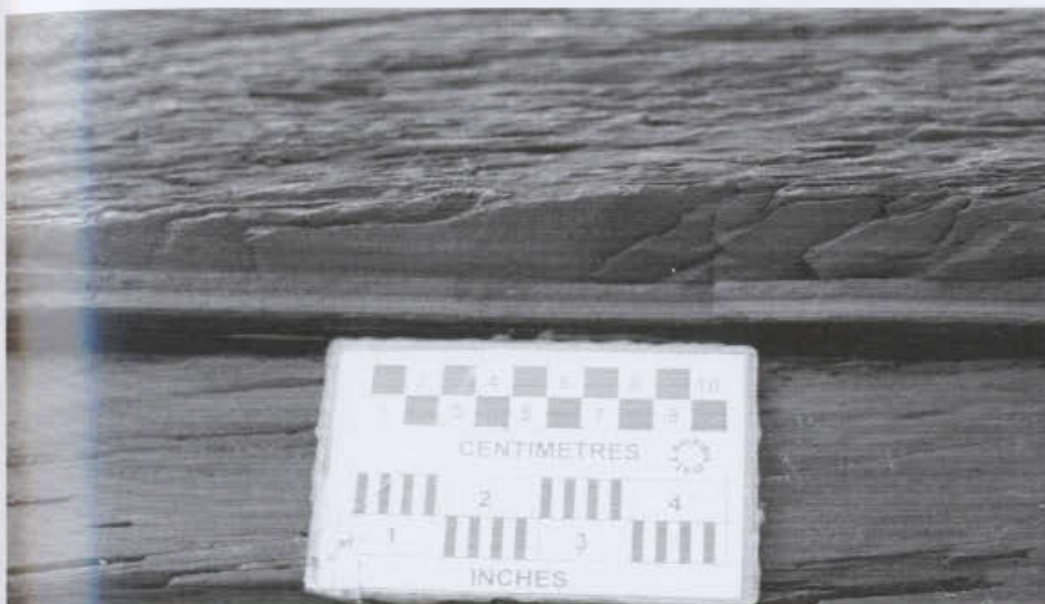


Plate 5. A very thin bed of subfacies D2.1E showing planar lamination. It is presented here to contrast it with facies D2.3 below. Rectangular scale has both centimetre and inch divisions.



Plate 6. Isolated and connected siltstone lenses of facies D2.2 in shale (white arrow). Thin and very thin laminae of facies D2.3 (black arrow). Rectangular scale has both centimetre and inch divisions.

Other lenses are present above siltstone beds and are connected to these beds by thin siltstone dykes. These dykes usually have an irregular shape and orientation.

#### **3.5.4. Interpretation of Facies D2.2**

The intervals or trains of isolated lenses of siltstone in shale are interpreted as isolated ripple lenses similar to subfacies D2.1B that were deformed by loading when silt ripples sank into underlying soft mud (Bouma, 1962). Massive siltstone lenses, or lenses that are connected to underlying siltstone beds by dykes or offshoots are interpreted as injection structures (Bouma, 1962, Dzulynski and Walton, 1965; Hiscott, 1979; Ma, 1996). The close association of these latter lenses with massive beds may suggest that these structures formed during the rapid expulsion of pore fluid and sediments, as dykes, following liquefaction of the massive beds. Cyclic loading due to seismic shocks may have been the cause of liquefaction in the Québec foreland basin (Hiscott, 1979).

#### **3.5.5. Structureless Siltstone (Facies D2.3): Description**

This is the second most common facies in Class D. It consists entirely of laminae (Plate 6) and very thin beds that are internally structureless and ungraded. Most of the beds are less than 3 cm thick.

#### **3.5.6. Interpretation of Facies D2.3**

These beds can be ascribed to deposition of the silt from suspension with no

subsequent traction deposition. Alternatively, the structureless part may have been deposited as a result of the “freezing” of the lower part of the flow while other sediments in the current were transported farther into the basin (Walker, 1965, 1967). An additional interpretation suggested by Walker (1965) is that the current may have been detached from the seabed as an interflow because of the higher density of the bottom waters. In this case, the sediment would settle from the interflow and there would be no seabed traction transport. It is unknown what the density of the bottom waters was at the time of deposition and thus this interpretation is speculative.

### **3.6. FACIES CLASS C (SANDSTONE-MUDSTONE COUPLETS AND MUDDY SANDSTONES)**

Sandstone beds of this class are the lower parts of sand-mud couplets of Pickering *et al.* (1989). They are the most common sandstone beds in the thesis area (Table 3.2). Facies of this class are grouped into two groups: disorganised (C1) and organised (C2). Organised facies are the most common, forming more than 98% of the beds of this class. The detrital composition of the different sandstone facies as determined by Enos (1965, 1969a,b) and Slivitzky *et al.* (1991) is shown in Appendix A7.

#### **3.6.1. Disorganised Sandstone Facies Group (C1)**

Only one facies is assigned to this group. These beds were termed type 2 greywacke by Enos (1965). They are characterised by a high percentage of muddy matrix

(up to 47%). Forty-two beds of this facies (termed here muddy sandstone) were observed in the thesis area.

#### 3.6.1.1. Muddy Sandstone Beds (Facies C1.1): Description

This facies consists of beds that range in thickness from less than 4 cm to about 40 cm (Table 3.2). Most are thin to medium beds while very thin beds are rare and thick beds are absent. The main characteristic of these beds is the presence of a high percentage of muddy material. Beds are mainly ungraded and most of the beds consist of very fine sand and mud. These beds contain variable proportions of mud clasts that range in size from 1-30 cm x 1-8 cm. Clasts are subangular to subrounded. Many of the beds contain scattered medium to coarse sand grains. Beds usually have sharp planar contacts (Plate 7). Only one bed was observed to have grooves at its base. The upper contacts with overlying shale vary from sharp to gradational. In some cases, muddy sandstone beds are difficult to distinguish from the shale. Muddy sandstone beds tend to occur with other sandstone beds in packets.

#### 3.6.1.2. Interpretation of Facies C1.1

Muddy sandstones beds are interpreted as debris flow deposits based on the lack of well developed grading to suggest deposition from suspension, and the lack of sedimentary structures to suggest tractional sediment transport. The solids in these debris flow were probably supported by matrix strength due to cohesion as a result of abundant



Plate 7. Facies Class C. P7.1. Muddy sandstone of facies C1.1. P7.2. A medium bed of facies C2.1 showing sharp upper and lower contacts. P7.3. Thick, massive bed of facies C2.1. P7.4. Several medium to thick beds of facies C2.1 forming a packet. The packet overlies a megaturbidite (arrow). Most of the mud cap of this megaturbidite is eroded. Hammer (circled) is 35 cm long. Jacob Staff divisions = 10cm. Rectangular scale has both centimetre and inch divisions.

mud matrix (Middleton and Hampton, 1976; Pickering *et al.*, 1989; Lowe and Guy, 2000). These beds are equivalent to “slurry sandstones” of other authors (e.g. Hiscott and Middleton, 1979).

### **3.6.2. Organised Sandstone Facies Group (C2)**

Sandstone beds of this group are the third most common type of sediment in the thesis area (Table 3.2). Diagnostic sedimentary structures and their vertical organisation are not unique to the Cloridorme Formation, but have been described from similar deposits elsewhere, both in modern and ancient settings. These deposits have been referred to as “classical turbidites” (Walker, 1978). Several facies are recognised in this group (Table 3.2). These facies are classified based on the sequence of sedimentary structures, type of sedimentary structure that characterises the basal part of beds, and the thickness of beds. Five facies are recognised: beds that start with a structureless division (Bouma, 1962,  $T_a$  division), facies C2.1; beds that start with a planar laminated division ( $T_b$ ), facies C2.2; beds that start with a cross lamination/climbing-ripple lamination ( $T_c$ ) or convolute lamination, facies C2.3; and the lower coarser parts of two types of megaturbidites, facies C2.4 and C2.5. Facies C2.4 and C2.5 beds are not recognised solely on the basis of their thickness because some of these beds may have thicknesses that are comparable to the thickness of other facies in this group. Facies C2.4 and C2.5 are instead recognised based on a combination of features such as exceptional lateral continuity, evidence of palaeoflow reversals in the bed, and presence of a pseudonodule division



between the lower sandy part and the overlying mud cap.

Sandstone beds of this class have a variety of thicknesses, sedimentary structures, types of bedding contacts and sole marks. These will be discussed in the next section. The sandstone beds are usually dark grey when fresh but weathered surfaces show a variety of shades of greyish green and grey.

#### 3.6.2.1. Sandstones with a Structureless Lower Division (Facies C2.1): Description

This is the most common facies in this class in terms of cumulative thickness and number of beds (Table. 3.2, Figure 3.8). Most of the beds of this facies are characterised by their massive appearance and sharp upper and lower contacts (Plate 7). Most are medium bedded while thin beds and thick beds are less common (Figure 3.9). More than 40% of the beds of this facies occur in amalgamated units. Poor to good normal grading was observed in 58% of the beds while 42% of the beds are ungraded. Grain size at the base of the bed ranges from very coarse sand-granule to silt-very fine sand, with a mean basal grain size of fine sand. The mean size of the bed tops is very fine sand (Table 3.3).

About 87% of the beds (subfacies C2.1A) consist of a structureless sandstone division overlain directly by shale (46%) or by an amalgamation surface (~41%). Grading is well developed in 34% of these beds while the remaining 66% are poorly graded or ungraded. Shale clasts are present in half of these beds; they may occur anywhere in the beds but tend to be more common in the upper parts of beds. These clasts range in size from a few centimetres to several centimetres; some of these clasts have their long axis

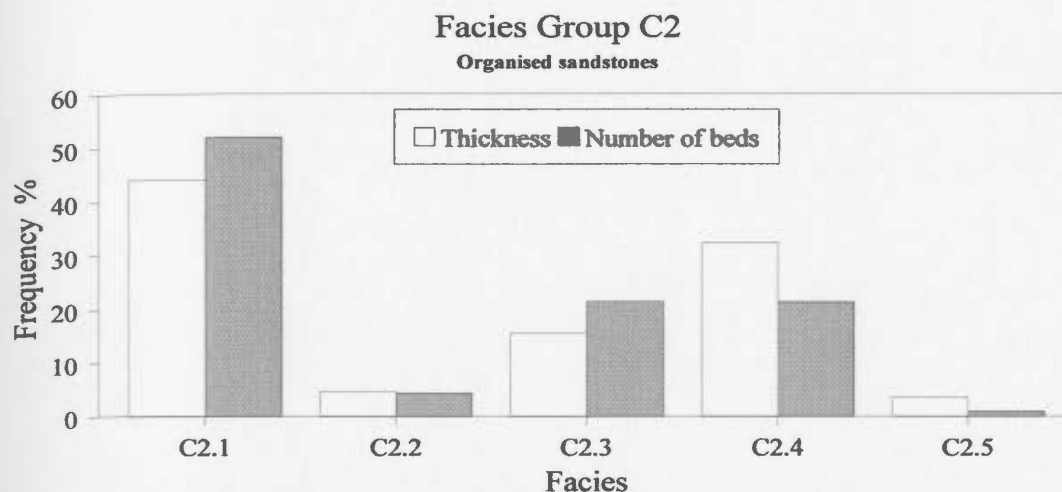


Figure 3.8. Relative proportions of the five facies of Group C2 (in percent) from all measured sections. Proportions are for the number of beds (grey pattern) and the total thickness (no pattern).

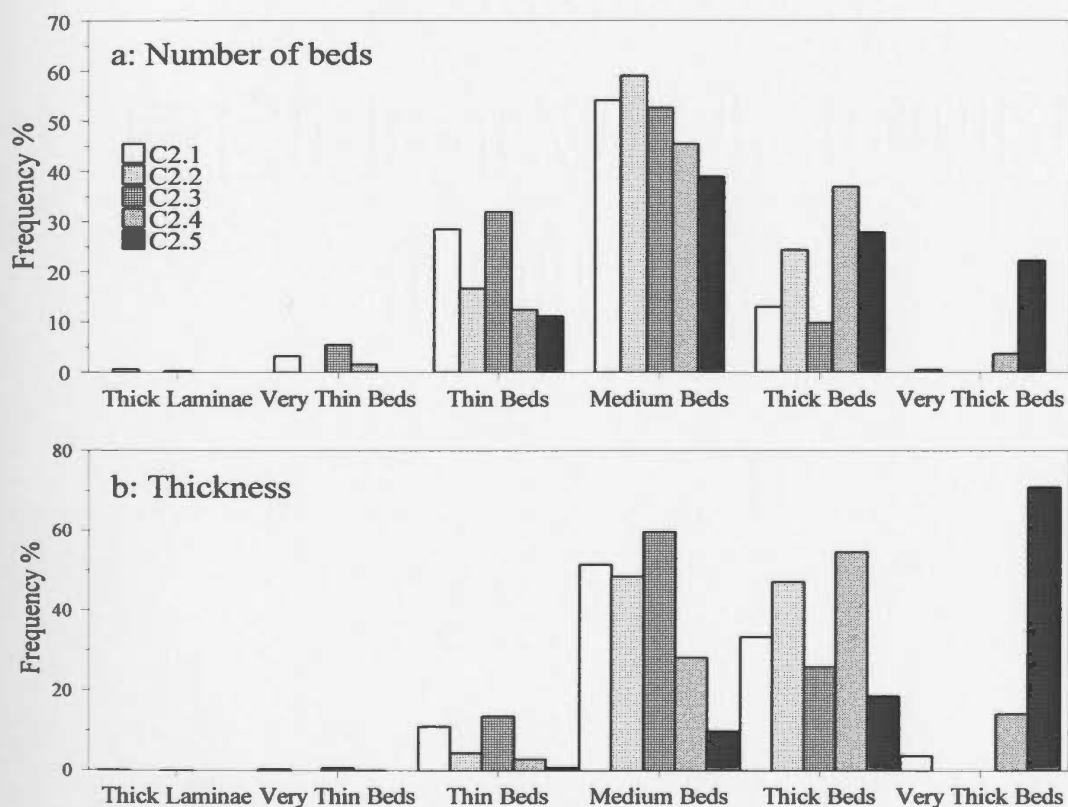


Figure 3.9. Relative proportions of the bed thickness categories of Ingram (1954) for each of the sandstone facies of Group C2. Proportions are for the number of beds (a) and the total thickness (b).

Table 3.3. Bed characteristics of facies C2.1 and its subfacies. For grain size, ST=silt, VFS=very fine sand, FS=fine sand, MS=medium sand, CS= coarse sand, VCS=very coarse sand, and GN=granule size. For grading, UN= ungraded, PR GR= poorly graded (1 phi size difference in grain size from the base to the top of the bed), GR WGR=graded to well graded (> 1 phi size difference from base to top).

	Facies or Subfacies	Total Thk. (m)	% of Thk	# of Beds	% of Beds	Bed Thickness (cm)		Grain Size				Normal Grading
						$\bar{x}$	Min / Max	$\bar{x}$ Basal	Min/Max	$\bar{x}$ Upper	Min/Max	
	C2.1	173.8	100	939	100	18.5	0.5/160	FS	ST-VFS/VCS-GN	VFS	ST-VFS/VCS-GR	42% UN 18% PR GR 40% GR-WGR
	C2.1 Non-Amal.	98.8	57	554	59	17.8	0.5/160	FS	ST-VFS/VCS-GN	VFS	ST-VFS/VCS-GR	44% UN 17% PR GR 39% GR-WGR
	C2.1 Amal.	75.0	43	385	41	19.5	1/115	FS	ST-VFS/VCS-GN	VFS	ST-VFS/CS	39% UN 21% PR GR 40% GR-WGR
Beds not in amalg. units	Subfacies C2.1A	79.1	46	465	49.5	17.0	0.5/160	FS	VFS/VCS-GN	VFS	ST-VFS/CS	50% UN 16% PR GR 34% GR-WGR
	Subfacies C2.1B	14.4	8	53	5.6	27.2	5.0/150	FS	ST-VFS/CS	ST-VF S	ST-VFS/FS-MS	5% UN 17% PR GR 78% GR-WGR
	Subfacies C2.1C	4.3	3	29	3.1	14.7	3.0/44	VFS-FS	VFS/MS-CS	ST-VFS	ST-VFS/MS	34% UN 28% PR 38% GR-WGR
	Subfacies C2.1D	1.0	1	7	0.7	14.1	4.0/24	FS	VFS/MS-CS	ST-VFS	ST-VFS/VFS-FS	28% PR GR 72% GR-WGR

Table 3.3. Continued

	Facies or Subfacies	Total Thk. (m)	% of Thk	# of Beds	% of Beds	Bed Thickness (cm)		Grain Size				Normal Grading
						$\bar{x}$	Min / Max	$\bar{x}$ Basal	Min/Max	$\bar{x}$ Upper	Min/Max	
Beds in amalg. units	Subfacies C2.1A	71.0	40.8	374	39.8	19.0	1/ 115	FS	ST-VFS/ VCS-GN	VFS	ST-VFS/ VCS-GN	39% UN 21% PR GR 40% GR-WGR
	Subfacies C2.1B	2.3	1.3	6	0.6	39	10/ 65	VFS-FS	ST-VFS/ MS	VFS	ST-VFS/ VFS-FS	33% UN 33% PR GR 33% GR-WGR
	Subfacies C2.1C	0.4	0.2	2	0.2	20.9	3.0/ 39.0	FS	ST-VFS/CS	ST-VFS	ST-VFS/ST-VFS	50% UN 50% GR-WGR
	Subfacies C2.1D	1.3	0.7	3	0.3	43.1	15/ 92.5	VFS-FS	ST-VFS/MS	VFS	ST-VFS/FS	33% UN 33% PR GR 34% GR-WGR

parallel to bedding with the remaining clasts do not have any preferred orientation. The lower contacts of the beds are mainly flat or wavy. Flutes were observed on the soles of 12% of the beds, while loads and grooves were observed on the soles of 12% and 8% of the beds, respectively. The upper contacts are sharp; in some instances, dykes and offshoots were observed to emanate from these beds into the overlying shale.

Fifty-nine beds consist of a lower structureless division overlain by a ripple laminated division (subfacies C2.1B). This is the second most common subfacies forming about 10% of the total thickness of facies C2.1. Six beds occur in amalgamated units. Beds in non amalgamated units have a mean bed thickness of ~27 cm (Table 3.3). The lower structureless division forms about 2/3 of the thickness of the beds and generally shows well developed normal grading. The upper division may consist of a single set of ripple lamination or 2-3 sets of climbing-ripple lamination. The ripple laminated division consists mostly of very fine sand or silt. In some beds, there is 1-4 cm-thick interval, at the top of the massive division and below the ripple laminated division, that has mud clasts that are usually 2-3 cm x 1-2 cm in size. Lower contacts of the beds are mainly flat to wavy. Flutes were observed on the soles of 17% of the beds; loads on 25% and grooves on 2%.

Thirty-one beds (subfacies C2.1C) have a lower structureless division followed by parallel lamination ( $T_{ab}$ ). These beds form about 3% of facies C2.1. Two of these beds occur in amalgamated units. The mean bed thickness is about 15 cm (Table 3.3). More than 65% of the beds show poor to good normal grading. The grain size at the base of

beds varies from very fine to coarse sand (mean size is fine sand) to silt-very fine sand at the top. More than 65% of the beds have a flat or wavy base with no sole marks. About 21% of the beds have flutes at their base, 12% have loads, and ~4% have grooves.

Only ten beds, three of which occur in amalgamated units, consist of a lower structureless division followed by parallel lamination and then ripple or climbing-ripple lamination (subfacies C2.1D). The thickness of each division is variable. Individual laminae in the middle parallel laminated division are 1-2 mm thick. The upper division consists of a single set of ripple lamination or two to three sets of climbing-ripple lamination similar to type A ripple-drift-cross-lamination of Jopling and Walker (1968). Normal grading is well developed in these beds. For the beds that do not occur in amalgamated units, the bases of three of the beds are flat while one bed has a wavy base. Flutes are present on the bases of two beds and loads on the base of one.

#### 3.6.2.2. Interpretation of Facies C2.1

Sandstone beds of this facies can be interpreted in different ways. Sandstone beds that show well developed normal grading and tractional sedimentary structures are interpreted as deposits from waning low density turbidity currents (Pickering *et al.*, 1989). Beds that have a lower structureless division followed by a rippled division without the development of an intermediate parallel laminated division (subfacies C2.1B) may suggest that deposition was too rapid for plane bed conditions to develop (Arnott and Hand, 1989). An alternative interpretation is that the massive division was deposited from the

highly concentrated head region of the current while the ripple lamination was formed by reworking of the deposited sediments by the tail of the turbidity current (Pickering *et al.*, 1989). The beds that have an upper division of climbing-ripple lamination (subfacies C2.1C) suggest that a combination of tractional transport and suspension deposition occurred, although tractional transport was dominant over suspension deposition, thereby producing climbing-ripple lamination without preservation of the stoss-side lamination (type A ripple-drift-cross-lamination of Jopling and Walker, 1968).

The interpretation of the origin of sandstone beds that are structureless (subfacies C2.1A) has recently been debated in the literature. Either deposition was from high concentration turbidity currents (Lowe, 1982, 1997; Pickering *et al.*, 1989; Bouma *et al.*, 1997; Hiscott *et al.*, 1998; Mulder and Alexander, 2001) or from sandy debris flows (Shanmugam, 1997, 2000; Shanmugam and Moiola, 1997). This debate still exists (Kneller and Buckee, 2000) and is beyond the scope of this thesis; nevertheless, the interpretation suggested below for these beds is consistent with their field characteristics.

Structureless beds form the majority (~90%) of the beds of facies C2.1. Less than half of these beds occur in amalgamated units and because most of the tractional sedimentary structures in this facies occur near the tops of the beds, evidence for these tractional structures may have been eroded in the amalgamated units. About 35% of the structureless beds show moderate to well developed normal grading consistent with deposition from turbidity currents (Middleton and Hampton, 1976; Pickering *et al.*, 1989; Middleton, 1993; Shanmugam, 1997, 2000). The remaining 65% of the beds that show

poor or no grading may have been deposited from high concentration turbidity currents or sandy debris flows. Some of these beds have flutes at their base. These scour marks confirm fluid turbulence in turbidity currents; laminar debris flows do not cut flutes (Shanmugam, 1997). Shanmugam (1997) utilises the presence of shale clasts to support a debris flow origin for similar beds. However, the origin of mud clasts in such beds is still poorly understood and cannot be used as an indicator of the flow rheology (Lowe, 1997). Many ideas have been suggested for the origin of such shale clasts (Johansson and Stow, 1995; Hiscott *et al.*, 1998). If the clasts were travelling behind the head of the flow; they could have been buried by sand and incorporated into beds that had already been partly deposited (Hiscott *et al.*, 1998). An alternative interpretation has been suggested by Mutti and Nilsen (1981). They propose that indurated shale clasts eroded from the underlying bed are incorporated into the lower part of the flow. These clasts may survive the high shear stress in the lower part of turbidity current and, because of their lower density relative to the denser basal part of the flow, will tend to move upward in the flow and may be preserved at the top of the beds.

The occurrence of clasts in some of the same beds that also exhibit well developed tractional structures or well developed normal grading argues in favour of turbidity current origin for all these features. Beds of the Cloridorme Formation are not unique in carrying mud clasts together with clear independent evidence of being turbidites (Walker, 1985).

Thus, structureless beds are interpreted to have been deposited from turbidity



currents. Beds with well developed normal grading may have been deposited from low concentration turbulent flows. Some tractional transport of the deposited sediments may have taken place and formed a variety of structures. Some beds may have been deposited rapidly from more concentrated flows (Mulder and Alexander, 2001). Rapid deposition from suspension prevents the development of tractional features (Arnott and Hand, 1989; Allen, 1991). During the deposition of some beds, the lower part of the flow may have become less turbulent, perhaps due to the high sediment concentration (Lowe and Guy, 2000). This high concentration layer may have separated as a quick bed or a lower inertia layer and “froze” due to an abrupt increase in intergranular friction (Middleton, 1970; Pickering *et al.*, 1989) or augmentation of mud content due to the shear-induced fragmentation of mud clasts (Lowe and Guy, 2000). Such basal high concentration zones have been termed sandy debris flows by Shanmugam (1997), but the preference in this thesis is not to recognise ephemeral parts of depositing currents as separate flows (Mutti *et al.*, 1999).

#### 3.6.2.3. Sandstones with a Parallel Laminated Lower Division (Facies C2.2): Description

This facies is the least common facies of this group (Figure 3.8). Only 78 beds have been recognised (Plate 8). Seven beds of this facies occur in amalgamated units. More than 50% of the beds have a lower parallel laminated division followed by ripple lamination or climbing-ripple lamination (Table 3.4). More than 60% of the beds are medium bedded (Figure 3.9). Beds outside amalgamated units are divided into three

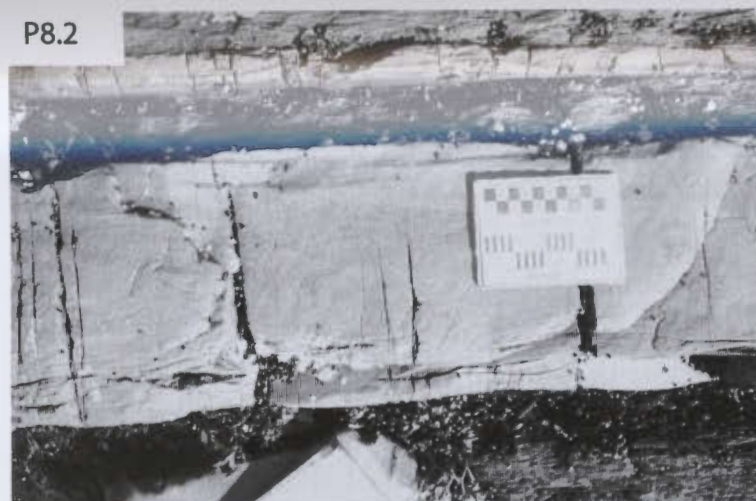


Plate 8. Facies C2.2 and C2.3. P8.1. Facies C2.2 with planar lamination in the lower 5 cm overlain by convolute lamination. P8.2. Facies C2.3 showing ripple lamination in the lower ~5 cm overlain by convolute lamination. The upper 3 cm has poorly developed ripple lamination. P8.3. Facies C2.3 with a single set of ripple lamination in the lower part that is overlain by ~12 cm of planar lamination that is overlain by wavy and convolute lamination. Lens cap = 5 cm. Jacob Staff divisions = 10cm. Rectangular scale has both centimeter and inch divisions.

Table 3.4. Bed characteristics of facies C2.2. Note that most of the beds that occur in amalgamated units belong to subfacies C2.2A. For abbreviations see Table 3.2.

	Facies or Subfacies	Total Thk. (m)	% of Thk.	# of Beds	% of Beds	Bed Thickness (cm)		Grain Size				Normal Grading
						$\bar{x}$	Min/Max	$\bar{x}$ Base	Min/Max	$\bar{x}$ Top	Min/Max	
	C2.2	18.1	100	78	100	23.2	4/77.0	FS	ST-VFS/CS-VCS	ST-VFS	ST-VFS/MS	27% UN 31% PR GR 42% GR-WGR
	C2.2 Non-Amal	17.2	95	71	91	24.2	4.5/77.0	FS	ST-VFS/CS-VCS	ST-VFS	ST-VFS/FS-MS	25% UN 30% PR GR 45% GR-WGR
	C2.2 Amal	0.9	5	7	9	12.4	4/22	VFS/FS	ST-VFS/MS-CS	VFS	ST-VFS/MS	43% UN 43% PR GR 14% GR-WGR
Beds not in amalg. units	Subfacies C2.2A	1.8	10	11	14	16.6	7.0/33.0	VFS/FS	ST-VFS/MS	VFS	ST-VFS/FS-MS	37% UN 45% PR-GR 18% GR-WGR
	Subfacies C2.2B	10.1	56	46	59	22	4.5/51.0	VFS-FS	ST-VFS/MS	ST-VFS	ST-VFS/VF S-FS	22% UN 28% PR-GR 50% GR-WGR
	Subfacies C2.2C	5.2	29	14	17.9	37.4	16/77.0	FS	ST-VFS/CS-VCS	ST-VFS	ST-VFS/ST-FS	29% UN 21% PR-GR 50% GR-WGR

subfacies. Beds that show only parallel lamination (subfacies C2.2A) are the least common. Only eleven such beds were observed. These beds range in thickness 7-33 cm (mean ~17 cm). Grain size is mainly very fine to fine sand at the base and very fine sand at the top (Table 3.4). Parallel lamination is defined by the presence of several 1-5 mm-thick laminae. The beds have sharp upper and lower contacts. The bases of the beds are planar or wavy. Flutes were observed on the sole of one bed while grooves were observed on another. Well developed normal grading occurs in about 18% of the beds while the remaining beds are ungraded or show poorly developed normal grading (Table 3.4).

Most of the beds of facies C2.2 consist of a parallel laminated division overlain by a division of ripple lamination/climbing-ripple lamination or a parallel laminated division overlain by convolute lamination (subfacies C2.2B; Table 3.4). The mean thickness of these beds is 22 cm. These beds have sharp upper and lower contacts. Most of the lower bedding planes are wavy or planar. Flutes were observed on the base of 10% of the beds. Other sole marks such as grooves and load casts are rare. Unlike beds of subfacies C2.2A, about 50% of the C2.2B beds show moderate to well developed normal grading. The parallel laminated division in this subfacies usually forms 25-35% of the beds. Parallel laminae are mainly planar and 1-5 mm thick. Climbing-ripple lamination is better developed as the upper division in thicker beds. Some ripple laminae are deformed into convolute lamination but in some beds, deformation may be so intense in some beds that geometry of the original ripple lamination cannot be established.

Beds of subfacies C2.2C have a lower parallel laminated division followed by a

ripple lamination or convolute lamination and an upper division of parallel lamination. No erosional contacts or truncations are present between the divisions. These beds are characterised by a greater mean thickness (~37 cm) than other sandstone beds of facies C2.2. Only 14 beds of this subfacies were observed. Most of these beds show poor to good normal grading. The lower bedding planes are sharp. About one third of the beds have planar lower contacts while the remaining beds have flutes or grooves. Loads were also observed on the soles of 3 beds. Thirteen of these beds occur in the PF and SH sections.

At the PF section, planar lamination characterises the lower division with laminae 2-5 mm thick. These planar laminae become slightly wavy or irregular near the upper part of the division. The middle division consists of ripple lamination/climbing- ripple lamination or convolute lamination. This middle division is overlain by a division of wavy or planar lamination some of which is muddy.

Beds at the SH section are thicker and may consist of several divisions of parallel or wavy lamination alternating with divisions of ripple or convolute lamination; the uppermost division is invariably planar or wavy lamination. The laminae in this uppermost division are 1-3 mm thick and contain a high proportion of silt and mud.

#### 3.6.2.4. Interpretation of Facies C2.2

These beds are interpreted as base-cut-out classical turbidites (Walker, 1970; Pickering *et al.*, 1989). The beds were deposited from waning low concentration turbidity

currents (Pickering *et al.*, 1989). The greater thickness of beds exhibiting several divisions suggests that these were deposited from relatively large flows. The lower, parallel laminated division was probably deposited under upper flow regime, plane-bed conditions while the upper part was deposited under lower flow regime conditions (Middleton and Hampton, 1976; Pickering *et al.*, 1989). Beds that exhibit climbing-ripple lamination suggest rapid fallout of sediment from suspension during deposition (Harms *et al.*, 1982). Deformation of some of these ripples may have been due to a combined effect of rapid deposition, and entrapment of pore fluids. Beds in the SH section that show several alternating divisions of ripple or convolute lamination with parallel lamination or wavy lamination, with no erosional surfaces or truncations between divisions (i.e., not an amalgamated unit), may have been formed beneath a “disturbed” flow (Van Tassell, 1981). This disturbance may have caused the flow to have a pulsating nature. Initiation of the flow by retrogressive failures might form pulsating currents (Larue and Provine, 1988). The pulsating nature of the flow might also have been due to the interaction of the current with the bottom topography (Haughton, 1994). The presence of these beds only in the SH and PF sections suggests local controlling factors (e.g., topography).

#### 3.6.2.5. Sandstones with a Basal Divisions of Ripple/Convolute Lamination (Facies C2.3):

##### Description

This facies is more common than facies C2.2 (Figure 3.8). More than three hundred beds start with ripple lamination, climbing-ripple lamination or convolute

lamination (Plate 8). About 10% of the beds occur in amalgamated units (Table 3.5). Beds that consist of only ripple lamination, climbing-ripple lamination or convolute lamination (subfacies C2.3A) are the most common, forming ~65% of the beds in facies C2.3. Beds that consists of multiple divisions of ripple lamination or climbing-ripple lamination or convolute lamination and parallel lamination (subfacies C2.3C), and beds consisting of ripple lamination or climbing-ripple lamination or convolute lamination followed by parallel lamination (subfacies C2.3B) are less common forming ~18% and ~9% of the beds of this facies, respectively. About 50% of the beds of facies C2.3 are medium bedded while 30% of the beds are thin (Figure 3.9).

Beds of this facies are characterised by sharp lower and upper contacts. The lower bedding planes are flat or slightly wavy (50% of the beds). Flutes occur on the bases of 26% of the beds and 19% of the beds have load casts on their bases. Grooves are rare. The mean basal and upper grain sizes are very fine sand, and very fine sand to silt, respectively (Table 3.5).

Subfacies C2.3A are dominant in amalgamated units of facies C2.3 (Table 3.5). One hundred and forty-one beds of this subfacies consist of 2-5 sets of climbing-ripple lamination with no preservation of stoss side laminae (type A ripple-drift-cross-lamination of Jopling and Walker, 1968). Fifty-five beds have a combination of ripple lamination and convolute lamination while only twenty-three beds exhibit only convolute lamination. Most of these beds lack well developed normal grading (Table 3.5) and have a mean basal grain size of very fine sand.

Table 3.5. Bed characteristics of facies C2.3. Note that most of the beds that occur in amalgamated units belong to subfacies C2.3A. For abbreviations see Table 3.2

	Facies or Subfacies	Total Thk. (m)	% of Thk	# of Beds	% of Beds	Bed Thickness (cm)		Grain Size				Normal Grading
						$\bar{x}$	Min/Max	$\bar{x}$ Base	Min/Max	$\bar{x}$ Top	Min/Max	
	C2.3	61.3	100	386	100	15.9	1.0/78.5	VFS	ST-VFS/VCS	ST-VFS	ST-VFS/CS-VCS	42% UN GR 36% PR GR 22% GR-WGR
	C2.3 Non-Amal.	55.3	90.3	351	90.0	15.8	1.0/77.0	VFS	ST-VFS/VCS	ST-VFS	ST-VFS/CS-VCS	39% UN GR 38% PR GR 23% GR-WGR
	C2.3 Amal	5.9	9.7	35	9.1	17	2.0/78.5	VFS/FS	ST-VFS/VCS	VFS	ST-VFS/CS-VCS	66% UN GR 17% PR GR 17% GR-WGR
Beds not in amalg. units	C2.3A	36.5	59.6	250	64.8	14.6	1.0/59.5	VFS	ST-VFS/VCS	ST-VFS	ST-VFS/FS-MS	47% UN GR 35% PR GR 18% GR-WGR
	C2.3B	4.1	6.7	33	8.5	12.4	3/38	VFS	ST-VFS/CS-VCS	ST-VFS	ST-VFS/FS	24% UN GR 48% PR GR 28% GR-WGR
	C2.3C	14.7	24.1	68	17.6	21.7	4.0/76.7	VFS	ST-VFS/MS	ST-VFS	ST-VFS/CS-VCS	19% UN GR 43% PR GR 38% GR-WGR



Beds of subfacies C2.3B show slightly better developed normal grading (Table 3.5). The upper parallel lamination usually mimics the ripple forms of the underlying division but these parallel laminae become more or less planar in the upper parts of the beds. Beds of subfacies C2.3C have multiple alternating divisions of parallel lamination and ripple lamination, and show better developed normal grading and a greater mean bed thickness than other subfacies (Table 3.5).

#### 3.6.2.6. Interpretation of Facies C2.3

These beds are interpreted as turbidites deposited from low concentration turbidity under lower flow regime conditions (Pickering *et al.*, 1989). The dominance of climbing-ripple lamination similar to type A ripple-drift-cross-lamination of Jopling and Walker (1968) in beds of subfacies C2.3A suggests that traction transport was relatively more important than fallout of sediment from suspension during the deposition of these beds (Jopling and Walker, 1968). Beds that show a combination of ripple/climbing-ripple lamination and convolute lamination were likely deposited rapidly, promoting syn-depositional or post-depositional deformation. The degree of deformation varies between beds, perhaps influenced by the degree of firmness of the underlying mud.

Beds of subfacies C2.3B were probably deposited from waning currents, so that the upper parallel laminated part accumulated during the dying stage of the flow. Beds of subfacies C2.3C that show multiple or alternating parallel and ripple laminated divisions are interpreted to have been deposited from pulsating currents like those that formed

subfacies C2.2C. The greater mean thickness of this subfacies suggests that pulsating conditions are favoured in bigger flows. This subfacies was observed in most of the sections and not restricted to sections SH and PF as with the case for subfacies C2.2C.

#### 3.6.2.7. Lower Parts of Type 1 Megaturbidites (Facies C2.4): Description

Megaturbidites in the thesis area have been studied previously by many workers and several ideas have been suggested for their origin (Skipper and Middleton, 1975; Hiscott and Pickering, 1984; Pickering and Hiscott, 1985; Edwards *et al.*, 1994). These megaturbidites have been used to correlate different parts of the Cloridorme Formation (Hiscott *et al.*, 1986; Pickering *et al.*, 1995).

Type 1 megaturbidites are common and distinctive in the thesis area. The lower coarser parts of these megaturbidites (facies C2.4) form a considerable proportion of the thickness of the sandstone facies in the thesis area (Table 3.2). Facies C2.4 is distinguished from facies C2.5 (the lower coarse parts of type 2 megaturbidites) by a better sorting, better normal grading, a variety of tractional sedimentary structures, and a greater number of structural divisions. Both facies are overlain by thick shale beds (megaturbidite caps). Three hundred and seventy-nine beds of facies C2.4 have been recognised in the thesis area (Plate 9), ranging in thickness from 2.5-151 cm with a mean thickness of 33.5 cm (Table 3.2). Most of these beds are medium to thick (Figure 3.9). Basal grain size of the beds ranges from very coarse sand-granules to very fine sand (mean basal grain size is fine-medium sand). The upper parts of the beds consist of very fine sand



P9.1



P9.2



P9.3



P9.4

Plate 9. Megaturbidites of facies C2.4. P9.1. Megaturbidite 20-FP1 showing a medium lower part and a thick mud cap (arrow shows layer thickness and top direction). P9.2. Megaturbidite 67-PF that is one of the thickest megaturbidites in the thesis area. P9.3. Megaturbidites in section SH (bed 39-SH (arrow)) and bed 41-SH (scale in rectangle). P9.4. Very thick megaturbidite 41-FP2. Jacob Staff scale divisions =10cm. Top is to the left for all

to silt. The mean grain size is medium sand.

It may be surprising to the reader that beds only 2.5 cm thick are assigned to a megaturbidite facies. The full megaturbidite thickness also includes the mud cap, which is commonly 5-10 times thicker (or more) than the sand bed at the base of the layer. The reasons for designating assigning these beds as megaturbidites have been listed earlier (§3.6.2). Pickering and Hiscott (1985,1995) also recognised some “megaturbidites” less than 70 cm thick (coarse base plus mud cap).

In most cases the grading is not gradual but stepwise. The maximum grain size is present in the basal few centimetres or in pockets at the base such as in flutes. In most cases, beds of facies C2.4 consist of several divisions, each having its own characteristic grain size and being separated from the division above by a sharp break in grain size which may be associated with a laminae or very thin bed of mud (parting) that is 0.5 - 2 cm thick. These mud partings are more common in thicker beds of this facies; in some cases, two or three partings are present at different levels within the same bed.

The number of sedimentary structural divisions or the alternations in the type of sedimentary structure range from 1 to 27. The number of divisions is related to the thickness of a beds; thicker beds have more structural divisions. Certain alternations of sedimentary structures occur many times in single beds and for convenience may be considered as a single structural division, analogous to the  $T_d$  turbidite division of Bouma (1962) which consists of an alternation of muddy and silty laminations. Three such divisions were recognised: one consists of several alternations of wavy lamination (usually

composed of siltstone) with muddy lamination, while the others consist of alternations of wavy laminations and/or pseudonodules with muddy laminations. These three different divisions usually occur in the upper parts of beds of facies C2.4. Planar lamination and cross bedding, where present, tend to occur in the lower parts of beds.

The lower bedding planes vary from irregular (60 % of beds) to flat (32.5%) to wavy (8%). Sole marks include flutes (52% of beds), loads (6% of beds) and grooves (1.5 % of beds).

In order to simplify the description of this facies, beds of facies C2.4 are divided into three groups based on bed thickness and the number of sedimentary structure alternations. Group A, 112 beds, are beds that are thinner than 18 cm. The average basal grain size is fine sand. The average number of structural divisions in this group is 3. Many of the beds of group A are restricted to the eastern part of the thesis area (detailed area A). Sole marks and structural divisions of most of these beds show one palaeocurrent trend. Group B, 204 beds (the most common), comprises beds 18-50 cm thick. The average basal grain size is medium sand. The average number of divisions is 5. Group C, 63 beds (the least common), consists of beds that are thicker than 50 cm. The average basal grain size is coarse sand. The average number of divisions or alternations is 8.

In order to investigate if the structural divisions follow a predictable sequence similar to the Bouma (1962) sequence, a Markov chain analysis was performed for each of the three groups of beds. A Markov property is recognised if the probability of occurrence of a particular state (sedimentary structure division in this case) depends on the identity of

the preceding state or states (division(s); Krumbein and Dacey, 1969).

The procedure for Markov chain analysis and how the different matrices are constructed is explained in detail in many references (Miall, 1973, 1982; Hiscott, 1981, 1982; Powers and Easterling, 1982; Davis, 1986) and will not be repeated here. An embedded Markov chain model is used, so that there are no transitions between a state (division) and itself (Krumbein and Dacey, 1969). A transition matrix (F), transition probability matrix (P) and difference matrix (D) were first constructed using the procedures in the references listed above. The independent trails matrix (R) and the normalised difference matrix (Z) were constructed using the procedures suggested by Powers and Easterling (1982). A FORTRAN program written by R.N. Hiscott (MARKOV.FOR) was used to compute the matrices (Appendix A5-2.1).

The size of the transition matrix (raw data) was 9x9 for group A beds and 10x10 for group B and C beds because no beds in group A have a cross bedded division (Appendix A5-2.2). The following states were recognised:

- Erosional base (state 0)
- Structureless division (1)
- Planar lamination (2)
- Ripple lamination (3)
- Climbing-ripple lamination (4)
- Convolute lamination and/or pseudonodules (5)
- Wavy lamination (6)

-Muddy lamination (7)

-Cross bedding (8)

-Mud cap (9)

The entries in the normalised difference matrix (Z) with absolute value > 2.0 are considered to indicate the presence of a Markov property (dependence on the previous state) because 95% of the standard normal distribution is enclosed between  $\pm 2$  and 99.7% between  $\pm 3$  standard deviations (Powers and Easterling, 1982).

The observed transition count matrix can be tested for the presence of first order Markov memory using a Chi squared ( $\chi^2$ ) test with  $(m-1)^2 - m$  degrees of freedom (Hiscott, 1981; Powers and Easterling, 1982). The presence or absence of Markov memory depends on whether the calculated value of  $\chi^2$  is more or less than the value from tables for the 5% significance level of a standard  $\chi^2$  distribution with the correct degrees of freedom. Chi squared ( $\chi^2$ ) was calculated as described by Powers and Easterling (1982), using the MARKOV.FOR program.

#### 3.6.2.8. Interpretation of Facies C2.4

The interpretation that follows considers only the features of facies C2.4 observed in individual sections. Skipper (1971), Skipper and Middleton (1975) and Skipper and Bhattacharjee (1978) interpreted some of the structures at the base of some megaturbidites beds (e.g., BT- 24 in the SH and RE sections) as antidunes deposited from turbidity currents. Pickering and Hiscott (1985) provided compelling evidence that these

structures are not antidunes but rather dunes that formed following the reflection of turbidity currents from barriers and basement highs. Many megaturbidites have been described in the literature from many parts of the world in both modern settings and ancient turbidite sequences (Ricci Lucchi and Valmori, 1980; Pilkey, 1988; Rothwell *et al.*, 1992). Reflected turbidity currents have been also studied experimentally and theoretically (Pantin and Leeder, 1978; Kneller, 1995; Edwards *et al.*, 1994).

Type 1 megaturbidites observed in this study are interpreted to have been deposited from large turbidity currents that travelled across the basin and may have been reflected several times during flow. These thick megaturbidites must have originated from large slope failures. Major slumps probably evolved into large scale turbidity currents that travelled across the basin, eroding into underlying beds as indicated by the presence of flute casts on the soles of beds of facies C2.4. Some of these flows may have not deposited any sediments during their initial pass across the basin floor (Pickering and Hiscott, 1985), but as the current slowed down different types of sedimentary structures formed as a result of the deceleration of the current. If reflections occurred, the reverse flow was slower and thus less competent than the flow that deposited the basal sand. The sediment grain size in the basal one or two divisions is much coarser than the overlying divisions; which show an opposite palaeocurrent trend.

Sharp grain size breaks and partings might suggest these are amalgamated units. Pickering and Hiscott (1985) provide compelling arguments, however, that these beds formed during a single depositional event: divisions always decline in grain size through a



single bed, and only this facies (and facies C2.5) are overlain by homogeneous mud caps commonly metres thick that indicate deposition from an exceptionally large-volume flow.

The predicted sequence of sedimentary structures based on Markov chain analyses is similar to the Bouma (1962) sequence. Group A beds show two main predicted sequences (Figure 3.10). Sequence 1 (~ 25% of the total) has a structureless basal division ( $T_a$ ), followed by a division of planar lamination ( $T_b$ ), followed by climbing-ripple lamination ( $T_{cc}$ ) and a mud cap. Note that  $T_{cc}$  refers to a  $T_c$  division consisting of climbing-ripple lamination while  $T_{cr}$  refers to a  $T_c$  division consisting of ripple lamination. A variation of this sequence is beds that only have a  $T_{cc}$  division followed by a mud cap, essentially a base-absent sequence (Pickering *et al.*, 1989). Sequence 2 (~30% of the total) starts with a ripple laminated division ( $T_{cr}$ ) above an erosional surface, followed by wavy lamination which is overlain by convolute lamination/pseudonodules or muddy lamination and then a mud cap. The main difference between these types of beds is the lack of wavy lamination, muddy lamination or convolute lamination/pseudonodules above the climbing-ripple lamination in sequence 1, and the lack of  $T_a$  and  $T_b$  divisions in sequence 2. The first sequence is interpreted to have been deposited from a relatively faster moving current that carried a large sediment load. Rapid deposition from suspension and traction transport controlled the deposition of these beds. The lower structureless division was probably deposited rapidly followed by upper flow regime plane bed conditions that formed the planar laminated division. A combination of traction and deposition from suspension took place during the deposition of the climbing-ripple lamination followed by deposition of

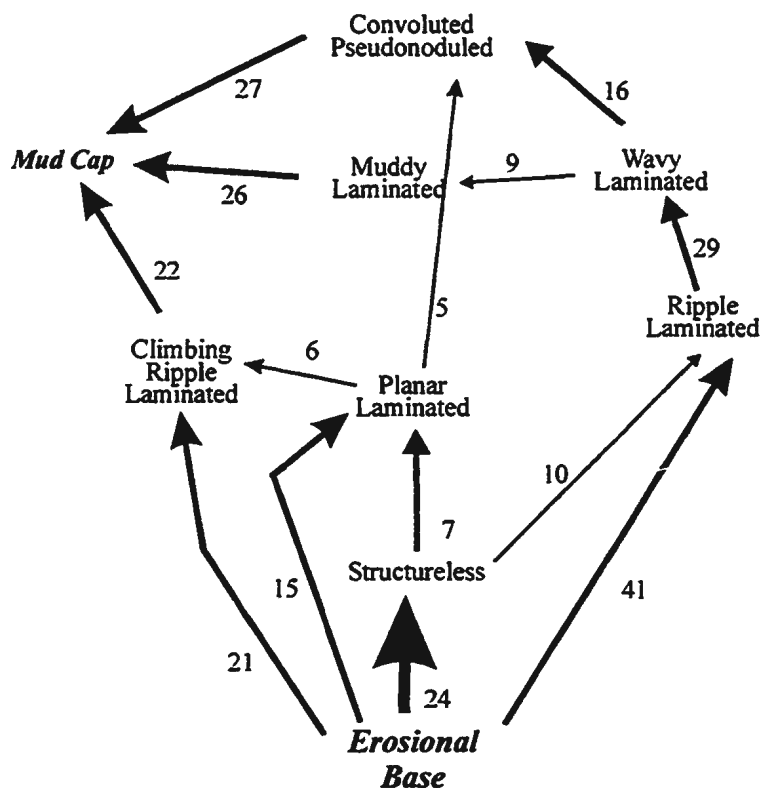


Figure 3.10. Transition diagram for group A beds of facies C2.4. Arrow weights are based on the values assigned to the transition in the normalised difference matrix. Three arrow weights are present: thick for values  $>6$  (e.g., Erosional base to structureless), medium for values 3-6 (e.g., erosional base to ripple lamination), thin for values  $<3$  but  $>2$ . The actual number of transitions is indicated. Only those transitions with significance at  $\geq 95\%$  are shown with an arrow.

mud from suspension. The rapid deposition of the mud prevented the segregation of very fine grains to form muddy laminae and silty laminae above the division of climbing-ripple lamination. These flows probably carried a large proportion of mud.

Sequence 2 beds suggest deposition from slower moving currents that perhaps carried smaller loads or a smaller proportion of mud than the flows that deposited sequence 1 beds. During deposition, traction may have been more dominant. Slow current speed is suggested by the lack of  $T_a$  and  $T_b$  divisions and slow deposition is suggested by alternating laminae of mud and very fine sand-silt. The segregation of the very fine sand-silt from finer grains may have occurred by any of a number of processes (Hesse and Chough, 1980; Stow and Bowen, 1980). The pseudonodule division present in the upper part of these beds was formed as a result of soft sediment deformation of some of the silt bands of the muddy lamination. Pickering and Hiscott (1985) suggested that the muddy and silty planar to wavy lamination may have formed when the silt-mud suspension was moving slowly back and forth after it became ponded on the basin floor.

Beds that show different base-cut-out sequences suggest differences in the current speeds of different flows. The occurrence of many beds of facies C2.4 belonging to group A in the eastern part of the thesis area suggests that most of these beds were deposited by one pass of a current moving from east to west. Megaturbidites that show bipolar palaeoflow directions suggest the return of the flow after being reflected or deflected against basin highs or margins (Pickering and Hiscott, 1985).

Group B beds of facies C2.4 also have three predicted sequences (Figure 3.11).

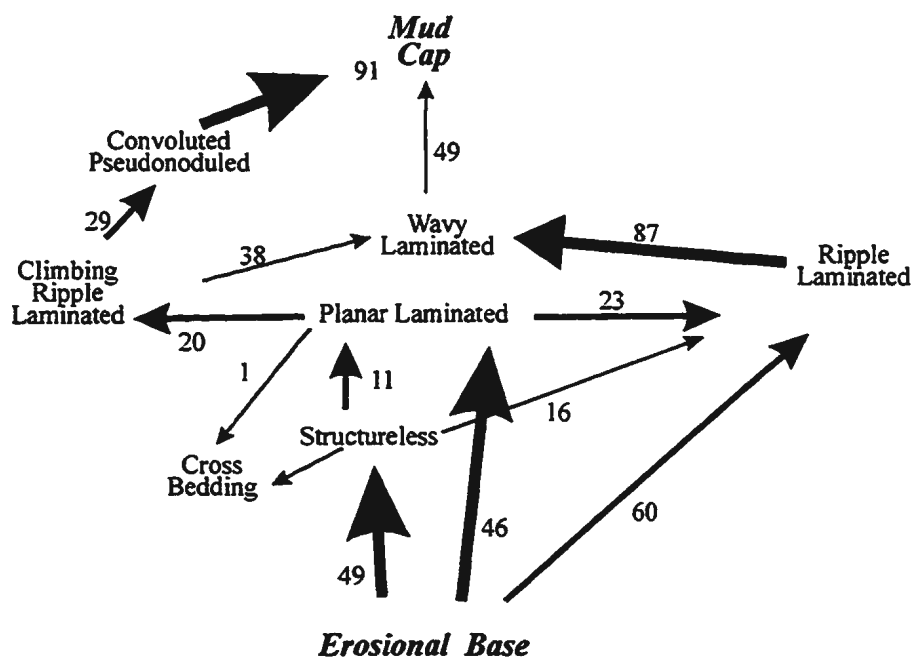


Figure 3.11. Transition diagram for group B beds of facies C2.4. Arrow weights are based on the values assigned to the transition in the normalised difference matrix. Three arrow weights are present: thick for values >6, medium for values 3-6, thin for values < 3 but >2. The actual number of transitions is indicated. Only those transitions with significance at  $\geq 95\%$  are shown with an arrow.

The main variation in the three sequences is whether the predicted sequence has climbing-ripple lamination or ripple lamination. About 25% of the beds start with ripple lamination overlying an erosional base (sequence 1). Sequences 2 and 3 have similar predicted lower divisions and the variation in these two predicted sequences is in what sequence of sedimentary structures overlies the planar laminated division. Sequence 2 (~15% total) has a structureless basal division ( $T_b$ ), followed by a division of planar lamination ( $T_p$ ), followed by climbing-ripple lamination ( $T_{cr}$ ), followed by convolute lamination and pseudonodules and a mud cap. Variation in this predicted sequence are base-absent sequence (Pickering *et al.*, 1989). Sequence 3 (~25% of total) differs from sequence 2 in that there is a ripple lamination ( $T_r$ ) instead of a climbing-ripple lamination ( $T_{cr}$ ) overlain by wavy lamination instead of convolute lamination and pseudonodules. Base-absent sequences are also present. The predicted sequences for group B beds are interpreted to have been deposited from decelerating currents. Differences nature of the sediment load in the flow and in the ratio of suspended load to bed load at the time of deposition are believed to account for these three sequences. Sequence 1 suggests deposition from decelerating currents that may have lacked coarser sediment to form a lower division of planar lamination. These coarser sediments may have been deposited elsewhere in the basin. The presence of ripple lamination instead of climbing-ripple lamination suggests a low ratio of suspended-load to bed-load transport. Sequence 2 with climbing-ripple laminations suggests high ratios of suspended load to bed load. The overlying convolute lamination and pseudonodules resulted from the soft-sediment

deformation and loading of these rapidly deposited sediments. Sequence 3, characterised by ripple lamination and wavy lamination, suggests longer duration bed-load transport and reworking to form ripples and wavy laminae. The presence of a basal structureless division or a division of planar lamination at the base of many of the beds of group B suggests currents with high velocities and perhaps high sediment concentration. At the onset of deposition, the lower structureless division was probably deposited rapidly from suspension followed by traction under upper flow regime plane bed conditions that formed the parallel laminated division. The mud drapes or partings that are present between some of the sedimentary structural divisions are interpreted to have been deposited from the tail of the flow that deposited the underlying sandy part. The presence of several of these mud partings in a single bed suggests successive passes of the current following reflections/deflections from basin-margin highs (Pickering and Hiscott, 1985; Edwards *et al.*, 1994).

Group C beds of facies C2.4 display sedimentary structures similar to the Bouma sequence (Figure 3.12). These sequences are interpreted to represent deposition from waning flows. A slight modification to the procedure used for beds of groups A and B was applied because many of these beds have intervals that consist of several alternations of wavy lamination, convolute lamination and pseudonodules. These repeating intervals have been grouped into a single division. Nine group C beds have cross bedding in the form of small dunes or megaripples in their lower parts. These structures were initially interpreted by Skipper and co-workers as antidune deposits but were later reinterpreted as

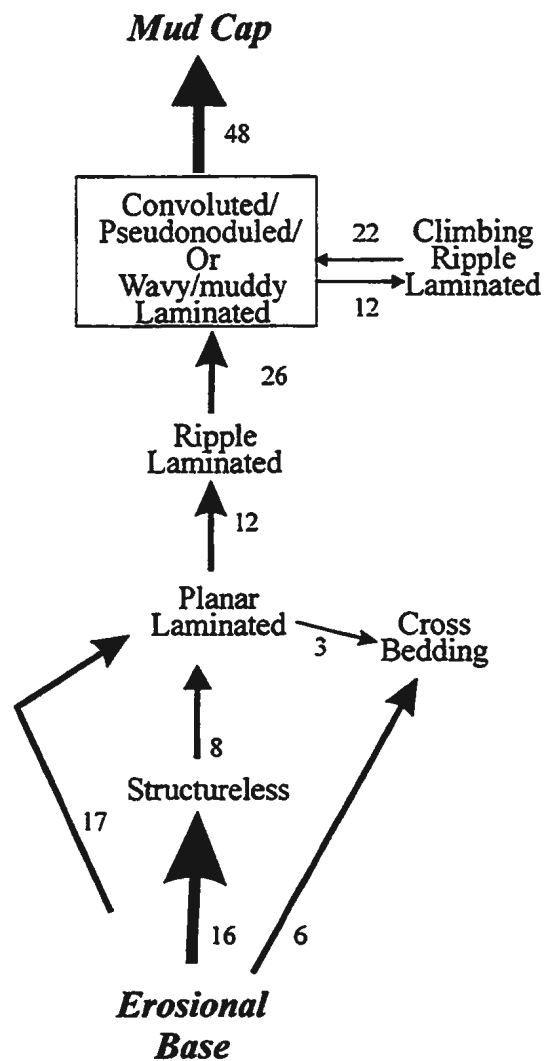


Figure 3.12. Transition diagram for group C beds of facies C2.4. Arrow weights are based on the values assigned to the transition in the normalised difference matrix. Three arrow weights are present: thick for values >6, medium for values 3-6, thin for values < 3 but >2. The actual number of transitions is indicated. Note that the wavy, muddy, convoluted and pseudonoduled divisions are combined for these beds (see text for details). Only those transitions with significance at  $\geq 95\%$  are shown with an arrow.

reflected flow deposits by Pickering and Hiscott (1985). Pickering and Hiscott (1985) suggested that these bedforms developed when bed-load transport (reworking) was dominant. They ascribed the rounding of the dune crests to erosion beneath reverse flows.

#### 3.6.2.9. Lower Parts of Type 2 Megaturbidites (Facies C2.5): Description

This facies is considerably less common than facies C2.4. Only eighteen beds have been recognised in the thesis area. Some of these beds are thick (e.g., beds BT-3 in FP1, RE, SH and PF sections), very distinctive, and serve as good marker beds for correlation (Chapter 4).

Thick beds of facies C2.5 may be divided into two parts: a lower, usually thin (1-10 cm-thick) part that is better sorted than the remainder, and an upper part that is characterised by pseudonodules of variable sizes. The upper part ranges in thickness from several centimetres to almost three metres. Lower bedding planes are flat to wavy, although flutes were observed on the soles of facies C2.5 beds in other parts of the Cloridorme Formation (Skipper and Middleton, 1975). These beds usually have thick mud caps (up to 5 m thick).

The lower part of the bed is either structureless or may show faint parallel lamination with individual lamina 0.2-0.5 cm thick. Poorly developed ripple lamination was observed in only one bed. This lower part has the coarsest grain size; in some beds, granules were observed at the base. The mean grain size in this basal part is usually coarse to medium sand. Normal grading or no grading characterises these basal parts. Thin beds



of facies C2.5 rarely have this lower part and if present in may be very thin (1-2 cm).

The upper boundary of the lower part is marked in some cases by a distinct break (depression) in the weathering profile. This depression is 1-2 cm thick and has a higher proportion of muddy material.

The upper division consists of very poorly sorted muddy sandstone or muddy siltstone that is characterised by the presences of pseudonodules of variable size and shape. Some of these pseudonodules have a slightly lighter colour than the muddy sandstone and siltstone in which they lie. These pseudonodules have been described in detail by Skipper and Middleton (1975). Slivitzky *et al.* (1991) incorrectly described this structure as conglomerate. Grading is poorly developed in this part, although the proportion of muddy material tends to increase upward.

#### 3.6.2.10. Interpretation of Facies C2.5

The characteristics of the beds of this facies suggest that different mechanisms deposited the lower and upper parts. The lower part shows better sorting and tractional structures while the upper part consists of pseudonodules that formed as a result of wet-sediment deformation. The marked break in grain size at the top of the lower part may have a similar origin to the parting in type 1 megaturbidites although no evidence of flow reflection was observed in beds of facies C2.5.

The flows that deposited these beds were probably turbulent at least in their frontal part as suggested by the presence of flutes at the base of equivalent beds in other parts of

the Cloridorme Formation (Skipper and Middleton, 1975). These flows probably carried a low proportion of medium to coarse sand and a high proportion of fine sand, silt and mud. As the flow moved across the basin, the coarse fraction accumulated rapidly to form a graded structureless part, or the coarse sediments was moved along the bed by traction to form parallel lamination and ripple lamination. Skipper and Middleton (1975) suggested that the segregation of the coarse sediment to the base of the flow may have produced a two-layer sediment gravity flow, with the lower part perhaps similar to what has been termed an inertia layer by Postma *et al.* (1988).

The mud parting that overlies the lower part of the bed in thick examples of facies C2.5 is interpreted to have been deposited from suspension after the first passage of the main flow across the basin (Pickering and Hiscott, 1985), implying that it later returned after reflection to deposit the remainder of the bed.

The upper part of the bed is interpreted to have formed as a result of deformation of rapidly deposited sediment (Skipper and Middleton, 1975). This sediment may have been deposited from reflected flows. The flows that deposited these pseudonoduled divisions probably consisted mostly of fine sand and mud initially carried in suspension and then dropped rapidly when the suspension became ponded on the basin floor (Pickering and Hiscott, 1985). This rapid deposition resulted in loading, deformation, and pseudonodules. The mud cap (facies Class E) that overlies the upper part was probably deposited from the ponded suspension. The large thickness of these mud caps suggests a large proportion of suspended mud (Pickering and Hiscott, 1985).

Thin beds of facies C2.5 that consist mostly of the pseudonoduled part were probably deposited from smaller but otherwise similar flows. These may have been distal or downcurrent fringes of larger flows that deposited their coarse load elsewhere in the basin (up-flow or up-current “proximal areas”).

Beds of facies C2.5 and C2.4 have similar characteristics such as the thick mud cap and great lateral continuity. These features may suggest a genetic relationship between the two facies (see Chapter 5).

### **3.7. FACIES CLASS B (SANDS)**

Two facies groups are recognised: disorganised and organised. Disorganised sandstone beds (facies group B1) are extremely rare. Organised sandstone beds (group B2) are more common but only form a small percentage of the total number of beds and total thickness of the measured sections (Table 3.2).

#### **3.7.1. Disorganised Sandstone Beds of Class B (Group B1)**

##### **3.7.1.1. Sandstones with fluid escape structures (Facies B1.1): Description**

One facies is recognised in this group. It is extremely rare (only six beds), representing < 0.02% all the beds in the thesis area. These beds occur associated with other sandstone beds in packets. The beds have sharp upper and lower contacts. Lower bedding planes may have grooves; otherwise, they lack any sole marks. The six beds of this group range in thickness from ~10 - 85 cm. The common feature of this facies is the

presence of fluid-escape structures that usually occur in the upper parts of beds. Two types of structures are recognised: pipes that range in length from a few centimetres to less than 20 cm, and are 1-3 cm wide; and small wispy structures that have a different colour or grain size than the beds in which they occur. Some of these pipes may be filled by coarse sand. Grain size of the beds varies from coarse sand to very fine sand. Four of the beds show poorly developed normal grading while the remaining two beds are ungraded. Shale clasts, up to 5 cm x 5 cm, are present in the upper part of some of these beds.

#### 3.7.1.2. Interpretation of Facies B1.1

These beds are interpreted to have been deposited rapidly based on the presence of the fluid escape pipes and wispy structures and the lack of tractional structures. The fluid escape pipes and wispy structures resemble type B pillars and type D stress pillars of Lowe (1975), respectively. These structures are related to liquefaction and fluidisation and pore-fluid escape due to rapid deposition. The sand may have been extensively fluidised and remobilised during rapid deposition (Stow and Johansson, 2000). The presence of shale clasts suggests erosion of more or less firm underlying mud.

The origin of such deposits that do not show well developed normal grading or tractional sedimentary structures have been debated recently. These debates centre on whether such rocks were deposited by high density turbidity currents (Pickering *et al.*, 1989; Mutti, 1992; Hiscott *et al.*, 1998, Lowe, 1997) or sandy debris flows (Shanmugam,

*et al.*, 1997; Shanmugam, 2000). The poorly developed normal grading tends to support deposition from turbidity currents while other properties such as the presence of mud clasts and poor lateral continuity have been used as evidence of a debris flow origin (*cf.* Shanmugam, 2000). The presence of shale clasts does not preclude deposition from turbidity currents because many deposits of turbidity currents showing well defined tractional sedimentary structures and normal grading also contain large and abundant shale clasts (Walker, 1992; Postma *et al.*, 1988). Lateral continuity will be discussed in Chapter 5.

### **3.7.2. Organised Sandstone Beds of Class B (Group B2)**

The facies in this group form more than 85% of Class B (Table 3.2). Two facies are recognised in this group: sandstone beds with near-horizontal stratification (facies B2.1); and sandstone beds consisting of two parts, called bipartite beds in this thesis (facies B2.2). Some beds of the bipartite facies have poorly developed grading or no grading so might be considered as disorganised facies, but other beds have lamination suggesting they are organised. Colour of the beds ranges from dark grey when fresh, to greyish green when weathered.

Sandstone beds of this group commonly occur in amalgamated units of two or more beds. About 66% of the sandstone beds that show near-horizontal stratification occur in amalgamated units, whereas about 5% of the bipartite beds occur in amalgamated units.

### 3.7.2.1. Sandstone Beds with Near-horizontal Stratification (Facies B2.1): Description

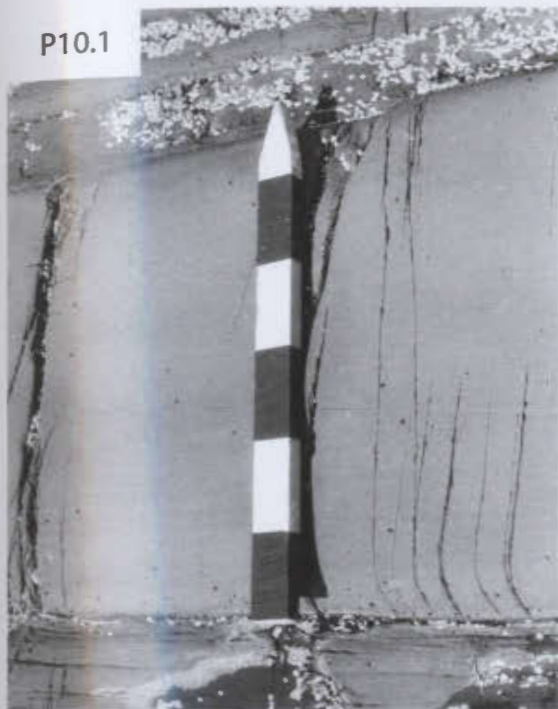
This facies is more common than the disorganised sandstone facies but only 56 beds belonging to this facies were recognised in all the sections of the thesis area. Beds of facies B2.1 that do not occur in amalgamated units range in thickness from 8-138 cm. Thinner and thicker beds of this facies are present but these are present in amalgamated units (Table 3.2). The mean bed thickness is ~ 38 cm. At outcrop scale, the beds are continuous. The basal grain size is quite variable, ranging from very fine sand to very coarse sand. Most of the beds are normally graded. Upper and lower contacts are sharp. Beds of this facies were not recognised as a separate facies or lithologic type by Enos (1965) and Slivitzky *et al.* (1991). They were included in type 1 or type 2 greywacke (Enos, 1965; Slivitzky *et al.*, 1991).

Most beds of this facies consist of three parts (Plate 10), listed here from base to the top:

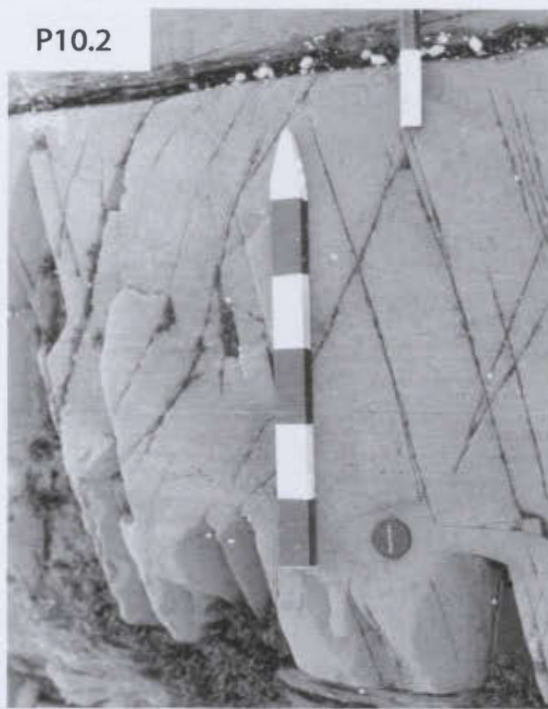
- A lower structureless division that ranges in thickness from a few centimetres to less than 20 cm. The basal few centimetres may show inverse grading followed by normal grading for the remainder. This lower division consists mainly of poorly sorted sediments and tends to be better developed in thicker beds. Some beds may show sole marks such as flutes or grooves.

- A middle division that ranges in thickness from a few centimetres to less than 30 cm. This division consists of 2-10 stratification bands. Each band ranges in thickness from a few millimetres to less than 3 cm and lies on a near-horizontal surface. Inverse

P10.1



P10.2



P10.3

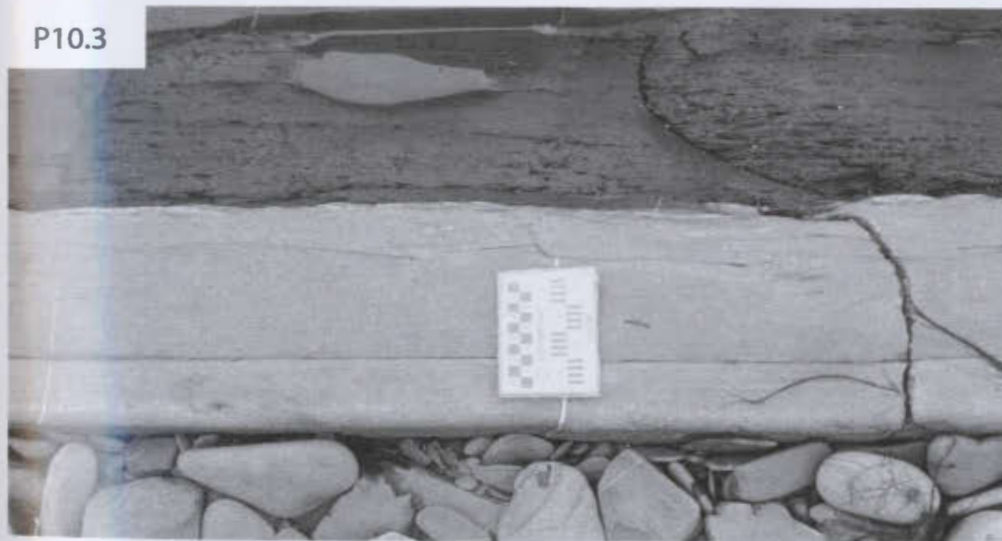


Plate 10. Facies B2.1 and B2.2. P10-1. Facies B2.1 with a poorly developed lower structureless division (lower ~10 cm) overlain by a division of near-horizontal stratification (10-20 cm thick) and a structureless top division (the rest of the bed). P10-2. Facies B2.1 showing a better developed lower structureless division (below the top of the camera lens cap) and a thicker middle division of near-horizontal stratification. P10-3. Facies B2.2 showing planar upper and lower contacts and a bedding joint in the lower third of the bed, Shale clasts are more common in the upper part of the bed than in the lower part.

grading is well developed in these thin bands and ranges from very fine sand at the base to coarse sand at the top of the band. Thicker bands have inverse grading only in their lowermost part; this is followed by poorly developed normal grading for the remainder of the band. In some beds, the thicknesses of the bands decreases from the base to the top of the interval.

-The top division of the bed is usually structureless, but the normal grading that starts at the base of the bed continues through this division. Shale clasts, some up to 10-20 cm in length, are common in some of the beds. Fluid escape structures, mostly type D stress pillars (Lowe, 1975), are locally present in this division.

#### 3.7.2.2. Interpretation of Facies B2.1

These beds are interpreted as deposits from high concentration turbidity currents (Hiscott and Middleton, 1979; Lowe, 1982; Pickering *et al.*, 1989; Kneller and Branney, 1995). The overall normal grading suggests deposition from a decelerating flow. The lower structureless division of the bed that shows normal grading suggests rapid deposition from suspension. The presence of inverse grading at the base of some beds suggests that dispersive pressure due to grain interaction may have been important during the onset of deposition (Middleton and Hampton, 1976). The lack of structures such as parallel lamination or cross stratification that Lowe (1982) recognised for the lower parts of the deposits of high density turbidity currents ( $S_1$  division of Lowe, 1982) suggests perhaps that deposition from suspension was so rapid that tractional structures did not



form (Arnott and Hand, 1989; Allen, 1991; Kneller and Branney, 1995). Hiscott (1994) also noted that near-horizontal stratification (his “spaced stratification”) is overlain and underlain by structureless sand.

The second division that consists of the near-horizontal stratification was designated as division  $S_2$  by Lowe (1982). Lowe (1982) suggested that individual inversely graded bands are formed as a result of the development of a moving layer at the base of the flow that is maintained by dispersive pressure and fed by the rain of grains from above. The separation of these layers takes place during periods of flow unsteadiness causing an increase in the concentration of sediments towards the base of the flow. The presence of several of these inversely graded bands is due to the continued fallout of sediments from the overlying current. After a moving layer collapses and “freezes”, a new layer (called carpet) is formed and a succession of layers form (Hiscott and Middleton, 1979; Lowe, 1982). Hiscott (1994) suggested that dispersive pressure cannot form inversely graded beds that are 5-10 cm thick as suggested by Hiscott and Middleton (1979) and Lowe (1982), and that it is only responsible for the inverse grading in the lowermost part (~1 cm) of each stratification band.

Hiscott (1994) instead suggested that the near-horizontal stratification may have formed as a result of deposition from a highly pulsating current where periods of erosion alternate with periods of suspension sedimentation. Hiscott (1994) termed this a sweep-fallout model. In the first phase, the downward sweep of a large eddy produces an erosional surface and inverse grading in the lowermost part of the band. This is followed

by a period of deposition from suspension that forms the remaining part of the band. The gradual upward decrease within the division in the thickness of individual bands is due to the gradual decrease in fallout rate as deposition progresses. Kneller and Branney (1995) suggested another, somewhat similar, mechanism for the deposition of these beds. They attributed the lower and upper parts of the beds to rapid deposition from suspension while the middle part showing near-horizontal stratification might form during periods of decreased fallout of sediments from suspension when dispersive pressure becomes a more dominant process allowing the formation of inversely graded bands. Kneller and Branney (1995) suggested that the alternation of periods of high and low sediment fallout from suspension is due to the unsteady nature of the flow created by bottom slope irregularities or heterogeneity in the grain concentration or grain-size distribution of the depositing current. Beds that have near-horizontal stratification at the base without the underlying structureless division resulted whenever the initial phase of rapid deposition from suspension did not take place.

The upper division of the bed that overlies the division of near-horizontal stratification and that is characterised by normal grading and fluid-escape features suggests renewed rapid deposition from a turbulent suspension, or perhaps a decline in eddy and vigour (in the case of the sweep-fallout model). The mud clasts that are present in this part were presumably eroded from underlying semi-consolidated mud deposits along the flow path.

### 3.7.2.3. Bipartite Sandstone Beds (Facies B2.2): Description

Beds of this facies are the most common in Class B. More than 200 beds have been recognised but they represent a small proportion of the total number of beds measured in the thesis area (Table 3.2). About 95% of these beds are overlain and underlain by shale while the remaining 5% occur in amalgamated units. Beds range in thickness from less than 4 cm to more than 40 cm, but most are medium beds (Table 3.6). The distinctive feature of these beds is the presence of a planar, flat joint that splits individual beds into two parts, or in rare cases three parts. This joint is called a bedding joint (Parkash, 1969). At outcrop scale, these beds are highly regular in thickness with sharp upper and lower contacts (Plate 10.3). As with other facies of this class, these bipartite sandstone beds tend to occur with sandstone packets. The two parts of these beds are hereafter referred to as the lower part and the upper part.

The lower part is usually coarser and better sorted than the upper part. Lower parts range in thickness from less than 1 cm to 23 cm (Table 3.6). Grain size at the base is mostly fine to very fine sand. Lower parts show poor to moderate normal grading. The variation in grain size from the base to the top of the part is usually less than 1 phi unit. More than 70% of these lower parts are structureless. Of the remaining 30%, about half have shale clasts while the other half show faint parallel lamination or near-horizontal stratification. The occurrence of shale clasts and parallel lamination or near-horizontal stratification together was not observed. The shale clasts vary in size, but are usually 1-10 cm x 1-2 cm. Clasts vary in shape from subangular to subrounded. They tend to occur

Table 3.6. Comparison of the thickness and grain size characteristics between the upper and lower parts of bipartite beds (Facies B2.2). Thickness is in centimetres. Grain size abbreviations are: VCS=very coarse sand; CS=coarse sand; MS=medium sand; FS=fine sand; VFS=very fine sand; and, SLT=silt. Almost half of the lower parts of beds have near-horizontal stratification while the other half have mud clasts. Fluid-escape structures and clasts were observed in one case. More than half of the upper parts of beds contain mud clasts. Siltstone clasts and mixtures of siltstone and mud clasts are rare. Six cases show a single set of ripple lamination while another seven cases have fluid-escape structures.

	Structureless lower part	Lower part with structures or clasts	Total lower parts	Structureless upper part	Upper part with structures or clasts	Total upper parts
Number	161	46	207	87	120	207
Thickness $\bar{x}$ (cm)	6.3	8.8	6.9	8.1	9.8	9.1
Thickness $\sigma$ (cm)	4	5	4	5	6	6
Min. thk. (cm)	0.8	2.2	0.8	1.1	2.2	1.1
Max. thk. (Cm)	23	23	23.5	36.3	30	36.3
Basal grain size, $\bar{x}$	VFS-FS	VFS-FS	VFS-FS	SLT-VFS	SLT-VFS	SLT-VFS
Basal grain size min.	SLT-VFS	SLT-VFS	SLT-VFS	SLT	SLT	SLT
Basal grain size max.	CS-VCS	MS-CS	CS-VCS	MS	MS	MS
Upper grain size, $\bar{x}$	VFS-FS	VFS-FS	VFS-FS	SLT-VFS	SLT-VFS	SLT-VFS
Upper grain size min.	SLT-VFS	SLT	SLT	SLT	SLT	SLT
Upper grain size max.	CS	FS-MS	SLT	FS-MS	MS	MS

close to the top of the part just below the bedding joint. Many of these clasts have their long axis parallel or sub parallel to the bedding joint. Shale clasts may also occur near the base or the middle of the lower part, but these are less common and smaller in size.

Siltstone clasts are extremely rare but, where present, they are smaller than the shale clasts and contain irregular laminae.

Parallel lamination or faint near-horizontal stratification are very poorly developed but occur as 2-5 laminae or bands anywhere in the lower part. Each band is a few millimetres thick. These structures are more common where the sediments are coarser and better sorted. Fluid-escape structures, similar to type D stress pillars of Lowe (1975), were observed in one case.

The bases of many of these beds are planar or flat although wavy and irregular bases with flutes, grooves and load casts were rarely observed. These sole marks, where present, preferentially occur in certain sections and stratigraphic levels or associated with lower bed parts characterised by relatively coarse grain size.

At the bedding joint there is a sharp grain-size break. The upper part is finer in grain size and contains more muddy material. The decline in grain size of the particles across this joint is about 1 phi unit.

The upper parts of these beds are usually thicker than the lower parts. Grain size in the base of the upper part is mostly silt to very fine sand (Table 3.6). Grading is more-or-less absent. The higher proportion of mud in the upper part compared to the lower part makes it darker (Plate 10.3). More than 50% of these upper parts contain shale clasts.

Fluid-escape structures similar to type D stress pillars of Lowe (1975) are present in about 10% of the occurrences.

Shale clasts in the upper part tend to occur either at or just above the bedding joint or concentrated near the top of the bed. Shale clasts that occur at or above the bedding joint are up to 20 x 5 cm in size and have their long dimension more-or-less parallel to the bedding joint. Clasts near the top of the upper part are usually smaller and have no apparent preferred orientation.

Parkash (1969) and Parkash and Middleton (1970) studied the texture and sedimentary structures of eight beds similar to the bipartite beds in the  $\beta 7$  member of the Cloridorme Formation in the area between Grande-Vallée and Petite-Vallée over a distance of about 3km. Some of the observations of these studies are listed below.

- Thin beds are laminated in upcurrent areas (near Petite-Vallée) but are massive in the downcurrent areas (near Grande-Vallée).

- Thick beds are structureless in both upcurrent and downcurrent areas.

- Shale and siltstone clasts are mostly less than 15 cm. These clasts may be present at the top of the bed or just above the bedding joint. Fragments are absent in thinner beds and beds that show laminations.

- Grains are typically aligned parallel to the current direction and are better aligned in the lower parts of the beds in the upcurrent areas, but the upper parts of beds show poor or no consistent grain orientation in the upcurrent areas. The best developed grain orientation was observed close to the bottom of the bed; the fabric becomes more

scattered upward in the bed.

- Grading is better developed in these beds in upcurrent areas. The lower parts of beds are coarse and have better developed grading. There is a sharp break in grain size at the bedding joint. There is little or no change in the mean grain size of the basal parts of beds in the upcurrent or downcurrent directions.

#### 3.7.2.4. Interpretation of Facies B2.2

Each bipartite bed is interpreted to have been deposited from a single turbidity current. It is believed that this current was carrying a high proportion of muddy material that affected its behaviour. In more than 200 examples observed, the bedding joint is planar. This is unlike amalgamated beds (2 events) which tend to have irregular scoured contacts. It is interpreted that bipartite beds were deposited by a turbidity current that evolved or split into two parts, probably during a late stage of flow just before deposition. The lower part may have had a high sediment concentration and the upper part a lower concentration. This situation is not unique and has been suggested for many turbidite deposits and has been observed in experiments (Middleton, 1967; Carter, 1975; Middleton and Hampton, 1976; Postma *et al.*, 1988; Kneller and Branney, 1995; Mutti *et al.*, 1999; Lowe and Guy, 2000).

The turbidity currents eroded and scoured part of the underlying seabed as suggested by the presence of flutes at the base of some of the beds. Some shale clasts eroded from underlying, somewhat firm mud may account for the mud clasts in the

bipartite beds. At some stage, a basal layer possessing a high sediment concentration developed probably due to a high rate of sediment fallout. The high concentration may have caused the apparent viscosity in the lower part of the flow to increase causing the flow to separate into two parts (Postma *et al.*, 1988; Mutti, *et al.*, 1999). This high concentration in the lower part probably developed when turbulence in the current was unable to maintain all the sediment that was rapidly settling out of suspension (Middleton, 1967; Postma *et al.*, 1988). The suppression of turbulence in the lower layer caused this part of the flow to become more-or-less laminar (Postma *et al.*, 1988). This layer has been termed an inertia flow layer in which the grains are supported by a combination of dispersive pressure, hindered settling and cohesion (Postma *et al.*, 1988; Kneller and Branney, 1995). The poorly developed grading observed in the lower part suggests little or no segregation of grains, perhaps due to the high sediment concentration.

Parallel laminations observed in some of the lower parts may have been formed by traction transport (Parkash 1969; Lowe and Guy, 2000). Alternatively, they may have formed in a way similar to near-horizontal stratification during periods of fluctuations in the rate of sediment fallout from suspension due to flow unsteadiness (Kneller and Branney, 1995). The tendency of many shale clasts to occur close to or above the bedding joint may suggest that some of these clasts actually moved along the interface between a lower inertia bed and an overlying more turbulent suspension. Postma *et al.* (1988) observed in their experiments that clasts travelled along the interface after being initially suspended in the head region of the flow, but subsequently were thrown into the wake of



the flow where they settled to the interface of the partially developed inertia-flow layer.

The upper part of the bed is believed to have been deposited from suspension as the current slowed down after the deposition of the lower inertia layer. The poor development of normal grading and the fluid-escape structures may suggest rapid deposition from suspension of sediments consisting of a high percentage of muddy material.

An alternative interpretation for the origin of bipartite beds is that the upper part of the bed was emplaced by a high concentration mudflow as suggested by McCave and Jones (1988). High density turbidity currents are initiated by slumping and evolve into a highly turbulent flow causing all sediments to disintegrate. Such flows have sufficient energy to erode underlying material and incorporate shale clasts. When these currents slow, McCave and Jones (1988) hypothesise that two layers develop: a lower coarse-grained dispersion (fine sand and silt) where shear is high, and an overriding and thicker clay rich mudflow characterised by high cohesion and viscosity. This may continue to move as a mudflow.

The greater amount of mud clasts in the upper part of each bed compared to the lower part suggests that the same process was repeatedly at work. Several ideas have been suggested by Johansson and Stow (1995) based on their observations and the work of others. The shale clasts may have been ripped from the underlying muddy substrate and incorporated into the basal more sandy part of the flow. The clasts would have moved upward in the flow because of strong shear, and if they were not completely disintegrated,

might have become concentrated at the top of the basal layer (Mutti and Nilsen, 1981; McCave and Jones, 1988). Some of the shale clasts, if sufficiently indurated, could have survived this shear. Clasts that broke down would have increased the viscosity of the lower part of the flow and perhaps promoted its rapid deposition by freezing. This is similar to the processes suggested for the formation of slurry flows (Lowe and Guy, 2000). Part of the muddy material may have been moved upwards with escaping fluid into the overlying part of the flow contributing to the mud component of the upper part of the bed (McCave and Jones, 1988).

The greater amount of mud clasts in the upper part of the bed suggests that these clasts were not broken, either because they were not subjected to a significant amount of shearing and may have been carried passively in a sort of slurry flow as suggested by McCave and Jones (1988), or because they were more indurated and thus did not break apart.

The presence of fluid-escape structures in the upper parts of these beds suggests pore-fluid expulsion from rapidly deposited sediments (Lowe, 1975).

Thus, it is apparent that the interpretation of bipartite beds is complicated and that they need additional study. Nevertheless, the characteristics observed during this study and others suggests that the formation of two parts of the bed took place due to some sort of separation of a single flow during its deposition. The high percentage of mud may have prevented the development of good grain size grading. The mud content likely reduced turbulence (Kneller and Branney, 1995; Lowe and Guy, 2000).

Shanmugam *et al.* (1997) and Shanmugam (2000) suggested that the lower part of such stratified flows is non-turbulent flow and therefore a sort of a debris flow. Others consider such flow transformations as a normal consequence of rapid deposition, and would use the name “high concentration turbidity current” for the long-distance transport and depositing current (Hiscott *et al.*, 1998, Lowe and Guy, 2000).

### 3.8. OTHER LITHOLOGIES

The other lithologies observed in the thesis area are carbonate beds and ash horizons. Carbonate beds, consisting mostly of dolomite or dolomitic limestone (Enos, 1969b), range in thickness from 2-75 cm and some consist of a number of oblate spheroidal masses at one stratigraphic level. They are very distinctive in the field and have brown or dark brown colour. They are resistant to weathering and brittle. These carbonate beds form a minor amount of the rocks in the study area (<1.5% of the measured sections). Enos (1969b) correlated some of these dolomite beds for distances of up to 10 km. Dolomite beds are believed to be of diagenetic origin (R. Hesse, Personal Communication, 1998); the oblate spheroidal bodies are concretions.

Several volcanic ash horizons were observed in the thesis area (Chapter 4). Individual layers range in thickness from a few millimetres to several tens of centimetres. Thinner layers are massive and consist mostly of clay sized particles. Some thicker ash horizons are internally laminated or cross laminated and contain variable proportions of silt and very fine sand particles. Ash beds are easily obscured because they are easily

weathered and eroded, or are covered by mussels. They are distinguished mostly by their light green to yellowish -blue colour. Thin ash layers that mostly consist of clay-size particles and are massive are interpreted to have been deposited by direct pelagic sedimentation. Thicker beds that show tractional sedimentary structures and a mixture of silt and fine sand were probably current deposited.

### 3.9. SUMMARY

The rocks present in the measured sections are dominated by shale (~67%) and more-or-less equal amounts of sandstone and siltstone. The shale beds range in thickness from less than 0.5 cm to 510 cm (mean ~14.5 cm). These shale beds are the mud caps of the underlying sandstone and siltstone facies and were probably deposited from the same flow that deposited these sandstones and siltstones. Some of the shale may have been deposited by other processes such as hemipelagic sedimentation, but there is no compositional evidence to permit recognition of hemipelagic muds.

Siltstone beds of Class D are the second most common facies class. Beds range in thickness from less than 0.5 cm to 95 cm (mean thickness ~4 cm). Ripple lamination and climbing ripple lamination are the most common sedimentary structures, present in ~80% of Class D beds and laminae. Some of the silty sediments were deformed during or after deposition. Most of the siltstone beds were deposited from low concentration turbidity currents.

Organised sandstone beds of Class C are the most common sandstone facies in the

thesis area (13.6 % of the total thickness of the measured sections). They exhibit a variety of sedimentary structures and show partial Bouma (1962) sequences. Most of these beds were deposited from low concentration turbidity currents. Megaturbidites (thick sand-mud couplets) are common and represent a significant proportion (~32%) of the Class C sandstone beds observed in the thesis area. The thickness of these couplets ranges from a few tens of centimetres to several metres. These beds were deposited from large flows that probably originated as a result of large slope failures. The megaturbidites exhibit a variety of sedimentary structures that show bidirectional sediment transport, suggesting that some of these flows may have been deflected and reflected several times against basin highs and basin margins (Pickering and Hiscott, 1985). A less common type of megaturbidite was also observed in the thesis area (3.5% of the thickness of Class C). These beds do not have well developed tractional sedimentary structures; instead, their lower parts have a large proportion of wet-sediment deformational structures (pseudonodules) that suggest less mature flows. These megaturbidites may have been deposited from flows that did not travel a long distance from where they originated as a large slope failure.

Sandstone beds of facies Class B are the least common beds. These beds do not show tractional structures (parallel/planar/cross laminations) like those of Class C. Instead they lack well developed normal grading and exhibit fluid escape structure suggesting rapid deposition from more concentrated turbulent flows.

Beds deposited from other types of sediment gravity flows such as debris flows and sediment slides are rare or absent. This suggests that the sections studied were located

away from the base-of-slope where these types of flows and deposits would likely be more common.

## **CHAPTER 4**

### **CORRELATIONS OF MEGATURBIDITES AND K-BENTONITES**

#### **4.1. INTRODUCTION**

Correlation of the sedimentary sequences at the studied localities is essential for achieving the objectives of this thesis. In this chapter, it will be shown, using several marker beds, that approximately 650 m of section exposed in the area extending from Anse à la Rogne to Pointe Séche (composite sections SH-SYE; Chapter 5) are equivalent to approximately 570 m of the section exposed from Le Brûlé to Pointe-à-la-Frégate (section PF), located approximately 14 km to the west. It will also be shown that approximately 420 m of section exposed in the area extending from Ruisseau à l'Ail to Pointe des Canes de Roches (composite section RE-PCDR) are equivalent to the lower 430 m of section SH-SYE and to the lower 420 m of section PF. Thus, a 420-650 m-thick sequence can be correlated over a distance of approximately 25 km (the distance between section PCDR and section PF). The other eight sections described from the thesis area, representing thinner sedimentary sequences, can be correlated with parts of this thicker sequence.

Two types of marker beds or horizons are used for correlation: megaturbidite beds (facies C2.4 and C2.5 and their caps), and altered volcanic ash (K-bentonites). Both types of marker bed are geologically instantaneous events characterised by their wide areal distribution (Huff, 1983; Normark *et al.*, 1993; Reading and Levell, 1996). K-bentonites

have been very useful in correlating stratigraphic sequences over large areas (Kolata *et al.*, 1996). They are especially useful for correlations in areas characterised by complex facies relationships or in areas where palaeontological control is poor or lacking (Huff *et al.*, 1992). Megaturbidites have been successfully correlated over large areas in both modern deep marine basins (Pilkey, 1988; Rothwell *et al.*, 1992; Weaver *et al.*, 1992) and ancient turbidite sequences (Ricci Lucchi and Valmori, 1980; Hesse, 1995a).

Correlation of the K-bentonite horizons across the entire study area will be used to divide the studied sequence into smaller stratigraphic intervals (time-slices). These time-slices are further divided into smaller slices or mini-slices on the basis of megaturbidite correlations. Details of the facies architecture in the time-slices are treated in Chapter 5. According to the North American Stratigraphic Code (1983), these time-slices may be considered as lithochronozones (Article 75, p. 869) defined as “*a non-hierarchical, but commonly small, formal chronostratigraphic unit*”. The thickness of these time-slices depends on the vertical distribution of the marker beds within individual sections. The final correlation is remarkably good (e.g., Figure 4.6), and together with the K-bentonite correlation, leave no doubt as to the position of the chronostratigraphic surfaces in outcrops of this part of the Cloridorme Formation.

## 4.2. CORRELATION OF MEGATURBIDITES

More than seventy megaturbidites (facies C2.4 and C2.5 plus their mud caps) were observed in the thesis area. These beds are numbered using arabic numerals from 1



through 71. The megaturbidites were correlated on the basis of facies type, thickness, thickness patterns of groups of beds, stratigraphic position, or a combination of these parameters. All these beds have been correlated between sections PF and SH-SYE while the lower sixty-three of these beds have also been correlated to the RE and PCDR sections. The labelling scheme used here for these beds is different from that used by Pickering and Hiscott (1985, 1995). Here, the bed number is given first, followed by the abbreviated name of the section where the bed occurs. For example, 23-FP1 means megaturbidite bed 23 exposed at section FP1. Pickering and Hiscott (1985, 1995) used the abbreviated section name followed by a numeral or a letter to indicate the beds (e.g., FPE-23; SH-P). Megaturbidites that are correlated across the entire area are renamed using two letters, BT (basin-wide turbidite), followed by a number that refers to the position of the bed in the sequence. For example, BT-3 is the third oldest measured megaturbidite that extends across the area. It corresponds to 3-SH at St-Hélier and 3-PF at Pointe-à-la-Frégate. There is no correspondence between bed numbers in this thesis and those of Pickering and Hiscott (1985, 1995), in part because some of their inferred correlations are incorrect.

Other beds of the same facies were observed in the study area. Some of these could not be correlated across the entire area mainly because of lack of exposures in certain sections. These beds are labelled with the addition of a letter following the number of the immediately underlying, more traceable, bed (e.g., 45a-PF overlies 45-PF but underlies 46-PF).

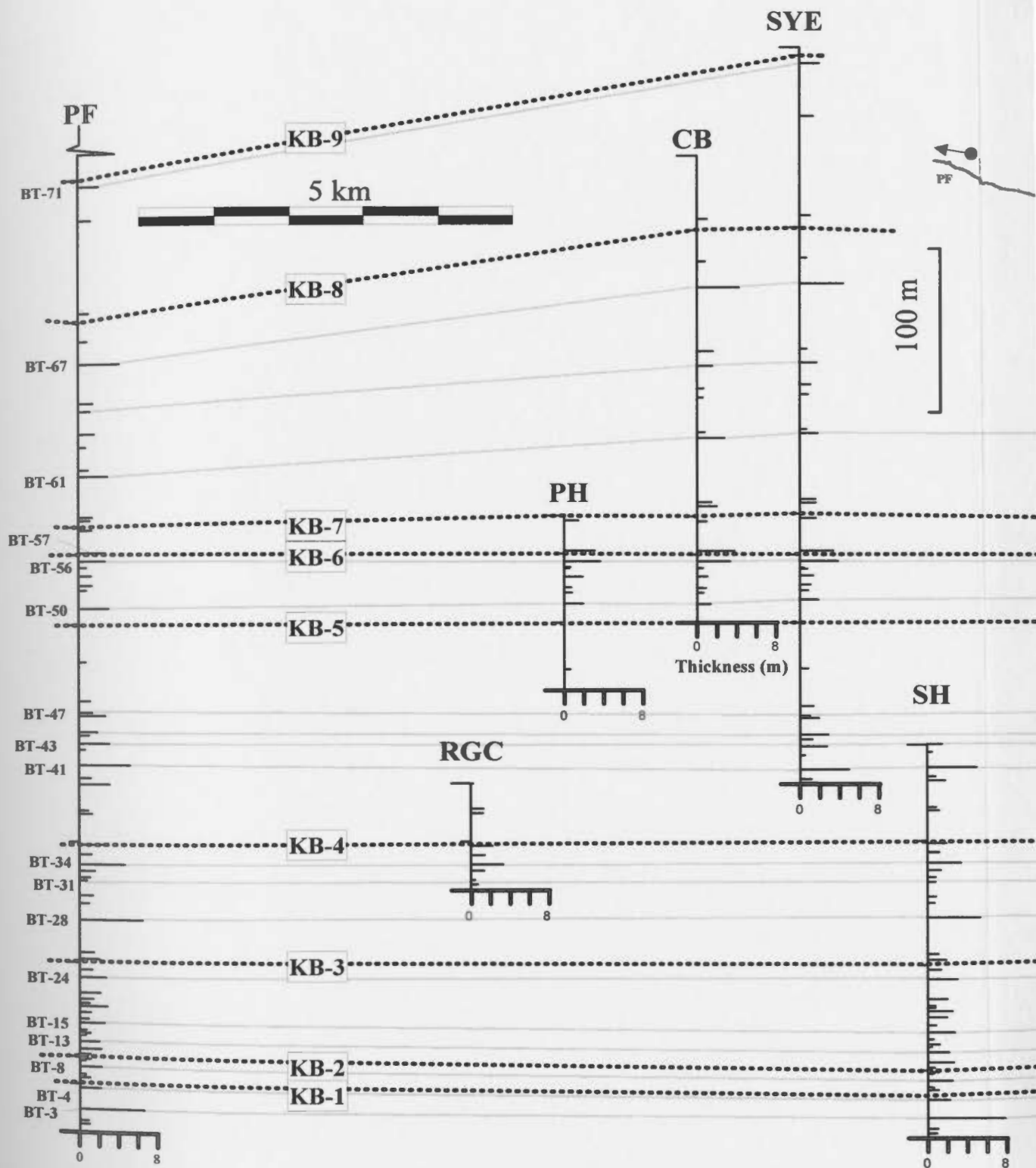
#### **4.2.1. Correlation Based on Megaturbidite Thicknesses and Stratigraphic Position**

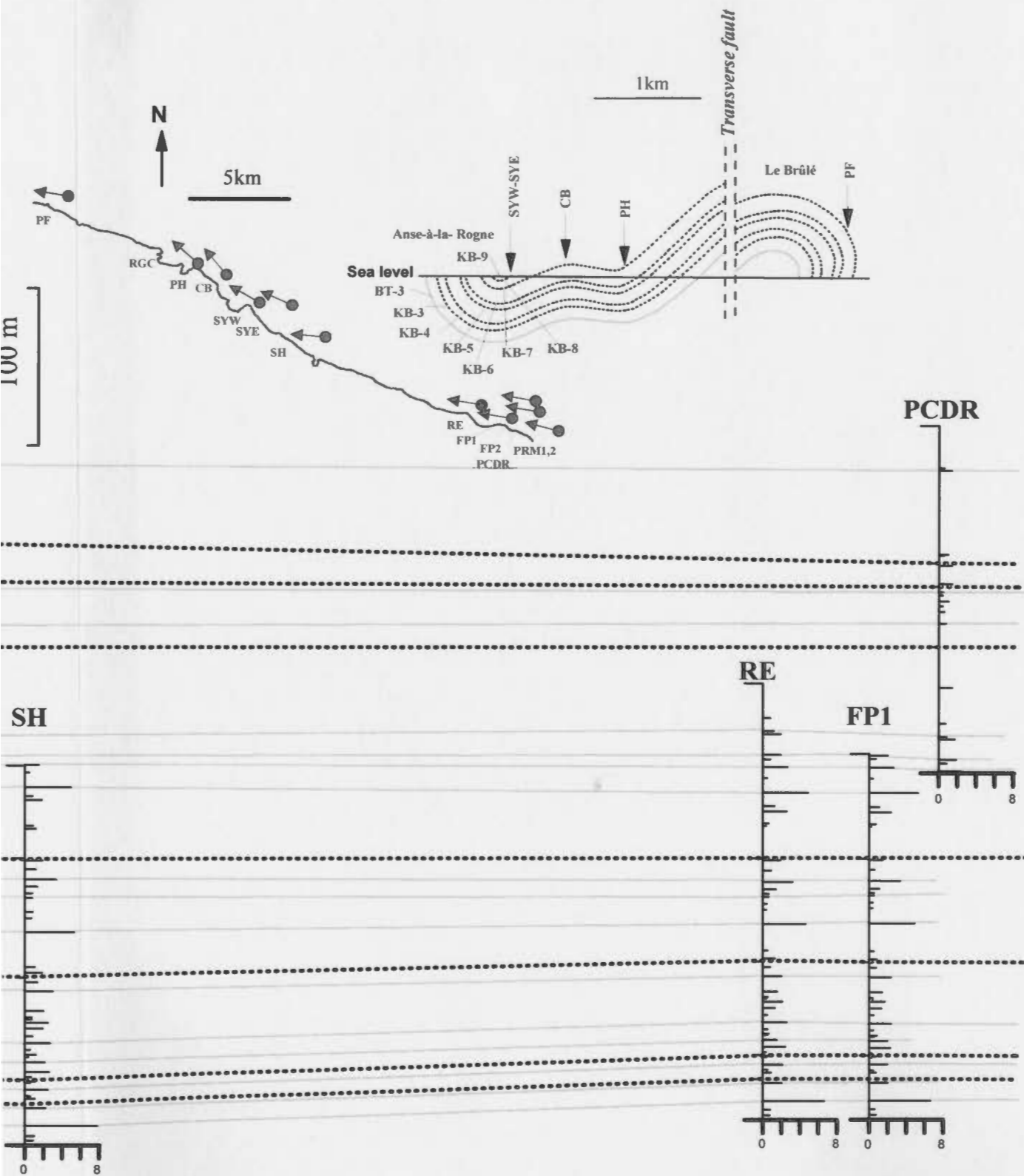
Megaturbidites vary in thickness from less than 1 m to more than 7 m. Lateral variations in the thickness of individual beds is minor except for beds in PCDR, so that bed thickness can be used as a guide to correlation. The stratigraphic positions of beds and groups of beds with particular thicknesses were also used for correlation (Figure 4.1).

Several very thick megaturbidites (thicknesses > 5 m) such as beds BT-3, BT-28, BT-41 and BT-67 can be correlated across the entire area based on thickness alone. BT-3 and BT-28 extend between PF, SH, RE and FP1 sections with minor variations in their thickness. BT-41 is correlated between PF, SYE, SH, RE and FP1 while BT-67 is correlated between sections PF, CB and SYE.

Sequences of megaturbidites and the nature of thickness variations of megaturbidites were also used for correlation (Figure 4.1). For example, between BT-3 and BT-28 there are 24 megaturbidites. In this interval, BT-4 is about 2 m thick but BT-5, BT-6 and BT-7 are much thinner. BT-6 and BT-7 are closely spaced and very thin and the overlying BT-8 is thicker at approximately 2 m. These patterns are recognisable from section to section.

Megaturbidites BT-14, BT-15 and BT-16 are easily recognised throughout the field area. These three beds are closely spaced vertically and BT-15 is almost twice as thick as beds BT-14 and BT-16. This pattern persists in sections PF, SH, RE and FP1. The sequence of megaturbidites from BT-31 to BT-40, together with KB-4 (§ 4.3), proved to be useful in correlating the short RGC section with sections PF, SH, RE and





FP1 (Figure 4.1).

Megaturbidites BT-39, BT-40 and BT-41 are important because they allow correlation of sections PF, SYE, SH, RE and FP1. BT-39 and BT-40 are closely spaced. BT-39 is twice as thick as BT-40 while BT-41 is much thicker than BT-39 and BT-40. This sequence is identical in sections PF, SYE, SH, RE and FP1 (Figure 4.1). Another sequence that correlates sections PF, SYE, RE and PCDR is from megaturbidites BT-43 to BT-47. This sequence starts with a thick megaturbidite (BT-43) followed by two closely spaced megaturbidites (BT-44 and BT-45) with BT-45 twice as thick as BT-44. Above megaturbidites BT-44 and BT-45, there are two closely spaced megaturbidites (BT-46 and BT-47) with BT-46 twice as thick as BT-47. These two correlations are important because they indicate that most of section SYE is stratigraphically above SH with only a small interval of overlap between the two sections. Hence, there is now no doubt that Pickering and Hiscott (1985, 1995) and Hiscott *et al.* (1986) miscorrelated sections CB, SYE and the upper part of PF with the sequence exposed in sections SH and FP1 and PCDR. They erroneously correlated megaturbidite BT-67 in sections PF, CB and SYE (their beds PF-14, CB-15 and SYE-20) with megaturbidite BT-28 in sections SH and FP1 (their beds SH-P and FP-37). They inferred the presence of a fault with a displacement of about 200 m in the small cove (Anse à la Rogne) that separates exposures of sections SH and SYE. The new correlation in this thesis requires no such fault. This was confirmed during conditions of a favourable very low tide and little and no waves, when the sand and silt packet present in the upper part of the SH section was traced

(walked-out) across Anse à la Rogne with no offset by faulting

Other beds and sequences that are important in correlation include megaturbidites BT-56 and BT-57 that correlate sections PF, PH, CB, SYE and PCDR. Correlation of section PCDR is partly based on KB-5 and KB-6 because there is a noticeable decrease in thickness of BT-56 and BT-57 at PCDR. Megaturbidites BT-58, BT-59 and BT-60 are also important because they correlate sections PF, CB, SYE, and PCDR, with support from the presence of K bentonite Horizon KB-7.

Type 1 megaturbidites are the most common type of megaturbidites in the thesis area while beds of facies C2.5 and their caps (type 2 megaturbidites) are less common. Two occurrences of type 2 megaturbidites were also correlated between several sections. One of the thickest megaturbidites (BT-3) was correlated between sections PF, SH, RE, and FP1. The other megaturbidite is bed BT-56a that is correlated between sections PF, PH, CB, SYE and PCDR.

#### **4.3. K-BENTONITE CORRELATIONS**

K-bentonite horizons have been recognised in the study area by Enos (1965) and Slivitzky *et al.* (1991). The word “horizon” is used here instead of layer or bed because individual bentonite occurrences vary in thickness and may consist of more than one layer or bed. Enos (1969a) was able to correlate a ~2 cm-thick ash layer over a distance of 3 km.

Nine different K-bentonites horizons (numbered KB-1 to KB-9) have been

recognised in the studied sequence. All nine horizons are present in stratigraphic order in section PF; in the other sections, fewer than nine of these horizons were observed because of limited stratigraphic thickness or poor exposure. In the PCDR section, KB-6 and KB-7 are located adjacent to faults and are replaced by quartz veins emanating from the faults.

Most of the K-bentonite horizons do not show any features indicative of deposition or reworking by currents, suggesting that they were formed by settling of volcanic ash through a tranquil water column (Figure 4.2). Horizons KB-5 and KB-8 exhibit tractional sedimentary structures (mainly ripple lamination), suggesting deposition or reworking by currents and were not chemically analysed (Figure 4.3). Nevertheless, these two reworked horizons are also used for correlation because they occur at a consistent stratigraphic position in all the sections where they are present. Resedimented or reworked ash beds have been used in correlating many thick sequences, especially in Japan (Tokuhashi, 1979).

The distribution of the different K-bentonite horizons in the measured sections has been shown in previous sections of the thesis and is summarised in Figure 4.1. The basic characteristics of each horizon and its stratigraphic position relative to basin-scale megaturbidites are listed in Table 4.1.

The nine K-bentonite horizons were investigated to see whether these different horizons can provide additional and independent support of the megaturbidite correlation presented above. The different K-bentonite horizons are present in a consistent stratigraphic position (in relation with correlated megaturbidites). If these different

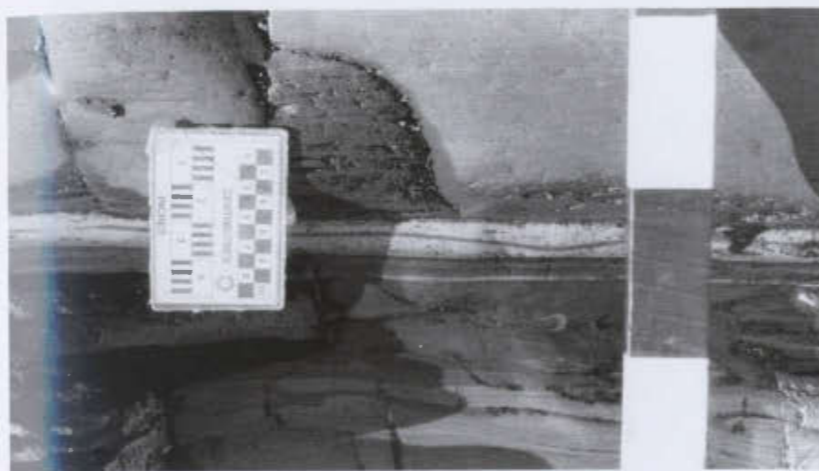


Figure 4.2. K-bentonite horizon 1 (KB-1) exposed at section FP1. The horizon consists of four massive layers. The layers lack any tractional sedimentary structures suggesting no reworking. Scale divisions =10 cm.



Figure 4.3. K-bentonite horizon 8 (KB-8) exposed at section SYW. The horizon consists of several layers. Some of the layers show tractional sedimentary structures suggesting their reworking by currents.



Table 4.1 Field characteristics of K-bentonite horizons and their stratigraphic position relative to megaturbidites. KB-1 consists of 4 layers; KB-2, KB-3, KB-4, KB-6, KB-7 and KB-9 consist of single layers; KB-5 consists of 1-8 layers while KB-8 consists of 1-4 layers.

KB horizon	Occurrence	Thickness (cm)	Thickness of individual layers (cm)	Stratigraphic position
<b>KB-1</b>	FP1, RE, PF	3 - 5	0.3 - 0.8	Above BT-4 cap
<b>KB-2</b>	FP1, RE, SH, PF	1 - 1.5	1 - 1.5	Above BT-10 cap
<b>KB-3</b>	FP1, RE, SH, PF	2 - 2.5	2 - 2.5	Above BT-25
<b>KB-4</b>	FP2, FP1, RE, SH, RGC, PF	1 - 5	1 - 5	Above BT-36
<b>KB-5</b>	PCDR, SYE, CB, PH, PF	20 - 85	1 - 30	Below BT-50
<b>KB-6</b>	PCDR, SYE, CB, PH, PF	1 - 2	1 - 2	Between BT-56 & BT-57
<b>KB-7</b>	PCDR, SYE, CB, PH, PF	1 - 3	1 - 3	Above BT-58
<b>KB-8</b>	SYE, SYW, CB, PF	10 - 50	1 - 30	Below BT-69
<b>KB-9</b>	SYE, PF	3 - 5	3 - 5	Above BT-71

K-bentonites horizons also have distinct chemical composition, then they would add considerable weight to the correlation of the sections based on megaturbidites alone.

#### **4.3.1. Correlation of K-bentonite Horizons Based on Chemical Fingerprinting**

The chemical composition of K-bentonites has been used in their correlation over large areas of eastern North America (Kolata *et al.*, 1996). Analyses of whole-rock samples have shown that many K-bentonites have a distinct chemical signature (Kolata *et al.*, 1986).

Forty-seven samples were collected from the nine K-bentonites. The samples were analysed using X-ray fluorescence (XRF) and inductively coupled plasma mass spectrometry (ICP-MS) (see Chapter 2). Of the forty-seven samples, ten were excluded from any further assessment because of contamination attributed to reworking (4 samples from horizons KB-5 and KB-8) or because they only occur in one section (6 samples). Numbering of the 37 remaining K-bentonite samples is based on their stratigraphic position in relation to the megaturbidites.

Major, minor and trace element compositions of the remaining 37 samples were tested for their usefulness in correlating the bentonite horizons across the entire thesis area. This was achieved in two steps. The first step was to test if the elemental concentration is distinct from one K-bentonite horizon to the next in a control group collected from four of the K-bentonite horizons in a set adjacent and well correlated sections (SH, RE and FP1). Only those four horizons had sufficient numbers of samples

for this type of analysis. The second step was to use any unique chemical signature to provide criteria to distinguish the K-bentonite horizons. These two steps were achieved by subjecting the chemical composition of the K-bentonite horizons to a series of commonly used statistical tests (Huff, 1983; Kolata *et al.*, 1986, 1996).

Discriminant function analysis was used to test if the K-bentonite horizons are chemically distinct and thus useful for correlation and discrimination. The discriminant procedure identifies a combination of variables (elemental compositions in this thesis) that best distinguish between groups of samples (each K-bentonite horizon defines a “group”).

The correlation of the K-bentonite horizons using the discriminant procedure was completed in two steps. First, horizons that had already been correlated with a high degree of confidence based on megaturbidites were selected as a control group and their elemental composition was compared using the discriminant procedure. The discriminant functions and coefficients that differentiated between the control-group samples (Figure 4.4a) were then used in the second step to assign K-bentonite samples with less certain stratigraphic position (or replicas) to one of the horizons in the control group. Using this procedure, a number of chemical elements were identified that best differentiate between the K-bentonite horizons. The procedure is explained in detail in Appendix A4.

The samples outside the control group are called “unknown samples” because they were initially not proven to come from one of the four control group horizons. Their sample numbers, however, indicate suspected correct assignment based on megaturbidite correlation alone. Hence, K-bentonite IV in the RGC section (Figure 4.4b) was

### Control group samples

159

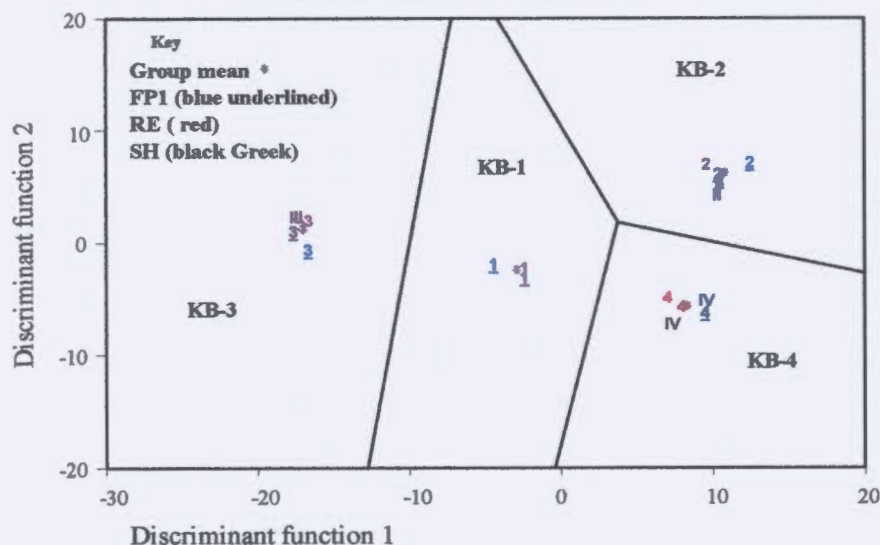


Figure 4.4a. Territorial map constructed from the two main discriminant functions calculated for 6 elements in the 18 control group samples. Asterisks are the means for each group. Boundaries are equidistant from pairs of group means. Samples from different sections have different font type (FP1= italics, RE bold, SH Greek). Numbers refer to K-bentonite horizons (e.g., 3= sample from KB-3 at FP1).

### "Unknown samples"

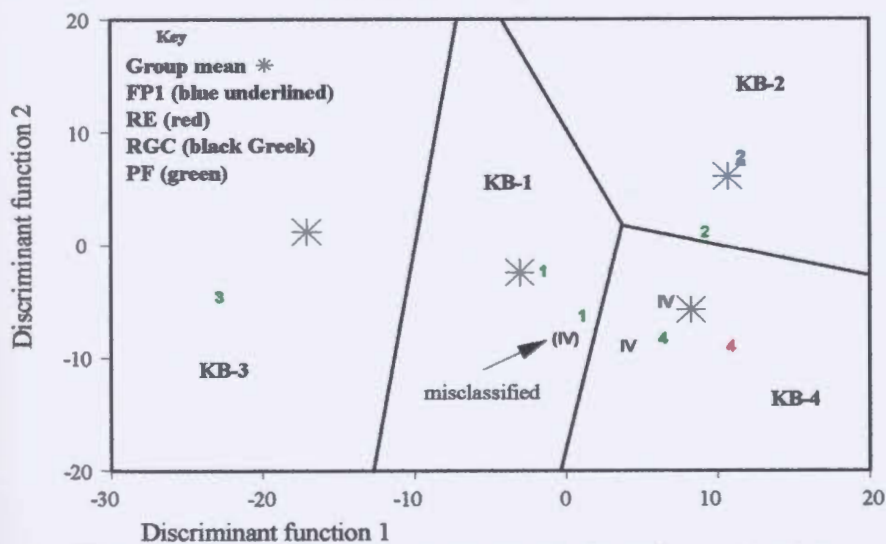


Figure 4.4b. Classification of 10 "unknown samples" as shown by their scores for the two main discriminant functions. Nine out of ten samples are classified correctly as anticipated from their stratigraphic position. The exception is one sample (IV) which fell in the field of KB-1 instead of KB-4.

considered, based on its stratigraphic position, to be KB-4. Confirmation of this assignment was as outcome of the geochemical typing of the control group, followed by discriminant function analysis to classify “unknown” samples.

Based on the megaturbidite correlations for the lower part of the studied succession, ten unknown samples taken from the PF, FP1, RE and RGC sections were classified using the discriminant coefficients and constants for the control-group. Remarkably, nine of the ten samples were successfully assigned to the K-bentonite horizon (group), to which they were believed to belong, as predicted from field relationships and megaturbidite correlation alone (Figure 4.1). The sample that was not classified as anticipated was one of three samples collected from two sampling sites in inferred horizon KB-4 in the RGC section. The other two samples were indeed classified as KB-4, leading to the conclusion that the third sample was anomalous.

Thus, chemically distinct K-bentonite horizons from the PF section are inferred to be equivalent, based on chemical composition, to corresponding horizons KB-1 to KB-4 in the SH, RE and FP1 sections. This confirms the original field-based correlations of K-bentonite horizons. Also, the single K-bentonite horizon at section RGC has chemistry matching KB-4 in the control group. The K-bentonite horizons and their sequence provide a dependable correlation tool because the matched K-bentonite beds occur in a consistent stratigraphic position relative to correlated megaturbidites: there are no stratigraphic mix ups (i.e., no cases where a K-bentonite horizon with KB-4 chemistry underlies a horizon with KB-2 chemistry). Field experience in locating these horizons supports this

conclusion. For example, KB-3, located above BT-25, is well exposed in sections FP1 and RE, but was not initially identified in the SH section, because of poor exposure. Subsequently, with considerable effort (digging) at SH at the correct stratigraphic position above BT-25.

For K-bentonite horizons KB-6, KB-7, and KB-9, the limited number of samples that could be collected (2 from KB-6, 3 from KB-7, and 4 from KB-9) restricts the number of statistical procedures or tests that can be applied because mean elemental abundances can not be well determined. The discriminant analysis procedure was not performed on these samples; instead, an F ratio was calculated for chemical data from these samples to identify the best discriminating elements (Table A5-3.3). The four immobile elements (Eu, Sc, Th, Ti) with the highest F ratios were selected and their concentrations were used to construct bivariate diagrams (Figure 4.5) in order to see if these K-bentonite horizons are distinct from each other (Kolata *et al.*, 1986).

The bivariate diagrams show that KB-9 is easily distinguished from horizons KB-6 and KB-7. The best clustering and distinction are observed in the  $\text{TiO}_2$  vs Sc,  $\text{TiO}_2$  vs Th and  $\text{TiO}_2$  vs Eu plots. Distinction between KB-6 and KB-7 is not possible using these four elements, perhaps because both horizons originated from the same volcano or set of volcanos. Horizon KB-6 occurs just a few tens of metres (ranging from 17-25 m) below KB-7, as compared to the hundreds of metres (200-280 m) that separate horizon KB-9 from KB-7. If the rate of sedimentation is assumed to not vary dramatically, then the shorter time between the eruptions that produced KB-6 and KB-7 might account for their

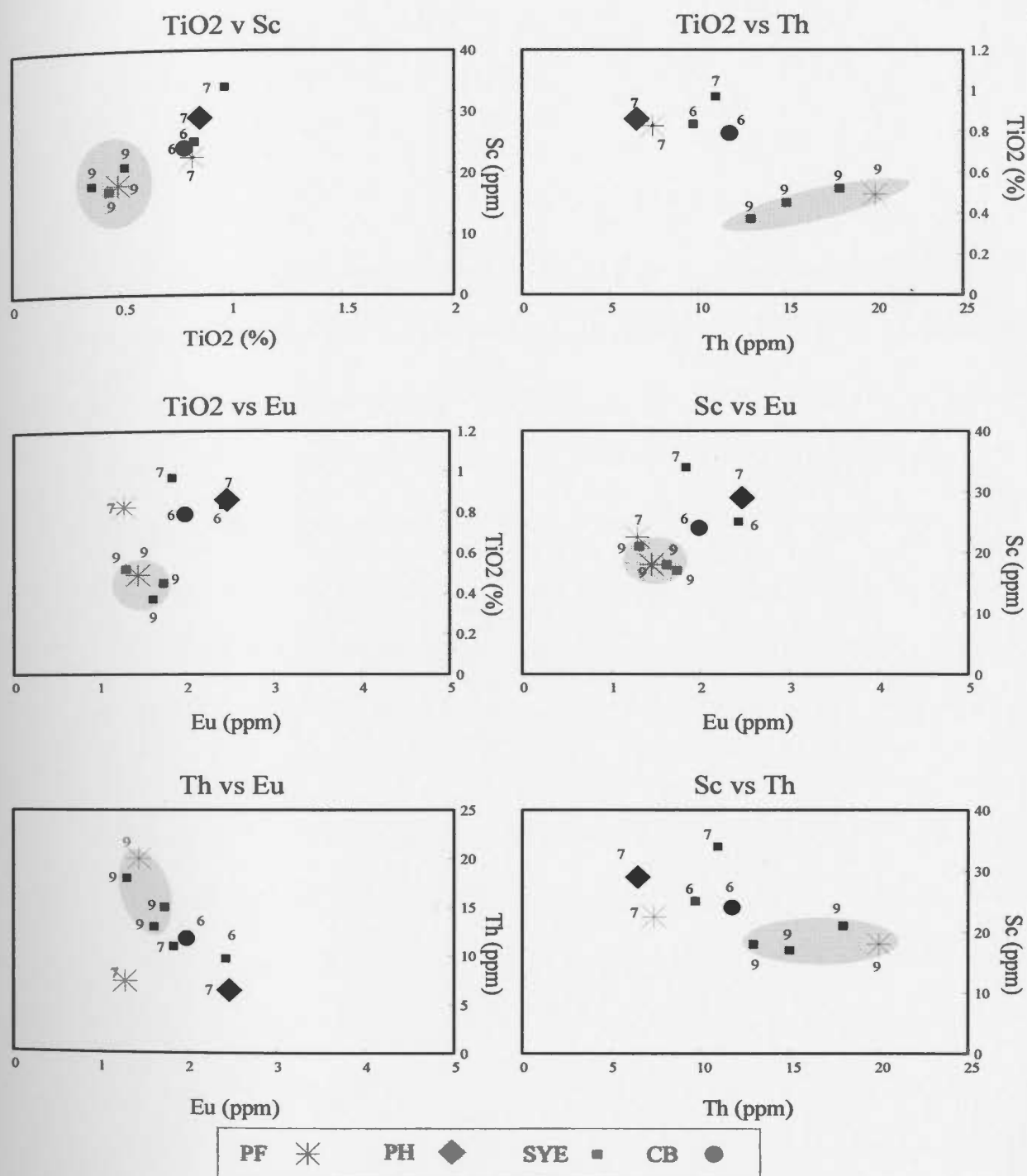


Figure 4.5. Scatter plots of the four most discriminating elements (based on their F ratios). K-bentonite horizon KB-9 is easily distinguished from horizons KB-6 and KB-7 on most plots. Distinction between KB-6 from KB-7 is not possible using these four elements. Note that symbols refer to sections (e.g., PF=\*) while the numbers refer to K-bentonite horizons (e.g., 9=KB-9).

similar composition.

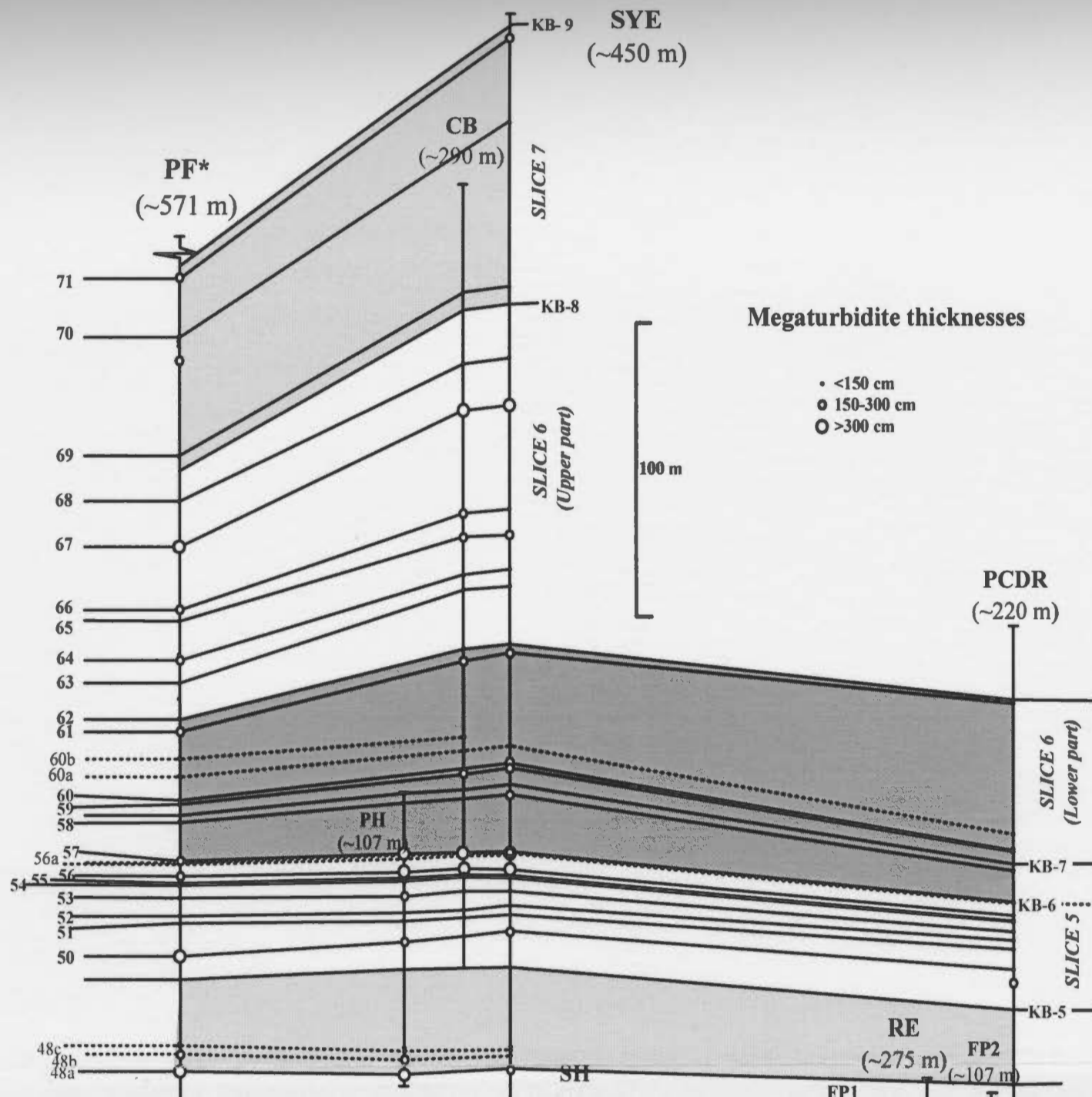
#### 4.4. CONCLUSIONS

Using chemical criteria to distinguish seven distinct K-bentonite horizons, and field evidence to correlate two other K-bentonite horizons (KB-5 and KB-7), it is possible to confirm the correlation of the studied sequence and to divide several long sections into seven time-equivalent slices that can be traced across the entire thesis area (Figure 4.6). The thicknesses of these slices depend of the spacing between the K-bentonite horizons: it is less in the lower part of the sequence (thinner slices 1, 2 and 3 with mean thicknesses of 33 to 71 m), and greater in the upper part of the sequence (thicker slices 4, 6, 7 with mean thicknesses of 100 to 158 m). The exception is slice 5, which has a mean thickness of 62m.

Each of the seven time-slices can be further divided into smaller intervals on the basis of megaturbidite correlations (§4.2). Megaturbidites occur more frequently in the lower part of the sequence than in the upper part. This permits most detailed investigation of the lower part of the sequence.

It should be emphasised that the durations of time-slices, sub-slices and mini-slices (Chapter 5) are unknown because the K-bentonite horizons are not dated. Also, the bases and tops of these slices are arbitrary placed at isochronous surfaces that are essentially randomly scattered throughout the succession, so the slice cannot be considered as architectural elements with particular genetic significance. Instead, each slice, sub-slice





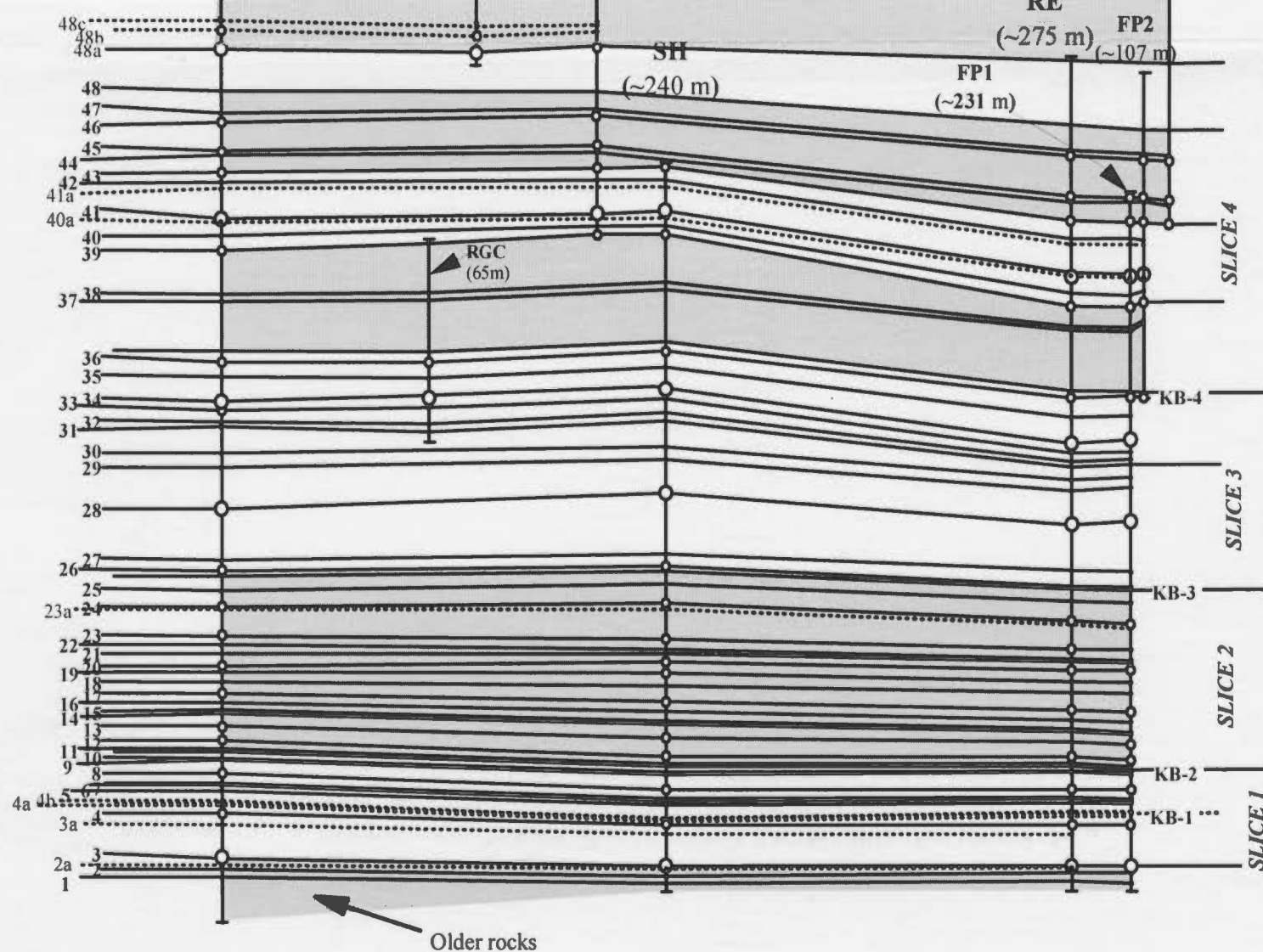


Figure 4.6. Divisions of the studied sequence into seven "time slices" based mostly on the correlations of K-bentonite horizons KB-2 to KB-5 and KB-7 to KB-9. The correlation of the base of time slice 1 is based on megaturbidite BT-3 that occurs across the area. Solid lines correlate between equivalent megaturbidites. Heavy solid lines correlate between equivalent K-bentonite horizons that are present in all the sections. Poor exposures in parts of some sections prevented the correlation of all megaturbidites and K-bentonites in the area (dashed correlation lines). Time slices are divided into mini-slices (see Chapter 5) based on correlated megaturbidites (numbered 1-71). Numbers in parenthesis under each section title indicate the thickness (in metres) of the sequence at each section. The correlated sequence in PF section is ~571 m although an additional ~200m of section above KB-9 were described in the field. Sections SYW, PRM1 and PRM2 are not shown to avoid crowding of the figure. Hatching and stippling are only for clarification of the correlations of some parts of slice 4 and 6. Note that most of slice 6 and all of slice 7 are not exposed in the PCDR section. Section PF and section PCDR are approximately 25 km apart (see Figure 3.1). Vertical exaggeration is ~87x.

and mini-slice is a time-stratigraphic unit which contains deposits that accumulated synchronously. Shapes of slices, and facies trends within slices, can be used to evaluate the sequential deposition of the lower part of the Cloridorme Formation, the subject matter of Chapter 5.

## **CHAPTER 5**

### **DEPOSITIONAL ENVIRONMENT, ARCHITECTURAL ELEMENTS AND DEPOSITIONAL HISTORY**

#### **5.1. INTRODUCTION**

The proceeding chapter investigates the different facies observed in the correlated time-slices (outlined in Chapter 4) in order to understand their lateral variability and the factors that may have affected their deposition and evolution (facies tract approach of Mutti, 1992). The detailed investigation presented here, at the smallest scale may allow the recognition of the two-dimensional shape of turbidite sediment bodies (i.e., architectural elements) within each time-slices. The architecture of these sediment bodies will be examined in detail. The depositional environment suggested for each time-slice will be based on the different facies and architectural elements identified within these time-slices. These elements represent sediment bodies formed in distinct sedimentary subenvironments. Finally, when all the time-slices and their constituent architectural elements have been discussed, the depositional environment of this part of the Cloridorme Formation will be constructed, using the information derived from time-slice 1 to time-slice 7.

It should be emphasised, that the thickness of each time-slice is controlled by the stratigraphic separation of K-bentonite horizons that mark the top and base of the time-slices (except for BT-3 which marks the base of time-slice 1, Chapter 4). Time-slices 1, 2,

3 and 5 are the thinnest time-slices.

The study presented in this chapter is done on two different scales. The first, at a regional scale, is based on the correlation of three composite sections compiled using the data collected from each of the detailed study areas (areas A, B and C; Chapter 2). Area B is located about 10-12 km WNW (at ~N75W relative to today's north) from area A (Appendix A5, A6). Section PF was measured in the area from Le Brûlé to Pointe-à-la-Frégate in the western part of the thesis area (detailed area C). Area C is located about 11-16 km NW of area B. Area C is about 22-26 km NW of area A (i.e., area C is 25-27 km from area A in a ~N60W direction). This regional-scale of the study allows delineation of the "external architecture" of turbidite bodies (Chapin *et al.*, 1994). The orientation of the studied sections with respect to palaeoflow directions are presented in figures 3.1 and 4.1.

The second, smaller scale of investigation will consider the more local changes within each detailed areas (i.e., the "internal architecture"). This is useful for understanding the architecture of turbidite bodies or facies that are characterised by rapid changes that may not be resolvable using the regional investigation.

In section PF (detailed area C, Chapter 2), all seven time-slices are present. Based on lateral correlation, an interval of about 12.5 m in time-slice 7 is not exposed due to faulting. The internal architecture could not be investigated in area C because of limited outcrop that permitted only one section to be measured.

In the middle part of the thesis area (detailed area B, Chapter 2), all seven time-slices are present and illustrated in composite section SH-SYE. Time-slices 1, 2 and 3 are

exposed in the lower to middle part of section SH; about 5.1 m of time-slice 1 is not exposed here. Time-slice 4 is divided into two parts: sub-slice 4-1, exposed in section SH, bounded at the base by KB-4 and at the top by the base of bed BT-43; and sub-slice 4-2, exposed in section SYE, bounded at the base by the base of bed BT-43 and at the top by KB-5. The division of a time-slice into sub-slices is applied to time-slice 4 and time-slice 6, and should not be confused with the term “mini-slice” which is widely used in this chapter for even thinner units which occur in many of the time-slices (§5.4). One fault observed in section SYE, time-slice 5, causes the loss of 2–4 m. Time-slices 6 and 7 are well exposed in the middle and upper parts of the SYE section. Several sections (SYW, CB, PH) were measured in different parts of area B. In these sections, parts of time-slices 5, time-slice 6, and parts of time-slice 7 are exposed. These sections are used to study the internal architecture of these three time-slices. The lateral distance between these sections is variable (Appendix A6).

In the eastern part of the thesis area (detailed area A), a composite section (RE-PCDR) was compiled from most of the RE section and all of section PCDR. Time-slices 1, 2, 3, and sub-slice 4-1 (bounded by the same markers as in area B) are well exposed in section RE. In section PCDR, sub-slice 4-2, time-slice 5 and part of time-slice 6 (sub-slice 6-1) are well exposed. The remaining part of time-slice 6 (above bed BT-63 to KB-8) and time-slice 7 are not exposed in section PCDR, thus the depositional history of the upper part of time-slice 6 and all of time-slice 7 will be based entirely on the study of the upper parts of composite sections PF and SH-SYE which are exposed in areas B and C.

Time-slices 1, 2 and 3 are exposed in both sections RE and FP1. Sub-slice 4-1 is exposed in sections RE, FP1, FP2 and PRM1 (Figure 2.2). Parts of sub-slice 4-2 are also exposed in sections RE and FP2, however, full exposure of this sub-slice occurs in section PCDR. The lateral distance between the equivalent beds in sections RE, FP1, FP2, PCDR, PRM1 and PRM2 varies from ~200 m to ~1700 m (Figure 2.2).

The geometry of the time-slices and mini-slices, and of sediment bodies within these is also outlined in this chapter. This is achieved by investigating the thickness variations of the time-slices, mini-slices and sediment bodies between the correlated sections at a regional and local scale. The thickness of the beds measured in the studied sequence is a function of the depositional thickness, and subsequent changes to this thickness caused by either compaction or, tectonic thinning and/or thickening. Bed thickness variation due to differential compaction and tectonic action is believed to be minor in most cases for composite sections in areas A, B and C. Nevertheless, as a precaution against over interpretation, a thickness variation is only considered important or significant if a particular mini-slice varies by  $\pm 10\%$  from the mean mini-slice thickness averaged over all three sections. Negative deviations indicate thinning whilst positive deviations indicate thickening (Ricci Lucchi, 1975; Table A5-4.1). Note that the variations in the thicknesses are over distances of more than 10 km between areas A, B and C.

Composite sections RE-PCDR and SH-SYE were measured in the same overturned fold limb and their present thickness is believed to have not been affected greatly by folding (Enos, 1965). Hence, no correction of bed thickness was applied to the

beds exposed in the sections of area A. Section PF was measured in the overturned limb of the fold exposed at Le Brûlé. The dip of the beds in this area is greater than the dip of the beds in composite sections SH-SYE and RE-PCDR (Chapter 2), raising the possibility that these rocks may have experienced a greater amount of thinning due to folding.

Composite section SH-SYE and sections SYW, CB and PH are used to study the internal architecture of time-slices 5, 6 and 7. Sections SYW, CB and PH were measured in the gently dipping (northern) limb of the syncline exposed at Pointe Séche. Detailed correlation of the beds between these three sections and composite section SH-SYE indicated that folding has affected the thickness of the beds differently in sections SYW, CB and PH in comparison to composite section SYE. Hence, corrections were made to the thickness of the beds in section PH, CB and SYW (Appendix A5).

The part of the Cloridorme Formation studied in this thesis lacks features or facies that indicate the presence of canyons, major erosional features, or channels, subsequently, these elements will not be discussed. Instead, the main characteristics of the four most relevant architectural elements will be dealt with and are illustrated and summarised in Figure 5.1 and Table 5.1. Some of these elements correspond to more than one architectural element of Mutti and Normark (1987, 1991) or Stow *et al.* (1996). The cross-sectional and planformal shapes of these elements are shown in Figure 5.1.

The correlation diagrams presented in this chapter are drawn with large vertical exaggeration. For example, time-slice 1 is drawn with a vertical exaggeration of ~750x. It is critical to account for this when deciding whether depositional elements are, for



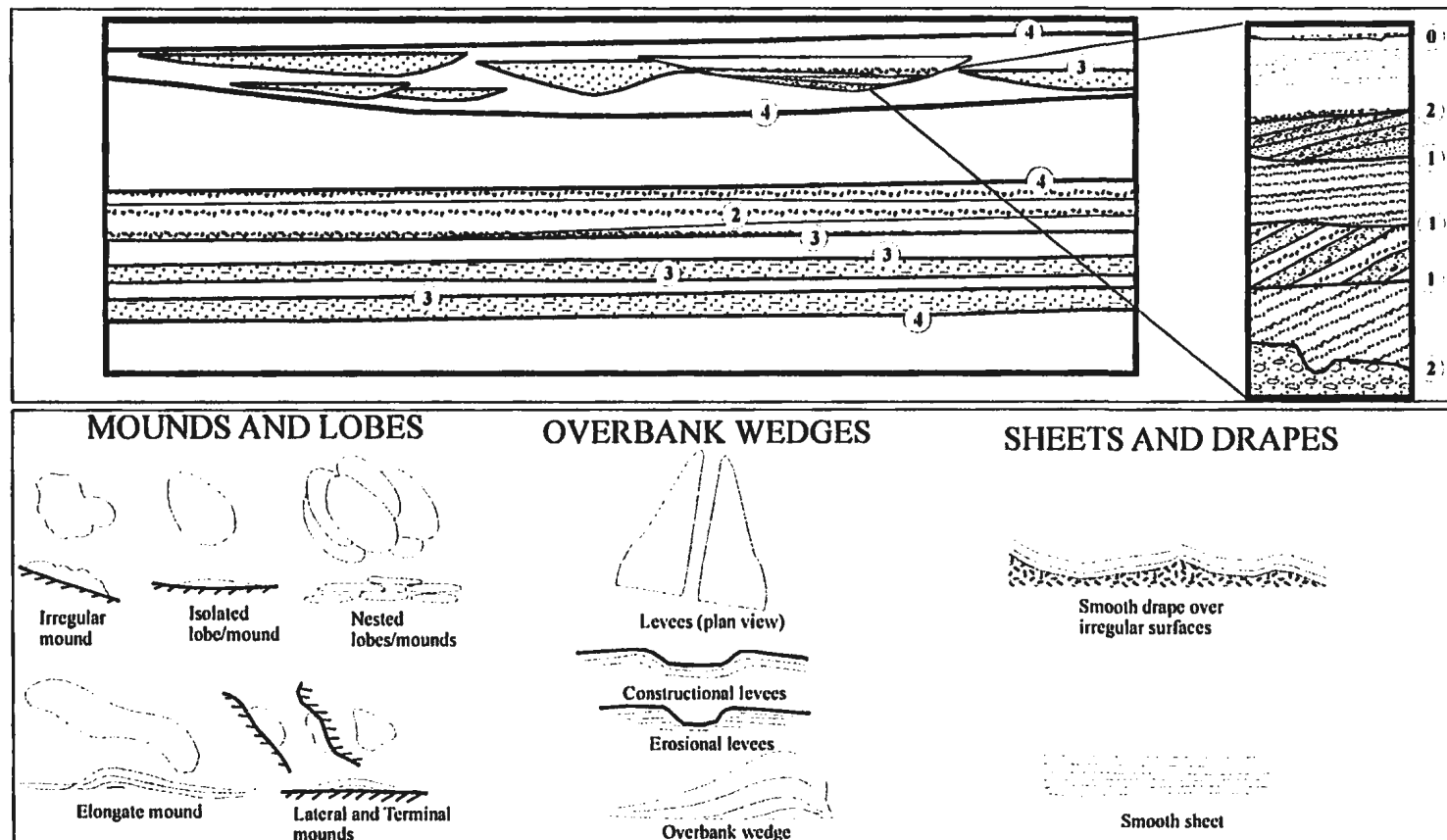


Figure 5.1. Upper panel shows bounding surface hierarchy in ancient deposits (modified from Pickering *et al.*, 1995). 0<sup>th</sup> order bounding surface delineates normal concordant bedding contact between strata. 1<sup>st</sup> order surface could be concordant or discordant and bounds beds or packets of beds (e.g., cross bedding sets). 2<sup>nd</sup> order surfaces bound sedimentary complexes of genetically related facies. 3<sup>rd</sup> order surfaces are major erosional surfaces, and separate groups of complexes (depositional bodies). 4<sup>th</sup> order surfaces are basin wide major erosional surfaces. Third and fourth-order surfaces delineate sediments equivalent to Mutti and Normark's (1987) fourth and third-order physical scale, respectively. First and second-order surfaces correspond to Mutti and Normark's (1987) fifth-order physical scale. The lower panel shows the different architectural elements relevant to this study; their shape in plan view is shown above the cross sectional view (modified from Stow *et al.*, 1996).

Architectural Element	Lobes and Mounds	Sheets and Drapes	Overbank Wedges	Megaturbidites
Size	Few metres to 100's m thick. Width varies from km to 100's km.	Thickness varies from metres to 1000's of metres. Cover areas that may reach 1000's km <sup>2</sup> .	100's m high and wedge out in 10's of km towards the basin margin.	Thickness varies from metres to 10's of metres. Single beds may spread over areas 100's km <sup>2</sup> .
Grain size	Sand with subordinate silt and mud.	Mud, silt and sand.	Mud dominates with subordinate silt and sand.	Boulder to silt and mud
Sedimentary structures	Thick bedded coarse sand packets, tabular and non-channelized, that alternate with thin bedded finer sediments. Scours common in some deposits.	Medium bedded and very thick bedded sands and megaturbidites are common, displaying a variety of tractional structures. Fine sand, silt with T <sub>c-e</sub> are common.	Graded mudstone units dominate. Thin bedded, current laminated fine sand and silt are common (T <sub>c</sub> , T <sub>d-e</sub> , T <sub>e</sub> ). Irregular upper and lower bed contacts.	Graded beds with sharp basal contacts. Thick mud caps. Structure varies from massive to current laminated.
Location in system	Downslope from channels.	Downslope from lobes or between channels.	Upslope from lobes. Adjacent to channels.	From basin margin to distal plain. Common in basin plain setting.
Plan view shape	Lobate to circular.	Flat with shape controlled by basin margins.	Paired triangular shape or wedge shape.	Very broad circular to lens shape.
Cross sectional shape	Plano-convex with a planar lower boundary. Tabular with variable lateral extent.	Even and parallel bedding surfaces that mimic underlying topography.	Wedge shape.	Tabular but taper in shape over 100's of km distances.
Comments	Constituent facies poorly known in modern lobes.	Some lobe deposits have a sheet-like geometry at outcrop scale.	Difficult to recognize the geometry in ancient systems. Individual beds correlated over 10's of km.	Believed to originate from large slumps and are good marker beds.

Table 5.1. Summary of the main features and characteristics of the architectural elements relevant to this study. Some of these elements combine more than one element discussed in other studies. This information is compiled from different sources (Mutti, 1977; Mutti and Normark, 1987, 1991; Pickering *et al.*, 1989, 1995; Hesse, 1995b; Stow *et al.*, 1996).

example, sheets or mounds.

## 5.2. ARCHITECTURE OF TURBIDITE BODIES

Architectural element analysis was first proposed for fluvial and aeolian deposits (Brookfield, 1977; Allen, 1983; Miall, 1985). An *architectural element* is defined by Miall (1985), as a “lithosome characterised by its geometry, facies composition, and scale, [that] represents a particular process or a suite of processes occurring within a depositional system”.

The application of architectural element analysis to turbidite bodies was first suggested by Mutti and Normark (1987). They identified both depositional and erosional elements. Mutti and Normark (1991) indicate that a depositional element consists of similar facies and facies associations that are different from the enclosing strata. Identification of the geometry of an architectural element requires the identification of bounding surfaces and their “order”, or hierarchy (Pickering *et al.*, 1995). For example, a deposit containing turbidite sands may consist of a variety of facies spanning scales from that of an individual graded bed to an entire basin fill. Mutti and Normark (1991) suggested a five-fold hierarchy. Their 5<sup>th</sup> order represents instantaneous events such as the deposition of individual beds, and their 1<sup>st</sup> order represents events lasting a million or tens of millions of years during which turbidite “complexes” are deposited and separated from one another by major unconformities. Mutti and Normark (1987; 1991) suggested a duration for the accumulation of deposits bounded by the different orders of bounding

surfaces. For example, turbidite complexes that form during periods of  $10^6$  to  $10^7$  years are bounded by 1<sup>st</sup> order surfaces, while turbidite stages that form during periods ranging from  $10^4$  to  $10^5$  years are bounded by 3<sup>rd</sup> order surfaces. Because turbidite systems vary considerably, and oversupplied turbidite systems may accumulate at rates too rapid to be resolved by biostratigraphy, strict adherence to the time frame proposed for deposits between the different bounding surfaces is not favoured or encouraged (Mutti and Normark, 1991; Stow *et al.*, 1996). Furthermore, Mutti and Normark *et al.* (1987; 1991) recognized nine architectural elements: (1) canyons, (2) major erosional features, (3) channels, (4) channel-lobe transition deposits, (5) overbank deposits or wedges, (6) lobes, (7) slope aprons, (8) basin-plains, and (9) megaturbidites. These elements are the building blocks of 3<sup>rd</sup>, 4<sup>th</sup>, and 5<sup>th</sup> order events in their hierarchical scheme.

Pickering *et al.* (1995) introduced a different architectural element scheme for turbidite systems (Figure 5.1). It is more similar to the scheme used for fluvial models (Miall, 1985), in that architectural elements are recognized based on the deposit geometry and the character of the facies within the specific element. Pickering *et al.* (1995) use a bounding surface hierarchy that allows for 4<sup>th</sup>, 5<sup>th</sup>, and 6<sup>th</sup> order features at the basin scale. Note that higher-numbered orders are smaller in size in the Mutti and Normark (1987, 1991) scheme, but larger in size in the Pickering *et al.* (1995) scheme. Unlike Mutti and Normark (1987), Pickering *et al.* (1995) did not specify any time frame for the deposits between their bounding surfaces; however they indicated that their 4<sup>th</sup> and 6<sup>th</sup> order surfaces are equivalent to Mutti and Normark's (1987) 3<sup>rd</sup> and 1<sup>st</sup> order surfaces,

respectively. Although some of these bounding surfaces may have their origin in sea-level changes, the reader should not confuse these different architectural-element bounding surfaces with orders of sea-level change reported in the literature (e.g., Emery and Myers, 1996, p. 17).

The architectural-element and bounding-surface schemes of Pickering *et al.* (1995) are adopted for this study because they are more detailed (larger number of bounding surfaces; Figure 5.1). However, it was difficult to distinguish 2<sup>nd</sup> from 3<sup>rd</sup> order bounding surfaces above and below sandstone and siltstone sheet elements.

Other architectural-element schemes for turbidite systems have been proposed, based on features such as laminae, beds and packets of beds as individual elements (Hurst *et al.*, 2000), or on the recognition of deposits of similar shape but with constituent facies that differ in texture as separate elements (e.g., sandstone sheet element and siltstone sheet elements of Carr and Gardner, 2000). Piper *et al.* (1999), using high-resolution boomer seismic-reflection data, recognized several architectural elements and subelements from the Hueneme and Dume submarine fans offshore California.

### **5.3. DATABASE, INTERPRETATION PROCEDURES AND ASSUMPTIONS**

The number of beds, mean bed thickness and total thickness of facies classes, facies and subfacies in the time-slices and mini-slices are presented in tables in a back-pocket CD ROM (Tables CD-T1 through CD-T7). The draughted sections (Appendix A3) and sections that are used in the correlation diagrams are based on field measurements,

recorded to the nearest 0.5 centimetre. Some thin laminae ( $< 0.3$  cm) are shown because they are useful in marking the top of megaturbidite caps. However, laminae  $< 0.3$  cm thick are not included in the number of beds presented in tables and figures in this chapter. Facies D2.3 is the most affected by the omission of thin laminae ( $< 0.3$  cm) because it contains many of these. The term “total thickness” used below refers to the cumulative thickness of a certain facies in a particular time-slice or mini-slice. For example, if a mini-slice contains 10 siltstone beds that are 3 cm thick each, then the total siltstone thickness in this mini-slice equals 30 cm. In descriptions and interpretations of the time-slices and mini-slices, the thickness and number of carbonate beds and ash horizons are excluded from the calculations of the thicknesses of time-slices, or the number of beds. The carbonates are diagenetic and the ashes are very thin.

To determine the depositional history for time-slice 1 and other time-slices in the thesis area, facies interpretation (Chapter 3) and the vertical and lateral facies relationships within each mini-slice were utilised. Only megaturbidite beds could be correlated between the three areas. Because biostratigraphic age data are limited and at a coarse scale of resolution, there are several unknowns that limit full determination of the depositional history. For example, sedimentation rates and the frequency and timing of events such as megaturbidite deposition are unconstrained. Other unknowns, include the precise amount of compaction and tectonic thinning and thickening. Another uncertainty is how useful palaeocurrent data are in indicating which sections were closer to the axial path of the depositing current and which sections were farther from this axial path. In the palinspastic

map (Figure A4.3), area A and area C are located along a traverse that lies in a WNW direction. Area B is located about 15° to the left of this traverse, as viewed from area A. This difference may be inconsequential for palaeocurrent data collected from ripple laminations (a large proportion of the measurements in most sections) because ripple orientations show considerable dispersion in nature (Graham 1988).

The majority of the palaeocurrent data suggest that the transport direction was from east to west (see also Pickering and Hiscott, 1985). Some megaturbidites have flutes or cross lamination indicating transport from west to east. So the terms “downflow” or “downcurrent” that are used in this chapter refer to flows moving east to west. Beds that show other palaeocurrent directions will be indicated in the text.

Two reasonably secure assumptions are used extensively in the interpretation of the depositional environment. The first is that megaturbidites and K-bentonites are instantaneous events that bound mini-slices and thicker time-slices of equal age. The second is that mini-slices or megaturbidites that show little or no variation in thickness between the three sections indicate an essentially flat sea bed during their deposition (Ricci Lucchi 1990, Ricci Lucchi and Valmori, 1980; Mutti, *et al.* 1994).

For figures showing long-distance correlations and short-distance correlations, the base of the mini-slice with the least thickness variation between areas A, B and C is used as a datum to align the sections. In some time-slices, several datums could have been selected. These datums are good indicators of the change in thickness of time-slices between the three areas.

The effect of compaction, and tectonic thickening and thinning, might have influenced the thickness of the beds and mini-slices, however, it is assumed that the beds and mini-slices in areas A and B (located in the same fold limb) have not changed in thickness relative to one another as a result of folding. Further, mini-slices in which there is little or no facies change from area A to B are assumed to have undergone similar amounts of compaction.

#### **5.4. TIME-SLICES**

Seven time-slices divide the sequence studied in this thesis. These are further divided into mini-slices based on correlation of megaturbidites (Chapter 4). Each time-slices varies in thickness and number of beds. The percent of each facies class that occurs in each time-slices and sub-slices is presented in Table 5.2.

##### **5.4.1. Description of Time-slice 1**

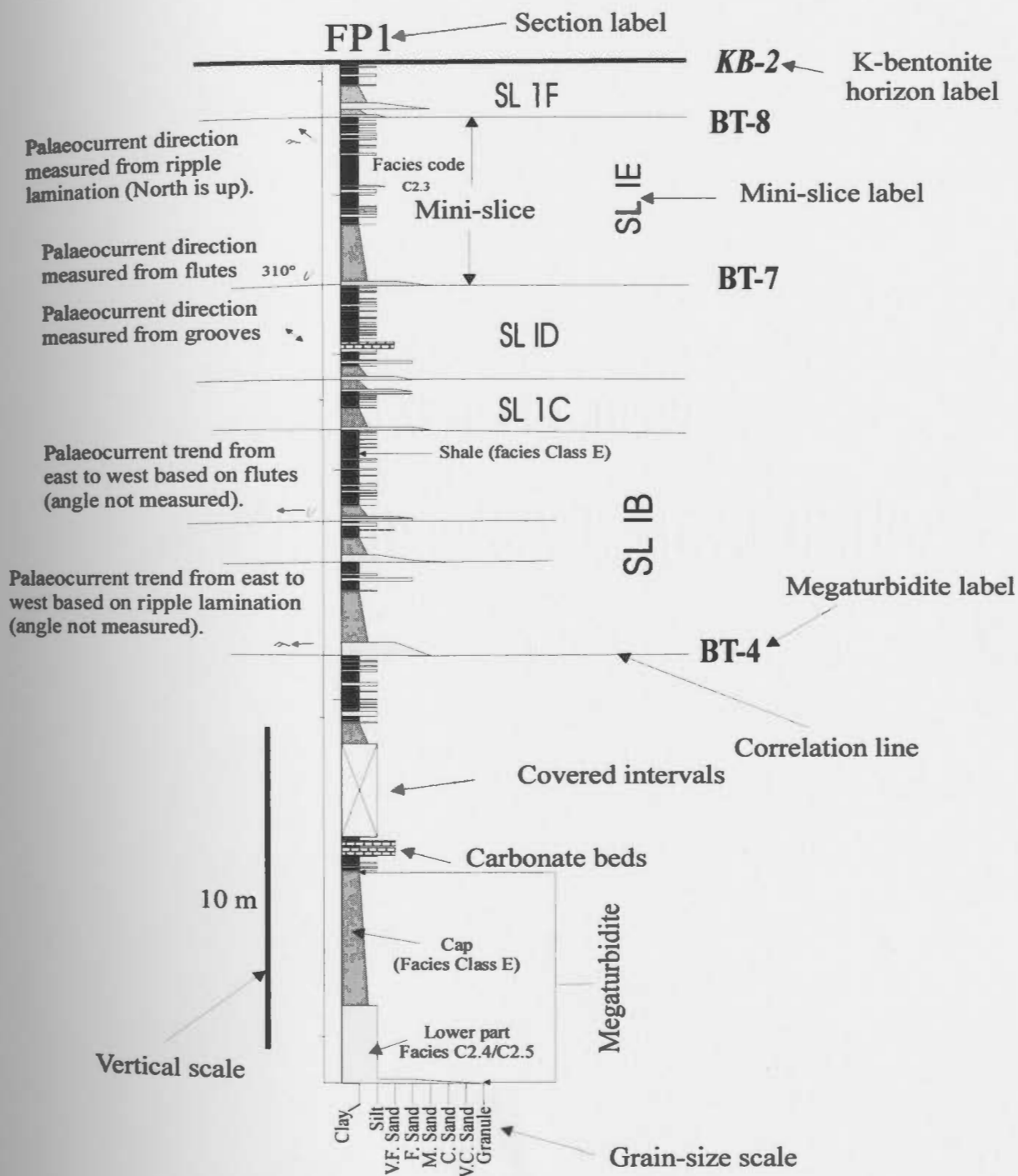
Time-slice 1, the thinnest time-slice, is exposed in areas A, B and C (Table 5.2). The base of megaturbidite BT-3 marks the base of this time-slice and K-bentonite horizon KB-2 marks its top. K-bentonite horizons and megaturbidites divide time-slice 1 in to six mini-slices (Figure 5.2). Mini-slices SL 1C through SL 1F are well exposed in areas A, B and C while parts of mini-slices SL 1A and SL 1B are covered in areas A and B. The external architecture of mini-slices SL 1C through SL 1F will be constructed using the data from all three areas, while only data acquired from areas A and C will be used to



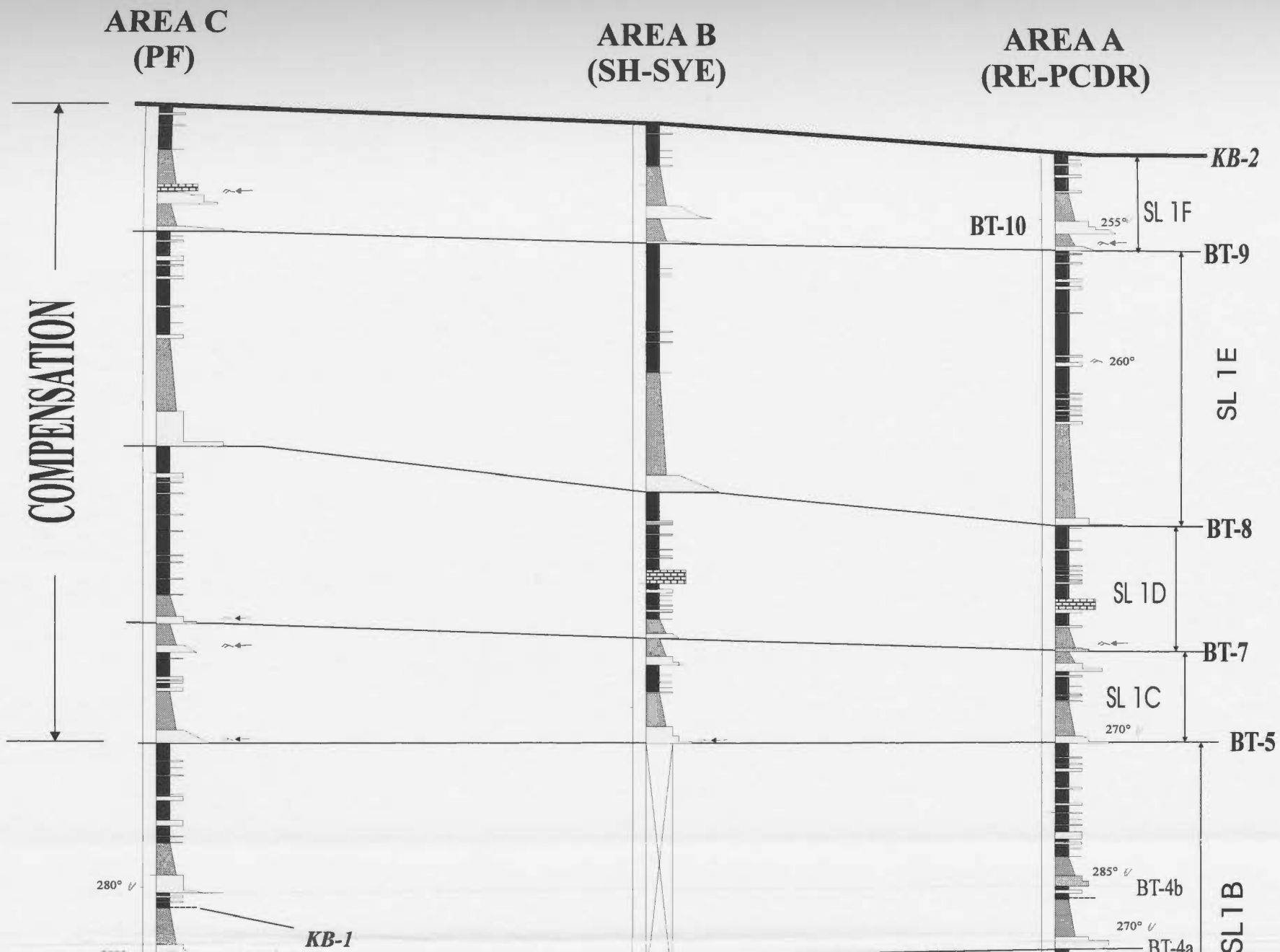
Table 5.2. Percentages of each facies class in the composite sections for each of the time slices. Slice 4 is divided into two sub-slices. The total thickness (TOT. THK) for each slice includes carbonate layers and covered intervals (C.INT). There are no covered intervals in composite sections PF and RE-PCDR. In time-slice 7 in PF, 12.5m were added to the thickness of the slice because some of the rocks in this slice were removed by faulting. SL1-2 is the data for the upper part of time-slice 1 (mini-slices SL 1C to SL 1F) because parts of mini-slices SL 1A and SL 1B are covered at composite section SH-SYE. Time-slices 4 and 6 are divided into sub-slices 4-1, 4-2 and 6-1, 6-2.

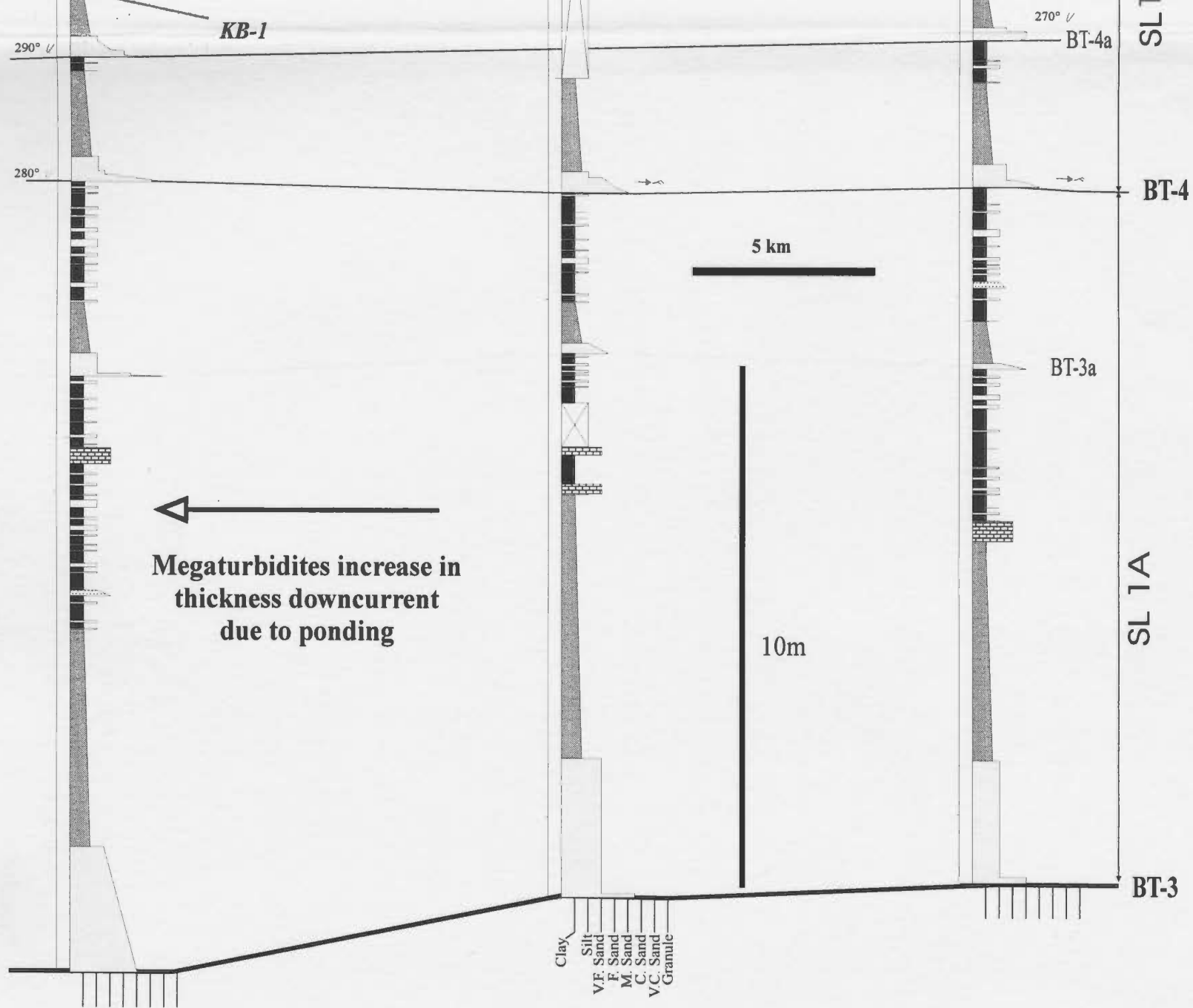
	COMPOSITE SECTIONS																
	PF						SYE-SH						RE-PCDR				
Time-slice/ Sub-slice	TOT. THK. (m)	C. INT (M)	B%	C%	D%	E%	TOT. THK. (m)	C. INT (m)	B%	C%	D%	E%	TOT. THK. (m)	B%	C%	D%	E%
SL 7	87.2	12.5	1.8	22.4	19.7	56.1	104.4	0	6.9	20.7	15.8	56.6	0	0	0	0	0
6-2	77.27	0	0	14.7	16.9	68.4	103.1	0.56	4.0	15.7	25.3	57.3	0	0	0	0	0
6-1	65.75	0	0.4	10.6	16.5	72.5	97.13	0	2.7	12.7	17.8	64.7	89.7	7.6	21.1	12.8	58.5
SL 5	43.0	0	0	12.5	14.8	72.7	41.5	0	0	10.2	11.1	78.7	38.7	1.4	9	26.6	63
4-2	73.7	0	0	10.5	17.7	71.8	77.2	0	0	8.9	18.9	72.2	80.1	2	11.6	19.2	67.2
4-1	58.5	0	0	9.0	14.8	76.2	57.4	0	0.5	14.2	20.2	65.1	55.9	0.8	17.5	13.7	68
SL 3	74.5	0	0	11.4	10.8	77.8	75.8	0	0	8.5	19.4	72.1	65.3	0	7.2	20.5	72.3
SL 2	57.8	0	0	11.6	9.7	78.7	64.2	0	0	11.5	6.1	82.4	58.6	0	6.4	13.4	80.2
SL 1	36.14	0	0	17.1	7.6	75.3	32.9	5.1	0	16.8	3.0	80.2	32.7	0	13.7	7.2	79.1

Key for the terms, symbols and patterns used in the correlation diagrams. The codes for facies C2.1 are not presented on these figures because they are numerous, so all non-coded sandstone beds are facies C2.1 beds.



**Figure 5.2. CORRELATED TIME SLICE 1**





examine the external architecture and facies relationships of mini-slices SL 1A and SL 1B.

The internal architecture and short-distance facies relationships for all mini-slices are investigated only in area A using sections FP1 and RE. Facies thicknesses and the number of beds for each facies and subfacies in mini-slices SL 1A and SL 1B in area A and area C are presented in Figure 5.3, while those for mini-slices SL 1C through SL1 F in the composite sections measured in areas A, B and C are presented in Figure 5.4.

Thicknesses and number of beds for some facies and subfacies that occur infrequently are not presented graphically; instead, these are available in Table CD-T1. Some facies and subfacies bed numbers are presented in pie graphs, which illustrate the variation in bed numbers for the mini-slices. Data for section FP1 is also summarised using pie graphs.

Shale comprises about ~80% of the thickness of time-slice 1. Sandstone and siltstone beds constitute considerably less (Table 5.2). Eleven megaturbidites (facies 2.4 and 2.5) with their thick mud caps (shale beds of Class E) are present in areas A and C.

Most of the sandstone beds of facies C2.4 show an increase in thickness from east to west. The most pronounced decrease in thickness is in area A. The lower parts of bed 8-PF and 3a-PF (facies C2.4) show a more pronounced increase in thickness. These two beds change from facies C2.5 in area C to facies C2.4 in areas B and A.

Sandstone beds of other facies are less common or absent in time-slice 1. Siltstone beds of facies D2.1 are more numerous in areas A and C in time-slice 1. In area B, siltstone beds of facies D2.2 and D2.3 are present in most of the time-slices. Siltstone beds assigned to different subfacies vary in numbers between the three areas (Figure 5.5).

Figure 5.3. Comparison of the facies thicknesses and number of beds for mini-slices SL 1A and SL 1B in the east (area A, composite section RE-PCDR), and west (area C, composite section PF). The total thickness and number of beds of mini-slice SL 1A increase from east to west. The number of beds of SL 1B decreases from east to west. Total thicknesses of facies classes increase from east to west due to ponding in a downflow direction (to the west). Siltstone subfacies D2.1A, D2.1B and D2.1D show a general decrease in total thickness and bed numbers from east to west while the other siltstone subfacies show an opposite trend. These mini-slices are shown in Figure 5.2 displaying the detailed correlation of time-slice 1.

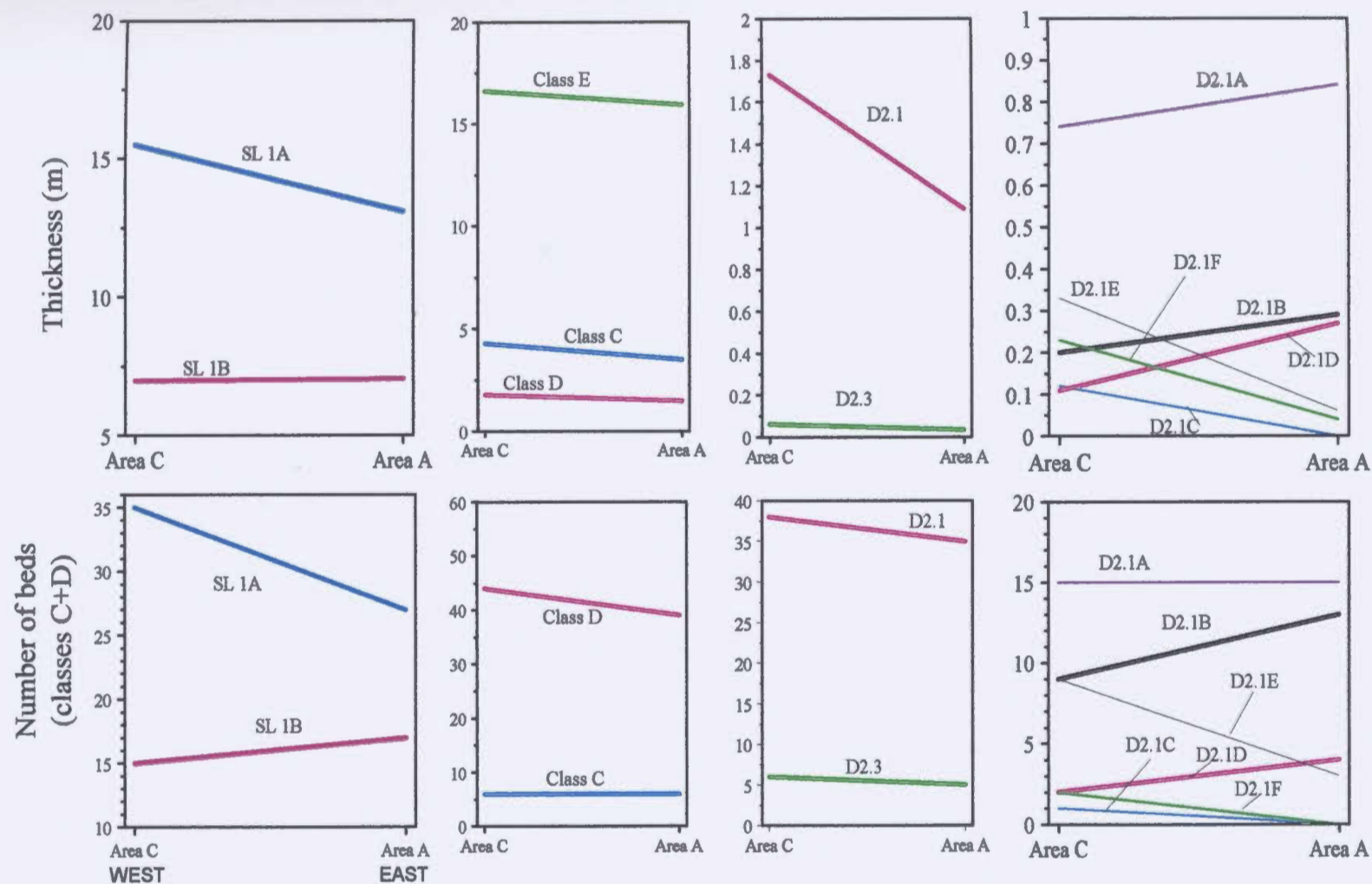
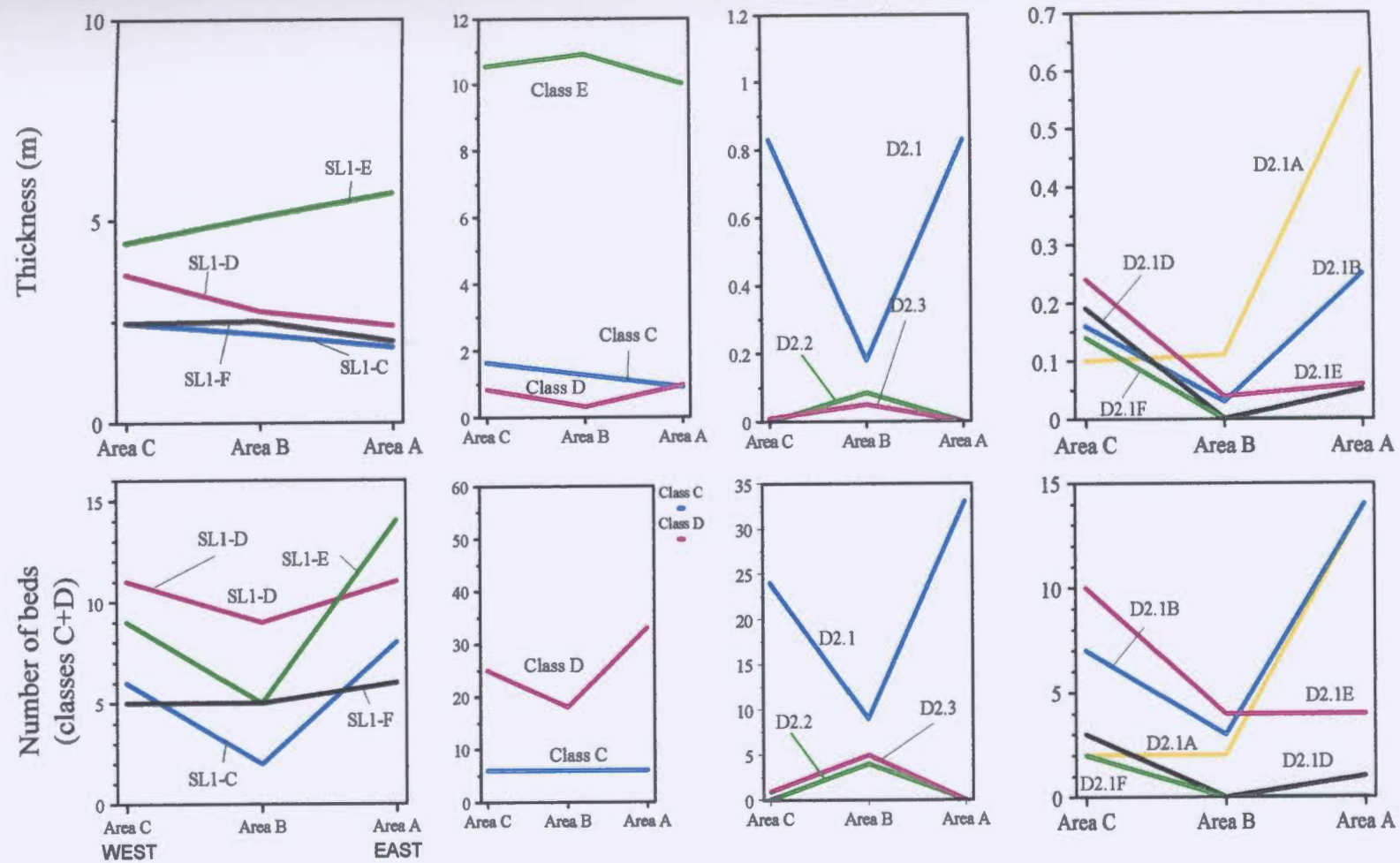




Figure 5.4. Comparison of the facies thicknesses and number of beds for mini-slices SL 1C through SL 1F in the east (area A), middle (area B) and west (area C). All the mini-slices except SL 1 E increase in thickness from east to west. There are less beds in the middle part of the area (area B). Class D beds have a greater total thickness and number of beds in area A and C. These mini-slices are shown in Figure 5.2.



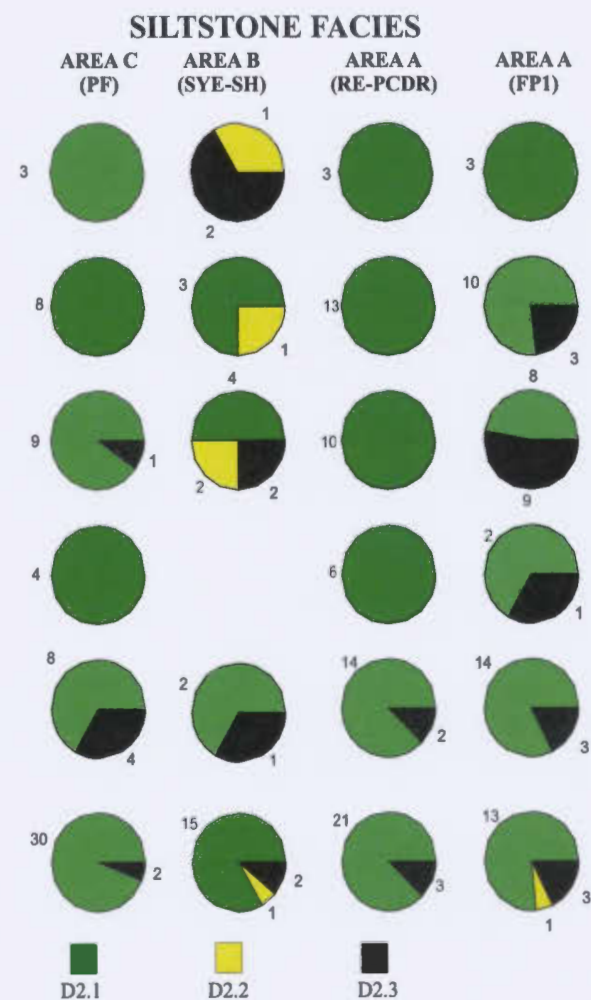
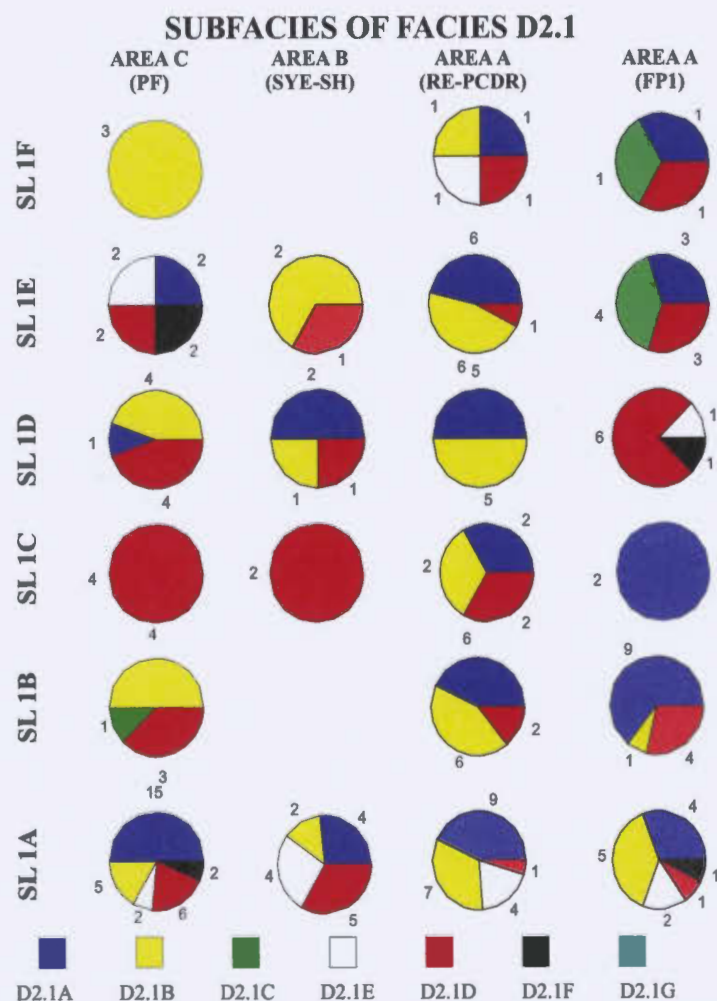


Figure 5.5. The number of siltstone beds assigned to different facies and subfacies in the mini-slices of time-slice 1 in areas A, B and C. Also included is the data from section FP1 for short distance correlation between sections RE and FP1 in area A. The number of beds and laminae assigned to each facies and subfacies is presented on each pie diagram.



Mini-slices SL 1A and SL 1B show no significant variation in thickness between areas A, B and C (Table A5-4.1). Mini-slices SL 1C, SL 1D and SL 1F increase in thickness towards the west while SL 1E decreases in thickness towards the west.

Short distance correlations (over a distance of ~1km) between sections FP1 and RE show that mini-slices SL 1C through SL 1F vary in thickness by tens of centimetres (Figure 5.6). Some of these mini-slices also show alternating thickness variations: if mini-slice thickness increases in one direction, then the overlying mini-slice increases in thickness in the opposite direction. This geometry is akin to the “compensation cycles” of Mutti and Sonnino (1981).

Facies C2.4 (lower parts of megaturbidites) show a slight variation in thickness between section FP1 and RE. Direct comparison of the thickness variations of correlated beds indicates that some beds in section RE are thicker by 5-10 cm than equivalent beds in section FP1. Basal grain size is slightly coarser for most of the beds of facies C2.4 in section RE than in section FP1.

Five beds assigned to other sandstone facies occur in time-slice 1 (Table CD-T1). Most of these beds occur in section FP1, area A. There is apparently the same number of siltstone beds and laminae in section RE (73 beds and laminae) and section FP1 (70). Beds of facies D2.1 are the most common. Beds of facies D2.2 are only present in section FP1 while beds of facies D2.3 are more numerous in section FP1 compared to section RE. Variations also occur in the proportion of siltstone beds assigned to subfacies between these two sections (Figure 5.5).

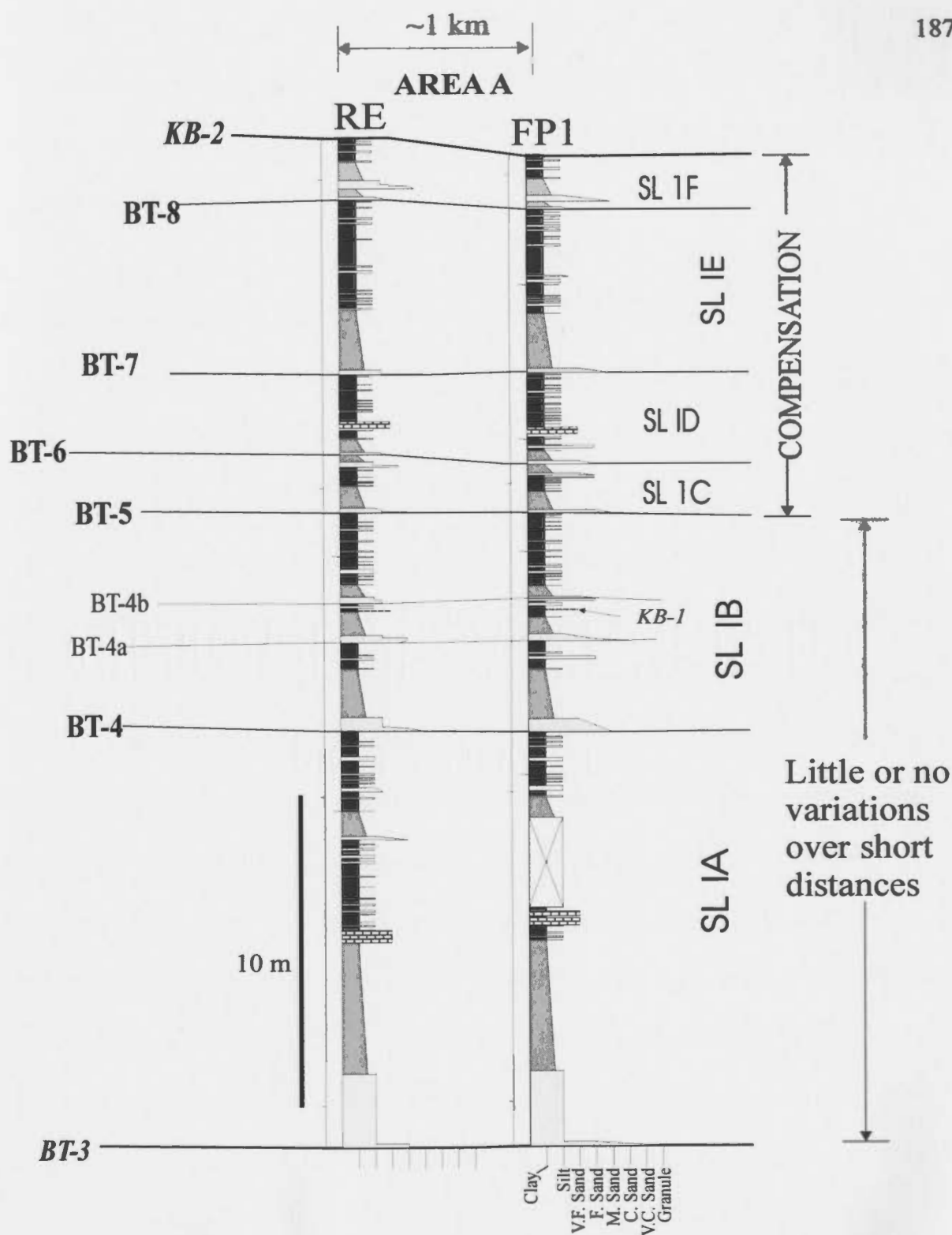


Figure 5.6. Detailed short distance correlation of time-slice 1 between sections FP1 and RE, separated by ~1000 m.

Only a few palaeocurrent measurements could be gleaned from the beds in this mini-slice, many of which were measured from flutes on megaturbidites. The main flow direction determined is shown in Figure 5.2.

#### 5.4.2. Interpretation of Time-slice 1

Time-slice 1 is dominated by shale, a large proportion as thick megaturbidites caps. Such megaturbidites (megaturbidite element) are interpreted from both modern deep-sea settings and ancient turbidites as basin-plain deposits of confined basins (Rothwell *et al.*, 1992; Mutti *et al.*, 1999). It is likely these megaturbidites originated from large slope failures that evolved into thick turbidity currents. The variation in thickness in successive time-slices, such as SL 1D and SL 1E, is interpreted to be due to compensation effects whereby a slight shift in the site of turbidity current deposition was a result of the variable relief on the sea bed created by the underlying mini-slice (Rothwell *et al.*, 1992). The increase in thickness of the megaturbidites from east to west suggests, they may have originated in the east and were forced to pond and fill deeper topography to the west (Ricci Lucchi, 1975; Rothwell *et al.*, 1992). The variation in sea bed-relief may have been caused by tectonic factors such as differential movement along buried faults (*cf.* Mutti *et al.*, 1978; Thornburg and Kulm, 1987; Miall, 1995). The relief may have been later flattened or smoothed by deposition of other megaturbidites (Pilkey, 1988).

The presence of a megaturbidite directly overlying another megaturbidite (e.g., BT-6 and BT-7, or BT-9 and BT-10) with no different facies or beds in between suggests

two successive failures (e.g. retrogressive failures).

Some megaturbidites, such as BT-4 and BT-10, show little change in the thickness of the lower part of the bed (facies C2.4). These beds have similar basal grain size suggesting that over a distance of more than 25 km, flow conditions varied little. Rothwell *et al.* (1992) recognised a downflow (proximal to distal) change in the sequence of sedimentary structures of the megaturbidites of the Madeira Abyssal Plain where beds that start with Bouma (1962)  $T_a$ ,  $T_b$  and  $T_c$  divisions in the upcurrent (proximal) areas show progressive base-cutout sequences in the distal areas over a distance of hundreds of kilometres. The lack of a proximal to distal change in the sequence of sedimentary structures in some of the thicker megaturbidites in time-slice 1 may be due to the short distance between the three area (~25 km) compared to the hundreds of kilometres in the Madeira Abyssal Plain. Mutti (1977) suggested that regularity of deposit thickness grain size is indicative of the flat sea bed characteristic of basin-plain settings. Thinner beds of facies C2.4 show more variability in the sequence of sedimentary structures and grain size between the sections. Small flows presumably are more affected by slight variations in bottom topography (Mutti *et al.*, 1978).

The observed facies change from facies C2.5 to C.4 in BT-3a and BT-8 is difficult to explain because no palaeocurrent indicators were observed in beds of facies C2.5. Beds 3a-PF (bed BT-3a at section PF) and 8-PF (facies C2.5) are structureless and have flat or wavy bases. Bed 3a-SH and 3a-RE (facies C2.4) have ripple laminations and climbing ripples in the middle parts indicating flow from west to east. Beds 8-SH and 8-RE (facies

2.4) have wavy laminations and no sole marks. If the flows from which these beds were deposited were travelling from west to east throughout deposition, then facies C2.5 changed to facies C2.4 in a downcurrent direction. It is suggested here that beds of facies C2.5 represent deposits of a transitional phase between a slump consisting of a mixture of sand, silt and mud, and a mature turbidity current characterised by good grain segregation (Walker, 1965). As the mixture of sand, silt and mud moves downflow it may increase in speed and incorporate water that will result in better mixing of the sediment and better size segregation of the grains. If this mixture is deposited before a critical degree of grain segregation develops, it will consist of poorly sorted deposit, similar to the majority of the beds of facies C2.5.

Most of the shale in time-slice 1 is interpreted to have been deposited from turbidity currents (Chapter 3), although part of this shale may have a hemipelagic origin. Some of the turbidite mud may have been deposited from flows similar to those that deposited the megaturbidites, but any coarser fractions must have been deposited elsewhere (*cf.* Rothwell *et al.*, 1992).

Siltstone beds are more prevalent compared to sandstone beds, particularly in areas A and C, however, they were not correlated between the sections. Siltstone facies in areas A and C show more similarity to each other than to siltstone facies in area B. The very thin beds and laminae of facies D2.3 that are more numerous in area B are interpreted as deposits from low density turbidity currents (Chapter 3). Beds of facies D2.2 are also interpreted as deposits of low concentration flows that were subsequently deformed by

loading to form isolated lenses of siltstone within shale. Siltstone beds of facies D2.1 are interpreted to have been deposited from low density turbidite currents that most likely had a higher sediment concentration than the flows that deposited beds of facies D2.2 and D2.3. The greater proportion of beds of facies D2.2 and D2.3 in area B (Figure 5.5) suggests that flows reaching this area were characterised by low sediment concentration.

Siltstone subfacies are also different between the areas A, B and C. Siltstones beds in area B are thin and consist dominantly of subfacies D2.1B (isolated “starved” ripples) and laminae and thin beds of subfacies D2.1E. Siltstone beds and laminae in area B also indicate deposition from flows characterised by low sediment concentration. Subfacies D2.1A is more numerous in areas A and C, where beds of subfacies D2.1A, consisting of climbing ripple laminated siltstone, are interpreted as deposits from flows in which rapid deposition of sediments from suspension was enhanced. Decrease in the number of beds of facies D2.1A between area A and C (Table CD-T1) suggests that flows that deposit climbing ripples do not travel long distances perhaps because most of the load settles from suspension before reaching the distal regions of the basin. Facies D2.1A probably changes to other siltstone facies downcurrent.

The difference in the proportion of siltstone facies and subfacies between areas A, B and C may reflect the different locations of areas A, B and C with respect to the paths of the depositing currents. Decrease in the number of siltstone beds in area B is interpreted to indicate that area B was located in a position marginal to the axes of flows depositing the siltstone beds, whilst areas A and C were located closer to the main paths of the flows.

Variation in bottom topography was most likely to be the strongest control on flow path direction. Low concentration flows are suggested to be more sensitive to slight bottom irregularities compared to the more concentrated and larger flows that deposited the megaturbidites (Mutti *et al.*, 1999). The change in the siltstone subfacies between areas A and C may represent downcurrent (i.e., proximal to distal) trends. In mini-slice SL 1A, there are more siltstone beds at area C than at both areas B and A. This may suggest that some flows that deposited siltstone beds in area C did not deposit sediment (bypassed) in areas A and B. This may also suggest that some beds in area C were deposited from flows that originated or were supplied from a source located between the two areas.

Alternatively, the greater number of beds in area C compared to areas A and B and their greater thickness suggests that area C was located closer to the main path of the flows that deposited these beds compared to area A, which was in a marginal location to the main path of the flow.

The internal architecture of time-slice 1 is similar to the external architecture, in that mini-slices show compensation cycles that are also interpreted to reflect bottom topography. Facies and subfacies vary between sections FP1 and RE. Some of the megaturbidites have thinner lower parts at FP1 compared to the same beds at RE. It is interpreted that these variations reflect slight variation in bottom topography between the area of section FP1 and the area of section RE. The area of section FP1 may have been located on a subtle topographic high. The flows that deposit megaturbidites are large and spread over large areas; a variation in megaturbidite thickness over distances of 1-2 km in

modern settings usually occurs in areas where bottom topography is irregular (*cf.* Rothwell *et al.*, 1992). The decrease in thickness and numbers of siltstone beds and laminae from section FP1 to RE may reflect downcurrent changes in the flow, prompted by variations in the bottom topography.

In summary, time-slice 1 consists of the deposits of large turbidity currents (megaturbidites) and shale also deposited by turbidity currents. Deposition was most likely in a basin-plain setting characterised by subtle bottom irregularities that controlled the thickness of the megaturbidite deposits (Hiscott *et al.*, 1986). Bottom topography may have been the result of movement along buried faults below the basin fill. No faults that might have been active during the deposition of time-slice 1 were observed in the field. However, syn-depositional fault movements have been proposed in similar tectonically active basins including deep sea trenches and foreland basins (Thonburg and Kulm, 1987; Miall, 1995).

Sandstone and siltstone beds are few in time-slice 1, implying that any source for sand-load turbidity currents was located far from the study area. Alternatively, the sediment source may have contributed mostly fine-grained material. Thickness and facies variations in the area are believed to result from the location of sections relative to axial flow paths. These paths were probably controlled by the bottom topography. The flows from which the megaturbidites were deposited were initiated as a result of large sediment failures that occurred mostly east of the thesis area.

The only architectural element observed in time-slice 1 is the megaturbidite



element that is characterised by more-or-less tabular two-dimensional geometry. These megaturbidites thicken in a westerly direction due to ponding of the flows in the west. Using the Pickering *et al.* (1995) architectural element scheme, these megaturbidites may be classified as smooth sheets or isolated (low-relief) mounds that are bounded by 0<sup>th</sup> order bounding surfaces (base of the lower coarse part of the beds and the top of the cap).

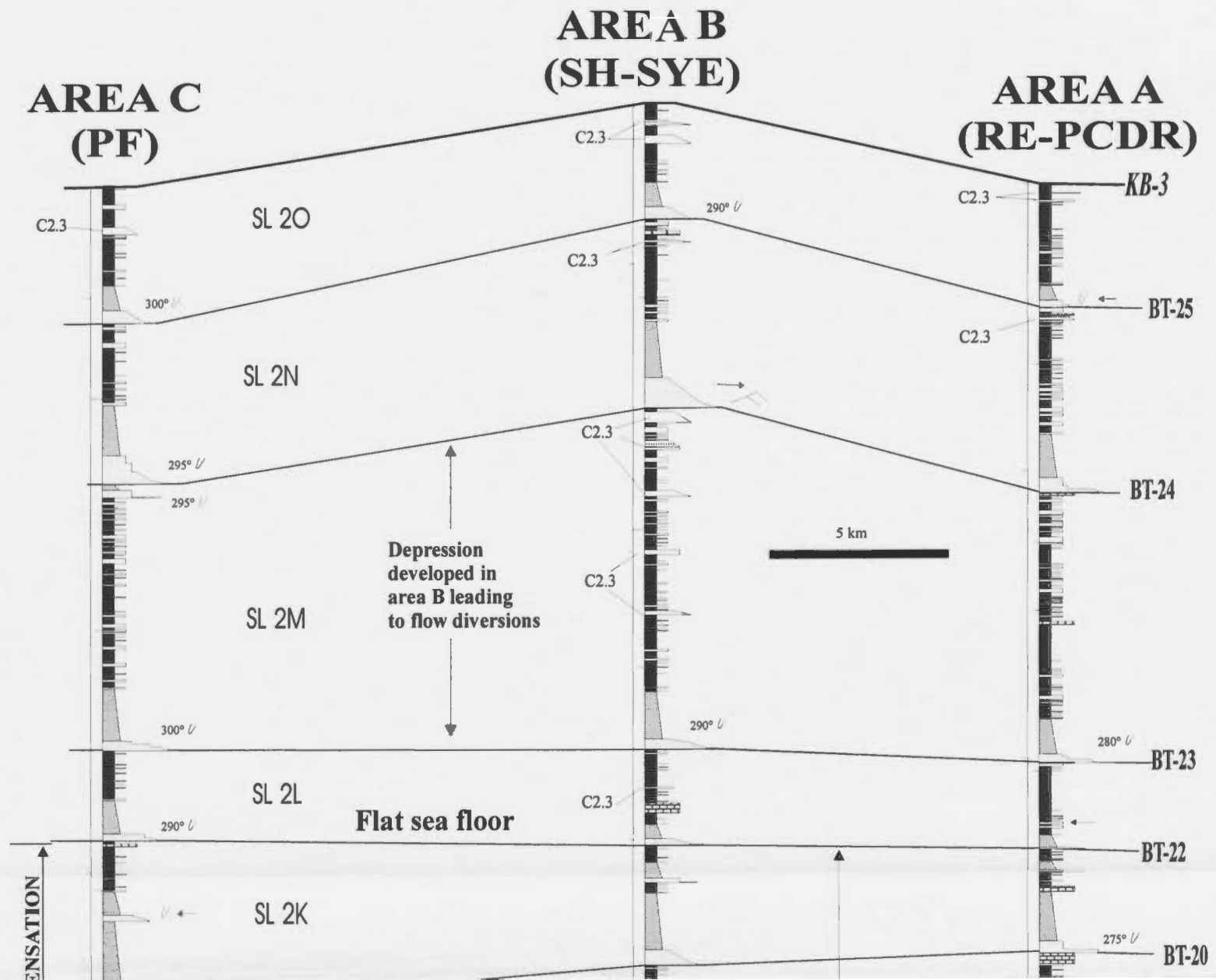
There is no evidence for significant differences in the degree of bed compaction in the three areas. Neither do the sediments in time-slice 1 show significant variations in the thickness of beds and mini-slices due to folding.

#### **5.4.3. Description of Time-slice 2**

Time-slice 2 is almost twice as thick as time-slice 1 (Table 5.2), and is well exposed in areas A, B and C. It is bounded by KB-2 at the base and KB-3 at the top (Figure 5.7). Shale comprises approximately 80% of the time-slice thickness. The total thickness of sandstone and siltstone varies from area to area. At area A, the total thickness of siltstone is greater than the total thickness of sandstone. This is different than in areas B and C where the reverse occurs and the total sandstone thickness is greater (Table 5.2).

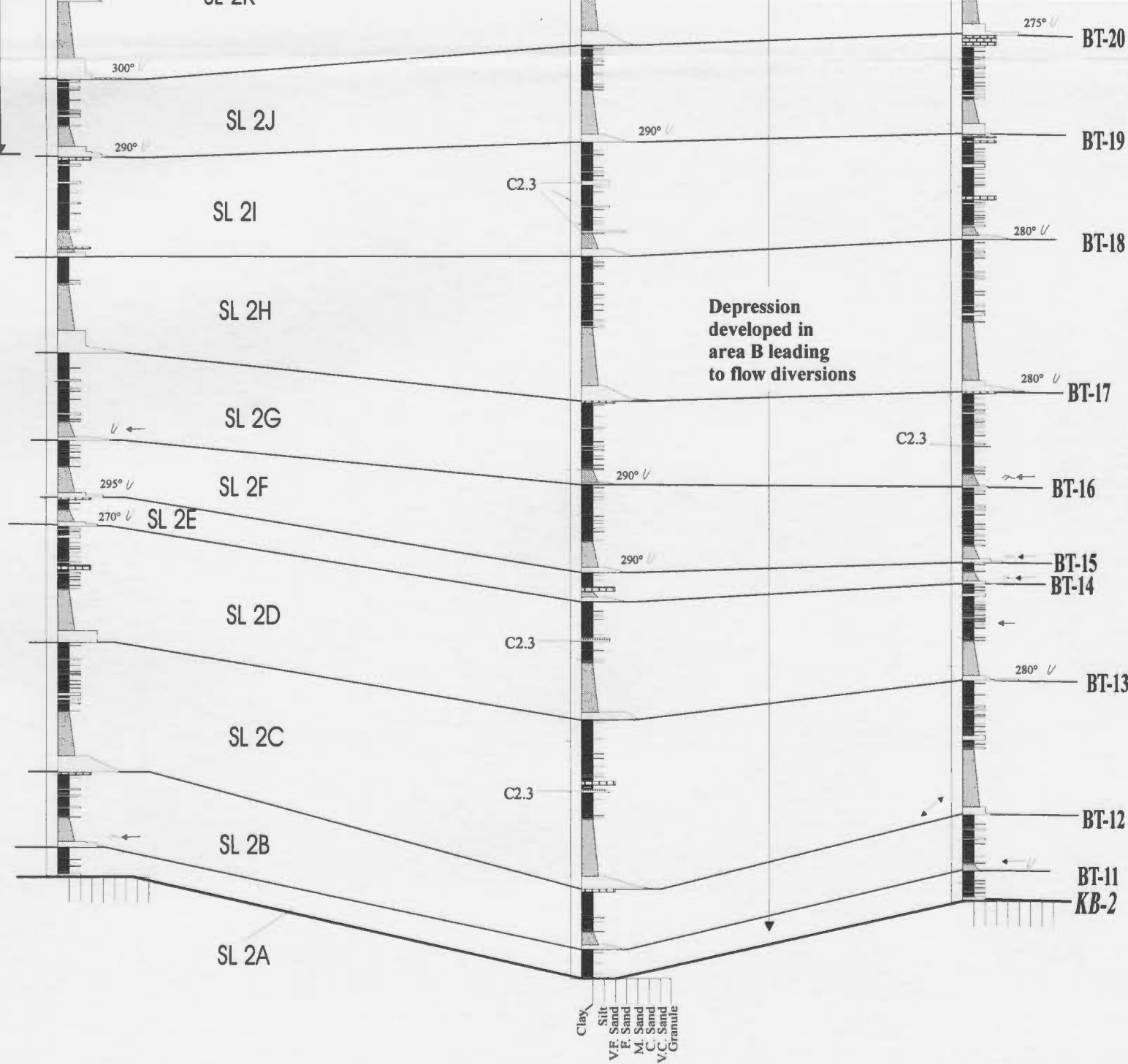
Based on megaturbidite correlations, this time-slice is divided into 15 mini-slices (numbered SL 2A through SL 2O), which show different thicknesses at different locations (Figure 5.7). In area B, several mini-slices are significantly thicker (+10-20%) than their mean thickness (Table A5-4.1), whereas in areas A and C some mini-slices are significantly thinner (-11 to -21%) than their mean thickness. Furthermore, some mini-

**Figure 5.7. CORRELATED TIME-SLICE 2**



10m

COMPENSAT



slices show alternating thickness variations resulting in an alternating thinning and thickening in one direction. Mini-slices SL 2G and SL 2L show little or no thickness variation between areas A, B and C but the mini-slices SL 2H through SL 2K, that occur between mini-slices SL 2G and SL 2L show variation in thickness in the three areas.

Sandstone and siltstone bed numbers and facies/subfacies thicknesses vary in different areas. Variation in the number of beds in each mini-slice in the three areas is presented in Table CD-T2 and Figure 5.8. The number of sandstone beds in time-slice 2 increases from area A to area B but then decreases westward. There is an increase in the number of sandstone beds of facies C2.3 in area B in mini-slice SL 2M. Sandstone beds of facies C2.1 and C2.2 occur only in section FP1 in area A (Table CD-T2).

Fifteen megaturbidites occur in time-slice 2 in areas A and B. A sandstone bed below 24-PF in area C was designated as a megaturbidite (23a-PF). This bed was not recognised as a megaturbidite in the other sections because of the lack of a thick mud cap, which may have been eroded in areas A and B. The lower parts of megaturbidite BT-12 and BT-13 change from facies C2.5 in area C to facies C2.4 in areas A and B.

Megaturbidites increase in thickness from east to west (Table A5-4.2), some of which increase in thickness by as much as 70% in area C (relative to their mean thickness). Megaturbidites in area A are significantly thinner (11-50% less than the mean). These variations in thickness of megaturbidites from east to west also holds for the lower coarse parts of most megaturbidites. Exceptions are the lower coarser part of BT-13, which does not change significantly in thickness from east to west and the lower coarser part of bed

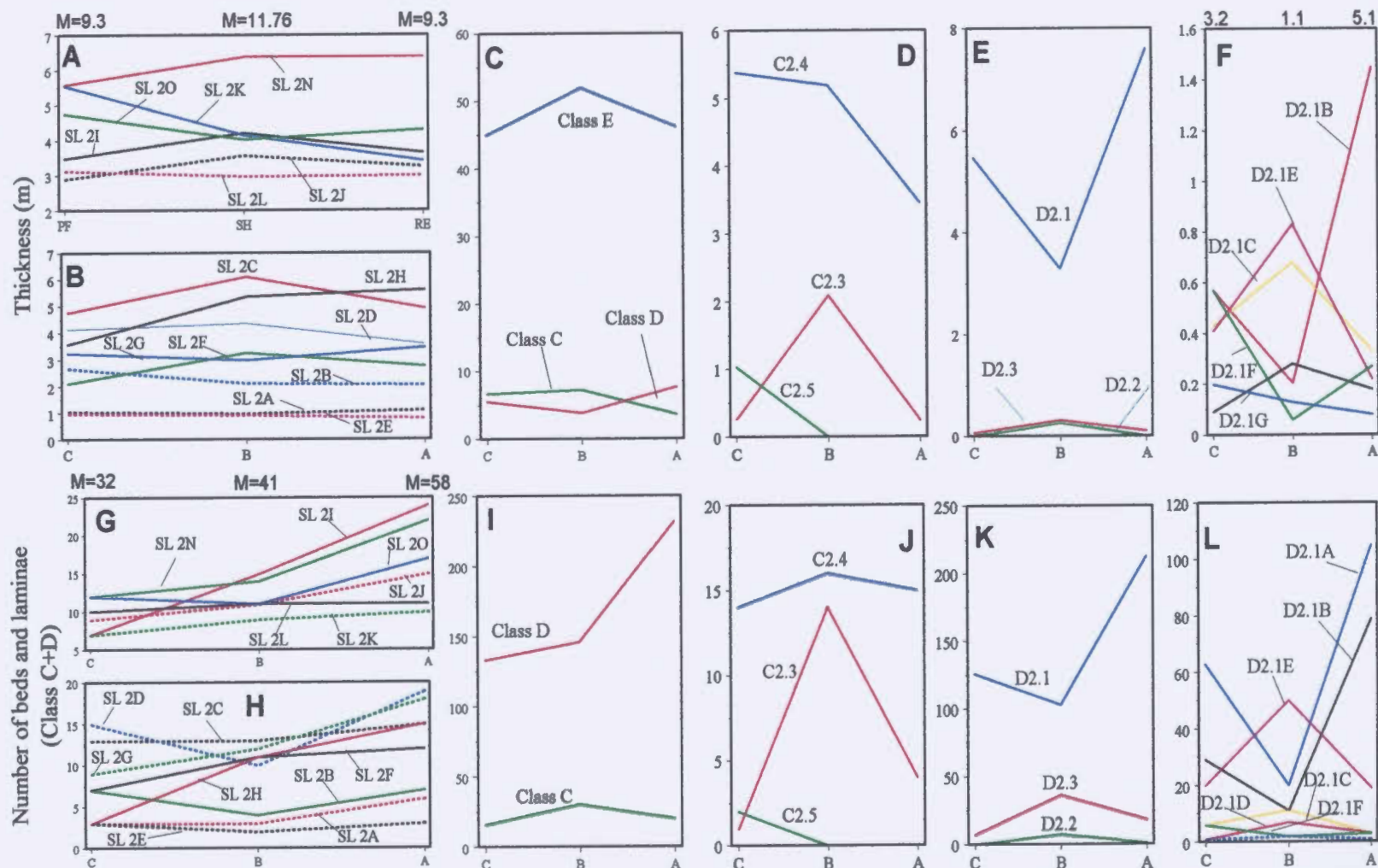


Figure 5.8. Comparison of the facies thickness and number of beds for time-slice 2 in the three areas of composite sections. A and B are the plots of the thickness of the mini-slices (values above A are for the thickness of mini-slice SL 2M in the three areas). C, E, and F are for the total thickness of facies and subfacies in time-slice 2. The numbers above F are the thickness of subfacies D2.1A. G and H are the total numbers of beds and laminae in the mini-slices (values above G are the numbers for mini-slice M). I, J, K and L are for the numbers of beds and laminae in time-slice 2.

BT-18 which is thicker in area B than in areas A and C.

A general westward decrease in the number of siltstone beds characterises most mini-slices. The number of siltstone beds assigned to facies D2.3 is greater in area B than in areas A and C. This tendency is maintained for both the entire time-slice and most of the mini-slices. In areas A and C, most of the siltstone beds are of facies D2.1 while beds of facies D2.3 are less common. Facies D2.2 are rare or absent in most mini-slices. In mini-slice SL 2M, more siltstone beds occur in areas B and C than area A. The siltstone facies and subfacies also vary in number and type in mini-slice SL 2M.

Siltstone beds assigned to different subfacies also show variations between the three areas (Figure 5.9). In general, there are more beds assigned to subfacies D2.1A in area A than in areas B and C, although area B has considerably fewer beds assigned to subfacies D2.1A. Beds assigned to subfacies D2.1E are more numerous in area B than in areas A and C (Figure 5.9).

For the short-distance correlations, mini-slices show variations in total thickness, and also in the thickness and numbers of component facies and subfacies between sections FP1 and RE (Table CD-T2, Figures 5.9, 5.10). Sandstone beds of facies C2.1, C2.2 and C2.3 are more common in section FP1 than in section RE where only a few beds of facies C2.3 are present (Table CD-T2). In section FP1, three sandstone beds of facies C2.3 are present in mini-slice SL 2O and three beds of facies C2.2 are present in mini-slices SL 2L (1 bed) and SL 2M (2 beds). Mini-slices SL 2I, SL 2J, SL 2M, and SL 2N have two or more sandstone beds of facies C2.3. Other mini-slices have a single bed or do not have any



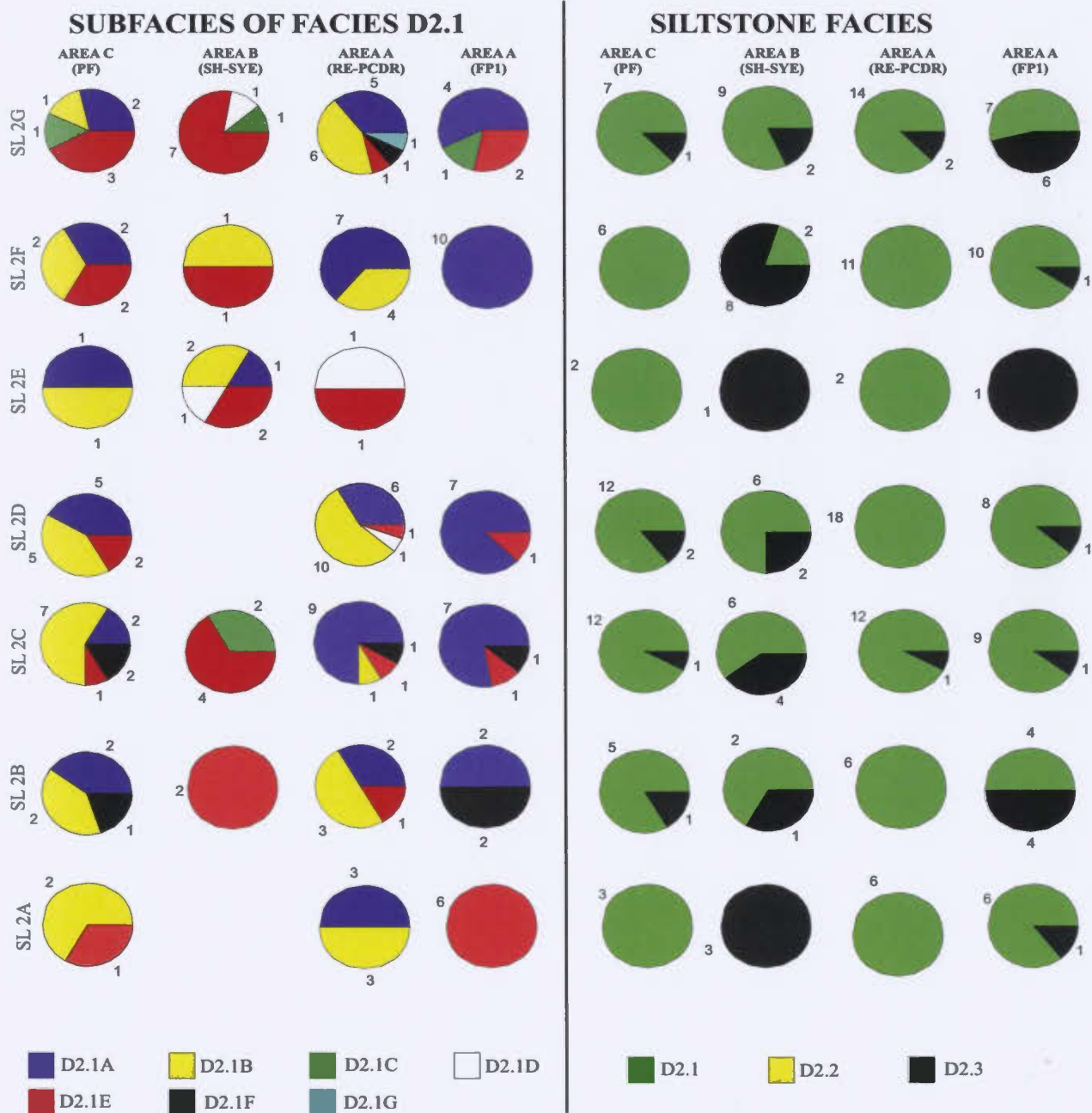
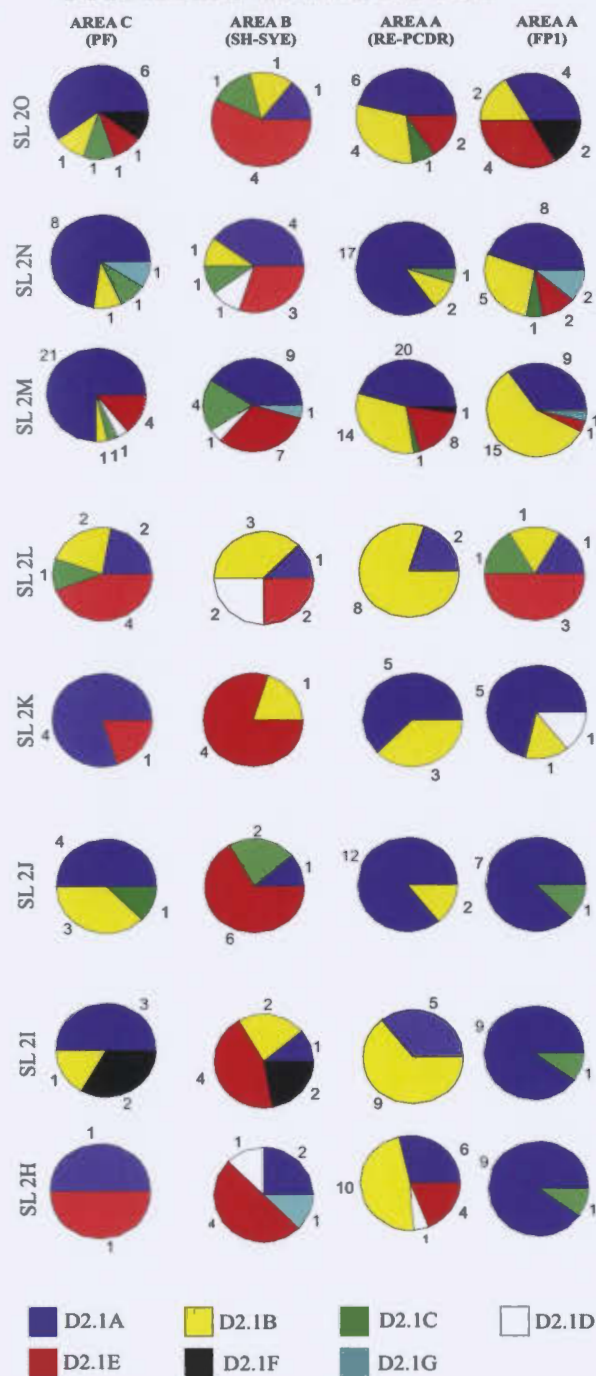


Figure 5.9. The number of siltstone beds and laminae assigned to different facies and subfacies in the mini-slices of time-slice 2 in areas A, B and C. Also included is the data from section FP1 for short distance correlation between sections RE and FP1 in area A. The number of beds and laminae assigned to each facies and subfacies is shown on the pie diagrams.

## SUBFACIES OF FACIES D2.1



## SILTSTONE FACIES

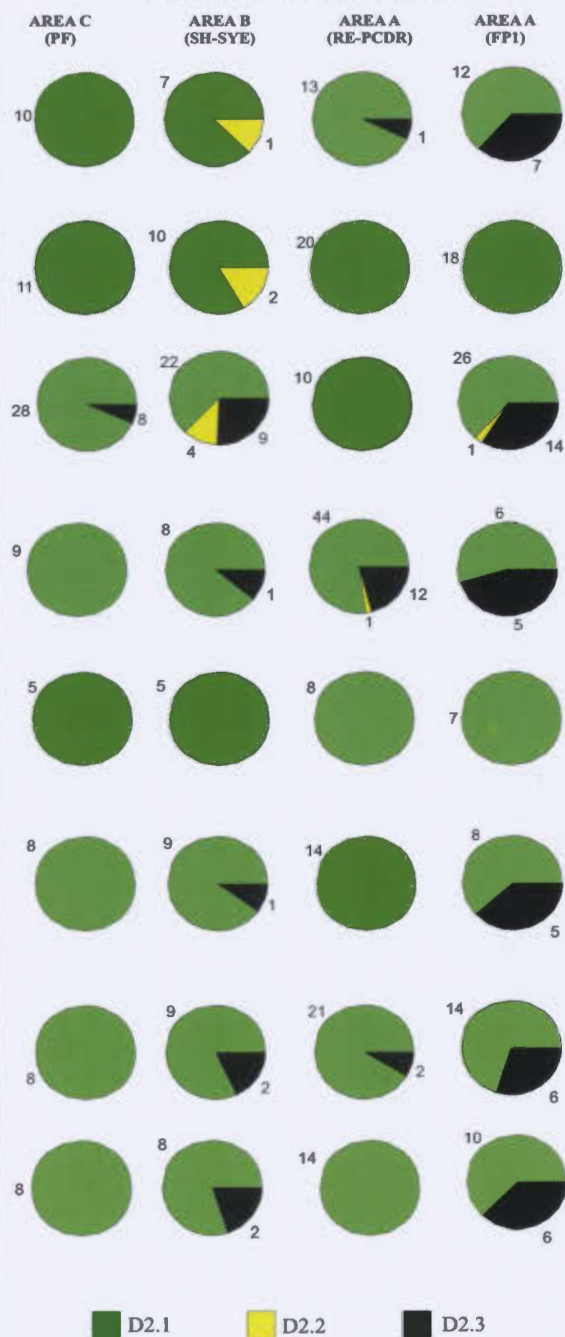
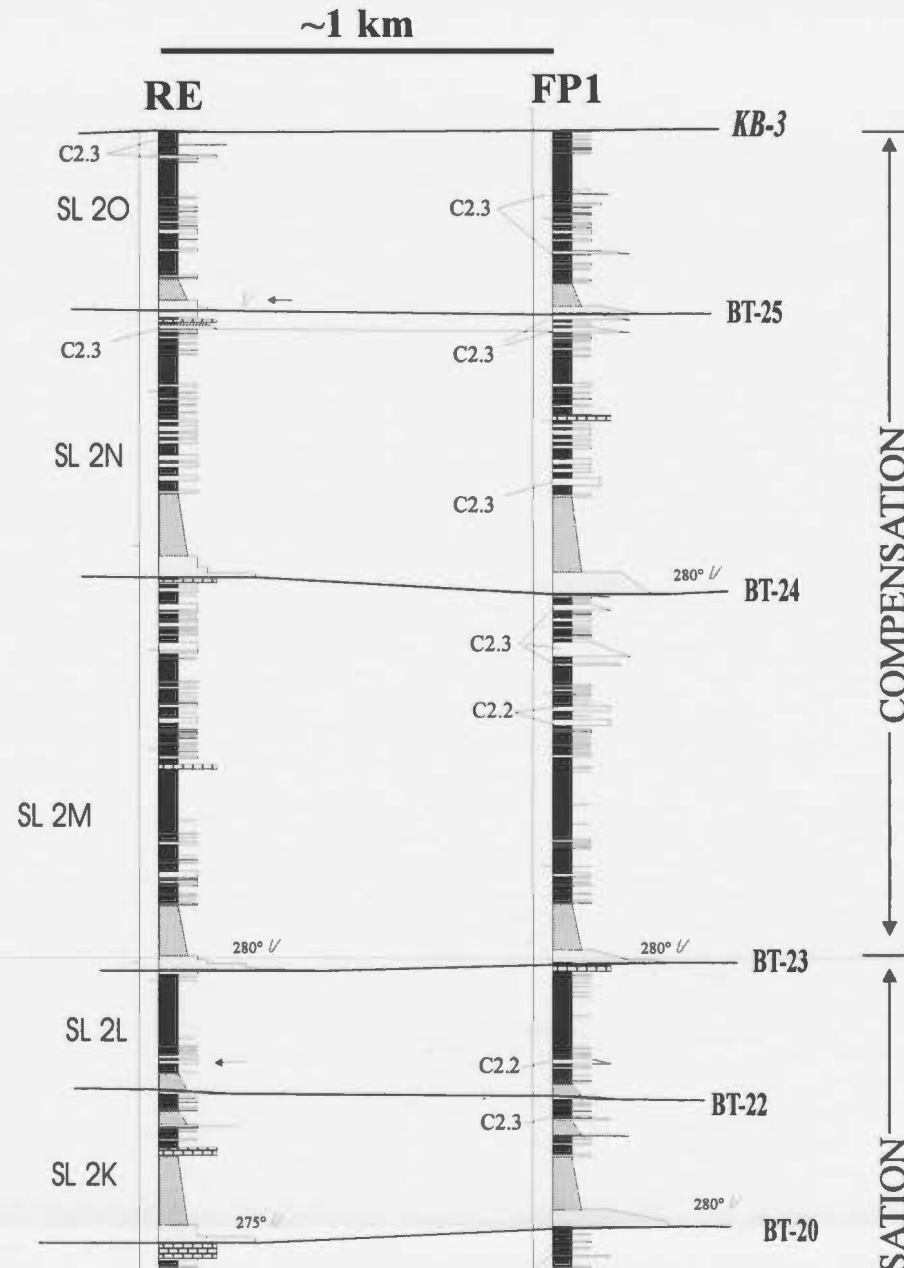
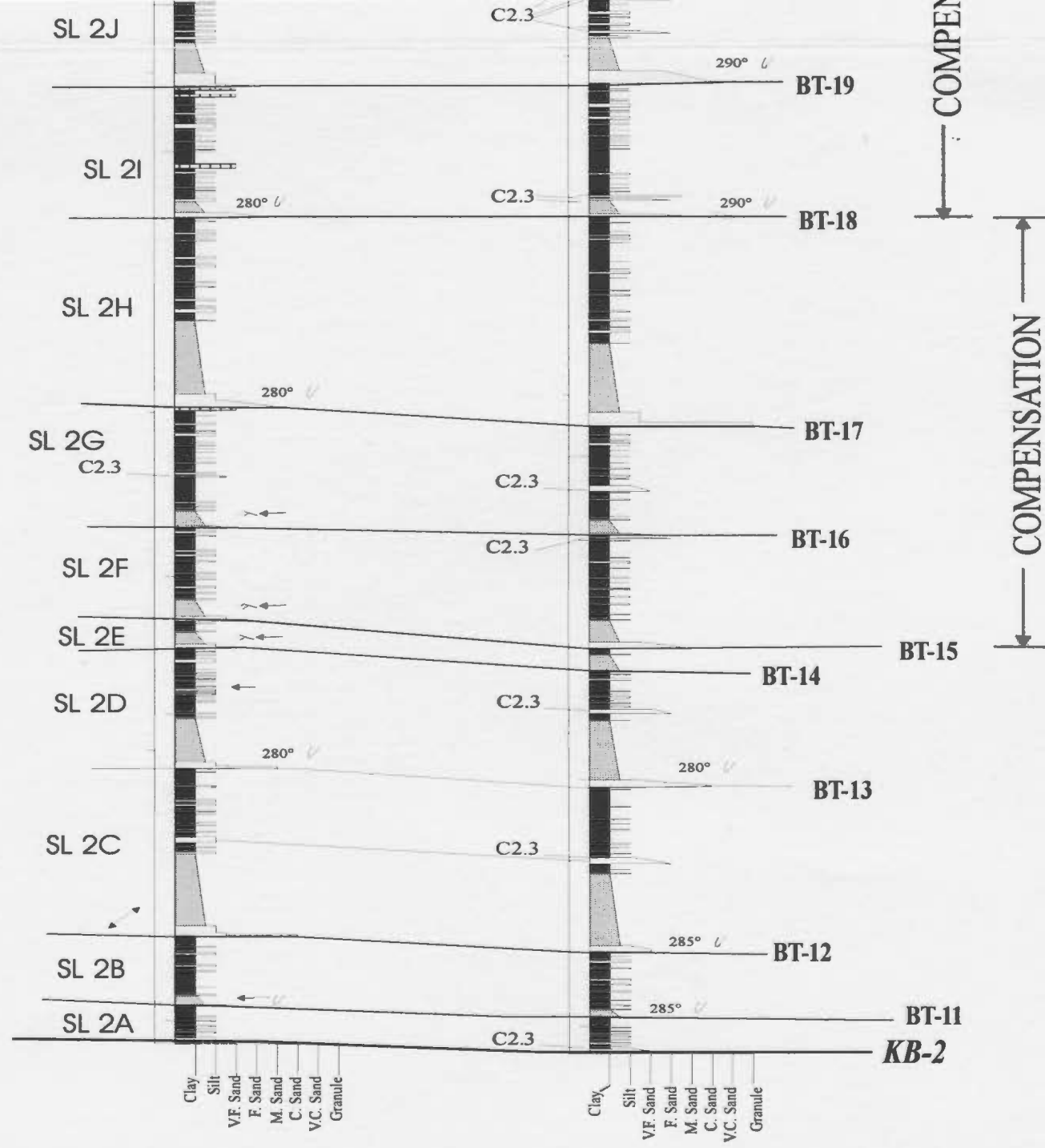


Figure 5.9. Continued.



**Figure 5.10. Short distance correlation of time-slice 2**





sandstone beds assigned to facies C2.3. At RE, only four beds of facies C2.3 are present (2 in mini-slice SL 2O, 1 in SL 2N and 1 in SL 2G). Individual beds could not be correlated between section FP1 and section RE.

Siltstone beds are only slightly more frequent in section RE (232 beds and laminae) than in section FP (204 beds and laminae). For most of the mini-slices, beds of facies D2.1 are more numerous in section RE than in section FP1 while beds of facies D2.2 are more numerous in section FP1. Siltstone subfacies show slight variation between sections FP1 and RE. These variations occur mostly in subfacies D2.1A, D2.1B and D2.1E (Figure 5.9). Other subfacies are rare or absent.

#### **5.4.4. Interpretation of Time-slice 2**

Depositional processes occurring during time-slice 2 were dominated by the accumulation of megaturbidites from large flows and thin siltstone beds and laminae from low density currents. Although similar to the depositional processes during time-slice 1, some mini-slices within time-slice 2 show pronounced thickness variations (Figure 5.7). In area B, some mini-slices increase in thickness significantly (Table A5-4.1). This is interpreted to be the result of deposition into a depression (*cf.* Ricci Lucchi and Valmori, 1980, Pickering and Hilton, 1998) which is most likely due to tectonic subsidence, perhaps as a result of movement along buried faults (*cf.* Mutti *et al.*, 1999).

Mini-slice geometry is controlled by the interplay of the rate of subsidence in area B and the rate of sediment deposition. When the rate of deposition was high relative to the

rate of subsidence, the depocentre at area B tended to fill up and a flat sea bottom was re-established. If however, the rate of subsidence or deepening in area B exceeded the rate of deposition, the thicknesses of the mini-slices are greater in area B.

During periods when the sea bed was more-or-less flat, the mini-slices tended to increase in thickness in area C, presumably due to ponding of megaturbidites and other muddy turbidites in the west. Rates of sedimentation are not known and may have varied considerably during the deposition of individual mini-slices.

The combined effects of rates of deposition and changing bottom topography are evident when comparison is made between the thicknesses and shapes of some mini-slices. For example, mini-slices SL 2A and SL 2G do not vary significantly (less than  $\pm 10\%$  of the mean thickness of the mini-slice) between the three areas, suggesting that the sea-bottom was more-or-less flat at the time of deposition (*cf.* Ricci Lucchi, 1990; Mutti *et al.*, 1994). Mini-slice SL 2B increases in thickness significantly in area C, probably due to ponding of megaturbidites to the west (Rothwell *et al.*, 1992). The development of a bathymetric depression in area B is suggested for mini-slices SL 2C and SL 2F. This depocentre trapped a proportion of the sediments that might otherwise have been deposited in area C.

The significant reduction in the thickness of the deposits in area C, especially for mini-slice SL 2F, supports this interpretation. The reduction in the thickness of shale in area C supports the interpretation that most of the shale is of turbidity-current origin rather than being hemipelagic (Chapter 3).

The variation in the mini-slice geometry and thickness is also observed in the

remaining mini-slices and is similarly attributed to the interaction between the rates and amount of deposition and rates of subsidence at area B.

In mini-slice SL 2M, the greater number and thickness of sandstone beds in area B compared to areas A and C is interpreted to be the result of the closer proximity of area B to the main paths of the depositing currents than area A. Sandstone beds below megaturbidite 24-SH may be laterally equivalent of the siltstone beds below megaturbidite 24-RE. This suggests that area A may have been in a position marginal to the paths of the depositing currents. In area C, the siltstone beds are thicker than those in area A, suggesting that the area was located closer to the paths of the flows that deposited the siltstone beds. The sandstone bed below bed 24-SH is probably equivalent to megaturbidite BT-24a but its mud cap was eroded by the current that deposited the overlying megaturbidite and hence it is not assigned to facies C2.4 in area B.

Differential compaction of the sediments below mini-slice SL 4M may also have affected the thickness of mini-slice SL 4M. The greater thickness and numbers of sandstone beds in mini-slice SL 4M in area B compared to areas A and C may have caused increased compaction of the underlying sediments at area B (Mutti *et al.*, 1978)

Mini-slices SL-2N and SL 2O show less significant changes in thickness between the three areas suggesting the filling of the area B depression and a reduction in bottom topography. In mini-slice SL 2N, beds of facies D2.1 decrease in number from east to west. Mean bed thickness also decreases from east to west (Table CD-T2). The number of beds and their mean thickness show a more pronounced decrease between areas A and B,

suggesting that area B may have been farther away from the flow paths that deposited the siltstone beds of facies D2.1. The decrease in the number and mean bed thickness of facies D2.1 beds between area A and C is less than between areas A and B suggesting that the flow paths were closer to both areas A and C, and farther from area B.

Short-distance correlation between section FP1 and RE shows that mini-slices of time-slice 2 display alternating thinning and thickening between these two sections, which is interpreted to be the result of compensation. Sandstone beds that are more common in section FP1 probably change into siltstone beds at section RE. Possible correlations may be made between some of the sandstone and siltstone beds in section FP1 and those in section RE (e.g., sandstone bed in SL 2C at FP1 with the thick siltstone above bed 12-RE, Figure 5.10). The change of subfacies between section FP1 and RE was likely to be partly controlled by shifting of the location of deposition due to variation in bottom topography.

In summary, deposits in time-slice 2 are similar to those in time-slice 1 in that they consist of megaturbidites and turbidite muds, deposited from large flows that traversed the the area. Siltstone and sandstone beds were deposited from low concentration turbidity currents. Bottom topography probably exerted greater influence on deposition of time-slice 2 than time-slice 1. The interaction between the rate of deposition and the rate of tectonic subsidence controlled the geometry of the mini-slices. During deposition of time-slice 2, area B experienced enhanced subsidence and acted as a depocentre trapping larger proportions of the sediment being transported across the area by currents moving from east to west. Facies C2.3 beds, deposited from low concentration turbidity currents, are

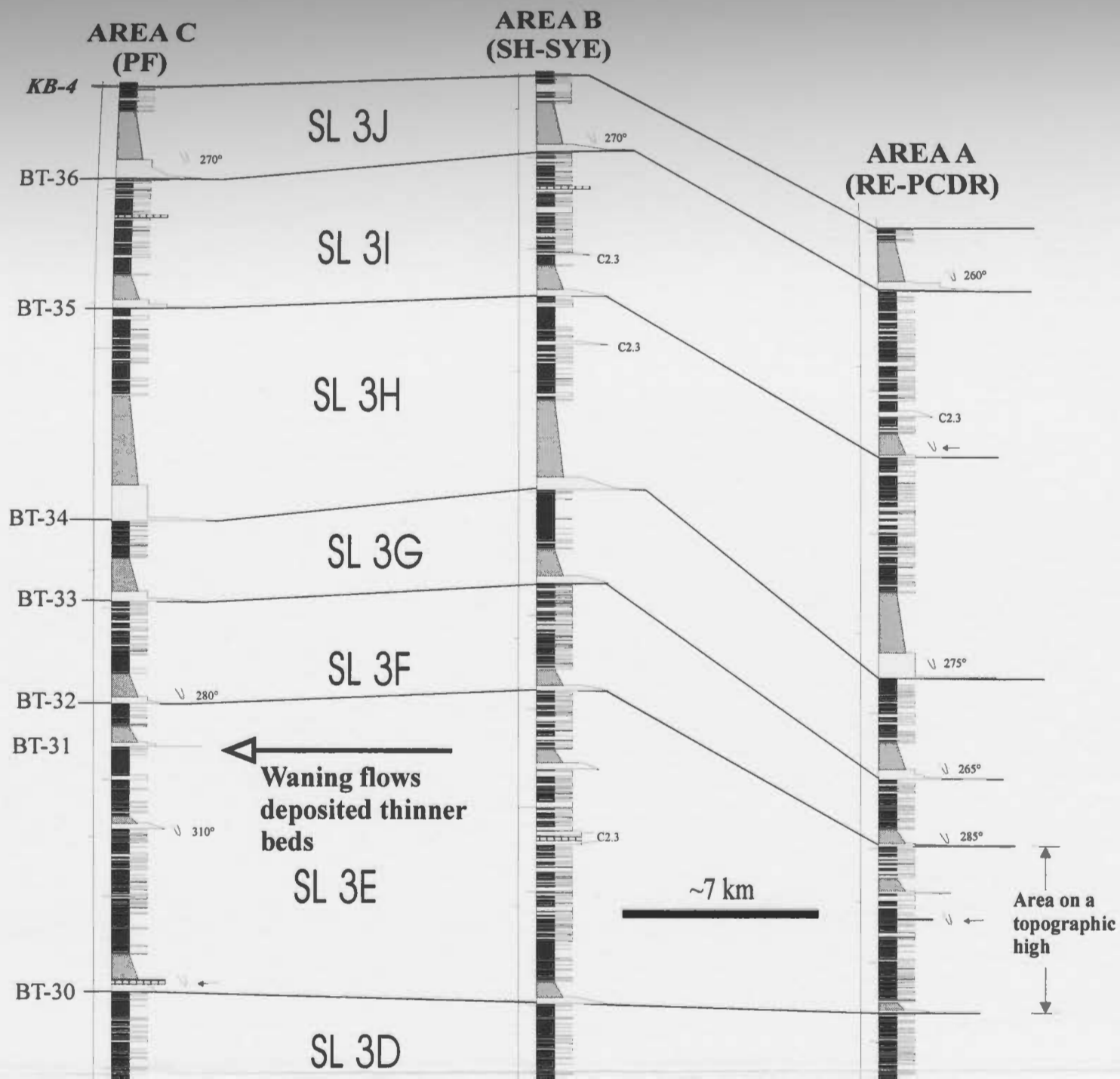
more common in area B (Table TD-2). Sea-bottom irregularities most likely controlled the transport paths of low concentration turbidity currents that deposited the siltstone beds (*cf.* Normark, 1985).

The depositional setting most representative of time-slice 2 is suggested to have been a basin-plain setting, where deposition was dominated by (i) large turbidity currents depositing megaturbidites and by (ii) low concentration turbidity currents initiated at a distal source and carried mostly silt and mud loads by the time they transited the thesis area. Megaturbidites are the dominant architectural element within time-slice 2 and they have a more-or-less tabular geometry and are bounded by 0<sup>th</sup> order bounding surfaces. The sandstone and siltstone beds within time-slice 2 do not cluster or form packets which may potentially suggest other architectural elements in the sense of Mutti and Normark (1987).

#### **5.4.5. Description of Time-slice 3**

Time-slice 3 is slightly thicker than time-slice 2 (Table 5.2) and is well exposed in areas A, B and C. It is bounded by KB-3 at the base and KB-4 at the top (Figure 5.11). This time-slice is about 10 m thinner at area A compared to areas B and C. Shale forms about 72% of this time-slice in areas A and B and approximately 78% of the total thickness at area C (Table 5.2). The total thickness of siltstone is two to three times the total thickness of sandstone in areas A and B. In area C, the total thickness of siltstone is slightly less than sandstone (Table CD-T3, Figure 5.12). Such thickness variations within this time-slice, therefore, suggest significant lateral facies changes.

**Figure 5.11. CORRELATED TIME-SLICE 3**





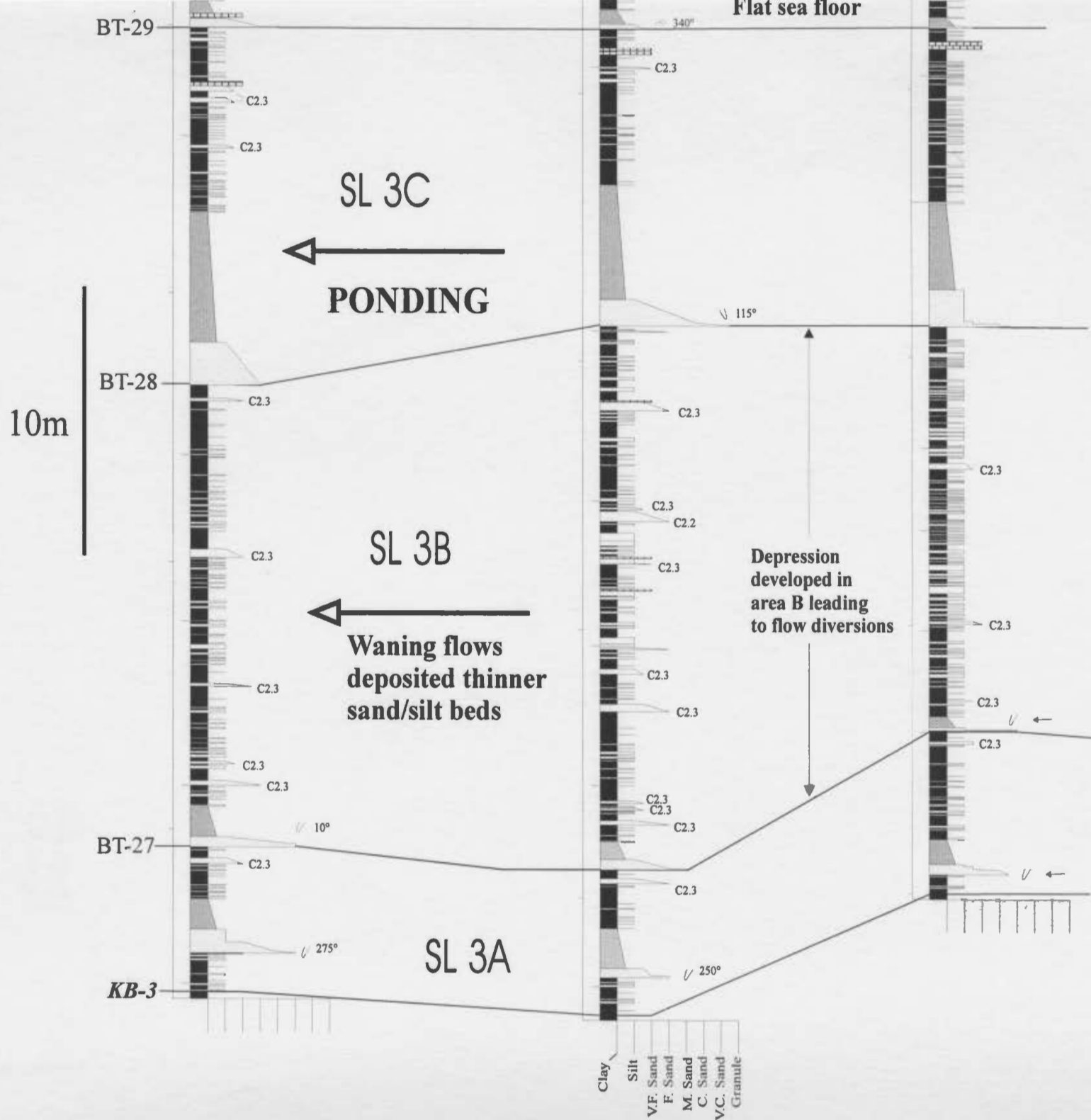
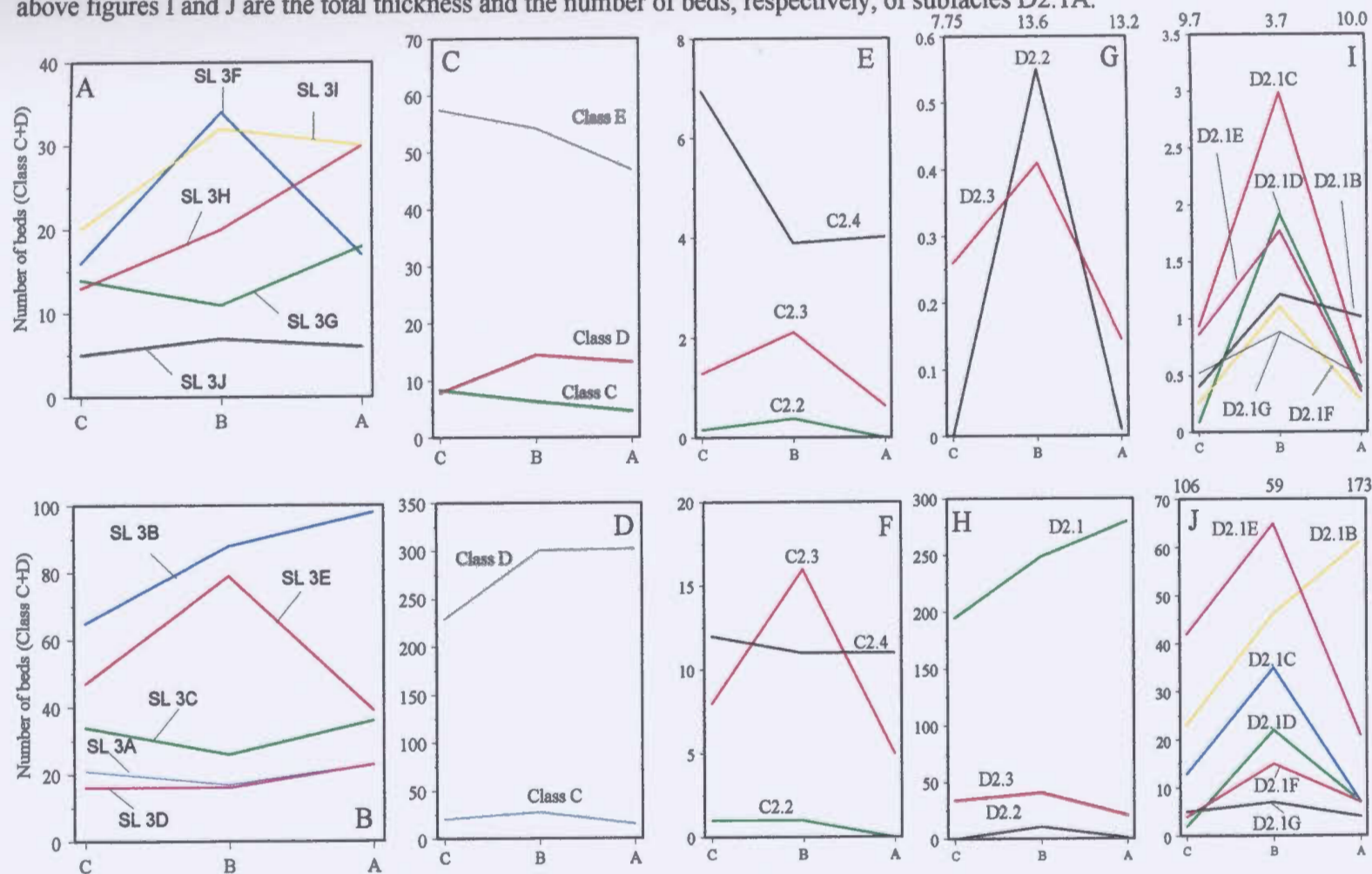


Figure 5.12. Comparison of the facies thicknesses and number of beds for time-slice 3 in the three areas of composite sections. A and B are plots of the bed numbers for each of the mini-slices. C, E, G and I are for the total thickness in metres of facies and subfacies. D, F, G and H show the number of beds. The values above Figure G are the thickness of facies D2.1. The values above figures I and J are the total thickness and the number of beds, respectively, of subfacies D2.1A.



Megaturbidite and K-bentonite horizons divide this time-slice into ten mini-slices (numbered SL 3A through SL 3J). These mini-slices vary in thickness between areas A, B and C. The degree of change is greater for some mini-slices than others, specifically, mini-slices SL 3B, SL 3E, SL 3F and SL 3J are significantly thinner at area A compared to areas B and C (Figure 5.11, Table A5-4.1).

The total thickness of sandstone and the total thickness of shale increases from east to west, while siltstones show a pronounced decrease in thickness from area B to area C. Mini-slices also differ in the number of component beds. There are more sandstone and siltstone beds in area B than in areas A and C (e.g., mini-slices SL 3F and SL 3E). In mini-slices SL 3 B and SL3I, the number of sandstone and siltstone beds differs slightly between areas B and A but there is a more distinct decrease in numbers in area C. For SL 3C and SL 3G, the number of sandstone and siltstone beds is less in area B than in areas A and C. The remaining mini-slices within time-slice 3 show little or no variation.

Megaturbidites show a significant increase in thickness from east to west (Table A5-4.2). One bed, 30a-PF, was observed in mini-slice SL 3E in area C but was not classified as facies C2.4 in the other areas. Sandstone beds of facies C2.3 are more numerous in SL 3B and SL 3E in area B compared to the other areas. In other mini-slices, sandstones of facies C2.2 and C2.3 are rare or absent.

Siltstone beds of facies D2.1 are the most prevalent in terms of total thickness and number of beds (Figure 5.12 G and H). Total thickness of facies D2.1 increases slightly between areas A and B, then decreases markedly in area C. The number of beds of facies

D2.1 decreases from east to west. Siltstone facies D2.2 and D2.3 have greater total thicknesses and number of beds in area B compared to areas A and C. Siltstone beds of subfacies D2.1A are more numerous in areas A and C compared to area B. The total thickness of subfacies D2.1A is also less at area B. Other subfacies are more common in area B and have greater total thicknesses (Figure 5.13).

For the internal architecture, sections FP1 and section RE show small differences in bed numbers and facies types (Figures 5.13, 5.14 and Table CD-T3). The lower parts of some megaturbidites (BT-26, BT28, BT-33) are thinner in section FP1 than in section RE. The lower part of megaturbidite BT-36 is thicker in section FP1 than in RE. Sandstone beds of facies C2.3 are more numerous in section FP1 than RE (mini-slices SL 3B and SL 3H). The number of siltstone beds in both sections FP1 and RE are similar, but facies change do occur between the two sections (Figure 5.13).

#### **5.4.6. Interpretation of Time-slice 3**

Deposition was dominated by accumulation of megaturbidites as in time-slice 2, but the number and total thickness of siltstone beds shows an overall increase in areas A and B compared to time-slice 2. The increase in the percentage of siltstone in areas A and B suggests an increase in supply and may reflect greater proximity to the source or channel terminations.

The changes in the thicknesses of the mini-slices and their facies are interpreted to have resulted from variations in the rate of deposition and the rate of change of bottom

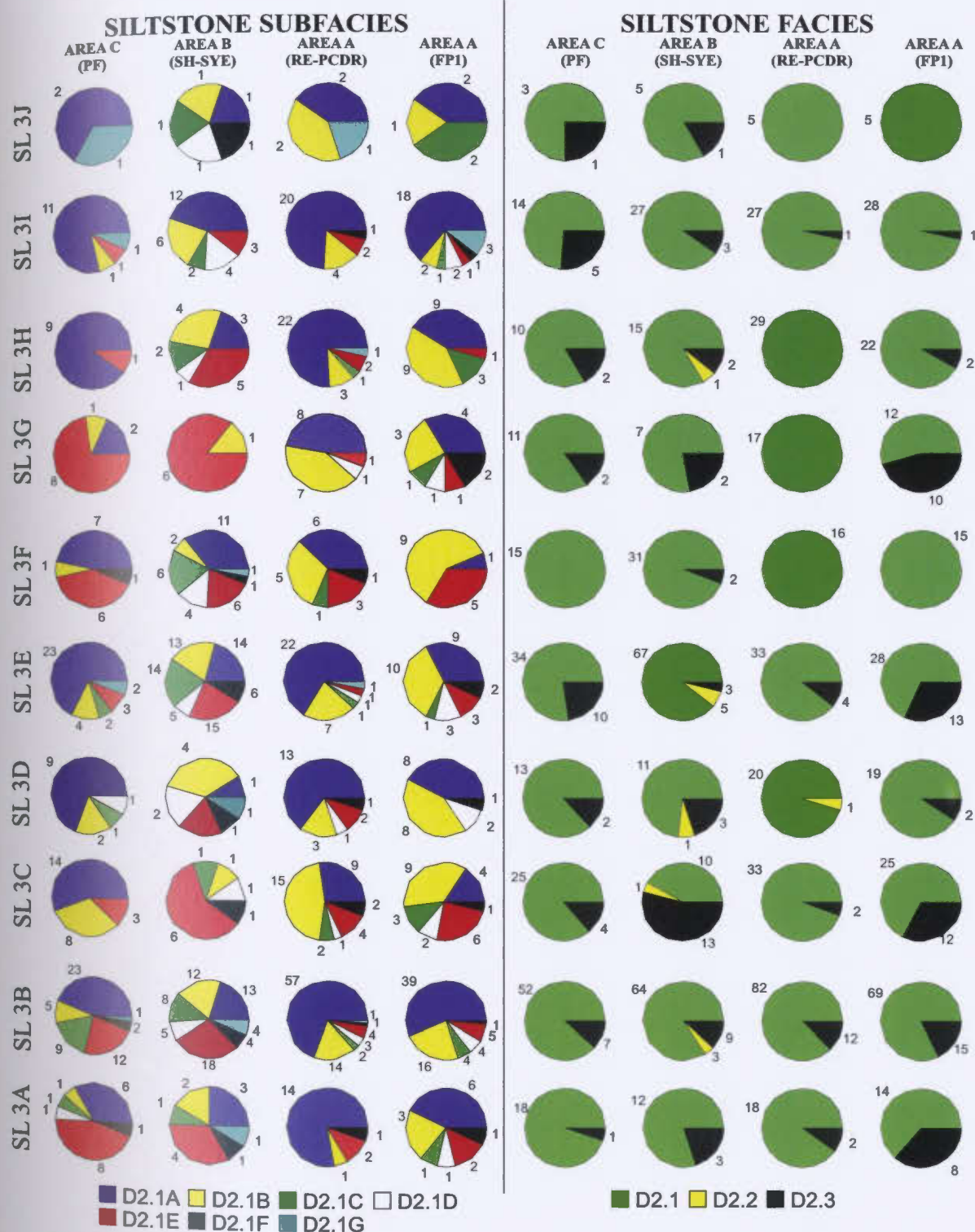
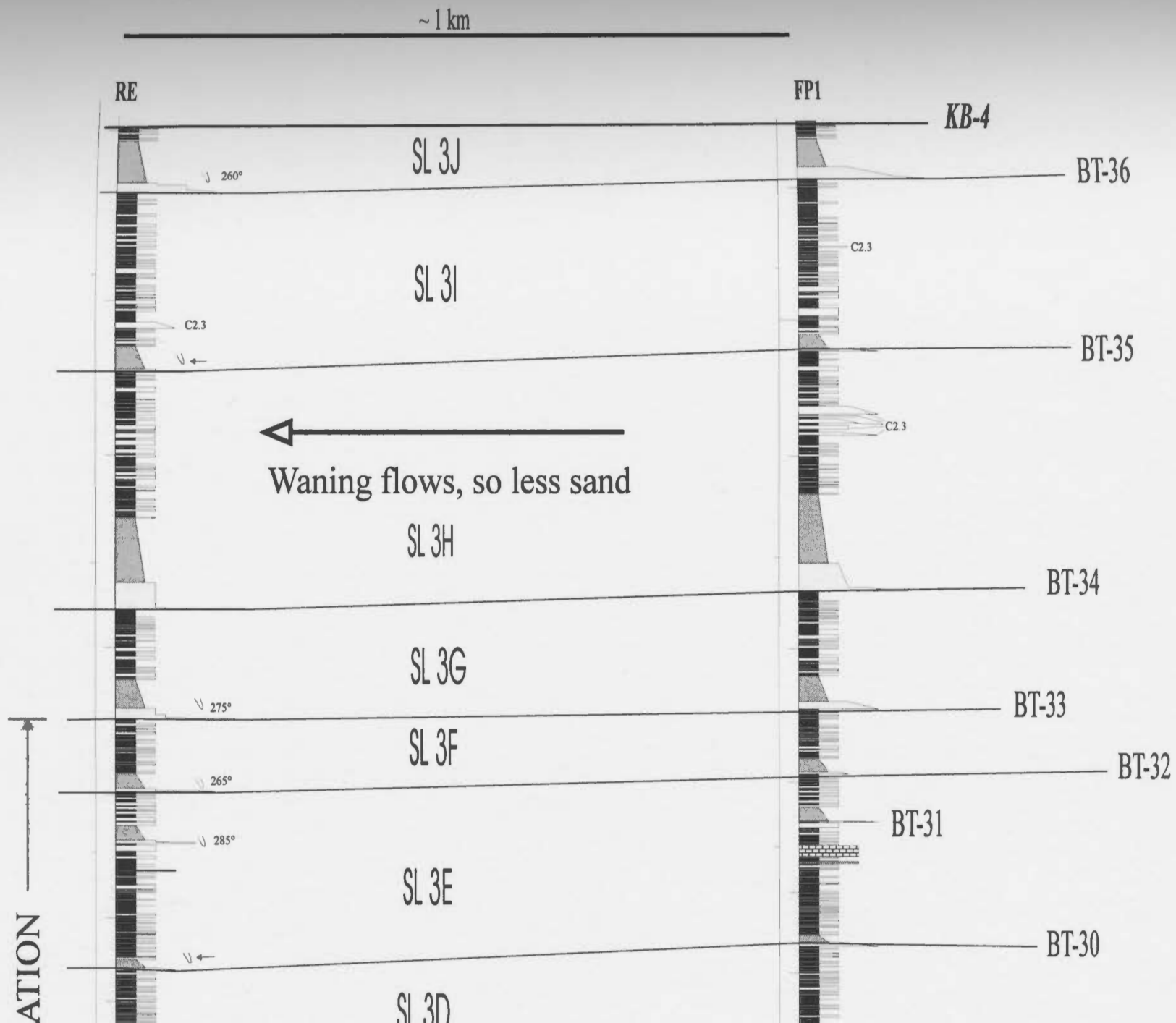


Figure 5.13. Numbers of siltstone beds assigned to the different facies and subfacies in the mini-slices of time-slice 3. These are compared between area A, B and C.

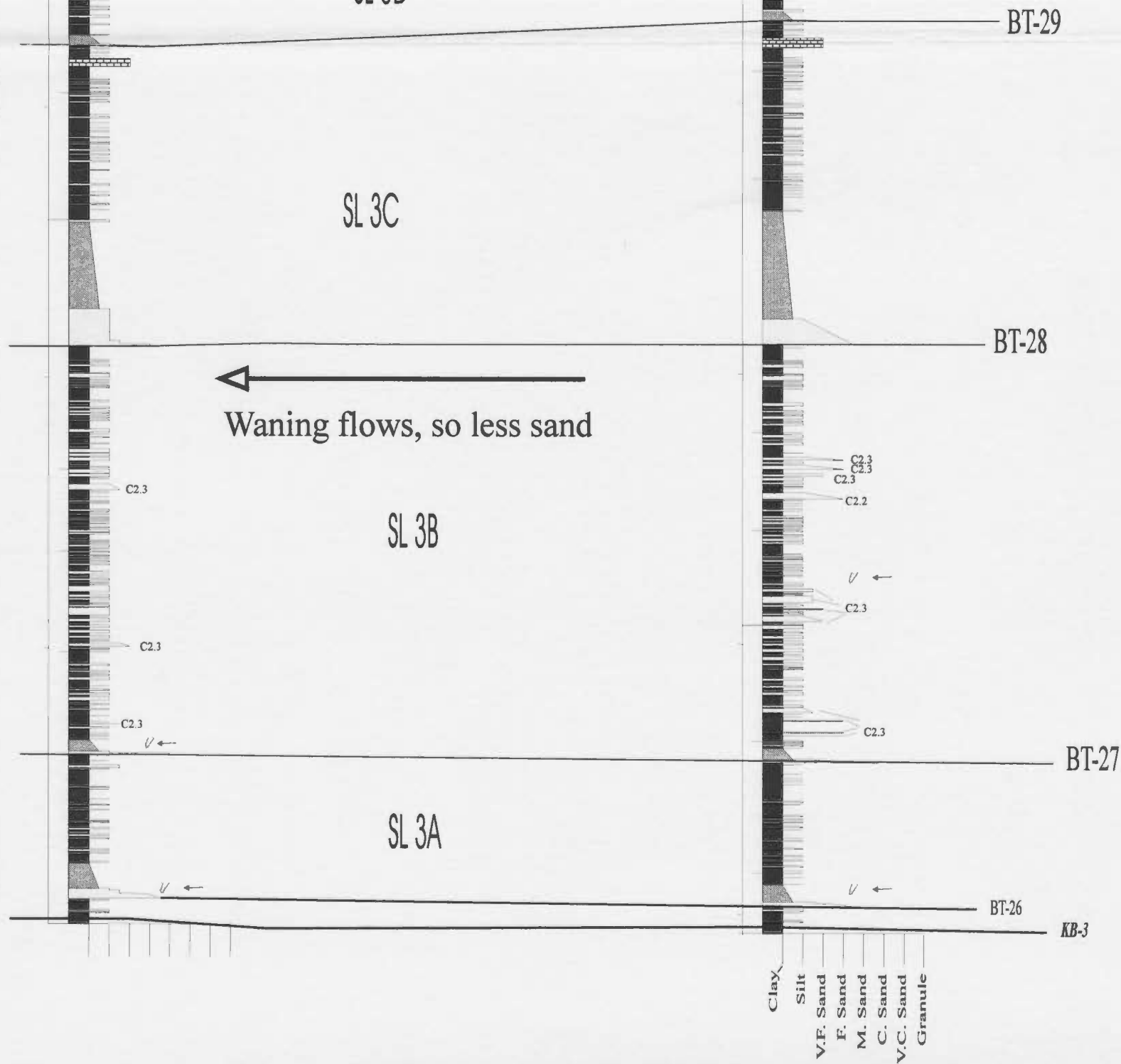
Figure 5. 14. Short distance correlation in time-slice 3





10m

COMPENS



topography. Changing in the bottom topography may have been caused by movement along buried faults (*cf.* Ricci Lucchi and Valmori, 1980; Mutti, *et al.*, 1999).

Mini-slices SL 3A, SL 3D and SL 3H display insignificant differences in thickness between areas A, B and C and result in a tabular shapes and geometry (e.g., SL 3D in Figure 5.11). Deposition of these mini-slices most likely occurred when the sea bottom was relatively flat. Nevertheless, decrease in siltstone bed number and thickness from east to west in these mini-slices does occur and is interpreted to represent a downflow facies change as a result of flow deceleration and deposition. Siltstone beds show a marked change in their total thickness, number and facies type between areas A and B and this is believed to indicate a marginal location of area B to the axial paths of the currents.

Ripple laminated and climbing ripple laminated siltstone beds (subfacies D2.1A) are the dominant subfacies and they tend to decrease in numbers between areas A and C, suggesting that conditions favourable to the formation of climbing ripples decreased in a downcurrent direction. These conditions may be related to the rates of settling from suspension and hence the rate of deceleration (Harms *et al.*, 1982).

Mini-slices SL 3C and SL 3J increase significantly in thickness towards area C, which is interpreted to result from compensation. In area C, mini-slices that underlie SL 3C and SL 3J (SL 3B and SL 3I) are thinner than in area B. This may have been caused by the trapping of the sediments in area B during the deposition of mini-slice SL 3B. Area B may have been a bathymetric low and as this depocentre filled up, more sediments may have reached area C.



Mini-slice SL 3B is significantly thicker in area B compared to both areas A and C. This difference is interpreted to indicate that area B was located in an area with lower sea bed elevation than area A. Due to the development of this bathymetric low and the resultant diversion of flows towards area B, only thin beds of siltstone and rarely, sandstone beds were deposited in area A. Four palaeocurrent measurements from the deposits of SL 3B in area A show a palaeoflow direction of  $295^{\circ}$ . In area B, palaeocurrent directions based on three measurements in the deposits of SL 3B have a mean value of  $260^{\circ}$ . One measurement in area C shows a palaeocurrent trend of about  $295^{\circ}$ . These palaeocurrent trends and the decrease in the siltstone bed thickness in area A compared to area B support the interpretation that area B was located in a sea-bottom low compared to area A at the time of deposition of mini-slice SL 3B.

Mini-slices SL 3E and SL 3F vary in thickness and component facies between areas A and area B. These changes are also interpreted to result from the effects of varying bottom topography. Deposits between BT-30 and BT-31 show a distinct facies change. Sandstones, siltstones and shales significantly decrease in total thickness in area A and this decrease is interpreted to be the result of area A being located on a bathymetric high. The flows that deposited thicker sediments in areas B and C may have been diverted away from the high at area A or may have increased speed, transiting the high, leading to less accumulation there. Megaturbidites 30-RE and 31-RE have significantly thinner lower sandy parts compared to equivalent megaturbidites in areas B and C, supporting the suggestion that area A may have been higher than the surrounding areas. Megaturbidites in

modern and ancient settings decrease in thickness in areas that are elevated above their surroundings (Ricci Lucchi and Valmori, 1980; Pilkey, 1988; Rothwell *et al.*, 1992; Mutti *et al.*, 1990). Thinning of turbidity current deposits as a current passes over areas of sea-bottom relief has also been suggested (Kneller, 1995). A more gradual thinning and fining of the sandstone and siltstone beds is observed from area B to area C for mini-slice SL 4E, which most likely reflects a downcurrent waning of the flows.

Megaturbidite 34a-PF may be equivalent to the sandstone beds in the middle of SL 3E in area B. It was not designated as a megaturbidite at area B because of its thin mud cap which was perhaps eroded in area B.

The subtle lensing of the sandstone and siltstone “packet” in mini-slice SL 3E would be impossible to recognise in most large outcrops and might also be difficult to image on seismic reflection profiles, unless high resolution instrumentation is used and the packet is close or near the sea bottom (Piper *et al.*, 1999). This siltstone packet may be considered as a gently lensing element consisting of stratified beds. The amount of siltstone in this element decrease in a downcurrent direction. This lens is bounded by 2<sup>nd</sup> or 3<sup>rd</sup> order bounding surfaces.

The main architectural elements within time-slice 3 are the megaturbidites, that have a more-or-less tabular geometry. The geometry of this element may change to a wedge or lense shape because it is affected by the bottom topography. Individual megaturbidites are bounded by 0<sup>th</sup> order bounding surfaces.

#### **5.4.7. Description of Time-slice 4**

Time-slice 4 ranges in thickness from 132 m to 136 m in areas A, B and C (Table 5.2). K-bentonite horizon KB-4 marks its lower boundary and KB-5 marks its upper boundary. Time-slice 4 is divided into two sub-slices. A lower sub-slice, sub-slice 4-1, is bounded at the base by KB-4 and at the top by the base of megaturbidite BT-43. The upper sub-slice, sub-slice 4-2 is bracketed by the base of BT-43 at the base and KB-5 at the top.

Facies and subfacies thicknesses and numbers vary between areas A, B and C (Figure 5.15). The two sub-slices are described and interpreted separately.

##### **5.4.7.1. Description of Sub-slice 4-1**

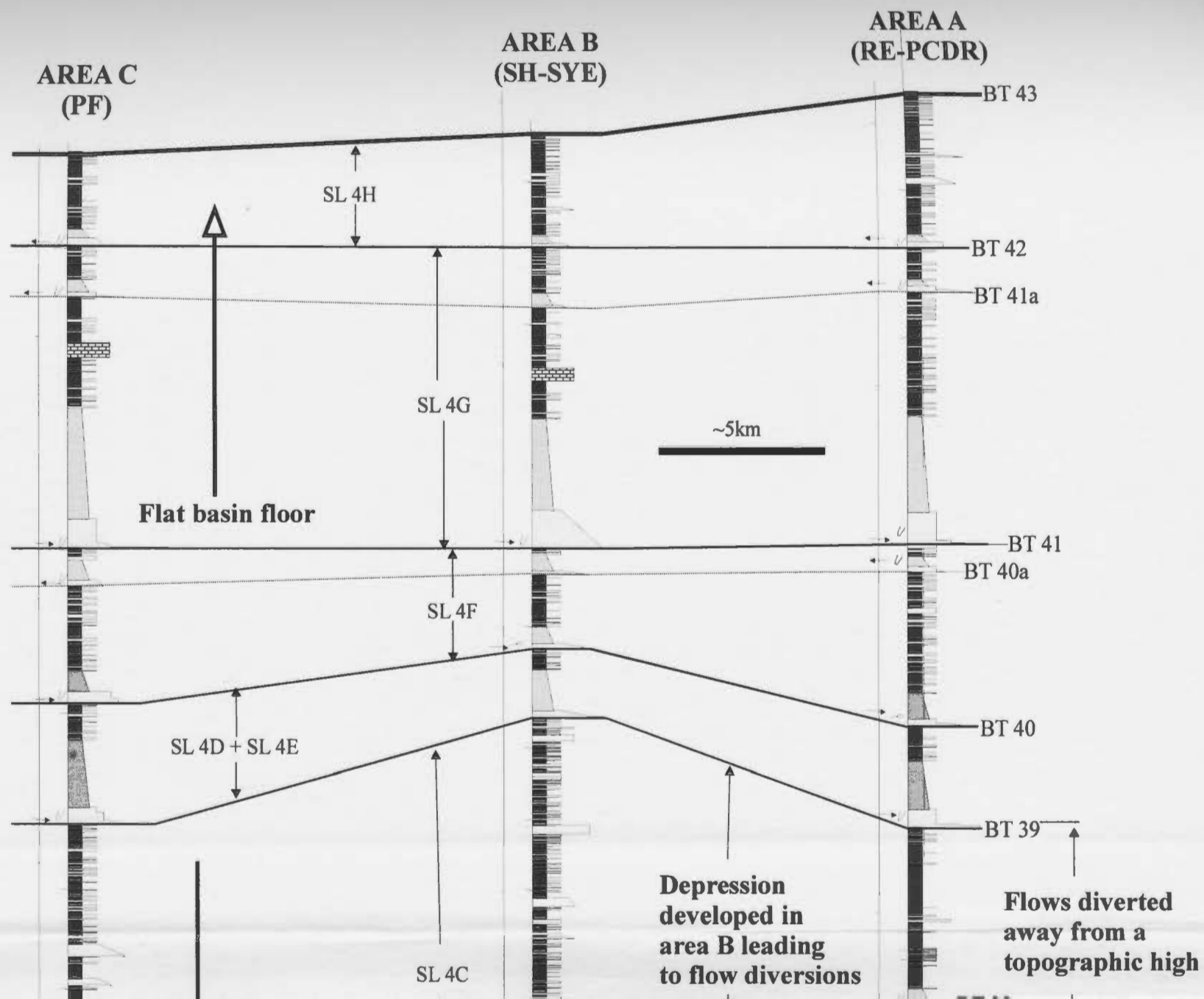
In sub-slice 4-1, shale forms 65-68% in areas A and B. In area C, shale forms greater than 76% (Table 5.2). The total thickness of siltstone is greater than the total thickness of sandstone in areas B and C. In area A, the total thickness of sandstone is more than the total thickness of siltstone (Table 5.2). The sandstone is mostly in the lower part of sub-slice 4-1 in area A.

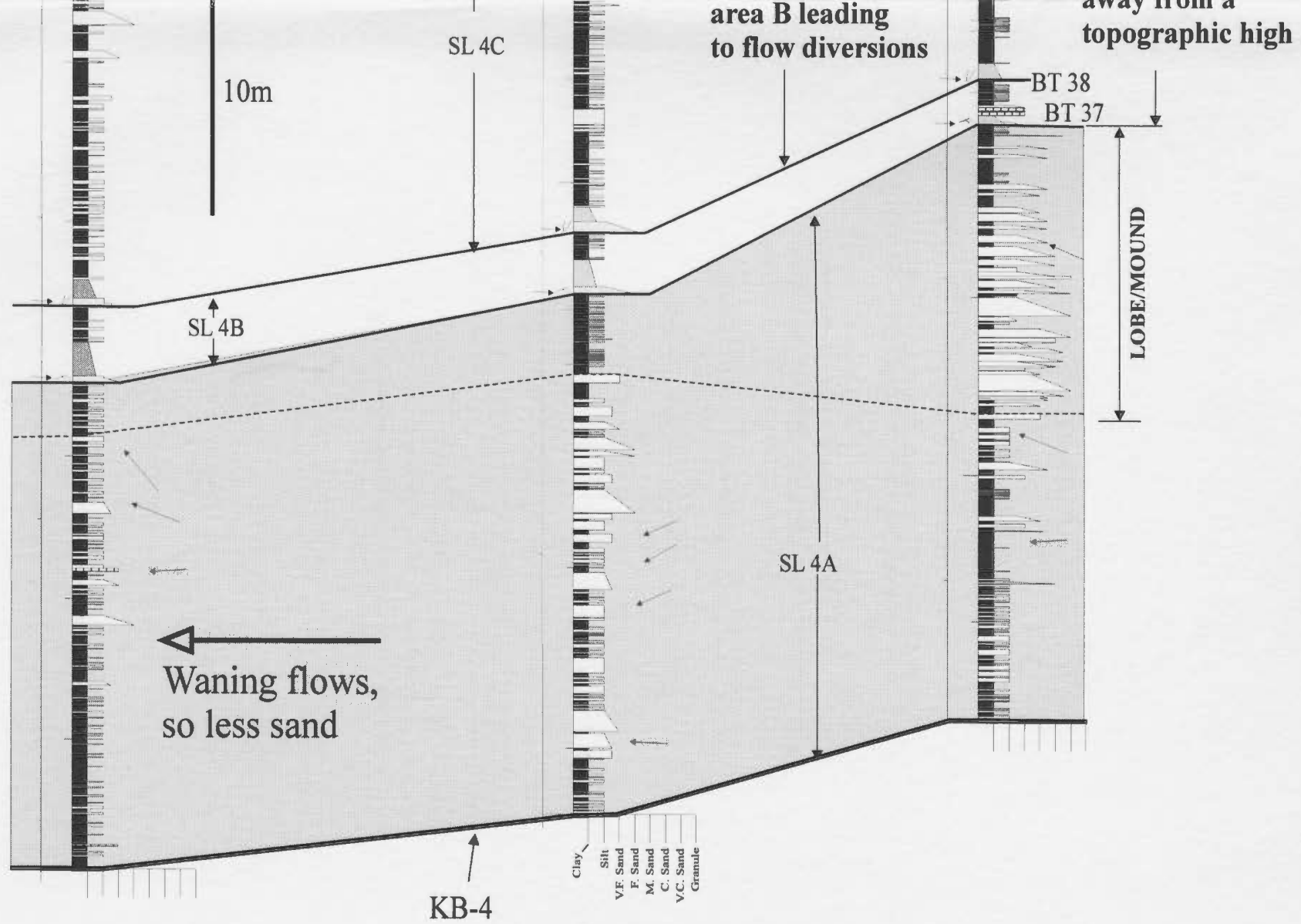
Megaturbidites and K-bentonite bed KB-4 divide sub-slice 4-1 into eight mini-slices (SL 4A through SL 4H) (Figure 5.16). Mini-slice SL 4D consists of megaturbidite BT-39.

The eight mini-slices that constitute sub-slice 4-1 vary in thickness, facies type and bed numbers between areas A, B and C (Figures 5.16 and Table CD-T4). Mini-slice SL



**Figure 5.16 CORRELATED SUB-SLICE 4-1**





4A, is significantly thicker (+~14%) in area A than areas B and C (Table A5-4.1). Mini-slice SL 4B is significantly thicker in area C (+29%) than in areas B and A. In area A, mini-slice SL 4B is significantly thinner (-35%) than in areas B and C. Mini-slice SL 4C is significantly thicker in areas B and C (+ 17-28%) compared to area A where it shows the most significant decrease in thickness (~-46%). Mini-slices SL 4D through SL 4F are significantly thicker in area C than areas A and B. Mini-slice SL 4G shows no significant difference in thickness between the three areas. The base of mini-slice SL 4G is therefore used as a datum in Figure 5.16. Mini-slice SL 4H is significantly thicker in area A than both areas B and C.

Megaturbidites also vary in thickness in the three areas. Megaturbidites 37-RE and 38-RE show a pronounced decrease in thickness in area A (-34 to -66%) compared to areas B and C (Table A5-4.2). Megaturbidites 39-SH and 40-SH show a significant decrease in thickness in area B compared to equivalent megaturbidites in areas A and C.

Sandstone beds of Class C other than facies C2.4 (the lower parts of megaturbidites) are present in sub-slice 4-1. A few sandstone beds of Class B are also present in sub-slice 4-1 (Table CD-T4), but these are not common. Most of the sandstone occurs in mini-slice SL 4A. Facies C2.1 is only present in area A in mini-slice SL 4A. Sandstone beds assigned to facies C2.2 and C2.3 are present in mini-slice SL 4A in areas A, B and C. In mini-slice SL 4A, sandstone beds in area A occur together as a sandstone packet. In area B, the sandstone beds in mini-slice SL 4A occur with medium to thick bedded siltstone beds and form a packet. There are no deep (>0.5 m) scours or channels at

the base of this packet. The beds that are in the lower part of the packet have a sheet-like geometry and display minimal variation in thickness for tens of metres in outcrops. In area C, sandstone beds in mini-slice SL 4A are least common. In other mini-slices, sandstone beds other than facies C2.4 are rare or absent (Figure 5.17).

Siltstone beds show variability in numbers and type of facies (Figure 5.17). Some of the mini-slices show a pronounced difference in the number of beds and facies and subfacies types. There are more siltstone beds in areas B and C compared to area A, particularly within mini-slices SL 4A and SL 4C. In mini-slice SL 4F, the number of siltstone beds is less in area B compared to both areas A and C. In mini-slices SL 4G and SL 4H, the siltstone beds show a decrease from east to west.

Flutes and ripple lamination of megaturbidites BT-37, BT-38, BT-39, BT-40 and BT-41 indicate a palaeoflow direction from west to east. Flutes and ripple lamination of megaturbidites BT-40a, BT-41a, BT-42, and BT-43 indicate an opposite palaeoflow direction from east to west (Figure 5.16).

In mini-slice SL 4A, more sandstone occurs at area A than in area B, but the combined total thickness of the sandstone and siltstone in area B is more than the combined total thickness of the sandstone and siltstone in area A. Total shale thickness in area A is greater than at area B. Palaeocurrent trends determined from sandstone beds in area A indicate a palaeocurrent direction  $\sim 280^\circ$  (mean of three measurements) for the beds in mini-slice SL 4A. In area B, the mean palaeocurrent trend is  $\sim 255^\circ$  (mean of four measurements) for mini-slice SL 4A, while in area C, palaeocurrent measurements show a



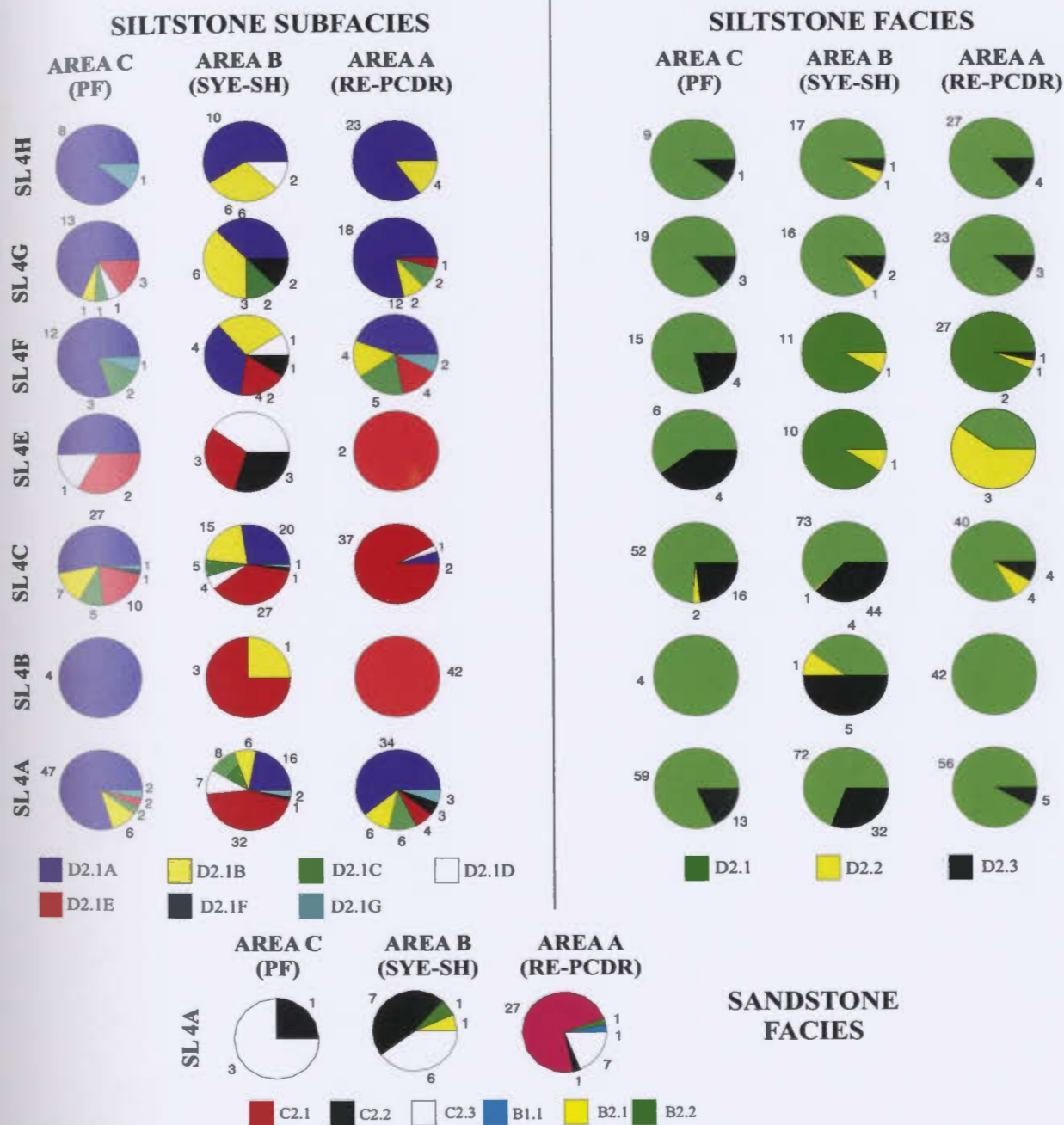


Figure 5.17. Numbers of sandstone and siltstone beds assigned to the different facies and subfacies in the mini-slices of sub-slice 4-1. These are compared between areas A, B and C. The number of sandstone/siltstone beds or laminae assigned to a facies or subfacies in each mini-slice is presented on each pie diagram.

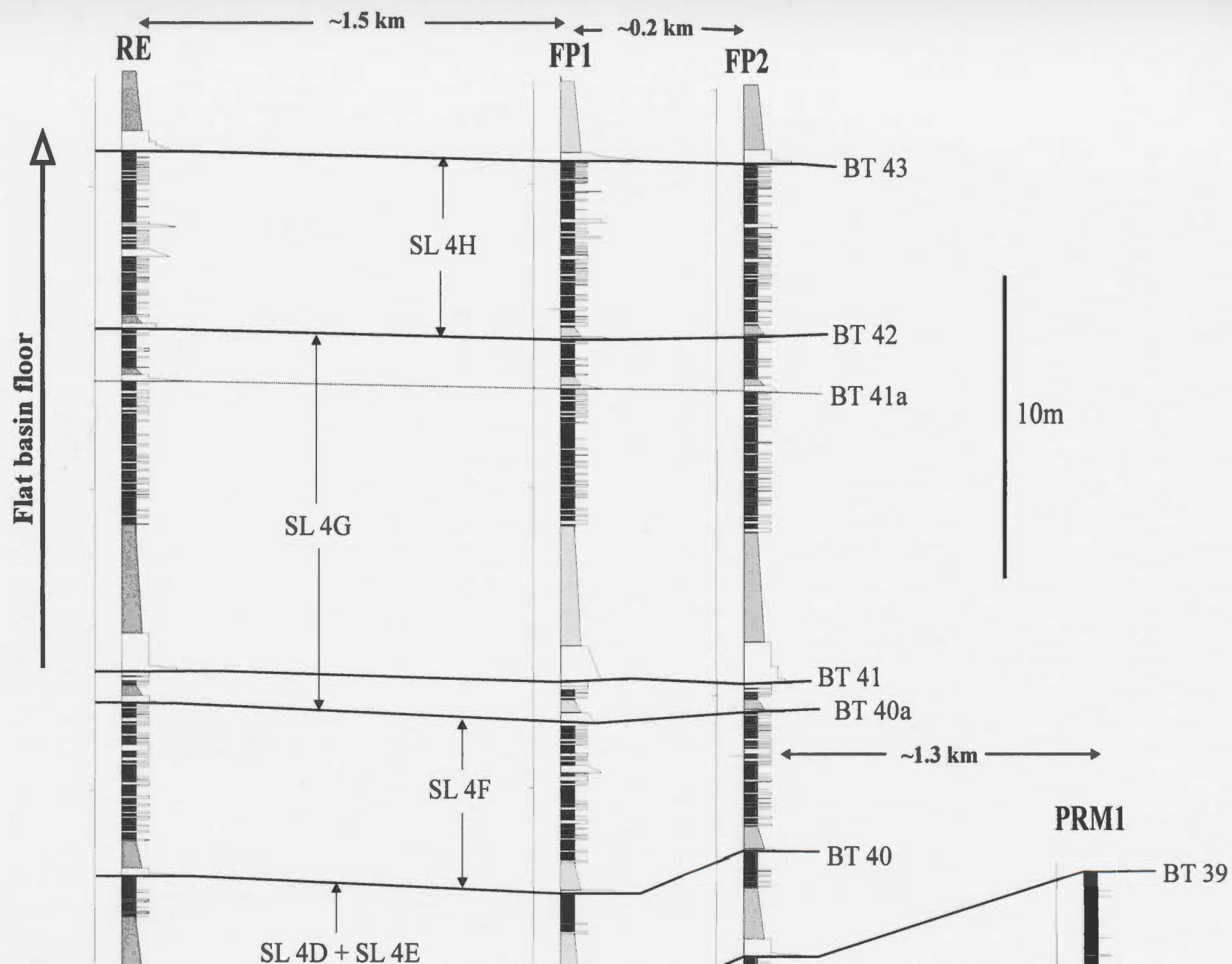
palaeoflow trend of 295° (mean of three measurements).

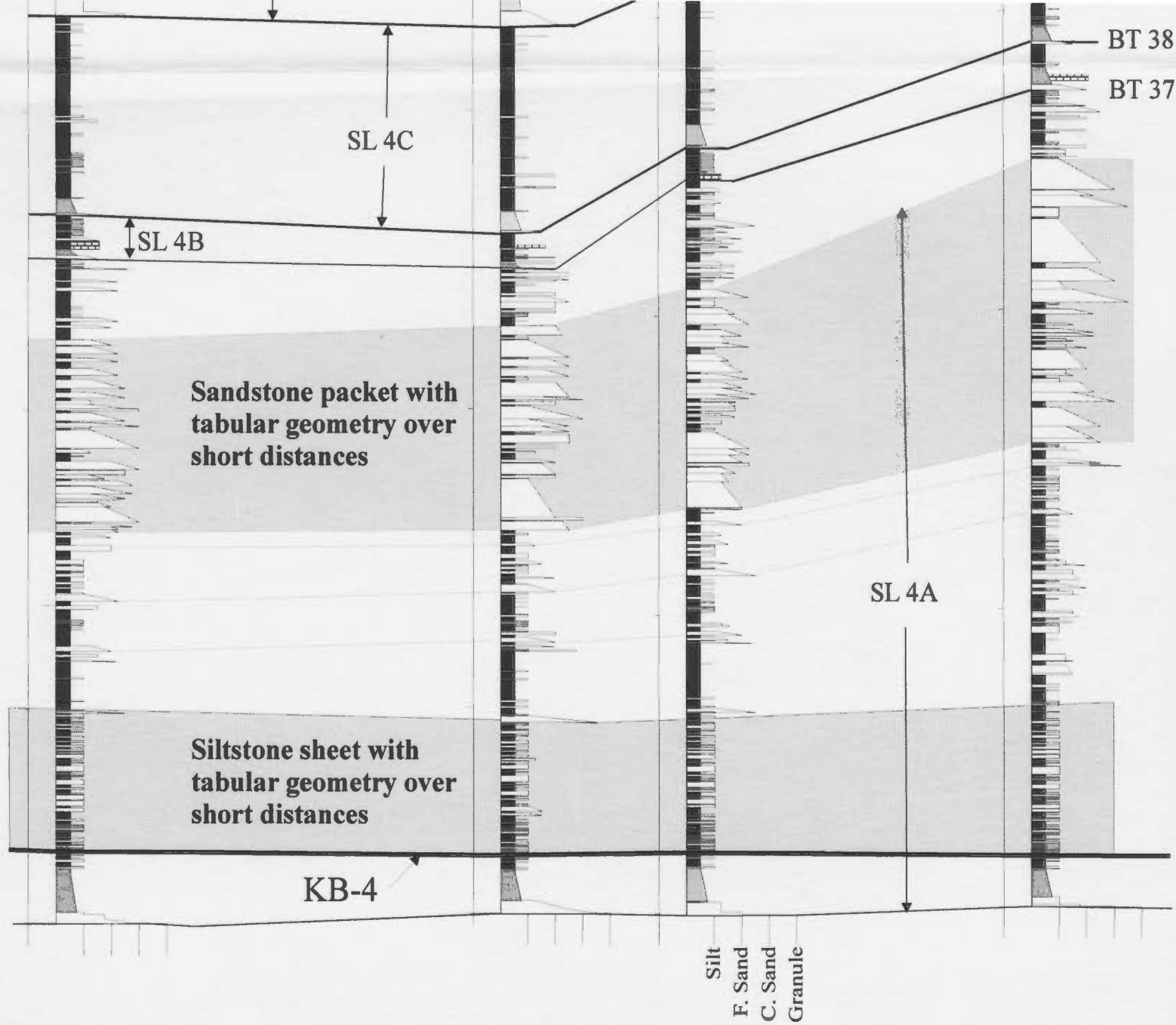
Mini-slices SL 4A, SL 4B and SL 4C occur in the lower part of section RGC, located between area B and area C (Figure 2.1; Table CD-T4). The thicknesses of these three mini-slices are similar to those thicknesses of the same mini-slices in area B, but they are thicker than in area C. Only one sandstone bed of facies C2.3 is present within mini-slice SL 4A. The other sandstone beds are the lower parts of megaturbidites. Siltstone beds of facies D2.1 in mini-slice SL 4A are more common in section RGC than in mini-slice SL 4A in areas B and A. Beds of facies D2.1 are rare in mini-slice SL4B in section RGC while in mini-slice SL 4C, the number of beds in section RGC is similar to areas B and C. Beds of facies D2.2 are rare in section RGC in mini-slices SL 4A, SL 4B and SL 4C. Beds of facies D2.3 are less common in section RGC for mini-slices SL 4A, SL 4B and SL 4C than in areas B and A. Siltstone beds assigned to subfacies D2.1A are more common in section RGC in mini-slice SL 4A than in areas B and A (Table CD-T4).

Sections RE, PF1, FP2 and PRM1 were used to determine the internal architecture of sub-slice 4-1. The distance between sections RE and FP1 is about ~1.5 km and the distance between sections PRM2 and FP2 is about 1.3 km. Sections FP1 and FP2 are about 200 m apart (Figure 5.18).

In mini-slice SL 4A, a sandstone packet, about 10 m thick, is present in all four sections. This packet consists mostly of facies C2.1 (Figure 5.18). Many beds in this packet are amalgamated, particularly, in section PRM1. In sections RE, FP1 and FP2 more beds occur in amalgamated units in the lower part of this packet than in the upper

**Figure 5.18. Short-distance correlation of sub-slice 4-1**





part. The sandstone packet is well defined and the transition from the lower part of the mini-slice (dominated by thin-medium bedded siltstone and subordinate sandstone) to the upper part of the mini-slice (consisting mostly of sandstone) is relatively abrupt. A well developed upward thickening or thinning, nor upward fining and coarsening sequences were not observed, except perhaps in the middle part of the packet in section FP2 and the upper part of the packet in section RE. None of these sequences were tested statistically, but Chen and Hiscott (1999) found no strong evidence for consistent asymmetric cycles in the Cloridorme Formation. Beds assigned to facies B2.2 are present in mini-slice SL 4A, especially in sections PRM1 and FP2. Beds of facies B2.2, usually occur below the thick sandstone beds and amalgamated units of sandstone. Beds of facies B2.2 are less common or absent in sections RE and FP1. A thick bed of subfacies D2.1A occurs near the upper part of this packet in sections PRM1 and FP2.

The lower part of mini-slice SL 4A consists of about 5 m of thin to medium siltstone beds alternating with shale. In sections RE, FP1 and FP2, a sandstone bed occurs in the upper part of this 5 m-thick interval, above which, 1-2 m of shale with few or no siltstone or sandstone beds occur in sections RE, FP1 and FP2. In section PRM1, there are several beds of facies B2.2 in this interval, above which, there is 2-3 m of alternating beds of sandstone and siltstone with shale occurs. Sandstone is more common in the lower part. Above this 2-3 m-thick interval is the main sandstone packet.

Mini-slices SL 4B through SL 4H show minimal variation between sections RE, FP1 and FP2 (Figure 5.19). Sandstone beds other than facies 2.4 are rare in these mini-

slices, although in section RE, there are more sandstone beds than in sections FP1 and FP2.

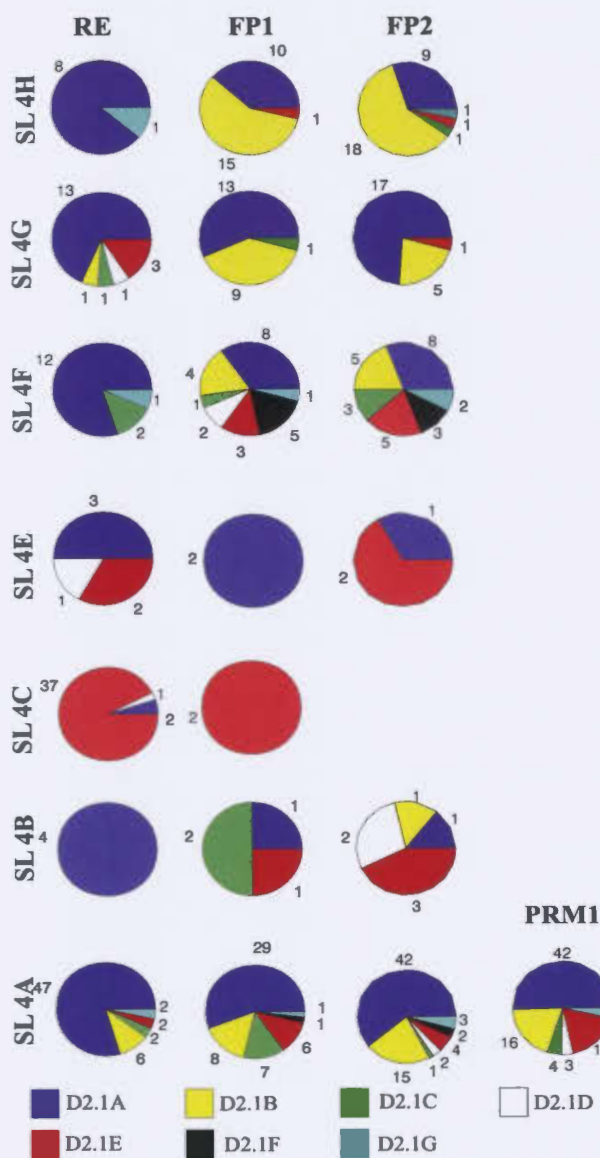
#### 5.4.7.2. Interpretation of Sub-slice 4-1

Sub-slice 4-1, unlike the older time-slices, has more sandstone and siltstone beds particularly, in areas A and B. Facies and thickness differences between the three areas appear to be restricted to mini-slices SL 4A through SL 4F. The differences in thickness of these mini-slices is interpreted to be due to interplay between deposition and bottom topography. Bottom topography is attributed to depositional and compactional effects, in addition to elevation differences due to tectonic subsidence and faulting. Minimal thickness variations in mini-slices SL 4G and SL 4H between areas A, B and C reflect little or no variations in bottom topography. This might be partly due to more rapid deposition of mini-slices SL 4G and SL 4H, resulting in less pronounced syn-depositional deformation in these two mini-slices than for the older mini-slices.

The sandstone packet in mini-slice SL 4A is interpreted to represent a lens or a mound consisting of tabular or wedge-shaped beds (Table 5.1). The constituent facies, tabular shape (on outcrop scale) and lack of deep channelling at the base of the packet are similar in many ways to lobe deposits (although a lobate shape is not evident) described from ancient turbidite deposits (Mutti and Normark, 1987; Mutti *et al.*, 1978, 1999) and many sandstone packets described from modern deep sea fans (Piper and Normark, 2001). The lack of well defined upward coarsening or thickening sequences suggests deposition



# SILTSTONE SUBFACIES



# SILTSTONE FACIES

226

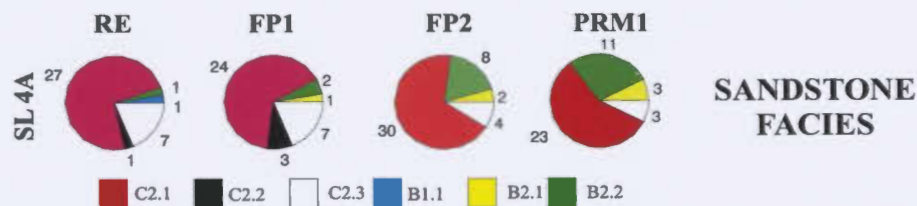
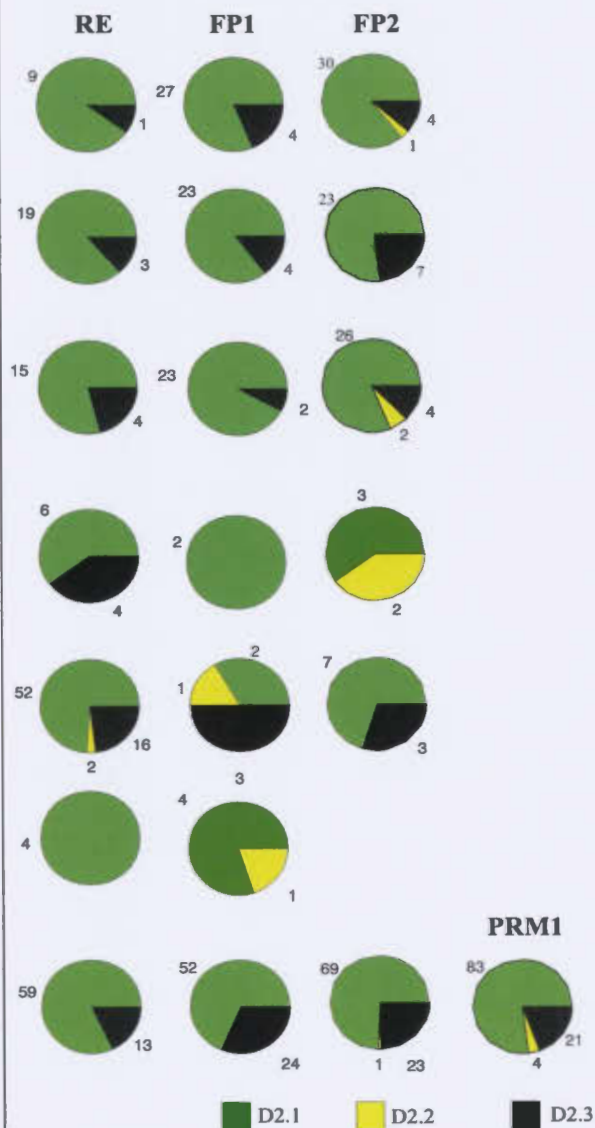


Figure 5.19. Numbers of sandstone and siltstone beds assigned to the different facies and subfacies in the mini-slices of sub-slice 4-1. These are compared over a short distance in area A. The number of sandstone/siltstone beds or laminae assigned to a facies or subfacies in each mini-slice is presented on each pie diagram.

was dominated by filling of topography generated by the deposition of beds and not progradation (Rozman, 2000). Alternatively, the lack of the upward coarsening/thickening sequences may be because these type of sequences are not widespread in such deposits (Chen and Hiscott, 1999).

Correlating individual beds of the sandstone packet between areas A and B is not possible, thus several interpretations for the lateral relationship of the beds of mini-slice SL 4A between areas A and B can be made. The lower part of mini-slice SL 4A in area A is a ~10 m-thick siltstone packet. This packet may represent a distal equivalent to more sandy deposits that accumulated east of the study area (*cf.* Mutti, 1977). The packet has many features similar to lobe fringe or distal lobe deposits described in both modern and ancient turbidites (Mutti, 1977; Pickering, 1981; Mutti and Ricci Lucchi, 1975; Mutti *et al.*, 1978,1999; Shanmugam and Moiola, 1991). If these are indeed distal lobe deposits, then they may have formed a bathymetric high on the sea bed. This high or mound may have controlled the deposition of sediments from subsequent flows. The more muddy interval above this siltstone packet may represent deposition of fine mud from dilute turbidity currents due to the diversion of subsequent currents away from the bathymetric high. Alternatively, this shale interval may reflect a reduction in the amount of sediments delivered to the area because of processes occurring farther east (upflow), such as channel switching, or more regional factors such as sea-level change.

The overlying sandstone packet consists mostly of facies C2.1 deposited from concentrated density currents (*cf.* Mulder and Alexander, 2001). The upward thinning and



fining trend in the upper part of the packet may reflect reduction in the rate and amount of deposition or perhaps the migration of the site of sand deposition away from the area of section RE because of compensation after a subtle mound had developed.

There are two alternative interpretations for the lateral relationship between beds within mini-slice SL 1A between areas A and B. The first (Figure 5.16) is that beds between KB-4 and the sandstone packet in area A (interpreted as distal lobe or lobe fringe deposits) are equivalent to all but the top ~3 m in area B (consisting of thin siltstone beds and laminae). The variations in bed thicknesses between these two equivalent intervals in areas A and B might reflect the position of these areas relative to the flow paths of the depositing currents. Area A might have been farther away from the axes of the flows than area B. In addition, area B might have been in a bathymetric low, compared to area A so that flows were diverted towards area B. The change in palaeocurrent direction to a more southerly directions (i.e., towards area B) may support the presence of a bathymetric low in area B during the deposition of most of the beds of mini-slice SL 4A in area B.

One of the reasons for this interpretation is that in area B mini-slice SL 4A consists of sandstone and siltstone and become more muddy in the upper part of the mini-slice. In area A, this vertical change in facies takes place in the lower half of the mini-slice. This interpretation suggests that the ~10 m thick sandstone packet forming the upper ~50% of the mini-slice SL 4A in area A is equivalent to the upper ~3 m interval of very thin siltstone beds and laminae in area B. The thinning and fining of the sandstone packet from area A to area B could reflect diversion of flows away from area B as a result of bottom

topography or that the flows that deposited sand that form packets do not continue for long distance downcurrent. If this interpretation is valid, then the sandstone packet in area A and the underlying siltstone and sandstone packet (best developed in area B) may have a shingled or nested form that was dictated by the depositional topography (*cf.* Bouma 2000; Piper and Normark, 2001) or facies type. Mini-slice SL 4A would be a series of shingled mounds. Beds similar to facies C2.1 have been shown to have limited lateral continuity at a higher level in the Cloridorme Formation (Enos, 1965; Ma, 1996).

The second alternative interpretation for the lateral relationship of the beds in mini-slice SL 4A is that the lower ~50% of the mini-slice in area A (consisting of thin-bedded siltstone, shale and a few sandstone beds) is equivalent to the lower ~50% of the more silty, sandy packet in area B. The variations in facies type and bed thicknesses might have been controlled by the location of both areas relative to the pathways of the depositing currents and perhaps topography. Area A may have been on a bathymetric high and/or located away from the axes of the depositing currents, while area B was located closer to the axes of the flows and/or in a bathymetric low. The sandstone packet in mini-slice SL 4A in area A would then be equivalent to the more sandy packet in the middle and upper part of mini-slice SL 4A in area B.

Beds of mini-slice SL 4A in area C represent the distal equivalents to the beds in area B. The beds in area C are similar to those in area B, but they are thinner and mini-slice SL 4A has more shale. This facies change may reflect downflow waning of the currents responsible for sediment deposition in area B. The variation in the thicknesses of

mini-slices SL 4A and SL 4B between areas A, B and C may be the result of differential compaction and the greater amount of compaction of shale compared to sandstone may account for part of the reduction in thickness of mini-slice SL 4A in area C and mini-slice SL 4B in areas A and B.

The deposition of the sandstone packet in the upper part of SL 4A in area A must have created a bathymetric high that controlled deposition patterns and caused flow diversions in mini-slices SL 4B through SL 4F. In these mini-slices, significant bed thickness and facies variations occur between areas B and A.

The fine grained facies of mini-slice SL 4B in area A, suggests the presence of a mound that behaved as an obstacle for flows from the east. The relief of this mound explains the thinness of megaturbidite BT-37 in area A (*cf.* Kneller, 1985, Pickering and Hiscott, 1985; Hiscott *et al.*, 1986).

Siltstone beds of subfacies D2.1A are restricted to area C and show a general palaeocurrent trend from east to west. Beds of subfacies D2.1A are not present in areas A and B, possibly due to depositional relief that diverted flows away from these areas. Only very thin beds and laminae of facies D2.2 and D2.3 and subfacies D2.1B and D2.1E are present in A and B suggesting that when the flows arrived the topographically high areas, they had low concentration that consisted mostly of silt.

During the deposition of mini-slice SL 4C, most of the sediments was diverted away from area A due to the mound that continued to act as an obstacle and divert most flows away from area A. Only mud or rarely thin siltstone were deposited from low

concentration turbidity currents in area A. Megaturbidite BT-38 thins in area A compared to areas C and B indicating the continued presence of a topographic high.

Siltstone beds in mini-slice SL 4C are thicker in area C than in area B. It is suggested that area C was located closer to the axes of the flow paths of the turbidity currents to explain this thickening. The presence of more siltstone beds exhibiting climbing ripple lamination (subfacies D2.1A) in area C than in area B further supports this. Climbing ripples indicate accelerated fallout from suspension and are generally observed closer to the inferred paths of decelerating turbidity currents.

The variation in the thickness of mini-slice SL 4C between areas C and B might be explained by greater compaction of older sediments under the weight of the greater total thickness of sandstone and siltstone in area B (*cf. Mutti et al., 1978*), or by greater tectonic subsidence in the vicinity of area B.

For mini-slices SL 4D through SL 4F, the distribution of facies and the difference in thickness was controlled mostly by variations in bottom topography. Megaturbidites BT-39 and BT-40 show flow from west to east suggesting that flows from the east were diverted away from area A on their first pass across the basin floor. These two megaturbidites may have accumulated during a short period of time, so that few other beds were deposited between them. BT-39 and BT-40 are thin in area B, probably due to the presence of a mound in that area. These beds are thicker in area A where muddy SL 4C would have compacted to provide additional accommodation space. Deposition of these megaturbidites in area A smoothed sea floor irregularities and filled depressions. Sea

floor topography was significantly reduced and became almost flat at the time of deposition of megaturbidite BT-40a, which shows an initial flow from the east, and megaturbidite BT-41 at the base of mini-slice SL 4G. Deposits above this level are essentially sheet-like (Figure 5.16).

Deposition of mini-slices SL 4G and SL 4H was dominated by low density turbidity currents carrying mostly silt and mud loads, interrupted by the deposition of megaturbidites from larger flows. Megaturbidites BT-41a, BT-42 and BT-43 show initial flow from east to west, indicating that flows initiated from the east were reaching the study area unimpeded, perhaps due to the burial of the obstacle that controlled the paths of flows below BT-41. These obstacles or irregularities in bottom topography were removed or smoothened mostly by the deposition of megaturbidites (*cf.* Pilkey, 1988).

Variation in the number and type of siltstone and sandstone facies within mini-slices SL 4G and SL 4H between areas A, B and C reflect downflow fining and thinning. The greater thickness of mini-slice SL 4H in area A may reflect closer proximity to the flows pathways. Alternatively, area A may represent a distal fringe of a sediment body developed east of the study area.

Regarding the internal facies architecture, the main variation between sections RE, FP1, FP2 and PRM1 is in mini-slice SL 4A. Minimal variation occurs within the facies of the lower part of this mini-slice between the four sections. This interval may represent a marginal part of a more sandy and silty packet in area B and perhaps farther to the east of area A. It has a sheet-like or a slightly lensing geometry between these four sections. The

shaly interval is interpreted to represent a period when the supply of coarser sediment was decreased as a result of topography-controlled diversion of turbidity currents or by a reduction of sediment supply to the entire area due to more regional (allocyclic) factors. Beds of facies B2.2 are more common in section PRM1 below the main sandstone packet and within packets under amalgamated units. They are interpreted to be genetically related to the deposition of the sandstones in the packets. These beds may have been deposited from concentrated flows that incorporated mud from the underlying substrate. The beds of facies B2.2 might also represent flows that were generated by the collapse of upslope channel banks due to undercutting.

Thick siltstone beds of subfacies D2.1A are interpreted to be the deposits of large flows that carried a large proportion of silt in suspension. These flows deposited the bulk of their load as they travelled over a mound or obstacle, formed by the deposition of the sandstone beds in the packet.

Variations in the bed thickness and the degree of amalgamation of the sandstone beds in the packet might reflect subtle bottom topography generated by deposition of the sandstone beds. Alternatively, thinning of the sandstone packet in section RE might reflect a more distal or marginal position in the sand body.

For mini-slices SL 4B through SL4G, little or no variation occurs between sections RE, FP1 and FP2. These mini-slices reflect a reduced sediment input to the area above the mound created by the sand packet. Slight variations in facies or subfacies reflect differences in the positions of the sections relative to the depositing currents and /or slight

variation in bottom topography. Mini-slices SL G and H have a tabular geometry and the siltstone facies and subfacies reflect downflow fining on a more-or-less flat seafloor.

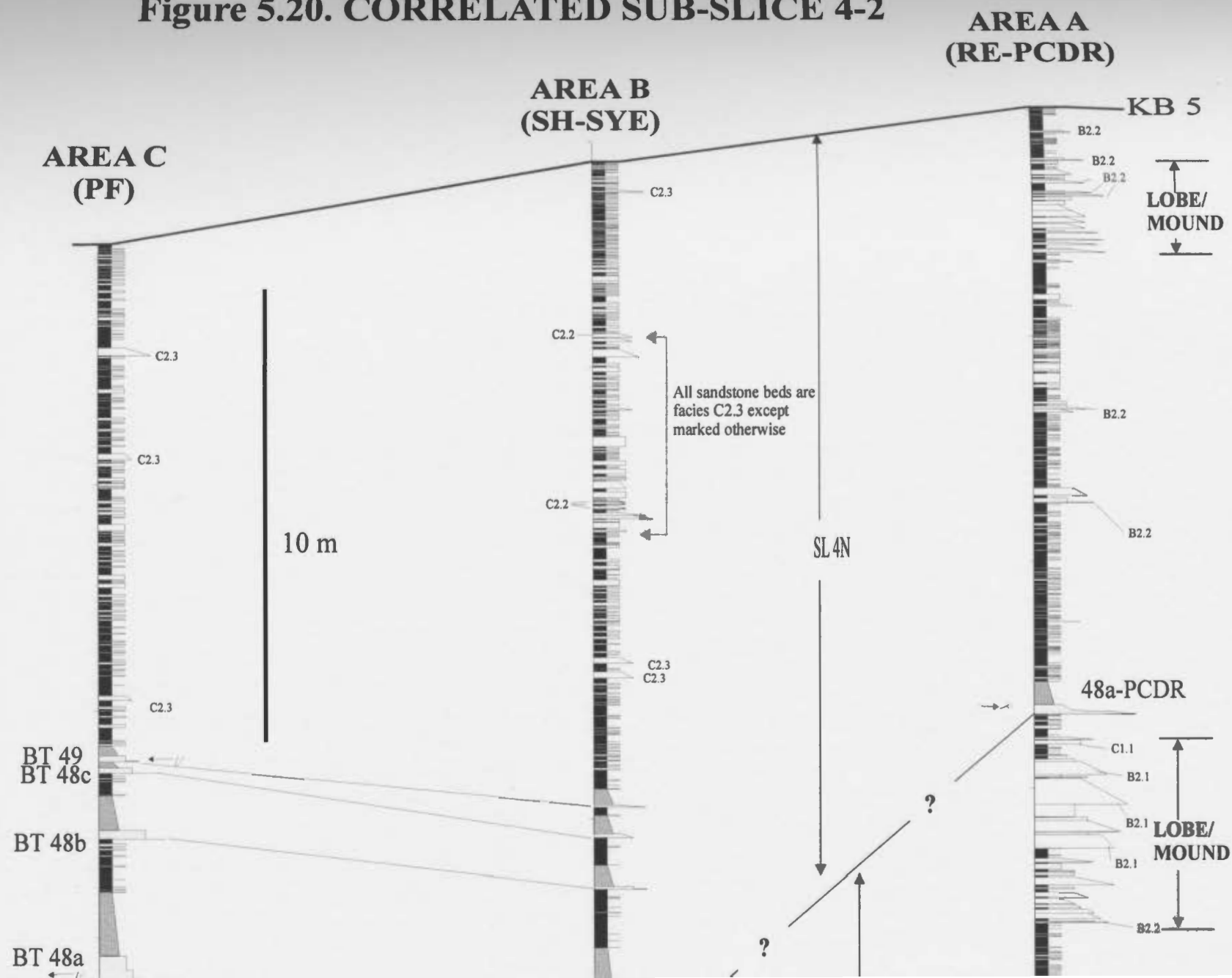
#### 5.4.7.3. Description of Sub-slice 4-2

In sub-slice 4-2, shale comprises about 72% of the sub-slice in areas B and C. In area A shale comprises about 67% of the total thickness of sub-slice 4-2 (Table 5.2). Total sandstone thickness is less than the total siltstone thickness in all three areas, including area A (unlike sub-slice 4-1; Table 5.2). The mini-slices also vary in thickness between the three areas (Table A5-4.1). Mini-slices SL 4I and SL 4J and SL 4K show the least variation across the area. The datum in Figure 5.20 is drawn at the base of SL 4K. Mini-slices SL 4L and SL 4M are significantly thicker in area A compared to areas B and C. Mini-slice SL 4N is significantly thicker in area B.

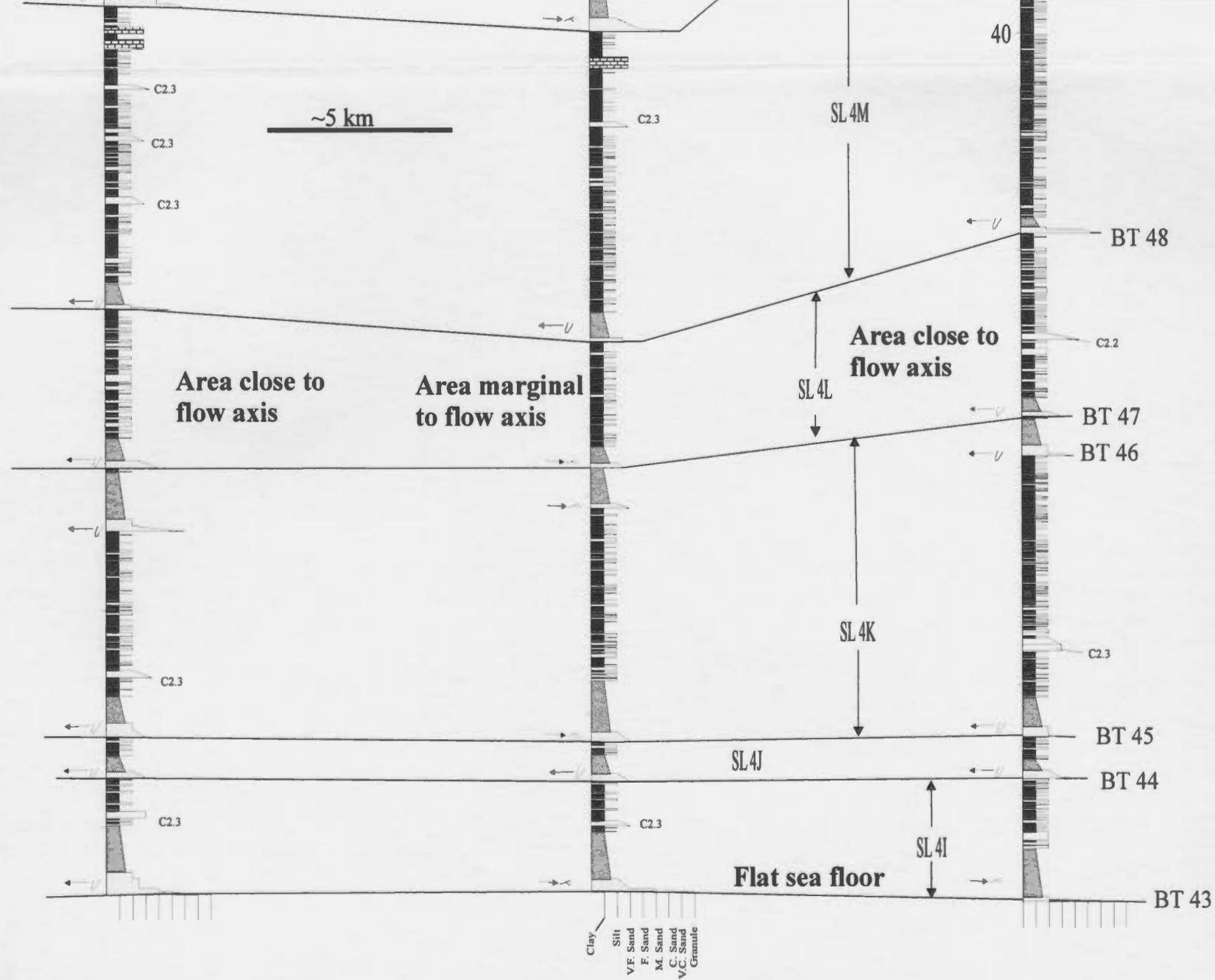
Megaturbidites and K-bentonite bed KB-5 divide sub-slice 4-2 into six mini-slices (SL 4I through SL 4N). Megaturbidites BT-48b, BT-48c and BT-49 are present only in areas B and C. The lower parts of megaturbidites 48b-PF and 48c-PF change from facies C2.5 in area C to facies C2.4 in area B. Megaturbidite BT-48a is assigned a lower case code because there is some uncertainty regarding its correlation between areas B and C. All megaturbidites that have flutes at their base indicate that the initial flow was from east to west (Figure 5.20). Some beds, without flutes at their base, have ripple lamination in their lower parts that suggest flow from west to east (Figure 5.20).

Megaturbidites vary in thickness between all three areas (Table A5-4.2).

**Figure 5.20. CORRELATED SUB-SLICE 4-2**





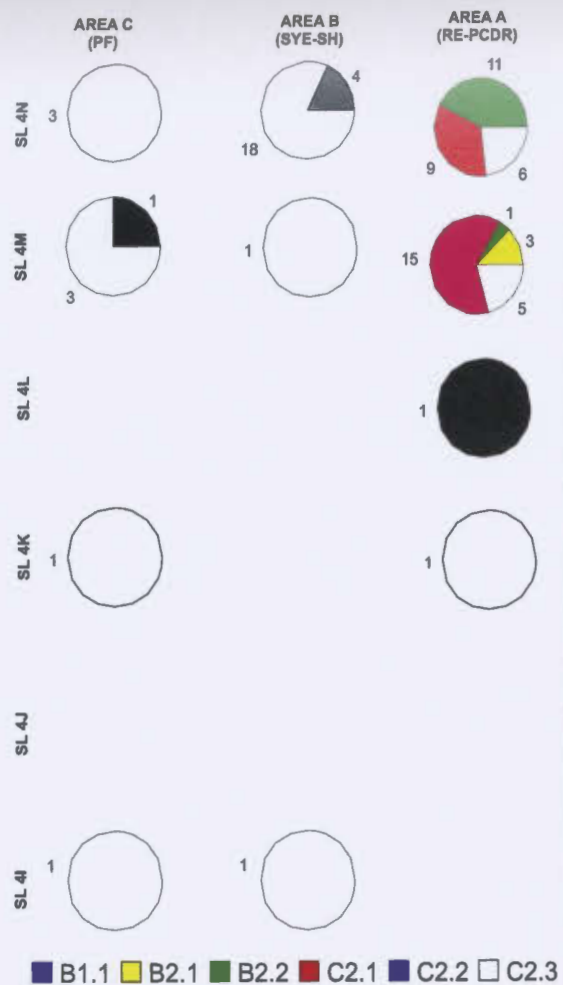


Specifically, megaturbidites BT-44, BT-45 and BT-48 are significantly thinner in area A than in areas B and C. Megaturbidites BT-46, BT-47, BT-48a are significantly thicker in area C than in areas A and B. Megaturbidite BT-43 is significantly thinner in area B than in areas A and C. Megaturbidite BT-48a shows the most pronounced decrease in thickness in area A and the most pronounced increase in thickness in area C.

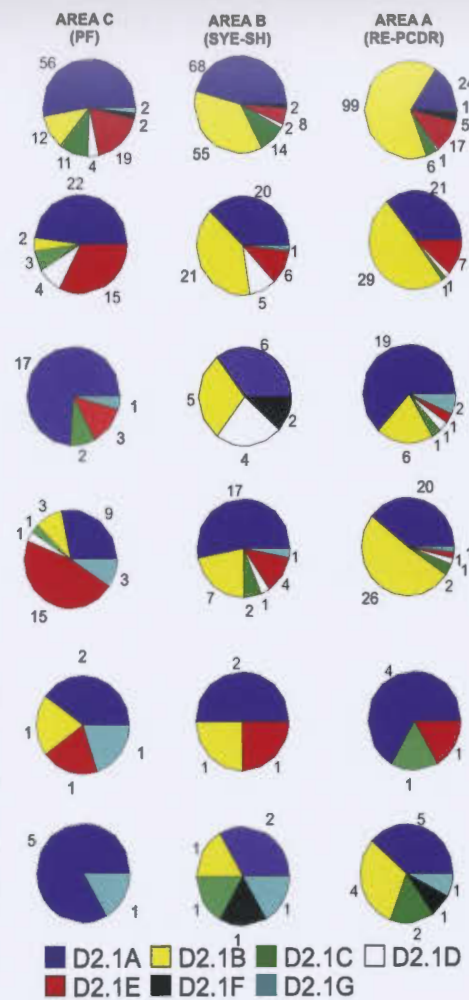
Sandstone beds other than facies C2.4 (the lower parts of megaturbidites) vary slightly in numbers between the three areas in mini-slices SL 4I through SL 4K (Figure 5.21). Greater variations in the numbers of sandstone beds between areas A, B and C characterises mini-slices SL 4M and SL 4N. In mini-slice SL 4M, sandstone beds of facies C2.1, C2.3, B2.1 and B2.2 form a packet in area A, however, this packet is not present in areas B and C, where there are significantly fewer sandstone beds. In mini-slice SL 4N, sandstone beds of facies C2.1, C2.3 and B2.2 form a packet near the top of the mini-slice in area A. Sandstone beds of facies C2.3 and C2.2 are common in area B. Sandstone beds in area B occur with other siltstone beds. Sandstone beds in areas A and B could not be correlated to adjacent composite sections. In area C, there are less than five sandstone beds of facies C2.2 and C2.3 in each of mini-slices SL 4M and SL 4N.

Siltstone beds show a general decrease in number from east to west (Figure 5.21) for mini-slices SL 4I through SL 4K. In these mini-slices, beds of subfacies D2.1A decrease in number from east to west, while other siltstone subfacies increase especially subfacies D2.1E. In mini-slice SL 4L fewer siltstone beds occur in area B than areas A and C. The thickness of the siltstone beds decreases significantly in area B in mini-slice SL 4L.

## SANDSTONE FACIES



## SILTSTONE SUBFACIES



## SILTSTONE FACIES

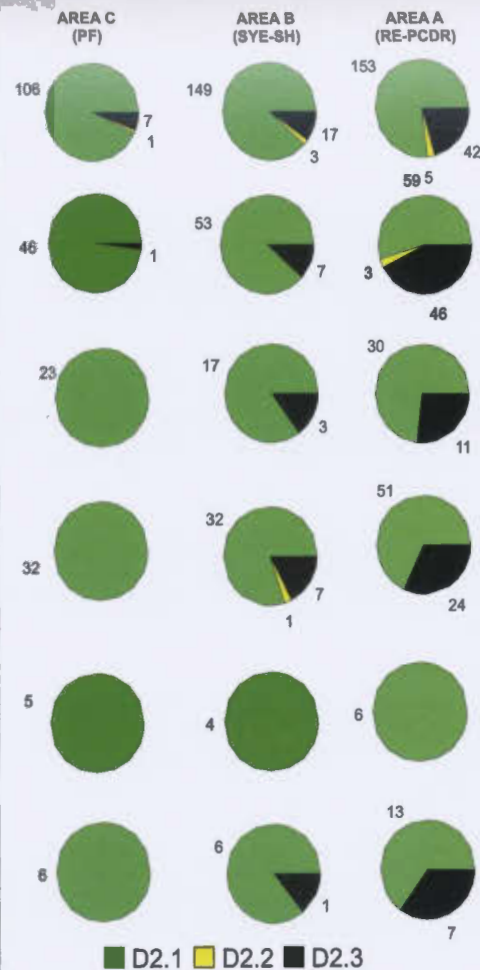


Figure 5.21. Numbers of sandstone and siltstone beds assigned to the different facies and subfacies in the mini-slices of sub-slice 4-1. These mini-slices are compared between area A, B and C.

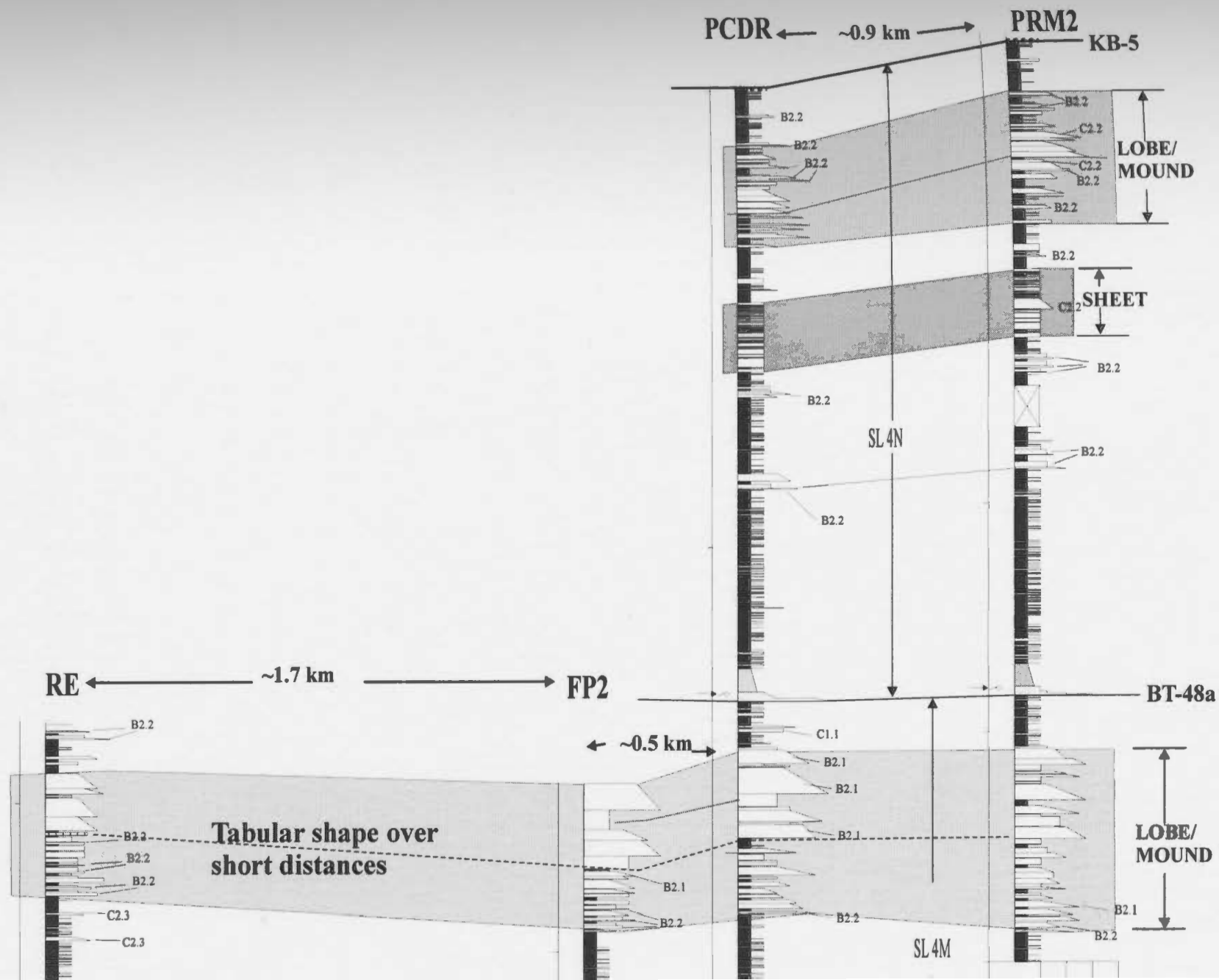
(Figure 5.21 and Table CD-T4). In mini-slice SL 4N, there is a decrease in the number of siltstone beds from east to west, but the siltstone beds in area A are dominated by subfacies D2.1B, in contrast to areas B and C, where siltstone beds assigned to subfacies D2.1A are most common.

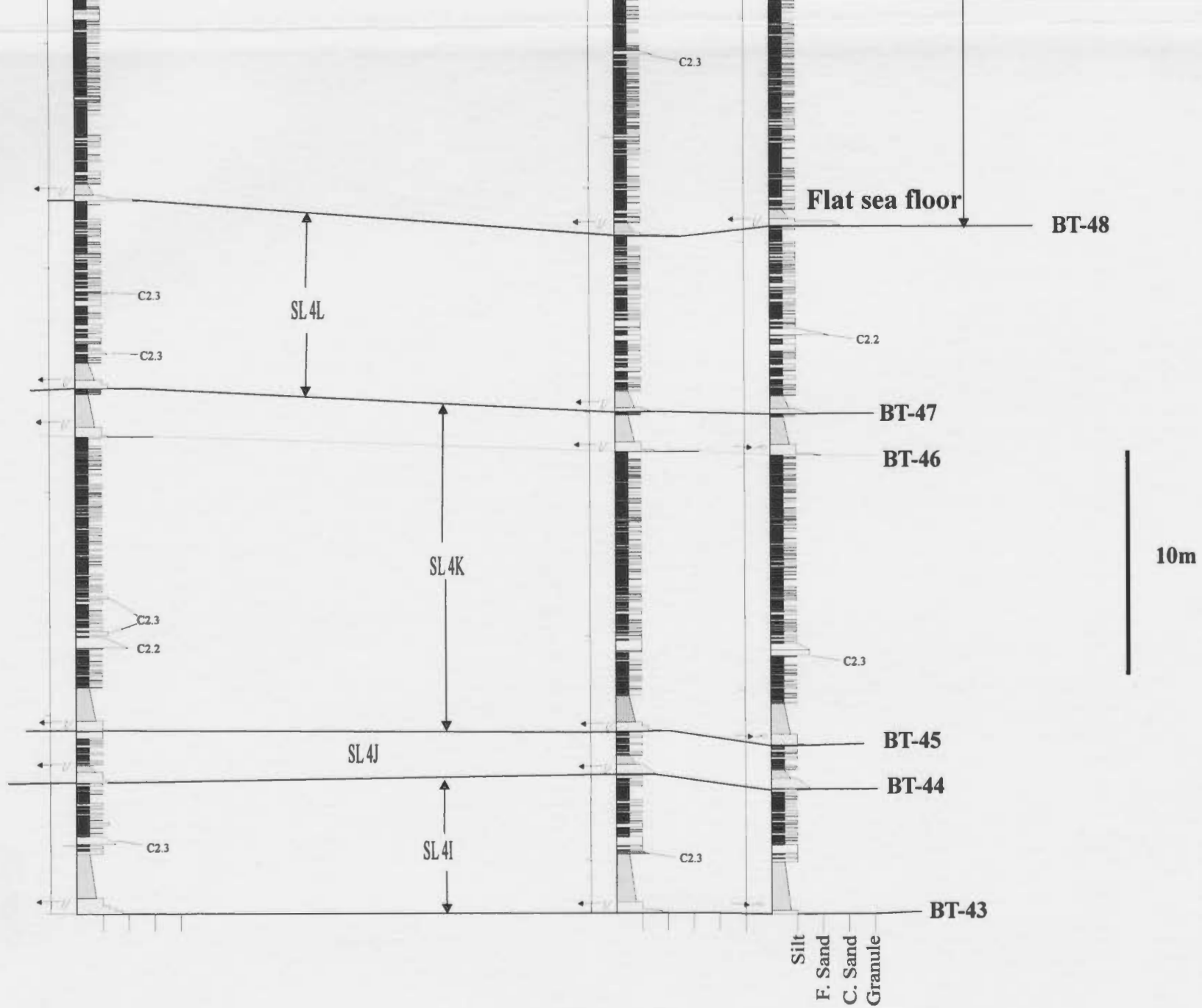
For the investigation of the internal architecture of sub-slice 4-2, sections RE, FP2, PCDR and PRM2 were used. The distance between section RE and section FP2 is ~1.7 km. The distance between section FP2 and section PCDR is about 0.5 km. The distance between sections PCDR and PRM2 is about 0.9 km (Figure 5.22).

Sandstone beds other than facies C2.4 and C2.5 are only common in mini-slices SL 4M and SL 4N. These sandstone beds form packets that are 5-8 m thick. The sandstone packet in mini-slice SL 4M may be divided into two parts: a lower part that consists of beds of facies B2.2, C2.1 and C2.3, and an upper part consisting of sandstone beds of facies C2.1, B2.1 and C2.3 that form amalgamated units. One thick siltstone bed of subfacies D2.1A occurs in the upper part of this packet in section FP2. A sandstone bed of facies C2.3 occurs approximately in the same position within the packet in section PCDR (Figure 5.22). In section PRM2, sandstone beds in the packet are thinner and less amalgamated than the beds in sections PCDR.

A second sandstone packet occurs in the upper part of mini-slice SL 4N in sections PCDR and PRM2. The beds in this packet are thinner than most of the beds in the packet in mini-slice SL 4M. The packet consists of sandstone beds of facies C2.1 that occur in amalgamated units and beds of facies B2.2 that lie above and below the amalgamated

**Figure 5.22. Short distance correlation of sub-slice 4-2**





units. In addition to sandstone beds that form packets in mini-slice SL 4N, there are several beds of facies B2.2 occurring in clusters of two to three beds in section PRM2 (Figure 5.22).

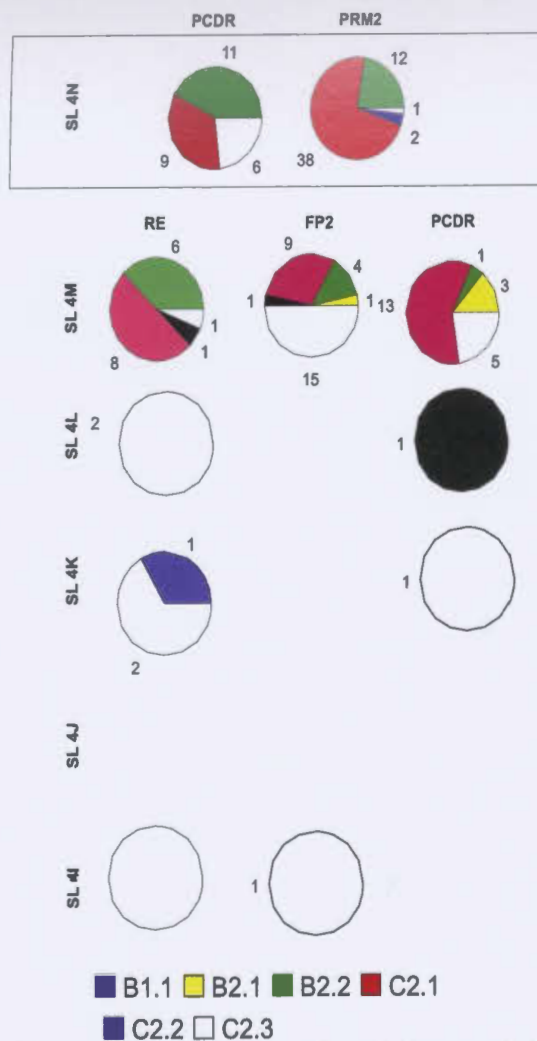
Siltstone facies show variations in the number of beds and the type of facies and subfacies between sections RE, FP2 and PCDR for mini-slices SL 4I through SL 4M (Figure 5.23). Similar variations are also observed in mini-slice SL 4N between sections PRM2 and PCDR. One packet of siltstone occurs in the middle of mini-slice SL 4N. This packet is 3-5 m thick and consists of medium to thick beds of subfacies D2.1C and D2.1G in addition to thin beds of subfacies D2.1A, B2.1B and B2.1E.

#### 5.4.7.4 Interpretation of Sub-slice 4-2

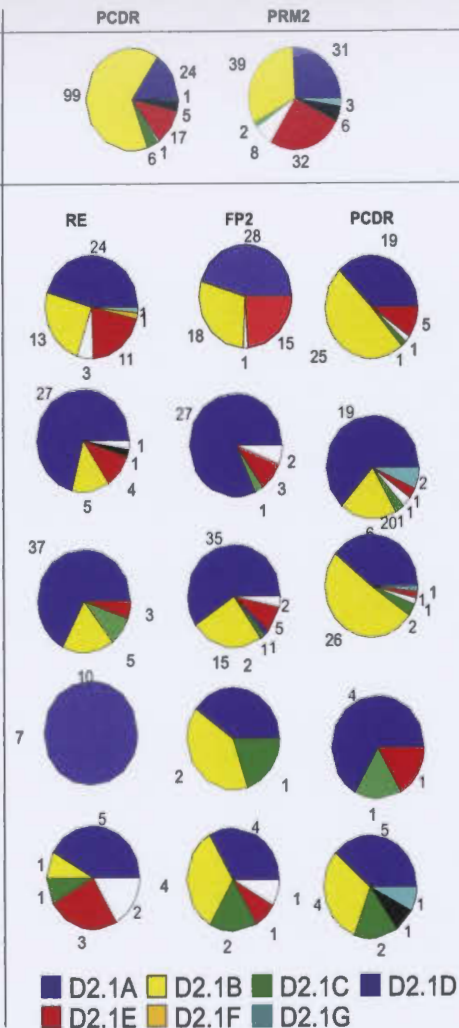
The mini-slices that form the lower part of this sub-slice (mini-slices SL 4I through SL 4L) show less pronounced variation in thickness and type of facies than mini-slices SL 4M and SL 4N. Except for the megaturbidites, the sediments in mini-slices SL 4I through SL 4L reflect deposition from low concentration flows carrying mostly silt and mud loads. These flows travelled from east to west and deposited thinner siltstone beds towards the west. Facies and subfacies variations likely also reflect the location of areas A, B and C relative to the pathways of the depositing currents. Thinner beds of siltstone in area B in mini-slice SL 4L compared to areas A and C may suggest that area B was not as close to the paths of the flows as areas A and C. The variations in the thickness of mini-slices might reflect greater deposition in the east closer to the source area of the flows.



## SANDSTONE FACIES



## SILTSTONE SUBFACIES



## SILTSTONE FACIES

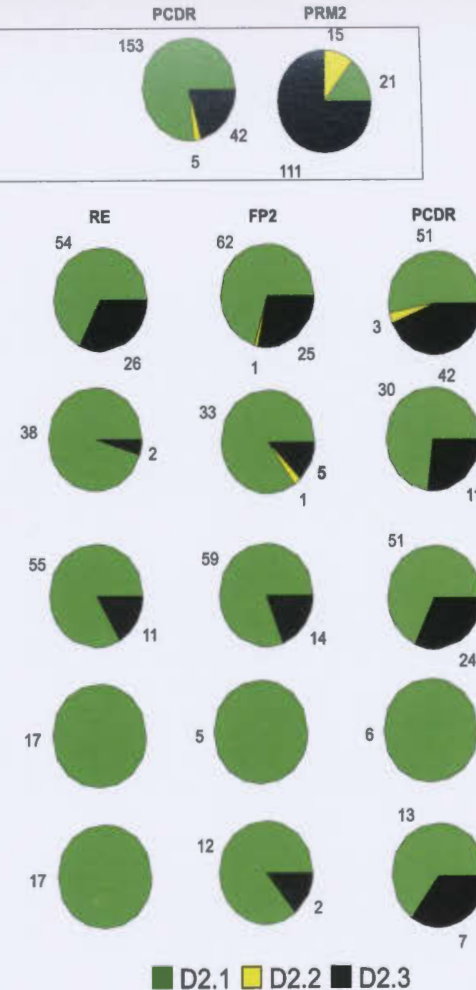


Figure 5.23. Numbers of sandstone and siltstone beds assigned to the different facies and subfacies in the mini-slices of sub-slice 4-2. These mini-slices are compared over a short distance between four sections in area A. Note that for mini-slice SL 4N, only two sections were compared.



Megaturbidites in mini-slices SL 4I to SL 4L increase in thickness from east to west, probably due to ponding of flows in the west (Hiscott *et al.*, 1986; *cf.* Rothwell *et al.*, 1992). It is believed, based on the orientation of flute marks on the bottom of megaturbidites, that the flows that deposited these layers were generated east of the thesis area.

Unlike time-slices 3, 2 and 1, variations in thickness of the mini-slices that could be attributed to bottom topography are not obvious. This does not, however, signify that bottom topography due to subsidence or compaction was not developed during the deposition of the lower part of sub-slice 4-1, rather, the sedimentation rate was sufficiently high to mask these effects compared to older mini-slices when sedimentation rates were possibly much lower.

In mini-slice SL 4M, sand was deposited in area A where it formed a ~5 m-thick packet. It is believed that this packet decreased in thickness west of area A. The lower part of the packet consists of thin to medium sandstone beds of facies C2.1 that show little or no amalgamation. The upward fining trend observed in these beds is not interpreted to have formed as a result of filling of a channel because no deep scours were observed below these packets in the field over the length of the outcrop (tens of metres). Further, upward fining trends are not reliable indicators of channel deposits (Chen and Hiscott, 1999). Instead, this trend is interpreted to be the result of compensation. One bed of facies B2.2 occurs below the packet and is interpreted to have been deposited from a concentrated flow that eroded part of the underlying muddy material and incorporated it

into the flow (*cf.* Pickering, 1981). The packet in area A must have formed a sediment mound on the sea floor (Figure 5.20) and affected deposition from subsequent flows.

An alternative interpretation of the correlation presented in Figure 5.20 is that megaturbidite 48a-PCDR is equivalent to BT-49 observed in areas B and C. This would require that the sandstone packet in area A diverted even the thick flow that deposited bed BT-48a in areas B and C. If this interpretation is true, then the flow that deposited the megaturbidite above the sandstone packet in area A must have thinned substantially as it moved from east to west, possibly as a result of the irregular bottom topography.

Mini-slice SL 4N shows significant variation in facies and thickness across the area, particularly between areas A and B. Megaturbidite BT-48a thins significantly in area A (as bed 48a-PCDR) probably due to the presence of a sediment mound in that area. Thinner megaturbidites, BT-48b, BT-48c and BT-49 were apparently diverted from area A. The lower parts of megaturbidites 48b-PF and 48c-PF change from facies C2.5 to facies C2.4 in area B because of the eastward-moving flows that deposited them were more mature as they reached area B after the incorporation of water promoted better grain segregation. Most flows in this interval bypassed area A and deposited mainly muddy and silty sediments in areas B and C. As the effect of the high topographic relief in area A was decreased due to deposition and probably compaction of the sediments below the sand packet, more flows generated in the east reached all three areas. Thicker siltstone and sandstone beds were deposited in areas B and C than in area A, possibly reflecting continued partial diversion of the flows from area A due to residual relief of the presence

of the sediment mound Mini-slice SL 4N is thicker in area B than in area C because more sand and silt were deposited in area B. This might have been controlled by greater compactional subsidence in area B.

Individual beds could not be correlated between areas A and B in mini-slice SL 4N although some speculated correlations are indicated on Figure 5.20. The siltstone packet in the upper third of mini-slice SL 4N in area A might be equivalent to some of the sandstone and siltstone beds in the middle of the mini-slice in area B. The siltstone packet might be analogous to the gently lensing subelement of the lower Hueneme Fan offshore California (Piper *et al.*, 1999). The greater thickness of mini-slice SL 4N in area B is due to flows bypassing area A due to its higher relief.

The upper sandstone packet in mini-slice SL 4N in area A is similar in its facies composition to the packet in mini-slice SL 4M in the same area. The packet in mini-slice SL 4N is, however, thinner and contains more beds of facies B2.2 in its lower part. This packet is also of limited lateral extent and perhaps had sufficient height to divert most of the flows away from area A; hence, more siltstone beds were deposited in areas B and C late in the deposition of mini-slice SL 4N.

For the internal architecture of sub-slice 4-2, the mini-slices do not show significant variation in thickness between sections RE, FP2, PCDR and PRM2, especially the lower mini-slices. The facies changes (Figure 5.23) in the lower mini-slices (SL 4I through SL 4L) reflect the downflow changes that take place as the currents lose part of their loads and momentum. Sandstone packets in mini-slices SL 4N and SL 4M have a

more-or-less tabular geometry over a short distance considered in area A (Figure 5.22).

The variations in facies and thicknesses of these packets probably reflects the effects of compensation and the location of the different sections with respect to the geometry of the sediment body that forms the packet.

#### **5.4.8. Description of Time-slice 5**

Time-slice 5 is bounded at the base by K-bentonite horizon KB-5 and at the top by KB-6. This is one of the thinnest time-slices. It ranges in thickness from 41.5 to 43 m in areas C and B and is about 39 m thick in area A. A fault observed in area B in mini-slice SL 5B, had stratigraphic displacement of approximately 4-5 m across it. Another inferred fault is present in area A in mini-slice SL 5G, because the thick megaturbidite BT-56 is missing in this area.

Comparison of bed numbers and total thicknesses between the three areas (Table CD-T5) is misleading because part of time-slice 5 is affected by faulting. Comparison of bed numbers and total thicknesses on the mini-slice scale is more accurate.

Megaturbidites and K-bentonite horizons divide time-slice 5 into seven mini-slices (SL 5A through SL 5G). These mini-slices vary significantly in thickness but there is some uncertainty regarding the thickness of mini-slice SL 5B in area B and mini-slices SL 5F and SL 5G in area A because of faulting. Mini-slice SL 5A is significantly thick in area B and significantly thin in area C ( $>\pm 10\%$  deviation from its mean thickness). Mini-slice SL 5B does not change in thickness between areas A and C. Mini-slice SL 5C shows no

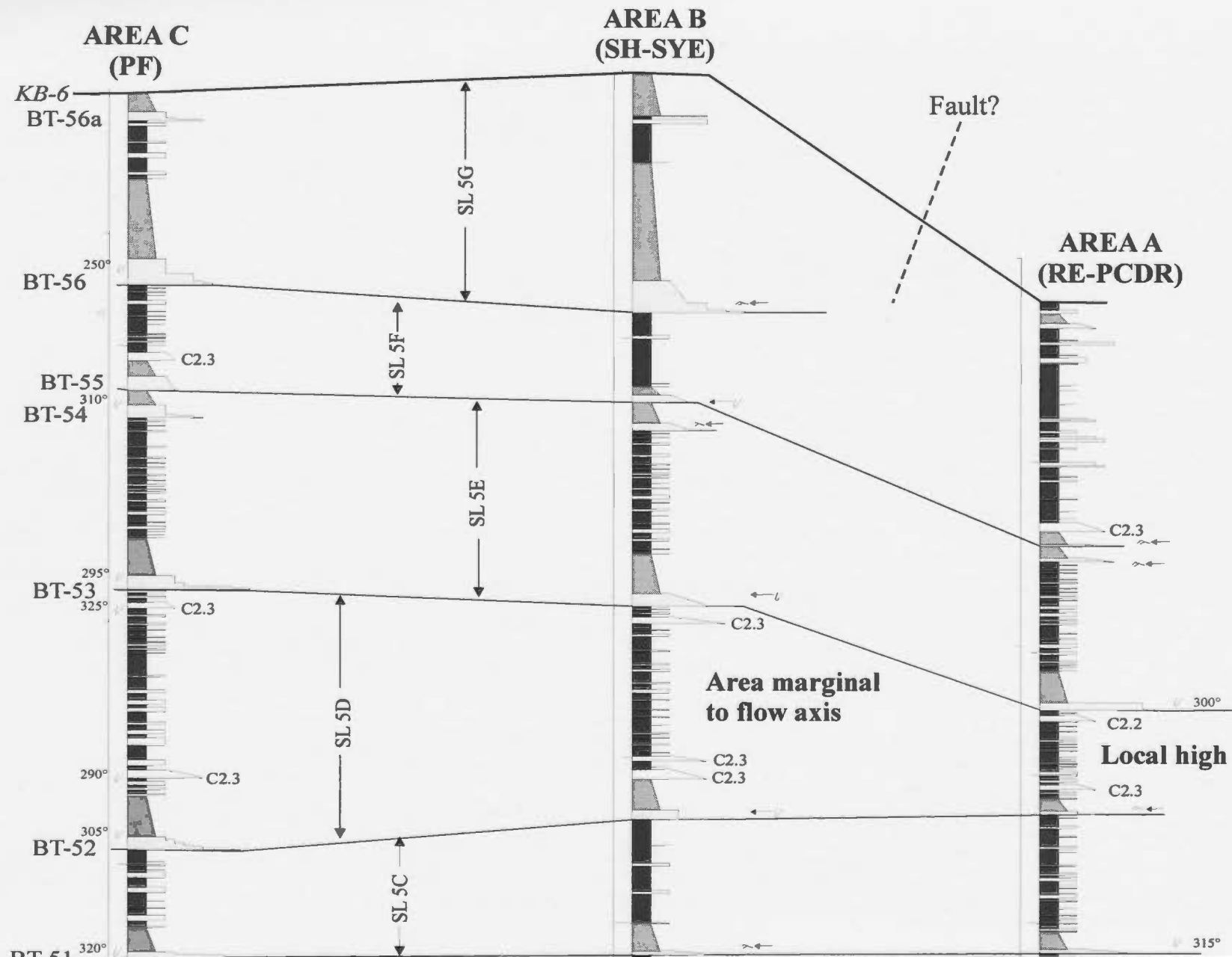
significant change in thickness in the three areas and so the datum in Figure 5.24 is placed at the base of this mini-slice. Mini-slice SL 5D is significantly thinner in area A than in areas B and C. Mini-slice SL 5E is only significantly thin in area A. Mini-slice SL 5F is thicker in area C than in area B and mini-slice SL 5G is thicker in area B than in area C (Table A5-4.1).

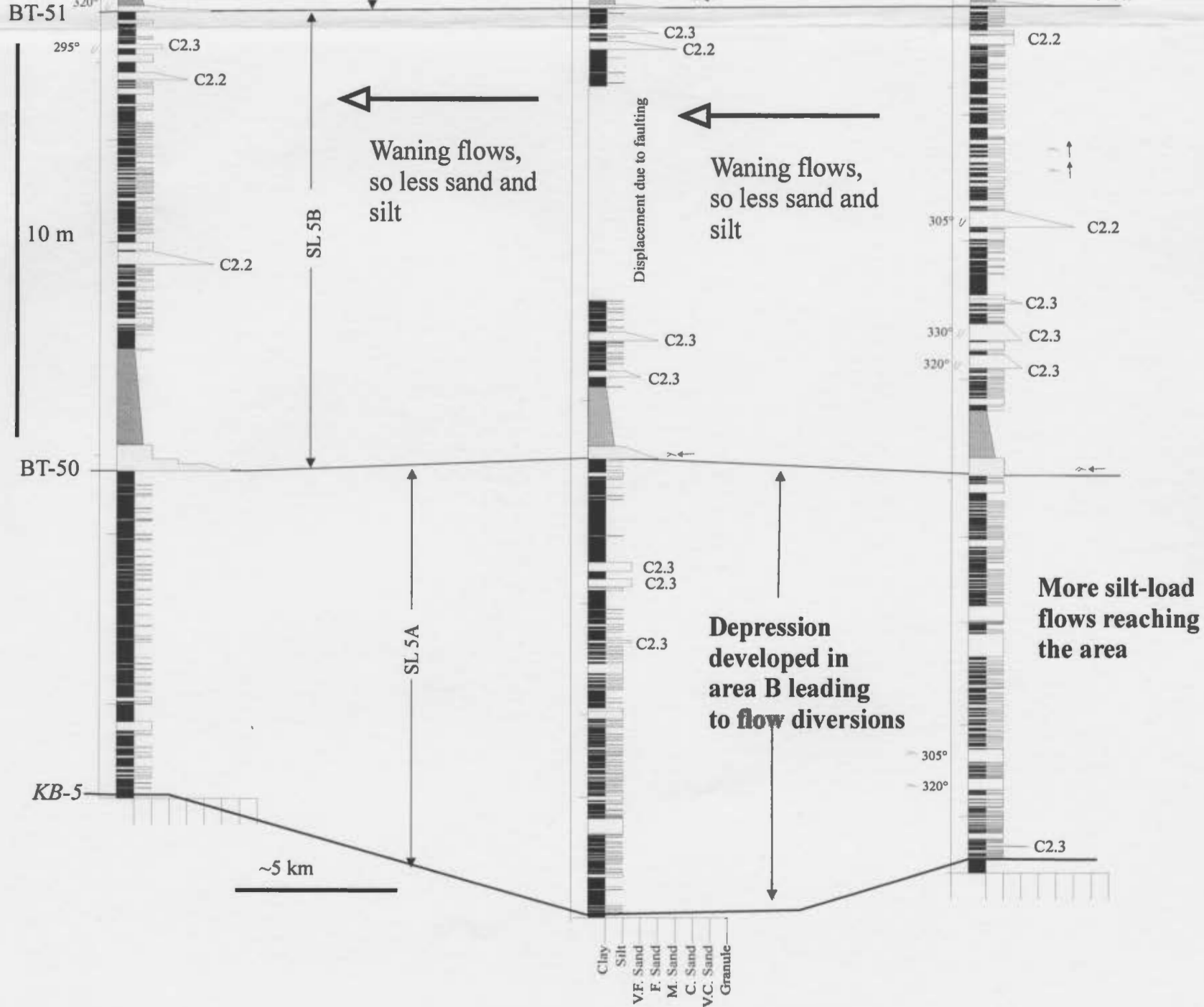
Megaturbidites are significantly thicker in area C and significantly thinner in area A. Only megaturbidites BT-50 and BT-55 are unusually thin in area B (Table A5-4.2). Most of these megaturbidites have flutes or ripple laminations indicating flow from east to west. All lower parts of the megaturbidites except BT-56a are assigned to facies C2.4. The lower part of megaturbidite BT-56a is assigned to facies C2.5.

Non-megaturbidite sandstone beds belong to facies C2.2 and C2.3. Less than 5 beds are present in any of the mini-slices, some of which are medium to thick bedded and may be tentatively correlated between the three areas (Figure 5.24).

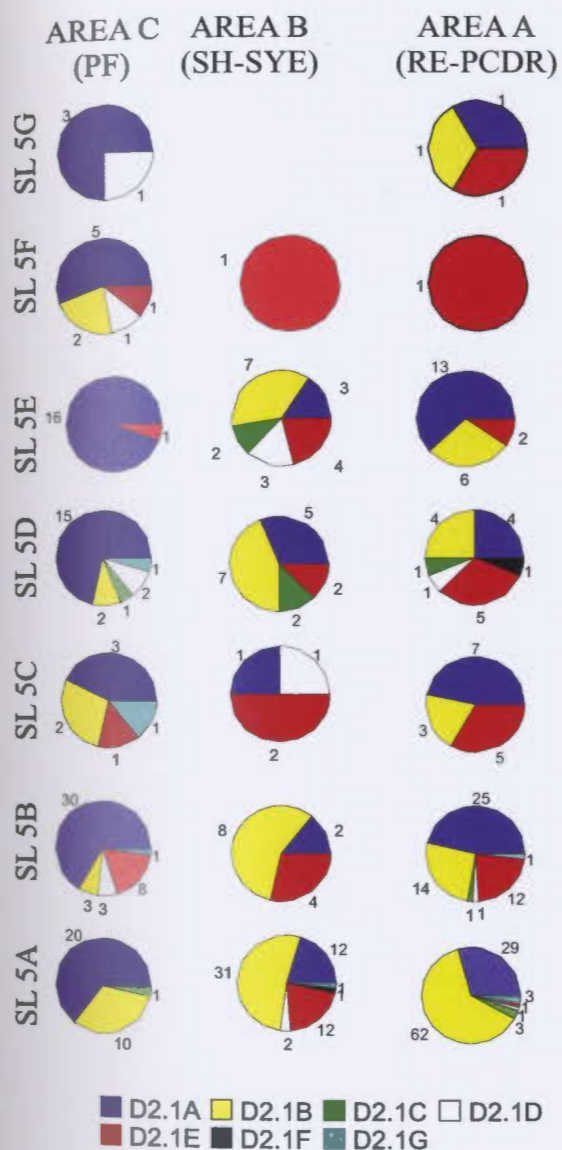
Siltstone beds decrease in number from east to west in mini-slice SL 5A, and between areas A and C in mini-slice SL 5B (Figure 5.25). In mini-slice SL 5C, siltstone beds are rare in area B. There is no pronounced change in the number of siltstone beds between areas A, B and C in mini-slices SL 5D and SL 5E (Figure 5.25). In mini-slices SL 5F and SL 5G, there are more siltstone beds in area C than in area B. Siltstone subfacies also vary between the three areas. In time-slice 5, siltstone beds of subfacies D2.1B are common and in some areas they are more common than subfacies D2.1A. Siltstone beds assigned to subfacies D2.1C, D2.1D and D2.1G are also present in some of the mini-slices

Figure 5.24. CORRELATED TIME-SLICE 5





## SILTSTONE SUBFACIES



## SILTSTONE FACIES

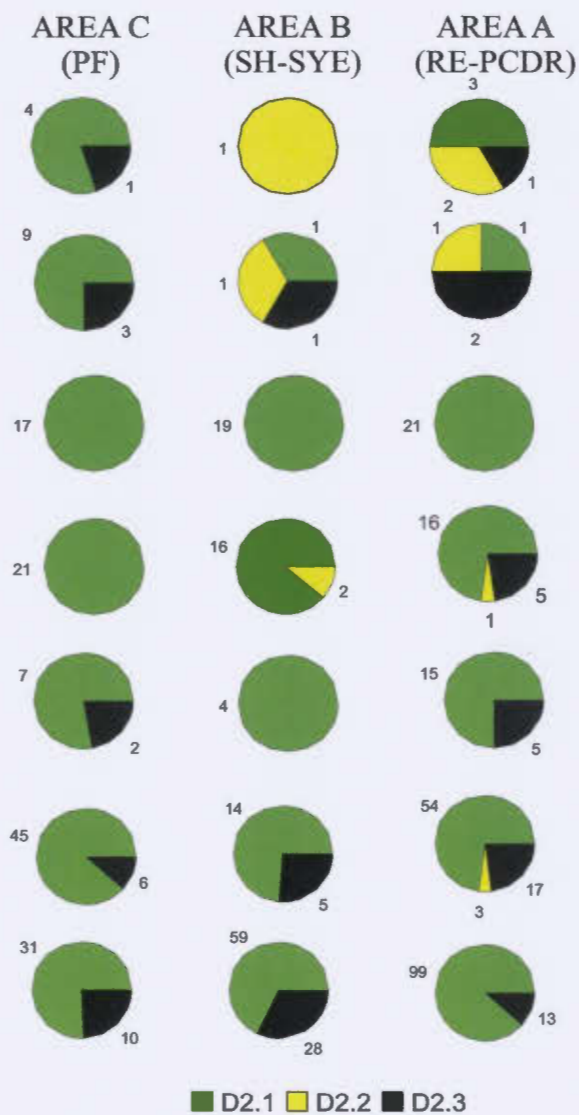


Figure 5.25. Numbers of siltstone beds assigned to the different facies and subfacies in the mini-slices of time-slice 5. These are compared between areas A, B and C.



(Figure 5.25). Some of the siltstone beds assigned to these three subfacies are medium to thick bedded in mini-slice SL 5A.

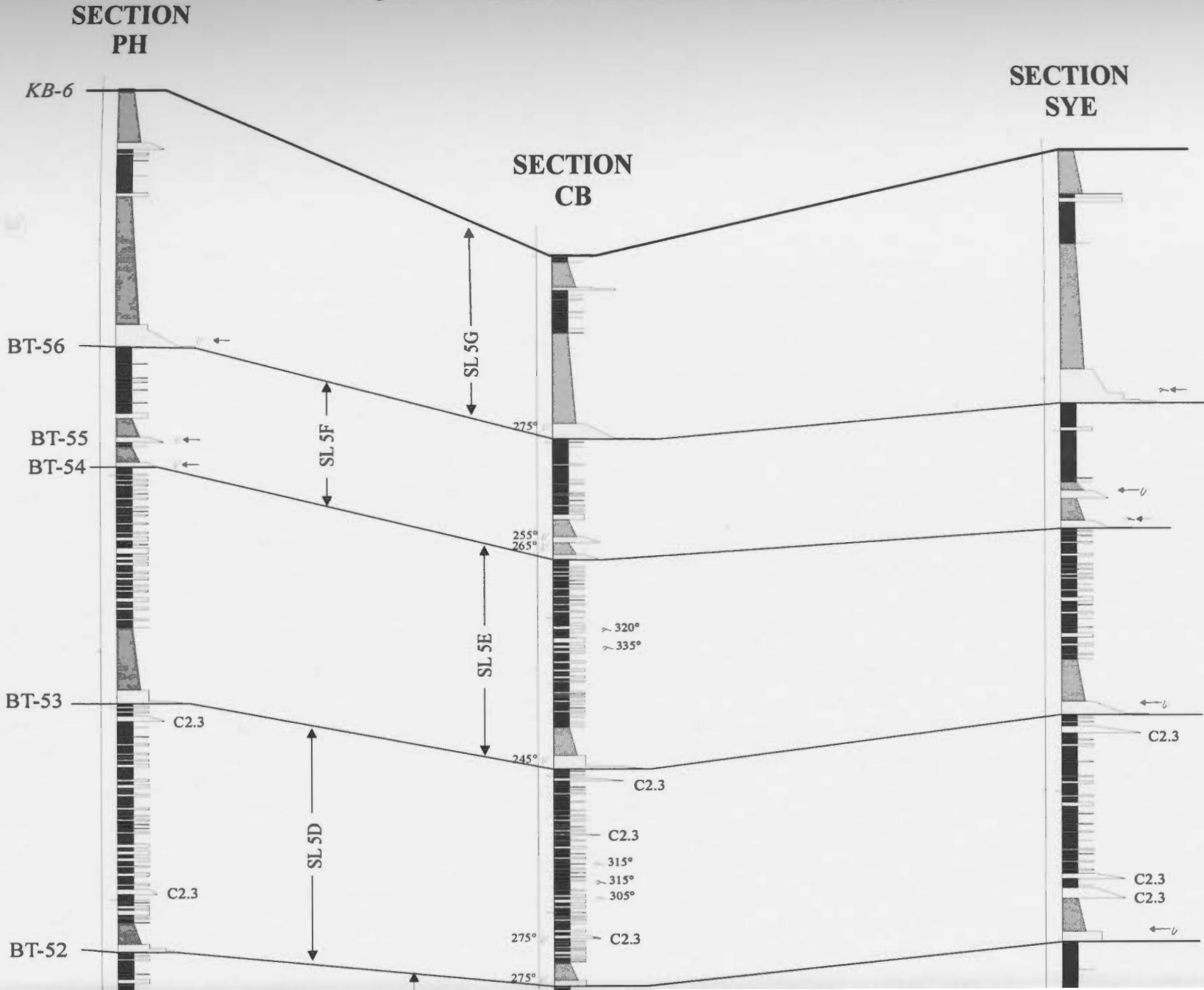
For the internal architecture of time-slice 5, three sections from area B are used. Section CB was measured in two different areas (Chapter 2). The distance between section PH and section CB in the lower part of time-slice 5 (between KB-5 and BT-52) is about 0.9 km. The distance between these two sections in the upper part of time-slice 5 (between BT-52 and KB-6) is about 2.2 km. The distance between section CB and section SYE varies from about 3 km in the lower part of time-slice 5 to about 2 km in the upper part of this time-slice (Figure 5.26).

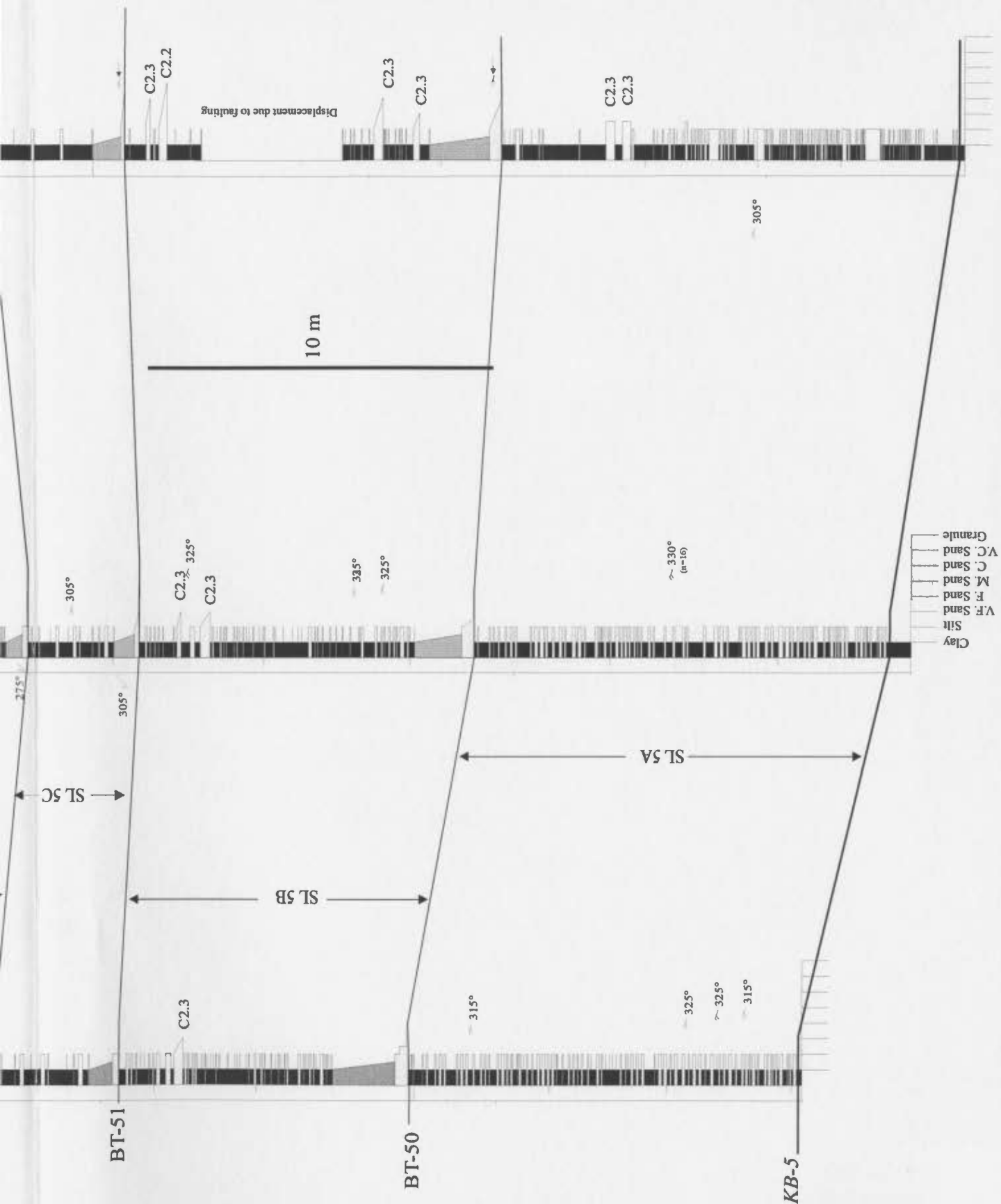
The thicknesses of the mini-slices vary between the three sections. Some mini-slices show a greater difference in thickness than others (Figure 5.26). Megaturbidites show slight variations in thickness between the three closely-spaced sections. Specifically, megaturbidites BT-56 and BT-56a show a pronounced decrease in thickness in section CB compared to sections PH and SYE.

It should be mentioned here that thickness of time-slice 5 as measured in the field for sections CB and PH is 30% thicker than what is presented in the thesis. This greater thickness is believed to have resulted because of folding, which was removed (all beds of time-slice 5 were reduced by about ~30%; Appendix A5).

Sandstone beds of facies C2.3 and C2.2 are present in three sections. These sandstone beds thin and fine from section SYE to sections CB and PH. Siltstone beds are assigned to different facies and subfacies and have similar abundances and character

**Figure 5.26. Short distance correlation of time-slice 5**





between sections PH and CB in mini-slices SL 5A, SL 5B and SL 5C. In section SYE, the number of siltstone beds is less in mini-slices SL 5A and SL 5C. Greater variation in the number and type of siltstone facies and subfacies between these three sections characterises mini-slices SL 5D through SL 5G (Figure 5.27).

#### **5.4.9. Interpretation of Time-slice 5**

Time-slice 5 was dominated by the deposition of thin to medium siltstone beds and more rarely sandstone beds, from low concentration turbidity currents. This depositional environment was occasionally interrupted by larger flows, depositing megaturbidites. The larger flows were possibly generated from sediment failure east of the study area. Slight variations in the thicknesses of the mini-slices reflect compensation and perhaps the combined effects of compaction and tectonic subsidence (*cf.* Mutti, 1992; Mutti *et al.*, 1999). Mini-slice SL 5A is characterised by a high proportion of siltstone beds that fine and thin from east to west. The greater thickness of mini-slice SL 5A in area B than in area A might indicate that the flows depositing the siltstone beds in area A, eroded the underlying muddy material. Alternatively, area B might have been a slight depression due to the greater compaction of the underlying sediments beneath the sands of time-slice 4. Beds thin considerably between areas B and C, probably due to the currents depositing most of their coarse load in area B.

Mini-slice SL 5A differs from other mini-slices by having a high proportion of siltstone beds, some of which are thick bedded. It is suggested that there was an increase

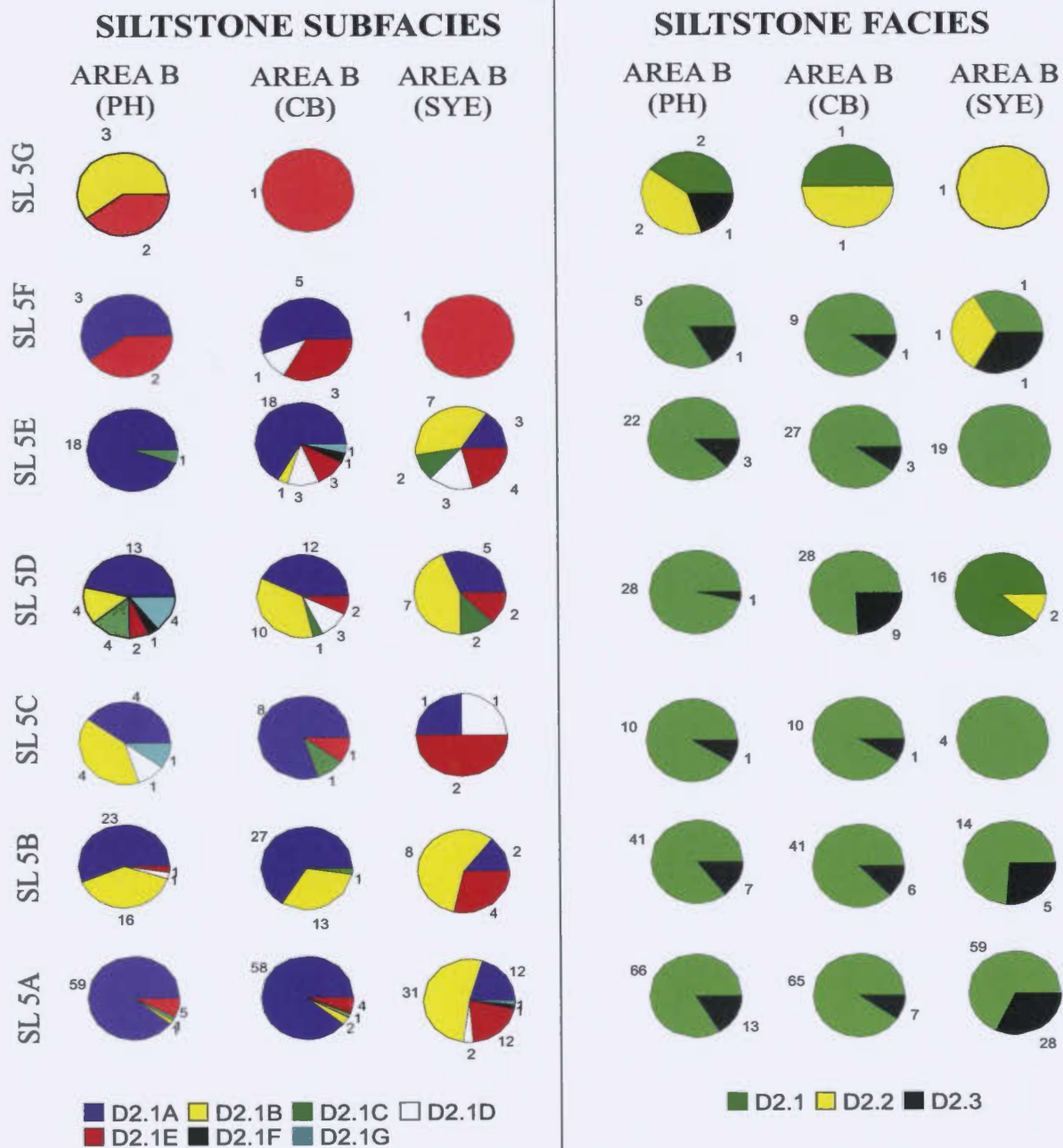


Figure 5.27. Numbers of siltstone beds assigned to the different facies and subfacies in the mini-slices of time-slice 5. These are compared over a short distance in area B.

in the amount of sediment reaching the thesis area at this time. More concentrated large flows reached the area and deposited some of the thick siltstone beds of subfacies D2.1G and D2.1F. Smaller flows deposited isolated “starved” ripples of subfacies D2.1B in area A, but did not continue farther west.

Mini-slice SL 5B also has many siltstone beds in addition to its sandstone beds; these decrease in number in area C compared to area A. Sandstone beds of facies C2.2 and C2.3 might be traceable across the thesis area in several of the mini-slices. This is different to other sandstone beds of facies C2.1 and beds of facies Class B in other time-slices, where they tend to cluster into packets (packets in time-slice 4).

Mini-slices SL 5C and SL 5E in areas A, B and C, and mini-slices SL 5F and SL 5G in areas B and C show variations in their thicknesses and facies that reflect downcurrent changes in the flows, caused by deceleration and loss of sediment load to deposition. Thickness variations in these mini-slices are likely due to compensation.

Mini-slice SL 5D shows a pronounced decrease in thickness in area A. This may reflect some local control in area A that limited deposition, such as local movement along buried faults leading to minor relative uplift (*cf.* Mutti, 1992; Pickering and Hilton, 1997).

For the internal architecture, mini-slice facies variation reflects probable downcurrent changes as the flows decelerated. The variations in thicknesses of the mini-slices probably reflects compensation, and, perhaps variations in the location of the sections relative to the axes of the depositing currents. Thinning of megaturbidites BT-56 and BT-56a in section CB might reflect variations in local bottom topography (*cf.*

Rothwell *et al.*, 1992).

In terms of architectural elements, megaturbidites are the most common element and these have different shapes controlled by bottom topography. They are bounded by 0<sup>th</sup> order bounding surfaces. Mini-slice SL 5A may reflect a change in the depositional conditions as more flows reached the area, perhaps because of increase in sediment supply, or switching and avulsion of channels east of the thesis area.

#### **5.4.10. Description of Time-slice 6**

Time-slice 6 is bounded by K-bentonite horizon KB-7 at the base and KB-8 at the top. Time-slice 6 is divided into two sub-slices, sub-slice 6-1 and sub-slice 6-2. Sub-slice 6-1 is present in areas A, B and C, while sub-slice 6-2 is present in areas B and C only. Therefore, the external architecture of sub-slice 6-2 will be based on the correlation of the composite sections in areas B and C.

##### **5.4.10.1. Description of Sub-slice 6-1**

Sub-slice 6-1 is bounded at the top by the base of megaturbidite BT-63. This sub-slice varies in thickness between areas A, B and C and is thickest in area B (~97 m) and thinnest in area C (~66 m). In area A it about 90 m thick (Table 5.2). The total thickness of shale forms between ~58% to 72% of the sub-slice. Although the percentage of shale decreases from west to east (Table 5.2), its total thickness is greater at area B than areas A and C (Figure 5.28). Sandstone beds of facies B2.1 and B2.2 decrease in number and

total thickness from east to west. Facies C2.1 and C2.3 decrease in number and total thickness from east to west, while sandstone beds of facies C2.2 and C2.4 show the opposite trend. Facies B1.1 and C1.1 are rare (Table CD-T6).

The total thickness of siltstone beds and the number of beds assigned to each siltstone facies are greater at area B than areas A and C. Not all siltstone subfacies bed numbers and total thicknesses are greater in area B than in areas A and C (Figure 5.28).

Mini-slices vary considerably in thickness between all three areas. All variations are more than  $\pm 10\%$  of the mean of thickness of each mini-slice (Table A5-4.1). The datum in figure 5.29 was placed at the top of mini-slice SL 6C as it shows the least difference in thickness between areas A, B and C (Table A5-4.1).

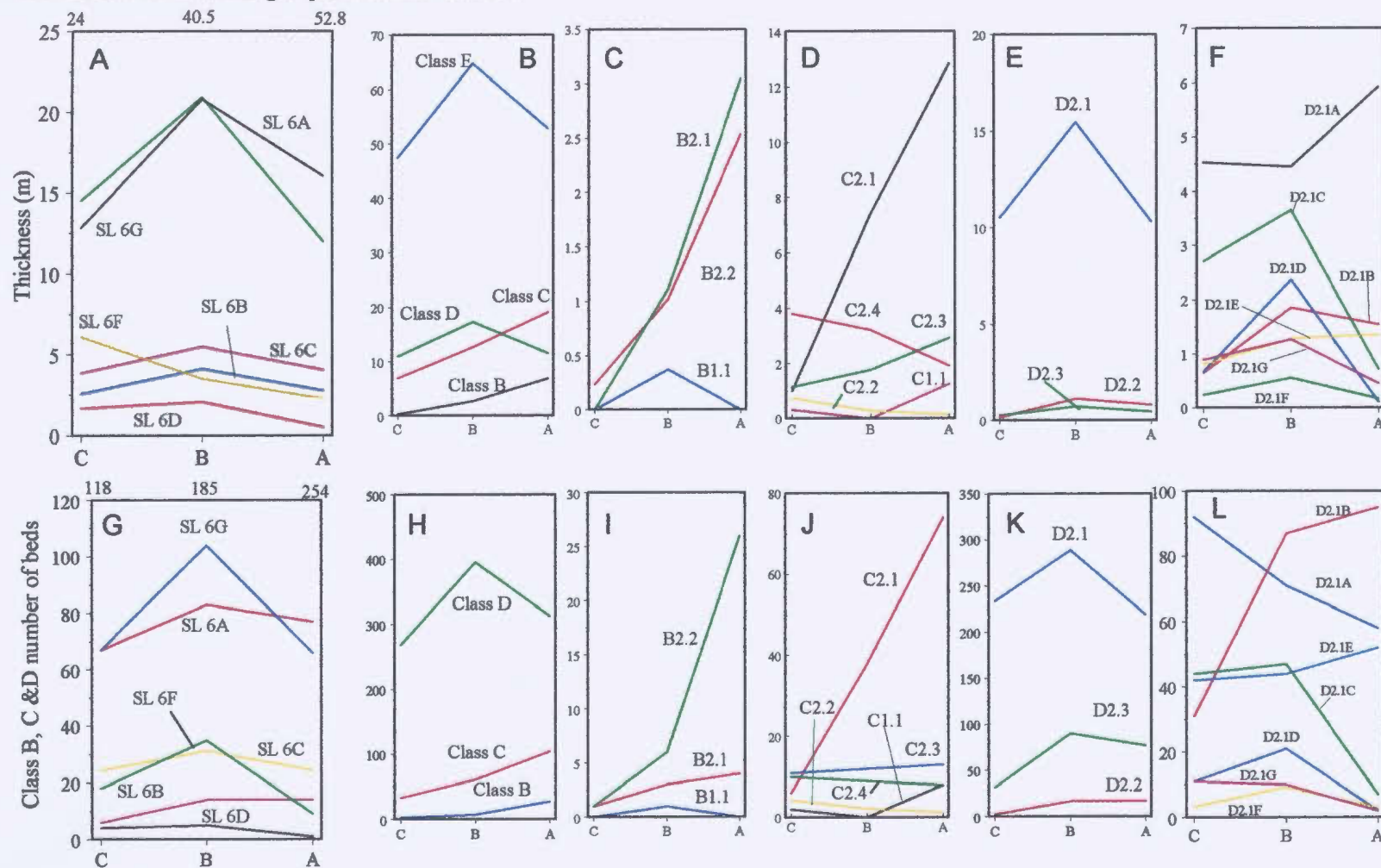
Mini-slices SL 6A, SL 6B, SL 6C, SL 6D and SL 6G are thicker at area B than areas A and C (Table A5-4.1). Mini-slice SL 6E is thicker at area A than areas B and C. Mini-slice SL 6F is thicker at area C than areas A and B.

Megaturbidites BT-57, BT-58 and BT-60 increase in thickness from east to west (Table A5-4.2). Megaturbidite BT-59 is slightly thicker at area B than area C and significantly thicker at area B than area A (Figure 5.29). Megaturbidites BT-61 and BT-62 are significantly thicker at area C than areas A and B. Variation in the thickness of these two megaturbidites between areas A and B is less pronounced (Table A5-4.2).

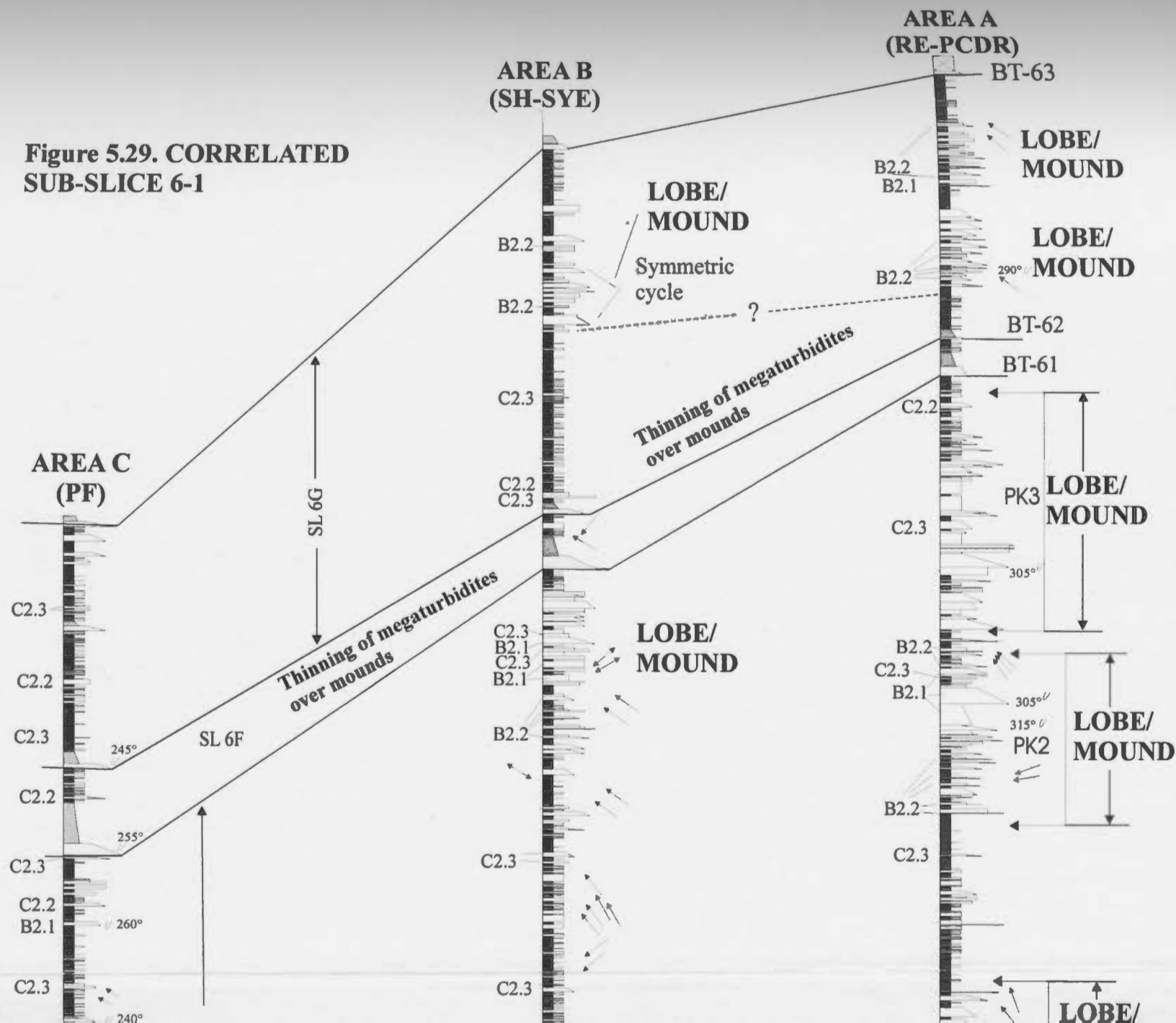
There is some uncertainty regarding the correlation of megaturbidite BT-63 because at area A no thick mud cap of megaturbidite 63-PCDR was observed due to poor exposure. The lower part of megaturbidite BT-63 is thicker at area B than area C. Some

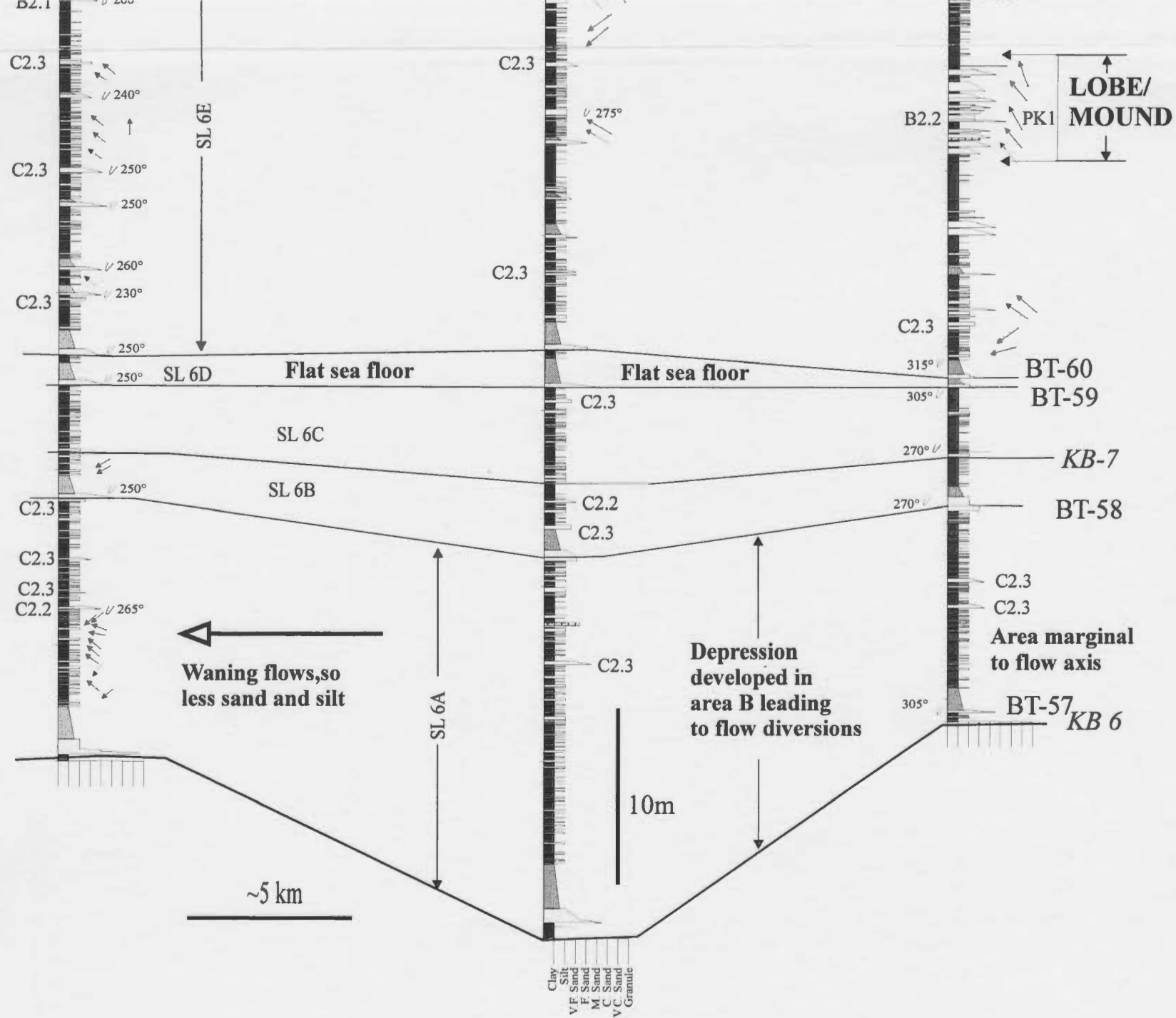


Figure 5.28. Comparison of the facies thicknesses and number of beds and laminae for sub-slice 6-1 between areas A, B and C. A is a plot of the thickness for each of the mini-slices. The values above A are for the thicknesses in mini-slice SL 6E. B, C, D, E, and F are for the total thicknesses in metres of facies and subfacies in sub-slice 6-1. G is plots of the number of sandstone and siltstone beds and laminae for each of the mini-slices. The values above G are for mini-slice SL 6E. H, I, J, K and L show the number of beds and laminae in sub-slice 6-1 for the facies groups, facies and subfacies.



**Figure 5.29. CORRELATED  
SUB-SLICE 6-1**





beds recognised as megaturbidites in mini-slice SL 6E could not be correlated with a high degree of confidence between areas B and C. Most of these megaturbidites are absent from area A (Figure 5.29).

All megaturbidites have either flutes or ripple lamination indicating flow from east to west (Figure 5.29). Some of the palaeocurrent trends show variations of several tens of degrees between different megaturbidites (Figure 5.29).

In mini-slices SL 6A, SL 6B, SL 6F, sandstone beds other than the lower parts of megaturbidites are rare or absent in most areas (Figure 5.30). In mini-slices SL 6E and SL 6G, sandstone beds of facies Class B and Class C are more common, particularly in areas A and B, where some of these sandstone beds occur in packets. Most sandstone in the packets are amalgamated beds of facies C2.1. Beds of facies B2.2 occur below the packets or in more muddy intervals between packets in area A. Several beds of facies B2.2 occur within a small interval in the upper part of mini-slice SL 6G in area A. Several thick to very thick beds of facies B2.1 are amalgamated in the packets of mini-slice SL 6E in area A. Well developed upward thickening, thinning, coarsening or fining sequences were not observed, except for a thin packet in mini-slice SL 6G located in area B. This packet consists of beds of facies C2.1 that coarsen and thicken upward followed by upward fining and thinning.

Siltstone beds assigned to different facies and subfacies are common in all mini-slices. Siltstone bed numbers differ between the mini-slices in the three areas (Figure 5.30). Subfacies D2.1C and D2.1B are more common than in the older mini-slices. Several

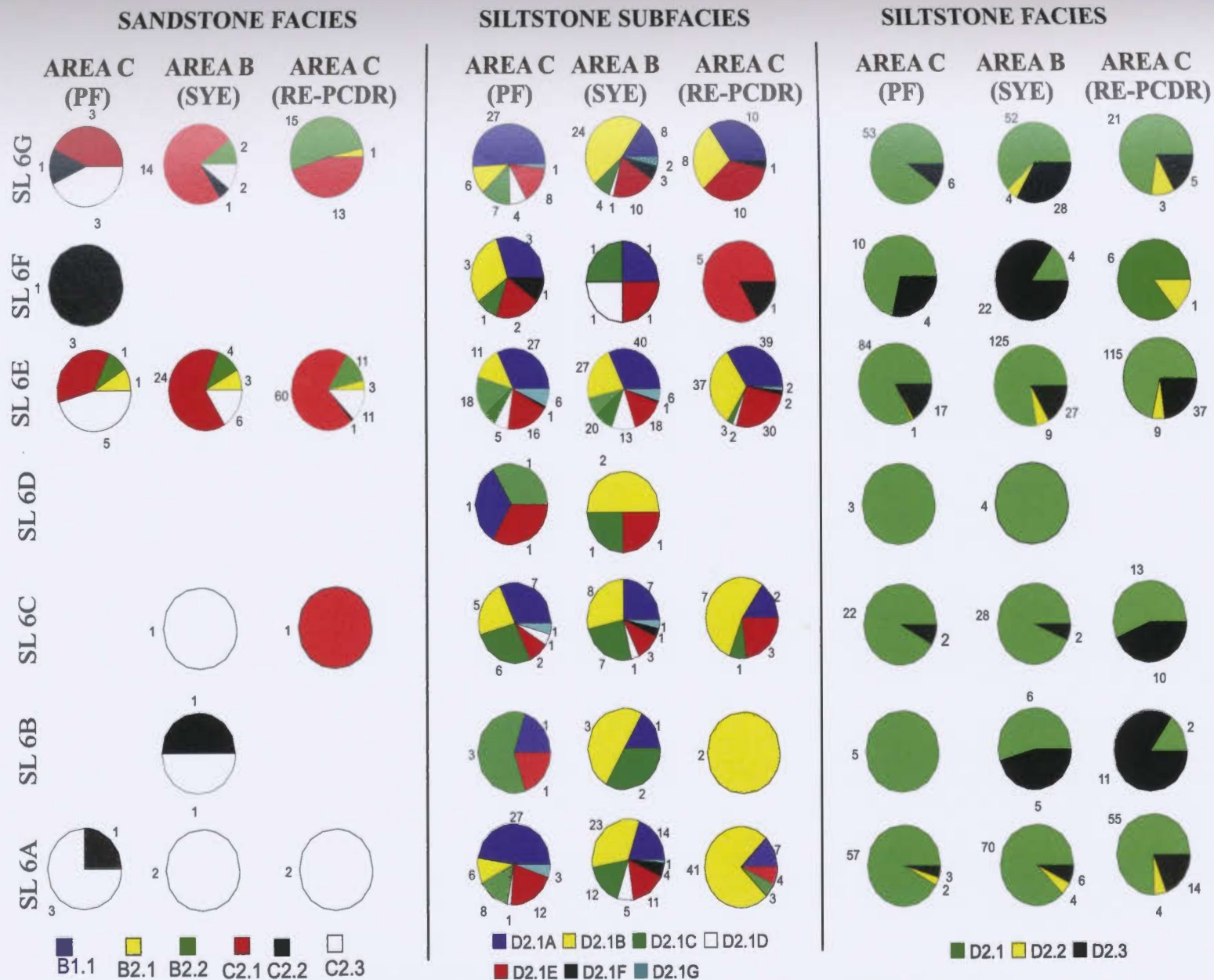


Figure 5.30. Numbers of sandstone and siltstone beds assigned to the different facies and subfacies in the mini-slices of sub-slice 6-1. These are compared between area A, B and C.



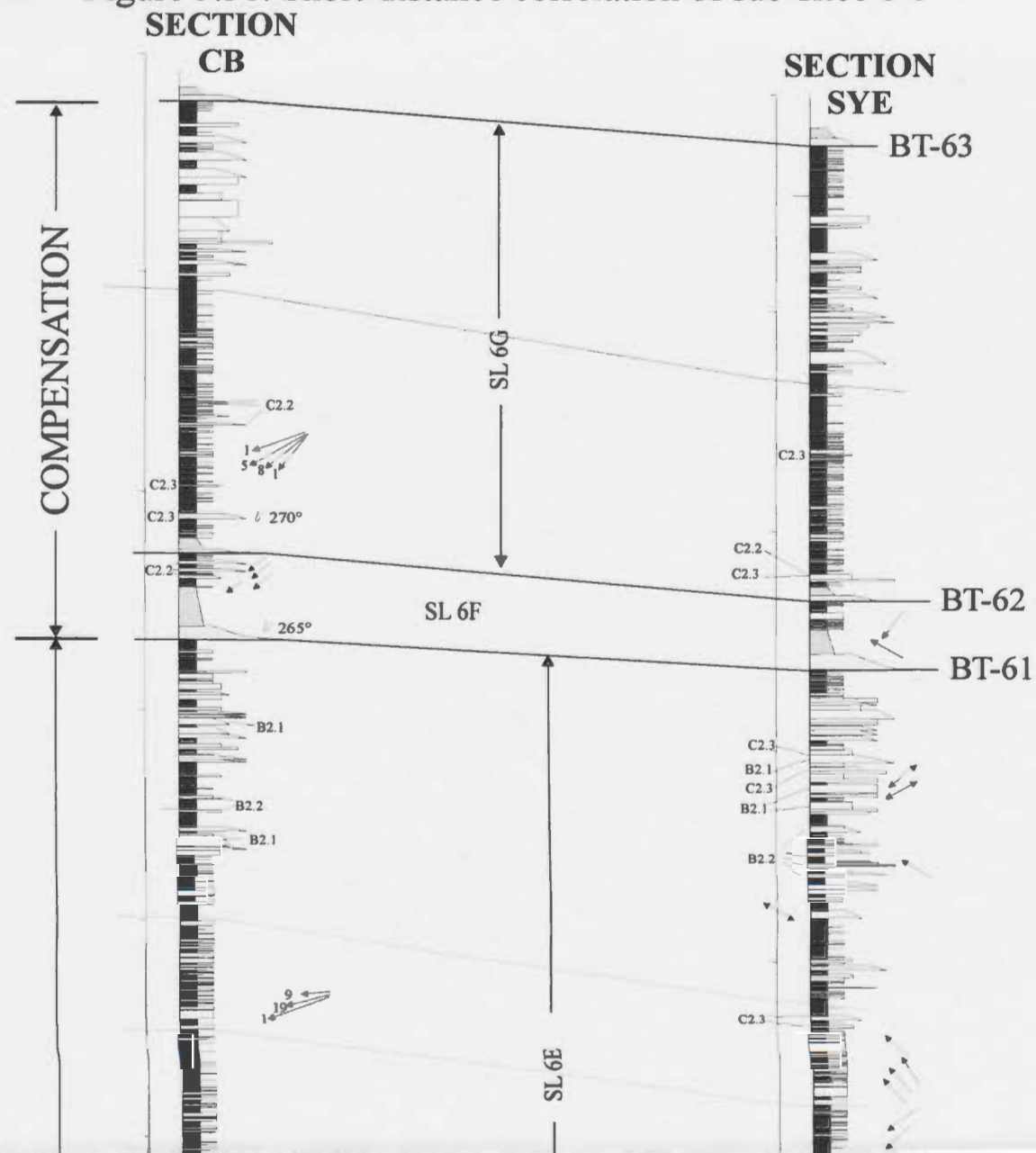
thick siltstone beds of subfacies D2.1A occur in the sandstone packets in mini-slice SL 6E, area A.

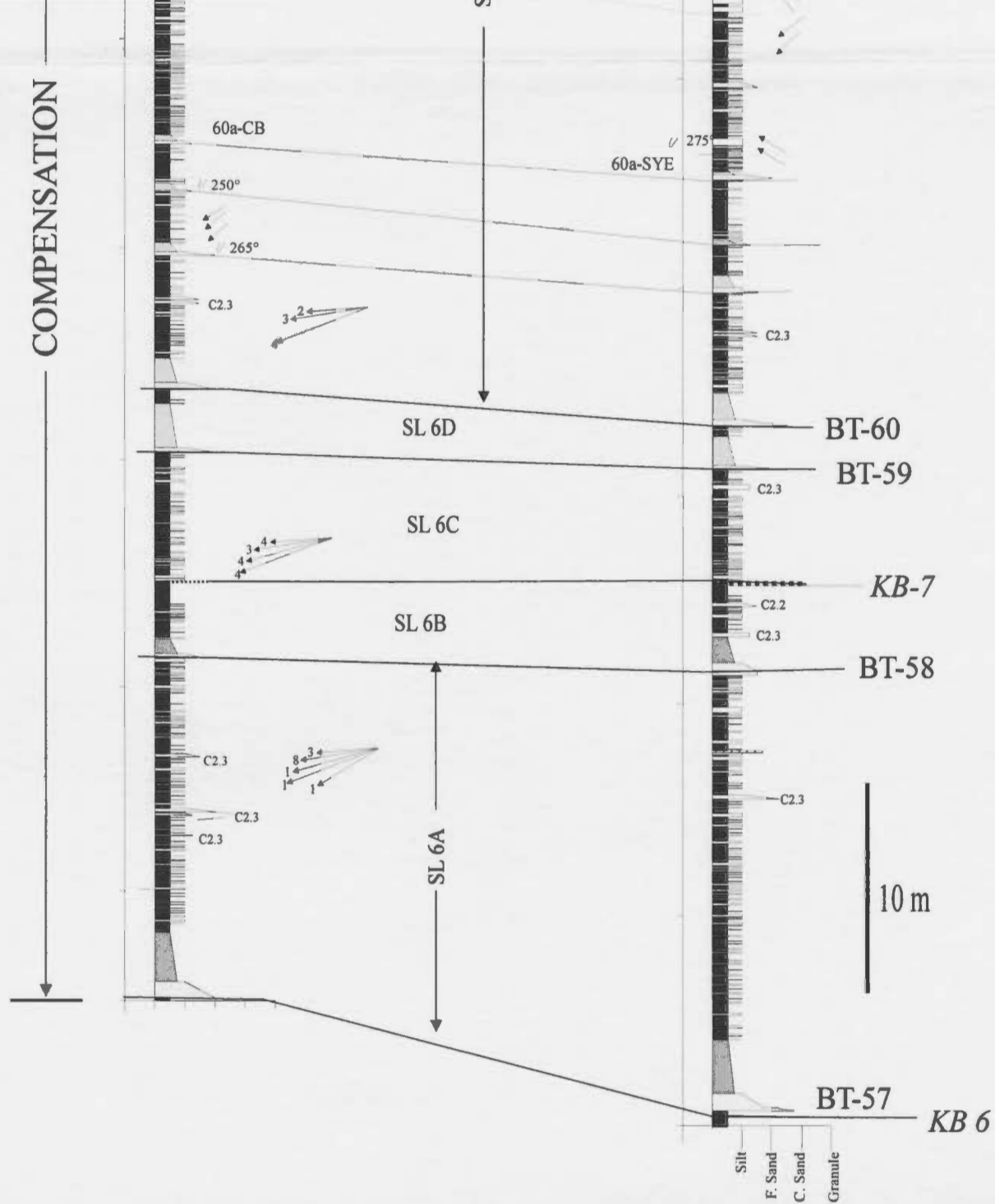
For the internal architecture of sub-slice 6-1, sections SYE and CB were used. These sections are ~1.7 to 2.5 km apart. There is a slight variation in the thicknesses of mini-slices SL 6B through SL 6G (Figure 5.31). SL 6A thins significantly from SYE to CB. Megaturbidites also vary in thickness between the two sections. Specifically, megaturbidites BT-57, BT-58 and BT-60 are thicker in section SYE than in section CB (Figure 5.31) while megaturbidite BT-59 is thinner. Megaturbidites BT-61 and BT-62 show minimal variation in their thickness between the sections, although their upper (mud cap) or lower parts may vary in thickness between sections SYE and CB.

Sandstone beds other than the lower parts of megaturbidites are only common in mini-slices SL 6E and SL 6G and are rare or absent in other mini-slices of this sub-slice (Figure 5.32). In mini-slice SL 6E, sandstone beds of facies C2.1, C2.3 and B2.2 are more common in section SYE. In mini-slice SL 6G, beds of facies C2.3 and B2.2 are present in section SYE, but absent in section CB. Beds of facies C2.1 are thicker in section CB than in section SYE (Figure 5.32).

Siltstone beds are less numerous in section CB than section SYE for mini-slices SL 6A, SL 6E, SL 6G and SL 6G (Figure 5.32). The other mini-slices show little or no variation in the numbers of siltstone beds assigned to different facies. Beds assigned to subfacies D2.1A are more common in section CB for all mini-slices except SL 6F. Beds assigned to subfacies D2.1B, D2.1C and D2.1E are more numerous in section SYE than

Figure 5.31. Short-distance correlation of sub-slice 6-1







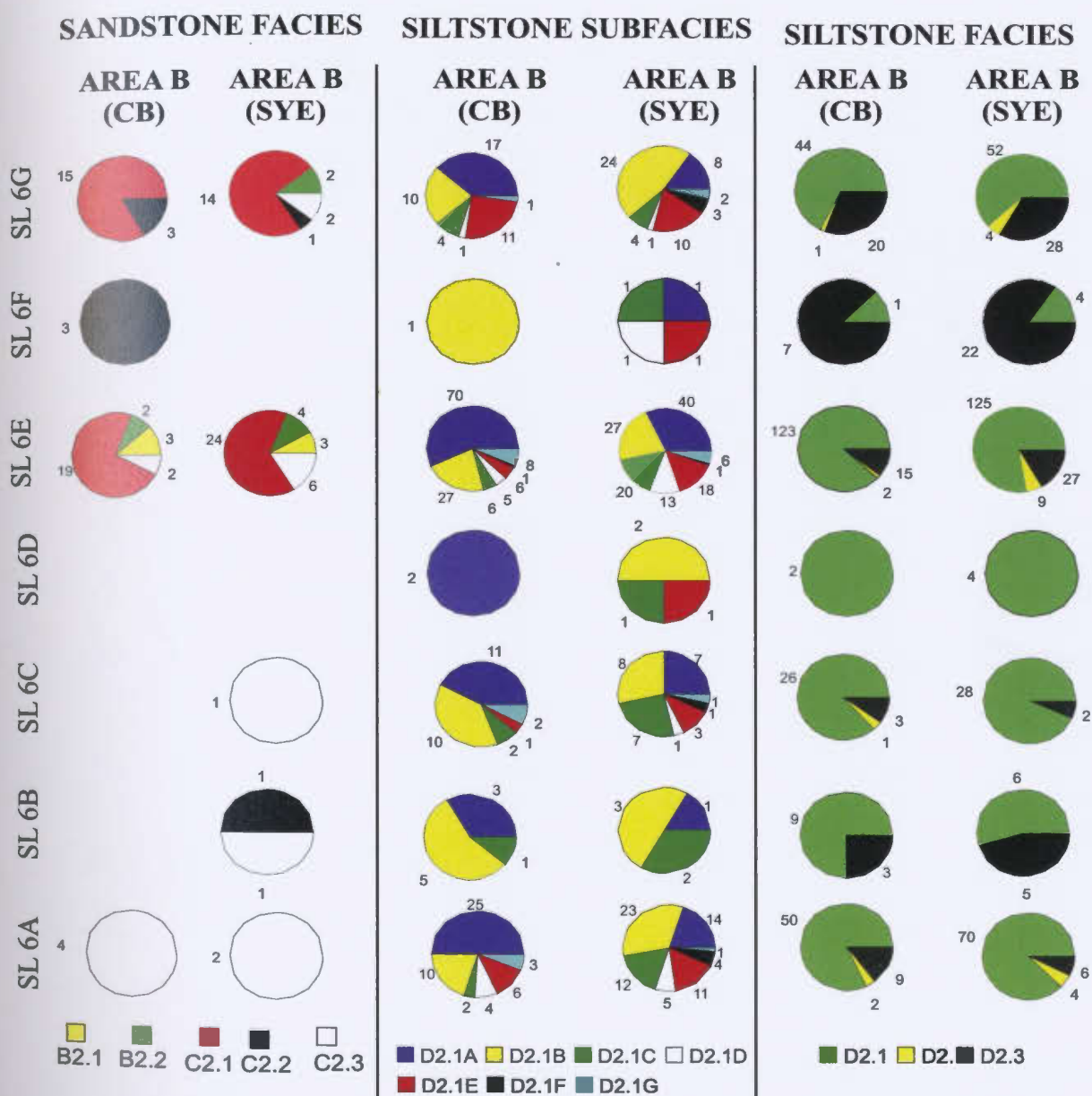


Figure 5.32. Numbers of sandstone and siltstone beds assigned to the different facies and subfacies in the mini-slices of sub-slice 6-1. These are compared over a short distance in area B.

section CB, for all the mini-slices. In mini-slice SL 6G subfacies D2.1E is more common in section CB than SYE. Other siltstone subfacies are rare or absent.

#### 5.4.10.2. Interpretation of Sub-slice 6-1

Sub-slice 6-1 has considerably more sandstone beds (as percent of the total thickness of the sub-slice and as number of beds) than time-slice 5. Most differences in the number of sandstone beds and their thickness are in mini-slices SL 6E and SL 6G.

The differences in mini-slices thicknesses are interpreted to be due to the interplay between deposition and bottom topography variations. Bottom topography is attributed to depositional relief, compactional and tectonic subsidence.

Mini-slice SL 6A is thickest in area B. Part of this variation in thickness may be due to bottom irregularities. Area B may have been in a topographic low compared to area A. Siltstone beds are thicker at area B (mean thickness is ~ 5cm) than area A (mean thickness ~ 2 cm) supporting this interpretation. Alternatively, area A may have been in a position marginal to the axial paths of the currents depositing the siltstone beds.

Megaturbidite BT-57 is thicker at area B than area A, supporting the interpretation that area B was a bathymetric low. The increase in the thickness of megaturbidite BT-57 in area C relative to area A is suggested to be due to ponding of the megaturbidite flows in the west. The decrease in thickness of siltstone beds and the facies changes between areas B and C is attributed to downcurrent changes as the flows decelerated.

An increase in the number of larger flows carrying silt and mud loads reaching the

area during the time of deposition of this mini-slice is thought to have occurred, suggesting proximity of the area to channel termination or an increase in the discharge. This is supported by the more common occurrence of thin beds and laminae of facies D2.2 and subfacies D2.1B than in older time-slices. Some of the flows deposited their loads rapidly, resulting in the formation of siltstone beds with convolute lamination (subfacies D2.1C). Sandstone beds are rare in this mini-slice, and it is suggested they were deposited from infrequent low density turbidity currents.

Depositional conditions did not change significantly during the accumulation of mini-slices SL 6B, SL 6C and SL 6D. Deposition was mainly from low concentration flows carrying silt and mud loads that were effected by bottom topography causing the axial paths of flows depositing sediments to be closer to area B than area A.

A pronounced variation in the type of facies is observed in mini-slice SL 6E between areas A, B and C. In area A, mini-slice SL 4E consists of packets of sandstone dominated by facies C2.1 and packets of siltstone. These packets alternate with more shaly intervals. In both areas A and B, the lower part of mini-slice SL 6E (lower ~15 m between BT-60 and packet PK1 in area A) shows a crudely similar vertical change in facies, consisting of an interval of siltstone overlain by a sandstone bed (megaturbidite ?) which might be correlatable between the two areas. Above this sandstone bed (megaturbidite ?) at areas A, an interval consisting of shale with two to three sandstone beds in the middle occurs. These sandstone beds may be equivalent to some siltstone beds in the middle of the same interval in area B. Correlation between areas B and C for the lower part of mini-

slice SL 6E is better constrained, because some beds with medium to thick mud caps can be correlated with confidence between these two areas (Figure 5.29). The beds in the lower part of this interval were deposited from low concentration turbidity currents carrying silt and mud loads. Infrequent, more sandy flows deposited sandstone beds of facies C2.3. The upper part of this interval was dominated by shale deposition from flows carrying mud loads. Periodic flows deposited sandstone beds in area A and siltstone beds in areas B and C. It is unknown if the two thick sandstone beds of facies C2.1 in area A below (PK1) are lateral equivalents to siltstone beds at the same level in areas B and C. In other time-slices, sandstone beds of facies C2.1 do not seem to continue for long distances in a downcurrent direction. Perhaps these two beds are more extensive because the flows became more efficient as they travelled in the downcurrent direction and incorporated muddy material (*cf.* Mutti *et al.*, 1999). This is unlike sandstone beds of the same facies that occur in packets where little or no mud was available for entrainment by passing turbidity currents.

The middle part of mini-slice SL 6E, above PK1 consists of sandstone and siltstone packets separated by more muddy intervals in area A and siltstone beds that cluster in poorly defined packets in area B. No bed clusters or packets are present in area C; here, laminae to thin beds of siltstone, and sandstone beds, alternate with shale. The upper part mini-slice SL 6E consists of ~30 m of medium to thick bedded sandstones and siltstones that form one or perhaps two packets in area A. In area B, the upper part of mini-slice SL 6E consists of interbedded sandstone beds of facies C2.1 and B2.2, and shale overlain by a

cluster (packet?) of sandstone beds that consist of a variety of facies. Only a few (<8 beds) sandstone beds are present in the upper part of mini-slice SL 4E in area C.

The sandstone packets in area A were deposited from high concentration turbidity currents. Some flows that deposited the sandstone beds may have continued to area B, where they deposited some siltstone beds. Some larger flows that deposited thick beds in the upper part of mini-slice SL 6E in area A may have continued onwards to areas B and C where they deposited some sandstone beds. Alternatively, a build-up mound of sand in area A might have acted as an obstacle that caused the diversion of subsequent flows away from area A. In this case, the packets developed in area B would not necessarily be lateral equivalents to the packets in area A. The first interpretation is preferred because of the observed vertical facies change observed in the upper part of mini-slice SL 6E. The upper part of this mini-slice in area A can be roughly divided into two packets. A lower packet (PK2), consisting of interbedded thin to medium sandstone beds of facies C2.1 and B2.2 in the lower part, overlain by two thick to very thick amalgamated beds of facies B2.1. The upper part of this packet consists of thin bedded sandstone and siltstone beds alternating with shale and it may be equivalent to the interval of alternating sandstone and shale below the sandstone packet observed at area B. It is believed that most beds that continue downcurrent are beds that were deposited from low concentration turbidity currents (facies C.2.3) and beds that are deposited from more muddy, efficient flows (facies B2.2). In contrast, beds deposited from high concentration flows (e.g., facies C2.1 and B2.1) do not continue downcurrent, perhaps, because the flows were controlled more

strongly by bottom topography. The upper packet in area A (PK3) consists of thick beds of facies C2.1 that may be lateral equivalents to the packet in the upper part of mini-slice SL 6E in area B. Thick beds of facies C2.1 in area A were probably deposited from large flows that continued downcurrent. In area C, low density turbidity currents deposited siltstone beds and some sandstone beds of facies C2.3 and C2.2. More rarely, high concentration turbidity currents reached area C and deposited sand beds of facies C2.1. These flows may have been the largest of the flows that deposited the packets observed in areas A and B.

The packets in the upper part of mini-slice SL 6E must have formed a mound-like feature in areas A and B. This is supported by significant thinning of megaturbidites BT-61 and BT-62. Flows that deposited BT-61 and BT-62 might have accelerated as they passed over the mound. The grain size at the base of these two megaturbidites is coarser at area A than areas B and C, consistent with the higher speed.

The presence of a mound or obstacle in area A was probably the cause of the deposition of thick beds of facies D2.1. The flows responsible for the deposition of these beds most likely deposited most of their loads as they moved up the slope of the obstacle (Kneller and Buckee, 2000).

The thickness variation of mini-slice SL 6E may be a function of compaction as well as differential sedimentation. Mini-slice SL 6E is more muddy at area C than areas A and B and is probably compacted relatively more at area C, accentuating the primary thickness difference.

For mini-slice SL 6F, variation in its thickness, bed thicknesses and facies are attributed to bottom topography created by mini-slice SL 6E. Most of the low concentration flows were diverted away from areas A and B toward area C. Only very low concentration flows reached areas A and B and deposited siltstone beds of facies D2.2 and D2.3.

The interval of thin siltstone beds and laminae in the lower part of mini-slice SL 6G at area A may be the equivalent of the thicker interval of siltstone and shale in the lower part of the mini-slice at area B (Figure 5.29, dashed line). The difference in thickness and facies is due to the presence of the sediment mound at area A. The sandstone packets at area A in the upper part of mini-slice SL 6G may be lateral equivalents to the sandstone packet and the overlying siltstone beds and laminae in area B. The symmetrical cycle observed in the packet in area B suggests lateral shifting of the locus of deposition due to compensation. At area C, most deposition was from low concentration turbidity currents that carried predominantly silt and mud loads. These may have been the same flows that deposited the sandstone beds in areas A and B, but bed-by-bed correlation is not possible.

In terms of architectural elements, the sandstone packets have a mound shape that tapers or decreases in thickness in a downcurrent direction. These mounds consist mostly of beds of facies C2.1 that show limited lateral continuity, particularly when they are amalgamated in packets. These packets are bounded at by 3<sup>rd</sup> order bounding surfaces.

Siltstone packets have a more sheet-like geometry and these sheets become more muddy and less well defined in a downcurrent direction. In areas where siltstones form

packets, they are bounded by 2<sup>nd</sup> or 3<sup>rd</sup> order bounding surfaces.

Between sections SYE and CB, the variation in the thickness of most of the mini-slices is probably due to compensation. Mini-slice SL 6A is significantly thicker in section SYE than in CB. This may reflect a slight variation in bottom topography between the two areas.

Most of the siltstone beds and laminae are thicker and more numerous in section SYE than in section CB. The thinning of the siltstone beds is probably due to downcurrent changes due to loss of sediment loads from the currents to deposition. The more common occurrence of beds with convolute lamination of subfacies D2.1C in section SYE than in section CB suggests that deposition may have been more rapid in section SYE causing the formation of convolute lamination. Alternatively the greater numbers of beds with convolute lamination in section SYE may have been caused by some external factor that had a greater effect in the area of section SYE than in section CB. Some of the beds of subfacies D2.1A that are more common in section CB may be equivalent to some of the beds of subfacies D2.1C in section SYE.

Some of the siltstone beds and laminae that cluster or form packets in parts of mini-slice SL 6E in section SYE thin and have thicker shale beds in CB reflecting down current deceleration of the deposition currents resulting in deposition of thinner siltstone beds and more mud. One siltstone packet in the middle of mini-slice SL 6E is tentatively correlated between sections SYE and CB. This packet slightly thins at CB suggesting it is lens-shaped. Siltstone beds in mini-slice SL 6G do not cluster to form packets; the



siltstone beds decrease in thickness and numbers between sections SYE and CB probably indicating the deceleration of the depositing flows in a downcurrent direction.

Sandstone beds that form the packet in the upper part of mini-slice SL 6E may be equivalent to the packet in the upper part of mini-slice SL 6E in section CB. Individual beds cannot be correlated. The decrease in the thickness of the sandstone beds and the decrease in the amount of amalgamation between section SYE and CB may suggest deceleration of dense flows in a downcurrent direction of slight variation in the location of the sections relative to the paths of the depositing currents. Flows that deposited beds of facies C2.1 may continue for some distance downflow and deposit beds of facies C2.1 in areas that are a few kilometres apart as observed in the lower part of sub-slice 4-1. The greater thickness and more amalgamation of the sandstone beds in the upper part of mini-slice SL 6G in section CB compared to section SYE suggests that section CB was probably located closer to the paths of the currents that deposited these sandstone beds than section SYE.

#### 5.4.10.3. Description of Sub-slice 6-2

Only a few metres of the lower part of sub-slice 6-2 are exposed in area A. The beds here are poorly exposed and are not considered in the proceeding discussion. This sub-slice will be investigated, instead, using the sections exposed in areas B and C. Sub-slice 6-2 is bounded by megaturbidite BT-63 at the base and K-bentonite horizon KB-8 at the top. Megaturbidites and KB-8 divide sub-slice 6-2 into six mini-slices (SL 6H through

SL 6M). Sub-slice 6-2 is ~103 m thick in area B and ~77 m thick in area C (Table 5.2). Shale forms ~68% of the total thickness of sub-slice in area C and ~57% in area B. All facies classes decrease in thickness and number of beds from area B to area C (Figure 5.33). Sandstone beds of facies C2.1 show a marked decrease in numbers and total thickness from area B to area C, while beds of facies C2.2 and C2.3 show the opposite trend. The total thickness and number of beds of facies C1.1 and C2.4 show minimal change between areas B and C. Siltstone beds of facies D2.1, D2.2 and D2.3 decrease in number and total thickness from area B to C. Facies D2.1 shows the most pronounced decrease (Figure 5.33). Subfacies D2.1A and D2.1B show a pronounced decrease in number from areas B to C. Subfacies D2.1G increases in number of beds from areas B to C. Other siltstone beds show little or no change in numbers between areas B and C.

Mini-slices SL 6H and SL 6I increase in thickness towards the west. Other mini-slices decrease in thickness between areas B and C. Mini-slices SL 6M and SL 6K show the most pronounced decrease in thickness from area B to area C. (Figure 5.34).

Megaturbidites including their mud caps, except BT-65, increase in thickness from area B to area C. Megaturbidite BT-65 decreases slightly in thickness from area B to area C (Table A5-4.2). All megaturbidites have either flutes or ripple lamination indicating an east to west flow direction (Figure 5.34). Some of the palaeocurrent measurements show variations of several tens of degrees between the various megaturbidites (Figure 5.34). Palaeocurrent trends from ripples show a greater degree of dispersion.

In mini-slices SL 6I, SL 6J, SL 6L and SL 6M, sandstone beds other than the

Figure 5.33. Comparison of the facies thicknesses and number of beds and laminae for sub-slice 6-2 between areas B and C. A is a plot of the thickness for each of the mini-slices. B, C,D,E, and F are for the total thicknesses in metres of facies and subfacies in sub-slice 6-2. The value above F is for the total thickness of subfacies D2.1A. G is plots of the number of sandstone and siltstone beds and laminae for each of the mini-slices. H, I, J, K and L show the number of beds and laminae in sub-slice 6-2.

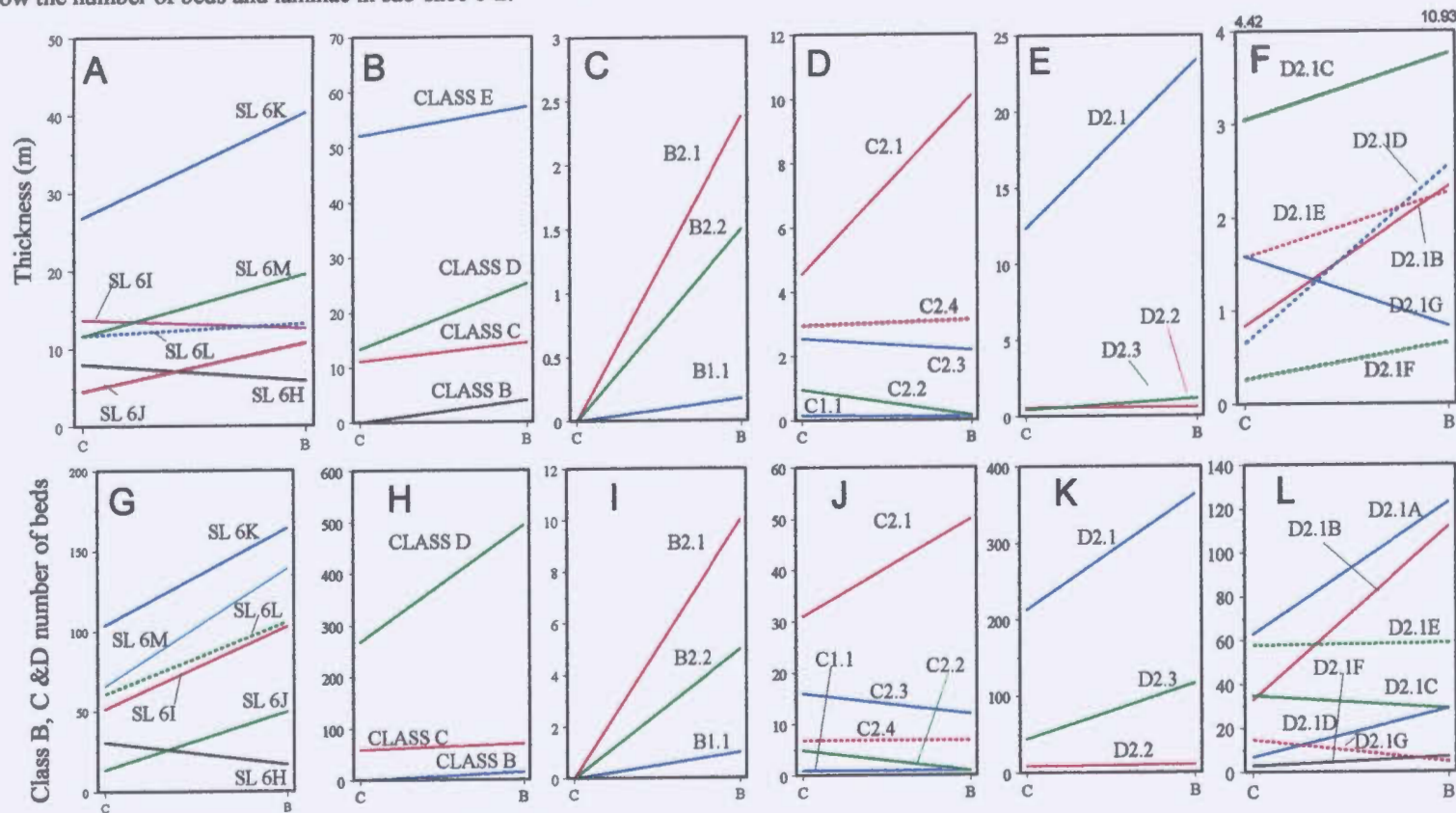
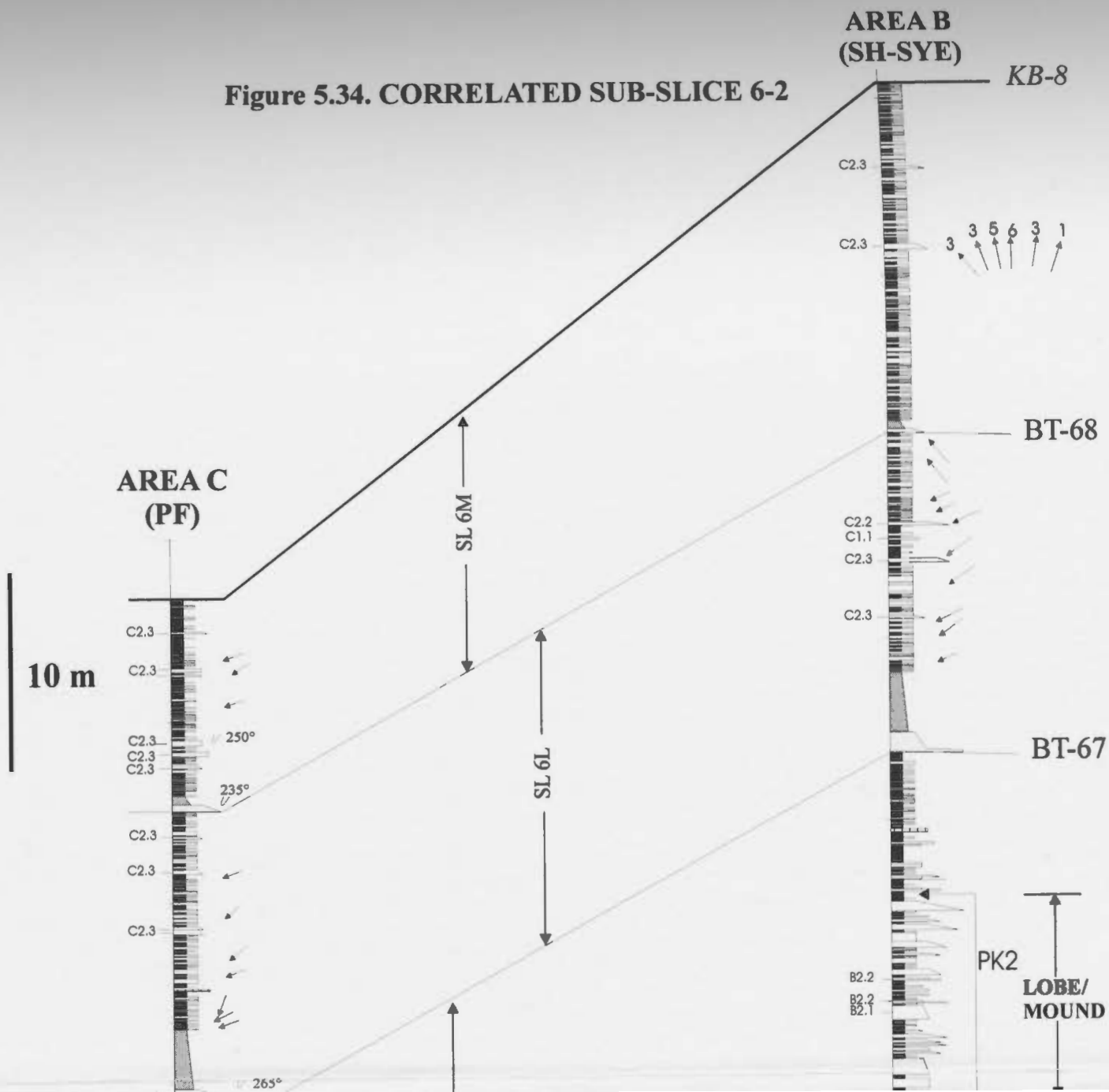
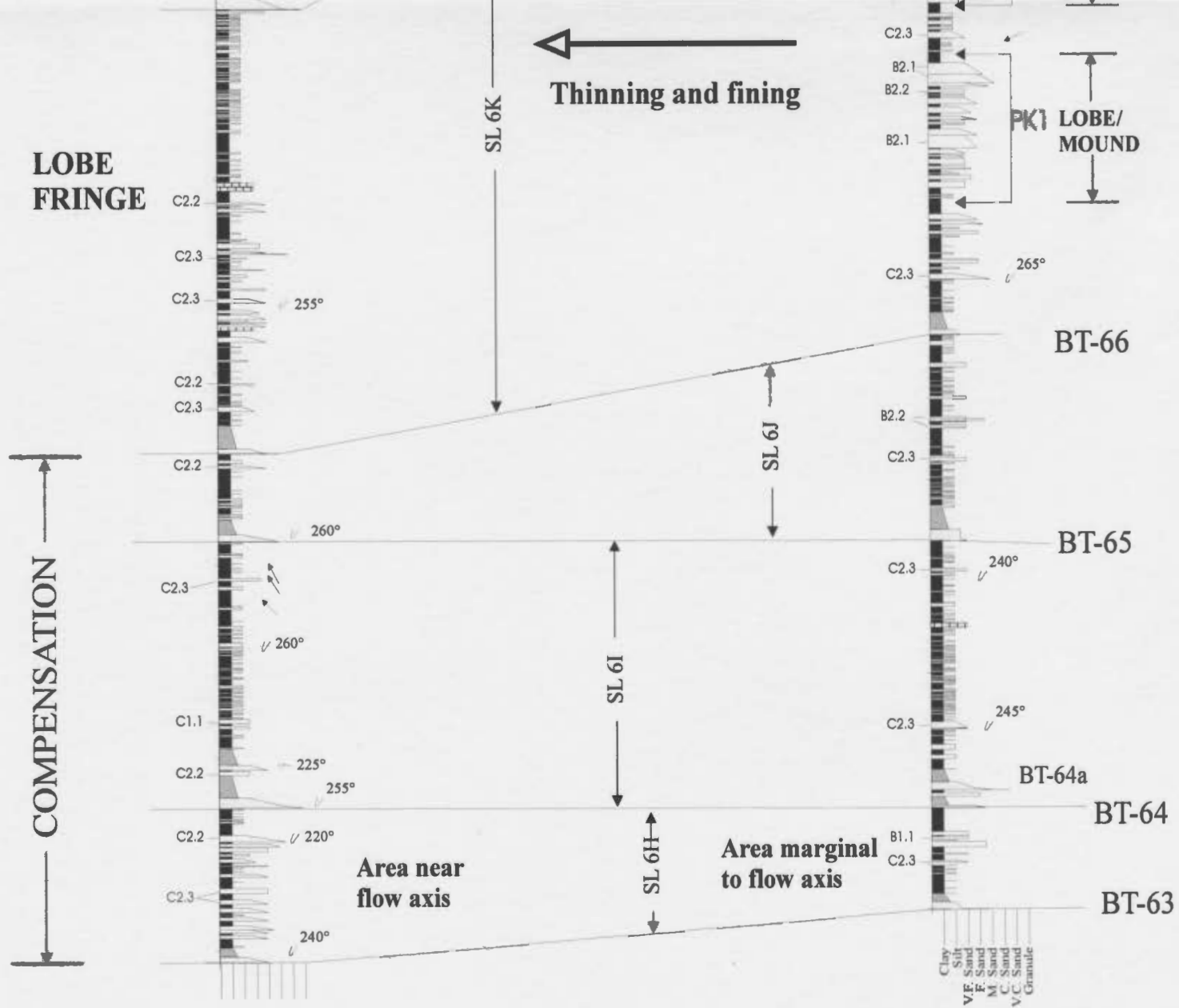


Figure 5.34. CORRELATED SUB-SLICE 6-2





lower parts of megaturbidites are rare or absent in areas B and C (Figure 5.35). In mini-slice SL 6H sandstone beds of facies C2.1 are predominant in area C, while in area B they are less common. In mini-slice SL 6K, sandstone beds of facies C2.1, B2.1, B2.2 and C2.3 are common in area B and form two packets (PK1 and PK2; Figure 5.34). Sandstone beds in area C are less common and do not form packets; instead, the sandstone beds alternate with shale beds, that are of similar thickness.

Siltstone beds are common in all mini-slices. They consist mainly of very thin beds and laminae in mini-slices SL 6H through SL 6K. In mini-slices SL 6L and SL 6M, the siltstone beds are very common (Figure 5.35). The total thickness of the siltstone in these two mini-slices is greater than the total thickness of shale in area B, but not in area C.

Sections SYE and CB are used to characterise the internal architecture. The lower parts of these two sections are ~2 km apart, while the upper part of these two sections is ~1 km apart. There is a slight variation in thickness of the mini-slices between the sections. Megaturbidites show slight variations in thickness (Figure 5.36). Sandstone beds are more common in section CB than in section SYE in mini-slices SL 6L and SL 6M. The majority of the sandstone beds are of facies C2.3. In mini-slice SL 6K, sandstone beds are more common in section SYE than in section CB, however, the packets that are present in section SYE persist in section CB. The number of siltstone beds is greater in section CB than section SYE in mini-slice SL 6H while in the other mini-slices the number of siltstone beds is greater in section SYE than in section CB. In mini-slice SL 6K, little variation occurs in the number of siltstone beds between the two sections. Siltstone beds assigned



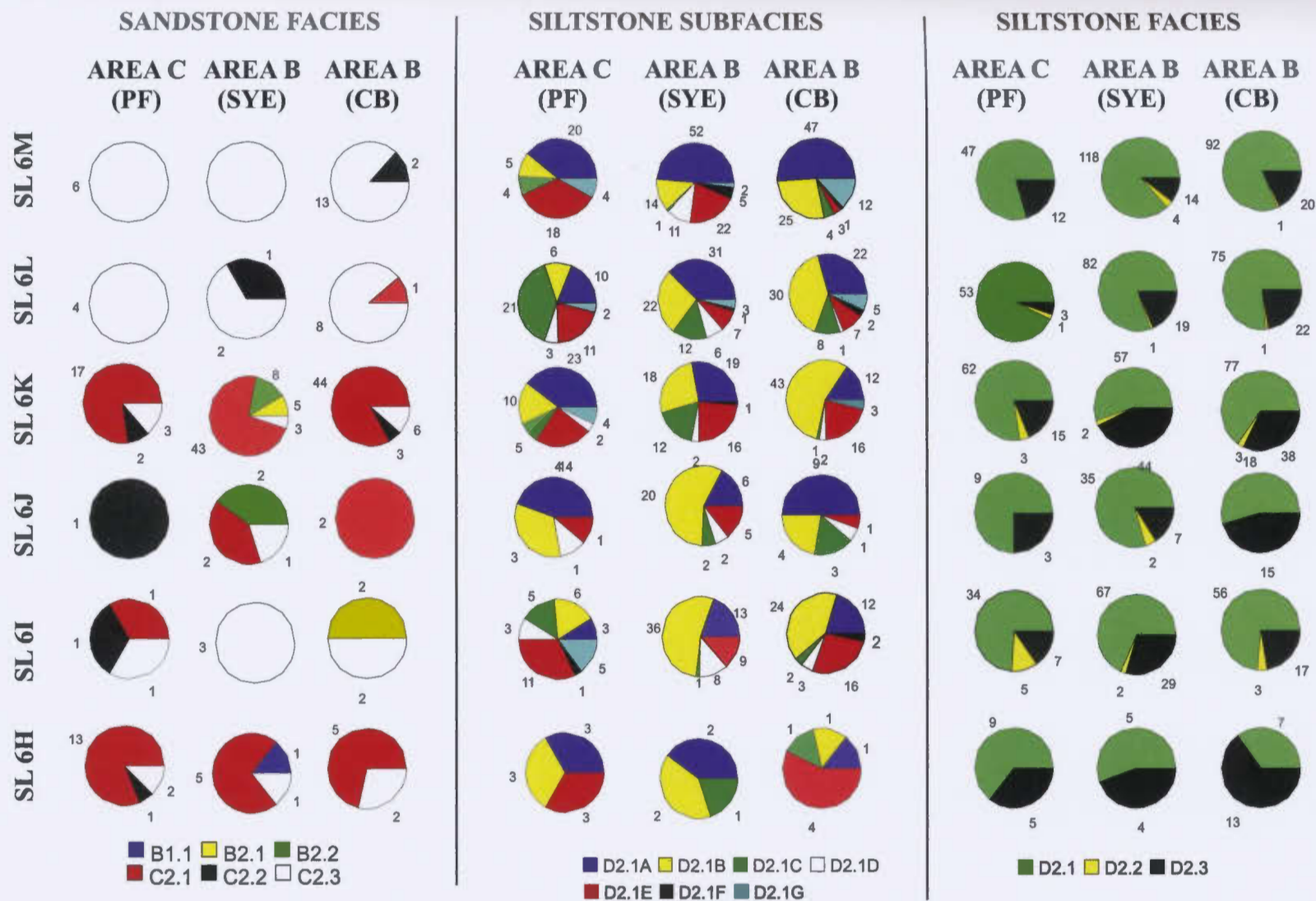
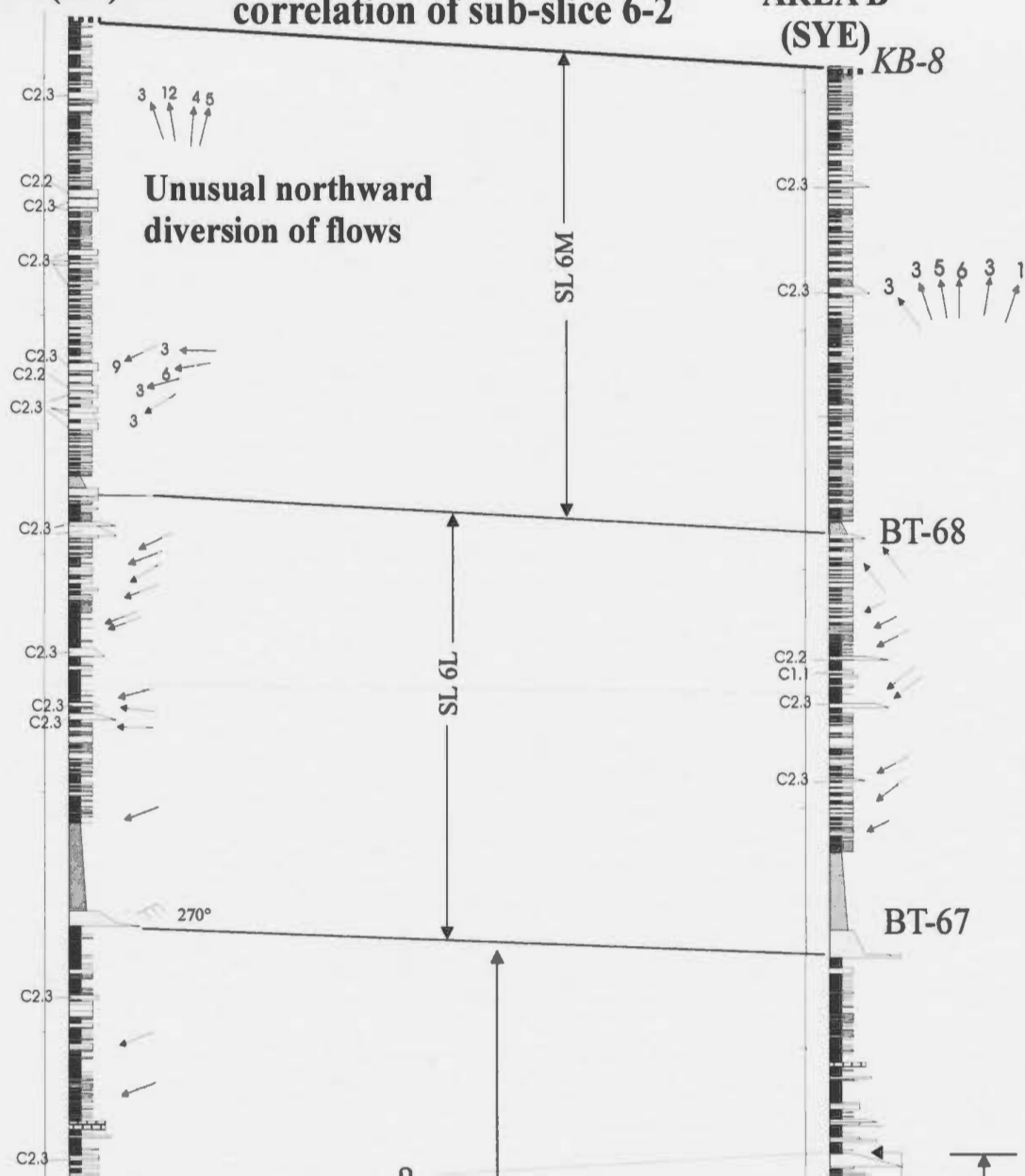


Figure 5.35. Numbers of sandstone and siltstone beds assigned to the different facies and subfacies in the mini-slices of sub-slice 6-2. These are compared between area B and C. Data for short distance comparison (section CB) is included.

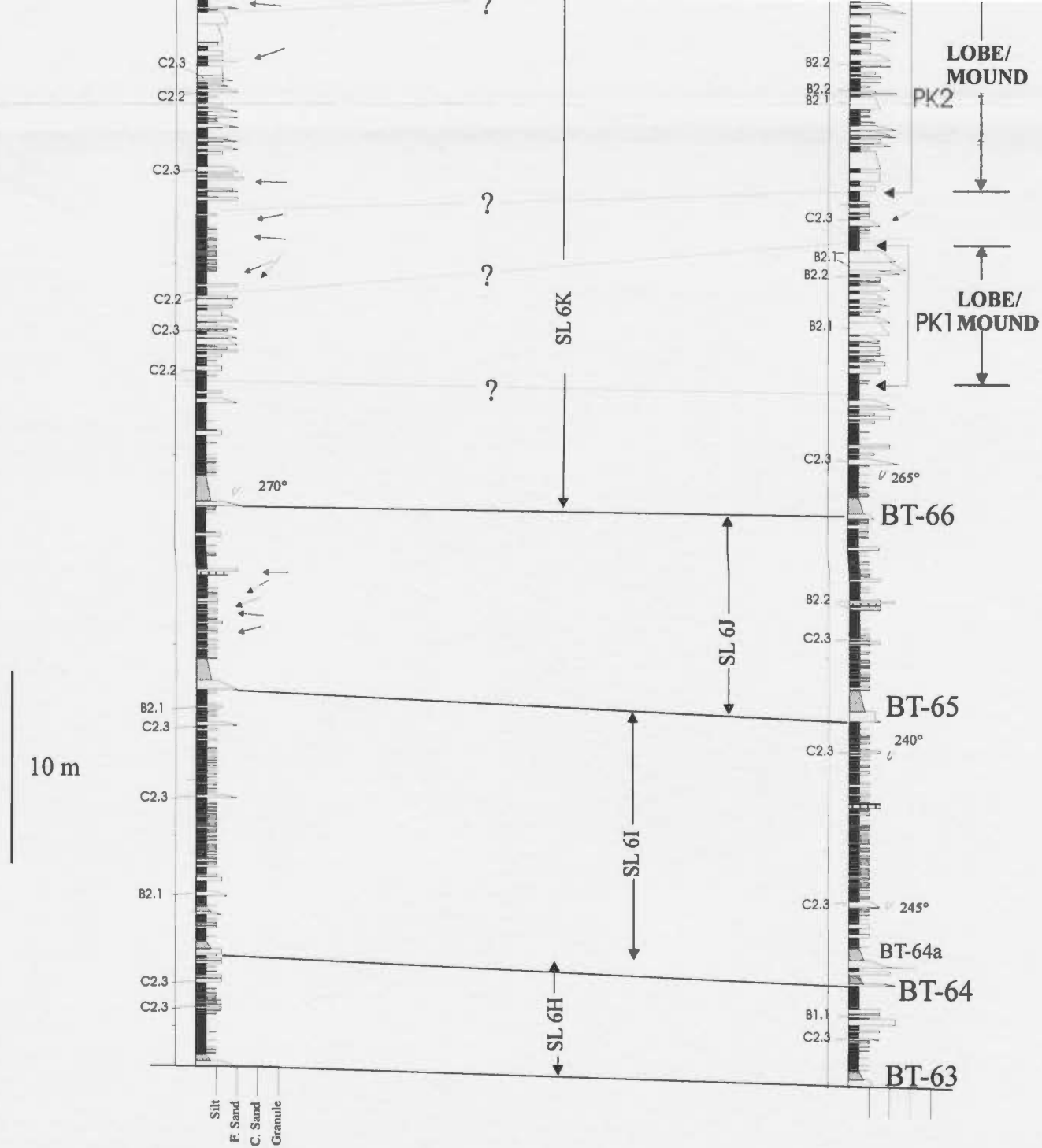
AREA B  
(CB)

Figure 5.36. Short-distance  
correlation of sub-slice 6-2

AREA B  
(SYE)







to different subfacies also show differences between the two sections. These variations are shown on Figure 5.35.

#### 5.4.10.4 Interpretation of Sub-slice 6-2

The sediments that constitute sub-slice 6-2 were deposited from low concentration flows that carried, for the most part, silt and mud loads that deposited thin to medium beds. Occasionally, some low concentration flows carried sand loads and deposited beds of facies C2.2 and C2.3. During the accumulation of mini-slice SL 6K, more concentrated flows deposited sandstone beds of facies C2.1, B2.1 and B2.2 in area B, where they clustered to form packets. Rarely, these concentrated flows continued to area C. The sandstone packets in area B shows a minimal degree of amalgamation, unlike the packets present in area A in sub-slice 6-1. One feature of sub-slice 6-2 is that mini-slices SL 6I and SL 6L vary little in thickness between areas B and C, suggesting a flat seafloor during the deposition of these mini-slices.

Mini-slice SL 6H has more sand in area C than area B. Area C may have been closer to the paths of the depositing currents than area B. This diversion of flows to area C is probably due to bottom topography variations caused by the greater accumulation of sediments in area B in the underlying mini-slice SL 6G. Hence, this variation in thickness is likely a compensation effect.

Megaturbidites BT 64 and BT 64a increase in thickness in area C, most likely due to ponding in the west. Variations in the siltstone facies and subfacies in mini-slice SL 6I

reflect downcurrent fining and decrease in sediment concentration of the flows.

Mini-slice SL 6J shows a pronounced thickness increase in area B compared to area C, suggesting a local control on deposition, either in area B or area C. A depression, perhaps due to faulting, may have developed in area B, or area C may have become a bathymetric high for similar reasons during the deposition of mini-slice SL 6J.

Mini-slice SL 6K shows a pronounced facies and thickness change between areas B and C. In area B, concentrated flows deposited sandstone beds of facies C2.1, B2.1 and B2.2, resulting in packets with little amalgamation. It is suggested that these packets are probably the distal equivalents of more sandy packets with a greater degree of amalgamation that developed east of the study area. It is also suggested here, that the difference in the thickness of mini-slice SL 6K between area B and C may be explained entirely by the greater compaction of more muddy sediments in area C. Downcurrent of area B, deposition was mainly from low concentration turbidity currents carrying silt and mud loads. A slight diversion of some of the flows from area C may have occurred due to a subtle bathymetric high in area B, caused by deposition of the sandstone packet.

It is suggested here that the packets that were deposited in area B of sub-slice 6-2 had a less convex upper surface than the packets of sub-slice 6-1 in area A. This is in agreement with the postulated shape of lobes proposed by Mutti (1992), where a greater degree of mounding in the upcurrent area occurs than in the downcurrent end.

Mini-slice SL 6L consists mostly of siltstone, where beds of subfacies C2.1A (with climbing ripples) are more common in area B, suggesting rapid deposition from

suspension. In area C, subfacies D2.1C beds are more common due to syn-depositional deformation resulting from rapid deposition of more soft muddy material between silt beds.

Mini-slice SL 6M has a few sandstone beds deposited from low concentration turbidity currents. Sandstone beds are slightly more common in area C than in area B suggesting perhaps that area C was closer to the flow paths than area B. Siltstone beds in area B, in mini-slice SL 6M, are more common and thicker than in area C. A particular characteristic of the siltstone beds in this mini-slice is the greater occurrence of subfacies D2.1A, with its climbing ripple lamination. Most of these beds show an unusual south to north trend. It is believed that beds of subfacies D2.1A were deposited rapidly, perhaps from flows that expand rapidly as they exited channels. The channels presumably had a more-or-less northerly course and did not occur near area C. In this case, area C was not downcurrent from area B.

For the internal architecture of the sub-slice 6-2, mini-slices do not show a significant difference in thickness between the two closely-spaced sections. The variation in thickness may be explained as a result of compensation and the position of the two sections relative to the axes of the depositing currents. The increased amount of sandstone in mini-slices other than SL 6K, suggests that section CB was closer to the axes of the depositing currents than section SYE. Flows that deposited the sandstone beds in packets in section SYE continued to section CB where the packets persist.

There are three main architectural elements observed in sub-slice 6-2. The first is

megaturbidites, which have a tabular, wedge or lens shape controlled by bottom topography. They are bounded by 0<sup>th</sup> order bounding surfaces. The second element is 10-15 m-thick sandstone packets that taper over distances of more than 10 km. These packets are bounded by 3<sup>rd</sup> order bounding surfaces and are mostly composed of sandstone beds of facies C2.1 that have a tabular shape at outcrop scale (10's - 100's m). These packets are lense-shaped over distances of 1-2 km. The beds become more muddy and thinner in a downcurrent direction. The third architectural element consists of packets of siltstone that are up to 20 m thick and composed of beds characterised by climbing ripple lamination. These packets have a sheet-like geometry on a local scale (1-2 km) but taper or have a lens shape over longer distances.

#### **5.4.11. Description of Time-slice 7**

Time-slice 7 is the upper-most time-slice in the studied sequence. It is exposed only in areas B and C and is bounded at the base by K-bentonite horizon KB-8 and at the top by KB-9. Three megaturbidites (BT-69, BT-70, BT-71) can be correlated between areas B and C. These three megaturbidites and KB-8 and KB-9 divide time-slice 7 into 4 mini-slices (SL 7A through SL 7D). Based on correlations, an estimated 12.5 m of section in mini-slice SL 7B at area B is missing due to faulting; thus, an evaluation of the external architecture of time-slice 7 will be limited to mini-slices SL 7A, SL 7B and SL 7D.

Flutes at the base of the megaturbidites indicate flow from east to west. Some beds identified as megaturbidites below BT-70 in area C, could not be correlated to similar beds

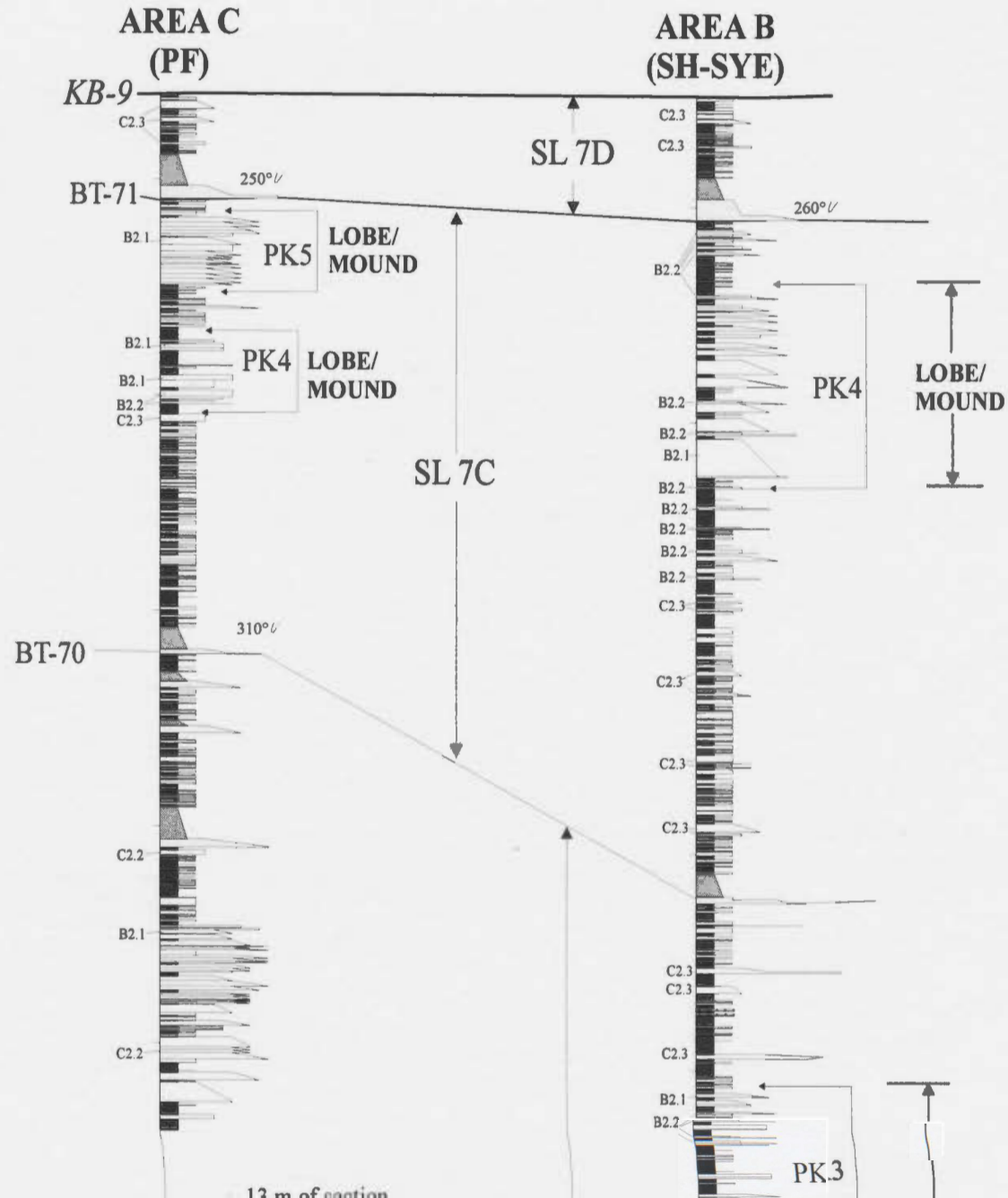
area B (Figure 5.37).

Mini-slices SL 7A, SL 7C and SL 7D are thinner in area C than area B (Figure 5.38). Facies and subfacies show variations in the number of beds and thicknesses in the different mini-slices between area B and area C (Figure 5.39). In mini-slice SL 7A, sandstone beds are rare. Siltstone beds are more common in area B than area C. Siltstone beds subfacies D2.1E are more common in area B. Other siltstone subfacies do not show much variation in bed/laminae numbers between the two areas.

In mini-slice SL 7B, sandstone beds are more numerous in area B than in area C. Sandstone beds in area B form three packets (Figure 5.37). Two lower packets (PK1 and PK2; Figure 5.37), are ~7-8 m thick, and consist of thin to thick bedded sandstone beds of facies B2.1, B2.2 and C2.1. These sandstone beds are interbedded with shale and only a few beds occur in amalgamated units. In area C, the sandstone packets are thin, and may be equivalent to the thicker packets in area B. Each packets at area C consists of a few beds of sandstone and siltstone (Figure 5.37). A thick packet, ~20 m thick occurs in the middle to upper part of mini-slice SL 7B in area B. This packet could not be correlated to area C because of faulting and will be discussed later in this section. In area B, some sandstone beds of facies C2.3 alternate with siltstone beds in the lower part of mini-slice SL 6B. In area C, thick beds of facies C2.2 alternate with siltstone beds in the lower part of mini-slice SL 6B.

In mini-slice SL 7C, sandstone beds are more numerous in area C than in area B. In area B, sandstone beds of facies C2.3 and B2.2 alternate with siltstone beds in the

**Figure 5.37 CORRELATED TIME-SLICE 7**



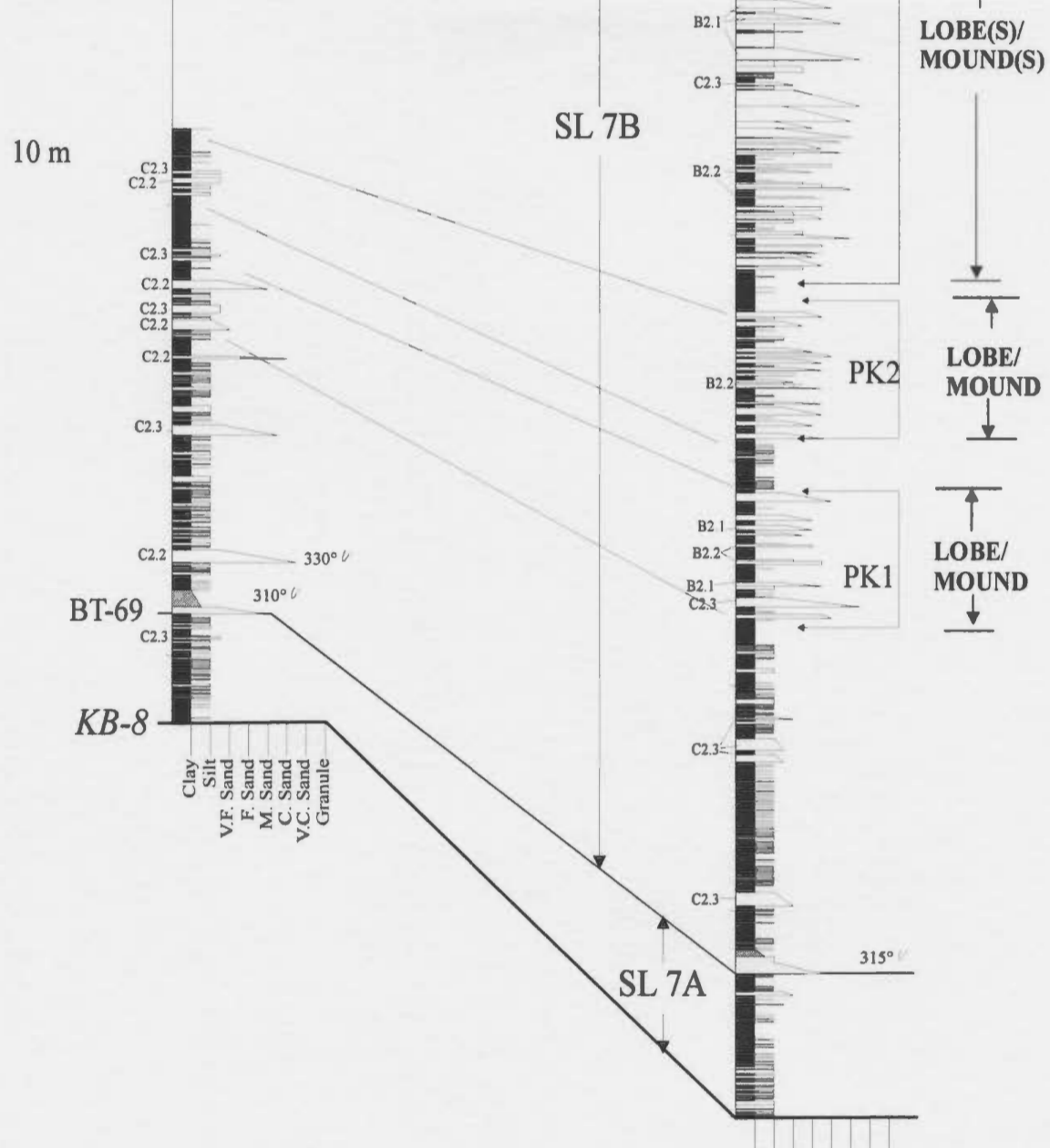
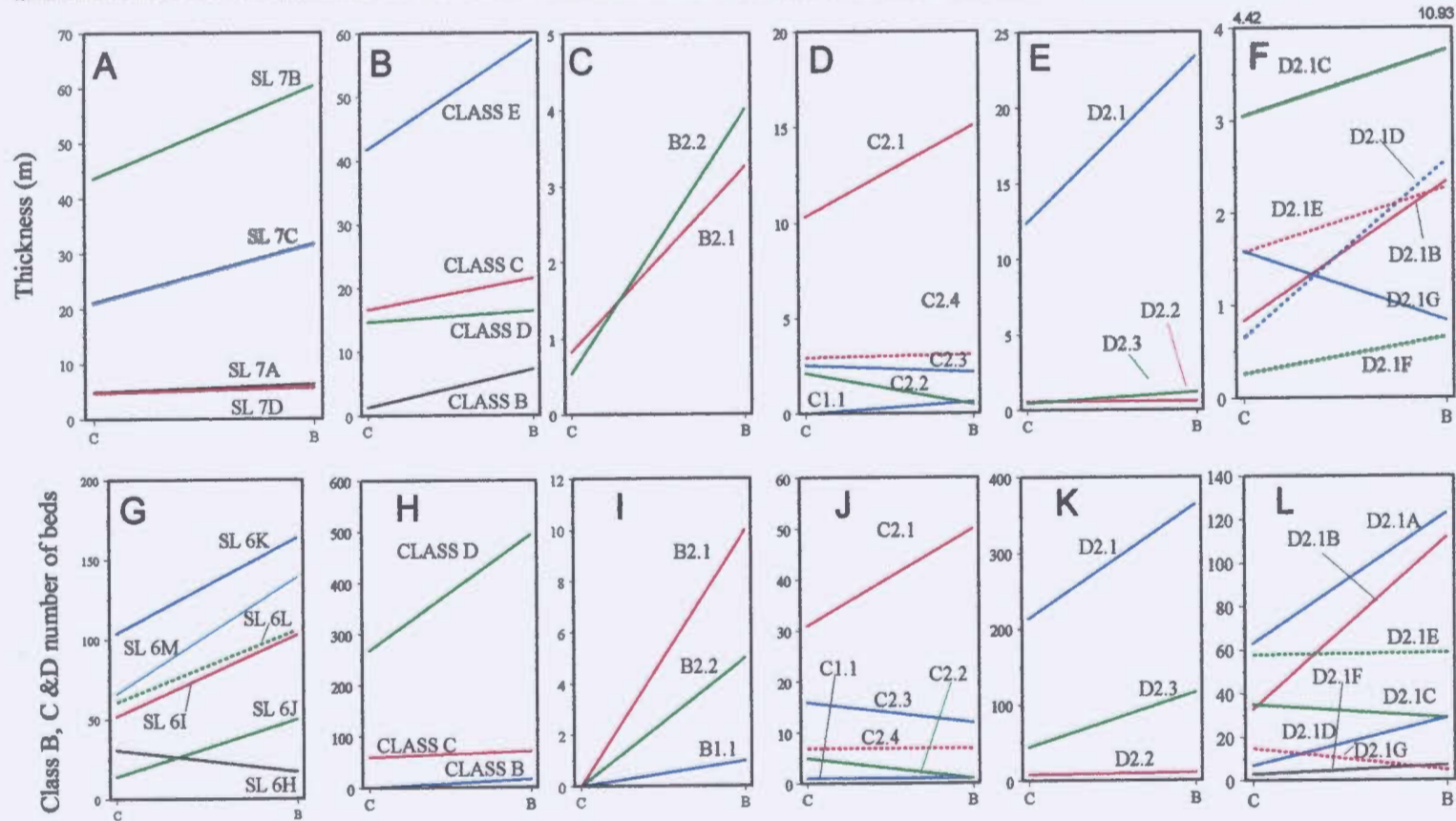




Figure 5.38. Comparison of the facies thicknesses and number of beds and laminae for sub-slice 6-2 between areas B and C. A is a plot of the thickness for each of the mini-slices. B, C,D,E, and F are for the total thicknesses in metres of facies and subfacies in sub-slice 6-2. The value above F is for the total thickness of subfacies D2.1A. G is plots of the number of sandstone and siltstone beds and laminae for each of the mini-slices. H, I, J, K and L show the number of beds and laminae in sub-slice 6-2.



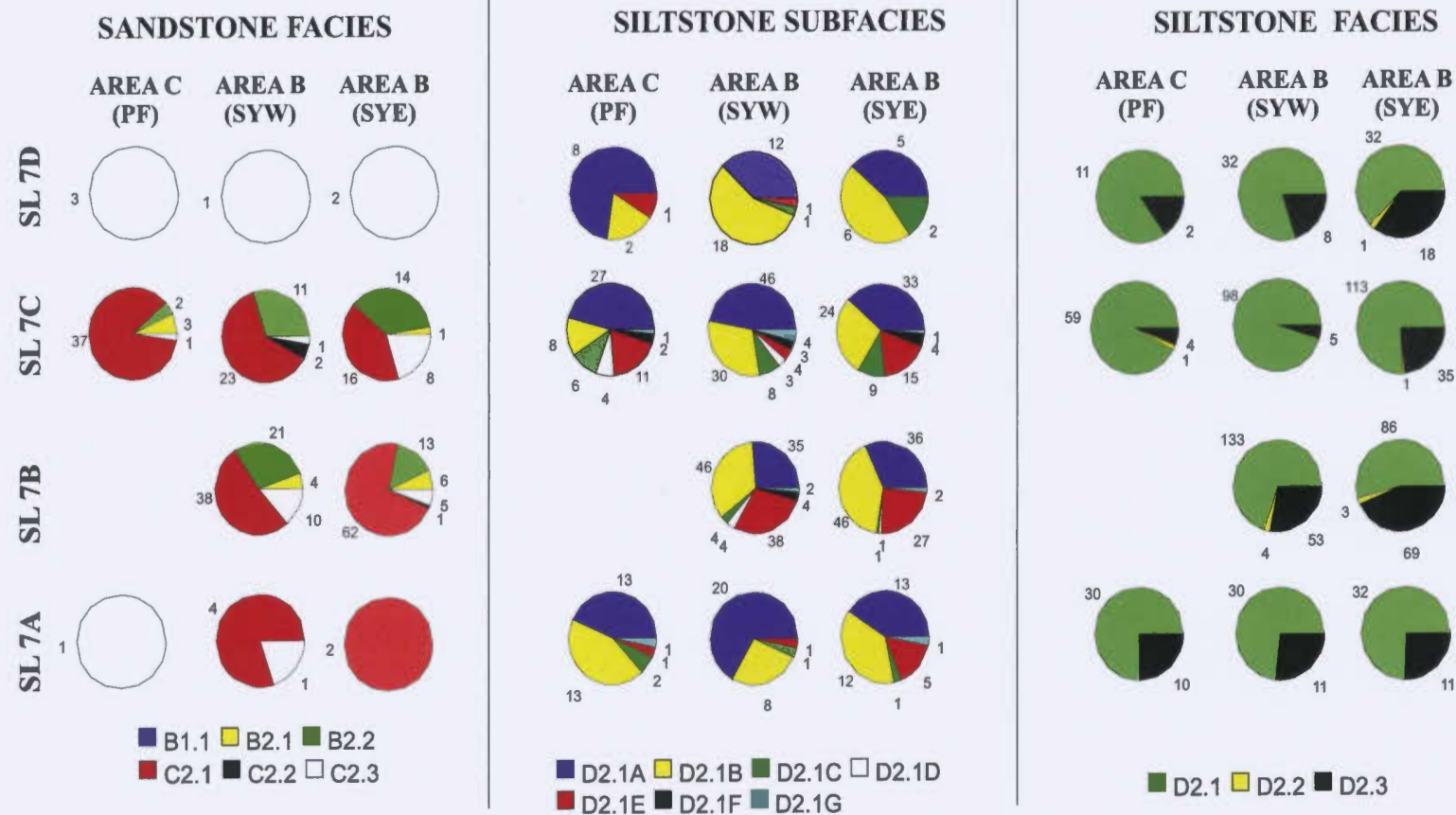


Figure 5.39. Numbers of siltstone and sandstone beds and laminae assigned to the different facies and subfacies in the mini-slices of time-slice 7. These are compared between areas B and C. Data for section SYW is for short-distance comparison of the number of facies and subfacies is also included

lower part of mini-slice SL 7C. Thick to medium bedded sandstone beds of facies C2.1, B2.1 and B2.2 form a ~ 10 m thick packet in the upper part of mini-slice SL 7C (PK4; Figure 5.37). Only a few sandstone beds in mini-slice SL 7C are amalgamated. In area C, no sandstone beds alternate with siltstone beds in the lower part of mini-slice SL 7C and in area C, they form two ~ 3-5 m thick packets (PK4 and PK 5; Figure 5.37). Medium to thick beds of facies C2.1, C2.3 and B2.2 form the lower packet (PK 4; Figure 5.37). Only two or three beds in PK4 are amalgamated, while PK5 consists mostly of medium to thick amalgamated beds of facies C2.1.

Siltstone beds are more common in mini-slice SL 7C in area B than in area C. Siltstone beds and laminae of facies D2.3 are considerably more common in area B (35 beds/laminae) than in area C (5 beds/laminae). Siltstone beds assigned to subfacies D2.1A and D2.1B decrease from area B to area C while subfacies D2.1E shows an opposite trend (Figure 5.39). Other siltstone subfacies are rare.

Mini-slice SL 7D is slightly thicker in area B than area C. Sandstone beds other than megaturbidites, show little or no variations between areas B and C. Siltstone beds are more common in area B than in area C. Facies D2.2 is more common in area B (18 beds/laminae) than area C (2 beds/laminae). Siltstone beds of facies D2.1 are more common in area B than in area C. Siltstone beds of subfacies D2.1B and D2.1C are more common in area B than in area C, while beds/laminae of subfacies D2.1A are more common in area C than in area B.

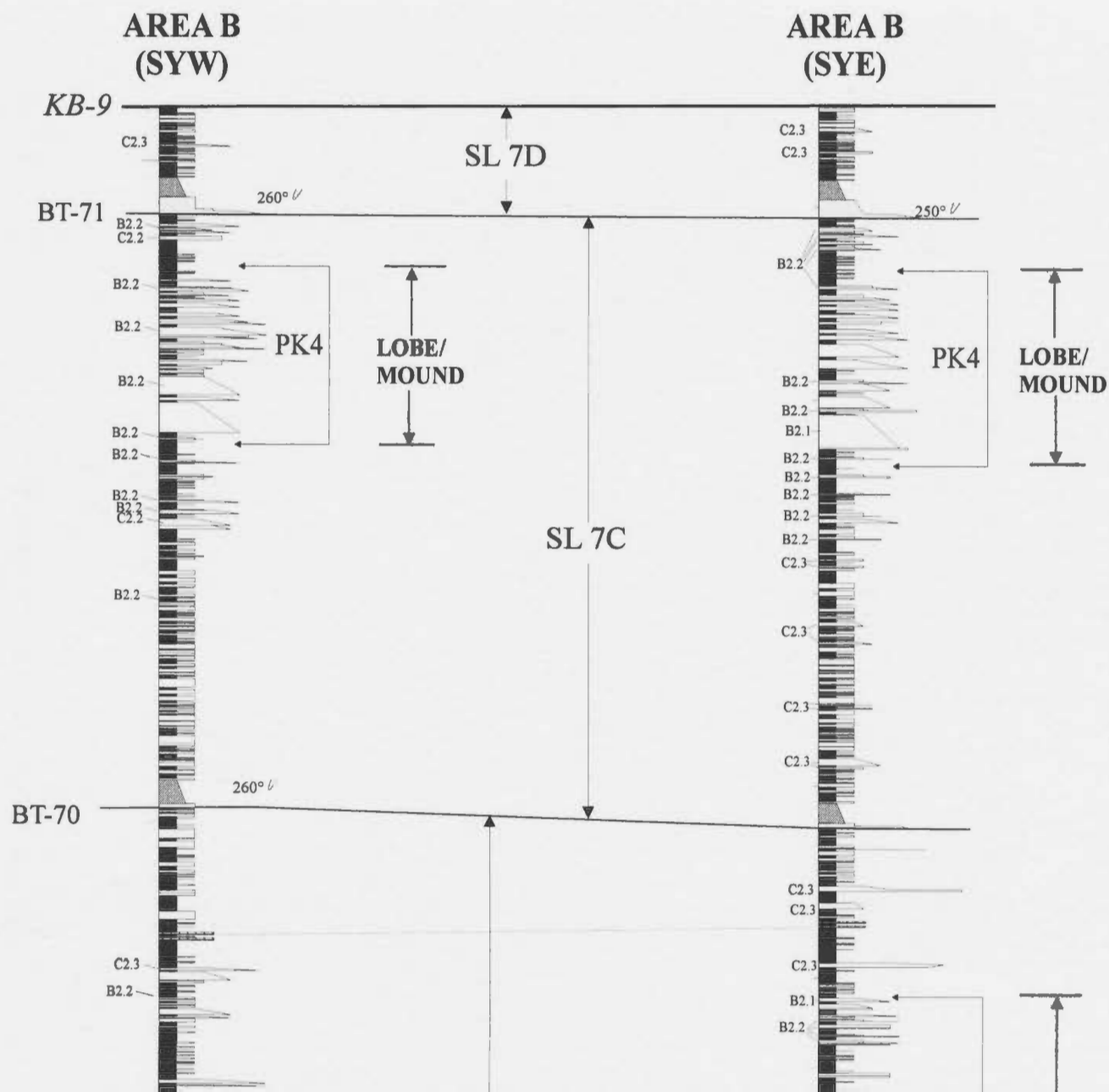
Sections SYW and SYE are used to investigate the internal architecture of time-

slice 7 (Figure 5.40). The distance between these two sections varies from ~0.5 km, in the lower part, to tens of metres in the upper part. Mini-slices SL 7D and SL 7C show only minor variations in the number of sandstone beds between sections SYE and SYW. Siltstone beds are more common in section SYE than in section SYW (Figure 5.39).

In mini-slice SL 7B, sandstone beds are more numerous in section SYE than in section SYW. Three sandstone packets are recognised in section SYE (Figure 5.40). The inferred equivalent packets are thinner in section SYW. Packet PK1 is 5 m thick in section SYE and consists mostly of facies C2.1 and some beds of facies B2.2. In section SYW, a package correlated to PK1 in section SYE is less well defined and consists of a few thin to medium sandstone beds of facies B2.2 and C2.3. The second sandstone packet (PK2; Figure 5.40), ~7-8 m thick in section SYE, consists of medium to thick beds of facies C2.1 that are mostly non-amalgamated. In section SYW, packet PK2 consists mostly of non-amalgamated medium beds of facies B2.2 and facies C2.1. The third packet in mini-slice SL 7B is ~20 m thick in section SYE and consists of medium to thick sandstone beds of facies B2.1, B2.2 and C2.1. Some thick siltstone beds of subfacies D2.1A occur in this packet. Some of the sandstone beds in this packet are amalgamated. In section SYW, PK3 is thinner (~15 m) and consists mostly of facies C2.1. Many of these sandstone beds are amalgamated.

Siltstone beds are more numerous in section SYW than section SYE in mini-slice SL 7B (Figure 5.39). Beds of facies D2.3 are more common in section SYE than in section SYW. Siltstone beds/laminae of subfacies D2.1E are more common in section

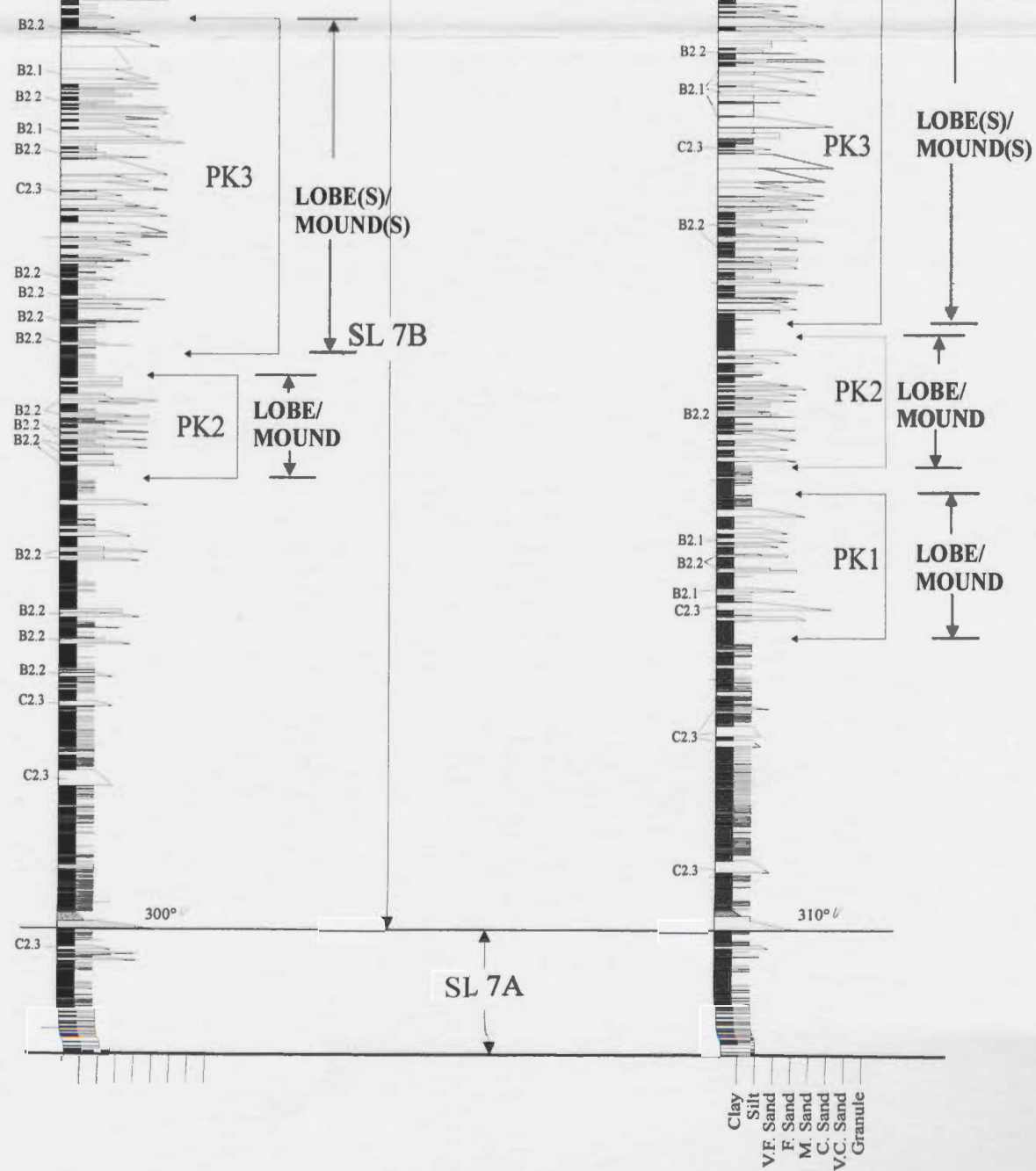
**Figure 5.40. Short-distance correlation of time-slice 7**



10 m

BT-69

KB-8



SYW than in section SYE while other siltstone subfacies show little or no variation between these two sections in mini-slice SL 7B.

In mini-slice SL 7C, there is little variation in the number of sandstone beds between sections SYE and SYW, although there is a difference in the type of facies (Figure 5.39). Siltstone beds are more common in section SYE than in section SYW. Beds of facies D2.1 and D2.3 are more common in section SYE than in section SYW. Siltstone beds/laminae of subfacies D2.1A are more common in section SYW than in section SYE while beds/laminae of subfacies D2.1E are more common in section SYE than in section SYW.

Mini-slice SL 7D shows little variation between sections SYE and SYW. However, siltstone beds of facies D2.3 are more numerous in section SYE and the subfacies of D2.1 vary in numbers between the two sections (Figure 5.39).

#### **5.4.12. Interpretation of Time-slice 7**

Low concentration flows deposited the siltstone beds of mini-slice SL 7A in areas B and C. The greater mini-slice thickness in area B may suggest slight variation in bottom topography. Sandstone and siltstone facies do not show a great variation in the type or number of facies and subfacies between the two areas.

The lower ~20 m of mini-slice SL 7B in area B may be tentatively correlated with the lower ~15 m of mini-slice SL 7B in area C. The siltstone beds and laminae in the lower part of mini-slice SL 7B in area B may be equivalent to the siltstone-rich interval in area C.



Siltstone beds and laminae in area C are thicker than those in area B, perhaps because area C was located closer to the paths of the depositing currents. Some sandstone beds occur with these siltstone beds; these beds are coarser in area C than in area B, supporting the hypothesis that area C was closer to the paths of the depositing currents.

The two lower sandstone packets in mini-slice SL 7B (PK1 and PK2 in Figure 5.37) in area B may be equivalent to two, less well developed clusters of sandstone and siltstone beds in area C. Packet PK1 in area B consists of beds of facies Class B (facies B2.1 and B2.2) while in area C, the equivalent packet consists of facies C2.2 and C2.3. It is suggested here, that some beds of PK1 in area B may have evolved or changed to facies C2.2 and C2.3 downcurrent towards area C. This speculation is based on good lateral continuity and downcurrent evolution of some beds of facies B2.2 in the other mini-slices. The overlying packet, PK 2, in area B shows less lateral continuity to area C than PK 1. This may be related to facies type. This packet consists mostly of beds of facies C2.1 that, in general, do not show good lateral continuity.

The lateral relationship of the remaining part of mini-slice SL 7B is unknown because part of the mini-slice is missing in area C due to faulting. Some of the beds that are recognised as megaturbidites in the upper part of SL 7B in area C may be lateral equivalents to some sandstone beds below BT 70 in area B, however, these were not recognised as megaturbidites in area B.

Mini-slice SL 7C is thicker in area B than area C. The lower part of the mini-slice consists of siltstone beds of different facies and subfacies that are thicker and more



common in area B than in area C. It is believed that this trend reflects downcurrent fining and thinning as the flows decelerated and deposited their loads. Sandstone beds of packet PK4 in the upper part of mini-slice SL 7C were deposited from concentrated flows, some of which may have continued to area C and deposited the sandstone beds of PK 4 in area B. Deposition of the upper packet in the upper part of mini-slice SL 7C was restricted to area C. This packet consists mostly of amalgamated beds of facies C2.1. Some beds have flutes at their base with a palaeocurrent trend that differs by as much as 60 degrees from other sandstone beds in this mini-slice in both areas B and C. This packet might have developed downflow from a local channel that did not influence area B.

Mini-slice SL 7D shows a slight thickening in area B compared to area C. More shale occurs in area B than in area C (Table CD T7). Some of the mud that formed the shale in area B might have been eroded in area C by the flows that deposited the thicker sand and silt beds in area C.

For the internal architecture of time-slice 7, mini-slices SL 7D and SL 7C do not show much variation in either facies or thickness. This is probably due to the fact that the upper parts of the two sections are spatially very close. The slight variation in facies and thickness of some beds is attributed to compensation.

For mini-slice SL 7A, the greater number of siltstone beds and laminae of subfacies D2.1A in section SYW than in section SYE, suggests that section SYW was closer to the paths of the flows than section SYE.

For mini-slice SL 7B, siltstone facies D2.3 are more numerous in section SYE than

in section SYW. Beds of facies D2.1 show the opposite trend. This suggests that some flows reaching section SYE had a small concentration of silt and deposited facies D2.3. Some of these flows may have deposited thicker laminae or beds of subfacies D2.1E in section SYW.

Sandstone beds of facies C2.1 decrease in number from section SYE to SYW. The sandstone packet 1 (PK1; Figure 5.40) thins towards SYW and becomes less defined. Packet 2 is more persistent from section SYE to section SYW, suggesting that some beds of facies C2.1 that form PK2 in section SYE change to facies B2.2 in a downcurrent direction. It is suggested that flows which first deposited facies C2.1 incorporated mud from the underlying substrate as soft mud clasts that disintegrated in the flow. This mud would have allowed the flows to continue farther downcurrent and perhaps deposit facies B2.2. Many beds of facies C2.1 in section SYE in PK2 are rich in mud clasts, supporting the above interpretation.

The thickest packet in mini-slice SL 7B, PK 3, consists of beds of facies C2.1 in both sections SYE and SYW. These beds were deposited from concentrated flows with sufficient momentum to continue to SYW. Some flows that deposited beds of facies C2.1 in SYE did deposit beds of other facies in section SYW, probably due to the incorporation of mud from the substrate. Thick siltstone beds of subfacies D2.1A were probably deposited from flows that exited channels and deposited most of their load as they encountered an elevated sea floor, formed by the deposition of the sand constituting PK3. The remaining part of mini-slice SL 7B consists mostly of siltstone beds and some

sandstone beds deposited from low-concentration flows.

There are four architectural elements in time-slice 7. The first is megaturbidites that vary in thickness and thus, geometry across the area. These megaturbidites are bounded by 0<sup>th</sup> order bounding surfaces. The second type of architectural element are the sandstone packets. Some packets consist of mostly medium sandstone beds that alternate with shale and show minor amalgamation (PK1, PK2 and PK4). Sandstone beds of these packets thin or become muddy in a downcurrent direction over distances of more than 10 km. Some packets appear to maintain their tabular or lens-shaped geometry for a distance of 1-2 km in a downcurrent direction. Other sandstone packets that consist mainly of medium to thick beds of facies C2.1, many of which are amalgamated. These packets have a wedge or lens shape and taper in a downcurrent direction over distances of 5-10 km. The lack of good lateral continuity of the sandstone beds is probably related to flow dynamics, whereby high concentration flows that deposited beds of facies C2.1 were sensitive to any slight variation in bottom topography, leading to rapid and localised deposition. However, some flows may have travelled farther following incorporation of mud from the substrate (*cf. Mutti et al., 1999*). The availability of mud for this purpose was enhanced when flow frequency decreased and were separated by longer periods of mud deposition. When flows were frequent, less mud was incorporated and deposition occurred rapidly resulting in amalgamated unit that form many of the packets. Sandstone packets are bound by 3<sup>rd</sup> order surfaces that delineate their external geometry.

The third architectural element is the siltstone packets, which have a sheet-like

geometry over distances of a few kilometres and a gently lensing geometry greater distances. These siltstone lenses or sheets are bounded by 2<sup>nd</sup> or 3<sup>rd</sup> order bounding surfaces.

The sandstone packet in the upper part of mini-slice SL 7C in area C may represent a different type of architectural element. It may be a local lens. This packet was not correlated over either a long or short distance, so its geometry is unknown.

## **5.5. SYNTHESIS OF DEPOSITIONAL ENVIRONMENTS AND DEPOSITIONAL HISTORY**

Several features observed in Pointe-à-la-Frégate Member of the Cloridorme Formation are characteristic of basin-plains and deep-marine turbidite systems. The most notable of these features include (i) the association of megaturbidite layers with other layers that have attributes of classical turbidites, (ii) the influx of coarse clastic sediments into a depositional environment otherwise characterised by deposition of mud, and (iii) the presence of sediment bodies that have many characteristics similar to deposits of modern submarine fans and ancient turbidite systems suggested to be fans. The interpretation of deep-marine turbidite deposits will invariably lead to comparison with submarine fans (Mutti and Normark, 1987, 1991; Mutti *et al.*, 1999; Piper *et al.*, 1999; Bouma, 2000; Piper and Normark, 2001) although in this study a “fan” shape was not observed and is not suggested.

The main criterion used in this thesis to distinguish a basin-plain environment from

a submarine fan system is the inferred two-dimensional geometry of some of the sandy deposits. Specifically, deposits that are interpreted as mounds are classified as submarine fan lobes whereas deposits with a more-or-less sheet-like geometry are classified as basin-plain deposits. The boundary between these two environments is identified in modern environments by a change in slope from gently inclined in the lower fan to essentially flat in the basin plain (Normark, 1970; Piper *et al.*, 1999). In ancient turbidite deposits, the boundary between the submarine-fan system and the basin plain can only be defined on the basis facies type and inferred geometry. This transition zone is characterised by a downcurrent change in facies where sandstone beds of the lobe or distal lobe thin and fine towards basin plain (Mutti *et al.*, 1999). This area has been referred to as the lobe fringe (Mutti *et al.*, 1978).

In terms of order of bounding surfaces used in this chapter, a 5<sup>th</sup> order surface is used to separate the submarine-fan system and the basin plain. Fourth order surfaces separate groups of sandstone bodies, each of which is interpreted as a lobe. Individual sandstone lobes are delineated by 3<sup>rd</sup> order surfaces while bodies of sheet sandstone and siltstone are delineated by 2<sup>nd</sup> or 3<sup>rd</sup> order surfaces. Lower rank bounding surfaces delineate other bodies that range from individual layers bounded by 0<sup>th</sup> order surfaces (e.g. megaturbidites) to 2<sup>nd</sup> order surfaces that delineate groups of beds.

Tectonics and sea-level changes were most likely the main external (autocyclic) factors controlling deposition of the studied sequence. These factors also controlled other local (autocyclic) factors such as channel switching. The sea-level curve for this period is

characterised by numerous rises and falls with two to four lowstands (Ross and Ross, 1995). This suggests that, during deposition of the studied sequence, sea level may have fluctuated considerably. Deciphering which factors had the greater control on the deposition of the studied sequence may be difficult. In the thesis area, the effect of tectonics on sedimentation may have been greater than the effects of sea-level fluctuations (*cf.* Bouma, 2000). The depositional history presented here is a synthesis of the depositional conditions that occurred during the accumulation of the deposits in the time-slices 1 through 7. The architectural elements observed in each of the time-slices are summarised in Table 5.3. The synthesis of the depositional environments is presented in Figure 5.41.

#### **5.5.1. Time-slice 1 to Time-slice 3**

The interval from the base of time-slice 1 to the top of time-slice 3 is interpreted to represent deposition in a basin-plain setting. Deposition was dominated by the accumulation of megaturbidites. The flows that deposited most of the megaturbidites were probably initiated by large sediment failures east of the study area. Many of these sediment failures evolved into mature turbidity currents, characterised by good grain-segregation by the time they reached the study area. The flows travelled across the length of the basin and some of them were reflected against the basin margins or basin highs (Pickering and Hiscott, 1985). Low density turbidity currents, initiated at a location distant to the thesis area, periodically reached the thesis area and deposited thin siltstone beds and laminae in

Table 5.3. Summary of the main characteristics of the time-slices and sub-slices with interpretations. The range of reader should read the slices in order starting with the time-slices 1(SL-1).

SLICE/ SUB-SLICE	THK (m)	CLASSES % B  C  D  E	ARCHITECTURAL ELEMENTS	O.B.S.	CONSTITUENT FACIES	
SL-7	87-104	4 21 19 56	Megaturbidites Sandstone mounds Siltstone sheets Sandstone lenses	0 3 2/3 2/3	C2.4 C2.1, B2.1, B2.2 D2.1, D2.2, D2.2 C2.1, B2.2	D to di lo
6-2	77-103	2 15 21 62	Megaturbidites Sandstone mounds Siltstone sheets	0 3 2/3	C2.4 C2.1, B2.1, B2.2 D2.1, D2.2	D la hi an
6-1	66-97	4 15 16 65	Sandstone mounds Megaturbidites Siltstone sheets	3 0 2/3	C2.1, B2.1, B2.2 C2.4 D2.1, D2.2	fe mi
SL-5	39-43	0 11 18 71	Megaturbidites	0	C2.4	De pa de irr co
4-2	74-80	1 10 19 70	Megaturbidites Sandstone mounds Siltstone lenses	0 3 2/3	C2.4 C2.1, B2.1, B2.2 D2.1	De in (st lov inf sli
4-1	56-59	0.5 13 16 70	Megaturbidites Sandstone sheets? Sandstone mounds	0 2/3 3	C2.4 C2.2, C2.3, D2.1E, A C2.1, C2.3	De sea col are Inc
SL-3	65-76	0 9 17 74	Megaturbidites Siltstone lenses	0 2/3	C2.4 D2.1C, D2.1E	Me ter A: tov
SL-2	58-62	0 10 10 80	Megaturbidites	0	C2.4, C2.5	Fa dep
SL-1	32-36	0 17 8 80	Megaturbidites	0	C2.4, C2.5	De tha

retations. The range of thickness of each slice/subslice (THK) is shown. O.B.S. = order of bounding surfaces. The

## CONSTITUENT FACIES

## INTERPRETATION

2.4 2.1, B2.1, B2.2 2.1, D2.2, D2.2 2.1, B2.2	Deposition from large flows that extended across the basin. The geometries of these layers are controlled by bottom topography. Mounds consist mostly of facies C2.1 deposited from concentrated flows that did not travel for long distances. Siltstone sheets were deposited from frequent low-concentration flows. Sandstone lenses formed by localized (in channels?) deposition of sand from concentrated flows.
2.4 2.1, B2.1, B2.2 2.1, D2.2 2.1, B2.1, B2.2 2.4 2.1, D2.2	Deposition is mainly from low concentration turbidity currents that deposited different type of siltstone facies and large flows that deposited megaturbidites. The flows were controlled by bottom irregularities. During periods of high sediment discharge, sandstone beds of facies C2.1, B2.1 and B2.2 were deposited from concentrated flows and formed mounds on the sea floor that acted as an obstacle for subsequent flows. These mounds were localized features that do not extend farther downcurrent. Some of the flows may have incorporated some of the underlying mud and travelled farther downcurrent. Siltstone sheets were deposited from frequent low-concentration flows.
2.4	Deposition dominated by large flows that extended across the area. Sand-load flows were less frequent and no packets or mounds were formed. Infrequent sand-load, low-concentration flows traveled across the area and deposited beds of facies C2.2 and C2.3. Sea-floor irregularities controlled deposit geometries. Some of these irregularities are attributed to movements of buried faults in area A. Silt-load flows were thicker and more concentrated and deposited thick silt beds in areas A and B. Flows waned downcurrent and deposited thinner beds.
2.4 2.1, B2.1, B2.2 2.1	Deposition of megaturbidites from large flows. Deposition of sand from concentrated flows. Most of the sandstone in mounds are amalgamated. The mounds diverted subsequent flows. Siltstone lenses consist of facies D2.1 (subfacies D2.1A, D2.1B, D2.1E and some thick beds of subfacies D2.1C and D2.1G. The silt was deposited from low concentration flows. Over short distances, the lenses have tabular geometries. Depositional factors have a greater influence on the geometry than subsidence due to higher rates of sedimentation in time-slice 4 compared to older slices.
2.4 2.2, C2.3, D2.1E, A 2.1, C2.3	Deposition of megaturbidites from large flows. Sandstone and siltstone packets may have formed mounds on the sea-floor and diverted subsequent flows. Sandstone beds in mounds are structureless and were deposited from concentrated flows. Sandstone beds in sheets are structureless in upcurrent areas but show Bouma sequences in area B and become more muddy farther down current. Over distances of 1-3 km, mounds and lenses are tabular. <u>Increase in the amount of sand reaching the area was due to the advance of a turbidite system from the east.</u>
2.4 2.1C, D2.1E	More sand and silt compared to time-slice 1 and 2 due to proximity to the source of sediments or channels terminations. Depressions in area B controlled the flows and more sand (facies C2.3) was deposited in area B. A structural high at area A resulted in a lens-shaped siltstone body. Sandstone and siltstone beds decrease towards the west due to waning flows. Megaturbidites increase in thickness westward due to ponding.
2.4, C2.5	Facies distribution and thickness are controlled by the interplay of subsidence and the rate of sediment deposition. Depressions in area B controlled the paths of the flows and focused these flows into area B.
2.4, C2.5	Deposition was on a flat basin floor from large flows that spread across the basin, and low-concentration flows that waned downcurrent (to the west).

DISTAL FAN

BASIN PLAIN

FAN FRINGE



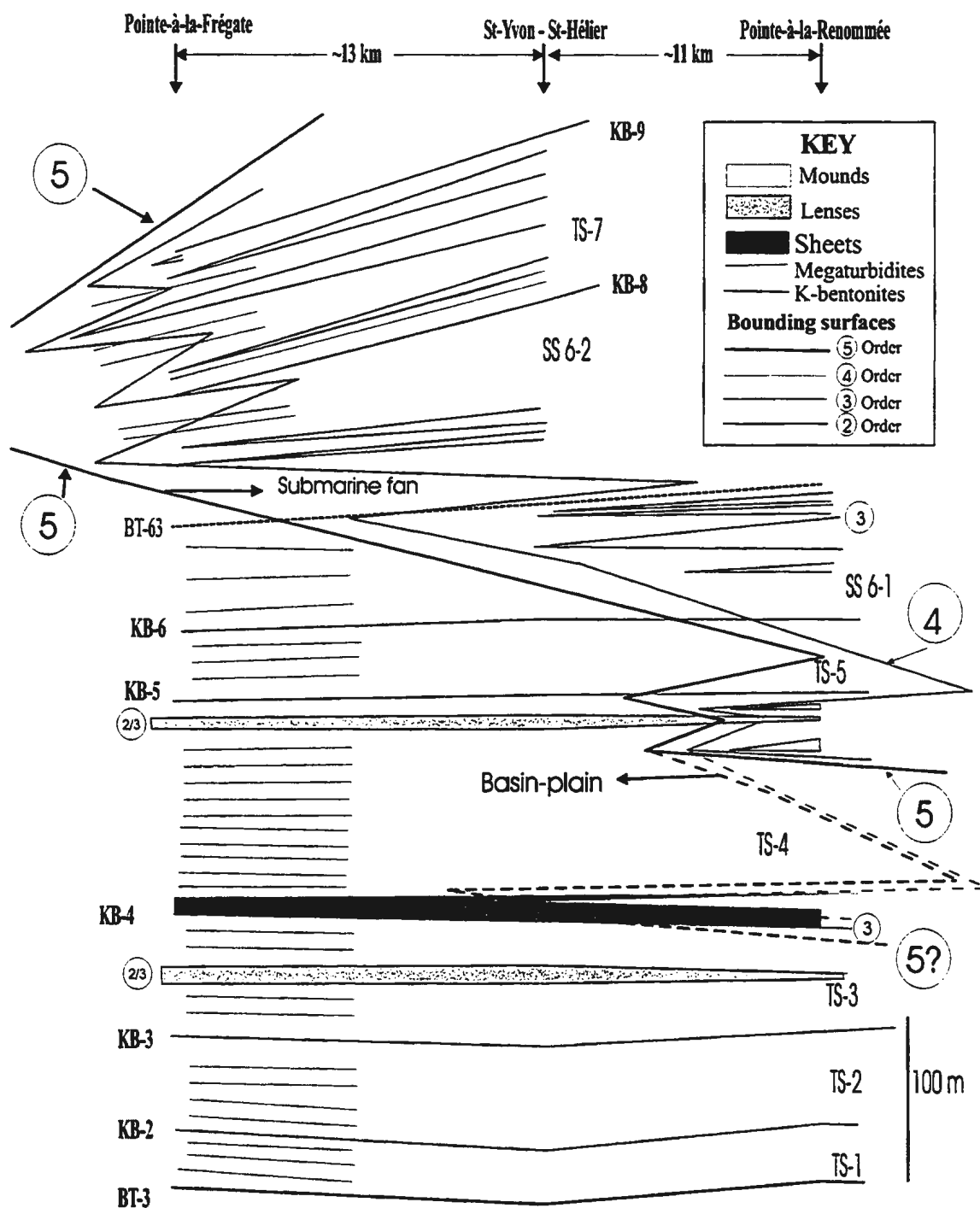


Figure 5.41. Schematic summary of the depositional history of the studied sequence. BT=basin turbidites, KB= K-bentonites, TS= time slices and SS are sub-slices. The numbers and positions of megaturbidites are schematic. Orders of bounding surfaces have no link to orders of sea-level change recognised by sequence stratigraphers.

the lower parts of this interval.

Sea-bottom irregularities had a pronounced effect on the deposition and geometry of the sediments in this interval. During deposition of the lower part of the interval, the sea bottom was more-or-less flat and the megaturbidites have a more-or-less tabular or wedge-shaped geometry. Wedging was due to ponding of megaturbidites to the west. During the remaining part of this interval, sea-bottom irregularities became more pronounced, probably due to movement along buried faults (*cf. Mutti et al.*, 1999). Several small depressions apparently developed, particularly in the middle part of the thesis area. These depressions and their bathymetry controlled the paths of the flows transiting the area. The interplay between rates of deposition and subsidence controlled the distribution of different facies and subfacies in the area and also, the geometry of megaturbidites and other architectural elements. When the rate of deposition was greater than the rate of subsidence, a flat sea-bottom developed; when the rate of subsidence exceeded deposition, bathymetric lows developed. Thicker deposits subsequently accumulated in these bathymetric lows because they intercepted the approaching flows. Areas on or near bathymetric highs were avoided by the flows and thus, experienced less deposition from more dilute flows. In the later part of this interval, more siltstone was deposited in the thesis area due to an increase in sediment supply, perhaps reflecting proximity to the source or channel terminations. Some of these silt-laden flows were frequent and formed siltstone packets with a lens-shaped geometry (gently lensing element; Figure 5.41). The geometry of these lenses was controlled by bottom

topography. This element is bounded by 2<sup>nd</sup> or 3<sup>rd</sup> order surfaces.

Earthquakes have been suggested as a cause for the large slope failures that evolve into large turbidity currents that deposit megaturbidites (Mutti *et al.*, 1994). Weaver *et al.* (1992) suggested that sea-level fluctuation may help trigger such large sediment failures. Both of these factors might explain the initiation of the flows that deposited the megaturbidites in the studied sequence.

Basin plains are considered as an architectural element by Mutti and Normark (1987; 1991), Normark *et al.* (1993) and Piper *et al.* (1999), however, they may include other elements such as megaturbidites, sheet sandstones, or lenses of sandstone or siltstone (Pilkey, 1988; Rothwell *et al.*, 1992; Piper *et al.*, 1999; Piper and Normark, 2001; and this study). It is suggested here, that basin plains can be considered as an architectural element bounded by 5<sup>th</sup> order bounding surfaces (*sensu* Pickering *et al.*, 1995); the basin plain can include other elements bounded by lower-order bounding surfaces.

#### 5.5.2. Time-slice 4

Time-slice 4 appears to represent a marked change in facies type in the area as seen in the increased numbers of sandstone and siltstone beds compared to older time-slices. Deposition was from large flows that deposited megaturbidites, and low density turbidity currents that deposited siltstone beds, some of which cluster to form packets.

Deposition of megaturbidites and siltstones was interrupted by periods when high-

density turbidity currents reached the eastern part of the thesis area and deposited sandstone beds, forming packets. Sandstone packets consist mostly of beds of facies C2.1 and are continuous over distances of 2-3 km. Over these distances, the sandstone beds thin and become less amalgamated. These packets have a tabular or a slightly lensing geometry over short distances. Some high density flows may have continued west and later deposited classical turbidites. Siltstone beds also form packets, which have a tabular shape on a local scale but taper in a downcurrent direction.

The sandstone packets cannot be correlated over distances of more than 10 km. Two alternative interpretations are suggested. Firstly, that the packet in the lower part of sub-slice 4-1 might represent a sediment mound, tapering abruptly westward. In this case, the mound may be similar to lobes of ancient turbidite deposits and modern fans (Mutti, 1992; Mutti *et al.*, 1999; Piper *et al.*, 1999; Bouma, 2000; Piper and Normark, 2001). If this deposit represents a lobe, then the depositional setting changed from that of a basin plain to a setting akin to a submarine-fan system. The 5<sup>th</sup> order bounding surfaces that Pickering *et al.* (1995) propose to separate submarine-fan systems would be located between this lobe and the basin plain. The lobe itself is bounded by a 3<sup>rd</sup> order surface. The 4<sup>th</sup> order surface is placed at an intermediate position between the 3<sup>rd</sup> and 5<sup>th</sup> order surfaces (Figure 5.41).

Alternatively, the sandstone and siltstone beds in the lower part of sub-slice 4-1 in areas B and C may be tabular or lens-shaped elements with 2<sup>nd</sup> or 3<sup>rd</sup> order bounding surfaces. If the sandstone packet in the lower part of sub-slice 4-1 is sheet-like rather than

a mound on the sea-floor, then the depositional setting for the lower part of time-slice 4 may still be a basin plain, characterised by deposition from sand-laden flows that continued downcurrent for tens of kilometres to deposit classical turbidites.

It is suggested here, that high-density flows that deposited sandstone facies C2.1 may have originated as hyperpycnal flows of fresh water and sediment generated during periods of increased river discharge (Piper *et al.*, 1999; Piper and Normark, 2001). Many studies have suggested that hyperpycnal flows can only occur if there is a high enough sediment concentration to overcome the higher density of seawater. Alternatively, some of the high-density flows may have been generated from river-mouth failures of sediments that consisted predominantly of sands. These high-density, low-efficiency flows, are unable to continue for long distances downcurrent unless they incorporate muddy material, resulting in an increase in flow efficiency. If this happens, flows pass gradually into dilute (low concentration) flows that deposit classical turbidites.

The sandstone packet in the upper part of sub-slice 4-2 does not continue laterally for more than 5 km. This packet is more confidently interpreted as a lobe that formed a sediment mound on the sea floor. The 4<sup>th</sup> and 5<sup>th</sup> order surfaces are placed between the 3<sup>rd</sup> third order surfaces that delineate the lobes and the basin plain deposits (Figure 5.41). Siltstone beds in sub-slice 4-2 that cluster into packets, are bounded by 2<sup>nd</sup> or 3<sup>rd</sup> order surfaces and have a sheet-like geometry on a local scale and a gently lensing geometry on a regional scale. These lenses are interpreted as low-density turbidity current deposits that may have been equivalent to coarse deposits east of the area. The lens shape is due to

bottom topography variability caused by deposition of the lobes.

### **5.5.3. Time-slice 5**

Time-slice 5 is thin and dominated by megaturbidites deposited from large flows and siltstone beds deposited from low concentration flows. The geometry of the megaturbidites was controlled by bottom topography. The reduced deposition of sand in the area during time-slice 5 suggests that sediment supply to the area was significantly reduced, possibly due to local factors such as channel switching and avulsion or deposition of sediment bodies east of the study area that caused diversion of subsequent flows away from the area. Other regional or local factors such as sea-level rise or faulting may have affected the supply of sediments to the area.

### **5.5.4. Time-slices 6 and 7**

Time-slices 6 and 7 include sandstone beds that cluster to form packets. The sandstone beds were deposited from high-density turbidity currents that carried sand loads and a small proportion of silt and mud. These flows may have been generated by river-mouth sediment collapse. When collapse was frequent, flows did not incorporate mud and therefore, deposited their loads rapidly after they exited confining channels. Some muddy sandstone beds (facies B2.2) that occur below these packets and within the muddier parts of packets were probably also deposited from high-density flows after they had incorporated soft mud from the underlying substrate. These flows were then able to travel

farther downcurrent and in doing so they may have removed most of the soft mud from the substrate, leaving little to be incorporated into subsequent flows.

#### **5.5.5. Post Time-slice 7**

Younger sandstone packets occur west of the thesis area in the  $\beta 7$  member of Enos (1965) in the Petite-Vallée and Grande-Vallée areas. Some of these packets been correlated to the  $\gamma 2$  member (Hiscott *et al.*, 1986), and might therefore indicate a further westward expansion of fan-like environments.

### **5.6. CONCLUSIONS**

The lower part of the Pointe-à-la-Frégate Member (*sensu* Slivitzky *et al.*, 1991) of the Cloridorme Formation was deposited in a basin-plain setting, characterised by a flat sea bottom. The degree of sea bottom irregularities increased during the deposition of the remaining part of the member. These irregularities were due to depositional, compactional and tectonic factors. Deposition was mostly from large flows generated from slope failures east of the study area. Siltstone beds were deposited from low density turbidity currents generated from a distant source. Similar conditions probably existed during the deposition of the underlying Manche-d'Épée Member.

Deposition during the middle part of the Pointe-à-la-Frégate Member was characterised by an increase in the amount of sand reaching the area. Deposition was still dominated by the accumulation of megaturbidites from large flows and siltstone beds from

low-density turbidity currents. Some sand was deposited from high-density turbidity currents, forming mounds on the seafloor, similar to those found along the distal edges of some modern submarine fans (Piper and Normark, 2001). Alternatively, these flows might have continued in a downcurrent direction and deposited the sand as sheets that became progressively more muddy. If the second alternative is valid, then the sand-prone sheets can still be considered part of a basin-plain setting (Cattano and Ricci Lucchi, 1995). The increase in the sediment supply to the study area during accumulation of the middle part of the Pointe-à-la-Frégate Member might have been caused by local factors within the basin such as channel switching, or more regional factors such as sea-level changes or tectonics. Bottom topography variation due to the interplay between deposition and subsidence played a major role in controlling flow paths of the currents and the resultant geometry of the sediment.

Accumulation of the upper part of the Pointe-à-la-Frégate Member was characterised by deposition of sand from high-density flows that formed mounds on the seafloor. This it thought to represent a deep marine setting, similar to the lower parts of some modern submarine fans, although a fan shape could not be demonstrated during this study. The increase in the sand amounts may reflects the combined effect of local and regional factors such as sea-level change, tectonics, advance of the submarine system over the thesis area and other local factors within the system.



## **CHAPTER 6**

### **BED THICKNESS DISTRIBUTION**

#### **6.1. INTRODUCTION**

The thickness of sedimentary beds is one of the basic properties measured when describing sedimentary sections. The amount of detail and precision of the measurements varies from study to study depending on the operator and the objectives of the study. The nature of the bed thickness of many sedimentary sequences has received varying amount of interest since the early 1950's and many studies have suggested that the thickness of sedimentary beds follows a certain statistical distribution. The bed thickness distribution of turbidites has received its fair share of interest over the past 50 years; recently, there has been an increase in this interest and in the sedimentological significance of particular bed thickness distributions.

Doubt as to what sedimentological information can be obtained from the study of bed thickness distributions has been expressed by Schwarzacher (1972,1975). He indicated that a bed thickness dataset may consist of more than one distribution and many different sedimentological processes could lead to deposition of beds with a similar bed thickness distribution. This skepticism and debate concerning what type of distribution best describes the thickness of turbidite beds, and its significance, may be partly due to the fact that previous studies used datasets with a small number of beds (Drummond, 1999). Nevertheless, turbidite bed thickness distributions still attract a lot of interest and many

new ideas have been introduced to explain the type of statistical distribution that best fits certain data (Carlson and Grotzinger, 2001; Talling, 2001). Because of this continued interest and the large dataset collected in this study, it was decided to test the nature of the bed thickness distribution of turbidites in the lower Cloridorme Formation and to speculate on what sedimentary factors may have been at play.

In the first part of this chapter, the more than 27,000 bed thickness measurements representing a variety of facies collected from the studied sections in the thesis area will be investigated without considering their vertical or lateral position within individual sections or between sections. The aim is to investigate if the different facies or subfacies follow different statistical distributions. For example, do siltstone beds and sandstone beds follow different distributions? What may cause part of the population to depart from the distribution that otherwise best fits the data? Finally, what are the geological factors, if any, that might logically control the type of distribution?

The presence or absence of a vertical change in the type of bed thickness distribution within individual sections, or the presence of lateral changes in the distribution type between sections, will be investigated towards the end of this chapter. Wherever there are lateral and vertical changes in processes or depositional environments deduced from other criteria (Chapter 5) an effort will be made to establish whether these changes are reflected in the bed thickness distributions. This approach is similar to how the bed thickness distributions of other turbidites sequences have been studied. The advantage in this study is that the facies have been described and interpreted in detail (Chapter 3). This

is unlike some other studies where bed thicknesses distributions of sandstone or siltstone bed are investigated without a clear understanding of the factors that might have affected their thickness.

A large number of statistical distributions might account for observed bed thickness datasets. The lognormal, exponential, and gamma distributions have commonly been cited in the literature as distributions that best describe the thicknesses of sedimentary beds including turbidite beds (Bokman, 1957; Pettijohn, 1957; McBride, 1962; Krumbein and Graybill, 1965; Ricci Lucchi, 1969; Hesse, 1975; Davis, 1986; Drummond and Wilkinson, 1996; Carlson, 1998; Drummond, 1999, Talling, 2001, Carlson and Grotzinger, 2001). The probability density function (pdf) of each of these distributions has one or more parameters (Figure 6.1; Table B1). The three main parameters are location, scale, and shape. The definitions of each of these parameters are presented here, adopted from the NIST/SEMATECH Engineering Statistics Internet Handbook. The 'location' is defined as the expected value of the parameter being measured. For a stable process, this is the value around which the process has stabilised. The 'scale' is defined as the expected amount of variation associated with the parameter. This tells us the range of expected values to either side of the location. The scale parameter stretches or compresses the pdf curve (Figure 6.1). The 'shape' describes how the values are distributed about the location. This tells us if the variation of the data is symmetric about the location or if it is skewed or possibly multimodal. The pdf curve changes in its form as the shape parameter changes (Figure 6.1).

The lognormal distribution is a common distribution and many geological variables are best fitted by it. If the bed thickness data are logarithmically transformed, then the data may be approximately normally distributed. Bokman (1957) proposed the logarithmic transformation of bed thickness data similar to the phi transformation applied to grain size data. If the distribution is lognormal then histograms with a logarithmic transformation of bed thickness data should have a symmetrical shape similar to the “bell”-shaped normal distribution curve. The statistical parameters of the distribution are easily obtained when the data are plotted on probability paper because lognormally distributed data plot as a straight line. The probability scale condenses the data in the middle part of the scale (~30-70% of the data) and expands the ends of the plot (< 10 % and > 90%). The slope of the line gives an indication of the degree of scatter of the bed thicknesses. Best fit lines (e.g., using linear regression analysis) are used to judge how well the data follow a lognormal distribution. Interpretation of best fit lines for logarithmically transformed data should be undertaken with caution (Talling, 2001; Swan and Sandilands, 1995).

In many cases, the thickness data do not plot as a single straight line when using probability-log scale, but instead, as two or more line segments, suggesting that the bed thickness population consists of several subpopulations reflecting deposition of beds by different processes or under varying conditions (McBride, 1962, Hesse, 1975, Hiscott, 1977). Others have suggested that segments may be explained in a variety of other ways including merging of data from several non-lognormal distributions (Walton *et al.*, 1980; Bridge, 1981).

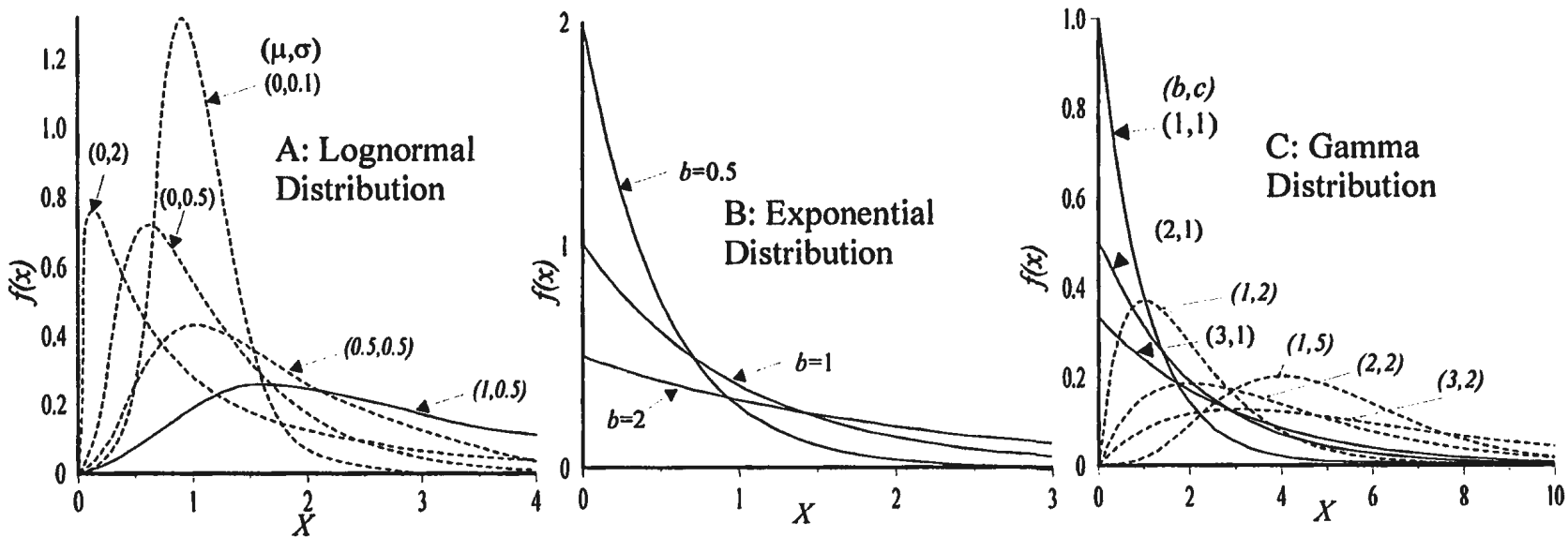


Figure 6.1. The three main types of distributions that have been suggested to best match turbidite bed thicknesses and against which the thickness data from this thesis will be tested. The parameters for each distribution are shown on the diagram. The lognormal distribution (A) is skewed to the right. The pdf,  $f(x)$ , starts at 0, increases until the mode and decreases after the mode. Two parameters, scale ( $\mu$ ) and shape ( $\sigma$ ) control this distribution. If  $\mu$  is constant, the skewness of the pdf increases as the  $\sigma$  value increases. If  $\sigma$  is greater than 1, the pdf rises sharply for very small values of  $x$ , follows the y axis, reaches the mode early, and then decreases sharply like the exponential distribution. The exponential distribution (B) has only one parameter: the scale parameter  $b$ , where  $b=1/\lambda$ . As  $b$  increases ( $\lambda$  decreases) the distribution is stretched out to the right; if  $b$  decreases, the distribution is squeezed towards the origin. The pdf starts at  $x=0$  at a level where  $f(x)=\lambda$  and decreases exponentially as  $x$  increases. It has a concave-upward shape. As  $x$  approaches infinity, the pdf approaches 0. The gamma distribution (C) has two parameters: the scale parameter ( $b$ ) and the shape parameter ( $c$ ). At a constant  $c$ , an increase in  $b$  tends to compress the distribution towards the x-axis, while an increase in  $c$  tends to make the distribution more symmetrical.

Talling (2001) suggests that the bed thickness distribution of turbidites (bed thicknesses of all the types of facies combined) in the Marnoso Arenacea Formation is a combination or summation of several lognormal subpopulations, each of which is associated with beds having a different basal Bouma (1962) division (facies or subfacies). He also notes that when beds are separated or classified based on basal grain size, each group or class plots as a lognormal distribution. Enos (1969a) indicated that the bed thickness distributions of sandstone and siltstone beds exposed in the area between Petite-Vallée and Grande-Vallée area approximately lognormal.

The exponential distribution (Table B1) has been suggested to best fit turbidite bed thickness data. Drummond and Wilkinson (1996) suggested that bed thickness data collected from the Rochers Penchés Member and Mont-Saint-Pierre Member of the Cloridorme Formation, and from other turbidite formations, are best fitted by the exponential distribution. Krumbein and Graybill (1965) suggested that the bed thickness of sedimentary beds could follow either the gamma distribution or the lognormal distribution.

In addition to the distribution types mentioned above, a great deal of interest has focussed on power-law scaling of turbidites in recent years (Hsu, 1983; Hiscott *et al.*, 1992, 1993; Rothman, *et al.*, 1994; Rothman and Grotzinger, 1995; Beattie and Dade, 1996; Malinverno, 1997, Carlson, 1998; Carlson and Grotzinger, 2001). If a power law distribution characterises turbidite bed thicknesses, then

$$N = aT^{-\beta}$$

where  $N$  is the number of beds thicker than  $T$ ,  $T$  is the bed thickness,  $-\beta$  is a scaling

exponent and  $a$  is a constant. The scaling exponent ( $-\beta$ ) is the value of the slope of a plot of  $N>T$  versus  $T$  on log-log paper. These plots may be fitted by a single line or several line segments.

Hiscott *et al.* (1992, 1994) and Beattie and Dade (1996) concluded that power-law scaling characterises turbidite beds triggered by earthquakes in the Izu Bonin forearc basin because both earthquakes and the thickness of turbidites have similar  $-\beta$  values of approximately -1. Rothman *et al.* (1994), Rothman and Grotzinger (1995), Pirmez *et al.* (1997), Carlson and Grotzinger (2001) related the  $-\beta$  value and its variation between correlated sections to internal factors within the basin related to depositional dynamics, erosion and amalgamation. Malinverno (1997) showed that different values of  $-\beta$  (i.e., different slopes for different segments of the  $N>T$  versus  $T$  plot) might be due to the presence of a relationship between bed thickness and bed length which depends on the bed volume. For example, larger flows and their deposits might spread over wide areas while smaller flows might be confined to topographic lows in the basin such as channels or depressions. Thicker beds will have the bigger  $\beta$  value. Recently, Winkler and Gawenda (1999) used the presence of a power law distribution (or the lack of it) for the thickness of turbidite beds of the Paleocene to lower Eocene Zumaya series in northern Spain to differentiate between climatic or tectonic factors as the main control on the deposition of these beds. Carlson and Grotzinger (2001) have suggested that different submarine fan subenvironments can be inferred from the shape of the cumulative power-law distribution curve because processes such as amalgamation and erosion are more common in certain

subenvironments and this is reflected in the shape and curvature of the power-law curve.

The methodology used to investigate the bed thickness distribution is given in Appendix B. This appendix includes the investigation carried out on some facies and subfacies bed thickness distribution.

## 6.2. CLASS E BED THICKNESS DISTRIBUTION

A total of 13,479 shale bed thicknesses were measured from all sections. Thicknesses were grouped into 5 cm-wide class intervals and then plotted as histograms (Figure 6.2a). A 5 cm-wide class interval seemed appropriate because the range of the bed thicknesses was about 510 cm, resulting in more than 100 classes.

The shale bed thickness distribution (Figure 6.2a) has a very high peak in the 5-10 cm class and a long tail of thicker beds. The shape of this distribution is most similar to the lognormal distribution (*cf.* Figure 6.1). The gamma and exponential distributions are less suitable as shown by the form of the distribution and the q-q plot, where most of the points (up to the 99<sup>th</sup> percentile) are better fitted by the lognormal distribution (Figure 6.2b).

The most common beds, are clustered mostly in the very thin and thin bed thickness range (1-10 cm), so processes responsible for the deposition of such beds were likewise common and significant. Many shale beds thicker than 140 cm are the mud caps megaturbidites.

On a probability-log plot (Figure 6.2c), a large percentage of the beds plot as



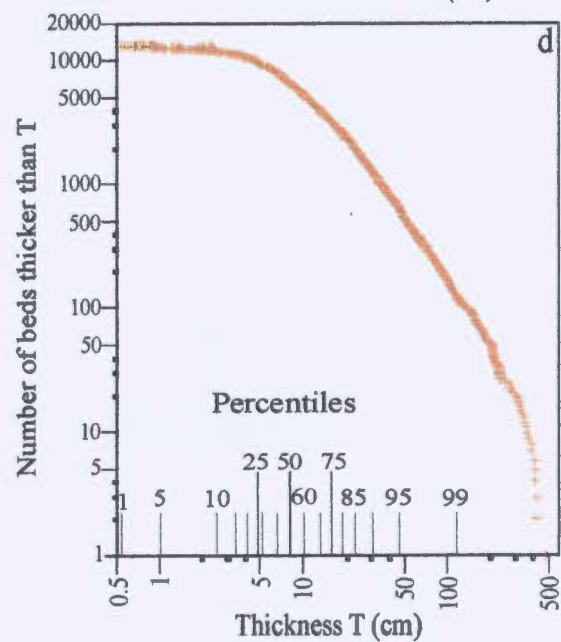
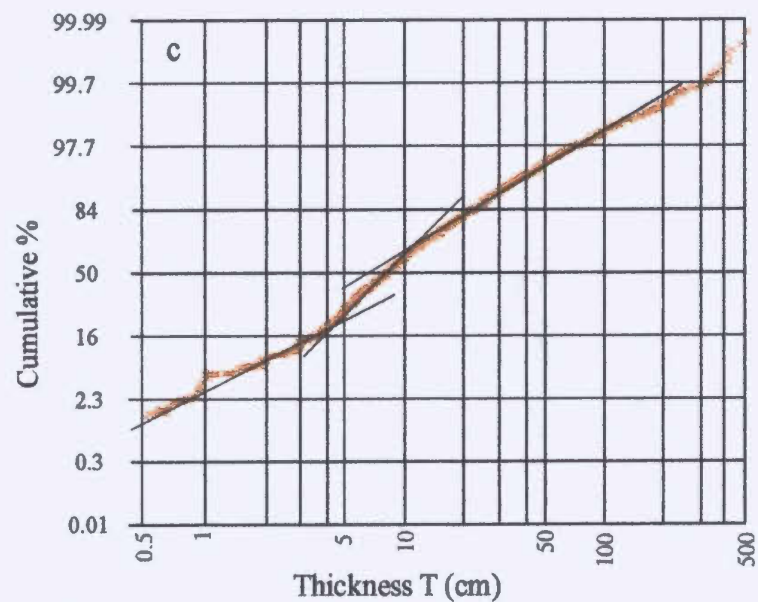
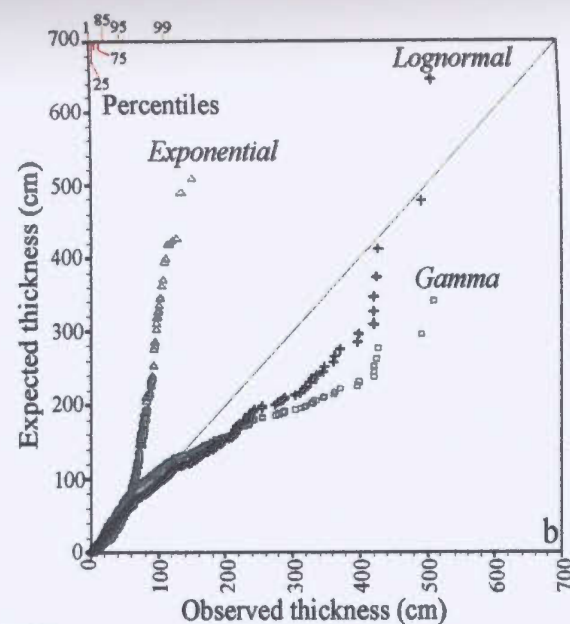
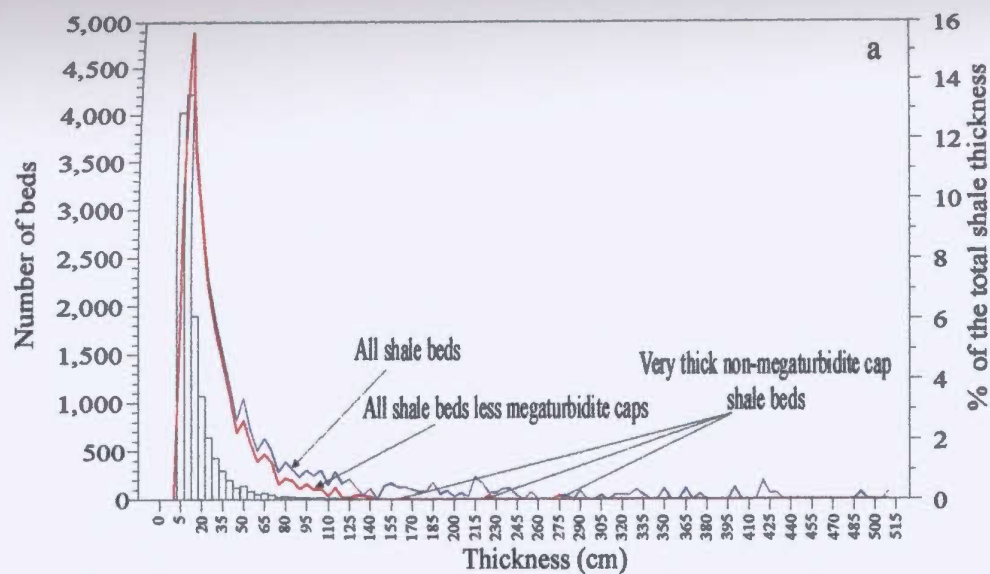
Figure 6.2:

a- Bed thickness distribution of the shale beds of Class E. The blue line represents the percent each class interval represents of the thickness of the shale. The rugged shape of this line is somewhat decreased when the thickness of the megaturbidite mud caps is removed and the data replotted.

b- q-q plot of the actual bed thicknesses of the shale beds *versus* the expected thickness for the lognormal (crosses), exponential (triangles) and gamma distributions (squares). The lognormal distribution best fits the data because beds that are as thick as 120 cm plot along the  $y=x$  line. However, this better fit relative to the other two distributions only pertains to an additional 5% of the population.

c- A probability-log plot of the bed thickness data can be three or more line segments (three are shown), suggesting two or three lognormal distributions. The first is for beds < 4cm thick representing ~16% of the of the population; the second for beds 4-10 cm thick (~45% of the population). A third segment may be fitted for beds that are 10-120 cm thick (~40% of the population).

d- Plot of  $N>T$  versus  $T$  of the data a line with two or more approximately straight segments. Note the inflection at ~4 cm, similar to the prominent break in the slope on the probability-log plot (part c).



straight line segments, suggesting distinct lognormal populations for various thickness populations. One population consists of beds less than 4 cm thick; these represent about 16% of the total number of shale beds (Table B2). The second population comprises beds 4-10 cm thick, and a third population corresponds to beds 10 - ~120 cm thick. Hesse (1975) suggested that turbidite mud plots more-or-less as a straight line while hemipelagic mud does not because of erosion by turbidity currents (*cf.* Nishiwaki, 1978). Do three segments in Figure 6.2c represent three different lognormal populations, or are they a single lognormal population that has been affected by certain factors that caused the segmentation of the line? If all shale beds thinner than ~120 cm belong to a single population, the decrease in slope at the left side of the plot (beds < 4 cm-thick) indicates a larger than expected range of bed thicknesses extending into very thin beds and laminae. Erosion or winnowing may have affected the thickness of the thinnest beds, but this is speculation. Alternatively, beds thinner than 4 cm may have formed by processes distinct from those that deposited the thicker beds.

For the main population, excluding megaturbidite caps, processes such as erosion, winnowing, or factors related to the size of the flow or its dynamics may have controlled the shale bed thickness. The tail of the thicker beds has a steeper slope than the line segments that characterise the rest of the population. The increase in slope for beds thicker than 300 cm is due to the presence of 21 beds which represent a very small percentage of the entire shale bed population of 13,479 beds. These 21 beds are the thick mud caps of megaturbidites. It is interpreted here that this change in the slope is a result of deposition

of thick megaturbidites and reflects the large volume of the slumps or slides responsible for these megaturbidites.

On the plot of  $N>T$  versus  $T$  (Figure 6.2d), a power law scaling is suggested by the linear trend of the central part of the plot. Ninety-eight percent of the beds (1<sup>st</sup> to 99<sup>th</sup> percentile) can be fitted by two lines. The most prominent trend is for beds that range in thickness from ~17 to 200 cm (Table B3); these beds represent ~22% of the population of shale beds and have a  $\beta$  value of 1.6 (Table B3). About 77% of the population consist of beds thinner than 17 cm. The  $\beta$  value of the segment representing beds 4-17 cm is about 0.9.

Segmentation of a power law plot has been attributed to variable depositional processes, or to spatial differences in the point of initiation or the spreadability of the current caused by different depositional processes such as levee spill-over or sheet flows (Malinverno, 1997; Pirmez *et al.*, 1997). Large flows tend to spread over a large area and thus have a large  $\beta$  value compared with smaller flows, perhaps confined in channels, levees or bottom depressions, which might have a small  $\beta$  value (Rothman and Grotzinger, 1995; Malinverno, 1997).

An alternative way to look at the power law plot is to argue for a single population that includes most of the beds (similar to the arguments for a single lognormal population above). Suppose that the segment of the line with a  $\beta$  of 0.9 represents this population (beds that are 4-17 cm representing ~55% of the population). Extending this line in the direction of thinner beds would lead to a higher number of beds than 13,000 suggesting

that thinner beds are under-represented because of erosion or difficulty in distinguishing very thin beds or individual shale layers.

In order to test whether the power law or lognormal distribution best characterise the thickness of the shale beds and laminae of Class E, the data were replotted on a single graph with two y-axes (Figure 6.3). It is concluded that the lognormal distribution better fits the data because a single more-or-less straight line encompasses a greater proportion of the beds than the linear trend (suggesting a power-law scaling) displayed on the plot of  $N>T$  versus  $T$ .

A subset of 137 beds  $\geq 100$  cm thick, representing thick mud caps of some megaturbidites, was investigated separately (Figure B2 in Appendix B). Both the lognormal and gamma distributions fit the data equally well (Figure B2 b,c), while beds  $>110$  cm thick could be fitted by a single lognormal distribution. Seismic activity has been suggested as a triggering mechanism for flows that deposit such megaturbidites (Mutti *et al.* 1988), while others have suggested that their initiation is controlled by fluctuations in sea level (Weaver, 1988). For these 137 beds (Figure B2d), the  $\beta$  value is  $\sim 2$ . This is within the range of  $\beta$  values noted for turbidites in seismically active areas (Hiscott *et al.*, 1992; Awadallah *et al.*, 2001), where power-law distributed earthquakes might control the triggering of failure events. The probability-log plot and the q-q plot show that the lognormal distribution provides a good fit for 80% of these thick mud caps.

To summarise, shale beds thickness is controlled by many factors such as erosion, volume of sediment carried in the turbidity currents and their spreadability that is

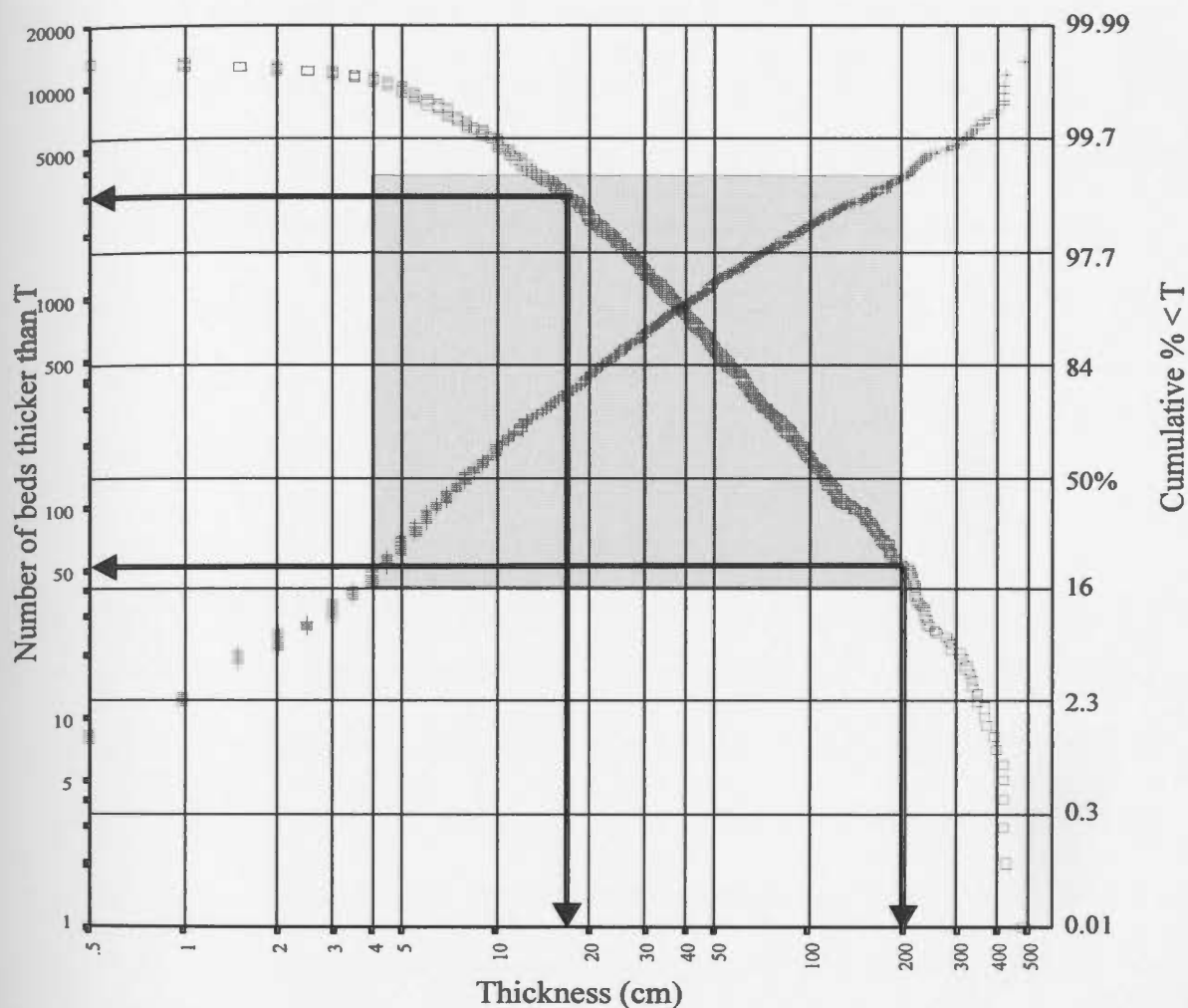


Figure 6.3. Comparison between the probability-log plot and log-log plot for the beds of Class E. The probability-log scale tends to compress the beds that are in the middle of the population (16-84%) and expands the graph for the very thin beds and laminae, and for the very thick beds (tails of the population). The log-log scale expands or spreads the very thick beds and compresses the thin beds into a small part of the graph. The bed thickness data of shale plots as segmented lines of both scales. Some of the segments are less obvious because of the nature of the scales. The lognormal distribution is apparently a better fit for the data than the power-law distribution because a greater proportion of the population (~82%, shaded area between cumulative % 16 to ~99, beds that are 4-200 cm thick) can be fitted by a more-or-less single straight line or line segments that do not vary very much in their slope. The most obvious trend that can be fitted by a single best fit line on the log-log plot of  $N>T$  versus  $T$  is that for beds 17 - 200 cm thick. These beds represent only ~23% of the shale beds. Other less obvious linear trends on the log-log plot may be more representative (e.g., Beds ~4 to ~20 cm thick, ~60 % of the beds; Table B2). This is because more than 60% of the beds of Class E are thin to very thin.

controlled by many interacting processes. It is believed that based on the data presented in chapters 3 and 5 that the thickness of shale beds is variable and influenced by many factors. The observed lognormal distribution for shale beds of the thesis area is probably a combination of several subpopulation (Talling, 2001). The  $N>T$  versus  $T$  plot of the shale bed thickness may be more informative, in that it was segmented with one segment suggesting a separate group of beds (megaturbidite caps) that were deposited from large flows, unlike other shale beds that were deposited from smaller flows that deposited non-megaturbidite sand-mud or silt-mud couplets.

### **6.3. CLASS D BED THICKNESS DISTRIBUTION**

This is the second most common facies class in terms of number of beds. A total of 11,249 siltstone beds were measured in different parts of the thesis area. These beds are interpreted to have been deposited from turbidity currents under variable conditions of traction transport and suspension deposition and a combination of traction and suspension. Siltstone bed thickness data for the entire Class D, individual facies and subfacies were tested to see if the different processes that formed the individual facies and subfacies affected the type of bed thickness distribution.

Thicknesses of the 11,249 beds were grouped into 5 cm class intervals and plotted as histograms (Figure 6.4). A 5 cm class interval seems appropriate because the range of bed thickness is about 95 cm.

The siltstone bed thickness distribution (Figure 6.4a) has a very high peak in the 0-

5 cm class and a long tail towards the thicker beds. About 90% of the beds are <10 cm thick (Table B2). The shape of this distribution is more similar to the exponential distribution or the gamma distribution. Experimentation with a bin size of 1 cm did not change the shape of the distribution. On the q-q plot, the gamma distribution fits the data better than the exponential distribution (Figure 6.4c). Beds thicker than 30 cm (0.5 % of the beds) are better fitted with a lognormal distribution.

On a probability-log plot, the data are best fitted by two linear trends (Figure 6.4c): a line for beds thinner than 4 cm and a line for beds thicker than 4 cm. This suggests the presence of two subpopulations of beds perhaps deposited by different processes or under different conditions. About 60% of the beds belong to the population that is less than 4 cm thick. The remaining population is that for beds > 4 cm thick. Beds thicker than 70 cm deviate from the lognormal trend followed by beds that are 4-70 cm thick. Beds of Class D that are > 70 cm tend to occur within sandstone packets or as amalgamated units.

On the  $N > T$  versus  $T$  plot (Figure 6.4c), three segments are observed: the first for beds < 4 cm thick (~60% of the beds), the second for beds 4~12 cm thick (32% of the beds) and the remaining segment is for beds > 12 cm thick (~7% of the beds). The segment that represents beds 4-12 cm thick on the  $N > T$  versus  $T$  plot is not apparent on the probability scale because of the compressed nature of the central part of the probability scale. Were the three different subpopulations deposited under different conditions? An answer was sought by studying individual facies separately.

All 9,013 beds of the graded stratified facies (D2.1) were investigated separately to



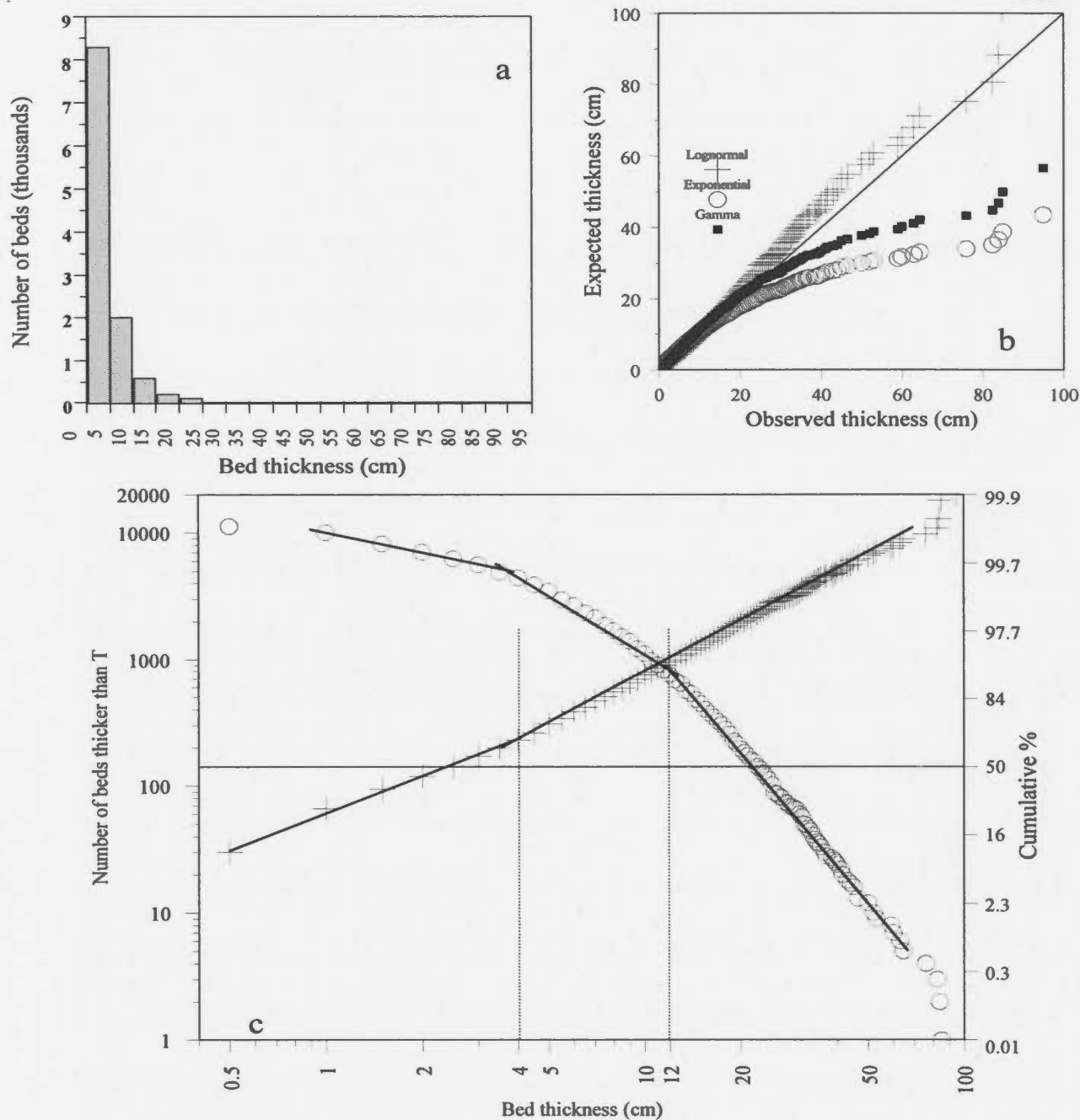


Figure 6.4. a: Histograms of the bed thickness data of facies Class D suggesting that the exponential distribution may be a better fit for the data. b: q-q- plot of the data; beds < ~20 cm thick most closely follow the gamma distribution whereas the lognormal distribution is a better fit for beds > 20 cm. c: Probability log plot suggests that the beds of Class D may be fitted by the lognormal distribution with two linear trends. Log-log scale shows that beds thicker than 12 cm clearly follow a power-law distribution. Other, less well defined linear trends could be fitted for beds < 12 cm (e.g., beds 4-12 cm thick).

see what type of distribution best fits these data (Figure 6.5). The removal of facies D2.2 and D2.3 from the bed thickness dataset of Class D decrease the exponential distribution parameter ( $\lambda$ ) (facies D2.1; Table B4). The lognormal and gamma distributions also provide a good fit for facies D2.1 beds (Figure 6.5b). The lognormal distribution better fits beds >30 cm, but these beds represent less than 3% of the population.

On the  $N > T$  versus  $T$  plot, there is little or no change in the shape of the plot of facies D2.1 from that of all facies Class D. Even the removal of more than 2000 beds of facies D2.3 from the dataset did little to change the shape of the plot because the thin beds of facies D2.2 plot in a narrow area of the graph and also because about 40% of the beds of facies D2.1 are very thin beds and laminae that plot in the same area.

Comparing the three siltstone facies on a probability-log plot (Figure 6.6a) shows that all three facies have more or less similar slope and that the facies D2.2 plot superimposed on facies D2.1. This may suggest that these two subpopulations have a common origin, for example if most of facies D2.2 beds were originally facies D2.1 beds that underwent syn-depositional and post-depositional deformation. Most of the beds of facies D2.3 plot with more or less the same slope, but in a different part of the graph because they are thinner. Overall, the thin nature of beds of facies D2.3 may suggest that the currents responsible for their deposition were characterised by low sediment loads or that the thinner beds were deposited in certain locations or during certain times when special conditions prevailed.

For the power-law scaling for facies D2.1 (Figure 6.6b, crosses) only beds thicker

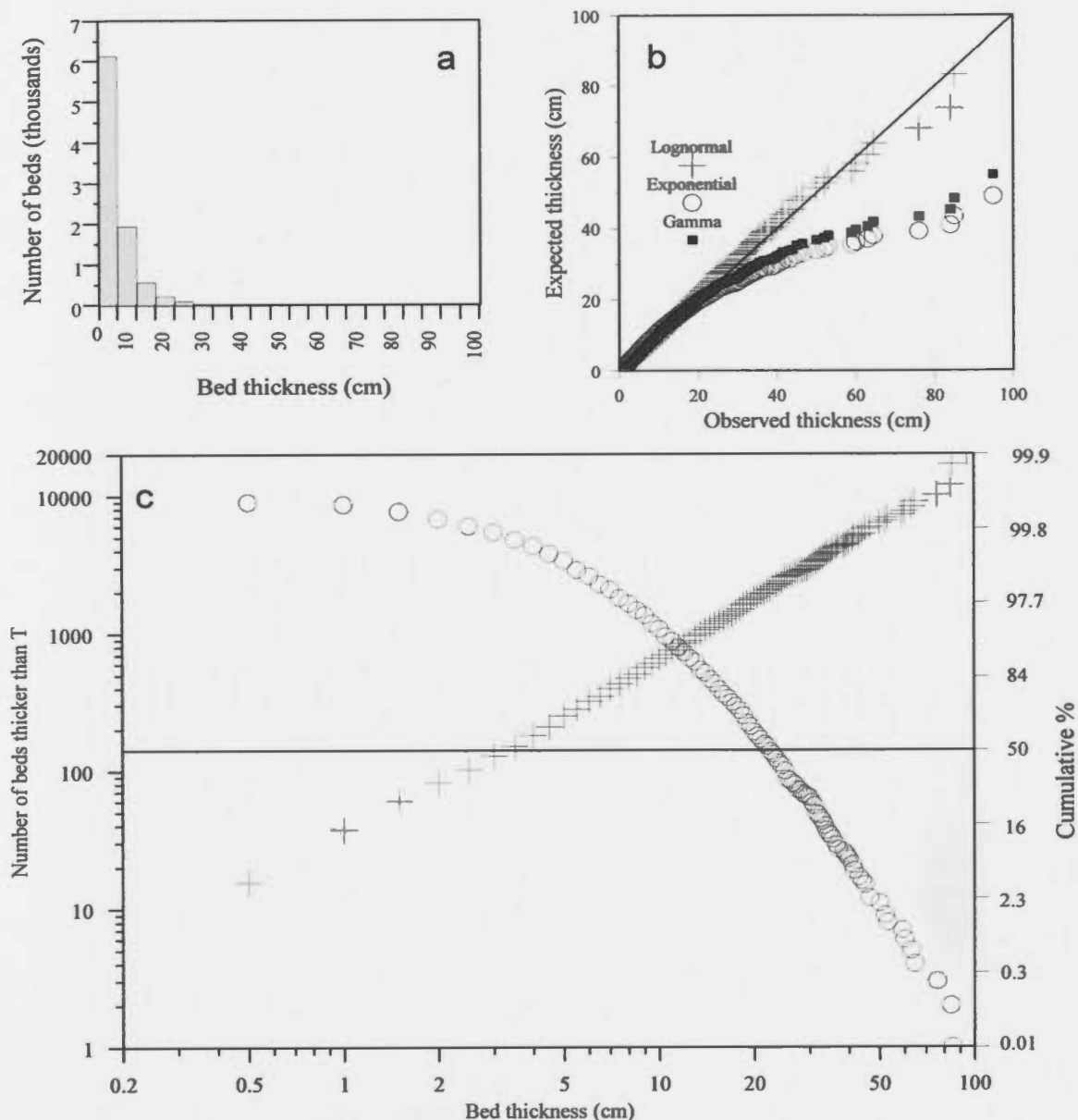


Figure 6.5. a: Histograms of bed thickness data for facies D2.1. The removal of facies D2.2 and D2.3 from the dataset did not change the shape of the histograms. The scale parameter  $\lambda=(1/b)$  decreased causing the histogram to be less peaked (compare with Figure 6.4). b: the q-q plot shows that the removal of facies D2.2 and D2.3 makes the lognormal distribution a better fit for the beds that are at the tails of the distribution. On the log-log plot, the shape does not change significantly from that of figure 6.4 because the thin beds of facies D2.3 that were removed from the dataset affected the shape on the probability scale, but not on the log-log scale because these beds plot in a small area of the graph.

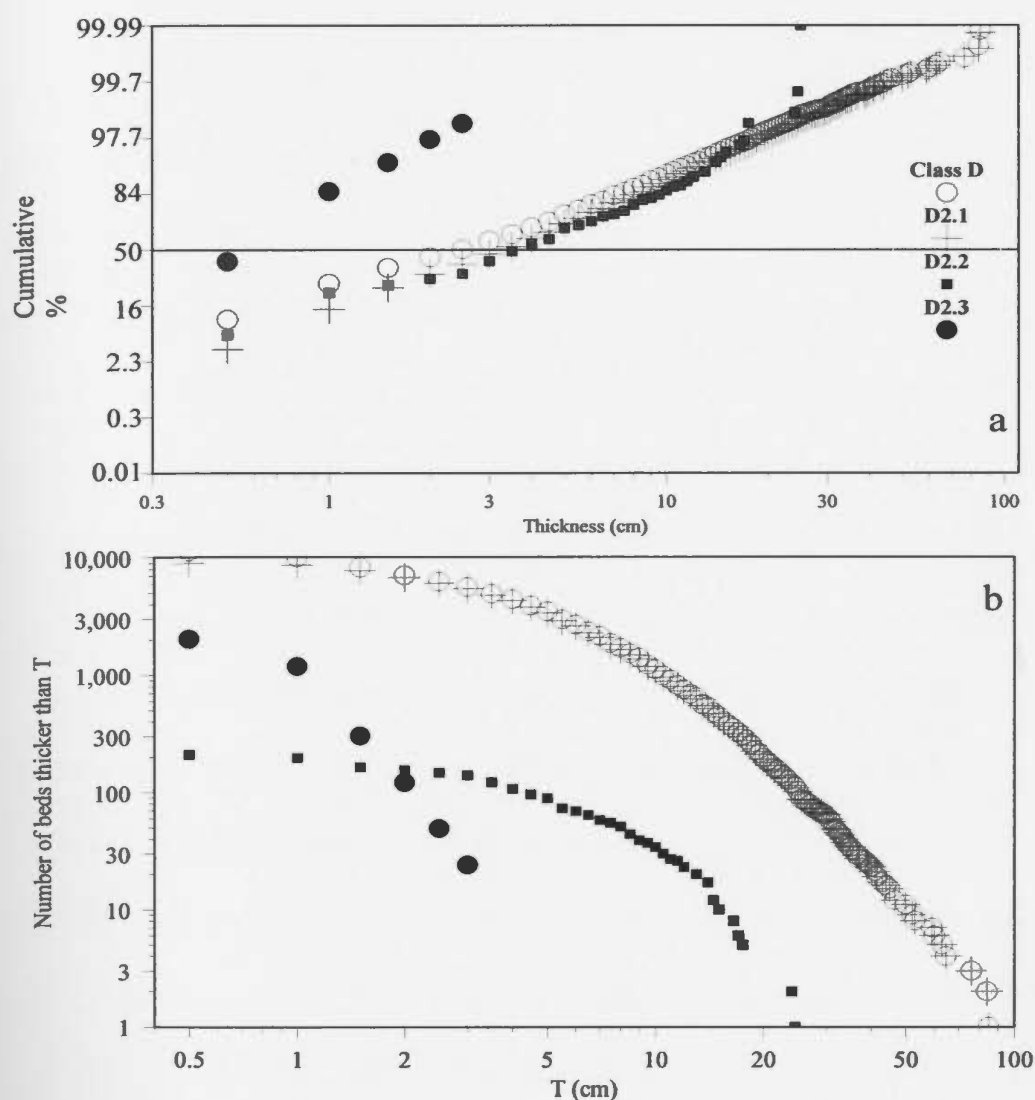


Figure 6.6. Comparison between the different siltstone facies of Class D. a: Facies D2.1 and D2.2 plot close to each other reflecting similar bed thicknesses range and perhaps similar origin. Beds of facies D2.3 plot away from the other facies because of their small thickness suggesting that the processes that deposited these facies is different in that it deposits thin beds with a narrow thickness range. b: log-log plot of the same data, here also facies D2.3 plots in a different area with a different slope suggesting perhaps certain depositional process or conditions that favour deposition of thin beds with a narrow thickness range. Note that although there are >1500 siltstone laminae of facies D2.3 their effect on the shape of the plot of all the siltstone beds of Class C is not well displayed because very thin beds and laminae plot in a narrow area atop the ordinate. Facies D2.2 beds plot in a different area because they are less common than facies D2.1 or D2.3. Their inclusion in the all Class C dataset has little effect on the plot of the bed of Class D, because of their small number, and their thickness falls in the same range where considerably much more beds of facies D2.1 occur.

than ~12 cm can be fitted to a linear trend ( $\beta=2.7$ ). These beds represent about 8% of the population. Most of the remaining beds do not show an obvious linear trend. Expanding or stretching of this other 92% of the data (plotting on larger paper for the thin beds only) permits two additional linear trends to be fitted: one for beds 3-12 cm thick and one for beds thinner than 3 cm. Beds 3-12 cm thick represent 52% of the beds of facies D2.1 and have a  $\beta$  of 1.34 while beds < 3 cm thick constitute 40% of the beds of facies D2.1 and have a  $\beta$  value of 0.3 (Figure B3, Table B3). The inclusion of facies D2.2 and D2.3 in the global Class D plot does not greatly modify the shape of the graph because most of the beds are very thin (facies D2.3) and plot in a small area of the graph. These very thin beds do, however, better define the segmented shape of the plot on an expanded scale because they are less than 3 cm thick and are numerous.

Individual subfacies of D2.1 plot with more or less the same slope on a probability log plot (Figure B3), but in different positions depending on their thickness suggesting that the type of subfacies is related to thickness, which may in turn be controlled by depositional processes (Talling, 2001). Subfacies D2.1A and D2.1B deviate from the trend of the other subfacies (Appendix B).

In summary, siltstone beds interpreted to have been deposited during conditions dominated by traction or a combination of traction and suspension are best fitted by the exponential or the lognormal distribution, based on q-q plots. A lognormal model adds ~ 5-10% more of the population. Departure from a single lognormal population (i.e., segmented probability plots) may reflect variations in flow characteristics for thinner and

thicker beds. Factors such as bottom topography (Chapter 5) and point of initiation may have influenced the type of bed thickness distribution.

#### **6.4. CLASS C BED THICKNESS DISTRIBUTION**

The thicknesses of 1,842 sandstone beds of Class C were grouped into 5 cm class intervals and then plotted as histograms (Figure 6.7a). A 5 cm class interval seemed appropriate because the range of the bed thicknesses was about 270 cm, resulting in more than 50 classes. A lognormal distribution is suggested by the histogram and the q-q plots (Figure 6.7a,b). There is a prominent mode thin and medium beds.

On a probability-log plot (Figure 6.7c), Class C data plot as a slightly curved (bowed) line that may be fitted by two or three line segments. The segmented lines suggest several lognormally distributed subpopulations. Beds 4-60 cm thick represent more than 80% of both the entire Class C bed population and the non-amalgamated beds population. Beds that occur in amalgamated units plot with the same trend as the entire Class C sandstone population, except that there is a deficiency in beds thicker than 50 cm. Beds that are thicker than 230 cm thick plot along a line with a slope which is different than the plot for most of the sandstone beds. This departure is due to the occurrence of four beds of facies C2.5 megaturbidites. It is interpreted that these beds were deposited from a very large and thick flow that spread over the entire thesis area (Malinverno, 1997). These four beds are emphasised by the nature of the probability



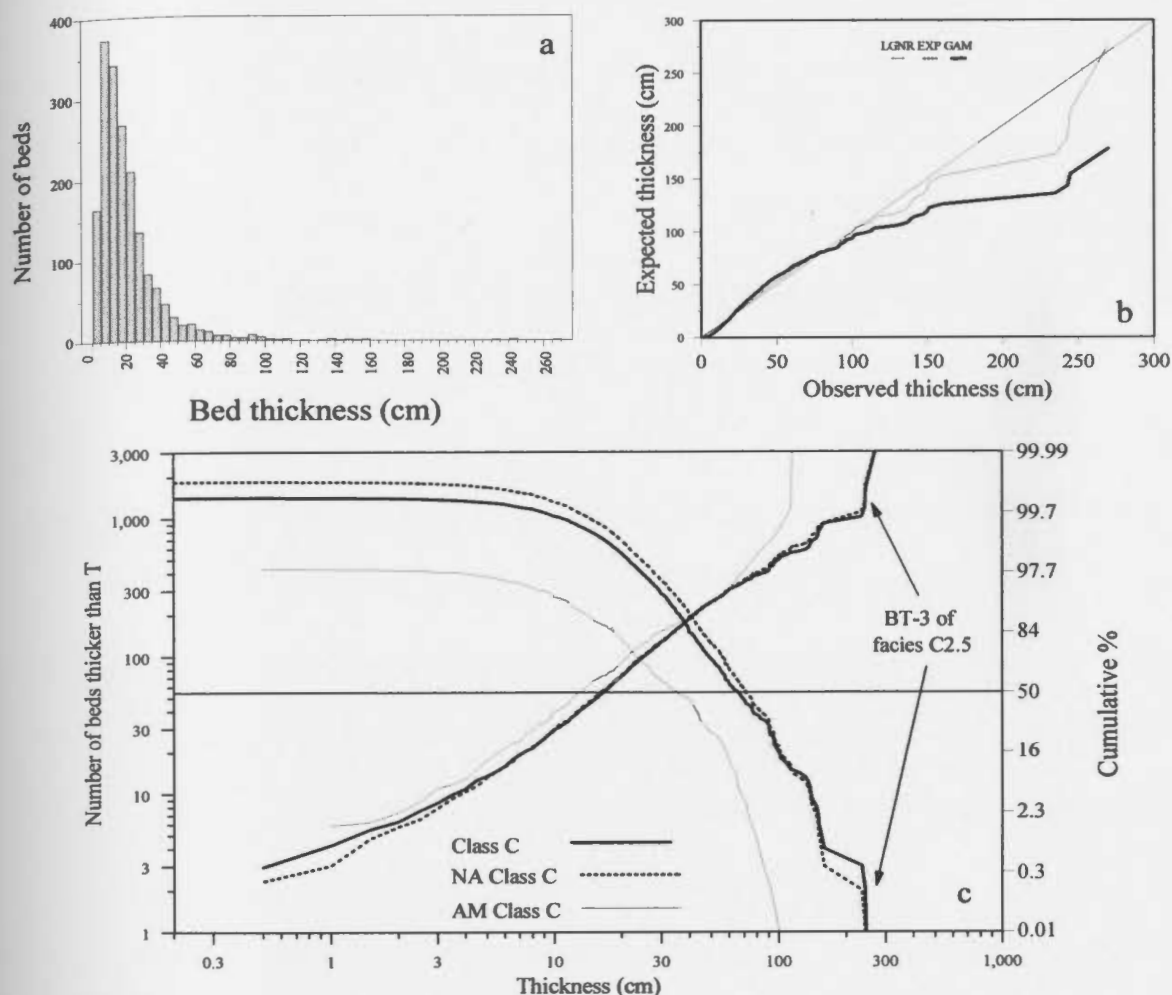


Figure 6.7. Facies Class C. a: histograms of all the beds of the Class suggest a lognormal distribution. This is also suggested by the q-q plot (b). Bed BT-3 occurs in four different locations and is the cause of the departure of the q-q plots for thickness  $> 2$  m. BT-3 is also an anomaly on the log-log (power-law) plot (c). Other thick beds (mostly megaturbidites) form a linear trend for beds that are thicker than 100 cm. Another linear trend in the global dataset for beds  $< 7$  cm can be observed. The amalgamated beds show linear trends for beds 9-50 cm thick and beds thicker than 50 cm.

scale which spreads the very thin or very thick beds (tails of the distribution). Beds that are 60-230 cm thick may also be fitted by a linear line segment. These beds form about 5 % of the population of the Class C beds. Most of these 60-230 cm-thick in Class C are megaturbidites.

On  $N>T$  versus  $T$  plots to test for power-law scaling, the full set of Class C beds and beds that do not occur in amalgamated units plot very close to each other. Beds that are 20-100 cm-thick, about 37% of the beds, have a  $\beta$  value of 2.0 (Table B3). About 25 beds (< 2% of all beds) which are thicker than 100 cm, deviate from this linear trend, and have a  $\beta$  value of 3. These beds are mostly megaturbidites (facies C2.4 and C2.5) or amalgamated beds; they partly account for the deviation from a single linear power-law trend. It is suggested here that the deviation from a single power-law trend for beds thicker than 20 cm is due to deposits from very large flows. Beds 7-20 cm thick represent 46% of the beds of Class C, and have no linear trend on this plot.

Amalgamated beds of Class C thicker than ~10 cm plot as a line with two segments. Beds 10-50 cm thick represent ~60% of the population of amalgamated beds with a  $\beta$  value of 1.3, while beds thicker than 50 cm represent 7% of the population and have a  $\beta$  of about 3.9. Comparing the slope of the line of amalgamated beds and the slope of the line for non-amalgamated beds suggests that the reduction in the slope of the line segment for amalgamated beds is due to the erosion of some of the thin beds and reduction in the thickness of thicker beds. The increase in the slope of the line segment for amalgamated beds that are thicker than 50 cm suggest that amalgamated beds are under-



represented. This is true for all sandstone beds in this part of the Cloridorme Formation. Very thick beds are rare and many of the thick sandstone beds observed are the lower parts of megaturbidites that rarely become amalgamated because of their thick mud caps.

In summary, the lognormal distribution seems to better fit the population of sandstone beds of facies Class C. Amalgamated beds form segments on probability plots and plots of  $N>T$  versus  $T$  with breaks at thickness of about 50 cm.

In Appendix B, different facies of Class C are investigated to in an attempt to answer the following questions. Do thickness data for facies or groups of beds that vary in certain internal properties (e.g., graded or ungraded, with clasts or without clasts) follow different types of statistical distribution or scaling values? What information can be obtained from these variations? For example, Rothman and Grotzinger (1995) suggested that debris flow deposits from the Kingston Peak Formation, California have a smaller power-law scaling value ( $\beta = 0.49$ ) compared to associated turbidites ( $\beta = 1.4$ ), which they explained to be due to different flow rheology. A synthesis of the results of the investigation presented in Appendix B is presented below.

Muddy sandstone beds (facies C1.1) interpreted as debris flow deposits have variable thicknesses that plot as several linear trends on probability-log plots (Figure B4) and have a power-law scaling parameter ( $\beta$  value) of 1.7 which is within the range of  $\beta$  value of other sandstone beds interpreted as turbidites (Table B3). It is suggested that for the Cloridorme Formation, turbidites and debrites can not be differentiated based on the  $\beta$  value. A more detailed investigation on a larger dataset is needed.

Beds of facies C2.1, characterised by a lower structureless division ( $T_a$ ) follow the lognormal distribution more clearly than the gamma or the exponential distribution (Figure B5). Deviation from a single linear trend on the probability-log plot is due to amalgamation especially for thick beds. On the log-log plot of  $N > T$  versus  $T$ , two linear segments are observed with  $\beta$  values of  $1.0 \pm 0.2$  and  $2.2 \pm 0.1$ . The presence of amalgamated beds in the dataset tends to make the linear segments more irregular and the  $\beta$  value smaller (i.e., gentler slope) than beds that do not occur in amalgamated units. The presence or absence of clasts does not significantly modify the shape of the log-log plot of  $N > T$  versus  $T$  (Figure B6). Grading or the absence of grading in beds of subfacies C2.1A has little effect of the  $\beta$  value each segment of the plot of  $N > T$  versus  $T$  (Table B3).

Subfacies C2.1B, C2.1C and C2.1D are beds that start with a structureless basal division but contain laminations (Bouma  $T_{ac}$ ,  $T_{ab}$ ,  $T_{abc}$ ). The bed thickness data of these three subfacies were combined in one set and tested. These beds are best fitted by several lognormal distributions. There are three segments on the log-log plot of  $N > T$  versus  $T$  of the bed thickness data of these three subfacies (Figure B7). The segmentation on both plots is controlled to some degree by the type of subfacies because  $T_{ac}$  beds (subfacies C2.1B) occur as thick beds while subfacies C2.1C and C2.1D tend to occur as thinner beds.

Beds of facies C2.2 (i.e., beds that start with planar laminations) are best fitted by the lognormal distribution, however, the thickness data of these beds do not plot as linear segment(s) on the log-log plot of  $N > T$  versus  $T$  for beds thicker than 13 cm (Figure B8). Beds thinner than 13 cm show a linear trend that is controlled by facies type and degree of

amalgamation.

Thick beds of facies C2.3 are best fitted by the gamma distribution while the thinner beds are best fitted by the lognormal distribution (Figure B9). Segmentation on both the probability-log plot and the log-log plot of  $N>T$  versus  $T$  may be controlled by subfacies type. This suggests that the type of subfacies is related to its thickness and is probably controlled by the type of flow that deposited the beds.

The lower parts of megaturbidites (facies C2.4 and C2.5) are best fitted by the lognormal distribution (Figure B10). There are several linear trends on the probability-log plot suggesting several lognormal populations. Bottom topography and the size of the initial flow controls the segmentation observed (Chapter 5).

In summary, the bed thickness distribution of the sandstone beds is related to subfacies type. Subfacies are classified based on the sequence of sedimentary structures observed in the beds. The sequence of sedimentary structures is related to the flow dynamics. This, indicates that under certain flow conditions, certain subfacies are deposited and form beds with a certain bed thickness population.

## **6.5. CLASS B BED THICKNESS DISTRIBUTION**

Beds of this class are uncommon in the thesis area where only 270 beds were measured and represent less than 1% of beds measured. Only 6 disorganised beds were observed in this thesis area. These six beds were not included in the bed-thickness distribution analysis. The remaining 264 beds belong to two organised sandstone facies.

Facies B2.1 consists of 56 beds, 36 of which occur in amalgamated units. This dataset is small in number and more than 64% of the beds occur in amalgamated units, the bed thickness distribution of this facies was not investigated. Facies B2.2 is more common (208 beds) and only 11 beds occur in amalgamated units. The bed thickness distribution of this facies was investigated to know which distribution best fits the data.

The lognormal distribution best describes 197 non-amalgamated beds of facies B2.2 (Figure 6.8a,b). On the probability-log scale and the log-log scale plots of  $N>T$  versus  $T$ , both lines are segmented. The first segment is for beds that are 8-16 cm thick (80 beds, or 38% of the beds) and have a  $\beta=0.9$  and the other segment is for beds that 16-42 cm thick (103 beds, or 50% of the beds) and have a  $\beta=4.1$  (Table B3). The power-law scaling value for the thicker beds is quite different than for other sandstone beds of similar thickness range of Class C. These facies are interpreted to have deposited by muddy, high concentration flows and are associated with sandstone packets.

## 6.6. COMPARISON BETWEEN FACIES CLASSES AND FACIES

Different facies classes are compared in this section to investigate if beds that have different texture follow a lognormal or a power law distribution. The four facies classes were first plotted on a probably-log scale (Figure 6.9a). All of the four classes do not show a single linear trend but the lines are stepped or bowed. The presence of absence of linear segments for the separate facies and subfacies are discussed elsewhere in this chapter and in Appendix B. The degree of departure from a linear trend is least for Class

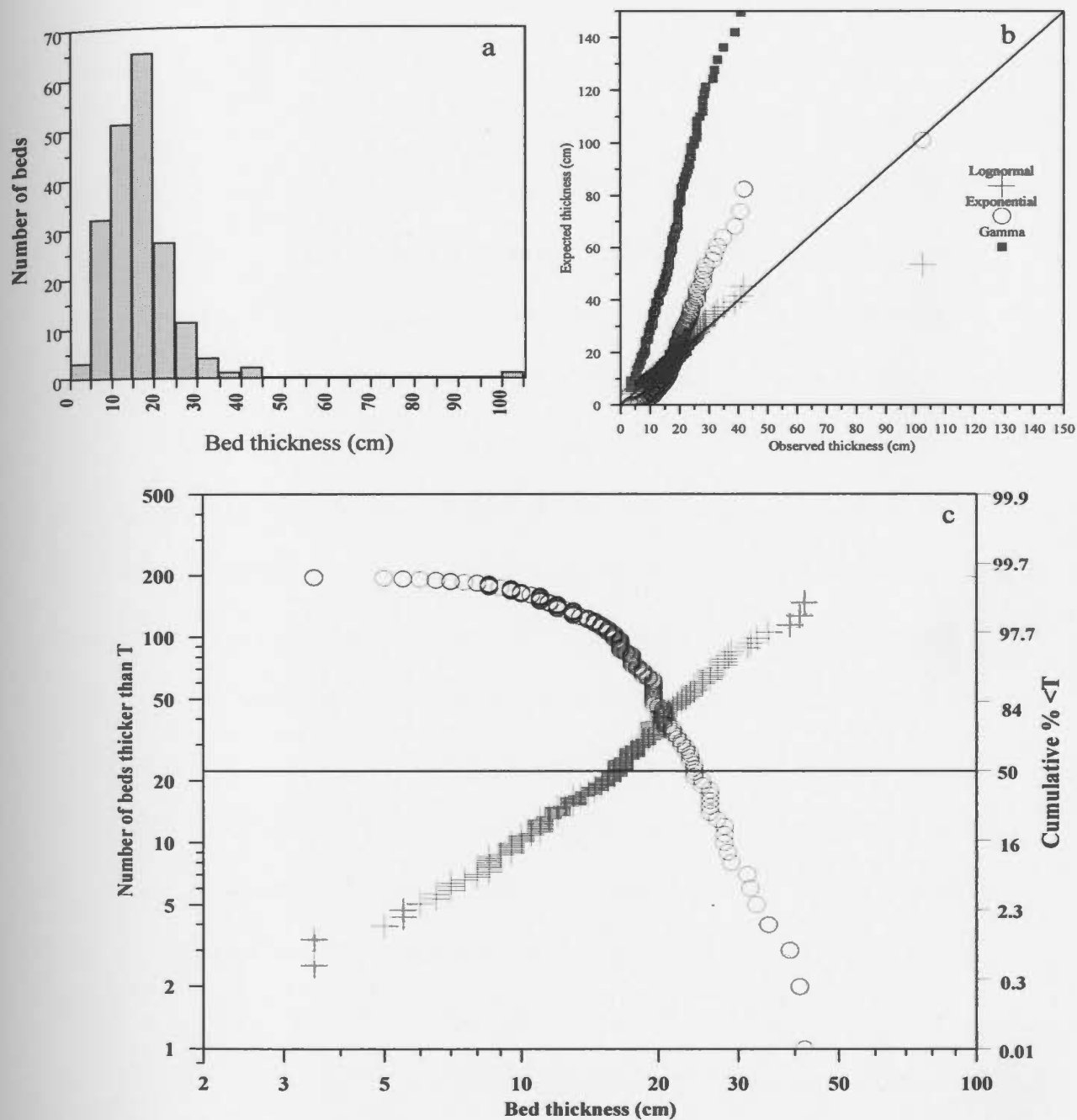


Figure 6.8. Facies B2.2. The lognormal distribution best fits the bed thickness data of this facies (a,b). The segmented nature of the data on both the probability-log and log-log plots suggests several subpopulations of bed thicknesses (c).

D and for beds less than ~70 cm for Class C. Class E and Class B show the most pronounced departure from a linear trend. These departures are because each class consists of more than a single population. For example, the bowing in the trend of Class E beds for thicknesses of 1-7 cm is because many of these beds are caps of thin and very thin beds of siltstone and sandstone (e.g., facies D2.3). The bowing of the trend of Class E for beds > 100 cm is because these are the mud caps of megaturbidites. Distinct subpopulations that are in the tails of the distribution are better displayed on the probability-log scale (e.g., megaturbidite caps in the Class E population).

Each class plots in a different place depending on the thickness of the beds in the class. The median thickness ranges from 2.5 cm for Class D to 16-17 cm for Classes B and C. This suggests that grain size might vary directly with the thickness of the beds (Talling, 2001). Other studies of turbidites have shown that some coarse sandstone beds are characterised by their thin nature (Mutti and Ricci Lucchi, 1972). Thin beds that are coarse in grain size (facies E of Mutti and Ricci Lucchi, 1972) are rare in the studied sections. Bed thickness and grain size are probably dependent on many factors that include flow size and velocity. For Class B, there is a change in slope for beds that are < 20 cm thick. This deviation is due to the 197 non-amalgamated beds of facies B2.2 (73% of the beds of Class B). About 75% of these 197 beds are less than 20 cm thick.

In order to compare all the beds from different classes for power-law scaling on a single plot log-log plot, the number of beds for each class (N) was converted to percentages. In this way it is easier to compare datasets that consist of different numbers

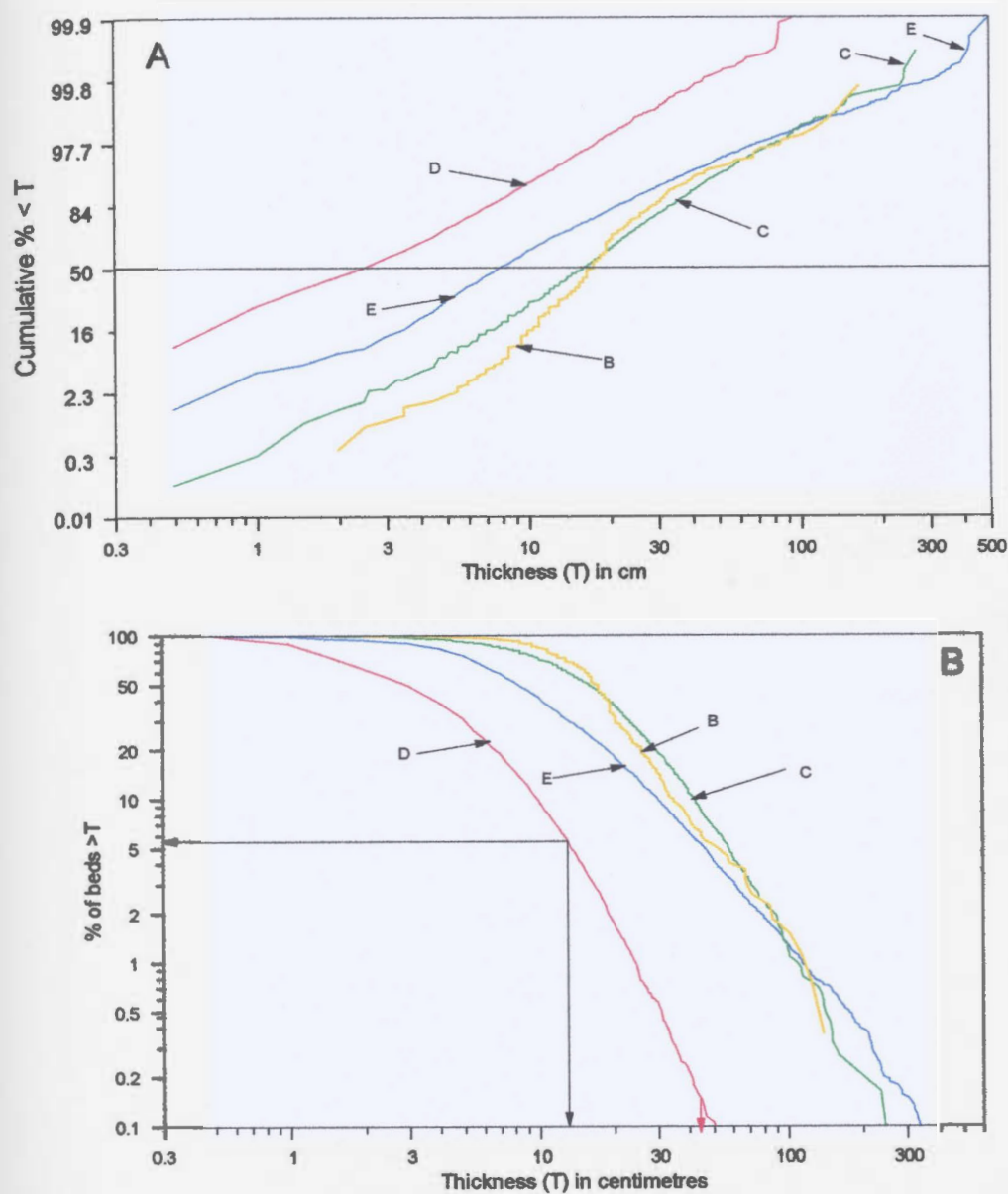


Figure 6.9. Comparison between the bed thickness data of the four facies classes observed in the thesis area using both a probability-log scale (A) and a log-log scale (B).

of beds. The four facies classes plot as segmented lines or show a linear trend for the thicker beds and a curved trend for the thinner beds (Figure 6.9b). The linear trends represent varying proportions of the population for each facies class. For example, the linear trend for facies Class D is for beds that are thicker than ~12 cm; these beds represent about 6% of the population. This 6% consists mostly of beds of subfacies D2.1F and D2.1G that tend to occur as very thick beds, and a few thick to very thick beds of subfacies D2.1A that tend to occur in sandstone packets (Chapter 5). The deposition of these thick beds is related to periods of increased sediment discharge. The thick beds of subfacies D2.1A formed when flows encountered and moved over an area of increased bottom topography. The linear trends for other facies classes probably reflect the summation of several lognormally distributed subpopulations (Talling, 2001). The point of the graph where the facies classes plot is related to both the grain size and the flow size. Sandstone beds of Classes C and B plot in the same area, while shale plots to the right of siltstone. This probably reflects that the flows that deposited many of the siltstone beds deposited thicker mud caps. This is also shown in where the area where the megaturbidite caps plot to the right of the sandstone beds. The relationship between grain size and thickness may not apply to the shale beds because most of the mud particles were not deposited as individual particles but rather as flocs of different sizes.

Non-amalgamated sandstone facies that display different sequences of sedimentary structures (facies and subfacies of Class C ) and some of the siltstone subfacies (D2.1A, D2.1D, D2.1F) were examined separately. The aim is to investigate if the thickness data of



beds that have similar basal structural division, or beds that have similar texture but have different structural divisions, plot differently on probability-log and log-log (power-law) plots. The percent of the number of beds is used instead of the actual number of beds because the number of beds differs between the facies or subfacies. The investigation of all the subfacies of Classes D and C is presented in Appendix B.

Siltstone beds plot in a different part of the graph than the sandstone beds on the probability-log plot (Figure 6.10a). This suggests that organised siltstone beds tend to be deposited as thin beds compared to organised sandstone beds. More than 70% of the beds of subfacies D2.1D ( $T_{bc}$ ) and subfacies D2.1F ( $T_{cd}$ ) have a median thickness greater than subfacies D2.1A ( $T_c$ ). This suggests that flows that deposit these beds may have been bigger compared to flows that deposited subfacies D2.1A. For the sandstone facies, facies C2.2 (beds that have a basal  $T_b$  division) have a greater median diameter than beds that have a structureless basal division ( $T_s$ ) or a basal division of ripples or climbing ripples ( $T_r$ ). This suggests that flows that deposited beds of facies C2.2 might have been bigger than those that deposited facies C2.1 and C2.3, regardless of the grain size. This is somewhat different to the observations of Talling (2001) who noted that beds that have a basal  $T_a$  or  $T_b$  division are usually thicker than beds that have a basal  $T_c$  division.

Talling (2001) suggested that the variation in the thickness of beds is due to the different concentration of the flows from which the beds are deposited. Concentrated flows will deposit beds that have a basal  $T_a$  or  $T_b$  division while low concentration flows deposit thinner beds. In the dataset from the Cloridorme Formation, this hypothesis is only

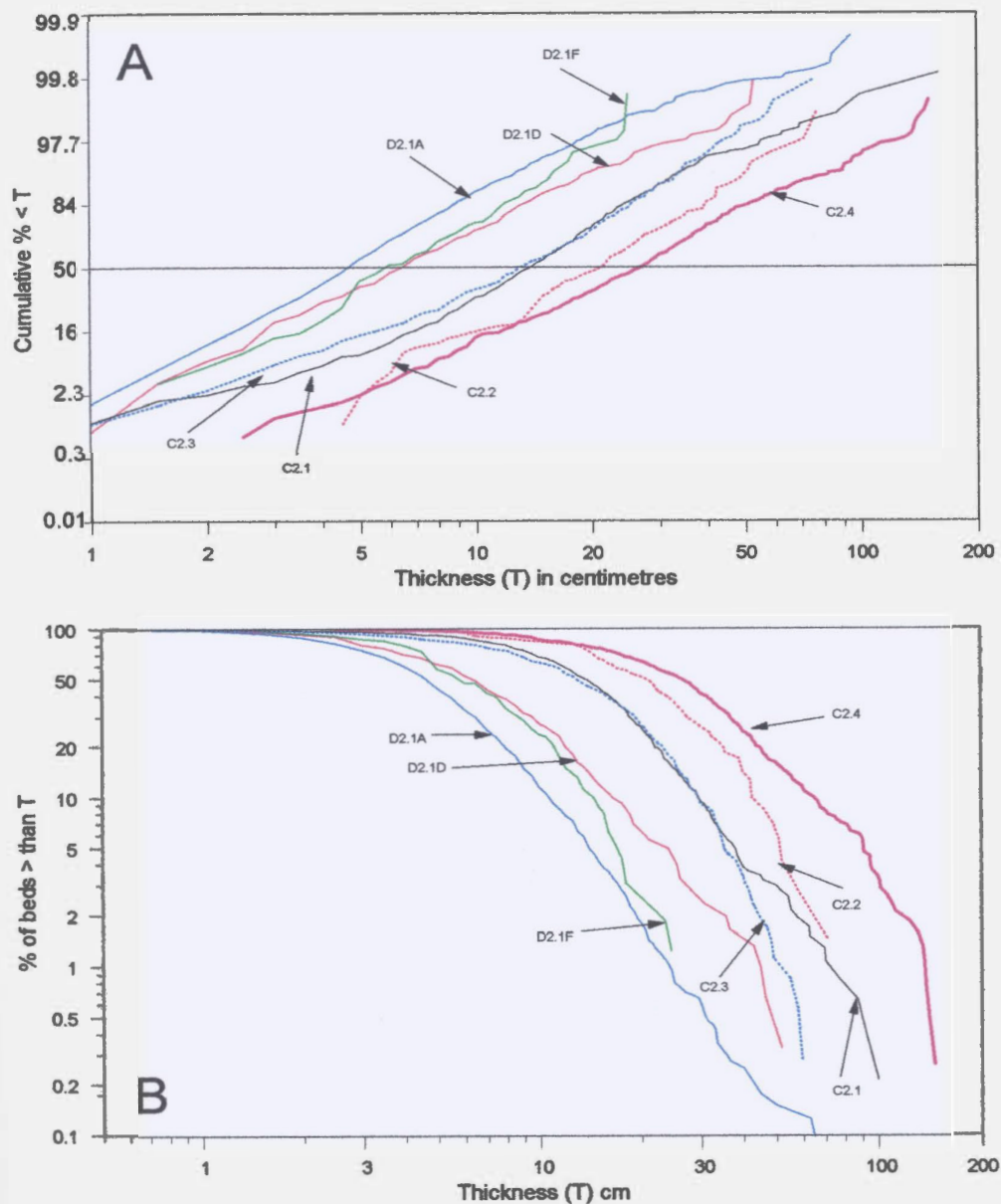


Figure 6.10. Comparison between the bed thickness data of facies and subfacies that have similar sequences of sedimentary structures but differ in texture, or have similar texture but differ in the sequence of sedimentary structures. Both a probability-log scale (A) and a log-log scale (B) are used.

supported for beds of facies C2.2 and C2.3, while other factors may control the bed thickness distribution of facies C2.1.

The lower part of megaturbidites (facies C2.4) represent a special case that is related to the large size of the flows from which they were deposited. Less than 1% of the megaturbidites are >100 cm, while about 4% are 90–130 cm thick). More than 50% of these megaturbidites are 30-90 cm thick. These distinct subpopulations are displayed as linear trends in Figure 6.10b.

Facies or subfacies that have similar sedimentary structures but differ in texture (facies C2.2 and subfacies D2.1D; facies C2.3 and D2.1A) show more-or-less a linear trend on Figure 6.10a, but plot in a different location on the graph which is related to the difference in the texture of the beds. On Figure 6.11B, these four bed-thickness datasets plot with more or less the same trend but in different locations on the graph depending on their texture.

## **6.7. LATERAL AND VERTICAL TRENDS IN BED THICKNESS DISTRIBUTIONS**

In this section, beds in each of the time-slices are compared to investigate what type of bed-thickness distribution best fits each set of data. Only the sandstone and siltstone beds and laminae were tested. Shale bed thicknesses were not tested. Data from time-slices 1 and 2 were combined into a single dataset because the number of beds is small. Because parts of time-slice 1 are not exposed in area B (mini-slices SL 1A and SL

1B), only the beds exposed in the upper part of time-slice 1 and all beds of time-slice 2 were analysed. The data from time-slice 5 were also not analysed because faulting has affected different intervals of this time-slice in areas A and B. When plotting the data as histograms (Figure B11) or on q-q plots (Figure B12), sandstone beds and siltstone beds were first plotted separately and then combined. When investigating if the data are best fitted by a lognormal or power-law distribution, only the combined file for sandstone and siltstone beds was used. The percent of beds thicker than T instead of the actual number of beds was used because the number of beds differs in the three

A general conclusion is that sandstone beds are best fitted by a lognormal or gamma distribution, while siltstone beds are best fitted by an exponential distribution or a gamma distribution. Because siltstone beds are more numerous than sandstone beds (by an order of magnitude in some time-slices), the combined datasets of the sandstone and siltstone bed thicknesses plot very much a like gamma distribution on the q-q plots (Figure B12). On Figure B11, the histograms for these combined datasets are very much like the exponential distributions of the siltstone alone. The small modes observed on these histograms for the combined datasets (e.g., time-slices 6 and 7) represent the sandstone beds.

The change in depositional environment from a basin-plain setting to a distal fan setting is not well displayed in these histogram plots because an increase in the number of sandstone beds is paralleled by a greater increase in the number of siltstone beds.

For time-slices 1 and 2, more than 95% of the data fall along a single straight line

on log-probability paper, suggesting a lognormal distribution (Figure 6.11). On log-log plots of the percent  $>T$  versus  $T$ , three segments can be fitted (Figure 6.11). Claims that the basin-plain deposits in the Cloridorme Formation follow a single linear trend (Carlson and Grotzinger, 2001) are not supported by this data. The first segment represents beds that are less than 5 cm thick; these account for about 80% of each population. The second segment is for beds 5-40 cm thick (~20% of the population) and a third segment is for beds thicker than 40 cm. The beds  $< 5$  cm thick are mostly the thin siltstone beds that dominate basin-plain deposits of time-slices 1 and 2. The second segment (beds 5-40 cm thick) corresponds to the megaturbidites and some of the sandstone beds of these time-slices. There are ~40-50 such sandstone beds (including the lower parts of megaturbidites) in each of areas A, B and C. The third segment is attributed to the very thick megaturbidites. The megaturbidites in areas B and C plot to the right of the beds of area A, and beds of area C plot to the right of area B, which might reflect the ponding of the megaturbidites in the west.

The bending of the plot of  $\%>T$  versus  $T$  for large  $T$  is due to an under-representation of very thick beds. The bending for small  $T$  is not attributed to amalgamation or erosion as suggested by Carlson and Grotzinger (2001) because erosion of beds that are 2-3 cm thick was not observed. Bending at very small values of  $T$  ( $<0.5$  cm) might be because many of the very thin laminae were not observed or not counted. Discrete bed-thickness subpopulations in time-slices 1 and 2 are attributed to different depositional processes. Specifically, there is a subpopulation of very thick beds deposited

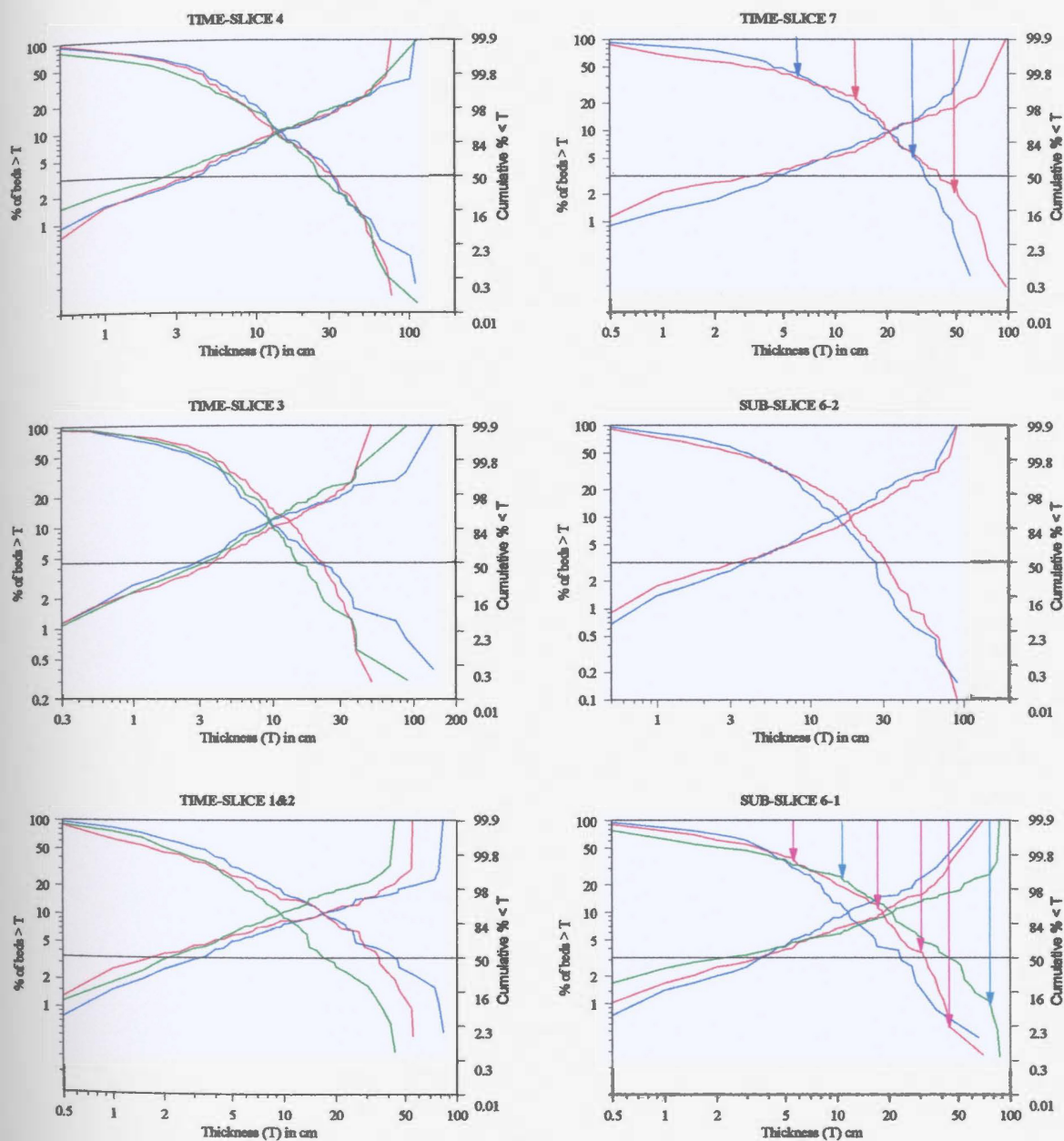


Figure 6.11. Comparison between bed thickness for a combined dataset of the sandstone and siltstone beds at areas A (green), B (red) and C (blue) in the time-slices of the thesis area.

from large flows, and a much larger subpopulation of very thin beds deposited from low concentration flows that were generated at a distant source.

For time-slice 3, the probability-log plot suggests an essentially lognormal distribution. Departure from a single linear trend is due to the presence of a small proportion of thick megaturbidites. On the %>T versus T plot, the bed thicknesses from the three areas have more-or-less the same slope. Departures for large values of T are due to the presence of megaturbidites that vary in thickness because of bottom topography. For beds less than ~40 cm thick, thicker beds are more abundant in area B than in areas A and C. The gentler slope of the % >T versus T curve for area C is attributed to the thinning of the beds in a downcurrent direction.

Time-slice 4 is interpreted to mark the transition from a basin-plain setting to a setting akin to distal submarine fans or fan fringes (Chapter 5). The probability-log graph shows a linear trend for the beds in all three areas, but departs from this trend for beds > 70 cm thick. The %>T versus T plot for power-law scaling is similar in slope for all three areas. The irregularities in the slope of the line are attributed to a combination of different factors. For area A, irregularities are due to amalgamation and the preferential deposition of beds in certain thickness ranges (i.e., beds in packets). Amalgamation is not common in areas B and C but preferential deposition as a consequence of bottom topography is believed to account for the irregularities. Without a detailed knowledge of the factors that control the thickness of the beds deposited, the irregularities in the curves for areas B and C might have been attributed incorrectly to amalgamation.

Sub-slice 6-1 consists of several packets of sandstone in area A that are interpreted as lobes. These lobes represent periods of increased deposition from high density turbidity currents. The lobes are better developed in area A than in area B and are mainly absent from area C. On a probability log-plot, the data from the three areas plot as segmented lines with two or perhaps three subpopulations. These segments are better displayed on the plot of %>T versus T.

For area A, one line segment is for 3 beds that are very thick (> 80 cm). The second segment is for beds 10-80 cm thick, the majority of which occur in packets (i.e., lobes). The third segment is for beds that are thinner than 10 cm. These subpopulations are also displayed on the histograms of Figure B11. The two segments for beds less than 80 cm thick are not differentiated on the probability-log plot.

For area B, the linear segments are more distinct. One segment is for ~10 beds that are ~30-45 cm thick. Another segment is for (~ 30) beds that are ~ 20-30 cm thick and the third segment is for beds that are ~5-20 cm thick. The distinct subpopulations correspond to beds in sandstone and siltstone packets. Some of these distinct population represent some of the modes observed in Figure B11 for sub-slice 6-1 in area B. Because beds in these packets are distinct in their thickness from the enclosing shale, they are better displayed on the plot of %>T versus T. Area C shows fewer linear segments because packets are not common there.

Sub-slice 6-2 is not exposed in area A and is therefore examined only in areas B and C. The bed-thickness data show two linear trends on a probability-log plot as two



linear trends similar to the other time-slices and sub-slices. The plot of %>T versus T does not display linear segments as in sub-slice 6-1 although there are several packets of sandstone beds that are interpreted as lobes. This is perhaps because there are many siltstone beds in the upper part of this sub-slice that mask the contribution of the sandstone beds. The two kinks in the plot for area C (Figure 6.11) are attributed to the presence of 2-3 megaturbidites that are much thicker than the other beds, and the presence of several medium sandstone beds that form a packet in the lower part of sub-slice 6-2 in area B (mini-slice SL 6H).

For time-slice 7, the lateral relationship between areas B and C is not well known because of faulting in area C. Segmentation is best displayed on the plot of %>T versus T for area B. The segments reflect discrete bed-thickness subpopulations related to the deposition of sandstone beds that form packets. The segmentation is well developed because most of the beds that do not occur in packets are thinner than the sandstone beds in the packets (i.e., the contrast in bed thickness is large). The irregular shape of the line in some of the segments is due to amalgamation.

## 6.8. CONCLUSIONS

The bed-thickness data for turbidites can be fitted by a number of statistical distributions. Sandstone beds are better fitted by lognormal distributions while siltstone beds more closely follow the exponential distribution. The shape of the distribution displayed on the histograms depends on the detail and resolution of field measurements.

The lognormal distributions might be combinations (mixtures) of different bed- thickness distributions (*cf.* Talling, 2001).

Investigating the bed-thickness data of turbidites that differ in their texture or sequence of sedimentary structures suggests that individual facies or subfacies might generally be described as lognormal. The different distributions for individual facies or subfacies might owe their origin to distinct flow processes that deposited beds with a limited bed-thickness range. For example, beds that display planar lamination at their base tend to be thick suggesting that they only form under conditions of increased sediment concentration or high rate of deposition.

Power-law scaling of turbidites has been suggested for many turbidite sequences. Earthquakes have been suggested as a triggering mechanism because both turbidites and earthquakes have a power-law scaling value of  $\sim 1$  ( $\beta = -1$ ). In the studied sections from the Cloridorme Formation, the log-log plots of  $N > T$  versus  $T$  (or  $\%>T$  versus  $T$ ) consist of segmented lines. One segment corresponds to thin or very thin beds. This is not unique to the Cloridorme Formation, and suggests that a simple explanation of earthquake-controlled initiation of turbidity currents cannot apply across the full range of bed types.

When investigating a power-law scaling for turbidites, it is important to look for linear trends in the thinner beds because they might not be clearly displayed on plots of  $N > T$  versus  $T$  especially where there is a mixture of thin and thick beds. When characterising a section or a sequence based on such plots, it is more accurate to use the beds that represent the majority of the population, which is in many cases the thin beds.

These beds may not represent a large proportions of the total thickness of the section or sequence studied (Drummond and Wilkinson, 1996; Malinverno, 1997).

In some cases, it has been possible to infer the cause of segmentation using  $N>T$  versus  $T$  plots. This should be attempted only after a clear understanding of the many variables that might control the thicknesses of the deposited sediments. Many of these variables may not be easily known. The interaction of many variables, and their variability temporally and spatially, make it difficult or impossible to use the shape of the plot of the bed-thickness data to predict depositional environments or subenvironments. This is at least the case in the studied sequence in the Cloridorme Formation, where variations in bottom topography during deposition were a major control on deposition, the distribution of different turbidite beds, and their thicknesses.

It is unknown how useful it might be to test different datasets from sequences elsewhere in the world deposited under different conditions. This would be a first step towards gaining a clear understanding of the range of variables that can affect deposition in order to relate the bed-thickness results to actual depositional processes and history. Such an expanded study is beyond the scope of this thesis

## **CHAPTER 7**

### **CONCLUSIONS AND RECOMMENDATIONS**

#### **7.1. SUMMARY AND CONCLUSIONS**

The Middle Ordovician lower Cloridorme Formation, between Pointe-à-la-Frégate and L'Anse-à-Valleau, northern Gaspé, Québec, was deposited first in a basin plain and subsequently in a setting similar to a modern distal submarine fan environment. The primary objective of this thesis is to better understand the depositional history of this part of the Cloridorme Formation, which was not well understood prior to this study. This objective was achieved through the detailed investigation of the facies in the area (Chapter 3), and the detailed delineation and mapping of architectural elements (Chapter 5) constrained by a precise stratigraphic framework based on the correlation of key beds (Chapter 4). The facies distribution and geometry of the deposits was controlled by an interplay between bottom topography and differential deposition. Variation in bottom topography was due to tectonics in addition to depositional and compactional factors. An understanding of the effects of these factors on deposition can only be achieved by this type of detailed study. The evolution of the depositional environment from a basin plain setting to a distal fan setting was due to the advance of a submarine fan system from the east of the area.

A basin-plain environment is suggested by the tabular geometry of the deposits, lack of any channel deposits or features suggesting channels (e.g., deep scours) and the

fine-grained nature of the facies. Sedimentation in this basin plain was dominated by the deposition of megaturbidites from large flows initiated from large sediment failures mostly east of the study area. This architectural element has a tabular to a slightly wedge-shaped geometry due to ponding of flows in the west. Sheet sandstone bodies, another architectural element of the basin plain, have a more-or-less tabular to slightly lensing geometry that is controlled by bottom topography. These sheet sandstone form 10-20 m-thick packets and consists of organised beds of sandstones and siltstone that have basal laminated divisions ( $T_b$  or  $T_c$ ). In upcurrent areas, these sheets may contain some structureless sandstone beds. The sandstone sheets become more shaly over distances of tens of kilometres in a downcurrent direction. Siltstone lenses, another architectural element of the basin plain, form 5-10 m-thick packets and consist of thin to medium beds of laminated siltstone and a few sandstone beds. They formed during periods of increased sediment supply and their lens shape is controlled by bottom topography. Over distances of 1-2 km, these lenses have a tabular shape. The siltstone lenses become more shaly in a downcurrent direction.

The distal part of a submarine-fan system is characterised by the presence of sandstone-lobe elements in addition to megaturbidite and siltstone-lens elements. The presence of such non-channelised sandstone-lobe deposits and the lack of deep scours beneath these lobes support a distal fan setting where channels are uncommon. The lobes are 10-20 m-thick packets of sandstone beds that do not continue for more than a few kilometres in a downcurrent direction. These lobes formed mounds on the sea floor and

controlled the deposition from subsequent flows. The lobes probably developed as flows exited confining channels. The lobes consist mostly of amalgamated beds of facies C2.1 and B2.1. These facies were deposited from concentrated flows that did not continue for a long distance in a downcurrent direction. These concentrated flows were strongly influenced by bottom topography. The downcurrent continuation of the concentrated flows was improved by the incorporation of mud into the flow, thus increasing their ability to maintain turbulence and travel farther downcurrent. The sandstone lobes have a tabular geometry over distances of 2-3 km but taper over longer distances. Amalgamation is more common in the upcurrent parts of the lobes. No well developed cyclicity in the bed thickness or grain size of the lobe deposits was observed in the area. A limited of cycles were observed, all attributed to compensation. Siltstone lenses and megaturbidites in the distal fan deposits are similar to those observed in the basin-plain deposits.

Two main factors controlled the deposition and geometries of the architectural elements in the lower Cloridorme Formation. The first factor was bottom topography which played a dominant role during the deposition of the lower part of the studied sequence. Movement along buried faults, especially in middle part of the thesis area, is believed to have controlled the geometry of the deposits. The inferred faults may have been reactivated structures that originally formed during the development of a passive margin along the Laurentian continental edge prior to the Taconic Orogeny. Subsequent foundering of the carbonate platform and loading by the thrust sheets conceivably reactivated these faults, leading to differential subsidence in the foreland basin.

The second factor was a progressive increase in sediment supply to the study area. More frequent sand-laden and silt-laden flows reached the area during the deposition of the middle and upper part of the studied sequence. These flows deposited their sediments forming lobes, sheets and lenses. The increase in the sediment supply was probably related to the progradation of a turbidite system from the east because of regional factors such as sea-level changes and/or tectonics.

Local factors such as the shape and size of the basin, channel switching, depositional features of the sediments and local tectonics also may have controlled the development and geometry of the different architectural elements of the lower Cloridorme Formation. Many of these local controls and factors are a consequence of the regional factors.

Bed thicknesses of the different facies and subfacies of the lower Cloridorme Formation may be described by any number of statistical distributions or a combination of many distributions. The bed thickness distribution of sandstone is best described as lognormal while siltstone bed thicknesses may follow either the exponential or gamma distribution. The nature of the bed thickness distribution depends on precisely how the bed thicknesses were measured and the resolution of the measurements (i.e., what is the minimum thickness being measured). The cumulative frequency distribution of sandstone and siltstone bed thicknesses follows a segmented power-law relationship. There are deviations from the linear trend displayed by the thicker beds, but these beds only represent a small part of each population. The nature of the log-log plots cause a wide part

of each power-law plot to be associated with only a small percentage of the beds. Great care must be exercised to avoid sweeping conclusions based on a striking linear trend that actually owes its origin to only a small portions of the beds.

There are many factors that control the nature of the bed thickness distribution. These factors and their interaction control the thickness of the beds deposited in all deep-marine and submarine-fan settings. As demonstrated in this study, predicting submarine fan depositional subenvironments based on the presence or absence of trends in turbidite bed-thickness plots should not be attempted before a detailed understanding is achieved for the factors that might have controlled the thicknesses of the beds deposited in these subenvironments.

## **7.2. RECOMMENDATIONS AND FUTURE WORK**

The detailed correlation and depositional history presented in this thesis provided the framework for some additional work that would add to the results of this study. The suggested additional work and recommendations are listed below.

The precise bed-by-bed correlation provides an excellent opportunity to initiate a study of the dynamics of the flows responsible for megaturbidite deposition. A selection of several laterally equivalent megaturbidites could be completely sampled and studied. Previous studies on megaturbidites of the Cloridorme Formation are restricted to field observations and limited fabric studies on one bed (Pickering and Hiscott, 1985; Edwards *et al.*, 1996). The only well documented study on megaturbidites is from the Madeira



Abyssal Plain (Rothwell *et al.*, 1992); however, this study was carried on cores that are more than 50 km apart and a full understanding on the dynamics of the flows that deposited those megaturbidites is still lacking.

A similar investigation could be undertaken for the sandstone beds of facies C2.1 that form a large proportion of the sandstone packets interpreted as lobes. This study might improve our understanding of the flow dynamics of these beds. The origin of these beds is still not well understood and is controversial. Some of these beds were tentatively correlated over a distance of a few kilometres, so their downcurrent evolution may be studied. Many of the studies that attempt to explain the origin of such beds are based on laboratory flume experiments or observations on single beds in single sections. A grain fabric study of some of beds in these lobes exposed in different areas would improve the understanding of the flow paths and perhaps illuminate why these beds are not laterally persistent. Palaeocurrent information from these lobes is limited because of the scarcity of flutes in amalgamated intervals. Even where not amalgamated, flutes are not common.

The results from this study necessitate a revision of the “formal” stratigraphy of the lower part of the Cloridorme Formation as proposed by Slivitzky *et al.* (1991). If the “formal” nomenclature proposed by them is maintained, it is at a minimum necessary to correct and clarify the following issues. First, the lower boundary of the Pointe-à-la-Frégate Member (PF) should be placed at the highest occurrence of facies C2.5 (G3 of Enos, 1965) as originally proposed by Enos (1969b) to separate his  $\beta 1$  member from the overlying  $\beta 2$  member. The highest occurrence of facies C2.5 is a ~ 7 m-thick bed of facies

C2.5 (BT-3, in this thesis) that is exposed very prominently in the area. Bed BT-3 also occurs in the Pointe-à-la-Renommée area (Pickering and Hiscott, 1985; 1995 and this study). Placing the boundary at the base of BT-3 would rectify the error in Enos (1965): he assigned coastal outcrops of the Pointe-à-la-Renommée area to the older  $\beta 1$  member, but detailed correlations show these to be equivalent to the section exposed at Anse à la Rogne and the section exposed west of Le Brûlé (Pickering and Hiscott, 1985; this study). Second, the position of the lower boundary of the PF Member in the Le-Brûlé area as mapped by Slivitzky *et al.* (1991) should be corrected by moving it from an inland position to where BT-3 is actually exposed in the wave-cut platform on the western side of the cove to the west of Le-Brûlé. The position of the lower boundary of the PF Member in the area east of Anse à la Rogne should be maintained because it is correctly placed at the base of bed BT-3 (Enos, 1965; Slivitzky *et al.*, 1991). Third, the relationship between the Pointe-à-la-Frégate Member and the Manche-d'Épée Member (ME) should be further investigated in detail. Key locations are the coastal exposures at Manche-d'Épée ( $\gamma 1$  member of Enos, 1965) and from Manche-d'Épée to Gros-Morne (type section of the ME Member of Slivitzky *et al.*, 1991), and the coastal outcrops east of the thesis area from Pointe-à-la-Renommée to Pointe Jaune. Detailed section measurements should be undertaken in these areas and ash beds, if present, should be sampled and analysed. The result of such an investigation could support or refute the time-equivalence suggested by Hiscott *et al.* (1986), who correlated the middle part of the PF Member exposed in the study area and the  $\gamma 1$  member of Enos (1965) located to the west of the study area.

Slivitzky *et al.* (1991) indicate that  $\gamma 1$  is equivalent to their Manche-d'Épée Member (1986). Fourth, the boundary between the Pointe-à-la-Frégate Member and the overlying Gros-Morne Member needs adjustment. It is placed by Slivitzky *et al.* (1991) at the base of sandstone packets at the first (eastern) headland at Pointe-à-la-Frégate. There are several sandstone packets in that area. If the boundary is located at the base of the lowest sandstone packet of the eastern headland, then the beds exposed in the syncline at Pointe Séche that extend to the west of Baie de Saint-Yvon also belong to the Gros-Morne Member of Slivitzky *et al.* (1991). Alternatively, it is recommended that the base of the Gros-Morne Member be placed at the base of a very thick (5-7 m) megaturbidite (BT-67) that is prominently exposed southeast of the headlands at Pointe-à-la-Frégate. As demonstrated in this thesis, megaturbidites are excellent marker horizons and are laterally persistent, unlike sandstone packets. However, this necessitates a detailed investigation of the lower part of the Gros-Morne Member in other areas. There are more than 200 m of section exposed above bed BT-67 in the Pointe-à-la-Frégate area, including some megaturbidites and several ash beds. Part of this section should be correlatable to the 245 m-thick type section of the Gros-Morne Member exposed west of Gros-Morne.

A better knowledge of the age of the studied sections is required in order to better understand the depositional history. A systematic and comprehensive collection of graptolites may help in achieving this goal. Existing graptolites collections are limited, partly because of the cleaved nature the shale. It also might be beneficial to date some of the ash horizons, although the resolution of the dates might be too coarse to accurately

constrain the detailed depositional history presented in this thesis. Nevertheless, improved U/Pb dating techniques are now able to date rocks of Ordovician age to the nearest  $\pm 1$  million years (Scott M. McLennan, Personal Communications, 2001). The ash beds described in this study are the best candidates for dating.

A more detailed investigation of the nature of the bed-thickness distributions might be helpful to determine whether or not submarine-fan and turbidite depositional environments and subenvironments can be characterised using this type of data. This characterisation should be attempted only after a clear understanding is developed concerning the factors that were operating in the depositional systems. Some of these factors might be difficult to know or constrain unless a detailed investigation similar to this study is completed in other well-exposed formations.

Finally, decompaction algorithms could be applied to the correlated time-slices to better understand original thickness variations and seabed topography. The present study has relied on rock thicknesses, and differential compaction has only been mentioned in a qualitative way when considering changing thicknesses of the time-slices from area A to area C. Proper decompaction must also consider thickness changes induced by folding and tectonic flattening. This would be a challenging project.

## REFERENCES

- ALLEN, J.R.L., 1982. *Sedimentary Structures, their Character and Physical Basis*, 2 vols: Amsterdam, Elsevier, 663pp.
- ALLEN, J.R.L., 1983. Studies in fluviatile sedimentation: bars, bar complexes and sandstone sheets (low-sinuosity braided streams) in the Brownstones (L. Devonian), Welsh Borders: *Sedimentary Geology*, v. 33, p. 237-293.
- ALLEN, J.R.L., 1991. The Bouma division A and the possible duration of turbidity currents: *Journal of Sedimentary Petrology*, v. 61, p. 291-295.
- ANDERSON, T. W., AND GOODMAN, L. A., 1957. Statistical inference about Markov chains: *Annals of Mathematical Statistics*, v. 28, p. 89-110.
- ARNOTT, R.W.C., AND HAND, B.M., 1989. Bedforms, primary structures and grain fabric in the presence of suspended sediment rain: *Journal of Sedimentary Petrology*, v. 59, p. 1062-1069.
- AWADALLAH, S.A.M., HISCOTT, R.N., BIDGOOD, M., AND CROWTHER, T.E., 2001. Turbidite facies and bed-thickness characteristics inferred from microresistivity (FMS) images of lower to upper Pliocene rift-basin deposits, Woodlark Basin, offshore Papua New Guinea, in Huchon, P., Taylor, B., and Klaus, A. (eds.), *Proceedings of the Ocean Drilling Program, Scientific Results*.
- BARNES, C.R., AND WILLIAMS, S.H., 1991. *Advances in Ordovician Geology*. Geological Survey of Canada Paper 90-9, 330p.
- BARNES, C.R., NORFORD, B.S. AND SKEVINGTON, D. 1981. *The Ordovician System in Canada*. International Union of Geological Sciences, 8, p. 1-27.
- BATES, R.L., AND JACKSON, J.A. 1987. *Glossary of Geology*. American Geological Institute, Alexandria, Virginia, 788pp.
- BEATTIE, P.D., AND DADE, W.B. 1996. Is scaling in turbidite deposition consistent with forcing by earthquakes?: *Journal of Sedimentary Research*, v. 66, p. 909-915.
- BERRY, W.B.N. 1960. Graptolite faunas of the Marathon region, West Texas. Texas University Publications No. 6005, 179pp.
- BERRY, W.B.N. 1962. Stratigraphy, zonation, and age of Schaghticoke, Deepkill, and

Normanskill Shale, Eastern New York: Geological Society of America Bulletin, v. 73, p. 695-718.

BERRY, W.B.N. 1970. Ordovician paleogeography of New England and adjacent areas based on graptolites, in E-an Zen, W.S. Whites, J. B. Hadly, and J.B. Thompson, (eds.), *Studies of Appalachian Geology, Northern and Maritime*: New York, Wiley Interscience, p. 23-34.

BEEDEEN, D.R., 1983. Sedimentology of some turbidites and rocks related rocks from the Cloridorme Group, Ordovician, Québec. MSc. thesis, McMaster University, Hamilton, Ontario, 254 pp.

BILLINGSLEY, P., 1961. Statistical methods in chains: *Annals of Mathematical Statistics*, v. 32, p. 12-40.

BIRON, S., 1973. Géologie de la région de Marsoui. Ministère des Richesses Naturelles du Québec, DP-244, p. 1-12.

BLOECHL, II, W.V., 1996. Sedimentation history and provenance of the Middle Ordovician Les Trois Rousseau Member of the Deslandes Formation: northern Gaspé Peninsula, Québec, Canada. MSc. thesis, University of California Santa Cruz. 227pp.

BOKMAN, JOHN W., 1957. Suggested use of bed thickness measurements in stratigraphic descriptions: *Journal of Sedimentary Petrology*, v. 27, p. 333 335.

BOUMA, A.H., 1962. *Sedimentology of some flysch deposits: a graphic approach to facies interpretation*: Amsterdam, Elsevier, 168p.

BOUMA, A.H., 1997. Reinterpretation of depositional processes in a classic flysch sequence (Pennsylvanian Jackfork Group), Ouachita Mountains, Arkansas and Oklahoma; discussions and reply: *American Association of Petroleum Geologists Bulletin*, v. 81, p. 449-491.

BOUMA, A.H., 2000. Fine-grained, mud-rich turbidite systems: models and comparisons with coarse-grained, sand-rich systems, in A.H., Bouma, and C.G. Stone, (eds.), *Fine-grained turbidite systems*. American Association of Petroleum Geologists Memoir 72/ Society of Sedimentary Research Special Publication No. 68, p. 9-20.

BRIDGE, J.S., 1981. Hydraulic interpretation of grain-size distributions using a physical model for bedload transport: *Journal of Sedimentary Petrology*, v. 51, p. 1109-1124.

BRISEBOIS, D., LACHAMAMBRE, G., AND PICHE, G., 1991. Carte Géologique, Péninsule de la Gaspé, Québec. Ministère des Richesses Naturelles du Québec, Carte 2146-DV 91-21.

BROOKFIELD, M.E., 1977. The origin of bounding surfaces in ancient aeolian sandstones: *Sedimentology*, v. 24, p. 303-332.

CARLSON, J.C. 1998. Analytical and statistical approaches towards understanding sedimentation in siliciclastic depositional system. PhD. thesis, Massachusetts Institute of Technology, Massachusetts, 954pp.

CARLSON, J., AND GROTZINGER, P.J., 2001. Submarine fan environments inferred from turbidite thickness distribution: *Sedimentology*, v. 48, p. 1331-1351.

CARR, M., AND GARDNER, M.H., 2000. Portrait of a basin-floor fan for sandy deepwater systems, Permian Lower Brushy Canyon Formation, West Texas, in A. H., Bouma, and C.G. Stone, (eds.), *Fine-grained turbidite systems*. American Association of Petroleum Geologists Memoir 72/ Society of Economic Paleontologists and Mineralogists Special Publication 68, p. 215-232.

CARTER, R.M., 1975. A discussion and classification of subaqueous mass-transport with particular application to grain-flow, slurry-flow and fluxoturbidites: *Earth-Science Reviews*, v. 11, p. 145-177.

CATTANO, A., AND RICCI LUCCHI, 1995, Long-distance correlation of sandy turbidites: a 2.5 km long cross section of Marnoso-Arenancea, Santeramo Valley, Northern Appennines, in Pickering, K.T., Hiscott, R.N., Kenyon, N.H., Ricci Lucchi, F., and Smith, R. (eds.), *Atlas of Architectural Styles in Turbidite Systems*, London, Chapman & Hall, p.303 -305..

CHAPIN, M.A., DAVIES, P., GIBSON, J.L., AND PETTINGILL, H.S. 1994. Reservoir architecture of turbidite sheet sandstone in laterally extensive outcrops, Ross Formation, western Ireland, in P. Weimer, A.H. Bouma, and B.F. Perkins (eds.), *Submarine Fans and Turbidite Systems*, Gulf Coast Section, Society of Economic Paleontologists and Mineralogists, Fifteenth Annual Research Conference, p. 53-68.

CHEN, C., AND HISCOTT, R.N., 1999. Statistical analysis of turbidite cycles in submarine fan successions: test for short-term persistence: *Journal of Sedimentary Research*, v. 69, p. 486-504.

COSSEY, S.P.J., 1994. Reservoir modelling of deepwater clastic sequences: mesoscale architectural elements, aspect ratios and producibility, in P. Weimer, A.H. Bouma, and B.F. Perkins (eds.), *Submarine Fans and Turbidite Systems*, Gulf Coast Section, Society of Economic Paleontologists and Mineralogists, Fifteenth Annual Research Conference, p. 83-93.

CLARK, J.D., AND PICKERING, K.T., 1996. *Submarine Channels: Processes and Architecture*: London, Vallis Press, 232pp.

DAVIS, J.C., 1986. *Statistics and Data Analysis in Geology*: New York, Wiley, 646pp.

DRUMMOND, C.N., 1999. Bed-thickness structure of multi-sourced ramp turbidites: Devonian Brallier Formation, Central Appalachian Basin: *Journal of Sedimentary Research*, v. 69, p. 115-121.

DRUMMOND, C.N., AND WILKINSON B.H., 1996. Stratal thickness frequencies and the prevalence of orderliness in stratigraphic sequences: *Journal of Geology*, v. 104, p. 118.

DZULINSKI, S., AND WALTON, E.K., 1965. *Sedimentary Features of Flysch and Greywackes*: Amsterdam, Elsevier, 274 pp.

EDWARDS, D.A., 1993. *Turbidity currents: dynamics, deposits and reversals*. Lecture Notes in Earth Sciences, v. 44: Berlin, Springer Verlag, 173 p.

EDWARDS, D.A., LEEDER, M.R., BEST, J.L., AND PANTIN, H.M., 1994. On experimental reflected density currents and the interpretation of certain turbidites: *Sedimentology*, v. 41, p. 437-462.

ELLS, R.W., 1883. Report on the geological formations in the Gaspé Peninsula: Geological Survey of Canada Report of Progress for 1882, Section DD, 32p.

EMERY, D., AND MYERS, K.J., 1996. *Sequence Stratigraphy*: Oxford, Blackwell, 297pp.

ENOS, P., 1965. Anatomy of Flysch- Middle Ordovician Cloridorme Formation, Northern Gaspé Peninsula, Ph.D. thesis, University of Yale, 145pp.

ENOS, P., 1969a. Cloridorme Formation, Middle Ordovician flysch, northern Gaspé Peninsula, Québec, Special Publication of the Geological Society of America, 117, 66pp.

ENOS, P., 1969b. Anatomy of flysch: *Journal of Sedimentary Petrology*, v. 39, p. 680-



723.

GARVER, J.I., ROYCE, P.R., AND SMICK, T.A., 1996. Chromium and nickel in shale of the Taconic foreland; a case study for the provenance of fine-grained sediments with an ultramafic source: *Journal of Sedimentary Research*, v. 66, p. 100-106.

GHIBAUDO, G., 1992. Subaqueous sediment gravity flow deposits: practical criteria for their field description and classification: *Sedimentology*, v. 39, p. 423-454.

GINGERICH, P. D., 1969. Markov analysis of cyclic alluvial sediments: *Journal of Sedimentary Petrology*, v. 39, p. 330-332.

GLOBENSKY, Y., 1978. *Geologie des basses-terres du Saint-Laurent*: Ministère de l'Energie et des Ressources Centre de Diffusion de la Geoinformation. Québec, p. 63.

GRAHAM, J., 1988. Collection and analysis of field data, in M. Tucker (ed.), *Techniques in Sedimentology*: Oxford, Blackwell, p. 5-62.

HARBAUGH, J. W., AND BONHAM-CARTER, G., 1970. *Computer Simulation in Geology*: New York, Wiley, 575pp.

HARMS, J.C., 1969. Hydraulic significance of some sand ripples: *Geological Society of America Bulletin*, v. 80, p 363-396.

HARMS, J.C., SOUTHARD, J.B., AND WALKER, R.G., 1982. *Structures and Sequences in Clastic Rocks*. Society of Economic Paleontologists and Mineralogists Short Course 9, 255pp.

HAUGHTON, P D.W., 1994. Deposits of deflected and ponded turbidity currents, Sorbas Basin, Southeast Spain: *Journal of Sedimentary Research* , v. 64, p. 233-246

HELLER, P.L., AND DICKINSON, W.R., 1985. Submarine ramp facies model for delta-fed, sand rich turbidite systems: *American Association of Petroleum Geologists Bulletin*, v. 69, p. 960-976.

HESSE, R., 1974. Long-distance continuity of turbidites: possible evidence for an Early Cretaceous trench-abyssal plain in the East Alps: *Geological Society of America Bulletin*, v. 85, p. 859-870.

HESSE, R., 1975. Turbiditic and non-turbiditic mudstones of Cretaceous flysch sections of the Eastern Alps and other basins: *Sedimentology*, v. 22, p. 387-416.

HESSE, R., 1982. Cloridorme Formation, in R. Hesse, G.V. Middleton, and B.R. Rust (eds.), Field Excursion Guide Book 7B: Paleozoic Continental Margin Sedimentation in the Québec Appalachians. Eleventh International Congress on Sedimentology, Hamilton, Ontario, Canada p.126-138.

HESSE, R., 1995a. Bed-by-bed correlation of trench-plain turbidite sections, Campanian Zementmergel Formation, Rhenodanubian flysch zone of the east Alps, in K.T. Pickering, R.N. Hiscott, R.N., N.H., Kenyon, F. Ricci Lucchi, and R.D.A., Smith (eds.), *Atlas of Deep Water Environments: Architectural Style in Turbidite Systems*: London, Chapman & Hall, p. 307-310.

HESSE, R., 1995b. Long-distance correlation of spillover turbidites on the western levee on the Northwest Atlantic Mid-ocean Channel (NAMOC), Labrador Sea, in K.T. Pickering, R.N. Hiscott, R.N., N.H., Kenyon, F. Ricci Lucchi, and R.D.A., Smith (eds.), *Atlas of Deep Water Environments: Architectural Style in Turbidite Systems*: London, Chapman & Hall, p. 276-281.

HESSE, R., AND CHOUGH, S.K., 1980. The Northwest Atlantic Mid-Ocean Channel of the Labrador Sea: II deposition of parallel laminated levee-muds from the viscous sublayer: *Sedimentology*, v. 27, p. 697-711.

HISCOTT, R.N., 1977. Sedimentology and Regional Implications of Deep-Water Sandstone of the Tourelle Formation, Ordovician, Quebec. Ph.D. Thesis, McMaster University, Hamilton, Ontario, 570pp.

HISCOTT, R.N., 1979. Clastic sills and dikes associated with deep-water sandstones, Tourelle Formation, Ordovician, Québec: *Journal of Sedimentary Petrology*, v. 49, p 1-9.

HISCOTT, R.N., 1980. Depositional framework of sandy mid-fan complexes of Tourelle Formation, Ordovician, Québec: *American Association of Petroleum Geologists Bulletin*, v. 64, p. 1052-1077.

HISCOTT, R. N., 1981. Chi-square tests for Markov Chain analysis: *Mathematical Geology*, v. 13, p. 69-80.

HISCOTT, R.N., 1984. Ophiolitic source rocks for Taconic-age flysch: Trace-element evidence: *Geological Society of America Bulletin*, v. 95, p. 1261-1276

HISCOTT, R.N., 1994. Traction-carpet stratification in turbidites-fact or fiction?: *Journal of Sedimentary Petrology*, v. 64, p. 204-208.

HISCOTT, R.N., AND MIDDLETON, G.V., 1979. Depositional mechanics of thick-bedded sandstones at the base of a submarine slope, Tourelle Formation (Lower Ordovician), Québec, Canada, *in* L.J. Doyle, and O.H. Pilkey, Jr., (eds.), *Geology of Continental Slopes*. Special Publication 27, Society of Economic Paleontologists and Mineralogists, p. 307-326.

HISCOTT, R.N., AND PICKERING, K.T., 1984. Reflected turbidity currents on an Ordovician basin floor: *Nature*, v. 311, p. 143-145.

HISCOTT, R.N., PICKERING, K.T., and BEEDEN, D.R., 1986. Progressive filling of a confined Middle Ordovician foreland basin associated with the Taconic Orogeny, Québec, Canada, *in* P.A., Allen and P. Homewood (eds.), *Foreland Basins*. Special Publication of the International Association of Sedimentologists, No. 8: Oxford, Blackwell Scientific Publication, p. 309 - 325.

HISCOTT, R.N., COLELLA, A., PEZARD, P., LOVELL, M.A., AND MALINVERNO, A., 1992. Sedimentology of Deep-water volcanoclastic, Oligocene Izu-Bonin forearc basin, based on formation microscanner images: *Proceedings of the Ocean Drilling Program*, v. 126, p. 75-96.

HISCOTT, R.N., COLELLA, A., PEZARD, P., LOVELL, M.A., AND MALINVERNO, A., 1993. Basin plain turbidite succession of the Oligocene Izu-Bonin intraoceanic forearc basin: *Marine and Petroleum Geology*, v. 10, p. 450-466.

HISCOTT, R.N., PICKERING, K.T., BOUMA, A.H., HAND, B.R., KELLER, B.R., POSTMAN, G., AND SOH, W. 1998. Basin floor fans in the North Sea: sequence stratigraphic models vs sedimentary facies, a discussion: *American Association of Petroleum Geologists Bulletin*, v. 81, p. 662-665.

HSU, K.J., 1983. Actualistic catastrophism, address of the retiring president of the International association of Sedimentologists: *Sedimentology*, v. 30, p. 3-9.

HUFF, W.S., 1983. Correlation of Middle Ordovician K-bentonite based on chemical fingerprinting: *Journal of Geology*, v. 91, p. 657-669.

HUFF, W.S., AND KOLATA, D.R., 1989. Correlation of K-bentonite beds by chemical fingerprinting using multivariate statistics, *in* T.A. Cross (ed.), *Quantitative Dynamic Stratigraphy*: New Jersey, Prentice Hall, p. 567-577.

HUFF, W.S., BERGSTRÖM, S.M., AND CELIATA, D.R., 1992. Gigantic Ordovician volcanic ash fall in North America and Europe: biological, tectonomagmatic, and event-

stratigraphic significance: *Geology*, v. 20, p. 875-878.

HURST, A., CRONIN, B., AND HARTLEY, A., 2000. Reservoir modelling sand-rich deep-water clastics: the necessity of down-scaling: *Petroleum Geoscience*, v. 6, p. 67-76.

INGRAM, R. L., 1954. Terminology for the thickness of stratification and parting units in sedimentary rocks: *Geological Society of America Bulletin*, v. 65, p. 937-938.

JENNER, G.A., 1996. Trace element geochemistry of igneous rocks: geochemical nomenclature and analytical geochemistry, in D.A. Wyman (ed.), *Trace Element Geochemistry of Volcanic Rocks: Application for Massive Sulfide Exploration*. Geological Association of Canada, Short Course Notes 12, p. 51-78.

JOHANSSON, M., AND STOW, D.A.V., 1995. A classification scheme for shale clasts in deep water sandstones, in A.J. Hartley and D.J. Prosser (eds.), *Characterization of Deep Marine Clastic Systems*. Geological Society Special Publications. Special Publication 94, p. 221-241.

JOPLING, A.V., AND WALKER, R.G., 1968. Morphology and origin of ripple-drift cross-lamination, with examples from the Pleistocene of Massachusetts: *Journal of Sedimentary Petrology*, v. 38, p. 971-984.

KESSLER, L.G. II, PRAVE, A.R., AND MCMILLEN, K.J., 1990. Origin of aggradational and multi-directional bedding in submarine density current deposits, Middle Ordovician, Québec and Newfoundland, Canada. The Thirteenth International Sedimentological Congress Abstracts, p. 266-267.

KESSLER, L.G. II, MCMILLEN, K.J., PRAVE, A.R. 1990. Sediment bypassing and sand deposition in muddy turbidites, Ordovician Cloridorme Formation, Gaspé, Québec, Canada. The Thirteenth International Sedimentological Congress Abstracts, p. 267-268.

KESSLER, L.G. II, PRAVE, A.R. MALO, M., BLOECHI, W.W., 1995. Mid-Upper Ordovician flysch deposition, northern Gaspé Peninsula, Québec; a synthesis with implications for foreland and successor basin evolution in the Northern Appalachian Orogen, in J.D. Cooper, M.L., Droser, and S.C. Finney, (eds.), *Ordovician odyssey; short papers for the Seventh international symposium on the Ordovician System*. Pacific Section, Society of Economic Paleontologists and Mineralogists. Field Guide 77, p 251-255.

KNELLER, B., 1995. Beyond the turbidite paradigm: physical models for deposition of turbidites and their implications for reservoir prediction, in A.J. Hartley, and D.J. Prosser,

(eds.), *Characterization of Deep Marine Clastic Systems*. Geological Society of London, Special Publication 94, p. 31-49.

KNELLER, B., AND BRANNEY, M.J., 1995. Sustained high-density turbidity currents and the deposition of thick massive sands: *Sedimentology*, v. 42, p. 607-616.

KNELLER, B., AND BUCKEE, C., 2000. The structure and fluid mechanics of turbidity currents: a review of some recent studies and their geological significance: *Sedimentology*, v. 47, p. 62-94.

KOLATA, D.R., FROST, J.K., AND HUFF, W.S., 1986. K-bentonite of the Ordovician Deborah Subgroup, upper Mississippi Valley: Correlation by chemical fingerprinting. Illinois State Geological Survey Circular, 537, 30p.

KOLATA, D.R., HUFF, W.S., AND BERGSTRÖM, 1996. Ordovician K-bentonite of eastern North America. Geological Society of America Special Paper 313, 84pp.

KRUMBEIN, W.C., AND GRAYBULL, F.A., 1967. *An Introduction to Statistical Models in Geology*. New York, McGraw Hill, 475pp.

KRUMBEIN, W.C., AND DACEY, M.F., 1969. Markov chains and embedded chains in geology: *Journal of the International Association of Mathematical Geology*, v. 1, p. 79-96.

LACHAMBRE, G., AND BRISEBOIS, D., 1990. Géologie de la Gaspésie, Cloridorme, Québec. Ministère de l'Énergie et des Ressources du Québec; Carte 2151 du DV 91-22.

LARUE, D.K., AND PROVINE, K.G., 1988. Vacillatory turbidites, Barbados: *Sedimentary Geology*, v. 57, p. 211-219.

LOGAN, W.E., 1883. Report on geology of Canada. Geological Survey of Canada, Report of Progress to 1863, 983pp.

LONGERICH, H.P., 1995. Analysis of pressed pellets of geological samples using wavelength-dispersive X-ray fluorescence spectrometry: *X-Ray Spectrometry*, v. 24, p. 123-136.

LOWE, D.R., 1975. Water escape structures in coarse-grained sediments: *Sedimentology*, v. 22, p. 157-204.

LOWE, D.R., 1982. Sediment gravity flows: II. Depositional models with special reference to the deposits of high-density turbidity currents: *Journal of Sedimentary*

Petrology, v. 52, p. 279-297.

LOWE, D.R., 1997. Reinterpretation of depositional processes in a classic flysch sequence (Pennsylvanian Jackfork Group), Ouachita Mountains, Arkansas and Oklahoma; discussions and reply: American Association of Petroleum Geologists Bulletin, v. 81, p. 449-491

LOWE, D.R., AND GUY, M. 2000. Slurry-flow deposits in the Britannia Formation (Lower Cretaceous), North Sea; a new perspective on the turbidity current and debris flow problem: Sedimentology, v. 47, p 31-70.

LYNCH, G., 1998. Characteristics of the Taconic orogenic front, northeastern Québec Appalachians. In Current Research, Geological Survey of Canada, 1998-D, p. 1-9.

LYNCH, G., AND ARSENAULT, O., 1997. Stratigraphy and deformation of the Humber Zone in Gaspésie, Quebec. In Current Research, Geological Survey of Canada, 1997-D, p. 1-8.

MA, C. 1996. Continuity of sandstone beds in the Ordovician Cloridorme Formation, Gaspé Peninsula, Québec. MSc. thesis, Memorial University of Newfoundland, 158pp.

MALINVERNO, A, 1997. On the power law size distribution of turbidite beds: Basin Research, v. 9, p. 263-274.

MARSHAK, S., AND MITRA, G. 1988. *Basic Methods of Structural Geology*: New Jersey, Prentice Hall, 446pp.

MCBRIDE, E. F., 1962. Flysch and associated beds of the Martinsburg Formation (Ordovician), Central Appalachians: Journal of Sedimentary Petrology, v. 32, p. 39-91.

MCCAVE, I.N., AND JONES, P.N., 1988. Deposition of ungraded muds from high-density nonturbulent turbidity currents: Nature, v. 333, p. 250-252.

MCGERRIGLE, H. W., 1954. An outline of the Geology of Gaspé Peninsula: Canadian Mining Journal, v. 75, p. 57-63.

MIALL, A.D., 1973. Markov chain analysis applied to an ancient alluvial plain succession: Sedimentology, v. 20, p. 347-364.

MIALL, A.D., 1982. Analysis of fluvial depositional systems. American Association of Petroleum Geologists Continuing Education Course Note Series. 20, 75pp.

- MIALL, A.D., 1985. Architectural, element analysis: a new method of facies analysis applied to fluvial deposits: *Earth-Science Reviews*, v. 22, p. 261-308
- MIALL, A.D., 1995. Collision-related foreland basins, in C.J. Busby and R.V. Ingersoll (eds.), *Tectonics of Sedimentary Basins*: Oxford, Blackwell, p. 393-424.
- MIDDLETON, G.V., 1967. Experiments on density and turbidity currents: III. Deposition of sediment: *Canadian Journal of Earth Sciences*, v. 4, p. 475-505.
- MIDDLETON, G.V., 1970. Experimental studies related to problems of flysch sedimentation, in J. Lejoie, (ed.), *Flysch Sedimentology in North America*. Geological Association of Canada Special Paper 7, p. 253-272.
- MIDDLETON, G.V., 1993. Sediment deposition from turbidity currents: *Annual Review of Earth and Planetary Sciences*, v. 21, p. 89-114.
- MIDDLETON, G.V., AND HAMPTON, M.A., 1976, Subaqueous sediment transport and deposition by sediment gravity flows, in D.J. Stanley, and D.J.P. Swift, (eds.), *Marine Sediment Transport and Environmental Management*: New York, Wiley-Interscience, p. 197-218.
- MIDDLETON, G.V., AND SOUTHARD, J.B., 1984. *Mechanics of Sediment Movement*. Society of Economic Paleontologists and Mineralogists Short Course 3, 401 p.
- MULDER, T., AND ALEXANDER, J., 2001. The physical character of subaqueous sedimentary density flows and their deposits: *Sedimentology*, v. 48, p. 269-299.
- MUTTI, E., 1977. Distinctive thin-bedded turbidite facies and related depositional environments in the Eocene Hecho Group (south-central Pyrenees, Spain): *Sedimentology*, v. 24, p. 107-131.
- MUTTI, E., 1992. *Turbidite Sandstone*: Milan, Agip, 275 pp.
- MUTTI, E, AND RICCI-LUCCI, F., 1972. Turbidites of the northern Apennines: introduction to facies analysis: *International Geological Reviews*, v. 20, p. 125-166.
- MUTTI, E., AND JOHNS, D.R., 1978. The role of sedimentary bypassing in the genesis of fan fringe and basin plain turbidites in the Hecho Group System (South-Central Pyrenees): *Memorie Società Geologica Italiana*, v. 18, p. 125-133.
- MUTTI, E., AND NILSEN, T. H., 1981. Significance of intraformational rip-up clasts in

deep-sea fan deposits: International Association of Sedimentologists second European Meeting Abstracts, Bologna, p. 117-119.

MUTTI, E., AND SONNINO, M., 1981. Compensation cycles: a diagnostic feature of turbidite sandstone lobes: International Association of Sedimentologists second European Meeting Abstracts, Bologna, p. 120-123.

MUTTI, E., AND NORMARK, W.R., 1987. Comparing examples of modern and ancient turbidite systems: problems and concepts, in J.K. Leggett and G.G. Zuffa, (eds.), *Marine Clastic Sedimentology: Concepts and case studies*: London, Graham and Trotman, p. 1-38.

MUTTI, E., AND NORMARK, W.R., 1991. An integrated approach to the study of turbidite systems, in P. Weimer, and M.H. Link, (eds.), *Seismic Facies and Sedimentary Processes of Submarine Fans and Turbidite Systems*: New York, Springer-Verlag, p. 75-106.

MUTTI, E., NILSON, C.H., AND RICCI-LUCCI, F., 1978. Outer fan depositional lobes of the Laga Formation (upper Miocene and lower Pliocene), east-central Italy, in D.J. Stanley, and G. Kelling, (eds.), *Sedimentation in Submarine Canyons, Fans and Trenches*: Stroudsburg, Dowden, Hutchinson and Ross, p. 210-233..

MUTTI, E., RICCI LUCCHI, F., SEGURET, M., AND ZANZICCHI, G., 1984. Seismoturbidites: a new group of resedimented deposits: *Marine Geology*, v. 55, p. 103-116.

MUTTI, E., DAVOLI, G., MORA, S., AND PAPANI, L., 1994, Internal stacking patterns of ancient turbidite systems from collisional basins, in P. Weimer, A.H. Bouma, and B.F. Perkins (eds.), *Submarine Fans and Turbidite Systems*. Gulf Coast Section, Society of Economic Paleontologists and Mineralogists, Fifteenth Annual Research Conference, p. 257-268.

MUTTI, E., TINTERRI, R., REMACHA, E., MAVILLA, N., ANGELLA, S., AND, FAVA, L. 1999. *An Introduction to the Analysis of Ancient Turbidite Basins from an Outcrop Prospective*. American Association of Petroleum Geologists Continuing Education Course Notes Series #39, 61pp.

NILSEN, T.H., 1980. Modern and ancient submarine facies: discussion of papers by R. G. Walkers and W. R. Normark: *American Association of Petroleum Geologists Bulletin*, v. 64, p. 1094-1112.



NISHIWAKI, N. 1978. Simulation of bed thickness distribution based on waiting time in the Poisson process. *International Congress on Sedimentology* 10, v. 2, p. 468-469.

NORMARK, W. R., 1970. Growth patterns of deep-sea fans: *American Association of Petroleum Geologists Bulletin*, v. 54, p. 2170-2195.

NORMARK, W.R., 1985. Local morphologic controls and effects of basin geometry on flow processes in deep sea basins, in G.G. Zuffa, (ed.), *Provenance of Arenites*, NATO-AI Series: Dordrecht, Reidel, p. 65-93.

NORMARK, W.R., POSAMENTIER, H., AND MUTTI, E., 1993. Turbidite systems: state of the art and future directions: *Review in Geophysics*, v., 31, p. 91-116.

NORTH AMERICAN COMMISSION ON STRATIGRAPHIC NOMENCLATURE, 1983. North American stratigraphic code: *American Association of Petroleum Geologists Bulletin*, v. 67, p. 841-875.

OJAKANGAS, R.W., 1968. Cretaceous sedimentation, Sacramento Valley, California: *Geological Society of America Bulletin*, v. 79, p. 973-1008.

PANTIN, H.M., AND LEEDER, M.R., 1987. Reverse flow in turbidity currents: the role of internal solitons: *Sedimentology*, v. 34, p. 1143-1155.

PARKASH, B., 1969. Downcurrent changes in sedimentary structures in Ordovician turbidite greywackes: *Journal of Sedimentary Petrology*, v. 40, p. 572-590.

PARKASH, B. AND MIDDLETON, G.V., 1970. Downcurrent textural changes in Ordovician turbidite greywackes: *Sedimentology*, v. 14, p. 259-293.

PEARCE, J.A., 1996. A user's guide to basalt discrimination diagrams, in D.A. Wyman, (ed.), *Trace Element Geochemistry of Volcanic Rocks: Application for Massive Sulfide Exploration*. Geological Association of Canada, Short Course Notes v. 12, p. 79-114.

PEARCE, J.A., AND CANN, J.R., 1973. Tectonic setting of basic volcanic rocks determined using trace element analyses: *Earth and Planetary Science Letters*, v. 19, p. 290-300.

PETT, J. W., AND WALKER, R. G., 1971. Relationship of flute cast morphology to internal sedimentary structures in turbidites: *Journal of Sedimentary Petrology*, v. 41, p. 114-128.

- PETTIJOHN, F.J., 1957. *Sedimentary Rocks*: New York, Harper & Row, 718pp.
- PICKERING, K.T., 1981. Two types of outer fan lobe sequence, from the late Precambrian Kongsfjord Formation submarine fan, Finnmark, north Norway: *Journal of Sedimentary Petrology*, v. 51, p. 1277-1286.
- PICKERING, K.T., 1987. Deep-marine foreland basin and forearc sedimentation: a comparative study from the Lower Paleozoic northern Appalachians, Québec and Newfoundland, in Leggett, J.K., and Zuffa, G.G., (eds.), *Marine Clastic Sedimentology*: London, Graham & Trotman, p. 190-211.
- PICKERING, K.T., AND HISCOTT, R.N., 1985. Contained (reflected) turbidity currents from the Middle Ordovician Cloridorme Formation, Québec, Canada: an alternative to antidune hypothesis: *Sedimentology*, v., 32, p. 373-394.
- PICKERING, K.T., AND HISCOTT, R.N., 1995. Foreland basin-floor turbidite system, Cloridorme Formation, Québec, Canada: long-distance correlation in sheet turbidites, in Pickering, K.T., Hiscott, R.N., Kenyon, N.H., Ricci Lucchi, F., and Smith, R. (eds.), *Atlas of Architectural Styles in Turbidite Systems*, London, Chapman & Hall, p.310 -316 .
- PICKERING, K.T., AND HILTON, V.C., 1997. *Turbidite Systems of Southeast France* :London, Vallis Press, 229 pp.
- PICKERING, K.T., HISCOTT, R.N., AND HEIN, F.J., 1989. *Deep Marine Environments: Clastic Sedimentation and Tectonics*: London, Unwin Hyman, 416pp.
- PICKERING, K.T., CLARK, J.D., SMITH, R.D.A., HISCOTT, R.N., RICCI LUCCI, F., AND KENYON, N.H., 1995. Architectural element analysis of turbidite systems, and selected topical problems for sand-prone deep water systems, in K.T. Pickering, R.N. Hiscott, R.N., N.H., Kenyon, F. Ricci Lucchi, and R.D.A., Smith (eds.), *Atlas of Deep Water Environments: Architectural Style in Turbidite Systems*, London, Chapman & Hall, p. 1-13.
- PILKEY, O.H., 1988, Basin plains; giant sedimentation events, in E.E. Clifton (ed.), *Sedimentologic Consequences of Convulsive Geologic Events*. Geological Society of America Special Paper 299, p. 93-99.
- PIPER, D.J.W., 1978. Turbidite muds and silts on deep sea fans and abyssal plains, in D.J., Stanley, and G. Kelling, (eds.), *Sedimentation in Submarine Canyons, Fans and Trenches*: Stroudsburg, Dowden, Hutchinson and Ross, p.163-175..

- PIPER, D.J.W., AND NORMARK, W.R., 2001. Sandy fans-from Amazon to the Hueneme and Beyond: American Association of Petroleum Geologists Bulletin, v. 85, p. 1407-1438.
- PIPER, D.J.W., HISCOTT, R.N., AND NORMARK, W.R., 1999. Outcrop-scale acoustic facies analysis and latest Quaternary development of Hueneme and Dume submarine fans, offshore California: Sedimentology, v. 46, p. 47-78.
- PIRMEZ, C., HISCOTT, R.N., AND KRONEN, J.D., JR, 1997. Sandy turbidite succession at the base of channel-levee system of the Amazon Fan revealed by FMS logs and cores: unravelling the facies architecture of large submarine fans, *in* Proceedings of the Ocean Drilling Program, Scientific Results, Flood, R.D., Piper, D.J.W., Klaus, A., and Peterson, L.C. (eds.), v. 155, p. 7-33.
- POSTMA, G., NEMEC, W., AND KLEINSPEHN, K.L., 1988. Large floating clasts in turbidites: a mechanism for their emplacement: Sedimentary Geology, v. 58, p. 47-61.
- POTTS, P.J., TINDLE, A.G., and WEBB, P.C., 1992. *Geochemical Reference Material Compositions*: Boca Raton, Whittles Publishing, Caithness, UK, CRC Press, Inc, 313pp.
- POWERS, D.W., AND EASTERLING, R.G., 1982. Improved methodology for using embedded Markov chains to describe cyclical sediments: Journal of Sedimentary Petrology, v. 52, p. 913-923.
- PRAVE, A.R., KESSLER, L.G., MALO, M., BLOEHL, W.V., AND RIVA, J., 2000. Ordovician arc collision and foredeep evolution in the Gaspé Peninsula, Québec; the Taconic Orogeny in Canada and its bearing on the Grampian Orogeny in Scotland: Journal of the Geological Society of London, v 157, p 393-400.
- RAMSAY, J. G., 1961. The effect of folding upon the orientation of sedimentary structures: Journal of Geology, v., 69, p. 84-100.
- READING, H.G., AND ORTON, G.J., 1991. Sediment caliber: a control on facies models with special reference to deep-sea depositional systems, *in* D.W., Müller, J.A., Mackenzie, and H. Weissert, (eds.), *Controversies in Modern Geology*, London, Academic Press, p. 85-111.
- READING, H. .G., AND RICHARDS, M. 1994. Turbidite systems in deep-water basin margins classified by grain size and feeder system: American Association of Petroleum Geologists Bulletin, v. 78, p.792-822.

READING, H.G., AND LEVELL, B.K., 1996. Controls on the sedimentary rock record, in H.G., Reading, (ed.), *Sedimentary Environments and Facies*, 3rd Edition: Oxford, Blackwell, p. 5-36.

RICCI LUCCHI, F., 1969. Channelized deposits in the middle Miocene flysch of Romagna (Italy): *Giornale di Geologia*, v. 36, p. 203-260.

RICCI LUCCHI, F., 1975. Miocene paleogeography and basin analysis in the Periadriatic Apennines, in C. Squyres, (ed.), *Guidebook to the Geology of Italy: Tripoli, Libya*, p. 129-236.

RICCI LUCCHI, F., 1981. The Marnoso-Arenacea turbidites, Romagna and Umbria Apennines, in F. Ricci Lucchi (ed.), *Excursion guide book, with contribution of sedimentology of some Italian basins. Second International Association of Sedimentologists European Meeting, Bologna*, pp. 229-303.

RICCI LUCCHI, F., 1990. Turbidites in foreland and on-thrust basins of the northern Apennines: *Palaeogeography, Palaeoclimatology, Palaeoecology*, v. 77, p. 51-66.

RICCI LUCCHI, F AND VALMORI, E. 1980. Basin-wide turbidites in a Miocene, over supplied deep-sea plain: a geometric analysis: *Sedimentology*, v. 27, p. 241-270.

RICHARDS, M.T., BOWMAN, M., READING, H.G., 1998. Submarine-fan systems I: characterisation and stratigraphic prediction: *Marine and Petroleum Geology*, v. 15, p. 689-717.

RIVA, J., 1968. Graptolite faunas from the Middle Ordovician of the Gaspé north shore: *Naturaliste Canadien*, v. 93, p. 1379-1400.

RIVA, J., 1974. A revision of some Ordovician graptolites of eastern North America: *Palaeontology*, v. 17, p. 1-40.

RIVA, J., AND MALO, M. 1988. Age and correlation of the Honorat Group, southern Gaspé Peninsula: *Canadian Journal of Earth Sciences*, v. 25, p. 1618-1628.

ROSS, C.A., AND ROSS, J.R.P., 1995. North American Ordovician depositional sequences and correlations, in J.D. Cooper, M.L., Droser, and S.C. Finney, (eds.), *Ordovician odyssey; short papers for the Seventh international symposium on the Ordovician System*. Pacific Section, Society of Economic Paleontologists and Mineralogists. Field Guide 77, p 309-313.

ROTHMAN, D.H., AND GROTZINGER, J.P., 1995. Scaling properties of gravity-driven sediments: Nonlinear processes in Geophysics, v. 2, p. 178-185.

ROTHMAN, D.H., GROTZINGER, J.P., AND FLEMINGS, P.B., 1994. Scaling in turbidite deposition: Journal of Sedimentary Research, v. 64, p. 59-67.

ROTHWELL, R.G., PEARCE, T.J., and WEAVER, P.P.E., 1992. Late Quaternary evolution of the Madeira Abyssal Plain, Canary Basin, NE Atlantic, Basin Research, v., 4, p. 103-131.

ROYCE, P.R., 1992. Provenance analysis of synorogenic strata using Cr and Ni concentrations in shale deposited during the Middle Ordovician Orogeny, western Newfoundland,. B.Sc. Thesis, Union College, Schenectady, New York.

ROZMAN, D.J., 2000. Characterization of a fine-grained outer submarine fan deposit, Tanqua-Karoo Basin, South Africa, in A. H., Bouma, and C.G. Stone, (eds.), *Fine-grained turbidite systems*. American Association of Petroleum Geologists Memoir 72/ Society of Economic Paleontologists and Mineralogists Special Publication 68, p. 279-289.

SCHWARZACHER, W., 1972. The semi-Markov process as a general sedimentation model, in Mathematical models of sedimentary processes, p. 247-268.

SCHWARZACHER, W., 1975. *Sedimentation Models and Quantitative Stratigraphy*: Amsterdam, Elsevier, 382 p.

SHANMUGAM, G., 1997. The Bouma Sequence and the turbidite mind set: Earth-Science Reviews, v. 42, p. 201-229.

SHANMUGAM, G., 2000. 50 years of the turbidite paradigm (1950s-1990s): deep-water processes and facies models-a critical prospective: Marine and Petroleum Geology, v. 17, p. 285-432.

SHANMUGAM, G., AND MOIOLA, R.J., 1988. Submarine fans: characteristics, models, classification, and reservoir potential: Earth-Science Reviews, v. 24, p. 383-428.

SHANMUGAM, G., AND MOIOLA, R.J., 1991. Types of submarine fan lobes: Models and implications: American Association of Petroleum Geologists, v. 75, p. 156-179.

SHANMUGAM, G., BLOCH, R.B., DAMUTH, J.E., AND HODGKINSON, R.J., 1997. Basin-floor fans in the North Sea: sequence stratigraphic models vs. sedimentary facies: reply: American Association of Petroleum Geologists, v. 81, p. 666-672.

SKIPPER, K., 1971. Antidune cross-stratification in a turbidite sequence, Cloridorme Formation, Gaspé, Québec: *Sedimentology*, v. 17, p. 51-58.

SKIPPER, K., AND MIDDLETON, G.V., 1975. The sedimentary structures and depositional mechanics of certain Ordovician turbidites, Cloridorme Formation, Gaspé, Québec: *Canadian Journal of Earth Sciences*, v. 12, p. 1934-1952.

SKIPPER, K., AND S. B. BHATTACHARJEE, S.B., 1978. Backset Bedding in Turbidites: A Further Example from the Cloridorme Formation (Middle Ordovician), Gaspé, Québec: *Journal of Sedimentary Petrology*, v. 48, p. 193-201.

SLIVITZKY, A., ST-JULIEN, P., AND LACHAMBRE, G., 1991. Synthèse géologique du Cambro-Ordovicien du nord de la Gaspésie. Ministère de l'Énergie et des Ressources du Québec MM-85-04, 40p.

SOUTHARD, J. B. AND MACKINTOSH, M. E., 1981. Experimental test of auto-suspension: *Earth Surface Processes and Landforms*, v. 6, p. 103-111.

SPSS, 1999. SPSS© Base 9.0 Application Guide, SPSS. © Inc, 444 N. Michigan Avenue, Chicago, Illinois, USA, 412pp.

ST-JULIEN, P., AND HUBERT, C., 1975. Evolution of the Taconian Orogen in the Québec Appalachians: *American Journal of Science*, v. 275-A, p. 337-362.

STANLEY, D. J., AND BOUMA, A. H., 1964. Methodology and paleogeographic interpretation of flysch formations: A summary of studies in the Maritime Alps, in A. H. Bouma and A. Brouwer, (eds.), *Turbidites*. Amsterdam, Elsevier, p. 34-64.

STELTING, C.E., BOUMA, A.H., AND STONE, C.G., 2000. Fine-grained turbidite systems: overview, in A.H., Bouma, and C.G. Stone, (eds.), *Fine-Grained Turbidite Systems*. American Association of Petroleum Geologists Memoir 72/Society of Economic Paleontologists and Mineralogists Special Publication No. 68, p. 1-8.

STOW, D.A.V., AND BOWEN, A.J., 1980. A physical model for the transport and sorting of fine-grained sediments by turbidity currents: *Sedimentology*, v. 27, p. 31-46.

STOW, D.A.V, AND JOHANSSON, M., 2000. Deep-water massive sands; nature, origin

and hydrocarbon implications, in D.A.V. and Mayall, M. (eds.), *Deep-water sedimentary systems; new models for the 21st century*: Oxford, Pergamon, p. 145-174.

STOW, D.A.V., AND PIPER, D.J.W., 1984. Deepwater fine-grained sediment: facies models, in Stow, D.A.V., and Piper, D.J.W., (eds.), *Fine-Grained Sediments: Deep-Water Processes and Facies*. Special Publication 15, Geological Society of London, p. 611-646.

STOW, D.A.V. AND TABAREZ, A.R., 1998. Hemipelagites; processes, facies and model, in M.S. Stoker, D. Evans and A. Cramp (eds.), *Geological Processes on Continental Margins; Sedimentation, Mass-Wasting and Stability*. Special Publications 129, Geological Society of London, p 317-337.

STOW, D.A.V., READING, H.G., AND COLLINSON, J.D., 1996. Deep seas, in H.G., Reading, (ed.), *Sedimentary Environments and Facies*: Oxford, Blackwell, p. 395-453.

SWAN, A.R.H., AND SANDILANDS, M., 1995. *Introduction to Geological Data Analysis*: Oxford, Blackwell Science, 446p.

TALLING, P.J., 2001. On the frequency distribution of turbidite thickness: *Sedimentology*, v. 48, p. 1297-1329.

THORNBURG, T.M., AND KULM, L.D., 1987. Sedimentation in the Chile Trench: depositional morphologies, lithologies, and stratigraphy: *Geological Society of America Bulletin*, v. 98, p. 32-52.

TOKUHASHI, S., 1979. Three dimensional analysis of a large sandy-flysch body, Mio-Pliocene Kiyumi Formation, Boso Peninsula, Japan: *Memoirs of the faculty of Science, Kyoto University, Series of Geology & Mineralogy*, v. 46, p. 1-60.

VAN HOORN, B., 1970. Sedimentology and paleogeography of an Upper Cretaceous turbidite basin in the south-central Pyrenees, Spain: *Leidse Geologische Mededelingen*, v. 45, p. 73-154.

VAN TASSEL, J., 1981. Silver abyssal plain carbonate turbidite: flow characteristics: *Journal of Geology*, v. 89, p. 317-333.

WALKER, R. G., 1965. The origin and significance of the internal sedimentary structures of turbidites: *Yorkshire Geological Society Proceedings*, v.35, p.1-32.

WALKER, R. G., 1967. Turbidite sedimentary structures and their relationship to

proximal and distal depositional environments: *Journal of Sedimentary Petrology*, v. 37, p. 25-43.

WALKER, R. G., 1969. Geometrical analysis of ripple-drift cross-lamination: *Canadian Journal of Earth Science*, v. 6, p. 383-391.

WALKER, R. G., 1970. Review of the geometry and facies organization of turbidites and turbidite-bearing basins, in J. Lejoie, (ed.), *Flysch Sedimentology in North America*. Special Paper 7, Geological Association of Canada, p. 219-251.

WALKER, R. G., 1978. Deep water sandstone facies and ancient submarine fans: models for exploration for stratigraphic traps: *American Association of Petroleum Geologists Bulletin*, v.62, p. 932-966.

WALKER, R.G., 1985. Mudstones and thin-bedded turbidites associated with the Upper Cretaceous Wheeler Gorge Conglomerates: a possible channel-levee complex: *Journal of Sedimentary Petrology*, v. 55, p. 279-290.

WALTON, E.K., STEPHENS, W.E., AND SHAW, M.S., 1980. Reading segmented grain-size curves: *Geological Magazine*, v. 117, p. 517-524.

WEAVER, P.P.E., ROTHWELL, R.G., EBBING, J., GUNN, D., AND HUNTER, P.M., 1992. Correlation, frequency of emplacement and source directions of megaturbidites on the Madeira Abyssal Plain: *Marine Geology*, v. 109, p. 1-20.

WILLIAMS, H., 1979. Appalachian Orogen in Canada: *Canadian Journal of Earth Sciences*, v. 16, p. 792-807.

WINCHESTER, J.A., AND FLOYD, P.A., 1977. Geochemical discrimination of different magma series and their differentiation products using immobile elements: *Chemical Geology*, v. 20, p. 325-343.

WINKLER, W, AND GAWENDA, P. 1999. Distinguishing climatic and tectonic forcing of turbidite sedimentation, and the bearing on turbidite bed scaling: Palaeocene-Eocene of northern Spain: *Journal of the Geological Society of London*, v. 156, p. 791-800.

WOODWARD, N.B., BOYER, S.E., AND SUPPE, J. 1989. Balanced Geological Cross-Sections. American Geophysical Union, Short Course in Geology, 132pp.



## **APPENDICES**

**APPENDIX A1**

**LOCATION OF THE ROCKS AND BEDS PRESENTED IN THE PLATES**

**APPENDIX A1: LOCATION OF THE BEDS PRESENTED IN THE PLATES**

The location of the photographs given in this table is with reference to their level within the sections presented in Appendix A2. For example, the bed of subfacies D2.1A presented in plate P2.1. is located at about 257 m above the base of the section.

**Plate 1.**

- P1.1. At ~ 20 m level in section FP2 between megaturbidites 38-FP2 and 39-FP2.
- P1.2. At ~155 m level in section PF.

**Plate 2.**

- P2.1. Lower ~10 m of section SYW.
- P2.2. At ~70 m level in section PCDR.

**Plate 3.**

- P3.1. At ~ 257 m level in section RE.
- P3.2. At ~ 102 m level in section SYW.
- P3.3. At ~188 m level in section SYE.
- P3.4. At ~21 m level in section SH.

**Plate 4.**

- P4.1. At ~ 160 m level in section SYE.
- P4.2. At ~ 186 m level in section SH.
- P4.3. At ~ 97 m level in section FP1.
- P4.4. At ~188 m level section SH.

**Plate 5.** At ~358 m level in section PF.

**Plate 6.** At ~20 m level in section PH

**Plate 7.**

- P7.1. At ~147 m level in section CB.
- P7.2. At ~278 m level in section SYE.
- P7.3. At ~110 m level in section CB.
- P7.4. At ~110 m level in section CB.

**APPENDIX A1. Continued****Plate 8.**

- P8.1. At ~101 m level in section PCDR.
- P8.2. At ~111 m level in section FP1.
- P8.3. At ~351 m level in section SYE.

**Plate 9. Megaturbidites.**

- P8.1. At ~73 m level in section FP1.
- P8.2. At ~469 m in section PF.
- P8.3. At ~215 m to 225 m level in section SH.
- P8.4. At ~41 m in section FP2.

**Plate 10.**

- P10.1. At ~48 m level in section PCDR.
- P10.2. At ~ 50 m level in section PCDR.
- P10.3. At ~765 m level in section PF.

**APPENDIX A2**

**DESCRIPTION OF THE AREAS OF THE MEASURED SECTIONS**

## **A2. DETAILED DESCRIPTION OF THE AREAS OF MEASURED SECTIONS**

### **A2.1. Sections RE, FP1, FP2, PCDR, PRM1 and PRM2 (Figure 2.2, Appendix A3)**

The RE section (802417) was measured in the wave-cut platform at the headland to the west of the mouth of Ruisseau à l'Ail (811410). Sections FP1 and FP2 were measured in the wave-cut platforms and headlands to the east (817412 and 817411, respectively).

The wave-cut platform at section RE is adequate for detailed measurements although some parts of this section are only exposed at very low tide. Some parts of the section were described from the cliff adjacent to the wave-cut platform. The beds are steeply dipping (Table 2.2) and one fault is present tens of metres east of the mouth of Ruisseau à l'Échalote. The stratigraphic displacement across this fault is approximately 210 m (west side up). Correlation of the beds between sections RE and FP1 suggest a fault occurs in the cove that separates these two sections. The stratigraphic displacement across this fault is estimated to be approximately 75 m (west side up).

The wave-cut platform at section FP1 is adequate for description at low tide. Cliff exposures are poor. Beds are steeply dipping (Table 2.2), and one fault is located in the area between sections FP1 and FP2. The stratigraphic displacement across this fault is a few metres (east side up).

In the FP2 section, beds are only exposed on a narrow wave-cut platform that is a few tens of metres wide. Beds are steeply dipping and no faults were observed within this

section. A cove separates section FP2 from section PCDR. Correlation of the beds between these sections suggests a fault in the cove. The stratigraphic displacement across this fault is estimated to be approximately 85 m (west side up).

Section PCDR was measured in the wave-cut platform at Pointe des Canes de Roches (826409). The base of the section is only observed at very low tide in the beach area near the dirt road leading to the Tourist Information Centre. The beds are steeply dipping (Table 2.2), and one fault near the top of the section has a stratigraphic displacement of approximately 23 m (east side up).

Section PRM1 was measured in the wave-cut platform at Pointe-à-la-Renommée (831407). Beds are steeply dipping or overturned (Table 2.2). The area of exposure is limited laterally to a few tens of metres.

Section PRM2 (827407) is located approximately mid-way between sections PCDR and PRM1. A fault is located to the west of this section and the stratigraphic displacement across this fault is about 45 m (west side up).

## **A2.2. Sections SH, SYE, SYW, CB, PH and RGC (Figures 2.3 and 2.4, Appendix A3)**

Section SH (710456) was measured in the wave-cut platform east of Anse à la Rogne. The exposure of the basal parts of the section is very poor because of boulder cover and some beds can only be observed at very low tide. The top 20 m of the section

can only be seen at very low tide and when wave action is negligible. The beds in this section are steeply dipping and four faults were observed in the middle to upper part of the section. The displacements across these faults vary from less than 5 m to more than 100 m (Figure 2.3).

Section SYE was measured in the wave-cut platform and the cliffs on the western side of Anse à la Ronge. The lower part of the section (704456) was measured in the cliff because of poor or no beach exposures. Good exposure of the upper part of the section was observed in the wave-cut platform at low tide. The top of the section is located in the hinge of the syncline south of Pointe Séche (685480). One fault with a displacement of about 2–4 m was observed in the lower part of the section.

Section SYW (696468) was measured in the wave-cut platform at Pointe Séche. The base of the section can be studied only at very low tide. The top of the section ends at the hinge zone of the syncline south of Pointe Séche. Dip of the beds in this section is less steep than equivalent beds exposed on the opposite limb of the syncline in section SYE (Table 2.2). Correlation of the beds between sections SYW and CB suggests a fault in the Baie de Saint Yvon separates these two sections. The stratigraphic displacement across this fault is estimated to be approximately 100 m (west side up).

Section CB was measured in two locations. The lower 21 m is only exposed in the wave-cut platform at Pointe Barreau (672487). In this area, the beds are gently dipping (Table 2.2) and one fault with an estimated stratigraphic offset of several tens of metres



(west side up) is located at the eastern part of Pointe Barreau in Anse à Breton. The remaining part of the CB section was measured in the wave-cut platform between hinges of the anticline at Cape Barré (680480) and the syncline at Pointe à Mimi (685473). The dip of the beds gradually increases from Cap Barré to Pointe à Mimi. No faults were observed in the area.

The beds outcropping between Pointe Barreau and Cap Barré are flat lying or very gently dipping (Table 2.2). The top of one particular bed (BT-53) covers most of the outcrop area. A small anticline occurs in this area (Figure 2.4).

Section PH (663490) was measured in the wave-cut platform at Pointe à Hubert on the western side of Anse du la Rivière du Petit Cloridorme (Figure 2.4). In this section, the dip of the beds is moderate (Table 2.2) and only the top few metres of the section were measured in the cliff above the platform. One fault was observed in the section and the displacement across the fault is a few tens of metres (west side up) (Figure 2.4). The hinge area of the syncline is well exposed in the cliffs on the west side of the cove and in the beach area about 300–400 m west of Pointe à Hubert.

Section RGC was measured in the small headland on the western side of Baie de Cloridorme (652495). The lower part of the section is exposed only at low tide. Here, the beds are moderately dipping (Table 2.2) and no faults were observed in the section, however, it is inferred, based on stratigraphy and correlation, that faults bracket the section at its base and top.

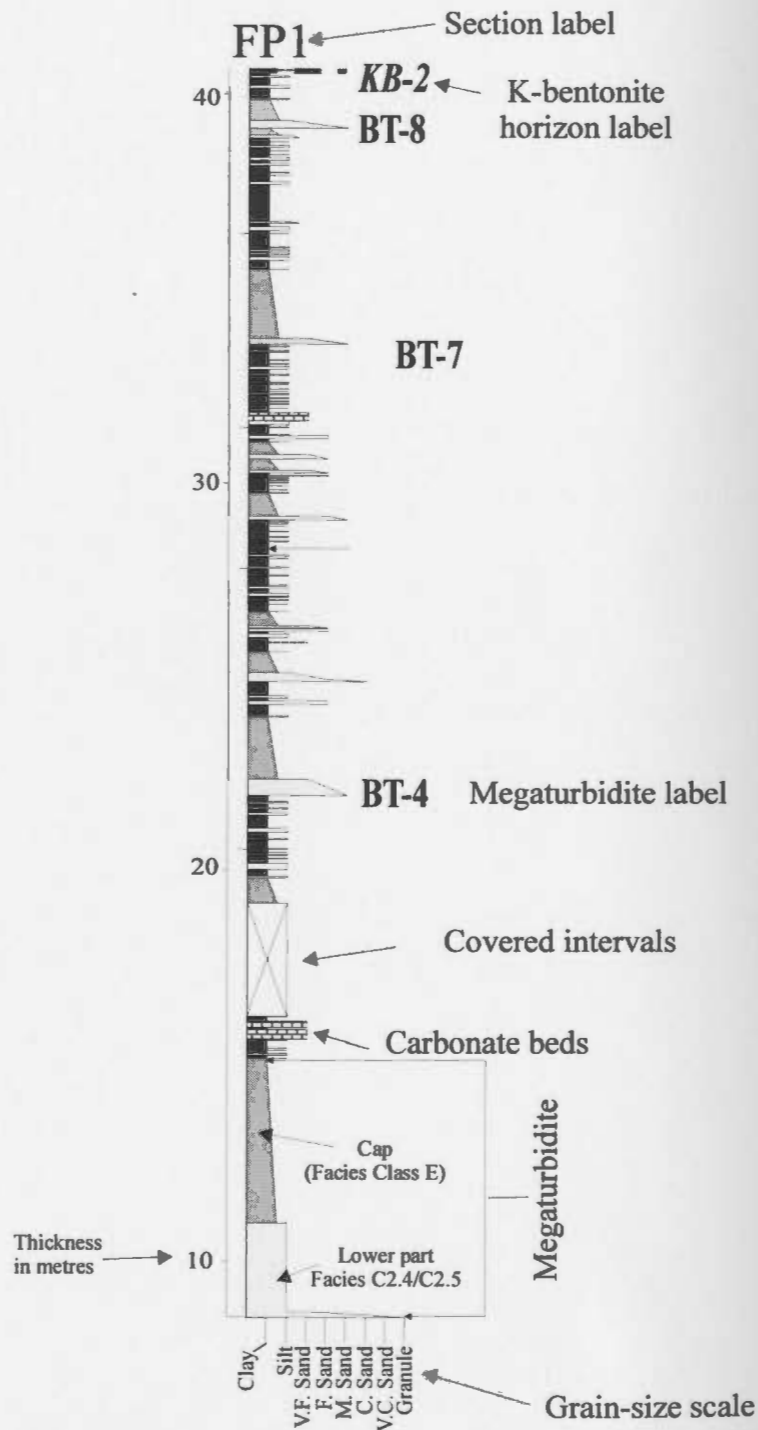
The area between section RGC and section PF contains the most structurally deformed sequence of the entire thesis area. This area was examined in detail in order to investigate whether the exposed beds could be correlated to parts of other sections. No marker beds were found to tie this section to other sections. It is believed that the beds exposed in this area are older than the sequence considered in this thesis. Other studies support this conclusion (Enos, 1965, 1969a, 1969b). Only a small area, extending laterally just a few tens of metres and located west of the Cloridorme wharf, is equivalent to part of the base of the studied sequence. This area is bounded by faults to the east and west.

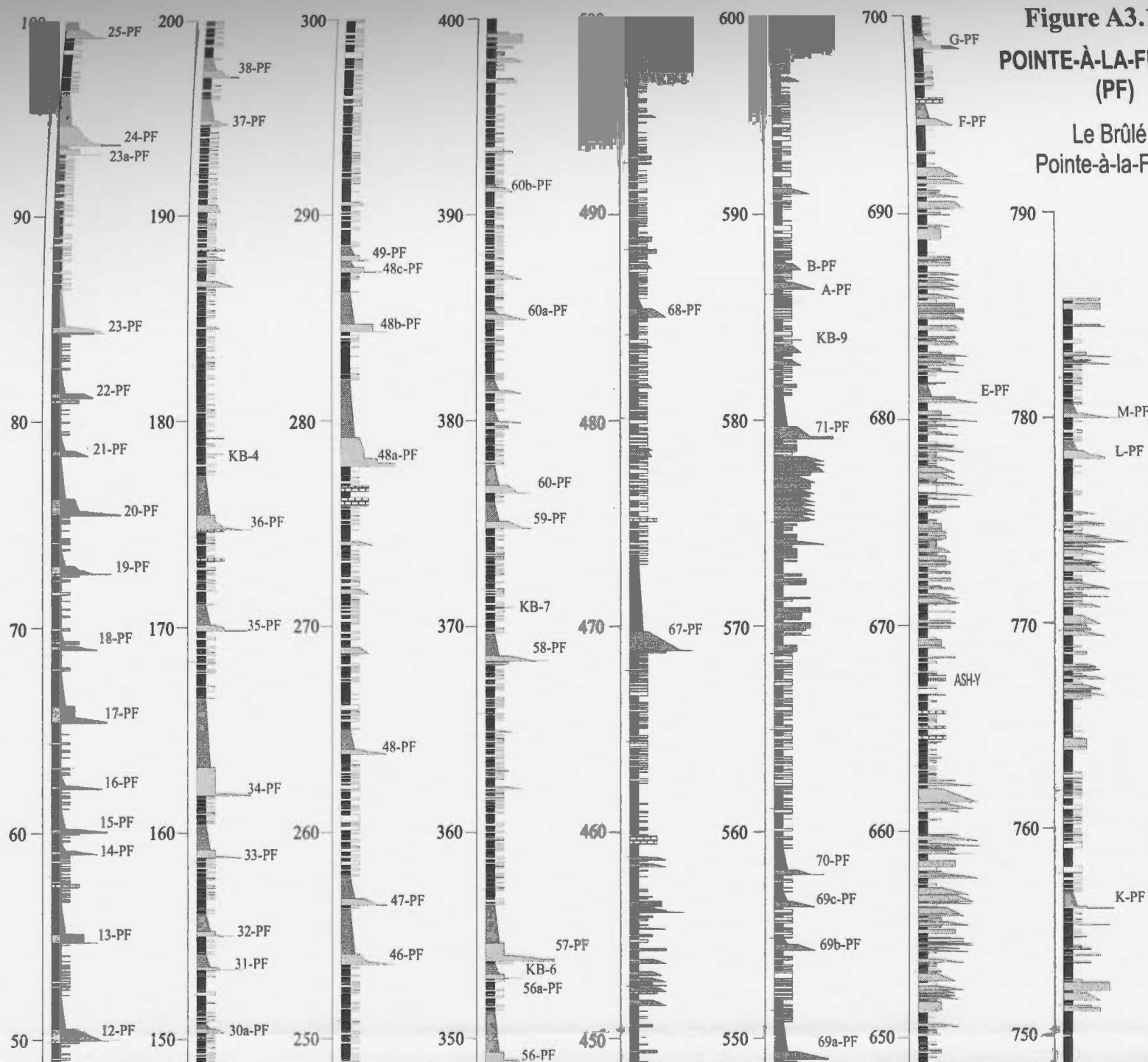
### **A2.3. Section PF (Figure 2.5, Appendix A3)**

The beds exposed in the wave-cut platform between Le Brûlé and Pointe-à-la-Frégate are overturned and dip towards the south (Table 2.2). The lower 238 m of this section (from the base to BT-43PF) was measured in a small unnamed headland west of Le Brûlé. The small cove between this unnamed headland and Cap Blanc was bypassed because it is highly faulted. The remainder of the section (from BT-43PF to the top of the section) was measured in the area extending west from Cap Blanc to the second headland west of Pointe-à-la-Frégate (592520). In this area, there are a large number of faults but the displacements across these faults are minor and easily unravelled.

**APPENDIX A3**  
**LOGS OF THE MEASURED SECTIONS**

**Key for the terms, symbols and patterns used in sections logs.**  
**Thickness is in metres. Some of the fill patterns may be different in different sections.**





**Figure A3.1**  
**POINTE-À-LA-FRÉGATE**  
**(PF)**  
 Le Brûlé to  
 Pointe-à-la-Frégate

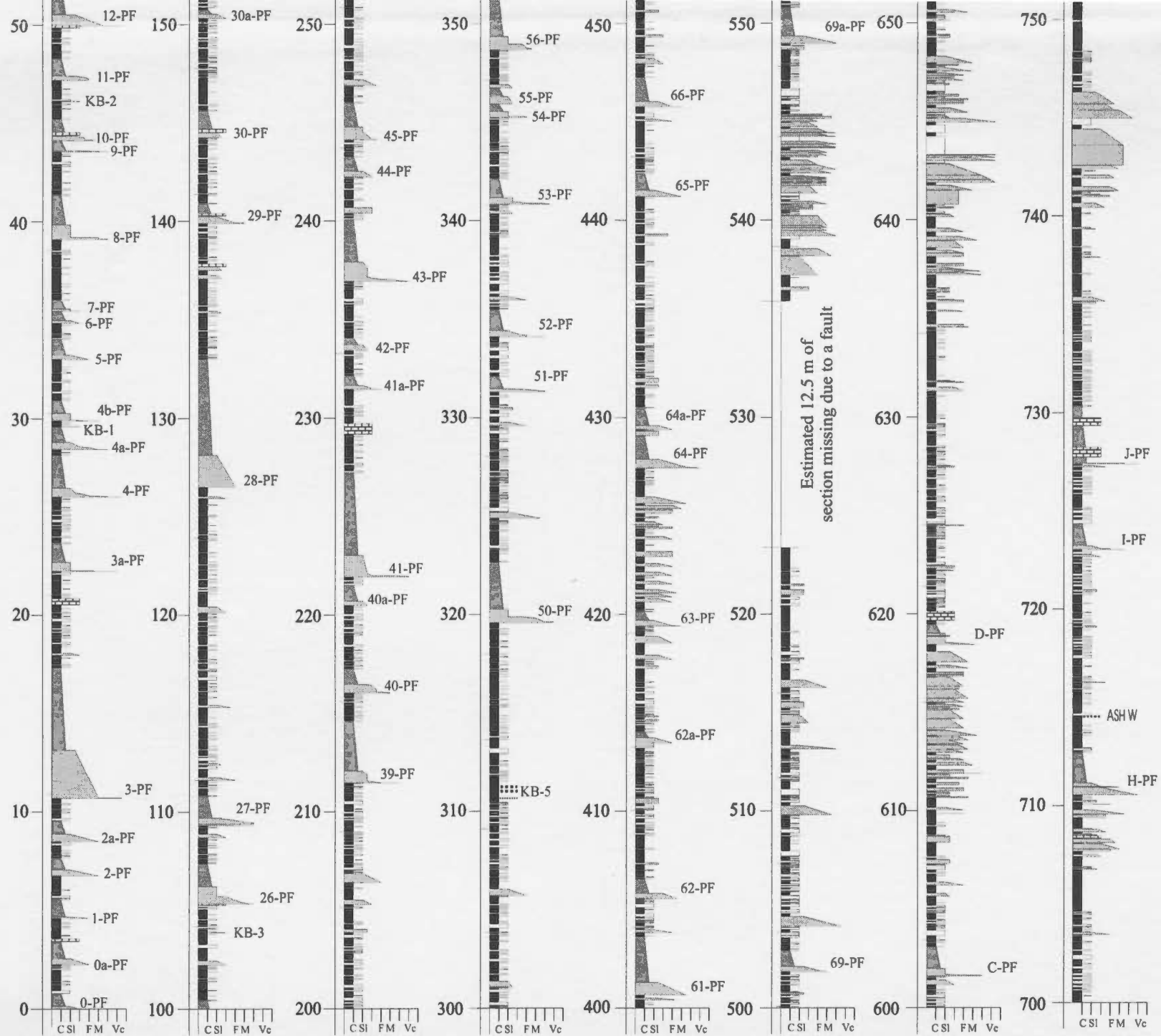
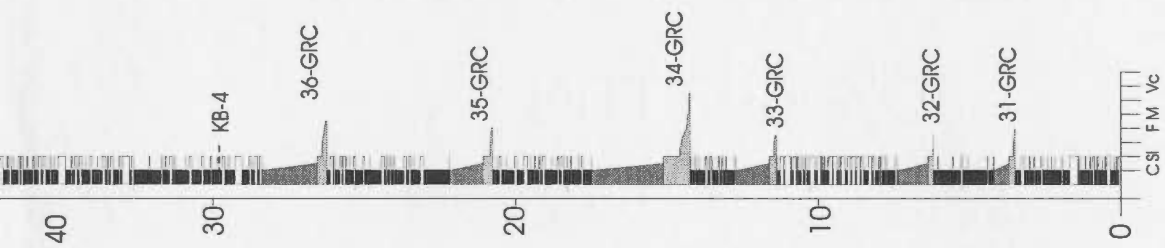


Figure A3.2

# **RIVIÈRE DU GRAND CLORIDORME (RGC)**

(Small Headland between wharf and beach)







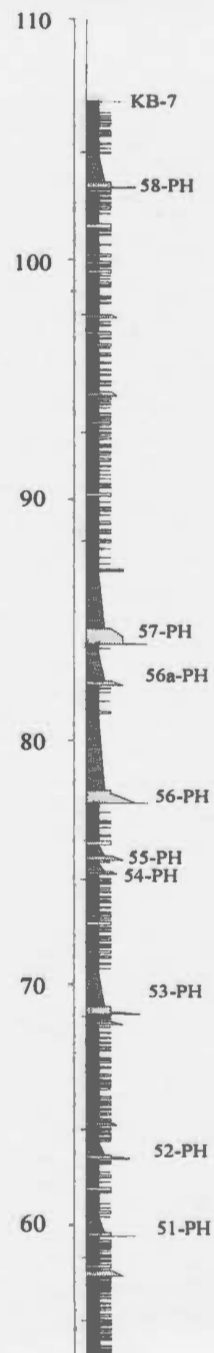


Figure A3.3

## POINTE À HUBERT (PH)

Section on the west side of  
Anse de Petit Cloridorme

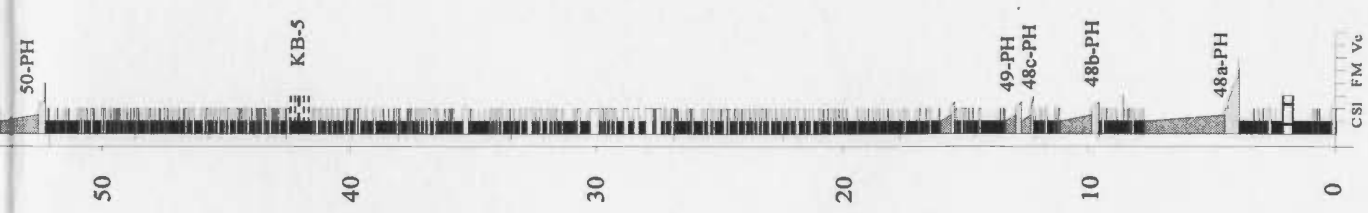
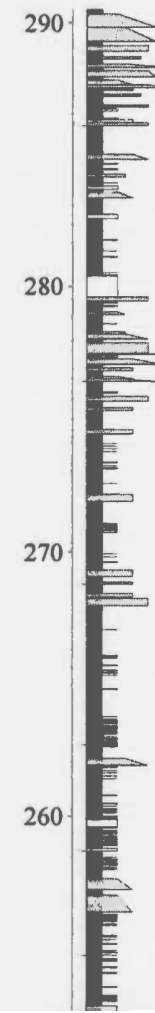
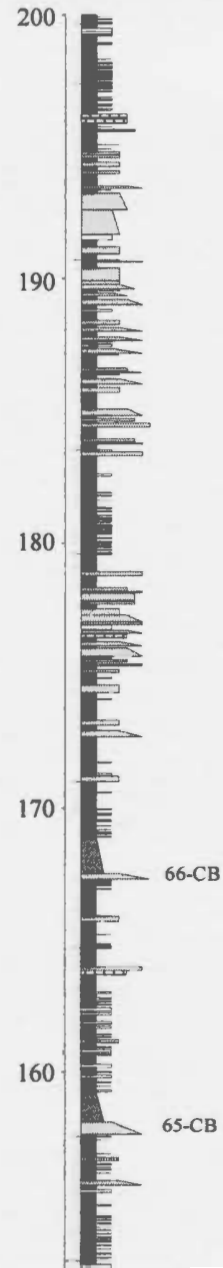
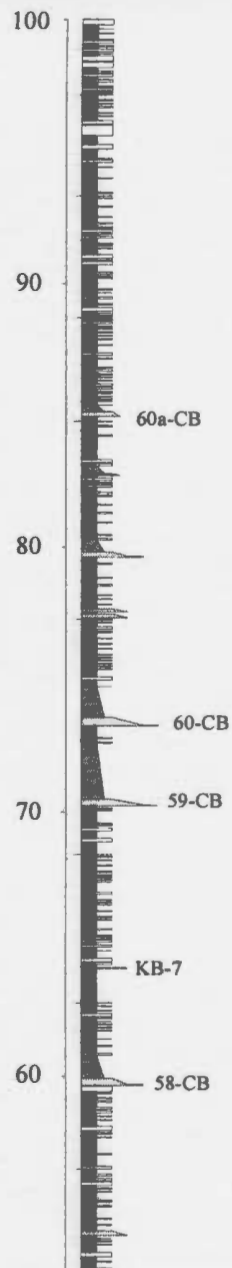
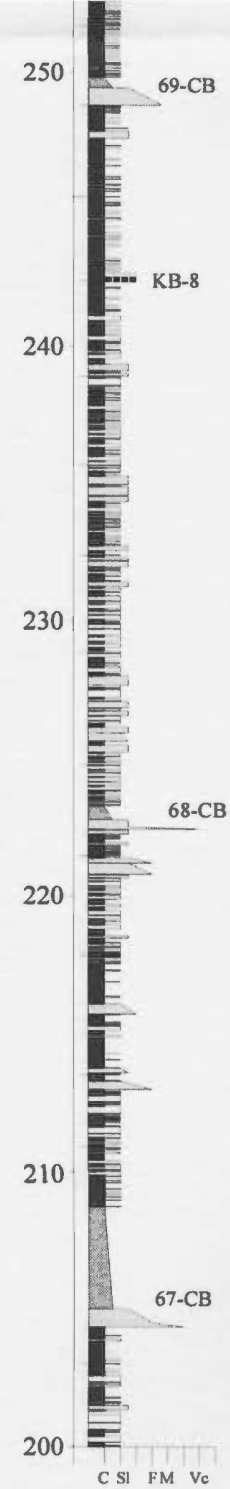
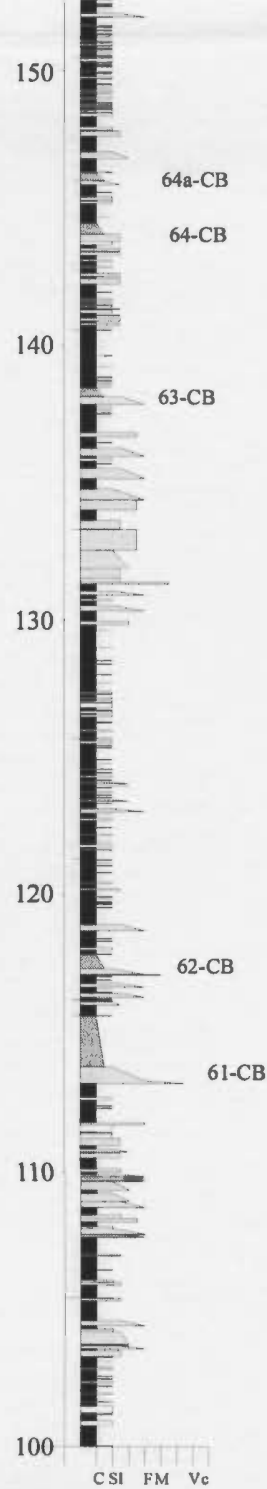
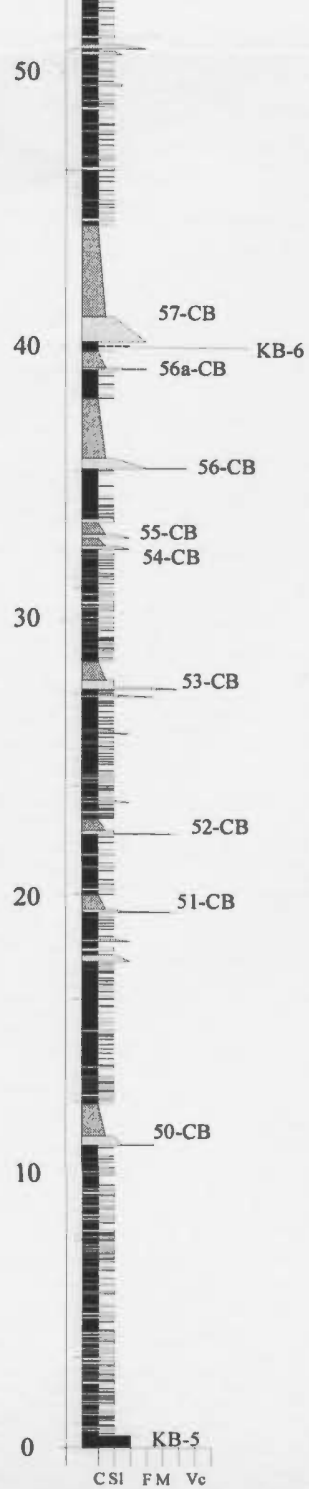


Figure A3.4

## CAP BARRÉ

Pointe Barreau to Cap Barré  
to Pointe à Mimi





70-SYW

100

90

80

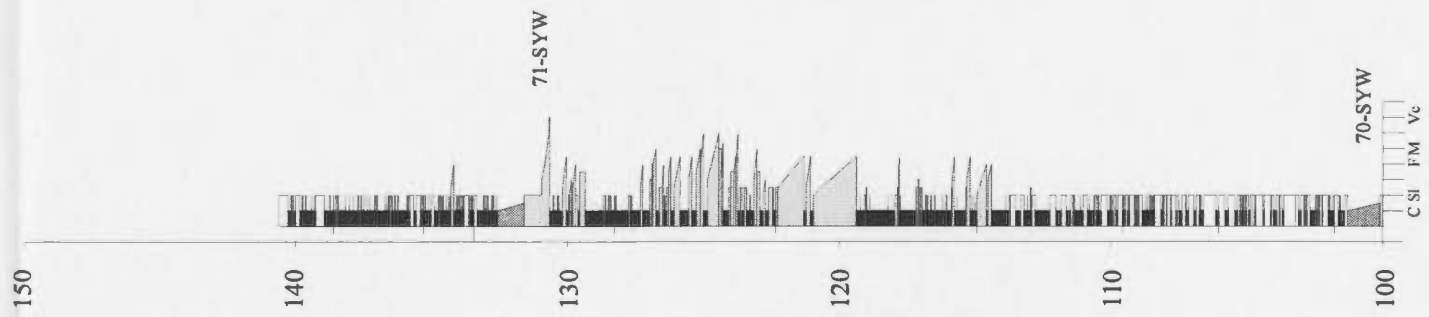
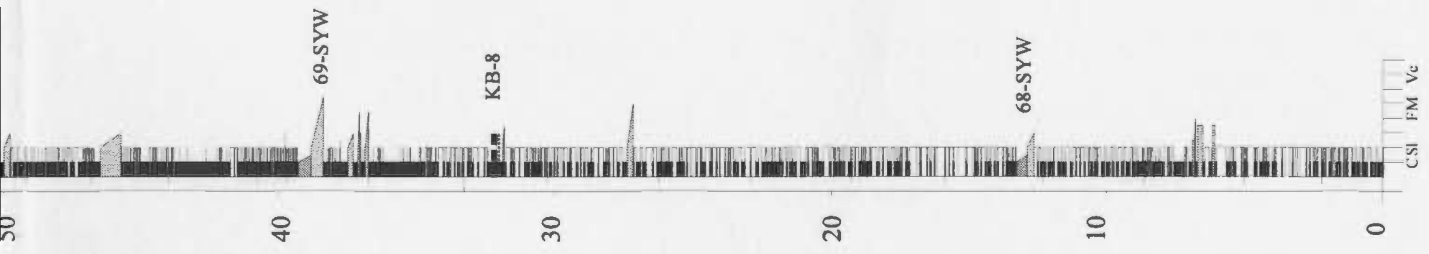
70

60

Figure A3.5

## ST. YVON WEST (SYW)

Northern limb of the syncline  
at Pointe Séche



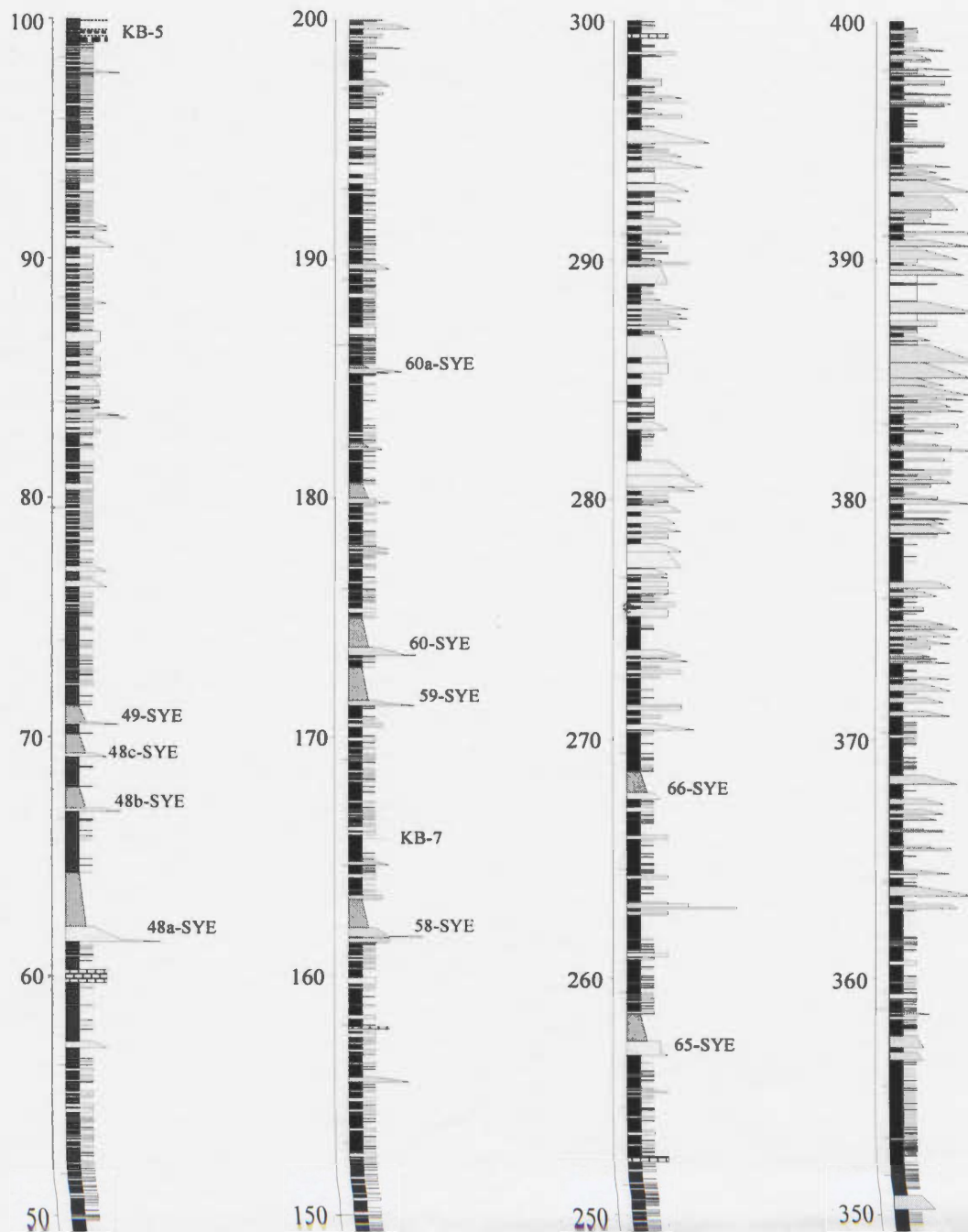
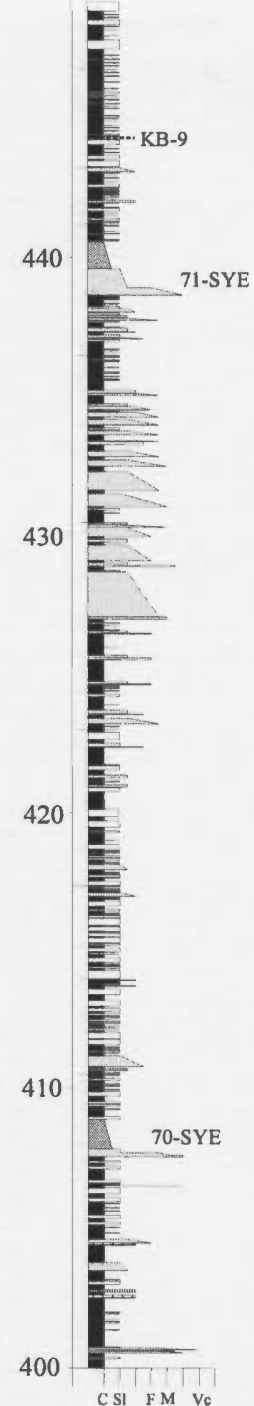
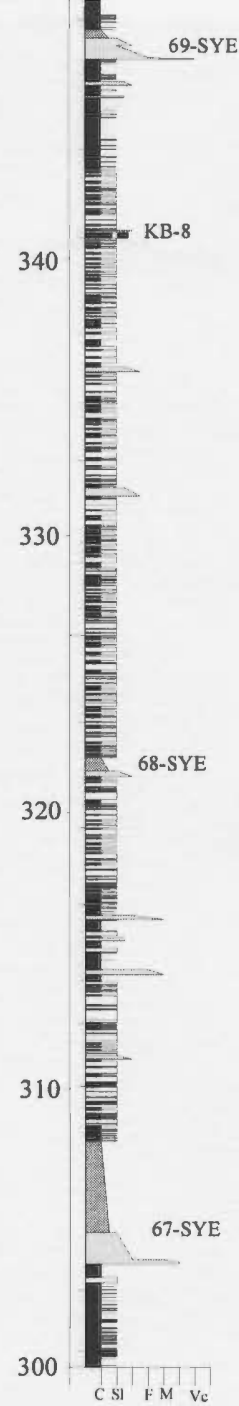
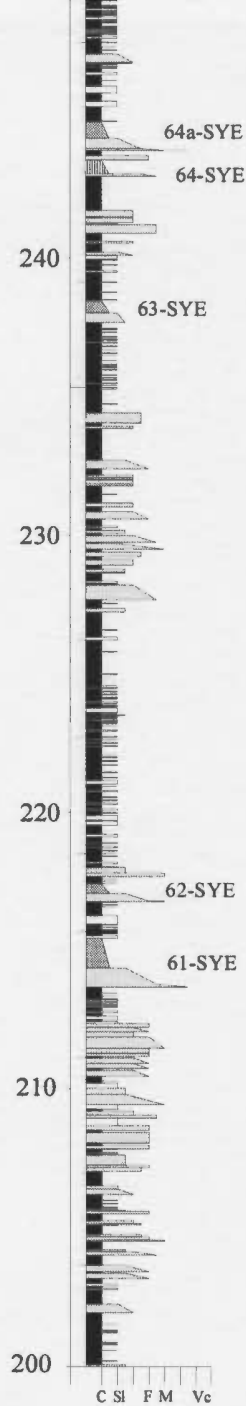
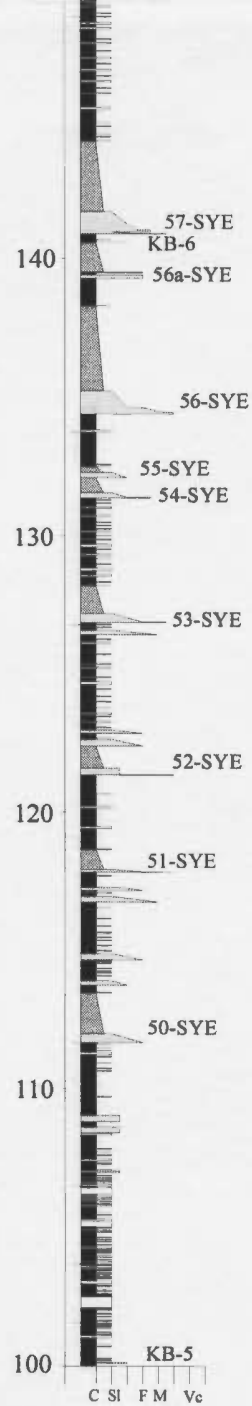
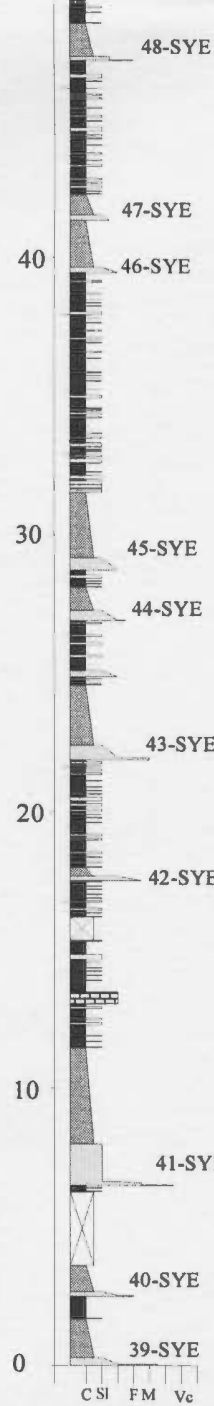


Figure A3.6  
**SAINT YVON EAST  
(SYE)**

Anse à la Rogne  
to  
Pointe Séche





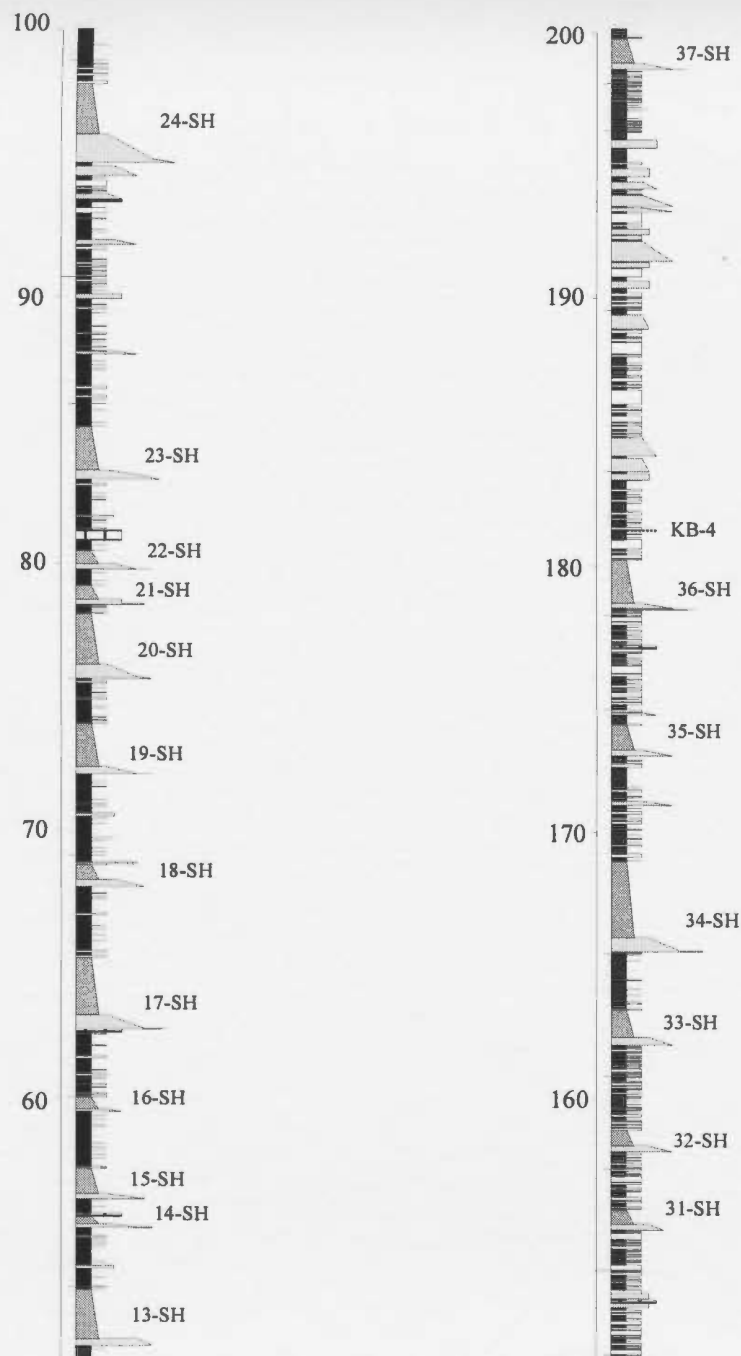
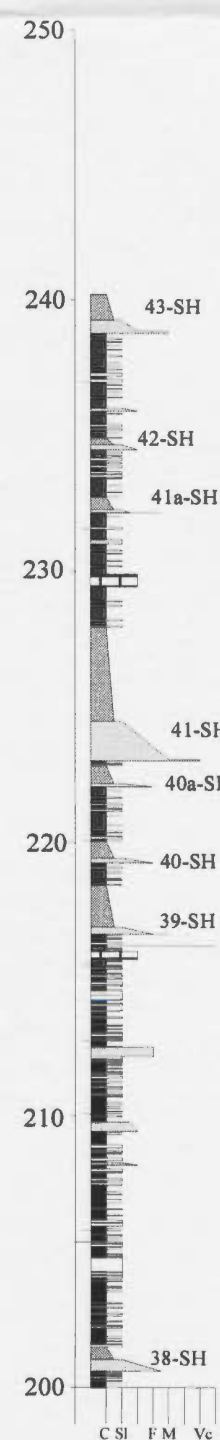
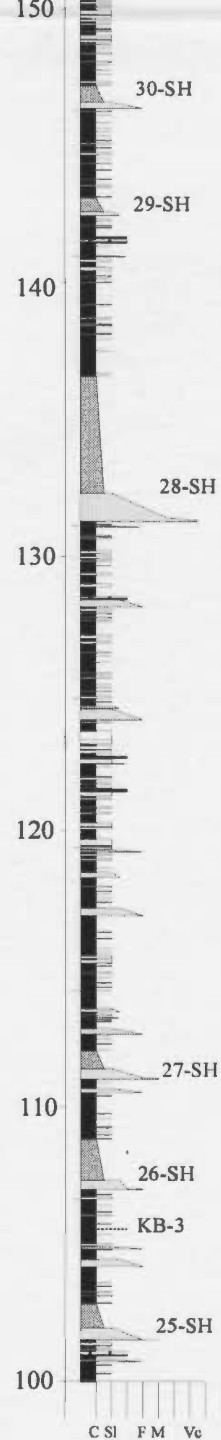
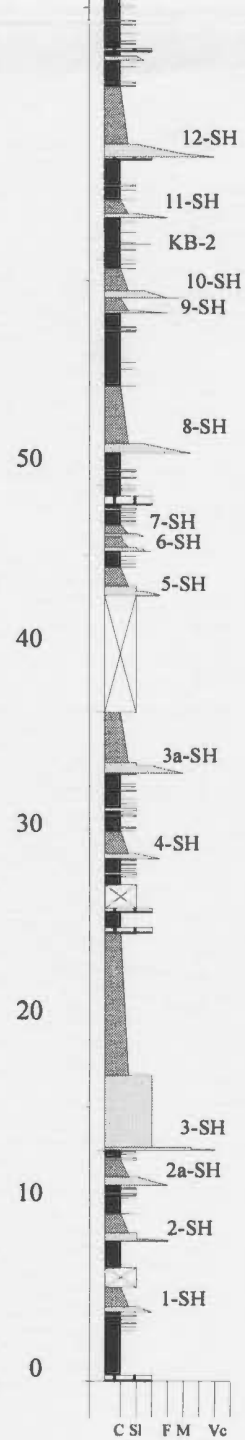


Figure A3.7

**SAINT-HÉLIER**

Saint-Hélier  
to  
Anse à la Rogne



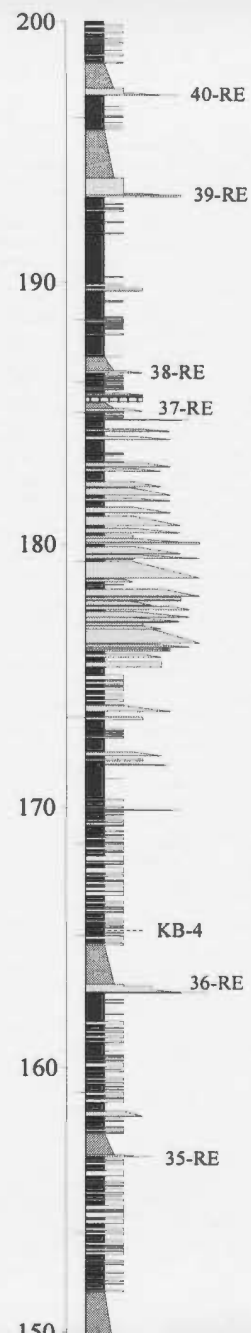
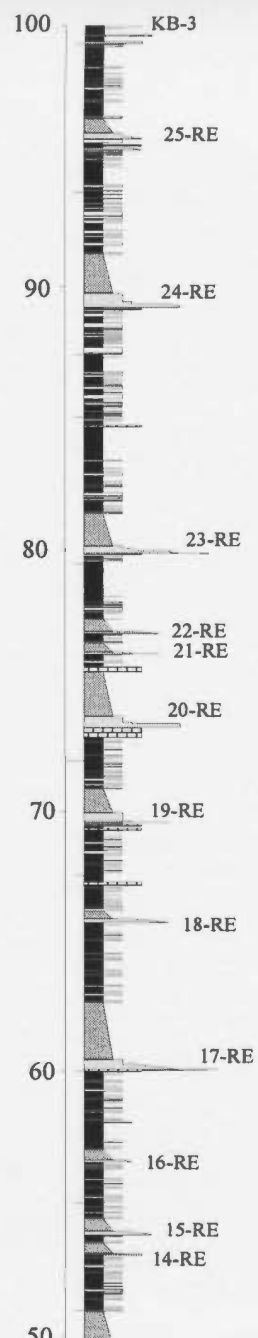
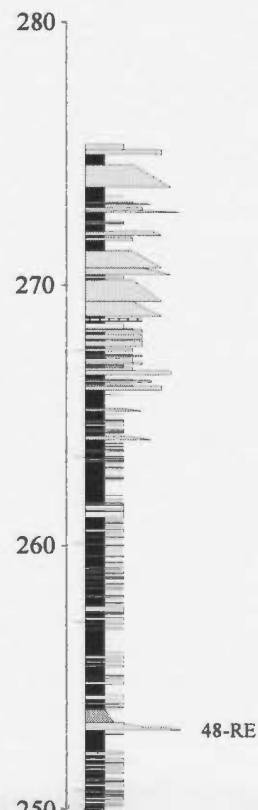
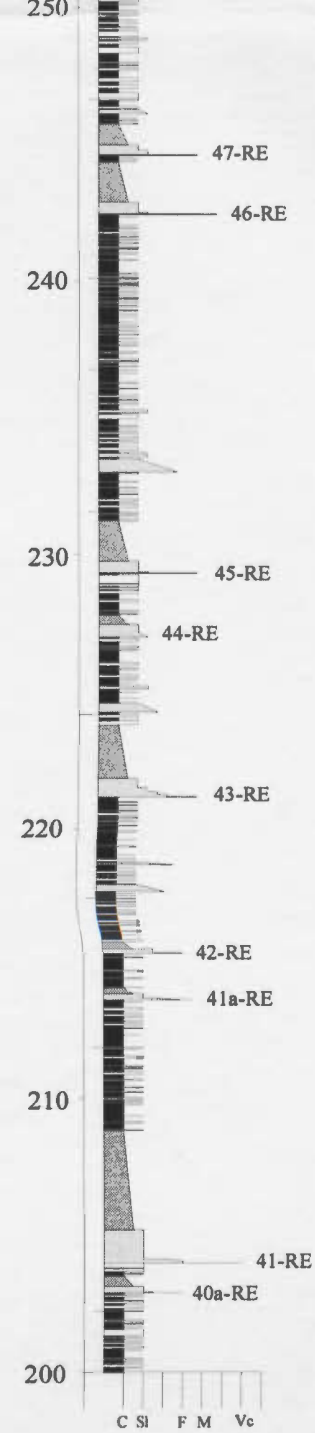
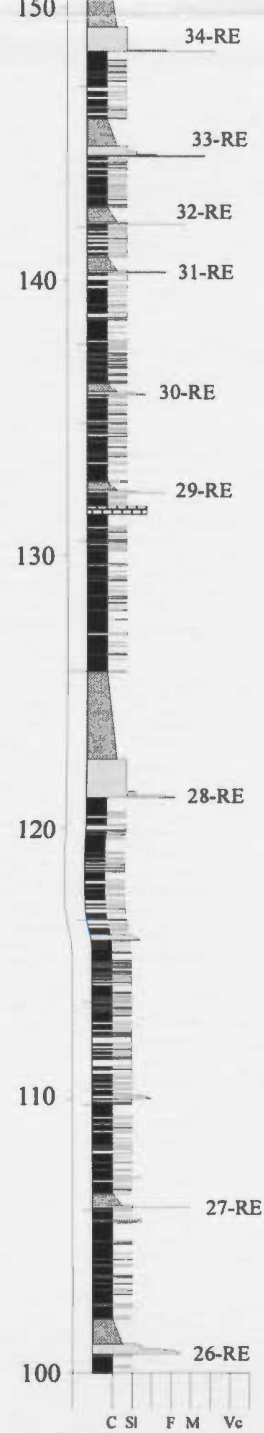
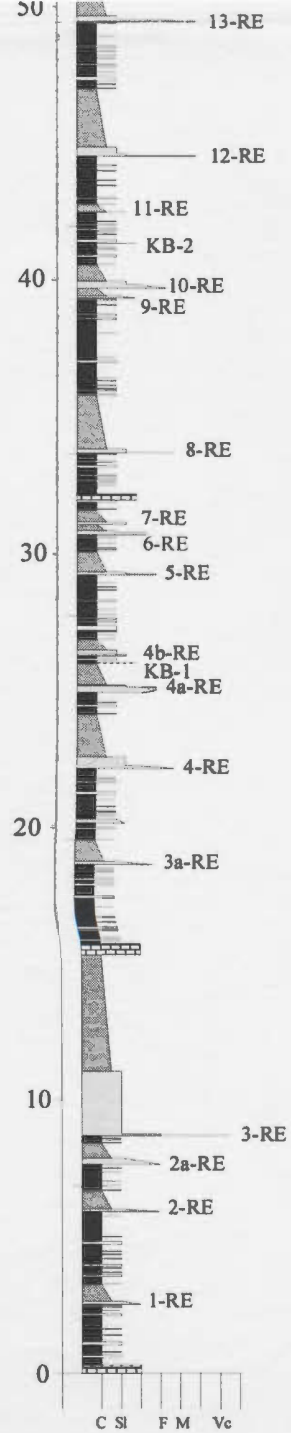


Figure A3.8

## RUISSEAU À L'ÉCHALOTE (RE)

Headland west of Ruisseau à l'Ail





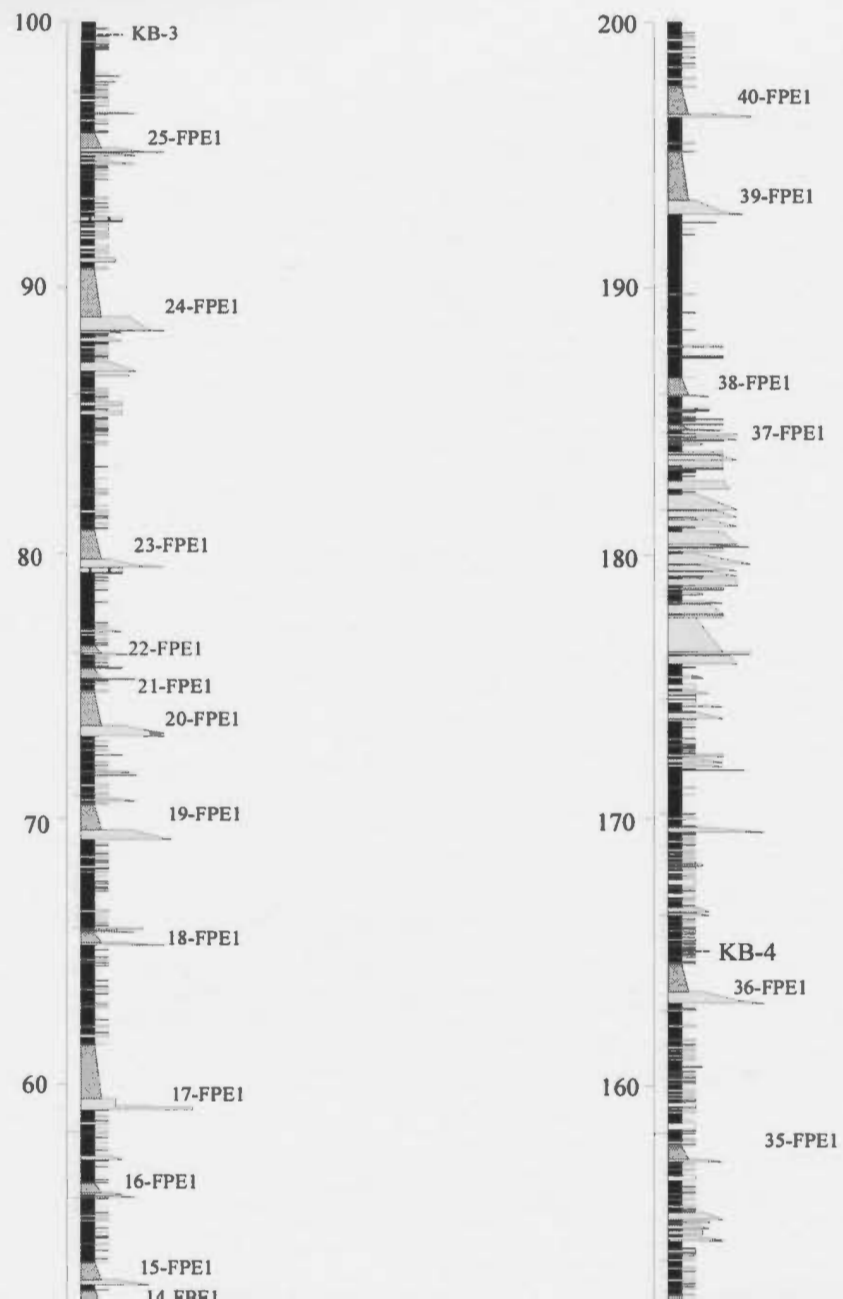


Figure A3.9

# FAME POINT (FP1)

Headland east of Ruisseau à l'Ail

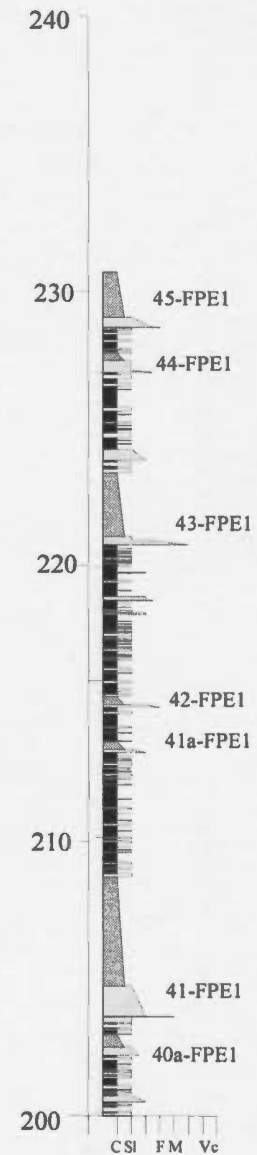
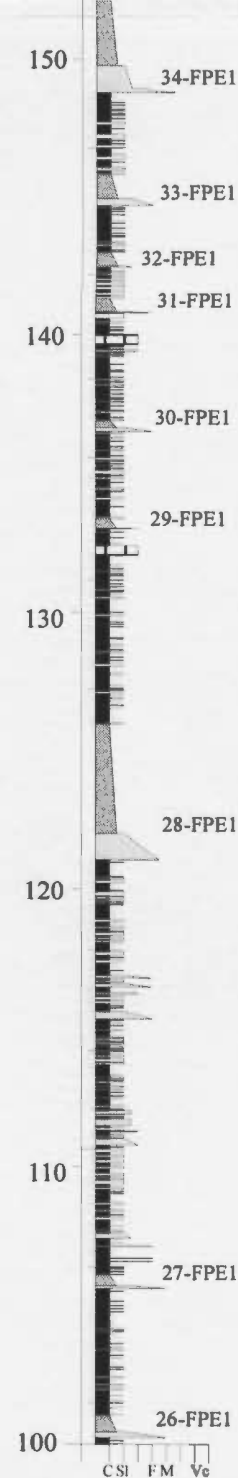
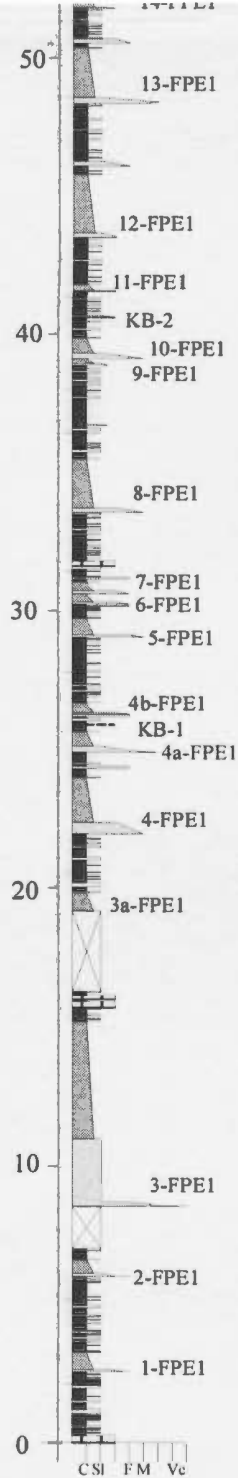
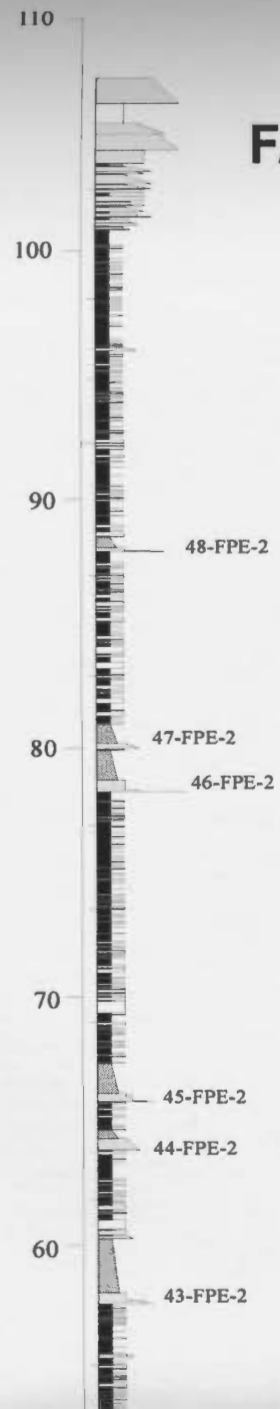
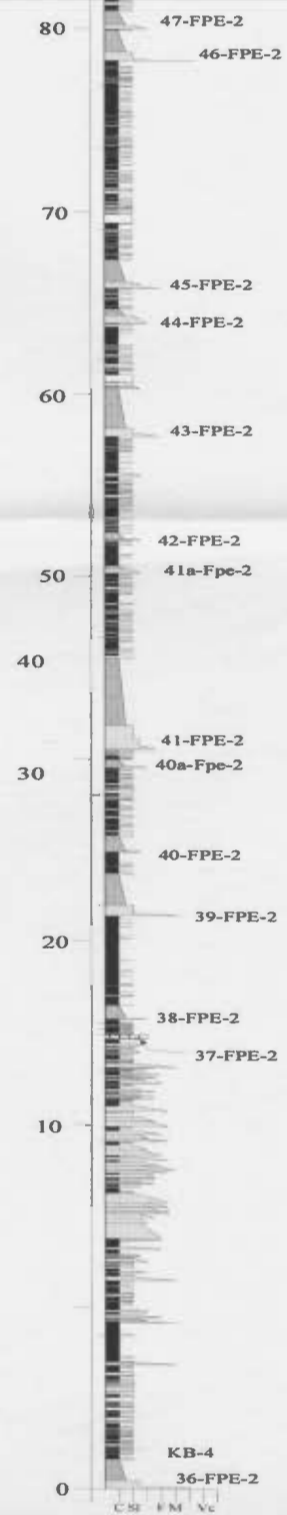


Figure A3.10  
**FAME POINT # 2**  
**(FP2)**







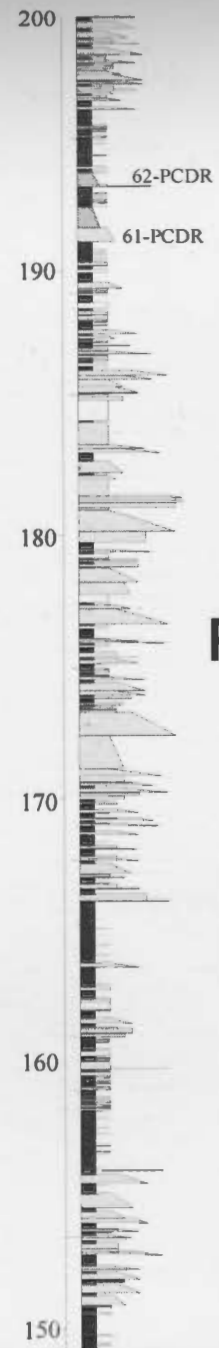
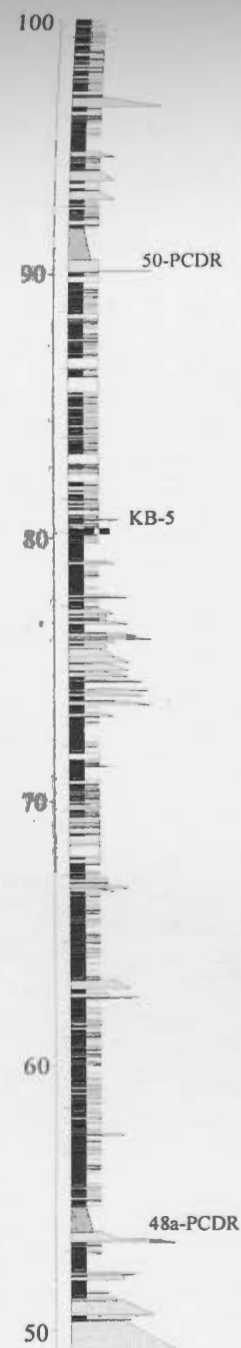


Figure A3.11

## POINTE DES CANES DE ROCHES (PCDR)

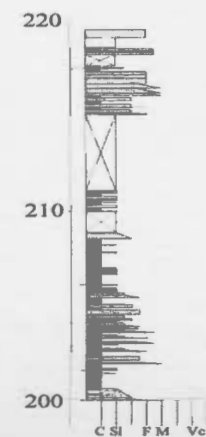
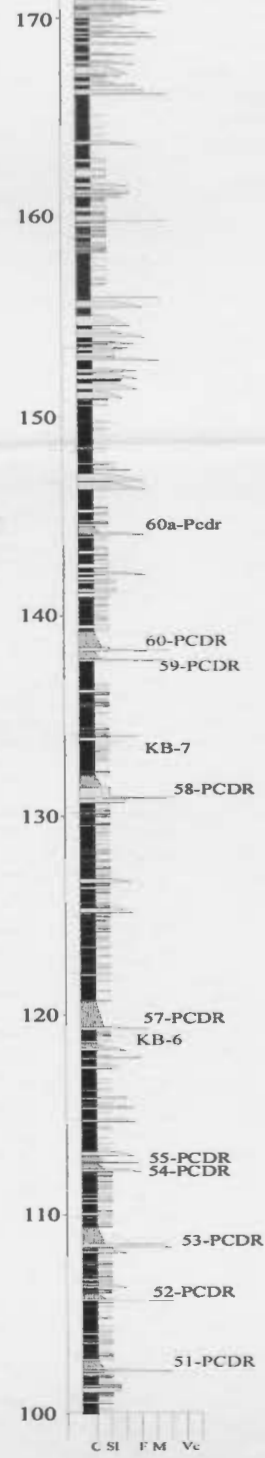
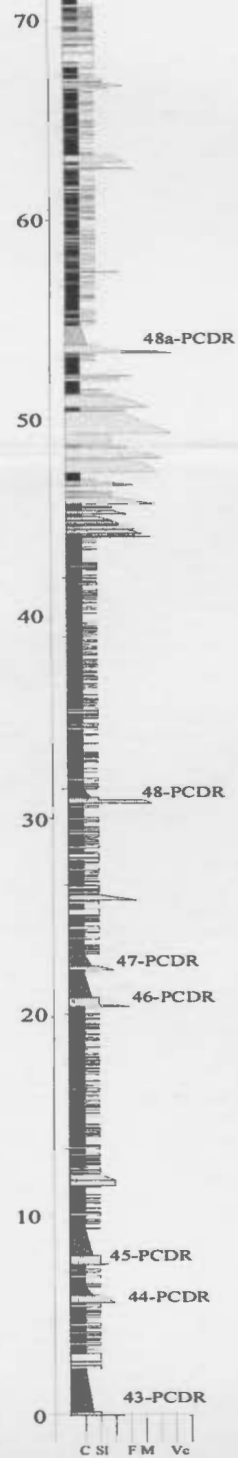


Figure A3.12

## POINTE À LA RENOMMÉE (PRM2)

## POINTE À LA RENOMMÉE (PRM1)

First Headland

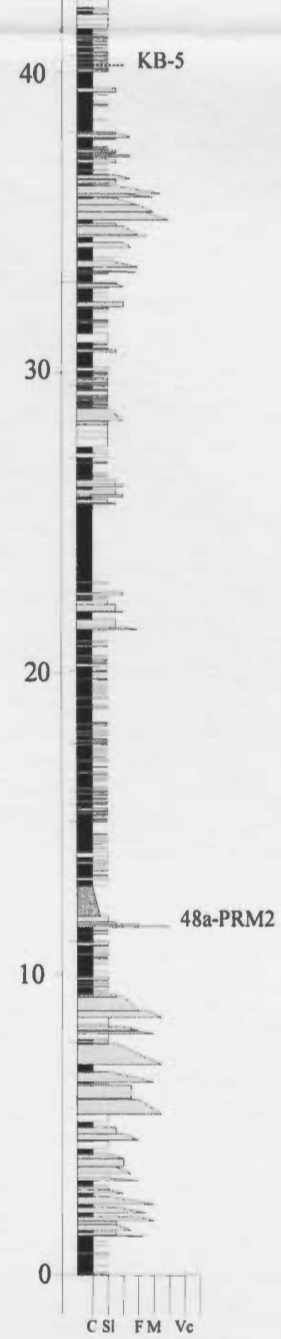
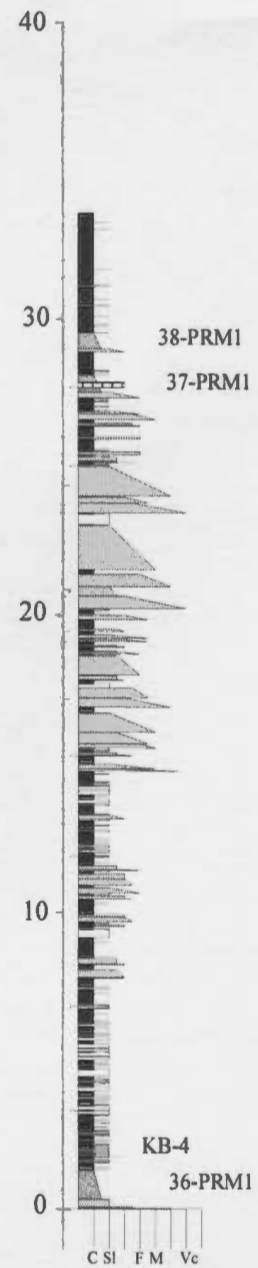
Second Headland

60

50

KR-5

# First Headland



**APPENDIX A4**  
**STATISTICAL METHODS USED FOR K-BENTONITE CORRELATIONS**

#### A4. PROCEDURE

Eighteen samples from K-bentonite horizons KB-1 to KB-4 in the Pointe-à-la-Renommée and St- Hélier areas (sections FP1, RE, and SH) were used as a control group. These eighteen samples (3 from horizon KB-1, 5 from horizon KB-2, 5 from horizon KB-3, and 5 from horizon KB-4) were collected from different exposures of these four horizons in the three sections, during different field seasons. The reason for choosing samples from these four horizons to serve as a control group is because the physical correlation of the sequence enclosed by horizons KB-1 and KB-4 in the area between Pointe-à-la-Renommée and St- Hélier is secure (Enos, 1965, p. 87; Skipper and Middleton, 1975) and, compared with other K-bentonite horizons, a greater number of samples were available from these horizons. The importance of good stratigraphic control for the control group samples has been stressed by Kolata *et al.* (1986). The control-group was used to investigate if any of these four horizons has a unique chemical fingerprint. Ten other samples ("unknowns"), mainly from the PF and RGC sections (8 samples), with expected equivalence (based on their position relative to megaturbidites) to horizons KB-1 to KB-4, were then tested against the results of the discriminant analysis on the control group to see if these ten samples could be unambiguously assigned to horizons KB-1, KB-2, KB-3 or KB-4.

Before statistically analysing the data, element mobility was considered. Immobile elements are those elements that remain conserved during secondary alteration processes

(e.g., weathering or low-temperature metamorphism: Winchester and Floyd, 1977; Huff and Kolata, 1989). Immobile elements have been used to differentiate between volcanic rocks originating from different magmas in different tectonic settings (Pearce and Cann, 1973). Thus, the immobile elements should also be useful in the differentiation of K-bentonite horizons originating from different magmas, or from a magma source that evolved through time (Huff, 1983; Kolata *et al.*, 1996). The following elements are considered mobile and were excluded from any further analysis (Kolata *et al.*, 1986; Wilson 1989; Jenner, 1996, Pearce, 1996): Ba, Sr, Rb, K, La, Mg, Mn, P, Si, Cs, and U . Elements for which most of the concentrations were below the limit of detection (As, Ag, In, Sb, Bi) were also excluded from further analysis.

Before performing the discriminant analysis, the concentrations for each element were evaluated graphically to see if the 95% confidence limits about the mean, for each of the four K-bentonite horizons, overlap (Figure A4.1). Elements with little or no overlap would be the best in discriminating between the K-bentonite horizons. Such elements are characterised by a different mean concentration from horizon to horizon but a small range of concentration within individual horizons (Table A4.1).

The Statistical Package for the Social Sciences (SPSS®) was used in the discriminant analysis. The data for the 18 control-group samples were entered into a computer file and subjected to stepwise discriminate analysis using the Wilks' lambda method. The computer program first identifies and ranks variables (elements) on how

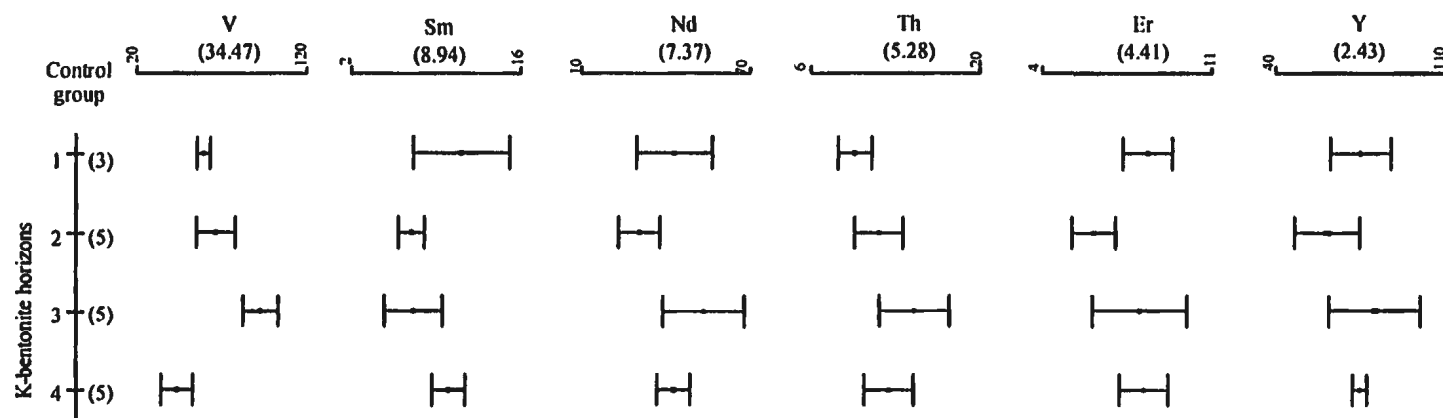


Figure A4.1. 95% confidence intervals for sample means for six elements arranged in decreasing F ratio (shown in parentheses under each element). Elements that are good in discriminating between the K-bentonite horizons are those that show a minimum of overlap. Vanadium (V) is an excellent discriminator between K-bentonite horizons KB-1 and KB-3, or KB-1 and KB-4, or KB-3 and KB-4 because the confidence intervals do not overlap. Vanadium alone cannot be used to distinguish between horizons KB-1 and KB-2. In this case, other elements such as Erbium (Er) may be used for discrimination. Elements that have a low F ratio such as Yttrium (Y) is not good discriminators because all 4 horizons have statistically indistinguishable concentrations.



Table A4.1. Mean and standard deviation for the chemical composition of all the samples in the four K-bentonite horizons of the control group. Number of samples in brackets.

	Horizon #1 (3)		Horizon #2 (5)		Horizon #3 (5)		Horizon #4 (5)	
Elem.	Mean	S.dev.	Mean	S.dev.	Mean	S.dev.	Mean	S.dev.
Na <sub>2</sub> O%	0.53	0.16	0.87	0.26	1.08	0.35	0.70	0.21
S	1316	1015	9910	9502	5104	3106	991.7	355.3
Cl	350	374	417.3	417.4	600.8	507	801.4	838.8
CaO%	0.45	0.18	0.66	0.66	0.47	0.10	0.40	0.10
Sc	39.33	4.73	31.22	7.10	32.28	3.39	28.31	6.38
TiO <sub>2</sub> %	1.39	0.01	1.41	0.15	1.58	0.21	0.76	0.05
Fe <sub>2</sub> O <sub>3</sub> %	4.37	0.70	7.15	2.88	6.60	1.91	3.53	0.15
V	59.33	1.53	66.60	9.26	92.80	8.32	43.60	7.40
Cr	20.67	6.43	44.60	49.57	48.40	8.32	19.00	16.73
Co	6.77	4.20	13.58	10.19	32.34	29.43	9.56	3.81
Ni	32.67	29.84	83.20	39.87	49.60	18.49	23.00	5.34
Cu	0.00	0.00	151.20	202.39	88.60	120.11	33.00	42.06
Zn	175.00	78.58	139.00	94.61	118.20	50.71	424.00	576.73
Ga	28.00	0.00	22.80	2.28	21.40	0.55	27.40	2.30
Ge	1.67	0.58	1.16	0.48	1.40	0.55	1.78	0.49
As	3.00	6.93	16.20	9.68	16.40	8.32	1.00	8.22
Y	75.0	5.00	61.00	11.92	78.40	15.85	74.20	2.39
Zr	358.9	10.79	414.56	32.95	472.94	87.47	423.44	19.39
Nb	10.67	0.58	10.96	0.78	13.16	1.28	10.68	1.01
Mo	1.77	0.72	6.88	3.16	7.02	8.37	1.22	0.65
Sn	4.00	0.00	4.00	0.71	4.20	0.45	5.20	1.10
Sb	2.33	3.26	2.46	2.10	1.02	0.39	1.06	1.15
La	27.23	3.25	22.34	6.59	62.06	10.22	36.86	4.35
Ce	71.20	7.42	57.74	13.62	135.78	26.12	84.74	8.11
Pr	8.93	1.07	6.87	1.50	13.99	2.60	9.50	1.07

Table A4.1. Continued

Elem.	Horizon #1 (3)		Horizon #2 (5)		Horizon #3 (5)		Horizon #4 (5)	
	Mean	STDS	Mean	STDS	Mean	STDS	Mean	STDS
Nd	43.13	5.42	30.48	5.99	53.56	11.73	42.92	4.82
Sm	11.07	1.60	6.96	0.85	7.08	1.92	10.00	1.10
Eu	2.43	0.39	1.60	0.22	1.33	0.37	1.82	0.18
Gd	10.50	1.54	6.28	0.66	6.56	2.12	9.42	0.74
Tb	1.97	0.21	1.32	0.08	1.50	0.35	1.78	0.08
Dy	12.87	1.10	9.04	0.71	11.40	2.30	11.98	0.73
Ho	2.67	0.21	1.94	0.17	2.56	0.50	2.58	0.19
Er	8.37	0.40	6.14	0.72	8.04	1.57	7.98	0.80
Tm	1.22	0.05	0.87	0.12	1.20	0.22	1.17	0.17
Yb	8.40	0.26	5.82	0.72	7.90	1.53	7.78	0.85
Lu	1.30	0.05	0.89	0.13	1.21	0.24	1.23	0.15
Hf	9.53	0.32	11.24	1.21	13.16	2.64	11.74	0.62
Ta	0.75	0.03	0.98	0.11	0.95	0.10	0.84	0.10
W	2.13	0.55	10.36	9.36	8.88	8.23	12.58	12.17
Tl	0.77	0.15	0.90	0.33	2.40	3.14	0.94	0.19
Pb	2707.7	4689	20.00	9.41	24.60	15.57	5.40	9.86
Th	9.67	0.57	11.69	1.64	14.66	2.35	12.51	1.67

they differentiate between different groups (horizons). Variables are selected for the analysis based on a high F ratio or low Wilks' lambda (Table A4.2). If the differences between the group means (i.e., means from K-bentonite horizon x to K-bentonite horizon y) are measurably larger than differences between samples within each group (i.e., each K-bentonite horizon considered alone), then the F ratio will be large (Table A4.2, Equation 4.1). The Wilks' lambda of a variable (chemical element) is defined as the ratio of the within-horizons sum of squares to the total sum of squares (SPSS® Base 9.0 Application Guide, 1999). The Wilks' lambda is the inverse of the discriminating power of the variables (elements) selected for the analysis, so a larger Wilks' lambda corresponds to a smaller discriminating power (Table A4.3). The Wilks' lambda values range from 0 to 1.

The calculated F ratio and Wilks' lambda values for 21 elements determined in the 18 control-group samples are ranked according to their discriminating power in Table A4.3. The best elements in decreasing order of discriminating power were: V, Ti, Ce, Pr, Gd, Eu, Sm, Nd, Tb, Nb, Dy, Yb, Ho, Lu, Th, Tm, Ta, Er, Hf, Zr and Y.

In the stepwise method, the program uses a stepwise selection criteria which starts by identifying the element that has between-group means that are most different, then it selects the next best element in the following step and investigates if the addition of this element improves the distinction between the horizons. The program continues to add and remove elements until it reaches a step where a combination of certain elements provides the best separation between the K-bentonite horizons and where the addition of new

Table A4.2 Equation used to calculate the F ratio of the different elements. An example of how the F ratio was determined for the element Vanadium in the control group samples is also given.

Equation 4.1

$$F \text{ ratio} = \frac{(\text{Between-horizons sum of squares})/(k-1)}{(\text{Within-horizons sum of squares})/(N-k)}$$

where  $N$  = total sample size;  $k$  = number of horizons.

The between-horizon sum of squares is calculated by subtracting the overall mean (mean of all the observations) from the mean of each horizon, then squaring the difference. Each squared value is multiplied by the number of samples in each horizon and results for all horizon are totalled (SPSS® Base 9.0 Application Guide, 1999).

The within-horizon sum of squares estimates the variability. It is calculated by multiplying each horizon's variance by the number of samples in each horizon, minus 1. The results are then totalled for all the horizons.

The between-horizons degrees of freedom (df) = number of horizons (4) minus 1 =3 while the within-horizons df = total number of samples (18) minus the number of horizons (4)=14.

Calculation of the F ratio for V for the 18 samples of the control group.

Beds	KB-1	KB-2	KB-3	KB-4	Total
#Samples	3	5	5	5	18
Mean	59.3	66.6	92.8	43.6	66.28
S.d.	1.53	9.26	8.32	7.40	20.40
	Sum of Squares		df	Mean Square	F
Between Horizon	6233.74		3	2077.92	34.47
Within Horizons	843.86		14	60.28	
Total	7077.6		17		

Table A4.3. F ratio and the Wilks' lambda values for the samples of the control group.

Variable	F ratio	Wilks' Lambda
V	34.4732	0.1192
TiO <sub>2</sub>	33.5412	0.1221
Ce	20.4771	0.1855
Pr	14.4805	0.2437
Gd	9.4199	0.3312
Eu	9.3647	0.3325
Sm	8.9497	0.3427
Nd	7.3757	0.3875
Tb	7.3106	0.3896
Nb	7.0470	0.3983
Dy	5.8797	0.4424
Yb	5.6144	0.4539
Ho	5.4351	0.4619
Lu	5.2977	0.4683
Th	5.2763	0.4693
Tm	4.6997	0.4982
Ta	4.6668	0.4999
Er	4.4059	0.5143
Hf	3.3818	0.5798
Zr	3.1962	0.5935
Y	2.4396	0.6566

Table A4.4. F ratio and the Wilks Lambda values for the samples of KB-6, KB-7, and KB-9.

Variable	F ratio	Wilks' Lambda
TiO <sub>2</sub>	9.9295	0.2611
Th	9.1733	0.2762
Sc	5.0357	0.4111
Eu	2.7489	0.5612
Sn	2.6573	0.5681
Ni	2.3792	0.5951
Pr	2.3121	0.6023
Nd	1.8663	0.6525
Sm	1.8464	0.6554
Cu	1.8153	0.6583
Ce	1.5971	0.6885
Y	1.5820	0.6898
Lu	1.4136	0.7139
Hf	1.3941	0.7152
Gd	1.2554	0.7361
Yb	1.1312	0.7567
Tm	0.9721	0.7836
Er	0.9112	0.7935
Sb	0.8735	0.8014
Ge	0.8736	0.8012
Zr	0.8222	0.813
Ho	0.6343	0.8472
Ta	0.6137	0.8517
Dy	0.5183	0.8716
V	0.4945	0.8763
Tb	0.3977	0.8986
Tl	0.3693	0.9054
Nb	0.2392	0.9362
Ga	0.0431	0.9883

elements does not improve the discrimination between the horizons (SPSS® Base 9.0 Application Guide, 1999).

For the control-group samples, the program selected the highest ranked element (V) in step 1. The program then selected elements in a sequential manner according to their ranking (lower lambda). So, in the second step, Ti was added and the program tested if the combination of V and Ti improved the discrimination between the four K-bentonite horizons. If not, then Ti was excluded and the next element down the list was considered, and so on for all the elements. The program continued this procedure until a combination of elements resulted in the best separation between the four K-bentonite horizons. The results of the stepwise analysis show that only six elements (V, Sm, Nd, Th, Er, Zr) are required for a satisfactory discrimination between the four K-bentonite horizons, each of which has a distinct chemical fingerprint.

The SPSS calculates and prints the discriminant function coefficients for each of the discriminating variables (elements); these can then be used to calculate the scores for each sample. For each case (sample), SPSS calculates its score by multiplying each coefficient by the value of the corresponding variable (element), sums the products and adds a constant (Equation 4.2).

$$D = B_0 + B_1 X_1 + B_2 X_2 + \dots + B_n X_n \dots \dots \dots (4.2)$$

Where  $X_i$  are the values of the independent variables (elemental concentrations),  $B_i$  are the

coefficients for individual variables, and  $B_0$  is a constant.

Three discriminant functions were obtained from the stepwise analysis of the control-group samples. The first function accounts for 80 % of the variance in the discriminant model, while the second and third functions accounted for 12% and 8 %, respectively (Table A4.5). The eigenvalue for the first function is the highest (171) while it is relatively small for the other two functions (27, 17). The highest eigenvalue corresponds to the eigenvector (discriminant function 1) in the direction of the maximum spread of the K-bentonite means. The second eigenvalue corresponds to the eigenvector (discriminant function 2) in a direction that has the second largest spread, etc. (SPSS® Base 9.0 Application Guide, 1999).

The results of the stepwise analysis show that only two functions, accounting for 92% of the sample variance, are sufficient to effectively distinguish the four K-bentonite horizons using the control-group samples (Figure 4.4).

For each of the 18 control-group samples, its discriminant score was calculated by substituting concentrations of the six elements in the sample into Equation 4.2, each multiplied by the discriminant coefficients (Table A4.6). This was done twice because two discriminant functions are employed. For example, consider sample PF-4-96, for which the six elements concentrations (in ppm) are: V=32, Sm=7.6, Nd=33, Th=11, Er=6.4, Zr=343. Using the coefficients in Table A4.6, the discriminant scores for this sample are:



Table A4.5. Properties of the discriminant functions for the control group samples of the four K-bentonite horizons.

Function	Eigenvalue	% of Variance	Cumulative %
1	171.48	79.58	79.58
2	26.81	12.44	92.02
3	17.20	7.98	100.00

Table A4.6. Discriminant function coefficients

	Function 1	Function 2	Function 3
V	-0.141	0.293	-0.214
Sm	5.544	1.495	-1.262
Nd	-1.057	-0.411	0.253
Th	2.218	-0.559	1.585
Er	-6.499	-2.450	-1.712
Zr	0.093	0.054	0.009
(Constant)	-10.85	-12.061	3.687

A38

$$D1 = 32 (-0.14) + 7.6 (5.543) + 33 (-1.056) + 11(2.22) + 6.4 (-6.498) + 343 (0.092) + (-10.85) = 6.338$$

$$D2 = 32 (0.293) + 7.6 (1.49) + 33 (-0.411) + 11 (-0.559) + 6.4 (-2.45) + 343 (0.053) + (-18.179) = 12.434$$

**APPENDIX A5**  
**FOLDING EFFECTS ON THE SECTIONS THICKNESSES**

## **A5. FOLDING EFFECTS ON THE SECTIONS THICKNESSES**

The aim of this thesis is to study the geometry and architecture of a foreland-turbidite basin sequence. Thus, it is important to evaluate factors that might have affected the deposits after deposition, in particular their thickness. Of greatest concern are post-depositional factors that might have affected certain parts of the sequence or certain areas more significantly than others. The degree of compactional or tectonic thinning can only be quantified if strain markers are present in the succession.

Attempts to find objects that could be used as strain markers, such as reduction spots or well preserved fossils, were unsuccessful. An alternative approach used here relies on a comparison of the thicknesses of precisely correlated individual layers, individual beds, groups of beds and stratigraphic intervals between sections located on different parts of the major folds in the area.

These correlations have shown that some intervals in some sections have greater thicknesses than the same intervals in other sections. Specifically, sections SYW, CB and PH have considerably greater thicknesses than equivalent intervals in the nearby SYE section, located on the other limb of the Pointe Séche syncline. (Figure A5.1). It is suggested here that these thickness variations are largely due to folding because such variations in thickness over short distances are not expected and were never observed in any other correlated sections that occur in the same limb of a folds. No such thickness variations were observed in the correlated sections SH, RE and FP1 that are spaced

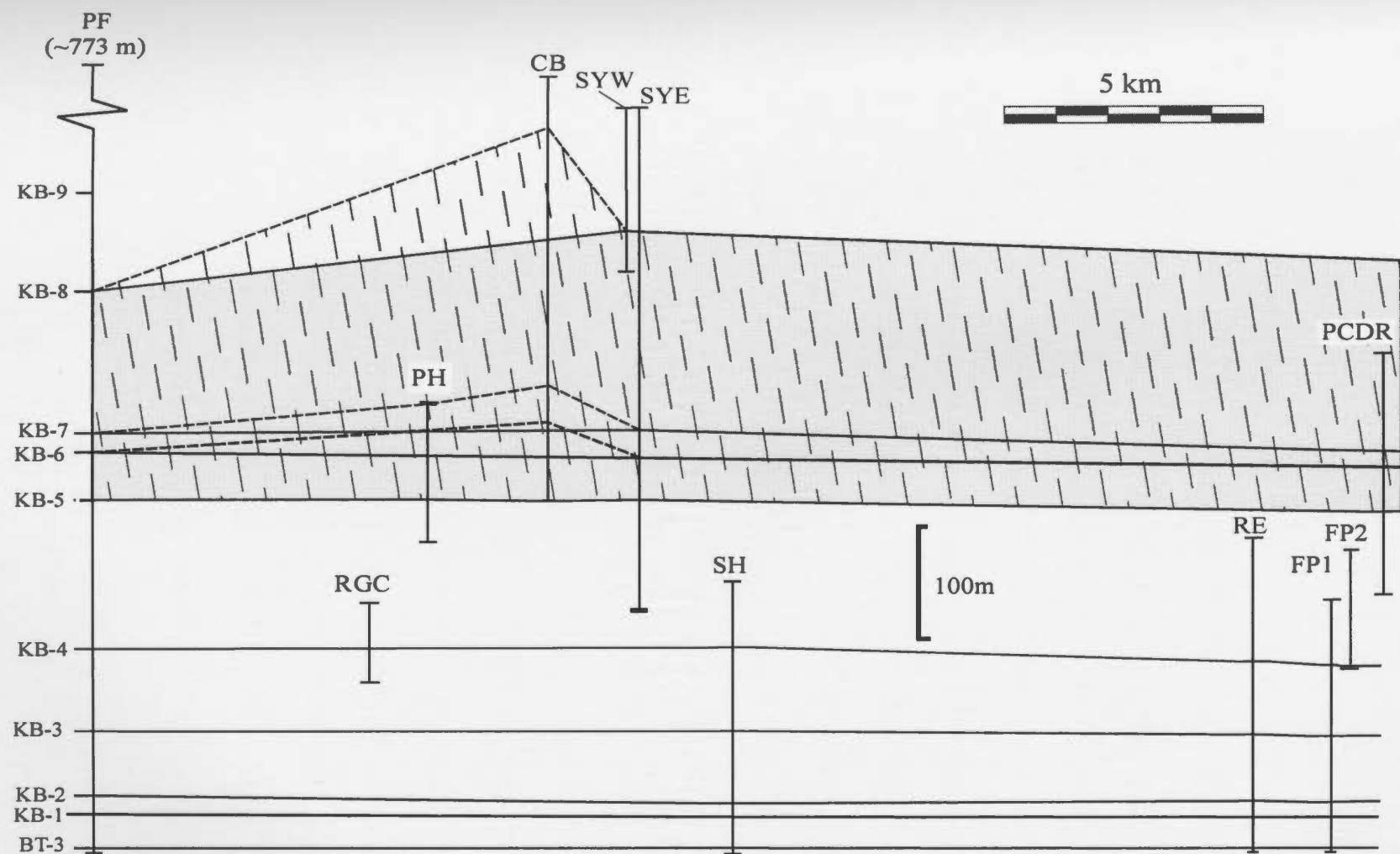


Figure A5.1. Correlation between the sections in the study area based on K-bentonite layers and basin-wide turbidites. This correlation shows that the sequences between BT-3 and KB-5 do not show any significant thickness variations. The sequences between KB-5 and KB-8 show significant thickness variations when the data from sections Cap Barré (CB) and Pointe à Hubert (PH) are considered in the correlations (dashed pattern). The same sequences show less significant thickness variations when the data from sections CB and PH are omitted (shaded pattern). The abnormal thicknesses of these two sections are attributed to structural effects (see text).

farther apart than sections SYE and CB. The facies types in all these sections are essentially the same. Another factor that affected the measured thicknesses is where the sections were measured on a fold. For example, the lower part of the SYE section was measured in the steeply dipping limb of a syncline whereas the upper part of the section was measured in the hinge of the syncline. The choice of where the sections were measured in the field was dictated by the available outcrop and outcrop quality.

In order to investigate the amount of variation in thicknesses between sections SYE and CB, a detailed correlation of these two sections was undertaken. First, based on precisely correlated marker layers, the two sections were divided into six intervals designated here as Interval A to Interval F (Figure A5.2). Secondly, within each of these intervals several individual layers were correlated (Figure A5.3). Based on these correlations, a tabulation of thickness variations for each interval in each section was obtained (Tables A5-1.A to A5-1.F). These data include thicknesses of individual layers, groups of layers bounded by precisely correlated layers, and entire intervals. These intervals compared between sections SYE and CB and cover thicknesses ranging from centimetres to tens of metres and to also include all types of facies in each interval.

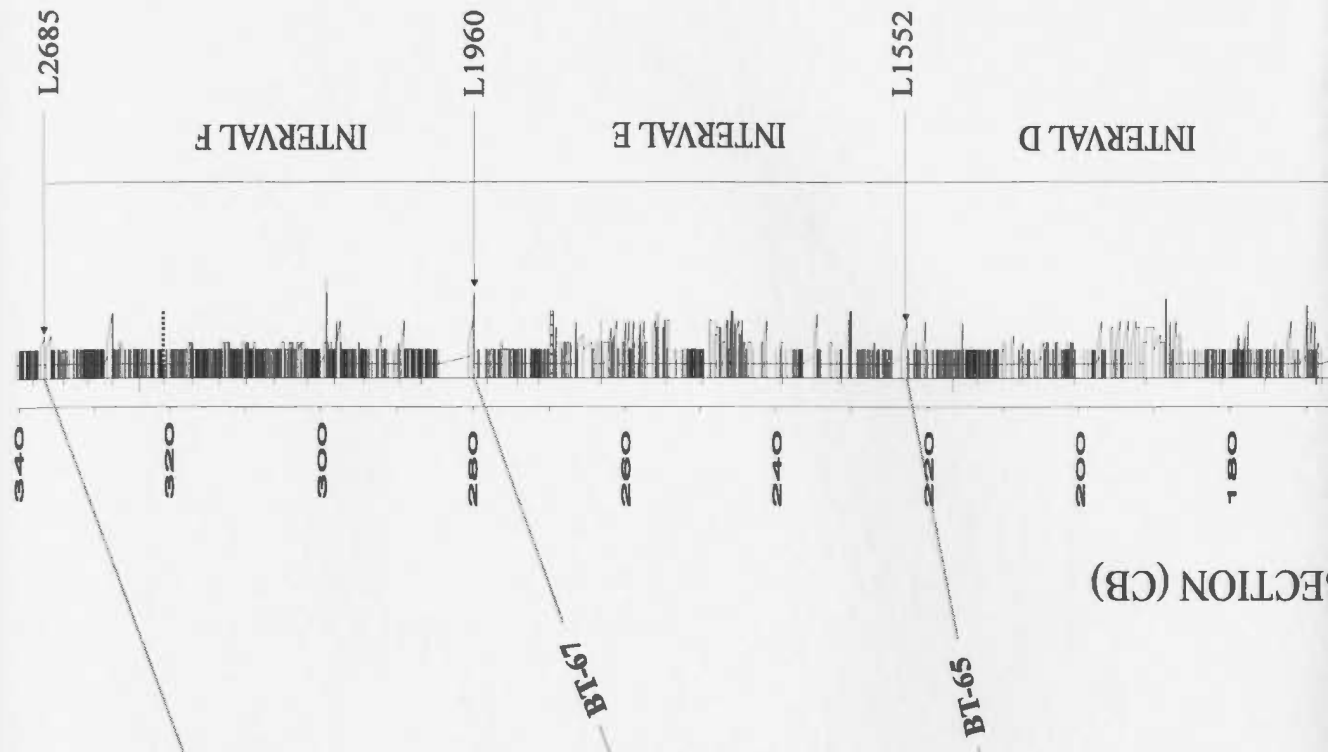
A linear regression analysis was performed for a plot of the thickness of equivalent intervals in the two sections, both interval by interval and for the entire dataset (Figure A5.4). The main conclusions are:

(1) Layers and groups of layers are thinner in section SYE than in section CB;

EAST SECTION (SYE)



SECTION (CB)



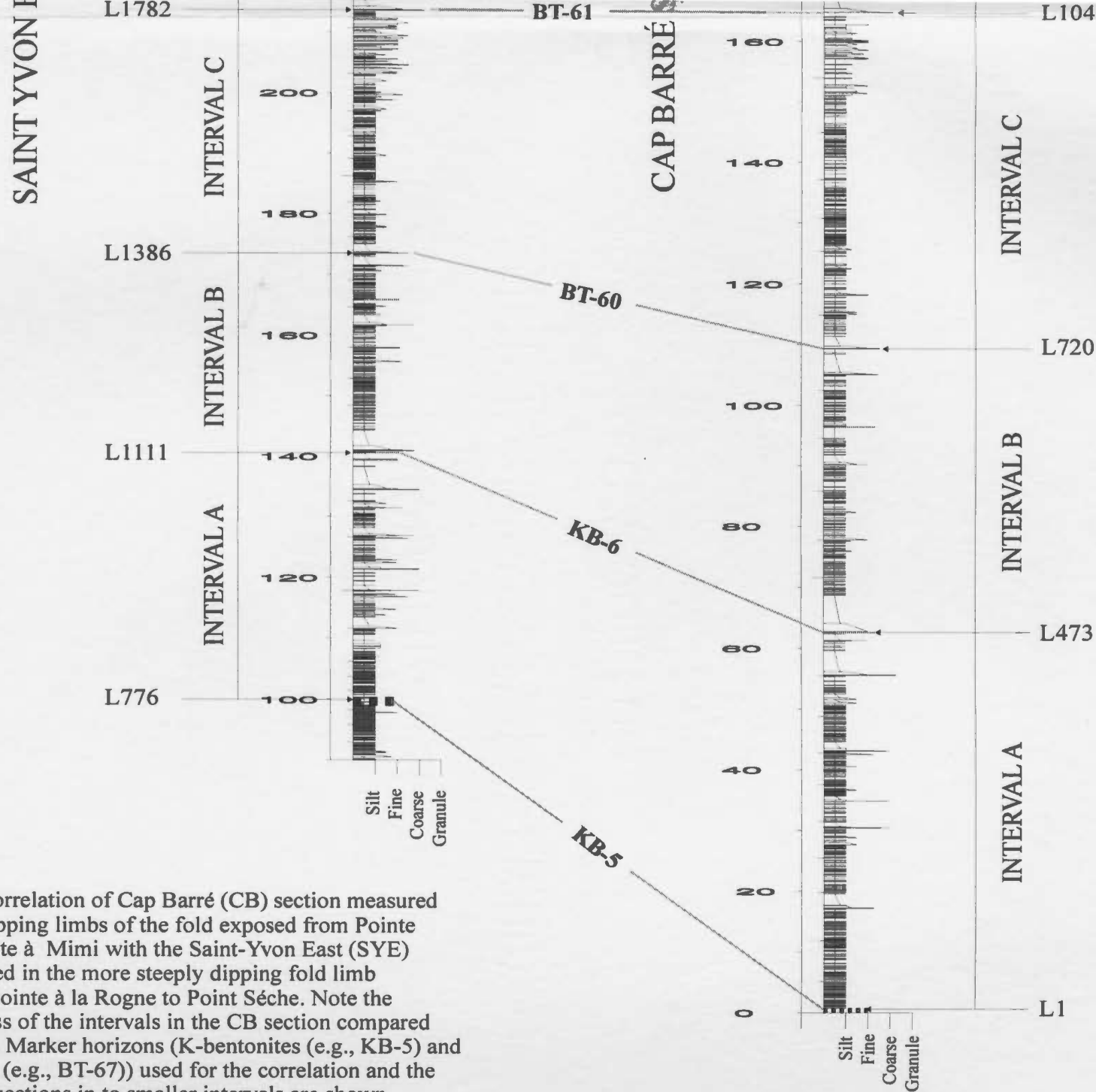


Figure A5.2. Correlation of Cap Barré (CB) section measured in the gently dipping limbs of the fold exposed from Pointe Barreau to Pointe à Mimi with the Saint-Yvon East (SYE) section measured in the more steeply dipping fold limb exposed from Pointe à la Rogne to Point Séche. Note the greater thickness of the intervals in the CB section compared to SYE section. Marker horizons (K-bentonites (e.g., KB-5) and basin turbidites (e.g., BT-67)) used for the correlation and the division of the sections in to smaller intervals are shown.



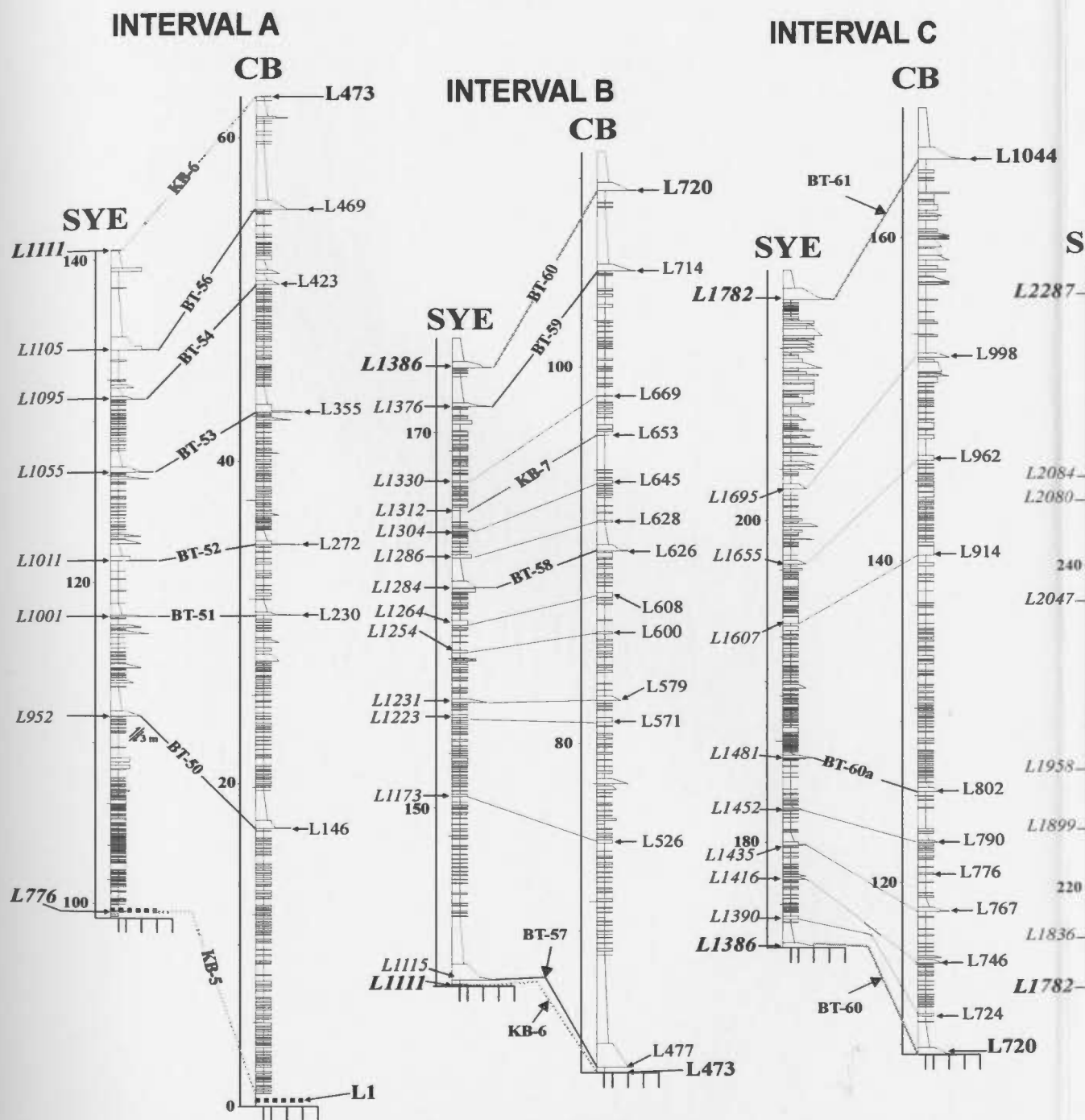
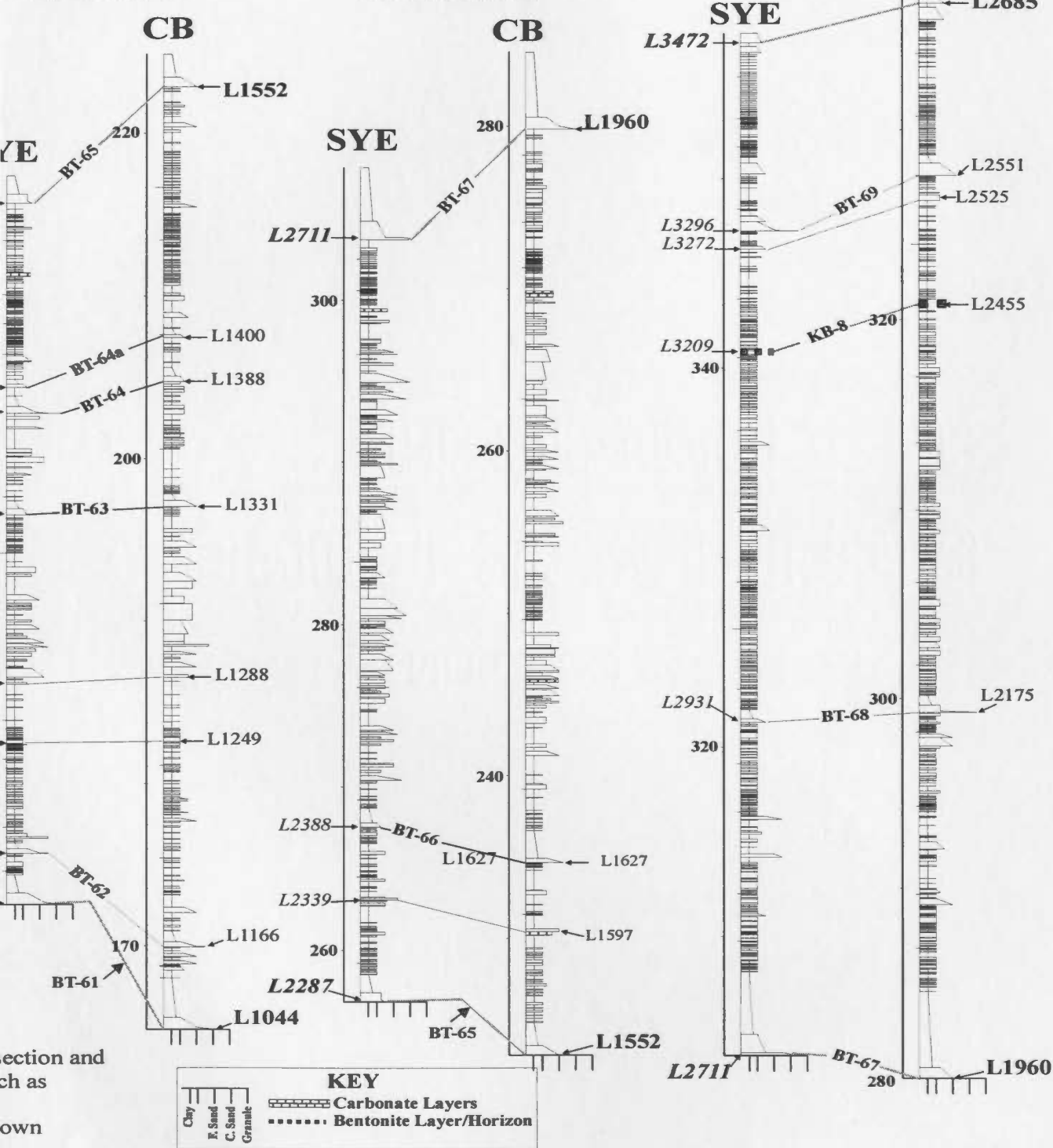


Figure A5.3. Details of each interval shown in Figure A5.2. Segments and individual beds correlated between SYE and CB section in each interval are used to calculate the amount of variation in bed thickness due to folding. Markers such as K-bentonite horizons (KB-5, KB-6, KB-7, KB-8) and basin turbidites (e.g. BT-50) that were correlated across the thesis area are shown. Bed numbers in the SYE section are labelled in italics font (e.g. *L1386*). Each interval has its own vertical scale.

## INTERVAL F

## INTERVAL D

## INTERVAL E



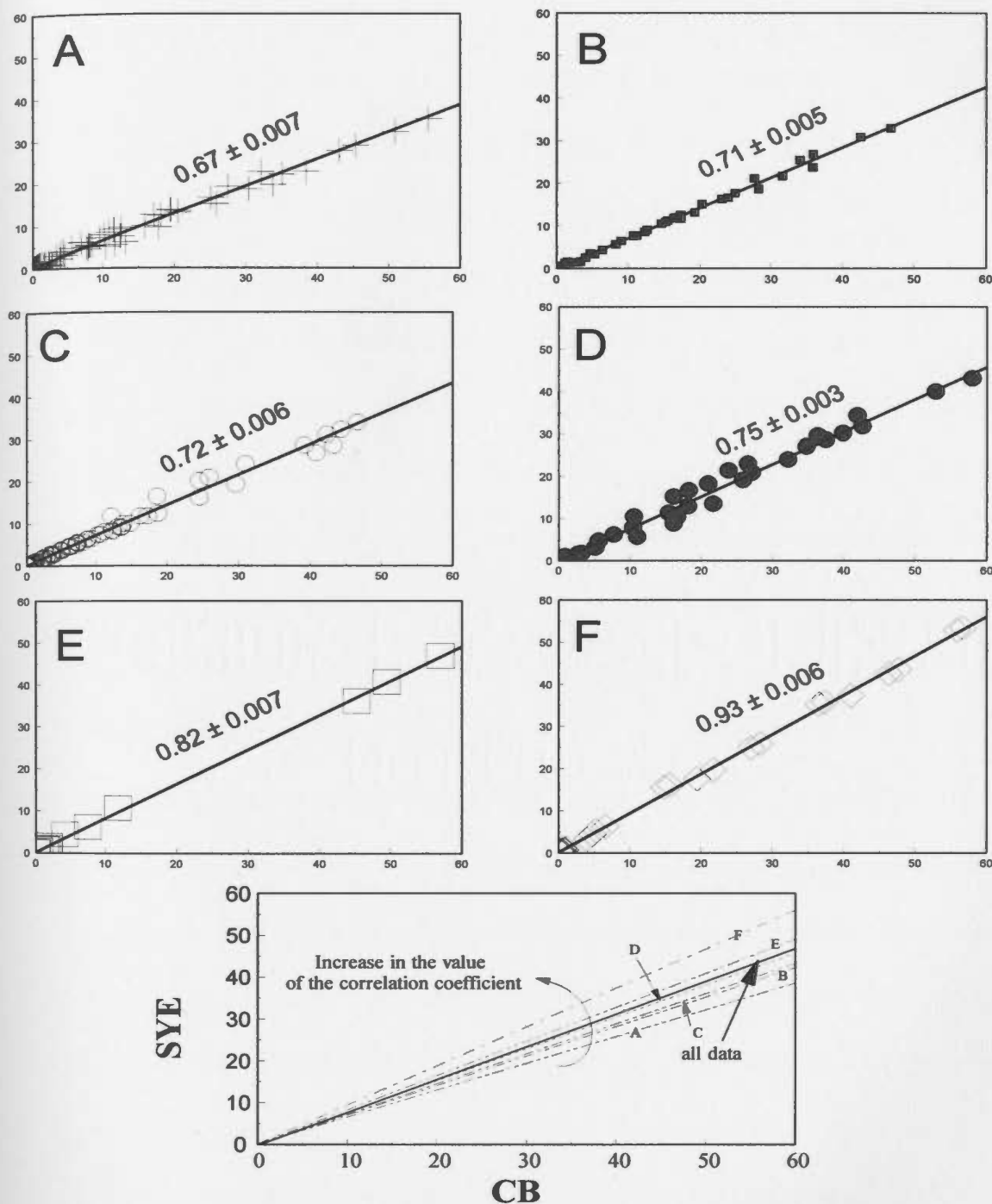


Figure A5.4. Regression analysis for the data-sets of bed thicknesses and interval thicknesses used to estimate the amount of structural thickening thickness of section Cap Barré (CB) relative to section St. Yvon east (SYE).

(2) The degree of thinning in the SYE section gradually decreases from the lower part of the section to the upper part of the section in that beds and intervals of the lower part of SYE may be ~ 67% of the thickness of the same beds and intervals in CB, whereas beds and intervals in the upper part are ~ 93% of the thicknesses at section CB.

It is concluded that section SYE, measured in the more steeply dipping fold limb, has undergone a greater amount of shortening compared to the CB section. The greater degree of thinning in the lower part of the SYE section compared to the upper part is probably a consequent of the position in the fold. Most of the lower parts of the SYE section was measured in the limb of the fold, whereas the upper part of the section was measured in the hinge area of the fold. Flow of rocks from the limb to the hinge of the fold would account for these variation.

All measured sections except SYW, CB, PH and RGC were measured in the overturned or steeply dipping limbs of folds. Hence, it was decided to adjust the thicknesses of sections PH, SYW and CB so that they are comparable to the thicknesses observed in section SYE, thus reducing the variations due to thickening and thinning on different fold limbs. Correction factors were applied to the field measured thicknesses for each interval in section CB and equivalent intervals in sections SYW and PH. No corrections were applied to section RGC because of its thinness and the fact that this section was not used in architectural and facies analysis in the thesis.

The corrections factors applied to thickness of each interval of section CB are

equivalent to the value of the correlation coefficient (slope of the regression line) for each of the six interval that were selected. For example, a correction factor of  $\sim 0.67$  was applied to the basal 62.55m of CB section (interval A). The value of the correction factor increases gradually where it is  $\sim 0.93$  for the top 34 m of the section CB.

Thus, the total thickness for section CB was adjusted from 370.9 m to 290.3 m. Section PH thickness was adjusted from 130.8 m to 106.6 m and section SYW was adjusted from 146 m to 140.6 m.

No correction was applied to sections located in the Pointe-à-la-Renommée area and Pointe à la Rogne (PRM1, PRM2, PCDR, FP2, FP1, RE and SH) because these sections were measured in the same fold limb and are inferred to have experienced comparable amounts of shortening. This also applies to the upper part of the PCDR section which is interpreted to be equivalent to the middle part of the SYE section.

In section PF, which is located further to the west, all beds are overtured (Table 2.2). Furthermore, the lower part of the section was measured near the hinge area of the anticline exposed at Le Brûlé while the middle and upper parts were measured away from the hinge area in the fold limb. Hence, the PF section may have experienced relatively more thinning than other sections. Because the PF section was measured away from the other sections, no corrections were applied to the field measurements. Nevertheless, potential thickness variations of the beds in this section will be considered when discussing the geometry and architecture of the facies and units.

Tables A5-1.A through A5-1.f. Data used to estimate the amount of variation in the thickness of the beds in section CB (columns 2-6) relative to section SYE (columns 7-11) because of tectonic effects. Section CB preserves a greater thickness because of less flattening by folding, and it was decided to normalise its thickness to SYE section in order to facilitate the thickness comparison. Each table refers to one interval in section CB (Figures A3.2 and A3.3). The first column indicates the interval or sub interval used: for example, interval AI is between bed L1 and bed L146. The second column refers to the used in the calculations. Individual and sets of beds were used. For example bed L2685, or two beds (e.g., L14 and L147) or several beds might form segments of varying thicknesses in the interval. The thickness is shown the 6<sup>th</sup> column. The thickness of the same equivalent segment in section SYE is presented in the 11<sup>th</sup> column (for bed numbers in columns 7&8) and is used in the regression analysis. The last column in the table indicates the facies for the beds or interval: sand, silt, mud, megaturbidite (mega), mud cap (cap) or a mixture of different lithologies.

Table A5-1A

Interval		CB				SYE				Thickness	Lithology
& sub inter.	Bed(s)	Bed	Level from	Level to	Thickness	Bed(s)	Bed	Level from	Level to		
AIVc	L470				0.98	L1110				1.07	CAP
AIVc	L469				0.11	L1109				0.21	SAND
AIVc	L469 + L470				1.09	L1109 + L1110				1.28	MEGA
AIVc	L455				3.45	L1106				3.03	CAP
AIVc	L454				0.585	L1105				0.825	SAND
AIVc	L454 + L455				4.035	L1105 + L1106				3.86	MEGA
AIVb	L426				0.64	L1098				0.2	CAP
AIVb	L425				0.225	L1097				0.19	SAND
AIVb	L425 + L426				0.865	L1097 + L1098				0.39	MEGA
AIVb	L424				0.445	L1096				0.54	CAP
AIVb	L423				0.22	L1095				0.175	SAND
AIVb	L423 + L424				0.665	L1095 + L1096				0.715	MEGA
AIVa	L356				1.09	L1056				1.01	CAP
AIVa	L355				0.5	L1055				0.33	SAND
AIVa	L355 + L356				1.59	L1055 + L1056				1.34	MEGA
AIVc	L469 →	L473	61.21	62.53	1.32	L1109	L1111	139.26	140.55	1.29	MIX
AIVc	L454 →	L469	55.57	61.21	5.64	L1105	L1109	134.41	139.26	4.85	MIX
AIVb,c	L425 →	L469	51.61	61.21	9.6	L1097	L1109	132.08	139.26	7.18	MIX
AIVb	L425 →	L454	51.61	55.57	3.96	L1097	L1055	132.08	134.41	2.33	MIX
AIVb,c	L425 →	L473	51.61	62.53	10.92	L1097	L1111	132.08	140.55	8.47	MIX
AIVb,c	L423 →	L469	50.95	61.21	10.26	L1095	L1109	131.35	139.26	7.91	MIX
AIVb,c	L423 →	L473	50.95	62.53	11.58	L1095	L1111	131.35	140.55	9.2	MIX
AIVa,b,c	L355 →	L469	43.09	61.21	18.12	L1055	L1109	126.82	139.26	12.44	MIX
AIVa,b	L355 →	L454	43.09	55.57	12.48	L1055	L1105	126.82	134.41	7.59	MIX
AIVa,b	L355 →	L425	43.09	51.61	8.52	L1055	L1097	126.82	132.08	5.26	MIX
AIVc	L454 →	L473	55.57	62.53	6.96	L1105	L1111	134.41	140.55	6.14	MIX
AIVb	L423 →	L454	50.95	55.57	4.62	L1095	L1105	131.35	134.41	3.06	MIX
AIVa	L355 →	L423	43.04	50.95	7.91	L1055	L1095	126.82	131.35	4.53	MIX
AIV	L355 →	L473	43.04	62.53	19.49	L1055	L1111	126.82	140.55	13.73	MIX
AIIIb	L272 →	L353	34.82	42.93	8.11	L1011	L1053	121.33	126.74	5.41	MIX
AIIIb	L272 →	L351	34.82	42.82	8	L1011	L1051	121.33	126.64	5.31	MIX
AIIIb	L272 →	L349	34.82	42.57	7.75	L1011	L1049	121.33	126.37	5.04	MIX
AIIIb	L349+350+351				0.25	L1049+50+51				0.3	MIX
AIIIb	L349+350+351+352				0.36	L1049+50+51+52				0.37	MIX
AIIIb	L349+350+351+352+353				0.4	L1049+50+51+52+53				0.4	MIX

Table A5-1A Continued

Interval & sub inter.	Bed(s)	Bed	CB Level from	Level to	Thickness	Bed(s)	Bed	SYE Level from	Level to	Thickness	Lithology
AIIIb	L349+350+351+352+353+L354				0.48	L1049+50+51+52+53+54				0.45	MIX
AIIIb	L353+L354				0.12	L1053+L1054				0.08	MEX
AIIIb	L354				0.08	L1054				0.05	MUD
AIIIb	L353				0.04	L1053				0.03	SILT
AIIIb	L351+L352				0.15	L1051+L1052				0.1	MEX
AIIIb	L352				0.11	L1052				0.07	MUD
AIIIb	L351				0.04	L1051				0.03	SILT
AIIIb	L349+L350				0.21	L1049+L1050				0.27	MEX
AIIIb	L350				0.08	L1050				0.09	MUD
AIIIb	L349				0.13	L1049				0.18	SAND
AIIIb	L273				0.66	L1012				0.785	CAP
AIIIb	L272				0.225	L1011				0.235	SAND
AIIIb	L272 + L273				0.885	L1011 + L1012				1.02	MEGA
AIIIa	L249				0.79	L1002				0.74	MUD
AIIIa	L248				0.21	L1001				0.1	SAND
AIIIa	L248 + L249				0.98	L1001 + L1002				0.84	MEGA
AIIIb	L272 → L355	34.82	43.07		8.25	L1011	L1055	121.33	126.82	5.49	MIX
AIIIa	L248 → L272	30.41	34.82		4.41	L1001	L1011	117.19	121.33	4.14	MIX
AIII	B248 → L355	30.41	43.07		12.66	L1001	L1055	117.19	126.82	9.63	MIX
AII	L234 → L248	28.75	30.41		1.66	L996	L1001	117.19	117.84	0.65	MIX
AII	L232 → L248	28.01	30.41		2.4	L994	L1001	117.07	117.84	0.77	MIX
AII	L230 → L248	27.6	30.41		2.81	L992	L1001	117.19	117.84	0.65	MIX
AII	L146 → L234	17.18	28.93		11.75	L952	L996	111.65	117.19	5.54	MEX
AII	L146 → L230	17.148	27.6		10.452	L952	L992	111.65	116.76	5.11	MIX
AII	L230 → L248	27.66	30.41		2.75	L992	L1001	116.76	117.84	1.08	MIX
AII	L230 → L234	27.66	28.75		1.09	L992	L996	116.76	117.19	0.43	MIX
AII	L234				0.165	L996				0.11	SAND
AII	L232+L233				0.545	C:L994+L995				0.12	SILT+MUD
AII	L233				0.36	L995				0.08	MUD
AII	L232				0.185	L994				0.04	SILT
AII	L230+L231				0.61	C:L992+L993				0.31	SAND+MUI
AII	L231				0.2	L993				0.09	MUD
AII	L230				0.41	L992				0.22	SAND
AII	L147				1.85	L953				1.49	MUD
AII	L146				0.51	L952				0.33	SAND
AII	L146+L147				2.36	L952+L953				1.82	MEGA
AII	L146 → L248	17.18	30.41		13.23	L952	L1001	111.65	117.84	6.19	MIX
AI	L1 → L146	0	17.18		17.18	L776	L952	99.07	111.65	12.58	MIX
A	L1 → L473	0	62.55		62.55	L776	L1111	99.18	140.55	41.37	MIX



Table A5-1B

Interval		CB			SYE						Lithology
& sub inter.	Bed(s)	Bed	Level from	Level to	Thickness	Bed(s)	Bed	Level from	Level to	Thickness	
BI,BII	L608	→ L720	87.75	109.33	21.58	L1264	L1386	159.69	173.43	13.74	MIX
BI,BII	L608	→ L714	87.75	105.09	17.34	L1264	L1376	159.69	171.35	11.66	MIX
BI,BII	L608	→ L669	87.75	98.44	10.69	L1264	L1330	159.69	167.31	7.62	MIX
BI,BII	L608	→ L657	87.75	96.73	8.98	L1264	L1316	159.69	166.14	6.45	MIX
BI,BII	L600	→ L720	85.81	109.33	23.52	L1254	L1386	158.24	173.43	15.19	MIX
BI,BII	L600	→ L714	85.81	105.09	19.28	L1254	L1376	158.24	171.35	13.11	MIX
BI,BII	L600	→ L669	85.81	98.44	12.63	L1254	L1330	158.24	167.31	9.07	MIX
BI,BII	L600	→ L655	85.81	96.57	10.76	L1254	L1314	158.24	165.97	7.73	MIX
BI,BII	L571	→ L720	81.11	109.33	28.22	L1223	L1386	154.77	173.43	18.66	MIX
BI,BII	L571	→ L714	81.11	105.09	23.98	L1223	L1376	154.77	171.35	16.58	MIX
BI,BII	L571	→ L669	81.11	98.44	17.33	L1223	L1330	154.77	167.31	12.54	MIX
BI,BII	L571	→ L655	81.11	96.57	15.46	L1223	L1314	154.77	165.97	11.2	MIX
BI,BII	L516	→ L720	73.51	109.33	35.82	L1163	L1386	149.69	173.43	23.74	MIX
BI,BII	L516	→ L714	73.51	105.09	31.58	L1163	L1376	149.69	171.35	21.66	MIX
BI,BII	L516	→ L669	73.51	98.44	24.93	L1163	L1330	149.69	167.31	17.62	MIX
BI,BII	L516	→ L655	73.51	96.57	23.06	L1163	L1314	149.69	165.97	16.28	MIX
BI,BII	L516	→ L645	73.51	93.81	20.3	L1163	L1304	149.69	164.72	15.03	MIX
BI,BII	L516	→ L627	73.51	90.2	16.69	L1163	L1284	149.69	161.68	11.99	MIX
BI,BII	L516	→ L624	73.51	89.87	16.36	L1163	L1282	149.69	161.45	11.76	MIX
BI,BII	L473	→ L720	62.55	109.33	46.78	L1111	L1386	140.55	173.43	32.88	MIX
BI,BII	L473	→ L714	62.55	105.09	42.54	L1111	L1376	140.55	171.35	30.8	MIX
BI,BII	L473	→ L669	62.55	98.44	35.89	L1111	L1330	140.55	167.31	26.76	MIX
BI,BII	L473	→ L655	62.55	96.57	34.02	L1111	L1314	140.55	165.97	25.42	MIX
BII	L669	→ L714	98.44	105.09	6.65	L1330	L1376	167.31	171.35	4.04	MIX
BII	L655	→ L714	96.57	105.09	8.52	L1314	L1376	165.97	171.35	5.38	MIX
BII	L655	→ L669	96.57	98.44	1.87	L1314	L1330	165.97	167.31	1.34	MIX
BII	L627	→ L669	90.2	98.44	8.24	L1284	L1330	161.68	167.31	5.63	MIX
BII	L627	→ L655	90.2	96.57	6.37	L1284	L1314	161.68	165.97	4.29	MIX
BII	L714				3.345	L1377+L1376				1.59	MEGA
BII	L714				2.99	L1377				1.374	CAP
BII	L714				0.355	L1376				0.215	SAND

Table A5-1B Continued

Interval		CB				SYE				Thickness	Lithology
& sub inter.	Bed(s)	Bed	Level from	Level to	Thickness	Bed(s)	Bed	Level from	Level to		
BII	L657				0.21	L1316				0.173	SILT
BII	L645				0.16	L1304				0.153	SAND
BII	L631				0.055	L1288				0.04	SILT
BII	L628+L627				1.55	L1285+L1284				1.585	MEGA
BII	L628				1.19	L1285				1.22	CAP
BII	L627				0.36	L1284				0.365	SAND
BII	L627 →	L720	90.2	109.33	19.13	L1284	L1386	161.68	173.43	11.75	MIX
BI	L571 →	L600	81.11	85.81	4.7	L1223	L1254	154.77	158.24	3.47	MIX
BI	L571 →	L579	81.11	82.26	1.15	L1223	L1231	154.77	155.61	0.84	MIX
BI	L526 →	L624	74.66	89.87	15.21	L1173	L1282	150.57	161.45	10.88	MIX
BI	L526 →	L618	74.66	89.26	14.6	L1173	L1274	150.57	161.05	10.48	MIX
BI	L526 →	L600	74.66	85.81	11.15	L1173	L1254	150.57	158.24	7.67	MIX
BI	L526 →	L571	74.66	81.11	6.45	L1173	L1223	150.57	154.77	4.2	MIX
BI	L516 →	L624	73.51	89.87	16.36	L1163	L1282	149.69	161.45	11.76	MIX
BI	L516 →	L600	73.51	85.81	12.3	L1163	L1254	149.69	158.24	8.55	MIX
BI	L516 →	L571	73.51	81.11	7.6	L1163	L1223	149.69	154.77	5.08	MIX
BI	L516 →	L526	73.51	74.66	1.15	L1163	L1173	149.69	150.57	0.88	MIX
BI	L624				0.26	L1282				0.193	SAND
BI	L618				0.1	L1274				0.051	SILT
BI	L610 →	L616	88.34	89.01	0.67	L1266	L1272	160.31	160.81	0.5	SILT
BI	L608				0.25	L1264				0.275	SILT
BI	L606				0.09	L1262				0.081	SILT
BI	L600				0.14	L1254				0.153	SILT
BI	L579				0.24	L1231				0.2	SAND
BI	L571				0.245	L1223				0.173	SILT
BI	L526				0.18	L1173				0.112	SILT
BI	L518 →	L522	73.85	73.97	0.12	L1165	L1167	149.91	150	0.09	SILT
BI	L516				0.1	L1163	L1165	149.69	149.91	0.07	SILT
BI	L477+L478				5.315	L1116+L1115				3.355	MEGA
BI	L478				4.04	L1116				2.55	CAP
BI	L477				1.275	L1115				0.79	SAND
BI	L473 →	L627	62.55	90.2	27.65	L1111	L1284	140.55	161.68	21.13	MIX
B	L473 →	L720	62.55	109.33	46.78	L1111	L1386	140.55	173.43	32.88	MIX

Table A5-1C

Interval		CB				SYE					Lithology
& sub inter.	Bed(s)	Bed	Level from	Level to	Thickness	Bed(s)	Bed	Level from	Level to	Thickness	
CH,CIII	L908	L1044	138.94	164.83	25.89	L1601	L1782	192.74	213.69	20.95	MIX
CH,CIII	L908	L988	138.94	152.61	13.67	L1601	L1695	192.74	201.94	9.2	MIX
CH,CIII	L876	L1044	133.88	164.83	30.95	L1516	L1782	189.57	213.69	24.12	MIX
CH,CIII	L876	L988	133.88	152.61	18.73	L1516	L1695	189.57	201.94	12.37	MIX
CH,CIII	L802	L1044	125.6	164.83	39.23	L1452	L1782	185.18	213.69	28.51	MIX
CH,CIII	L790	L1044	122.47	164.83	42.36	L1452	L1782	182.63	213.69	31.06	MIX
CH,CIII	L790	L802	122.47	125.6	3.13	L1452	L1481	182.63	185.18	2.55	MIX
CH,CIII	L776	L1044	120.47	164.83	44.36	L1446	BT#61	181.47	213.69	32.22	MIX
CH,CIII	L776	L802	120.47	125.6	5.13	L1446	L1481	181.47	185.18	3.71	MIX
CH,CIII	L768	L1044	118.19	164.83	46.64	L1436	L1782	179.78	213.69	33.91	MIX
CH,CIII	L768	L802	118.19	125.6	7.41	L1436	L1481	179.78	185.18	5.4	MIX
CH,CIII	L768	L790	118.19	122.47	4.28	L1436	L1452	179.78	182.63	2.85	MIX
CH,CIII	L768	L776	118.19	120.47	2.28	L1436	L1446	179.78	181.47	1.69	MIX
CI,CH	L754	L802	115.31	125.6	10.29	L1418	L1481	177.86	185.18	7.32	MIX
CI,CH	L754	L790	115.31	122.47	7.16	L1418	L1452	177.86	182.63	4.77	MIX
CI,CH	L754	L766	115.31	120.47	5.16	L1418	L1446	177.86	181.47	3.61	MIX
CI,CH,CIII	L724	L988	111.75	152.61	40.86	L1390	L1695	175.22	201.94	26.72	MIX
CI,CH	L724	L802	111.75	125.6	13.85	L1390	L1481	175.22	185.18	9.96	MIX
CI,CH	L724	L790	111.75	122.47	10.72	L1390	L1452	175.22	182.63	7.41	MIX
CI,CH	L724	L766	111.75	120.47	8.72	L1390	L1446	175.22	181.47	6.25	MIX
CI,CH,CIII	L720	L988	109.32	152.61	43.29	L1386	L1695	173.43	201.94	28.51	MIX
CI,CH	L720	L908	109.32	138.94	29.62	L1386	L1601	173.43	192.74	19.31	MIX
CI,CH	L720	L876	109.32	133.88	24.56	L1386	L1516	173.43	189.57	16.14	MIX
CI,CH	L720	L802	109.32	125.6	16.28	L1386	L1481	173.43	185.18	11.75	MIX
CI,CH	L720	L790	109.32	122.47	13.15	L1386	L1452	173.43	182.63	9.2	MIX
CI,CH	L720	L766	109.32	120.47	11.15	L1386	L1446	173.43	181.47	8.04	MIX
CIII	L1045+1044				3.175	L1783+1782				1.8	MEGA
CIII	L1045				2.42	L1783				1.1	CAP
CIII	L1044				0.755	L1782				0.7	SAND
CIII	L998				0.25	L1695				0.32	SAND

Table A5-1C Continued

Interval		CB				SYE					Lithology
& sub inter.	Bed(s)	Bed	Level from	Level to	Thickness	Bed(s)	Bed	Level from	Level to	Thickness	
CIII	L962				0.295	L1655	L1655	197.25	197.25	0.26	SAND
CIII	L916				0.18	L1609	L1609	194.03	194.03	0.19	SILT
CIII	L914				0.227	L1607	L1607	193.55	193.55	0.43	SILT
CIII	L998	→ L1044	152.61	164.83	12.22	L1695	L1782	201.94	213.69	11.75	MIX
CIII	L962	→ L1044	146.2	164.83	18.63	L1655	L1782	197.25	213.69	16.44	MIX
CIII	L962	→ L998	146.2	152.61	6.41	L1655	L1695	197.25	201.94	4.69	MIX
CIII	L914	→ L1044	140.31	164.83	24.52	L1607	L1782	193.55	213.69	20.14	MIX
CIII	L914	→ L998	140.31	152.61	12.3	L1607	L1695	193.55	201.94	8.39	MIX
CIII	L914	→ L1044	140.31	164.83	24.52	L1607	L1782	193.55	213.69	20.14	MIX
CII	L912				0.227	L1605				0.26	SILT
CII	L908				0.114	L1601				0.12	SILT
CII	L876				0.205	L1561				0.235	SILT/SAND
CII	L874				0.35	L1559				0.015	SILT
CII	L803+L802				0.6	L1481				0.37	mega
CII	L803				0.34	L1481				0.15	cap
CII	L802				0.26	L1481				0.22	sand
CI	L802				0.26	L1481				0.22	SILT
CI	L791+L790				0.53	L1452				0.28	MEGA
CI	L791				0.42	L1452				0.18	CAP
CI	L790				0.11	L1452				0.1	SAND
CI	L788				0.11	L1458				0.09	SILT
CI	L776				0.09	L1446				0.06	SILT
CI	L768+L769				0.88	L1436				0.81	MEGA
CI	L769				0.62	L1436				0.59	CAP
CI	L768				0.26	L1436				0.22	SAND
CI	L767				0.3	L1435				0.07	MUD
CI	L766				0.08	L1434				0.06	SILT
CI	L764				0.05	L1432				0.06	SILT
CI	L763				0.32	L1431				0.2	MUD

Table A5-1C Continued

Interval		CB				SYE					Lithology
& sub inter.	Bed(s)	Bed	Level from	Level to	Thickness	Bed(s)	Bed	Level from	Level to	Thickness	
CI	L762				0.08	L1430				0.1	SILT
CI	L754				0.16	L1418				0.11	SAND
CI	L752				0.21	L1416				0.13	SAND
CI	L751				0.1	L1415				0.07	MUD
CI	L750				0.044	L1414				0.03	SILT
CI	L749				0.1	L1413				0.07	MUD
CI	L748				0.035	L1412				0.03	SILT
CI	L747				0.21	L1411				0.23	MUD
CI	L746				0.11	L1410				0.07	SILT
CI	L744				0.08	L1408				0.09	SILT
CI	L736				0.027	L1402				0.02	SILT
CI	L734				0.05	L1400				0.04	SILT
CI	L732				0.045	L1398				0.044	SILT
CI	L730				0.04	L1396				0.03	SILT
CI	L728				0.053	L1394				0.044	SILT
CI	L726				0.035	L1392				0.04	SILT
CI	L724				0.14	L1390				0.177	SILT
CI	L768	→ L790	118.19	122.47	4.28	L1436	L1452	179.78	182.63	2.85	MIX
CI	L768	→ L776	118.19	120.47	2.28	L1436	1446	179.78	181.47	1.69	MIX
CI	L762	→ L776	116.68	120.47	3.79	L1430	1446	179	181.47	2.47	MIX
CI	L754	→ L790	115.31	122.47	7.16	L1418	L1452	177.86	182.63	4.77	MIX
CI	L754	→ L776	115.31	120.47	5.16	L1418	1446	177.86	181.47	3.61	MIX
CI	L754	→ L768	115.31	118.19	2.88	L1418	L1436	177.86	179.78	1.92	MIX
CI	L754	→ L762	115.31	116.68	1.37	L1418	1430	177.86	179	1.14	MIX
CI	L744	→ L802	114.23	126.6	12.37	L1408	L1481	177.04	185.18	8.14	MIX
CI	L744	→ L790	114.23	122.47	8.24	L1408	L1452	177.04	182.63	5.59	MIX
CI	L744	→ L776	114.23	120.47	6.24	L1408	1446	177.04	181.47	4.43	MIX
CI	L744	→ L768	114.23	118.19	3.96	L1408	L1436	177.04	179.78	2.74	MIX
CI	L744	→ L762	114.23	116.68	2.45	L1408	1430	177.04	179	1.96	MIX
CI	L744	→ L754	114.23	115.31	1.08	L1408	1418	177.04	177.86	0.82	MIX

Table A5-1C Continued

Interval			CB			SYE						Lithology
& sub inter.	Bed(s)		Level from	Level to	Thickness	Bed(s)	Bed	Level from	Level to	Thickness		
CI	L736	→	L802	113.05	126.6	13.55	L1402	L1481	176.19	185.18	8.99	MIX
CI	L736	→	L790	113.05	122.47	9.42	L1402	L1452	176.19	182.63	6.44	MIX
CI	L736	→	L776	113.05	120.47	7.42	L1402	1446	176.19	181.47	5.28	MIX
CI	L736	→	L768	113.05	118.19	5.14	L1402	L1436	176.19	179.78	3.59	MIX
CI	L736	→	L762	113.05	116.68	3.63	L1402	1430	176.19	179	2.81	MIX
CI	L736	→	L754	113.05	115.31	2.26	L1402	1418	176.19	177.86	1.67	MIX
CI	L736	→	L744	113.05	114.23	1.18	L1402	1408	176.19	177.04	0.85	MIX
CI	L724	→	L802	111.75	126.6	14.85	L1390	L1481	175.22	185.18	9.96	MIX
CI	L724	→	L790	111.75	122.47	10.72	L1390	L1452	175.22	182.63	7.41	MIX
CI	L724	→	L776	111.75	120.47	8.72	L1390	1446	175.22	181.47	6.25	MIX
CI	L724	→	L768	111.75	118.19	6.44	L1390	L1436	175.22	179.78	4.56	MIX
CI	L724	→	L762	111.75	116.68	4.93	L1390	1430	175.22	179	3.78	MIX
CI	L724	→	L754	111.75	115.31	3.56	L1390	1418	175.22	177.86	2.64	MIX
CI	L724	→	L744	111.75	114.23	2.48	L1390	1408	175.22	177.04	1.82	MIX
CI	L724	→	L736	111.75	113.05	1.3	L1390	1402	175.22	176.19	0.97	MIX
CI	L720	→	L802	109.32	126.6	17.28	L1386	L1481	173.43	185.18	11.75	MIX
CI	L720	→	L790	109.32	122.47	13.15	L1386	L1452	173.43	182.63	9.2	MIX
CI	L720	→	L776	109.32	120.47	11.15	L1386	1446	173.43	181.47	8.04	MIX
CI	L720	→	L768	109.32	118.19	8.87	L1386	L1436	173.43	179.78	6.35	MIX
CI	L720	→	L762	109.32	116.68	7.36	L1386	1430	173.43	179	5.57	MIX
CI	L720	→	L754	109.32	115.31	5.99	L1386	1418	173.43	177.86	4.43	MIX
CI	L720	→	L736	109.32	113.05	3.73	L1386	1402	173.43	176.19	2.76	MIX
CI	L720	→	L724	109.32	111.75	2.43	L1386	L1390	173.43	175.22	1.79	MIX
CIII	L913	→	L1044	140.31	164.83	24.52	L1607	L1782	193.55	213.69	20.14	MIX
CI	L720	→	L768	109.32	125.6	16.28	L1386	L1481	173.43	185.18	11.75	MIX
C	L720	→	L1044	109.32	164.83	55.51	L1386	L1782	173.43	213.69	40.26	MIX

Table A5-1D

Interval		CB					SYE					Lithology
& sub inter.	Bed(s)	→	Bed	Level from	Level to	Thickness	Bed(s)	Bed	Level from	Level to	Thickness	
DI,D2	L1249	→	L1552	180.91	222.83	41.92	L1899	L2287	222.48	256.8	34.32	MIX
DI,D2	L1249	→	L1400	180.91	207.43	26.52	L1899	L2084	222.48	245.47	22.99	MIX
DI,D2	L1249	→	L1388	180.91	204.72	23.81	L1899	L2080	222.48	243.88	21.4	MIX
DI,D2	L1249	→	L1331	180.91	197.02	16.11	L1899	L2047	222.48	237.68	15.2	MIX
DI,D2	L1249	→	L1288	180.91	186.49	5.58	L1899	L1958	222.48	227.2	4.72	MIX
DI,D2	L1166	→	L1552	169.94	222.83	52.89	L1836	L2287	216.81	256.8	39.99	MIX
DI,D2	L1166	→	L1400	169.94	207.43	37.49	L1836	L2084	216.81	245.47	28.66	MIX
DI,D2	L1166	→	L1388	169.94	204.72	34.78	L1836	L2080	216.81	243.88	27.07	MIX
DI,D2	L1166	→	L1331	169.94	197.02	27.08	L1836	L2047	216.81	237.68	20.87	MIX
DI,D2	L1166	→	L1288	169.94	186.49	16.55	L1836	L1958	216.81	227.2	10.39	MIX
DI,D2	L1044	→	L1552	164.83	222.83	58	L1782	L2287	213.69	256.8	43.11	MIX
DI,D2	L1044	→	L1400	164.83	207.43	42.6	L1782	L2084	213.69	245.47	31.78	MIX
DI,D2	L1044	→	L1388	164.83	204.72	39.89	L1782	L2080	213.69	243.88	30.19	MIX
DI,D2	L1044	→	L1331	164.83	197.02	32.19	L1782	L2047	213.69	237.68	23.99	MIX
DI,D2	L1044	→	L1288	164.83	186.49	21.66	L1782	L1958	213.69	227.2	13.51	MIX
DII	L1400	→	L1552	207.43	222.83	15.4	L2084	L2287	245.47	256.8	11.33	MIX
DII	L1388	→	L1552	204.72	222.83	18.11	L2080	L2287	243.88	256.8	12.92	MIX
DII	L1388	→	L1400	204.72	207.43	2.71	L2080	L2084	243.88	245.47	1.59	MIX
DII	L1331	→	L1552	197.02	222.83	25.81	L2047	L2287	237.68	256.8	19.12	MIX
DII	L1331	→	L1400	197.02	207.43	10.41	L2047	L2084	237.68	245.47	7.79	MIX
DII	L1331	→	L1388	197.02	204.72	7.7	L2047	L2080	237.68	243.88	6.2	MIX
DII	L1288	→	L1552	186.49	222.83	36.34	L1958	L2287	227.2	256.8	29.6	MIX
DII	L1288	→	L1400	186.49	207.43	20.94	L1958	L2084	227.2	245.47	18.27	MIX
DII	L1288	→	L1388	186.49	204.72	18.23	L1958	L2080	227.2	243.88	16.68	MIX

Table A5-1D Continued

Interval		CB		SYE									
& sub inter.	Bed(s)	Bed	Level from	Level to	Thickness	Bed(s)	Bed	Level from	Level to	Thickness	Lithology		
DII	L1288 → L1331	L1331	186.49	197.02	10.53	L1958	L2047	227.2	237.68	10.48	MIX		
DII	L1288 → L1288	L1288	186.49		0.19	L1958	L1958	227.2		0.12	SAND		
DII	L1331+L1332331+L13		197.02		0.785	L2047+L2048)47+L2		237.68		0.81	MEGA		
DII	L1332 → L1332	L1332	197.02		0.42	L2048	L2048	237.68		0.46	CAP		
DII	L1331 → L1331	L1331	197.02		0.365	L2047	L2047	237.68		0.35	SAND		
DII	L1401+L1400401+L14		207.43		0.57	L2085+L2084)85+L2		245.47		0.51	MEGA		
DII	L1401 → L1401	L1401	207.43		0.36	L2085	L2085	245.47		0.3	CAP		
DII	L1400 → L1400	L1400	207.43		0.21	L2084	L2084	245.47		0.21	SAND		
DII	L1389+L1388389+L13		204.72		0.875	L2081+L2080)81+L2		243.88		1.05	MEGA		
DII	L1389 → L1389	L1389	204.72		0.52	L2081	L2081	243.88		0.63	CAP		
DII	L1388 → L1388	L1388	204.72		0.355	L2080	L2080	243.88		0.42	SAND		
DII	L1332+L1331332+L13		197.02		0.785	L2048+L2047)48+L2		237.68		0.81	MEGA		
DII	L1332 → L1332	L1332	197.02		0.42	L2048	L2048	237.68		0.46	CAP		
DII	L1331 → L1331	L1331	197.02		0.365	L2047	L2047	237.68		0.35	SAND		
DI	L1249 → L1249	L1249	180.91		0.1	L1899	L1899	222.48		0.05	SILT		
DI	L1166+L1167166+L11		169.94		0.965	L1836+L1837)36+L1		216.81		0.645	MEGA		
DI	L1167 → L1167	L1167	169.94		0.68	L1837	L1837	216.81		0.36	CAP		
DI	L1166 → L1166	L1166	169.94		0.285	L1836	L1836	216.81		0.285	SAND		
DI	L1044+L1045044+L10		164.83		3.17	L1782+L1783)82+L1		213.69		1.8	MEGA		
DI	L1045 → L1045	L1045	164.83		2.42	L1783	L1783	213.69		1.1	CAP		
DI	L1044 → L1044	L1044	164.83		0.75	L1782	L1782	213.69		0.7	SAND		
DI	L1249 → L1288	L1288	180.91	186.49	5.58	L1899	L1958	222.48	227.2	4.72	MIX		
DI	L1166 → L1288	L1288	169.94	186.49	16.55	L1836	L1958	216.81	227.2	10.39	MIX		
DI	L1166 → L1249	L1249	169.94	180.91	10.97	L1836	L1899	216.81	222.48	5.67	MIX		
DI	L1044 → L1249	L1249	164.83	180.91	16.08	L1782	L1899	213.69	222.48	8.79	MIX		
DI	L1044 → L1166	L1166	164.83	169.94	5.11	L1782	L1836	213.69	216.81	3.12	MIX		
DI	L1044 → L1288	L1288	164.83	186.49	21.66	L1782	L1958	213.69	227.2	13.51	MIX		
D	L1044 → L1552	L1552	164.83	222.83	58	L1782	L2287	213.69	256.8	43.11	MIX		



Table A5-1E

CB						SYE						
Interval & sub inter.	Bed(s)	Bed	Level from	Level to	Thickness	Bed(s)	Bed	Level from	Level to	Thickness	Lithology	Reg-line
E	L1627+L1629				1.95	L2388+L2389				1.16	MEGA	1.2901111
E	L1628				1.69	L2389				0.89	CAP	1.08612892
E	L1627				0.26	L2388				0.27	SAND	-0.035773
E	L1597				0.17	L2340				0.195	SAND	-0.1063822
E	L1552+L1553				2	L2287+L2288				1.69	MEGA	1.32933844
E	L1553				1.4	L2288				1.13	CAP	0.85861035
E	L1552				0.6	L2287				0.56	SAND	0.2309729
E	L1627 →	L1960	234.63	279.84	45.21	L2388	L2711	267.52	303.72	36.2	MIX	35.2296063
E	L1597 →	L1960	230.38	279.84	49.46	L2340	L2711	263.04	303.72	40.68	MIX	38.5639302
E	L1597 →	L1627	230.38	234.63	4.25	L2340	L2388	263.04	267.52	4.48	MIX	3.09456877
E	L1552 →	L1627	222.83	234.63	11.8	L2287	L2388	256.8	267.52	10.72	MIX	9.01789722
E	L1552 →	L1597	222.83	230.38	7.55	L2287	L2340	256.8	263.04	6.24	MIX	5.68357326
E	L1552 →	L1960	222.83	279.84	57.01	L2287	L2711	256.8	303.72	46.92	MIX	44.4872587

Table A5-1F

Interval & sub inter.	CB					SYE					
	2	3	4	5	6	7	8	9	10	11	12
	Bed(s)	Bed	Level from	Level to	Thickness	Bed(s)	Bed	Level from	Level to	Thickness	Lithology
F3	L2685				0.45	L3472				0.52	SAND
F3	L2683				0.64	L3470				0.34	SAND
F3	L2552+L2551				1.1	L3296+L3297				1.07	MEGA
F3	L2552				0.43	L3297				0.3	CAP
F3	L2551				0.67	L3296				0.77	SAND
F3	L2525				0.29	L3272				0.16	SAND
F2	L2176+L2175				0.92	L2932+L2931				0.665	MEGA
F2	L2176				0.52	L2932				0.48	CAP
F2	L2175				0.4	L2931				0.185	SAND
F1	L1960+L1961				4.71	L2712+L2711				4.42	MEGA
F1	L1961				4	L2712				3.28	CAP
F1	L1960				0.71	L2711				1.14	SAND
F2,F3	L2175 →	L2685	299.24	336.63	37.39	L2931	L3472	321.31	357.11	35.8	MIX
F2,F3	L2175 →	L2683	299.24	335.78	36.54	L2931	L3470	321.31	356.6	35.29	MIX
F2,F3	L2175 →	L2551	299.24	327.57	28.33	L2931	L3296	321.31	347.24	25.93	MIX
F2,F3	L2175 →	L2525	299.24	326.27	27.03	L2931	L3272	321.31	346.27	24.96	MIX
F2,F3	L2175 →	L2455	299.24	320.96	21.72	L2931	L3209	321.31	341	19.69	MIX
F1,F2,F3	L1960 →	L2685	279.84	336.63	56.79	L2711	L3472	303.72	357.11	53.39	MIX
F1,F2,F3	L1960 →	L2683	279.84	335.78	55.94	L2711	L3470	303.72	356.6	52.88	MIX
F1,F2,F3	L1960 →	L2551	279.84	327.57	47.73	L2711	L3296	303.72	347.24	43.52	MIX
F1,F2,F3	L1960 →	L2525	279.84	326.27	46.43	L2711	L3272	303.72	346.27	42.55	MIX
F1,F2	L1960 →	L2455	279.84	320.96	41.12	L2711	L3209	303.72	341	37.28	MIX
F3	L2455 →	L2685	320.96	336.63	15.67	L3209	L3472	341	357.11	16.11	MIX
F3	L2455 →	L2683	320.96	335.78	14.82	L3209	L3470	341	356.6	15.6	MIX
F3	L2455 →	L2551	320.96	327.57	6.61	L3209	L3296	341	347.24	6.24	MIX
F3	L2455 →	L2525	320.96	326.27	5.31	L3209	L3272	341	346.27	5.27	MIX
F3	L2455 →	L2685	320.96	336.63	15.67	L3209	L3472	341	357.11	16.11	MIX
F2	L2175 →	L2455	299.24	320.96	21.72	L2931	L3209	321.31	341	19.69	MIX
F1	L1960 →	L2175	279.84	299.24	19.4	L2711	L2931	303.72	321.31	17.59	MIX
F	L1960 →	L2685	279.84	336.63	56.79	L2711	L3472	303.72	357.11	53.39	MIX

**APPENDIX A6**  
**PALINSPASTIC MAP CONSTRUCTION**

## **A6. PALINSPASTIC MAP CONSTRUCTION**

A palinspastic map was produced by balancing a cross section drawn in the middle part of the thesis area. A palinspastic map is defined as “a map that shows the distribution of the stratigraphic units prior to deformation” (Marshak and Mitra, 1988). The main objective for this exercise is to obtain a rough estimate for the location of the sections measured in this thesis relative to each other at the time of deposition. It is by no means a detailed or rigorous analysis of the structure in the area which is beyond the scope of this thesis.

Enos (1969b) produced a synthesised cross section transverse to the shoreline from Petite Vallée to St-Hélér (Enos, 1969b, Plate 1). In this cross section, fold axes were telescoped or projected along the strike. Based on field evidence, Enos’ (1969b) interpretation of the structures of the area depicted in this cross section is correct and is supported by other regional and local studies carried out subsequently (Lynch and Arsenault, 1997; Lynch, 1998).

A cross section similar to Enos’ (1969b) cross section was used for the construction of the palinspastic map but instead of using his members, the marker horizons that separate the time-slices described in this thesis were used instead (Figure A6.1a). The cross section was constructed along a traverse (A-A’) which is perpendicular to the strike of the thrust fault south of Anse à la Rogne (Figure A6.2). This thrust fault marks the contact between the Deslandes Formation and the Cloridorme Formation (Figure 2.1).

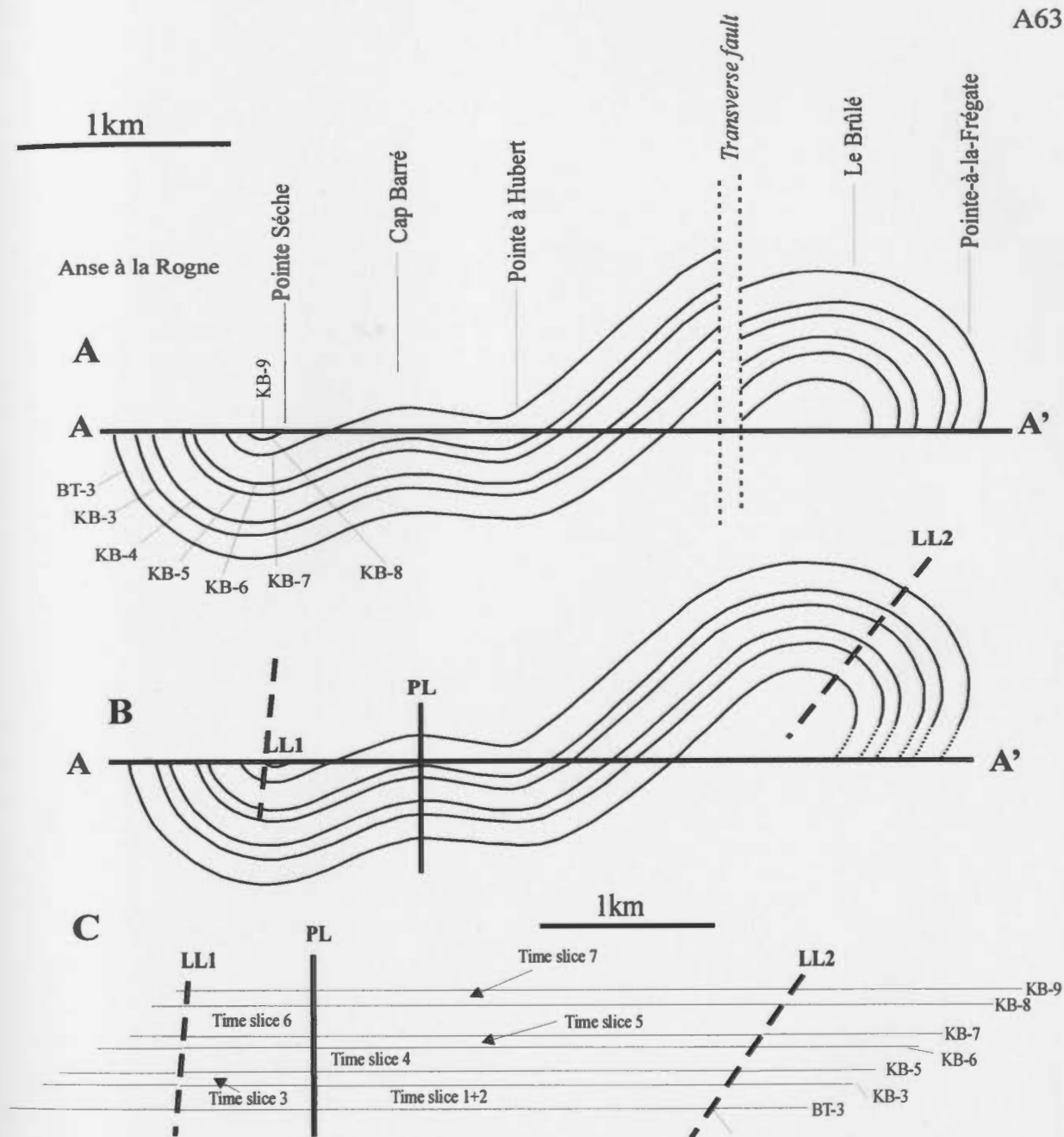


Figure A6.1. The deformed state cross section (A) with all the marker horizons, folds and the transverse fault. B shows the same section after the offset due to the transverse fault has been removed. The location of the pin line (PL) and loose lines (LL 1 and LL 2) are shown. C shows the undeformed state cross section where the beds have been drawn as horizontals. The time slices are also shown. Note that the loose lines are not vertical, but have a consistent trend making this restored cross section admissible.

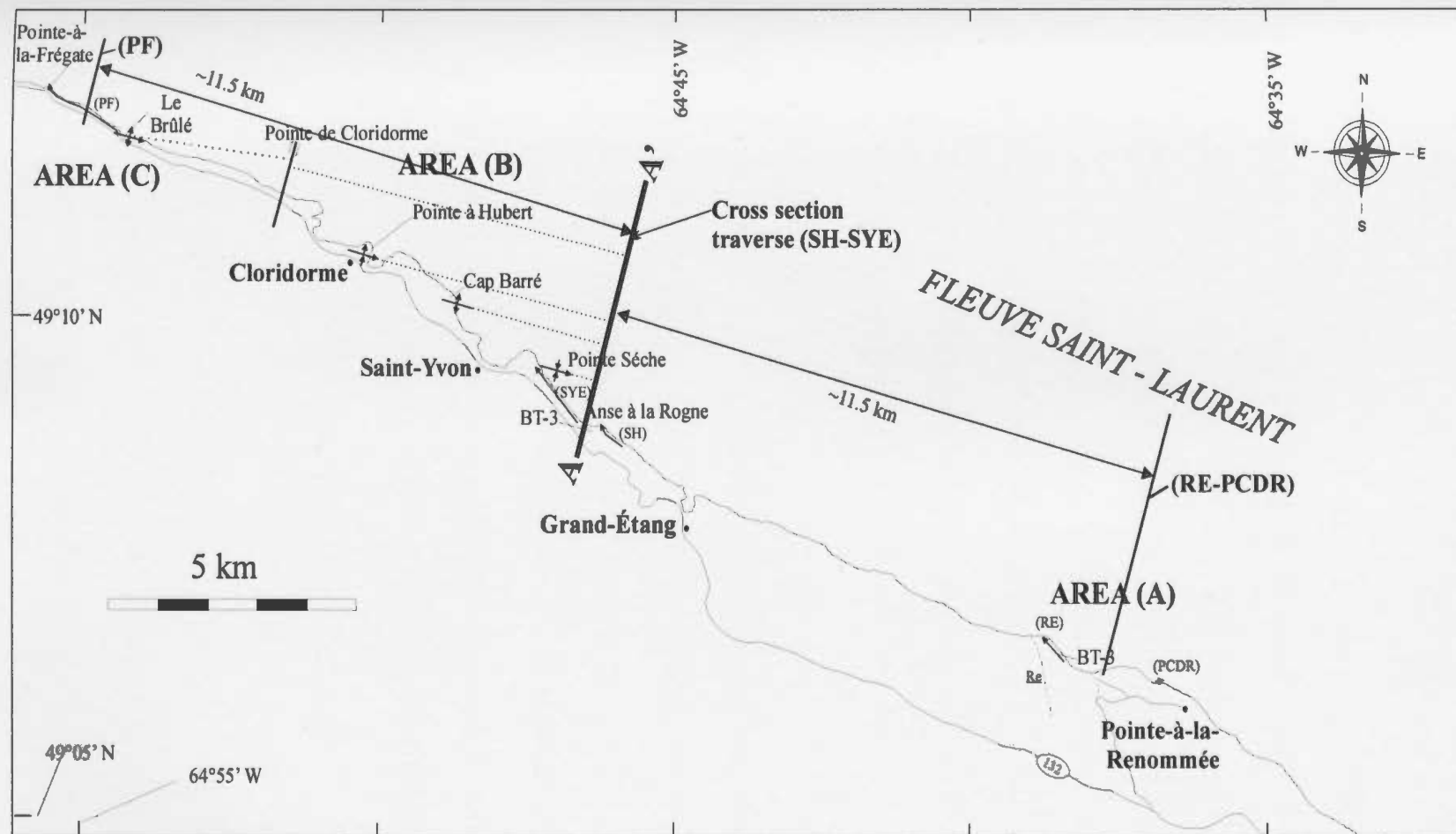


Figure A6.2 Map showing the location of the traverse (A-A') along which the cross section in Figure A4.1 was drawn. Also shown are the two antclines at Cap Barré and Le Brûlé and two synclines at Pointe Séche and Pointe à Hubert. The axes of these folds were projected along the strike towards the cross section traverse (dotted lines). Also shown are the location of three composite sections (PF, SH-SYE, RE-PCDR) used in this thesis to study the depositional environments and architectural elements.

The trend of this traverse is N15E. The anticline axes at Le Brûlé and Cap Barré and the syncline axes at Pointe à Hubert and Pointe Séche were projected along the strike towards the traverse. Enos (1969b) showed the presence of one major transverse fault west of Pointe de Cloridorme. Enos (1969b) estimated the horizontal component of movement along this fault to be 350-900m. When constructing the deformed state cross section, this fault was drawn in the same location and with the same separation suggested by Enos (1969b). This amount of displacement could not be verified in the field, so a  $\pm 0.5$  km (uncertainly) is added to the area of section PF.

A line length balance method was used to restore the section. This method was used for its simplicity. The displacement along the transverse fault was removed before the section was restored (Figure A6.1b). Because no undeformed rocks are present in this section, a local pin line was drawn perpendicular to bedding in the area of the anticline at Cap Barré (Marshak and Mira, 1988). In this area, the beds are very gently dipping (Figure 2.5). Two loose lines were drawn perpendicular to bedding (Woodward *et al.*, 1989). The first is located at the syncline at Pointe Séche; the second loose line was drawn in the hinge area of the anticline at Le Brûlé.

The bed length along each of the marker horizons from the pin line to each of the loose lines was measured. To draw the undeformed state cross section (Figure A6.1c), the pin line was fixed, the bed length of each of the marker horizons on both sides of the pin lines were drawn as horizontal lines using the length of each of the marker horizons to

represent the bedding planes before deformation. The restored loose lines are not perpendicular to the bedding in the restored cross section. Nevertheless, the restored cross section is admissible because the loose lines geometries are consistent (Marshak and Mitra, 1988).

The stratigraphic framework showing the undeformed state cross section is shown in Figure A6.1c. The restoration suggests that the distance along this traverse between the projected position of KB-9 at Pointe-à-la-Frégate and the anticline at Cap Barré is about 4 km while the distance between the projected position of bed BT-3 south of Anse à la Rogne and the anticline at Cap Barré is ~1.7 km.

To produce the palinspastic map, it is necessary to consider where the sections were measured relative to the folds. This is especially important for composite sections that were measured over a large area. For example, BT-3 at the base of the sequence in composite section SH-SYE was measured about 0.9 km east of the traverse A-A' (as measured perpendicular to the line of the traverse) while KB-9 that marks the top of time-slice 7 was measured in the syncline hinge at Pointe Séche about 1.2 km west of the traverse. So, the rocks exposed at the base of composite section SH-SYE and those exposed at the top are separated in the field by more than 2 km. Thus, the beds in this composite section may be considered to represent small segments of a section that gradually shifts in a NW direction from the lower part of the section to the upper part of the section. This separation of parts of single sections may not be critical in the long



distance correlation. No short distance correlation was carried out between section SH and section SYE because of limited overlap and poor exposure.

After restoration, the projected top of time-slice 7 (KB-9) exposed at Pointe-à-la-Frégate intersects the cross section traverse about 4 km ( $\pm 0.5$  km) from the point where the hinge of the anticline at Cap Barré intersects the same traverse A-A'. Horizon KB-9 is projected a 11.5 km to the WNW to pinpoint the location of the top of time-slice 7 in PF section at the time of deposition. The base of time-slice 1 (BT-3) was measured at Le Brûlé, about 2 km from Pointe-à-la-Frégate. As with composite section SH-SYE, the sequence measured in the PF sequence may be considered as small segments of a section that gradually shifts in a NW direction from the lower part of the section at Le Brûlé to the upper part of the section at Pointe-à-la-Frégate. Because of the uncertainty in the amount of displacement that took place along the transverse fault, the area where section PF is located on the palinspastic map (Figure A6.3) is enlarged. Only one section was measured in this area, so no short distance correlations are undertaken in this area.

For the sections in area A, a composite section RE-PCDR encompasses time-slices 1,2,3 and part of time-slice 4 exposed in the RE section and time-slice 5 and part of time-slice 6 exposed in section PCDR. Skipper (1975) suggested the presence of several faults between area A and area B (between composite sections RE-PCDR and SH-SYE). The offset along these faults was removed before producing the map. Because the sections in area A are in the same fold limb as the syncline at Anse à la Rogne, the position of the bed

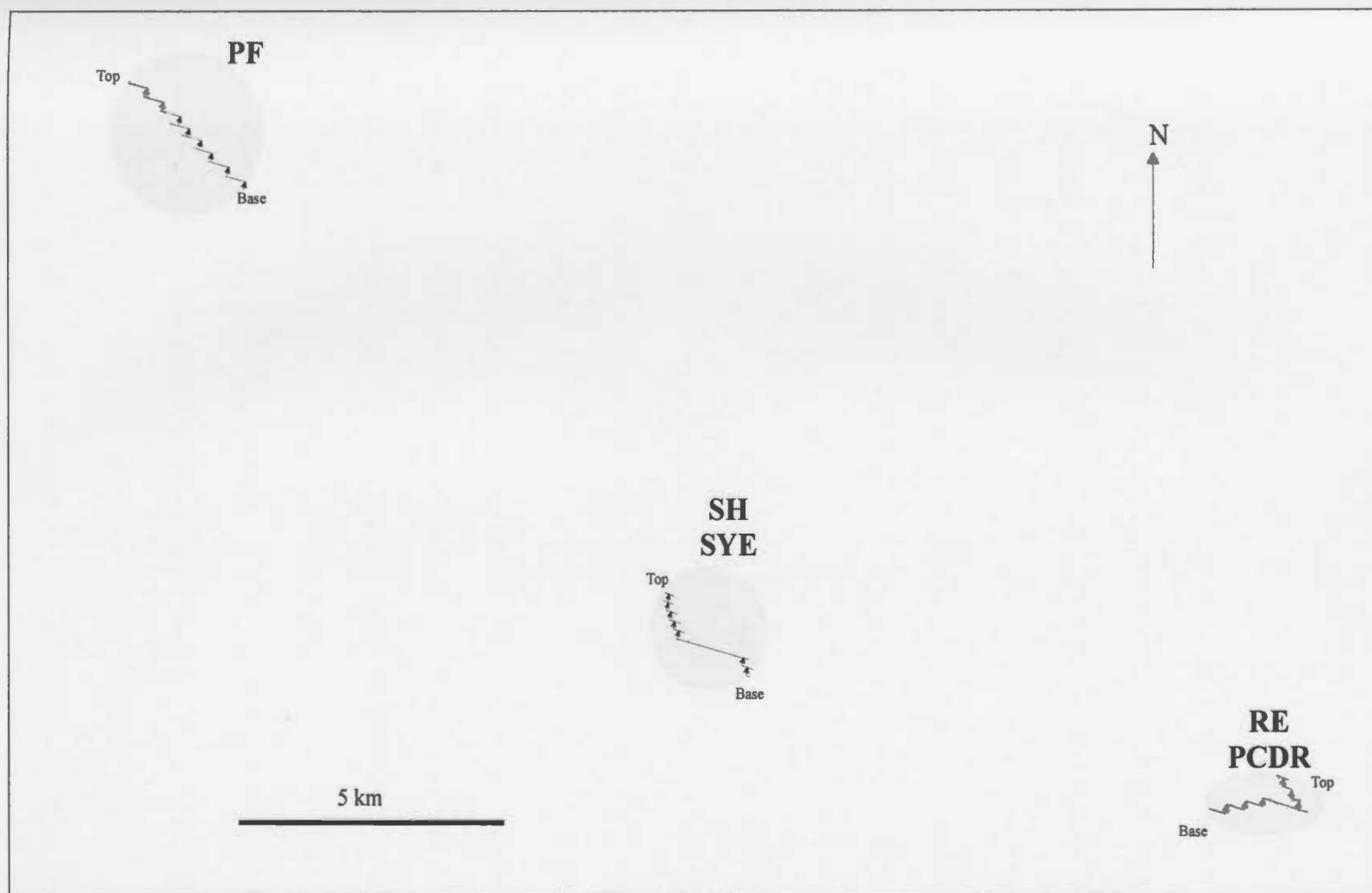


Figure A6.3. Palinspastic map showing where each composite sections was located at the time of deposition. For explanations refer to the text.

BT-3 at RE was determined by projecting the same bed exposed in the base of the composite section SH-SYE approximately 9 km along the strike (in an ESE direction). Section PCDR was measured about 2.2 km east of RE. Because of the shape of wavecut platform in the area, section RE was measured in a NW direction while PCDR were measured in a NE direction. Unlike the other sections, the sequence measured in the composite section RE-PCDR may be considered as small segments of a section that gradually shifts in a NW direction for ~ 50% of the sequence and in a NE direction for the upper ~ 50% of the sequence.

The palinspastic map shows that the three areas are not located along a single traverse of line. Area B is located about 10-12 km to the WNW direction as viewed from area A (~N75W direction) while area C is located at about 22-26 km in an approximately N60W direction as viewed from area A. These restored areas locations are used in interpreting some of the palaeocurrent trend seen in the different areas.

For the short distance correlations, closely spaced sections were used. It is important to consider the relative position of measured parts of each time-slice because, in figures showing sections and correlations, the sections are drawn vertically and the distance between the upper part and the lower part of sections is shown to be constant. For Area A, time-slices 1, 2 and 3 are only present in sections RE and FP1. The trend along which these two sections were measured is different (Figure 2.2). Section RE was measured in a NW direction while section FP1 was measured in a NE direction. So when comparing the facies

in these three time-slices it is important to note that at the time of deposition, the rocks present in time-slice 1 were deposited closer to each other than the rocks present in the younger time-slices including the lower part of time-slice 4 (Figure A5.1 and Figure 2.2).

Different parts of time-slice 4 are exposed in the other sections (FP2, PCDR, PRM1 and PRM2). The lines of these sections have variable trends controlled by the outcrop exposure. The upper part of section FP1 and section FP2 have more or less the same trend (Figure 2.2). So at the time of deposition, the distance between the areas where the beds in lower part of SL4 accumulated did not vary considerably from the separation distance for the middle part of time-slice 4. Beds exposed in the middle part of time-slice 4 PCDR (base of the exposure, Figure 2.2) were probably deposited closer to section FP2 than beds exposed in the upper part of SL4 in section PCDR. For sections PRM1 and PRM2 (Figure 2.2) compared to section PCDR, beds exposed in the older equivalent time-slices were probably deposited relatively farther apart compared to beds in younger equivalent time-slices.

In area B, the measured sections are located in different limbs of folds and some of them were measured over long distances. The upper part of time-slice 6 and time-slice 7 are exposed in sections SYE and SYW. Because of the nature of the outcrop, the upper part of time-slice 7 in these sections is only a few tens of metres apart, while the lower part of the section SYW and equivalent part of section SYE were measured ~ 0.5 km apart. These distance variations may be insignificant when comparing certain even-thickness

facies, but other facies such as those of Class B and C may vary in character over short distances.

Time-slices 5, 6 and part of time-slice 7 are exposed in the CB section (Figure 2.4). When comparing the beds in these time-slices with those in similar time-slices at section SYE it must be considered that, at the time of deposition, the beds in lower time-slice may have been more than 2 km apart while the beds in the upper time-slices may have been only several hundreds of metres apart. The same applies when comparing sections PH and CB. Time-slice 5 and the lower part of time-slice 6 are exposed in section PH. Most of time-slice 5 in sections CB was measured in a small area at Pointe Barreau (Figure 2.4, Chapter 2) which is located about 1 km from equivalent rocks in section PH. At the time of deposition, beds exposed in time-slice 6 in sections PH and CB were probably deposited more than 3 km apart.

These considerations should be remembered when comparing sections that are drawn as vertical lines elsewhere in the thesis.

## **APPENDIX A7 TABLES**

**A7-1: Chapter 2 tables**

**A7-2: Chapter 3 tables**

**A7-3: Chapter 5 tables**

Table A7-1.1. Analytical precision and limits of detections (D.L.) for trace elements and some major elements in the standard reference materials analysed with the Cloridorme K-bentonite samples using the XRF technique at MUN. Accepted concentrations in each standards are from Potts *et al.* (1992). Standards AGV-1, DNC-1, JG-2, and BCR-1 were analysed once during the course of the bentonite analysis. Except where % is indicated, all concentrations are in parts per million (ppm).

Spec.	D.L.	DTS-1 (n = 4)				BHVO-1 (n = 4)				SY-2 (n = 4)			
		Potts	Mean	s.d.	% s.d.	Potts	Mean	s.d.	% s.d.	Potts	Mean	s.d.	% s.d.
Na <sub>2</sub> O%	0.01	0.02	0.32	0.0	1.0	2.26	2.38	0.01	0.3	4.31	4.22	0.0	0.4
MgO%	0.01	49.58	49.58	0.02	0.0	7.23	7.03	0.01	0.1	2.69	3.06	0.0	0.3
Al <sub>2</sub> O <sub>3</sub> %	0.01	0.19	0.21	0.0	0.9	13.80	14.1	0.02	0.2	12.04	12.78	0.0	0.4
SiO <sub>2</sub> %	0.01	40.58	39.46	0.14	0.3	49.94	49.15	0.06	0.1	60.05	63.95	0.12	0.2
P <sub>2</sub> O <sub>5</sub> %	0.003	0.002	<LD	0.0	0.0	0.27	0.28	0.0	1.5	0.43	0.42	0.0	0.7
S	11	12.0	723.0	13.0	1.9	102	723.0	13.0	1.8	160.0	512	12	2.3
Cl	20	11.0	771.0	47.0	6.1	92	821.0	5.0	0.6	140.0	507	21	4.1
K <sub>2</sub> O%	0.002	0.00	0.04	0.0	4.3	0.52	0.50	0.01	1.3	4.44	4.34	0.0	0.1
CaO%	0.002	0.17	0.15	0.0	1.8	11.40	11.11	0.01	0.0	7.69	7.99	0.0	0.1
TiO <sub>2</sub> %	0.006	0.00	0.01	0.0	0.0	2.71	2.79	0.01	0.4	0.14	0.12	0.0	2.5
MnO%	0.002	0.12	0.13	0.0	1.3	0.17	0.17	0.0	0.4	0.32	0.31	0.0	0.6
Fe <sub>2</sub> O <sub>3</sub> %	0.005	8.68	9.33	0.01	0.1	12.23	12.33	0.02	0.2	6.31	6.31	0.0	0.1
Sc	7.0	4.0	<LD	0.0	0.0	32	32.0	1.0	3.1	7.0	9.0	1.0	11.1
Ba	21.0	2.0	<LD	0.0	0.0	139	127.0	5.0	3.9	460.0	450.0	5.0	1.2
V	6.0	11.0	9.0	1.0	11.1	317	317.0	5.0	1.6	50.0	51.0	3.0	5.9
Ce	39.0	0.0	0.0	0.0	0.0	39	<LD	0.0	0.0	175.0	145.0	15.0	10.3
Cr	7.0	3990	3990	22.0	0.5	289	312.0	3.0	0.9	10.0	2.0	3.0	0.1
Ni	5.0	2360	2360	11.0	0.5	121	116.0	4.0	3.8	11.0	11.0	2.0	18.2
Cu	4.0	7.0	7.0	2.0	28.6	136	137.0	2.0	1.4	5.0	3.0	2.0	66.7
Zn	3.0	46.0	30.0	2.0	6.7	105	101.0	3.0	2.5	248.0	233.0	3.0	1.5
Ga	2.0	1.0	<LD	0.0	0.0	21.0	23.0	1.0	4.3	29.0	27.0	1.0	3.7
As	13.0	0.0	0.0	0.0	0.0	0.0	0.0	0.0	0.0	17.0	16.0	4.0	25
Rb	0.7	0.06	0.2	0.2	0.0	11.0	9.3	0.2	2.3	217.0	220.0	0.5	0.2
Sr	1.1	0.32	<LD	0.0	0.0	403.0	410.5	0.9	0.2	271.0	271.0	0.7	0.2
Y	0.6	0.04	<LD	0.0	0.0	27.6	25.5	0.2	0.7	128.0	118.0	0.4	0.4
Zr	1.1	4.0	0.6	0.3	50	179.0	185.0	0.9	0.5	280.0	296.0	2.8	1.0
Nb	0.7	2.2	0.0	0.0	0.0	19.0	21.8	0.4	1.6	29.0	35.1	0.2	0.5
Pb	4.0	12.0	9.0	1.0	11.1	2.6	7.0	1.0	14.2	85.0	86.0	2.0	2.5
Th	3.0	0.01	<LD	0.0	0.0	1.08	<LD	0.0	0.0	379.0	347.0	2.0	0.5
U	3.0	0.004	<LD	0.0	0.	0.42	<LD	0.0	0.0	284.0	290.0	2.0	0.6

Table A7-1.1 continued.

Spec.	D.L.	SY-3 (n = 4)				PACS-1 (n = 4)			
		Potts	Mean	s.d.	% s.d.	Potts	Mean	s.d.	% s.d.
Na <sub>2</sub> O%	0.01	4.12	4.07	0.01	0.2	4.40	4.30	0.01	0.2
MgO%	0.01	2.67	2.96	0.01	0.3	2.41	3.74	0.02	0.4
Al <sub>2</sub> O <sub>3</sub> %	0.01	11.75	12.49	0.08	0.7	12.23	12.29	0.06	0.5
SiO <sub>2</sub> %	0.01	59.62	62.5	0.26	0.4	55.7	61.36	0.15	0.2
P <sub>2</sub> O <sub>5</sub> %	0.003	0.54	0.53	0.0	0.3	0.23	0.32	0.00	1.3
S	11	510	780.0	17.0	2.2	13200	13200	56.0	0.4
Cl	20	150	561.0	54.0	9.6	23900	23900	89.0	0.4
K <sub>2</sub> O%	0.002	4.23	4.15	0.03	0.7	1.50	1.59	0.01	0.6
CaO%	0.002	8.26	8.06	0.02	0.2	2.92	3.10	0.02	0.7
TiO <sub>2</sub> %	0.006	0.15	0.13	0.0	2.8	0.70	0.78	0.01	1.2
MnO%	0.002	0.32	0.30	0.00	0.7	0.06	0.06	0.00	0.9
Fe <sub>2</sub> O <sub>3</sub> %	0.005	6.49	6.20	0.01	0.2	6.96	7.47	0.01	0.2
Sc	7.0	7.0	<LD	0.0	0.0	0.0	0.0	0.0	0.0
Ba	21.0	450	449.0	7.0	1.5	0.0	0.0	0.0	0.0
V	6.0	50.0	14.0	5.0	35.7	127	155	3.0	1.8
Ce	39.0	2230	2230.0	25.0	1.1	0.0	0.0	0.0	0.0
Cr	7.0	11.0	10.0	0.3	0.1	113	126	4.0	2.9
Ni	5.0	11.0	11.0	2.0	18.2	44	42.0	1.0	2.4
Cu	4.0	17.0	18.0	0.5	0.1	452	398	3.0	0.7
Zn	3.0	244.0	233.0	3.0	1.5	824	801	3.0	0.4
Ga	2.0	27.0	27.0	1.0	3.7	0.0	0.0	0.0	0.0
As	13.0	19.0	<LD	0.0	0.0	211	211	6.0	0.8
Rb	0.7	206.0	201.7	0.8	0.4	0.0	0.0	0.0	0.0
Sr	1.1	302.0	296.8	1.1	0.4	277	277.9	0.9	0.3
Y	0.6	718.0	600.4	1.5	0.2	0.0	0.0	0.0	0.0
Zr	1.1	320.0	350.0	1.9	0.5	0.0	0.0	0.0	0.0
Nb	0.7	148.0	253.0	0.5	0.2	0.0	0.0	0.0	0.0
Pb	4.0	133.0	140.0	3.0	2.1	404	350	1.0	0.4
Th	3.0	1003.0	923.0	5.0	0.6	0.0	0.0	0.0	0.0
U	3.0	650.0	742.0	2.0	0.3	0.0	0.0	0.0	0.0



Table A7-1.1 continued.

Spec.	D.L.	AGV-1 (n = 1)		DNC-1 (n = 1)		JG-2 (n = 1)		BCR-1 (n = 1)	
		Litr.	MUN.	Litr.	MUN.	Litr.	MUN.	Litr.	MUN.
Na <sub>2</sub> O%	0.01	4.26	3.81	1.87	2.03	3.55	3.6	3.27	3.28
MgO%	0.01	1.53	1.46	10.05	10.03	0.04	0.11	3.48	2.92
Al <sub>2</sub> O <sub>3</sub> %	0.01	17.14	16.47	18.30	18.57	12.41	13.36	13.64	13.80
SiO <sub>2</sub> %	0.01	58.79	59.78	47.04	43.75	76.95	76.07	54.06	55.6
P <sub>2</sub> O <sub>5</sub> %	0.003	0.49	0.46	0.09	0.09	0.00	0.00	0.36	0.38
S	11.0	26.0	645.0	392.0	1138.0	9.0	532	410	953
Cl	20.0	119	623.0	37.0	997.0	0.0	0.0	59.0	645.0
K <sub>2</sub> O%	0.002	2.91	2.75	0.23	0.26	4.72	4.50	1.69	1.73
CaO%	0.002	4.94	4.84	11.27	11.01	0.80	0.77	6.95	6.76
TiO <sub>2</sub> %	0.006	1.05	1.02	0.48	0.45	0.04	0.05	2.24	2.27
MnO%	0.002	0.09	0.10	0.15	0.15	0.02	0.02	0.18	0.18
Fe <sub>2</sub> O <sub>3</sub> %	0.005	6.76	6.80	9.93	10.09	0.92	1.06	13.41	13.26
Sc	7.0	12.0	16.0	31.0	36.0	2.0	<LD	33.0	35.0
Ba	21.0	1226.0	1259.0	114.0	141.0	67.0	72.0	681.0	709.0
V	6.0	121.0	115.0	148.0	146.0	3.0	<LD	407.0	423.0
Ce	39.0	67.0	57.0	11.0	<LD	46.0	39.0	54.0	63.0
Cr	7.0	10.0	8.0	285.0	299.0	8.0	7.0	16.0	14.0
Ni	5.0	16.0	5.0	247.0	241.0	2.0	<LD	13.0	5.0
Cu	4.0	60.0	56.0	96.0	87.0	0.0	0.0	19.0	20.0
Zn	3.0	88.0	68.0	66.0	44.0	13.0	3.0	130.0	129.0
Ga	2.0	20.0	21.0	15.0	13.0	19.0	17.0	22.0	23.0
As	13.0	1.0	1.0	0.0	0.0	1.0	<LD	9.0	<LD
Rb	0.7	67.3	70.1	4.5	3.5	297	288.1	47.2	49.5
Sr	1.1	662	685.5	145	143.0	16.0	14.6	330.0	346.6
Y	0.6	20.0	17.3.0	18.0	16.3	89.0	71.4	38.0	34.1
Zr	1.1	227.0	247.0	41.0	35.9	97.0	88.1	190.0	204.5
Nb	0.7	15.0	17.0	3.0	1.6	15.0	15.4	14.0	14.6
Pb	4.0	36.0	36.0	3.0	10.0	33.0	31.0	14.0	20.0
Th	3.0	6.5	5.0	0.0	0.0	30.0	28.0	6.0	6.0
U	3.0	0.9	1.0	0.0	0.0	13.0	12.0	2.0	<LD

Table A7-1.2. Analytical precision and limits of detections (D.L.) for the trace elements in the standard reference materials analysed with the Cloridorme K-bentonite samples using ICP-MS technique at Activation Laboratories. Accepted concentrations in each standards are from Potts *et al.* (1992). Standard GXR-1 was fortified with Cr and Ni (Eric Hoffmann, Activation Laboratories, personal communications, 1997). All concentrations are in parts per million (ppm).

Elem.	D.L.	STM-1 (n = 5)				MAG-1 (n=5)			
		Potts	mean	s.d.	% s.d.	Potts	mean	s.d.	% s.d.
V	5.0	9	9.2	0.2	0.0	140	135.6	3.1	2.3
Cr	10.0	4	<LD	0.0	0.0	97	107.7	2.3	2.1
Co	0.5	0.9	1.4	0.1	7.6	20.4	21.1	0.4	2.0
Ni	10.0	3	<LD	0.0	0.0	53	57.5	5.5	8.8
Cu	10.0	5	<LD	0.0	0.0	30	31.1	0.5	1.6
Zn	10.0	235	233.7	2.7	1.1	130	140.1	17.5	12.5
Ga	1.0	36	35.3	0.1	0.3	20	22.2	0.5	2.1
Ge	1.0	1.4	1.5	0.0	3.6	0.0	<LD	0.0	0.0
As	5.0	5	<LD	0.0	0.0	9.0	8.1	0.1	1.1
Rb	0.5	118	115.5	1.3	1.1	149	149.3	1.4	1.0
Sr	0.1	700	693	1.9	0.3	146	141.4	1.4	1.0
Y	1.0	46	42.4	0.6	1.4	28	25.4	0.3	1.0
Zr	0.5	1210	1268	9.3	0.7	126	125.3	1.9	1.5
Nb	1.0	268	267.9	0.2	0.1	12	19.2	1.0	5.1
Mo	0.5	5.2	4.3	0.3	6.4	1.6	1.3	0.1	10.5
Ag	0.5	0.08	<LD	0.0	0.0	0.1	<LD	0.0	0.0
In	0.2	0.12	0.11	0.00	3.4	0.2	<LD	0.0	0.0
Sn	1.0	6.8	7.7	0.2	2.9	3.6	3.2	0.3	8.5
Sb	0.1	1.7	1.7	0.0	3.3	1.0	0.9	0.0	1.6
Cs	0.5	1.5	1.6	0.0	1.9	8.6	8.6	0.1	1.3
Ba	1.0	560	575	8.1	1.4	479	476.3	5.7	1.2
La	0.1	150	152.3	2.9	1.9	43	42.2	0.7	1.6
Ce	0.1	259	260.9	0.9	0.3	88	84.5	1.0	1.2
Pr	0.05	19	25.1	0.4	1.7	9.3	9.8	0.1	1.4
Nd	0.1	79	79.9	0.3	0.4	38	37.2	0.4	1.0
Sm	0.1	12.6	12.6	0.2	1.4	7.5	7.4	0.1	1.6
Eu	0.05	3.6	3.4	0.0	2.3	1.6	1.4	0.0	2.4
Gd	0.1	9.5	10.3	0.2	2.0	5.8	5.7	0.1	1.6
Tb	0.1	1.55	1.5	0.0	0.7	1.0	0.9	0.0	1.2
Dy	0.1	8.1	8.0	0.1	1.3	5.2	5.1	0.1	1.1
Ho	0.1	1.9	1.4	0.0	1.3	1.0	1.0	0.0	1.2
Er	0.1	4.2	4.6	0.0	1.1	3	2.8	0.0	1.7
Tm	0.05	0.7	0.7	0.0	0.8	0.4	0.4	0.0	1.9
Yb	0.1	4.4	4.3	0.0	0.8	2.6	2.5	0.0	1.0
Lu	0.04	0.6	0.6	0.0	1.4	0.4	0.4	0.0	2.4
Hf	0.2	28	29.4	0.4	1.2	3.7	3.6	0.0	1.3
Ta	0.05	18.6	18.5	0.0	0.4	1.1	1.4	0.1	5.1
W	0.5	3.6	3.7	0.2	5.6	1.4	1.8	0.1	7.9
Tl	0.1	0.3	0.3	0.0	5.3	0.6	0.3	0.0	2.9
Pb	5.0	17.7	21.4	0.7	3.1	24	26.1	0.9	3.3
Bi	0.3	0.1	0.2	0.0	7.6	0.3	<LD	0.0	0.0

Table A7-1.2 continued .

Elem.	D.T	BIR-1 (n = 5)				DNC-1 (n = 5)			
		Potts	mean	s.d.	% s.d.	Potts	mean	s.d.	% s.d.
Th	0.1	31	28.7	0.8	2.7	11.9	11.5	0.2	2.1
U	0.1	9.1	8.5	0.2	2.2	2.7	2.7	0.1	2.1
V	5.0	313.0	318.8	6.0	1.9	148	143.7	2.8	1.9
Cr	10.0	382.0	378.4	4.5	1.2	285	264.4	4.0	1.5
Co	0.5	51.4	52.0	0.4	0.7	54.7	54.1	0.5	0.1
Ni	10.0	166.0	166.9	1.2	0.7	247.0	246.7	3.1	1.3
Cu	10.0	126.0	124.9	1.3	1.0	96.0	97.5	1.6	1.6
Zn	10.0	71.0	86.9	15.1	17.4	66.0	80.5	33.1	41.1
Ga	1.0	16.0	16.2	0.2	1.1	15.0	13.9	0.1	1.0
Ge	1.0	1.5	1.5	0.0	3.3	1.3	1.3	0.1	5.4
As	5.0	0.0	0.0	0.0	0.0	0.0	0.0	0.0	0.0
Rb	0.5	0.3	0.8	0.1	9.6	4.5	4.1	0.1	2.4
Sr	0.1	108.0	112.0	0.9	0.8	145.0	140.9	1.5	1.1
Y	1.0	16.0	14.9	0.1	1.0	18.0	15.9	0.2	1.4
Zr	0.5	22.0	21.6	0.7	3.4	41.0	37.8	1.3	3.4
Nb	1.0	2.0	2.3	0.3	15.1	3.0	2.4	0.3	10.5
Mo	0.5	0.5	0.8	0.3	46.2	0.7	0.5	0.2	33.0
Ag	0.5	0.0	0.0	0.0	0.0	0.0	0.0	0.0	0.0
In	0.2	0.0	0.0	0.0	0.0	0.0	0.0	0.0	0.0
Sn	1.0	0.7	1.1	0.3	24.2	0.0	0.0	0.0	0.0
Sb	0.1	0.6	1.1	0.1	4.8	1.0	1.0	0.1	5.5
Cs	0.5	0.5	<LD	0.0	0.0	0.0	0.0	0.0	0.0
Ba	1.0	7.7	10.7	0.6	5.6	114.0	101.8	0.9	0.9
La	0.1	0.9	0.7	0.0	3.2	3.8	3.7	0.1	1.7
Ce	0.1	2.5	2.1	0.1	2.7	10.6	8.0	0.0	0.6
Pr	0.05	0.5	0.4	0.0	2.2	1.3	1.1	0.0	1.1
Nd	0.1	2.5	2.4	0.0	1.3	4.9	4.8	0.1	1.2
Sm	0.1	1.1	1.2	0.1	5.1	1.4	1.5	0.0	1.0
Eu	0.05	0.5	0.5	0.0	2.7	0.6	0.6	0.0	1.9
Gd	0.1	1.9	1.4	0.0	3.3	2.0	1.6	0.1	3.3
Tb	0.1	0.4	0.4	0.0	2.9	0.4	0.4	0.0	3.5
Dy	0.1	2.4	2.6	0.0	1.2	2.7	2.7	0.1	2.3
Ho	0.1	0.5	0.6	0.0	1.9	0.6	0.6	0.0	2.7
Er	0.1	1.8	1.6	0.0	1.8	2.0	1.8	0.0	1.8
Tm	0.05	0.3	0.3	0.0	1.1	0.3	0.3	0.0	2.5
Yb	0.1	1.7	1.7	0.0	1.5	2.0	2.0	0.0	1.7
Lu	0.04	0.3	0.3	0.0	3.2	0.3	0.3	0.0	4.3
Hf	0.2	0.6	0.7	0.0	5.1	1.0	1.1	0.1	6.5
Ta	0.05	0.1	0.1	0.0	15.5	0.1	0.2	0.0	8.4
W	0.5	0.2	0.5	0.1	22.7	0.2	1.1	0.1	12.9
Tl	0.1	0.01	<LD	0.0	0.0	0.03	<LD	0.0	0.0
Pb	5.0	3.0	32.1	1.0	3.1	6.0	16.1	0.2	1.3
Bi	0.2	0.02	<LD	0.0	0.0	0.02	<LD	0.0	0.0
Th	0.1	0.03	<LD	0.0	0.0	0.2	0.3	0.0	5.6

Table A7-1.2 continued.

Elem.	D.L.	W-2 (n = 7)				MRG-1 (n = 7)			
		Potts	mean	s.d.	% s.d.	Potts	mean	s.d.	% s.d.
U	0.1	0.1	<LD	0.0	0.0	0.1	<LD	0.0	0.0
V	5.0	182.0	171.0	2.5	1.5	61	51.9	1.3	2.6
Cr	10.0	93.0	94.4	1.8	1.9	430.0	435.7	9.3	2.1
Co	0.5	0.03	<LD	0.0	0.0	0.2	0.1	0.01	7.8
Ni	10.0	70.0	72.2	4.8	6.7	193.0	186.4	2.8	1.5
Cu	10.0	103.0	109.5	1.4	1.3	134.0	129.2	1.7	1.3
Zn	10.0	77.0	75.0	6.1	8.2	191.0	198.7	8.5	4.3
Ga	1.00	20.0	18.0	0.3	1.8	17.0	18.5	0.4	1.9
Ge	1.0	1.0	1.4	0.1	5.3	1.4	1.6	0.1	6.2
As	5.0	1.0	<LD	0.0	0.0	5.0	<LD	0.0	0.0
Rb	0.5	20.0	20.0	0.3	1.6	8.5	7.7	0.1	1.4
Sr	0.1	194.0	192.5	2.7	1.4	266.0	274.7	3.5	1.3
Y	1.0	24.0	20.2	0.2	0.9	14.0	12.3	0.1	0.9
Zr	0.5	94.0	77.6	6.3	8.1	108.0	103.4	0.8	0.7
Nb	1.0	7.9	7.2	0.3	4.4	20.0	20.0	0.3	1.4
Mo	0.5	0.6	0.6	0.1	9.5	0.9	1.5	0.1	8.4
Ag	0.5	0.0	0.0	0.0	0.0	0.0	0.0	0.0	0.0
In	0.2	0.0	0.0	0.0	0.0	0.0	0.0	0.0	0.0
Sn	1.0	0.0	0.0	0.0	0.0	3.6	3.5	0.2	5.7
Sb	0.1	0.8	0.8	0.0	2.9	0.9	0.7	0.0	3.4
Cs	0.5	1.0	0.9	0.9	1.9	0.6	0.7	0.0	3.2
Ba	1.0	182.0	171.0	2.5	1.5	61.0	51.9	1.3	2.6
La	0.1	11.4	10.8	0.2	1.5	9.8	9.3	0.1	1.2
Ce	0.1	24.0	22.9	0.2	1.0	26.0	25.4	0.2	0.7
Pr	0.05	5.9	2.9	0.0	1.3	3.4	3.7	0.0	0.9
Nd	0.1	14.0	12.9	0.2	1.2	19.2	18.1	0.2	1.2
Sm	0.1	3.3	3.4	0.1	1.8	4.5	4.6	0.1	2.6
Eu	0.05	1.1	1.1	0.0	0.9	1.4	1.4	0.0	2.0
Gd	0.1	3.6	3.1	0.1	2.9	4.0	3.5	0.1	3.2
Tb	0.1	0.6	0.6	0.0	1.4	0.5	0.6	0.0	1.6
Dy	0.1	3.8	3.9	0.1	2.1	2.8	3.0	0.1	2.0
Ho	0.1	0.8	0.8	0.0	1.7	0.5	0.5	0.0	1.1
Er	0.1	2.5	2.2	0.0	2.1	1.1	1.3	0.0	1.4
Tm	0.05	0.4	0.4	0.0	2.2	0.1	0.1	0.0	5.6
Yb	0.1	2.1	2.1	0.1	2.8	0.6	0.8	0.0	3.5
Lu	0.04	0.3	0.3	0.0	3.0	0.1	0.1	0.0	7.1
Hf	0.2	2.6	2.5	0.1	2.9	3.8	3.8	0.0	1.1
Ta	0.05	0.5	0.5	0.0	5.5	0.8	0.8	0.0	2.9
W	0.5	0.3	0.5	0.5	103.7	0.3	0.5	0.4	76.1
Tl	0.1	0.2	0.1	0.0	8.4	0.04	<LD	0.0	0.0
Pb	5.0	9.0	9.5	0.4	4.0	10.0	6.9	0.4	5.5
Bi	0.2	0.03	<LD	0.0	0.0	0.19	<LD	0.0	0.0
Th	0.1	2.2	2.2	0.0	1.4	0.9	0.8	0.0	2.2
U	0.1	0.5	0.5	0.0	1.4	0.2	0.2	0.0	1.9

Table A7-1.2 continued.

Elem.	D.L.	SY-3 (n = 5)				GXR-1 (n = 5)			
		Potts	mean	s.d.	% s.d.	Litr.	mean	s.d.	% s.d.
V	5.0	50.0	50.0	0.7	2.7	76.0	84	0.9	2.1
Cr	10.0	11.0	11	0.8	4.1	13.0	800	9.6	2.4
Co	0.5	8.8	4.6	0.1	1.7	7.8	6.0	0.1	2.0
Ni	10.0	10	<LD	0.0	0.0	41.0	4094	202	4.9
Cu	10.0	17.0	22	0.4	3.4	1110.0	1109	5.2	1.0
Zn	10.0	244.0	261	11.2	8.6	760.0	754	3.8	1.0
Ga	1.0	27.0	40.0	0.4	2.0	14.0	14.0	0.0	0.5
Ge	1.0	1.4	3.2	0.0	2.1	13.0	3.2	0.1	6.4
As	5.0	19.0	22.0	0.2	2.2	401.0	427	0.8	0.4
Rb	0.5	206.0	210	0.9	0.9	14.0	3.8	0.0	1.8
Sr	0.1	302.0	3129	1.7	1.1	259.0	294	2.3	1.6
Y	1.0	718.0	720	0.2	0.1	0.0	<LD	0.0	0.0
Zr	0.5	320.0	340	1.8	1.1	38.0	38	0.8	4.2
Nb	1.0	148.0	19.4	0.8	0.8	1.2	6.4	0.2	6.8
Mo	0.5	0.6	1.8	0.2	17.8	18.0	18	0.3	2.8
Ag	0.5	0.0	<LD	0.0	0.0	31.0	31	0.4	2.6
In	0.2	0.0	<LD	0.0	0.0	0.8	0.8	0.0	0.4
Sn	1.0	6.5	6.8	0.3	8.7	55.0	53.4	0.2	0.7
Sb	0.1	0.3	0.6	0.0	5.9	116.0	124	1.0	1.6
Cs	0.5	2.5	2.8	0.0	1.9	3.0	2.8	0.0	2.8
Ba	1.0	450.5	445	2.8	1.2	680.0	671	5.3	1.6
La	0.1	1340.0	1337	3.2	0.5	7.5	8.0	0.1	3.3
Ce	0.1	2230.0	2256	19.1	1.7	17.0	15	0.1	1.3
Pr	0.05	223.0	123	0.0	0.0	0.0	0.0	0.0	0.0
Nd	0.1	670.0	734	4.4	1.2	16.4	8.6	0.1	1.7
Sm	0.1	109.0	128	0.8	1.2	2.7	3.0	0.1	6.3
Eu	0.05	17.0	17.2	0.0	0.6	0.7	0.6	0.0	5.0
Gd	0.1	105.0	118	1.9	3.2	4.2	3.2	0.0	2.3
Tb	0.1	18.0	21.4	0.1	1.4	0.8	0.9	0.0	1.9
Dy	0.1	118.0	134	0.9	1.3	4.3	5.0	0.1	2.4
Ho	0.1	29.5	28.4	0.1	0.8	0.0	0.0	0.0	0.0
Er	0.1	76.8	87.4	0.5	1.2	0.0	0.0	0.0	0.0
Tm	0.05	11.6	13.6	0.1	1.1	0.4	0.4	0.0	1.5
Yb	0.1	62.0	70.2	0.9	2.5	1.9	2.4	0.0	3.9
Lu	0.04	7.9	8.8	0.1	1.5	0.3	0.4	0.0	5.3
Hf	0.2	9.7	7.2	0.1	2.7	1.0	1.0	0.0	4.0
Ta	0.05	30.0	21.8	0.1	0.9	0.2	0.4	0.0	3.3
W	0.5	1.1	2.6	0.1	8.0	0.0	0.0	0.0	0.0
Tl	0.1	1.6	1.5	0.0	1.2	0.0	0.0	0.0	0.0
Pb	5.0	133.0	131	0.7	1.0	720	980	14.7	3.0
Bi	0.2	0.27	0.2	0.0	8.4	1380.0	1378	2.7	0.4
Th	0.1	1003.0	1003	0.6	0.1	2.4	2.5	0.1	3.6
U	0.1	650.0	648	1.7	0.5	33.0	32.4	0.4	2.3

## Appendix A7-2.1

MARKOV.FOR - A FORTRAN 77 PROGRAM USED FOR MARKOV CHAIN ANALYSIS

MARKOV.FOR

This program calculated transition probability matrix, independent transition matrix, difference matrix and the normalized difference matrix observed-expected)/SQRT (expected)-values that exceed absolute (2.0) are beyond the 95% value for normally distributed differences)). For a pre-tabulated NxN transition matrix with zeros along the main diagonal, the input is the raw transition matrix, which is designed to test 1st, 2nd, or higher order Markov properties. The difference matrix is tested using a Chi-Squared test with the null hypothesis being that there is no difference between the independent probability matrix and the observed transition probability matrix. References for the test statistics are given in the program. For general background, see Miall (1973) and for the iterative fitting of row and column totals, see Powers and Easterling C (1982).

Author R.N. Hiscott

```

      INTEGER F(20,20),T,SI(20),SJ(20),DF(2)
      DIMENSION CHISQ(2),P(20,20),R(20,20),D(20,20),SR(20),
1  D1(20,20),A(20),B(20),A2(20),B2(20),ASUM(20),BSUM(20),
1  PI(20),PJ(20),RI(20),RJ(20),DI(20),DJ(20),D1I(20),D1J(20)
      CHARACTER*12 FILE1,OUTF
      CHARACTER FF
      FF=CHAR(12+128)
      WRITE(*,*) 'INPUT FILE NAME'
      READ(*,5002) FILE1
      WRITE(*,*) 'OUTPUT FILE NAME'
      READ(*,5002) OUTF
      open(unit=7,file=file1,status='old')
      open(unit=4,file=outf,status='new')
9991 FORMAT(1X,A1)
1000 FORMAT(I2)
1001 FORMAT(14(I3,2X))
1002 FORMAT(' ',I3)
2000 FORMAT(15(I8))
2001 FORMAT('///' TRANSITION MATRIX (RAW DATA)'///)
2002 FORMAT('////' TRANSITION PROBABILITY MATRIX'///)
2003 FORMAT(15(F9.3))
2004 FORMAT('////' INDEPENDENT TRIALS MATRIX'///)
2006 FORMAT('////' DIFFERENCE MATRIX'///)

```

```

2012 FORMAT(/' NO. OF ITERATIONS FOR ROW AND COLUMN FITTING')
2013 FORMAT(///// ' MATRIX NO.', I5)
2008 FORMAT(////10X, ' TEST EQUATION', 8X, ' CHISQ', 8X, ' D.F.'//
1/16X, ' 1', 12X, F9.3, 9X, I2//16X, ' 2', 12X, F9.3, 9X, I2)
2009 FORMAT(15(F9.2))
2010 FORMAT(////10X, ' NORMALIZED DIFFERENCE MATRIX'////)
2011 FORMAT(12('*****'))
5002 FORMAT(A12)
      WRITE(*,*) 'ENTER NTEST'
      READ(*,1000) NTEST

C
C
*****
C
      NTEST IS THE NUMBER OF SEQUENCES TO BE CHECKED
C
C
*****
C
      NTALLY=0
C
C
*****
C
      N IS THE SIZE OF THE SQUARE MATRIX TO BE TESTED
C
C
*****
C
12  CONTINUE
      NMATX=NTALLY+1
      WRITE(4,2013) NMATX
      WRITE(4,2012)
      DO 41 L=1,20
        A(L)=0.
        B(L)=0.
        A2(L)=0.
        B2(L)=0.
        ASUM(L)=0.
        BSUM(L)=0.
        SI(L)=0
        SJ(L)=0
        PI(L)=0.
        PJ(L)=0.
        RI(L)=0.
        RJ(L)=0.
        DI(L)=0.
        DJ(L)=0.
        D1I(L)=0.
        D1J(L)=0.
        SR(L)=0.
        D(L,L)=0.
        D1(L,L)=0.

```

```

41  R(L,L)=0.
    CHISQ(1)=0
    CHISQ(2)=0
    NITER=0
    T=0
    PT=0.
    RT=0.
    DT=0.
    DLT=0.
    write(*,*)'inpt size of the matrix "N" '
    READ(*,1000) N
    READ(7,*) ((F(I,J),J=1,N),I=1,N)
    DO 20 I=1,N
    DO 10 J=1,N
    SI(I)=SI(I)+F(I,J)
10  T=T+F(I,J)
20  CONTINUE
    DO 30 J=1,N
    DO 40 I=1,N
40  SJ(J)=SJ(J)+F(I,J)
30  CONTINUE
    DO 50 I=1,N
    A(I)=FLOAT(SI(I))/FLOAT(N-1)
    DO 60 J=1,N
    IF(SI(I).NE.0) GO TO 14
    P(I,J)=0.0
    GO TO 13
14  P(I,J)=FLOAT(F(I,J))/FLOAT(SI(I))
    PI(I)=PI(I)+P(I,J)
    PT=PT+P(I,J)
13  IF(J.EQ.I) GO TO 60
    ASUM(J)=ASUM(J)+A(I)
60  CONTINUE
50  CONTINUE
    DO 71 J=1,N
    DO 72 I=1,N
    PJ(J)=PJ(J)+P(I,J)
72  CONTINUE
71  CONTINUE
    DO 16 J=1,N
    B(J)=FLOAT(SJ(J))/ASUM(J)
    DO 17 I=1,N
    IF(I.EQ.J) GO TO 17
    BSUM(I)=BSUM(I)+B(J)
17  CONTINUE
16  CONTINUE
24  NITER=NITER+1
    NCHK=0
    WRITE(4,1002) NITER
    DO 51 J=1,N
    A2(J)=FLOAT(SI(J))/BSUM(J)
    B2(J)=FLOAT(SJ(J))/ASUM(J)
    TESTA=ABS(A2(J)-A(J))*A2(J)

```



```

TESTB=ABS(B2(J)-B(J))*B2(J)
IF(TESTA.GT.0.01) NCHK=1
IF(TESTB.GT.0.01) NCHK=1
A(J)=A2(J)
B(J)=B2(J)
ASUM(J)=0.
BSUM(J)=0.
51  CONTINUE
    IF(NCHK.EQ.0) GO TO 18
    DO 19 I=1,N
    DO 21 J=1,N
    IF(I.EQ.J) GO TO 21
    BSUM(I)=BSUM(I)+B(J)
21  CONTINUE
19  CONTINUE
    DO 22 I=1,N
    DO 23 J=1,N
    IF(I.EQ.J) GO TO 23
    ASUM(I)=ASUM(I)+A2(J)
23  CONTINUE
22  CONTINUE
    GO TO 24
18  CONTINUE
    DO 52 I=1,N
    DO 53 J=1,N
    IF(I.EQ.J) GO TO 53
    R(I,J)=A(I)*B(J)
    RI(I)=RI(I)+R(I,J)
    RT=RT+R(I,J)
    D(I,J)=F(I,J)-R(I,J)
    DI(I)=DI(I)+D(I,J)
    DT=DT+D(I,J)
    D1(I,J)=D(I,J)/SQRT(R(I,J))
    D1I(I)=D1I(I)+D1(I,J)
    D1T=D1T+D1(I,J)
53  CONTINUE
52  CONTINUE
    DO 73 J=1,N
    DO 74 I=1,N
    RJ(J)=RJ(J)+R(I,J)
    DJ(J)=DJ(J)+D(I,J)
    D1J(J)=D1J(J)+D1(I,J)
74  CONTINUE
73  CONTINUE

```

C  
C

```

*****
C
C   R(I,J) ARE VALUES OF ELEMENTS IN THE INDEPENDENT TRAILS
C   MATRIX. P(I,J) ARE VALUES OF ELEMENTS IN THE TRANSITION
C   PROBABILITY MATRIX. D(I,J) ARE VALUES OF ELEMENTS IN THE
C   DIFFERENCE MATRIX. D1(I,J) ARE VALUES OF ELEMENTS OF THE NORMAL-
C   IZED DIFFERENCE MATRIX (POWERS & EASTERLING, 1982, P. 922).
C
C
*****

      WRITE(4,9991) FF
      WRITE(4,2001)
      DO 31 I=1,N
31   WRITE(4,2000) (F(I,J),J=1,N),SI(I)
      WRITE(4,2011)
      WRITE(4,2000) (SJ(J),J=1,N),T
      WRITE(4,2002)
      DO 32 I=1,N
32   WRITE(4,2003) (P(I,J),J=1,N),PI(I)
      WRITE(4,2011)
      WRITE(4,2003) (PJ(J),J=1,N),PT
      WRITE(4,9991) FF
      WRITE(4,2004)
      DO 33 I=1,N
33   WRITE(4,2003) (R(I,J),J=1,N),RI(I)
      WRITE(4,2011)
      WRITE(4,2003) (RJ(J),J=1,N),RT
      WRITE(4,2006)
      DO 34 I=1,N
34   WRITE(4,2003) (D(I,J),J=1,N),DI(I)
      WRITE(4,2011)
      WRITE(4,2003) (DJ(J),J=1,N),DT
      WRITE(4,9991) FF
      WRITE(4,2010)
      DO 36 I=1,N
36   WRITE(4,2009) (D1(I,J),J=1,N),D1I(I)
      WRITE(4,2011)
      WRITE(4,2009) (D1J(J),J=1,N),D1T

C
C *****
C
C   FIRST CALCULATE CHISQ(1) VALUE FROM BILLINGSLEY (1961, P.17)AND
C   GINGERICH (1969, P.331).
C
C *****
C

      DO 70 I=1,N
      DO 80 J=1,N
      IF(I.EQ.J) GO TO 80
      IF(SI(I).EQ.0.OR.R(I,J).EQ.0) GO TO 80
      CHISQ(1)=CHISQ(1)+(F(I,J)-R(I,J))**2/R(I,J)
80  CONTINUE

```

```

70  CONTINUE
    DF(1)=(N-1)**2-N
C
C *****
C
C  SECONDLY CALCULATE CHISQ(2) VALUE FROM ANDERSON AND GOODMAN
C  1957)AND HARBAUGH AND BONHAM-CARTER (1970, P.121) CORRECTED AS
C  OUTLINED IN LETTER FROM DAVID ATTWOOD, JAN 4, 1982.
C *****
C
C  DO 90 I=1,N
C  DO 100 J=1,N
C  IF(F(I,J).EQ.0.OR.SJ(J).EQ.0) GO TO 100
C  CHISQ(2)=CHISQ(2)+2.*FLOAT(F(I,J))*ALOG(F(I,J)/R(I,J))
100 CONTINUE
90  CONTINUE
    DF(2)=(N-1)**2-N
    WRITE(4,2008) CHISQ(1),DF(1),CHISQ(2),DF(2)
    NTALLY=NTALLY+1
    IF(NTALLY.EQ.NTEST) GO TO 11
    GO TO 12
11  WRITE(4,9991) FF
    STOP
    END

```

Table A7-2.2A. Matrices used in Markov chain analysis of facies C2.4 group A beds.

TRANSITION MATRIX (RAW DATA)									
	0	1	2	3	4	5	6	7	9
0	0	24	15	41	21	1	10	0	0
1	0	0	7	10	3	1	1	1	0
2	0	0	0	6	6	5	3	1	0
3	0	0	0	0	3	6	29	4	16
4	0	0	0	2	0	5	11	5	22
5	0	0	0	3	2	0	9	1	27
6	0	0	0	6	5	16	0	9	26
7	0	0	0	1	0	2	4	0	16
9	20	0	0	0	0	0	0	0	0

TRANSITION PROBABILITY MATRIX									
	0	1	2	3	4	5	6	7	9
0	0.00	0.21	0.13	0.37	0.19	0.01	0.09	0.00	0.00
1	0.00	0.00	0.30	0.44	0.13	0.04	0.04	0.04	0.00
2	0.00	0.00	0.00	0.29	0.29	0.24	0.14	0.05	0.00
3	0.00	0.00	0.00	0.00	0.05	0.10	0.50	0.07	0.28
4	0.00	0.00	0.00	0.04	0.00	0.11	0.24	0.11	0.49
5	0.00	0.00	0.00	0.07	0.05	0.00	0.21	0.02	0.64
6	0.00	0.00	0.00	0.10	0.08	0.26	0.00	0.15	0.42
7	0.00	0.00	0.00	0.04	0.00	0.09	0.17	0.00	0.70
9	1.00	0.00	0.00	0.00	0.00	0.00	0.00	0.00	0.00

INDEPENDENT TRAILS PROBABILITY MATRIX									
	0	1	2	3	4	5	6	7	9
0	0.00	6.59	6.01	21.20	11.67	10.40	20.84	5.76	29.53
1	1.44	0.00	1.23	4.34	2.39	2.13	4.26	1.18	6.04
2	1.31	1.22	0.00	3.94	2.17	1.93	3.87	1.07	5.49
3	4.17	3.91	3.56	0.00	6.92	6.17	12.35	3.42	17.51
4	2.95	2.76	2.52	8.89	0.00	4.36	8.73	2.42	12.38
5	2.72	2.55	2.32	8.20	4.51	0.00	8.06	2.23	11.42
6	4.44	4.16	3.79	13.39	7.37	6.57	0.00	3.64	18.64
7	1.43	1.34	1.22	4.31	2.37	2.11	4.23	0.00	6.00
9	1.57	1.47	1.34	4.74	2.61	2.33	4.66	1.29	0.00

DIFFERENCE MATRIX									
	0	1	2	3	4	5	6	7	9
0	0.00	17.41	8.99	19.80	9.33	-9.40	-10.84	-5.76	-29.53
1	-1.44	0.00	5.77	5.66	0.61	-1.13	-3.26	-0.18	-6.04
2	-1.31	-1.22	0.00	2.06	3.83	3.07	-0.87	-0.07	-5.49
3	-4.17	-3.91	-3.56	0.00	-3.92	-0.17	16.65	0.58	-1.51
4	-2.95	-2.76	-2.52	-6.89	0.00	0.64	2.27	2.58	9.62
5	-2.72	-2.55	-2.32	-5.20	-2.51	0.00	0.94	-1.23	15.58
6	-4.44	-4.16	-3.79	-7.39	-2.37	9.43	0.00	5.36	7.36
7	-1.43	-1.34	-1.22	-3.31	-2.37	-0.11	-0.23	0.00	10.00
9	18.43	-1.47	-1.34	-4.74	-2.61	-2.33	-4.66	-1.29	0.00

NORMALISED DIFFERENCE MATRIX									
	0	1	2	3	4	5	6	7	9
0	0	6.78	3.67	4.3	2.73	-2.92	-2.37	-2.4	-5.43
1	-1.2	0	5.21	2.72	0.4	-0.77	-1.58	-0.16	-2.46
2	-1.14	-1.11	0	1.04	2.6	2.21	-0.44	-0.07	-2.34
3	-2.04	-1.98	-1.89	0	-1.49	-0.07	4.74	0.32	-0.36
4	-1.72	-1.66	-1.59	-2.31	0	0.31	0.77	1.66	2.74
5	-1.65	-1.6	-1.52	-1.82	-1.18	0	0.33	-0.82	4.61
6	-2.11	-2.04	-1.95	-2.02	-0.87	3.68	0	2.81	1.7
7	-1.19	-1.16	-1.1	-1.59	-1.54	-0.08	-0.11	0	4.09
9	14.71	-1.21	-1.16	-2.18	-1.61	-1.52	-2.16	-1.13	0

CHISQ  
598.32

D.F.  
55

Table A7-2.2B. Matrices used in Markov chain analysis of facies C2.4 group B beds.

TRANSITION MATRIX (RAW DATA)										
	0	1	2	3	4	5	6	7	8	9
0	0	49	46	60	28	2	10	0	0	0
1	0	0	11	16	8	1	9	1	1	0
2	0	0	0	23	20	5	8	0	1	0
3	0	0	1	0	7	31	87	8	0	13
4	0	0	0	3	0	29	38	9	0	24
5	0	0	0	8	15	0	16	11	0	91
6	0	0	0	33	21	27	0	11	0	49
7	0	0	0	2	3	8	11	0	0	16
8	0	0	0	0	0	1	1	0	0	0
9	12	0	0	0	0	0	0	0	0	0

TRANSITION PROBABILITY MATRIX										
	0	1	2	3	4	5	6	7	8	9
0	0.00	0.25	0.24	0.31	0.14	0.01	0.05	0.00	0.00	0.00
1	0.00	0.00	0.23	0.34	0.17	0.02	0.19	0.02	0.02	0.00
2	0.00	0.00	0.00	0.40	0.35	0.09	0.14	0.00	0.02	0.00
3	0.00	0.00	0.01	0.00	0.05	0.21	0.59	0.05	0.00	0.09
4	0.00	0.00	0.00	0.03	0.00	0.28	0.37	0.09	0.00	0.23
5	0.00	0.00	0.00	0.06	0.11	0.00	0.11	0.08	0.00	0.65
6	0.00	0.00	0.00	0.23	0.15	0.19	0.00	0.08	0.00	0.35
7	0.00	0.00	0.00	0.05	0.08	0.20	0.28	0.00	0.00	0.40
8	0.00	0.00	0.00	0.00	0.00	0.50	0.50	0.00	0.00	0.00
9	1.00	0.00	0.00	0.00	0.00	0.00	0.00	0.00	0.00	0.00

INDEPENDENT TRAILS PROBABILITY MATRIX										
	0	1	2	3	4	5	6	7	8	9
0	0.00	10.17	12.19	34.81	22.77	24.45	43.32	8.24	0.40	38.67
1	0.74	0.00	3.05	8.71	5.70	6.12	10.84	2.06	0.10	9.68
2	0.91	3.12	0.00	10.68	6.99	7.50	13.29	2.53	0.12	11.86
3	2.66	9.17	10.98	0.00	20.52	22.03	39.03	7.42	0.36	34.84
4	1.74	5.98	7.17	20.47	0.00	14.38	25.47	4.84	0.23	22.74
5	2.40	8.27	9.90	28.29	18.51	0.00	35.21	6.69	0.32	31.42
6	2.69	9.27	11.11	31.73	20.76	22.29	0.00	7.51	0.36	35.25
7	0.62	2.15	2.57	7.34	4.80	5.15	9.13	0.00	0.08	8.15
8	0.03	0.10	0.12	0.35	0.23	0.25	0.44	0.08	0.00	0.39
9	0.22	0.77	0.92	2.62	1.72	1.84	3.26	0.62	0.03	0.00

DIFFERENCE MATRIX										
	0	1	2	3	4	5	6	7	8	9
0	0.00	38.83	33.82	25.19	5.23	-22.45	-33.32	-8.24	-0.40	-38.67
1	-0.74	0.00	7.95	7.29	2.30	-5.12	-1.84	-1.06	0.90	-9.68
2	-0.91	-3.12	0.00	12.32	13.01	-2.50	-5.29	-2.53	0.88	-11.86
3	-2.66	-9.17	-9.98	0.00	-13.52	8.97	47.97	0.58	-0.36	-21.84
4	-1.74	-5.98	-7.17	-17.47	0.00	14.63	12.53	4.16	-0.23	1.27
5	-2.40	-8.27	-9.90	-20.29	-3.51	0.00	-19.21	4.31	-0.32	59.58
6	-2.69	-9.27	-11.11	1.27	0.24	4.71	0.00	3.49	-0.36	13.75
7	-0.62	-2.15	-2.57	-5.34	-1.80	2.85	1.87	0.00	-0.08	7.85
8	-0.03	-0.10	-0.12	-0.35	-0.23	0.75	0.56	-0.08	0.00	-0.39
9	11.78	-0.77	-0.92	-2.62	-1.72	-1.84	-3.26	-0.62	-0.03	0.00

NORMALISED DIFFERENCE MATRIX										
	0	1	2	3	4	5	6	7	8	9
0	0.00	12.17	9.69	4.27	1.10	-4.54	-5.06	-2.87	-0.63	-6.22
1	-0.86	0.00	4.55	2.47	0.96	-2.07	-0.56	-0.74	2.86	-3.11
2	-0.95	-1.77	0.00	3.77	4.92	-0.91	-1.45	-1.59	2.52	-3.44
3	-1.63	-3.03	-3.01	0.00	-2.98	1.91	7.68	0.21	-0.60	-3.70
4	-1.32	-2.45	-2.68	-3.86	0.00	3.86	2.48	1.89	-0.48	0.27
5	-1.55	-2.88	-3.15	-3.81	-0.82	0.00	-3.24	1.66	-0.57	10.63
6	-1.64	-3.05	-3.33	0.23	0.05	1.00	0.00	1.27	-0.60	2.32
7	-0.79	-1.46	-1.60	-1.97	-0.82	1.25	0.62	0.00	-0.29	2.75
8	-0.17	-0.32	-0.35	-0.59	-0.48	1.51	0.85	-0.29	0.00	-0.63
9	24.98	-0.88	-0.96	-1.62	-1.31	-1.36	-1.81	-0.79	-0.17	0.00

CHI SQ.  
953.89

D.F.  
71

Table A7-2.2C. Matrices used in Markov chain analysis of facies C2.4 group C beds.

TRANSITION MATRIX (RAW DATA)										
	0	1	2	3	4	5	6	7	8	9
0	0	16	17	8	7	0	3	0	6	0
1	0	0	8	2	1	1	1	1	0	0
2	0	0	0	12	5	6	6	1	3	0
3	0	0	1	0	1	6	18	2	0	0
4	0	0	1	1	0	7	15	2	0	6
5	0	0	3	1	5	0	14	3	0	36
6	0	0	2	6	12	19	0	5	0	12
7	0	0	0	0	0	7	3	0	0	5
8	0	0	0	3	0	2	4	1	0	0
9	2	0	0	0	0	0	0	0	0	0

TRANSITION PROBABILITY MATRIX										
	0	1	2	3	4	5	6	7	8	9
0	0.00	0.28	0.30	0.14	0.12	0.00	0.05	0.00	0.11	0.00
1	0.00	0.00	0.57	0.14	0.07	0.07	0.07	0.07	0.00	0.00
2	0.00	0.00	0.00	0.36	0.15	0.18	0.18	0.03	0.09	0.00
3	0.00	0.00	0.04	0.00	0.04	0.21	0.64	0.07	0.00	0.00
4	0.00	0.00	0.03	0.03	0.00	0.22	0.47	0.06	0.00	0.19
5	0.00	0.00	0.05	0.02	0.08	0.00	0.23	0.05	0.00	0.58
6	0.00	0.00	0.04	0.11	0.21	0.34	0.00	0.09	0.00	0.21
7	0.00	0.00	0.00	0.00	0.00	0.47	0.20	0.00	0.00	0.33
8	0.00	0.00	0.00	0.30	0.00	0.20	0.40	0.10	0.00	0.00
9	1.00	0.00	0.00	0.00	0.00	0.00	0.00	0.00	0.00	0.00

INDEPENDENT TRAILS PROBABILITY MATRIX										
	0	1	2	3	4	5	6	7	8	9
0	0.00	2.73	5.83	5.91	5.63	9.96	13.17	2.56	1.51	9.70
1	0.10	0.00	1.49	1.51	1.44	2.55	3.37	0.66	0.39	2.48
2	0.25	1.75	0.00	3.78	3.60	6.38	8.43	1.64	0.97	6.21
3	0.21	1.48	3.17	0.00	3.06	5.42	7.16	1.39	0.82	5.28
4	0.24	1.69	3.61	3.66	0.00	6.16	8.14	1.59	0.94	6.00
5	0.51	3.56	7.63	7.73	7.36	0.00	17.21	3.35	1.98	12.68
6	0.49	3.45	7.38	7.48	7.13	12.61	0.00	3.25	1.92	12.28
7	0.11	0.75	1.60	1.62	1.54	2.73	3.60	0.00	0.41	2.65
8	0.07	0.49	1.04	1.06	1.01	1.78	2.36	0.46	0.00	1.74
9	0.02	0.11	0.25	0.25	0.24	0.42	0.55	0.11	0.06	0.00

DIFFERENCE MATRIX										
	0	1	2	3	4	5	6	7	8	9
0	0.00	13.27	11.17	2.09	1.37	-9.96	-10.17	-2.56	4.49	-9.70
1	-0.10	0.00	6.51	0.49	-0.44	-1.55	-2.37	0.34	-0.39	-2.48
2	-0.25	-1.75	0.00	8.22	1.40	-0.38	-2.43	-0.64	2.03	-6.21
3	-0.21	-1.48	-2.17	0.00	-2.06	0.58	10.84	0.61	-0.82	-5.28
4	-0.24	-1.69	-2.61	-2.66	0.00	0.84	6.86	0.42	-0.94	0.01
5	-0.51	-3.56	-4.63	-6.73	-2.36	0.00	-3.21	-0.35	-1.98	23.32
6	-0.49	-3.45	-5.38	-1.48	4.88	6.39	0.00	1.76	-1.92	-0.28
7	-0.11	-0.75	-1.60	-1.62	-1.54	4.28	-0.60	0.00	-0.41	2.35
8	-0.07	-0.49	-1.04	1.94	-1.01	0.22	1.64	0.54	0.00	-1.74
9	1.98	-0.11	-0.25	-0.25	-0.24	-0.42	-0.55	-0.11	-0.06	0.00

NORMALISED DIFFERENCE MATRIX										
	0	1	2	3	4	5	6	7	8	9
0	0.00	8.04	4.62	0.86	0.58	-3.16	-2.80	-1.60	3.65	-3.11
1	-0.32	0.00	5.32	0.39	-0.37	-0.97	-1.29	0.42	-0.62	-1.58
2	-0.50	-1.32	0.00	4.22	0.74	-0.15	-0.84	-0.50	2.06	-2.49
3	-0.46	-1.22	-1.22	0.00	-1.18	0.25	4.05	0.51	-0.91	-2.30
4	-0.49	-1.30	-1.37	-1.39	0.00	0.34	2.40	0.33	-0.97	0.00
5	-0.71	-1.89	-1.67	-2.42	-0.87	0.00	-0.77	-0.19	-1.41	6.55
6	-0.70	-1.86	-1.98	-0.54	1.83	1.80	0.00	0.97	-1.38	-0.08
7	-0.33	-0.86	-1.26	-1.27	-1.24	2.59	-0.32	0.00	-0.64	1.44
8	-0.26	-0.70	-1.02	1.89	-1.00	0.16	1.07	0.80	0.00	-1.32
9	15.51	-0.34	-0.49	-0.50	-0.49	-0.65	-0.74	-0.33	-0.25	0.00

CHI SQ.      D.F.  
340.797      71

Table A7.3.1. Thickness of mini-slices of the time-slices in each of the areas of composite sections. Shown also in the mean thickness of each mini-slice and the percent difference of each mini-slice compared to the mean thickness of the mini-slice in the three areas.

MINI-SLICE	AREA C	AREA B	AREA A	MEAN ALL	C % DIF.	B % DIF.	A % DIF.
SL 7D	4.80	5.80	NA	5.30	-9.43	9.43	NA
SL 7C	21.20	31.60	NA	26.40	-19.70	19.70	NA
SL 7B	56.10	60.50	NA	58.30	-3.77	3.77	NA
SL 7A	5.20	6.50	NA	5.85	-11.11	11.11	NA
SL 6M	11.67	19.59	NA	15.63	-25.34	25.34	NA
SL 6L	11.785	13.27	NA	12.53	-5.93	5.93	NA
SL 6K	26.86	40.305	NA	33.58	-20.02	20.02	NA
SL 6J	4.565	10.705	NA	7.64	-40.21	40.21	NA
SL 6I	13.775	12.625	NA	13.20	4.36	-4.36	NA
SL 6H	8.05	5.84	NA	6.95	15.91	-15.91	NA
SL 6G	12.825	20.81	16.065	16.57	-22.59	25.61	-3.03
SL 6F	6.1	3.52	2.265	3.96	53.98	-11.15	-42.83
SL 6E	23.99	40.455	52.785	39.08	-38.61	3.53	35.08
SL 6D	1.67	2.075	0.52	1.42	17.47	45.96	-63.42
SL 6C	3.85	5.51	4.075	4.48	-14.03	23.04	-9.01
SL 6B	2.57	4.125	2.755	3.15	-18.41	30.95	-12.54
SL 6A	14.66	20.935	11.99	15.86	-7.58	31.98	-24.41
SL 5G	4.975	6.135	4.28	5.13	-3.02	19.59	NA
SL 5F	2.725	2.325	2.03	2.36	15.47	-1.48	NA
SL 5E	5.12	5.255	4.23	4.87	5.17	7.94	-13.11
SL 5D	6.715	5.47	2.7	4.96	35.34	10.25	-45.58
SL 5C	3.085	3.49	3.565	3.38	-8.73	3.25	5.47
SL 5B	11.73	6.205	12	9.98	17.55	NA	20.26
SL 5A	8.515	12.27	9.735	10.17	-16.30	20.61	-4.31
SL 4N	32.90	37.80	29.03	33.24	-1.02	13.70	-12.68
SL 4M	12.13	12.46	21.67	15.42	-21.32	-19.21	40.53
SL 4L	8.50	7.19	9.67	8.45	0.51	-14.93	14.42
SL 4K	12.40	12.67	14.18	13.08	-5.21	-3.19	8.40
SL 4J	1.91	1.85	1.92	1.89	0.70	-2.20	1.50
SL 4I	5.31	4.79	5.62	5.24	1.40	-8.63	7.22
SL 4H	3.46	4.32	5.91	4.56	-24.12	-5.37	29.50
SL 4G	10.96	11.05	11.32	11.11	-1.34	-0.57	1.91
SL 4F	5.92	3.75	3.75	4.47	32.33	-16.22	-16.11
SL 4E	1.42	0.84	1.33	1.20	18.83	-29.71	10.88
SL 4D	3.15	1.80	2.55	2.50	26.17	-28.10	1.94
SL 4C	14.51	15.84	6.72	12.35	17.46	28.18	-45.64
SL 4B	2.48	2.04	1.25	1.92	28.94	6.07	-35.01
SL 4A	15.99	16.57	19.85	17.47	-8.48	-5.16	13.65

Table A7-3.1 Continued.

MINI-SLICE	AREA C	AREA B	AREA A	MEAN ALL	C % DIF.	B % DIF.	A % DIF.
SL 3J	3.66	2.98	2.39	3.01	21.59	-1.00	-20.60
SL 3I	4.75	5.42	6.21	5.46	-13.02	-0.75	13.76
SL 3H	7.99	7.28	8.18	7.82	2.22	-6.87	4.65
SL 3G	3.01	3.51	3.77	3.43	-12.24	2.33	9.91
SL 3F	3.82	4.04	2.45	3.44	11.15	17.56	-28.71
SL 3E	10.58	11.64	6.18	9.47	11.74	22.94	-34.68
SL 3D	4.22	3.94	3.62	3.93	7.44	0.31	-7.75
SL 3C	13.25	10.94	10.86	11.68	13.41	-6.36	-7.05
SL 3B	17.20	20.02	15.14	17.45	-1.45	14.70	-13.25
SL 3A	5.38	5.46	6.11	5.65	-4.78	-3.36	8.14
SL 2O	4.76	4.03	4.31	4.37	9.01	-7.71	-1.30
SL 2N	5.59	6.39	6.38	6.12	-8.66	4.41	4.25
SL 2M	9.30	11.76	9.30	10.12	-8.09	16.22	-8.14
SL 2L	3.14	2.98	3.01	3.04	3.22	-2.17	-1.05
SL 2K	5.55	4.15	3.42	4.37	26.87	-5.04	-21.82
SL 2J	2.89	3.57	3.26	3.24	-10.80	10.19	0.62
SL 2I	3.47	4.21	3.65	3.78	-8.12	11.47	-3.35
SL 2H	3.57	5.36	5.63	4.85	-26.44	10.44	16.00
SL 2G	3.23	2.97	3.45	3.22	0.41	-7.67	7.25
SL 2F	2.12	3.25	2.75	2.71	-21.67	20.07	1.60
SL 2E	0.97	0.93	0.81	0.90	7.58	2.59	-10.17
SL 2D	4.15	4.36	3.59	4.03	2.89	8.10	-10.99
SL 2C	4.77	6.12	4.94	5.27	-9.64	16.06	-6.42
SL 2B	2.67	2.12	2.06	2.28	16.88	-7.13	-9.75
SL 2A	1.05	0.97	1.10	1.04	0.96	-6.73	5.77
SL 1F	2.46	2.50	2.00	2.32	6.11	7.62	-13.73
SL 1E	4.45	5.08	5.66	5.06	-12.11	0.33	11.78
SL 1D	3.66	2.76	2.39	2.94	24.63	-6.02	-18.62
SL 1C	2.46	2.18	1.86	2.17	13.54	0.62	-14.15
SL 1B	6.97	6.45	7.05	6.82	2.15	-5.47	3.32
SL 1A	15.04	13.30	13.08	13.81	8.91	-3.66	-5.25



Table A7.3.2. Thickness of megaturbidite layers (lower coarser part (facies C2.4/C2.5) and cap) in the three areas where composite sections were measured. Shown also is the mean thickness of each megaturbidite and the percent difference of each megaturbidite compared to the mean thickness in the three areas.

Marker	AREA C	AREA B	AREA A	Mean	C % DIF	B % DIF	A % DIF
<b>KB-9</b>							
71	270	198	NA	234	16	-16	NA
70	153	135	NA	144	6	-6	NA
69C	104	NA	NA	104	0	NA	NA
69B	92	NA	NA	92	0	NA	NA
69A	224	NA	NA	224	0	NA	NA
69	138	106	NA	122	13	-13	NA
<b>KB-8</b>							
68	133	67	NA	100	33	-33	NA
67	513	441	NA	477	8	-8	NA
66	180	116	NA	148	22	-22	NA
65	156	170	NA	163	-4	4	NA
64A	131	105	NA	65	100	-100	NA
64	213	51	NA	159	34	-34	NA
63	104	81	NA	93	12	-12	NA
62A	83	0	NA	41	100	-100	NA
62	127	65	53	82	56	-21	-35
61	365	180	134	226	61	-21	-41
60B	58	NA	NA	19	NA	NA	NA
60A	67	74	NA	47	43	57	NA
60A2	81	26	NA	36	127	-27	NA
60A1	66	74	41	60	9	23	-32
60	178	157	98	144	24	9	-32
59	157	159	52	123	28	30	-58
<b>KB-7</b>							
58	163	159	113	145	13	10	-22
57	367	336	140	281	31	20	-50
<b>KB-6</b>							
56a	96	127	NA	74	29	71	NA
56	341	386	39	255	34	51	-85
55	118	39	38	65	82	-40	-42
54	101	73	40	71	42	2	-44
53	167	135	102	134	24	0	-24
52	173	104	40	106	64	-2	-62
51	95	82	55	77	23	6	-29
50	376	182	167	242	56	-25	-31
<b>KB-5</b>							
49	100	80	NA	60	67	33	NA
48c	54	97	NA	50	7	93	NA
48b	194	103	NA	99	96	4	NA

Table A7-3.2. Continued.

Marker	AREA C	AREA B	AREA A	Mean	C % DIF	B % DIF	A % DIF
48A	563	292	142	332	70	-12	-57
48	144	135	72	117	23	15	-38
47	173	95	82	117	49	-19	-30
46	330	188	170	229	44	-18	-26
45	254	282	183	240	6	18	-24
44	136	122	83	114	20	8	-27
43	418	147	235	267	57	-45	-12
42	92	42	42	59	57	-28	-28
41A	88	58	46	64	38	-9	-28
41	640	492	486	539	19	-9	-10
40A	122	75	59	85	43	-12	-31
40	164	81	123	123	34	-34	0
39	375	180	255	270	39	-33	-6
38	125	87	60	91	38	-4	-34
37	157	117	35	103	52	14	-66
KB-4	2	5	3	3	-37	42	-5
36	340	187	188	238	43	-22	-21
35	157	116	90	121	30	-4	-26
34	611	337	318	422	45	-20	-25
33	199	131	140	157	27	-16	-11
32	137	79	62	93	48	-15	-33
31	96	77	61	78	23	-1	-22
30A	67	0	0	22	200	-100	-100
30	147	84	41	91	62	-7	-55
29	120	68	38	75	59	-10	-50
28	810	530	460	600	35	-12	-23
27	187	106	49	114	64	-7	-57
26	292	183	131	202	45	-9	-35
KB-3	6	2	3	4	64	-46	-18
25	177	131	76	128	38	2	-41
24	375	299	202	292	28	2	-31
23A	74	NA	NA	25	200	NA	NA
23	248	198	153	200	24	-1	-23
22	163	71	52	95	71	-26	-46
21	124	73	38	78	58	-7	-52
20	366	248	211	275	33	-10	-23
19	157	190	129	159	-1	20	-19
18	99	82	47	76	30	8	-38
17	338	272	257	289	17	-6	-11
16	69	54	50	58	20	-6	-13

Table A7-3.2. Continued.

Marker	AREA C	AREA B	AREA A	Mean	C % DIF	B % DIF	A % DIF
15	131	116	61	103	28	13	-41
14	78	38	48	55	43	-31	-12
13	200	210	150	187	7	13	-20
12	223	260	245	243	-8	7	1
11	134	65	30	76	76	-15	-61
<b>KB-2</b>							
10	123	108	84	105	17	3	-20
9	67	53	36	52	29	2	-31
8	224	248	209	227	-1	9	-8
7	71	39	51	54	32	-27	-5
6	78	56	40	58	35	-3	-31
5	132	105	86	108	23	-3	-20
4B	140	NA	60	67	110	NA	-10
<b>KB-1</b>							
4A	156	0	101	86	82	NA	18
4	263	220	203	229	15	-4	-11
3a	143	98	93	111	28	-12	-17
3	665	780	660	702	-5	11	-6

Table A7.4.1. Petrology of the greywackes and calcilutites facies of <sup>1</sup>Enos (1965, 1969a,b) and <sup>2</sup>Slivitzky *et al.* (1991). Calcareous wacke was type 4 greywacke by <sup>2</sup>Slivitzky *et al.* (1991) who also identified a 5th type of wacke that they term lithic wacke.

Facies	Grains					Matrix and cement	
	Detrital grains	Quartz	Feldspar	Rock fragments	Accessory Minerals	Argillaceous matrix	Carbonate matrix and cement
Type 1 greywacke <sup>1,2</sup>	65	60	10	25	5	17	17
Type 2 greywacke <sup>1,2</sup>	50	62	13	20	5	45	7
Type 3 greywacke <sup>1,2</sup>	70	16	1	83	0	20	10
Calcareous wacke <sup>1,2</sup>	55	65	15	20	0	11	32
Lithic wacke <sup>2</sup>	~90	65	10	22	5	~10	0
Calcilutite 1 <sup>1</sup>	26	80	15	3	2	11.6	62.4
Calcilutite 2 <sup>1</sup>	34.1	65	17.5	6.5	10.6	18	47.9
Silty carbonates <sup>2</sup>	35	85	15	0	0	10	55
Cal. Argillaceous siltstone <sup>2</sup>	45	?	?	0	0	35	20
Silty calcilutite <sup>2</sup>	25	?	?	10	tr	0	65
Silty cal. claystone <sup>2</sup>	25	?	?	10	tr	0	65
Dol. mudstone/silty claystone/clay-shale <sup>2</sup>	30	?	?	10	tr	55	15
Sandy cong. mudstone/dol. cong. mudstone <sup>2</sup>	50	48*	6*	38*	3	30	20
Calc. claystone/argill. calcilutite <sup>2</sup>	10	?	?	0	tr	40	50

**APPENDIX B**  
**BED THICKNESS DISTRIBUTION**

## APPENDIX B: BED THICKNESS DISTRIBUTION

### B1. METHODOLOGY

In order to assess which type of bed thickness distribution best fits the datasets collected from the studied sections, the following steps were taken. First, the general shape of the bed thickness distribution was obtained. Individual thickness measurements were binned into thickness classes. A large number of classes was used in most cases to obtain detailed plots. A 5 cm class interval was used in most cases because this resulted in plots with 10 or more class intervals. For each class, beds with a thickness equal to the upper limit of the class interval is included within the interval. For example, for class interval 0 - 5 cm, all beds that are  $>0$  cm and  $\leq 5$  cm are included in this class interval. Recall that bed measurements were made to the nearest 0.5 cm. Beds of thinner than 0.5 cm (mostly from Class D) represent less than 1% of beds, were rounded upward to 0.5 cm. Facies D2.3 was affected the most by rounding because a large percentage of this facies occurs as laminae. Histograms of the number of beds in each class were then plotted in various formats. A preliminary appreciation of the type of distribution was obtained from a visual inspection of these histograms.

The second step was to test which theoretical distribution best fit the data: the lognormal, exponential, or gamma distribution. This was done by producing a quantile-quantile plot (q-q plot) for each dataset investigated. This is a common method in data distribution analysis (Chamber *et al.*, 1983). In the q-q plot, for each actual bed thickness

an expected bed thickness is calculated. This expected thickness is calculated as if the distribution was one of the three candidate distributions. The parameters for each of the distributions were calculated from the actual bed thickness data. Each bed thickness measurement was plotted against its expected thickness to produce a q-q plot. If the actual bed thickness closely matches the expected thickness for a specified distribution, then points defining the plot will fall near the line  $y = x$ . The best clustering of points along the line  $y=x$  indicates which of the three distributions best fits the data. This is done by comparing, on a single plot, actual versus expected thicknesses for the three distributions. The details and instructions on how to construct a q-q plot and characteristics of these plots are explained in detail in Chambers *et al.* (1983).

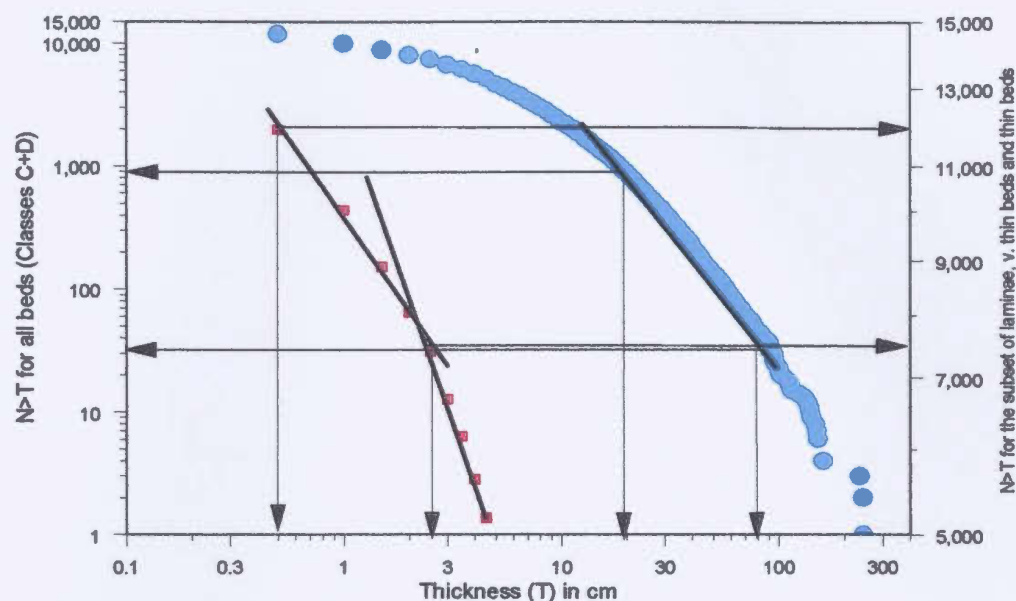
A plot of the bed thickness *versus* the cumulative percent was also generated. Bed thickness was plotted using a log scale on the x-axis while the cumulative percent of the number of beds was plotted using a probability scale on the y-axis. This plot shows whether the data are lognormally distributed, and whether there is a single population or several subpopulations. These plots are referred to hereafter as probability-log plots.

The data were treated differently when testing for power law distributions. The bed thicknesses were sorted in ascending order (thinner to thicker beds) and the number of beds thicker than  $T$  (the thinnest bed) were counted. The number of beds thicker than  $T$  ( $N > T$ ) was plotted (along the y-axis) against thickness  $T$  (along the x-axis) using a log-log scale. A best-fit line (or lines) was drawn by hand. This line is referred to hereafter as power law trend. The slope of this line (or lines) was calculated to obtain the scaling

parameter  $\beta$ . Each facies class, facies group and facies was tested to investigate if it follows a power law distribution and to see if the scaling exponent  $\beta$  varies between facies (Table B3).

A log-log scale expands small values and compresses large values, so when plotting  $N>T$  versus  $T$  (bed thickness), thicker beds are overemphasised because they plot over a large area of the graph even though they may represent only a small proportion of the bed population but this may represent a considerable percent of the total thickness of the beds being tested. Thin beds are masked or may not be well displayed on a log-log plot because they plot in a small area in the upper part of the graph, even though they account for a large proportion of the population. This has resulted in the interpretation of many turbidite bed thickness populations as power law distributions with a certain  $\beta$  value based on fitting a straight line to points corresponding to a small number of thick beds, while thinner beds that represent most of the population beds are overlooked (Figure B1). When this is done, the  $\beta$  value obtained may only reflect the scaling value of a small part of the population, specifically the thicker beds. This may lead to misleading conclusions about the dominant or most frequent processes responsible for the deposition of most of the beds (Malinverno, 1997). Greater care should be exercised when interpreting bed thickness dataset that consists of a large number of thin beds. In this case, it may be better to calculate a  $\beta$  for the thin beds (the majority of the dataset) and then consider other linear trends for the thicker "less common" beds as deviations from the main trend. Deviations or departures that manifest themselves as bends at the ends of a  $N>T$  versus  $T$





	Total Thk. (m)	Total #	% of Total Thk.	% of Total #	% Sand	% Silt
<b>All Class C+D</b>	887.54	13,096	100	100	14	86
<b>Beds 0.5 to 2.5 cm</b>	68.73	4498	7.8	34	1	99
<b>Beds 2.5 to 4.5 cm</b>	81.38	2222	9.2	17	1	95.6
<b>Beds 40 to 90 cm</b>	100.51	183	11.3	1.4	88.5	11.5

Figure B1. All the sandstone and siltstone bed thicknesses combined in a single dataset and plotted (blue circles). The main linear trend is for 183 beds that are 40 - 90 cm thick and represent a small percent (1.4%) of the combined dataset but account for 11.3 % of the total thickness of the sandstone and siltstone beds and laminae. There are no distinguishable linear trends for beds < 40 cm for the plot of the combined dataset. However, if a subset of thinner beds (red filled squares) is plotted on a different scale (2nd Y-axis on the right) other linear trends are observed. Each of these linear trends for the thinner beds represent a larger percent of the combined dataset but a small proportion of the total thickness of sandstone and siltstone.

plot are important in understanding bed thickness populations but they may be caused by less common and perhaps less significant processes (in terms of the proportion of the total bed population). The cause of the bending or departure should be investigated to rule out artifacts caused by limitations of the measuring techniques or procedures. For example, bed thickness data obtained from Formation Microscanner images lacks or under-represent very thin beds ( $<2.5$  cm) that cannot be resolved by the instrument (Hiscott *et al.*, 1992). The number of shale beds is surely under-represented because it is often difficult to distinguish thinner beds.

In order to decide if a power law or a lognormal distribution best characterises the bed thickness population, a single graph is constructed with log-thickness on the x-axis, and two variables on the y-axis: Y1, the number of beds thicker than T ( $N>T$ ) using a log scale; and Y2, the cumulative percent of the number of beds thinner than T using a probability scale (e.g., Figure 6.3). The number of measurements is large (about 27,000) and data reduction was applied in order to produce clear and meaningful plots. This data reduction was applied only when producing the graphs. All results and statistical parameters for different facies were done before the data reduction (Tables B3 and B4).

The scaling parameter is calculated by measuring the slope of the lines on the  $N>T$  versus T. These lines are best fit lines that are usually drawn by hand. Drawing best fit lines for the thinner beds on the  $N>T$  versus T were done on expanded scales (not presented in the thesis), to calculate the  $\beta$  values for these linear trends because many of these plots do not show straight line segments but a curve instead. As indicated above, this

is because of the nature of the log scale. Figure B2 is for the subset of facies Class E that represents the mud caps of megaturbidites.

## **B2. BED THICKNESS DISTRIBUTION FOR SILTSTONE SUBFACIES**

Each subfacies of the graded stratified facies (D2.1) have a different sequence of sedimentary structures, yet all are interpreted to have been deposited from turbidity currents. Each subfacies was investigated to assess whether the lognormal distribution or the power-law distribution better fits the bed thickness data. All subfacies were plotted in a single probability-log plot (Figure B3). Subfacies D2.1A, D2.1C, D2.1E and D2.1G plot with more or less the same slope. The position where the beds plot is controlled by thickness. Subfacies D2.1G and D2.1C have the largest median thickness of about 7-13 cm and formed as a result of syn- and post-depositional deformation that occurred most commonly in thicker beds that were deposited rapidly. On the other hand subfacies D2.1B and D2.1E were deposited from flows that carried smaller loads that were deposited as thin beds and laminae (e.g., isolated "starved ripples" of subfacies D2.1B).

Subfacies D2.1A has a wide range of thicknesses. Subfacies D2.1D and D2.1F do not have a consistent slope and may consist of several subpopulations. Subfacies D2.1D and D2.1E plot with a different slope than the rest, suggesting different depositional conditions (Talling, 2001). Other factors such as bottom topography or point of initiation may have contributed to the different bed thickness characteristics of the subfacies.

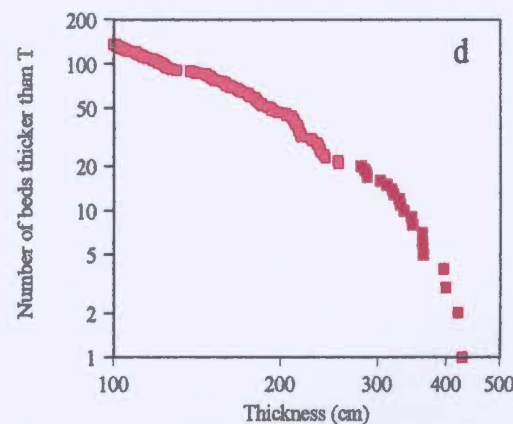
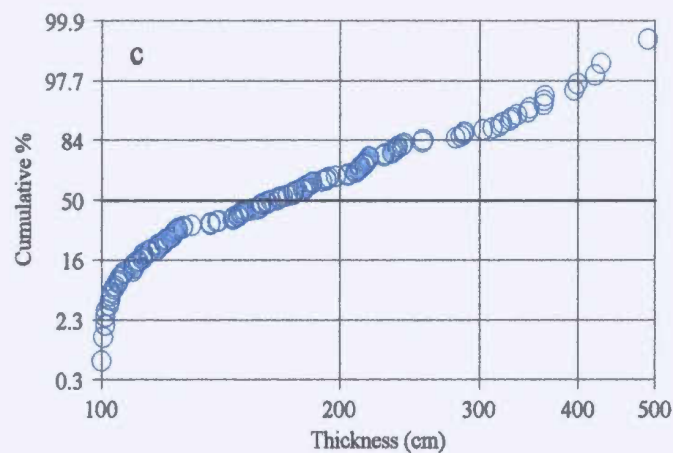
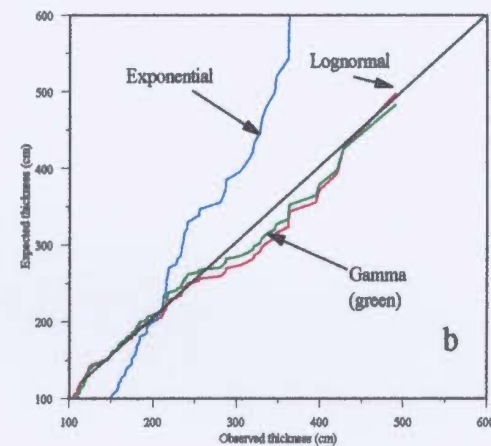
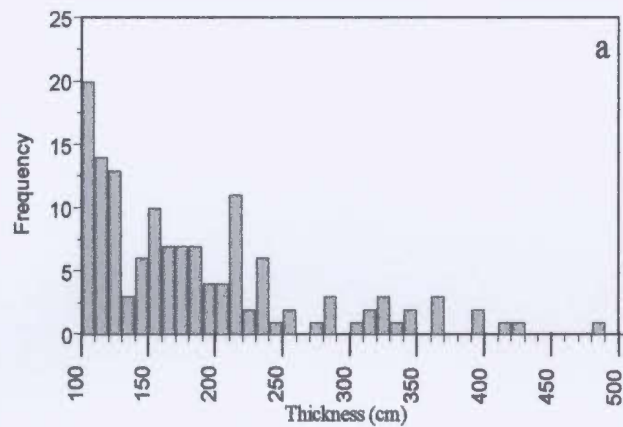


Figure B2. a- Bed thickness distribution of the 138 megaturbidite mud caps that are >100 cm thick. Note the ragged peaks and troughs. b: q-q plot of the bed thickness of the megaturbidite caps *versus* the expected thicknesses for lognormal, exponential and gamma distributions. The lognormal and gamma distributions best fit the data because they plot along the  $y=x$  line. c: Probability-log plot of the bed thickness data shows that ~80 % of these caps can be fitted by a single straight line. d:  $N>T$  versus  $T$  plot of the data shows that most of the beds can be fitted in one line. The slope of the line ( $\beta$ ) = ~2.

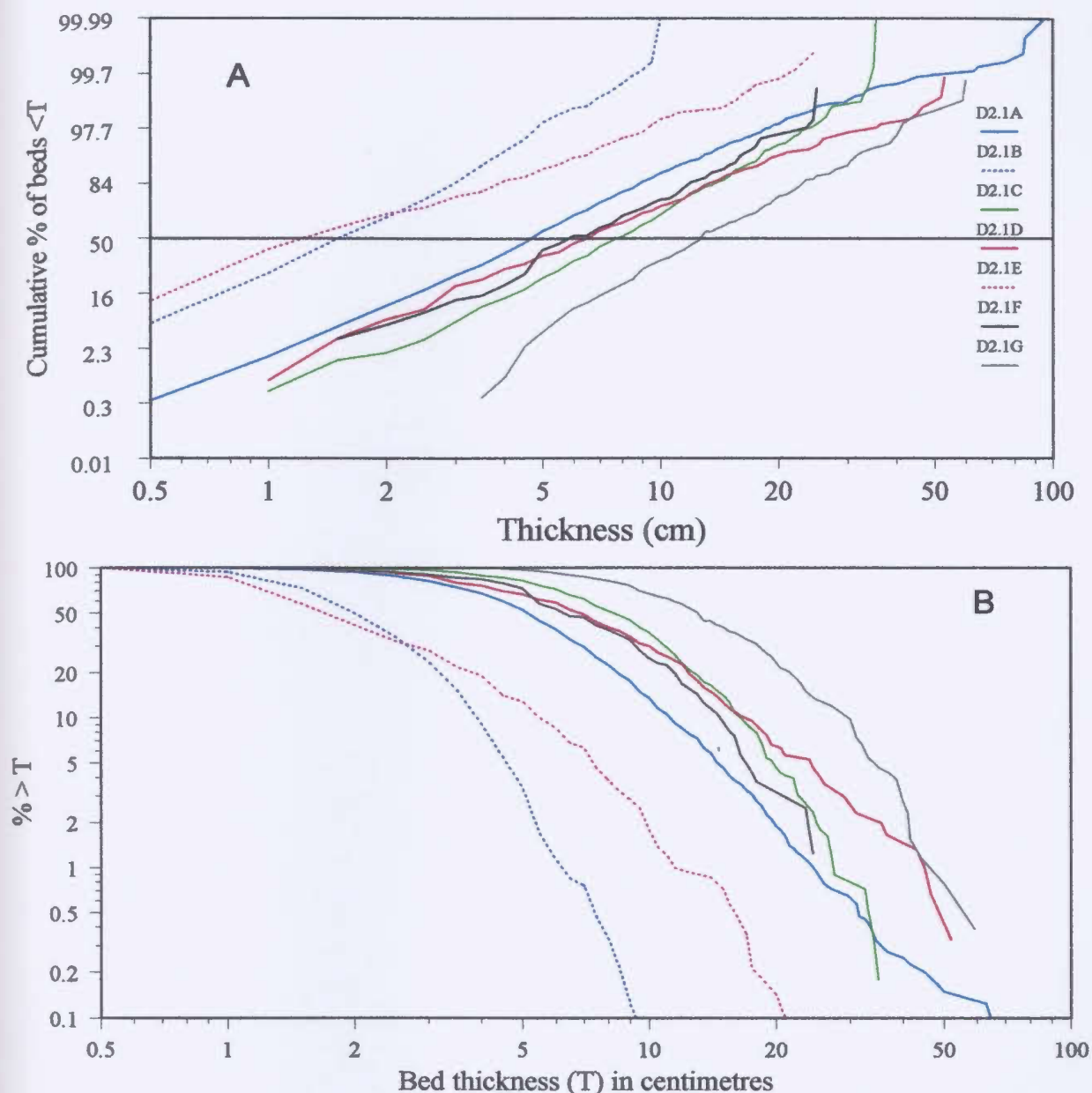


Figure B3. Comparison between the different subfacies of facies D2.1 on probability-log plot (A) and log-log plot (B). In A, subfacies D2.1B and D2.1E plot in a different part of the diagram because of their thin nature (50% < 2cm-thick) and subfacies D2.1B has a steeper slope because it only occurs as laminae, very thin and thin beds. Beds of subfacies D2.1C and D2.1G have the largest median thickness. Subfacies D2.1 D and D2.1C have inconsistent slope. B: log-log plot of %>T versus T of the subfacies, many of which do not have a well defined linear trend. It is interesting to note that plots for subfacies D2.1C and D2.1F have a similar shape. Subfacies D2.1B plots in a separate part of the graph with a different slope suggesting that beds of this subfacies formed under special conditions.

For power law scaling,  $N > T$  versus  $T$  was used to compare the subfacies (Figure B3). Some subfacies have better defined linear trends than others. For most of the subfacies, two linear trends were observed: one for the thinner beds with a  $\beta$  value of about  $1.0 \pm 0.3$ ; and one for thicker beds with a  $\beta$  of about  $2.5 \pm 0.3$ . Beds 3-10 cm thick of subfacies D2.1B have a  $\beta$  of 4.2 and beds of subfacies D2.1F that are 1.5-5 cm thick have only one linear trend ( $\beta = 0.3$ ). The  $\beta$  values presented here and in Table B3 were calculated from expanded plots of  $N > T$  versus  $T$ .

### **B3. BED THICKNESS DISTRIBUTION FOR SANDSTONE FACIES AND SUBFACIES**

Facies C1.1 are the only disorganised sandstone beds of group C1 (Table 3.1). These are interpreted as debris flow deposits. Only 42 beds were observed in the thesis area. On the probability-log plot, there is one more-or-less linear trend (Figure B4). On the  $N > T$  versus  $T$  plot, a  $\beta$  value of about 1.7 is obtained for beds that are 8-25 cm thick (33 beds). The  $\beta$  for beds 8-25 cm thick is within the range of  $\beta$  values for other sandstone beds of Class C interpreted as turbidites, but is different than the value of 0.49 obtained by Rothman and Grotzinger (1995). Their small  $\beta$  value indicate a wider range of deposit thickness. However, Rothman and Grotzinger (1995) only studied 24 beds. Larger datasets of debrite bed thickness should be tested before any conclusion can be made about what are representative scaling parameters for these types of deposits.



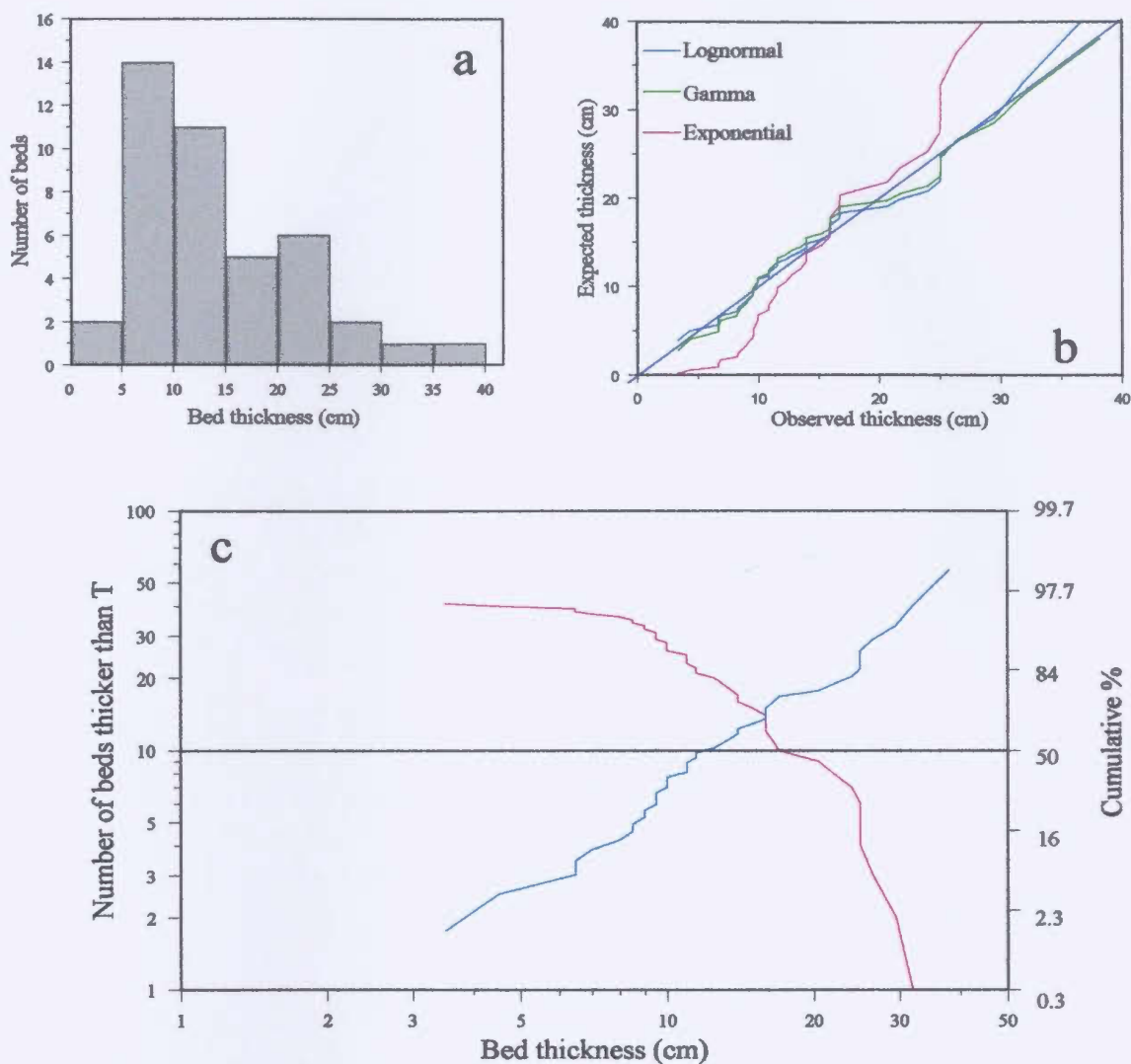


Figure B4. Muddy sandstone beds of facies C1.1. a: Histograms suggest a lognormal distribution while the q-q plot (b) suggests either a lognormal or a gamma population. On the probability-log plot, one more-or-less linear trend could be seen. On the log-log plot, beds 8-25 cm thick follow a linear trend.

Factors other than flow rheology might control the  $\beta$ .

Organised sandstones group C2 are more common than disorganised sandstone beds. Eighteen hundred (1800) beds were measured from the different sections in the thesis area. These beds have a variety of internal sedimentary structures, grading, and amount of clasts. They are interpreted as turbidites deposited from high to low concentration flows. Most of the beds of facies C2.1 are structureless or have a lower structureless division (Bouma  $T_a$  division). Some beds contain clasts, some show well developed normal grading, while others are massive. Facies C2.2 and C2.3 exhibit laminations ( $T_b$ ,  $T_{bc}$ ,  $T_{cd}$ ) and are interpreted as classical turbidites. Facies C2.4 and C2.5 are megaturbidites formed by deposition of unusually large flows. All Class C facies are tested below to see if the different facies or subfacies follow different statistical distributions or are characterised by different distribution parameters or scaling values.

Facies C2.1 is the most common facies of this group. Beds of facies C2.1 tend to occur in packets. Of the more than 939 beds measured, 40% (385 beds) occur in amalgamated units. Approximately 50% of the 557 non-amalgamated beds contain shale clasts and/or are ungraded. Only 89 beds have Bouma  $T_{ab}$ ,  $T_{ac}$  and  $T_{abc}$  divisions (Table 3.2).

Beds of Facies C2.1 follow a lognormal distribution more clearly than the gamma and exponential distributions (Figure B5a,b). On the probability-log plot (Figure B5c), a lognormal population is also suggested by the linear trend. Deviation from a single linear trend is interpreted to be due to amalgamation. This is more apparent for the thin beds



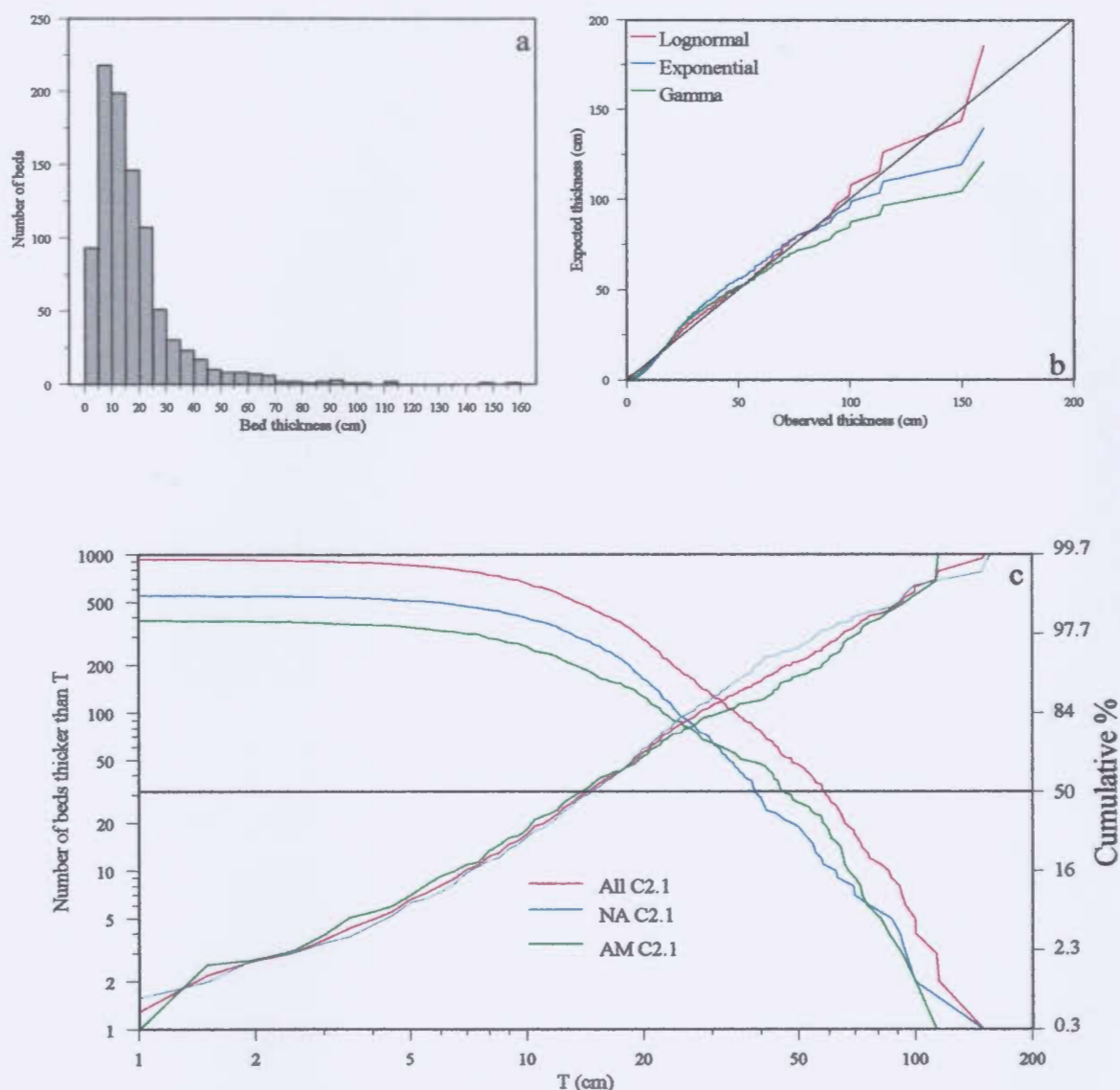


Figure B5. Beds of facies C2.1 follow a lognormal distribution (a,b). In c, a lognormal population is suggested by the linear trend of the plot of the bed thickness, although there are deviations from a single lognormal population. On the log-log plot, all datasets plot as a line with two straight segments representing 70-80% of the beds. Note the cross-over between AM C2.1 beds and NA C2.1 beds.

where the slope of the linear trend becomes gentler. The decrease in slope suggests an increase in the range of bed thicknesses relative to a single lognormal population. A best-fit line to a single lognormally distributed population would intersect the y-axis at a cumulative percentage value  $< 0.1\%$ . Instead, the linear trend with the gentler slope intersects the y-axis at  $\sim 2\%$  (i.e., beds that are at least 1 cm thick represent about 2% of the population). These small variations are emphasised because the tails of the distribution are expanded by the probability scale. The increase in the number of beds that are 1-5 cm thick may suggest that these beds form a separate population of sandstone beds formed under conditions different from the rest of the beds. Eighty seven beds of facies C2.1 are  $< 5$  cm. Closer inspection shows that almost 50% of these beds occur in amalgamated units while the remaining 50% are spatially restricted to specific parts of the sequence or in certain sections. For thick beds, amalgamation seems to be the main cause for the departure from a lognormal distribution. The departure is most obvious for beds that range in thickness from 30-70 cm (115 beds). About 50% of these 115 beds occur in amalgamated units.

On the log-log plot of  $N>T$  versus  $T$ , datasets have more than one linear segment. Two segments, one for the thinner beds and one for the thicker beds, account for 75-80% of the beds (Table B3). The power-law exponents ( $\beta$ ) for all C2.1 beds and beds that do not occur in amalgamated units are similar for each of the two segments ( $\beta = 1.0 \pm 0.2$  for thinner beds and  $\beta = 2.2 \pm 0.1$  for thicker beds). Beds thicker than 40 cm that occur in amalgamated units have a  $\beta$  value of 3.2. These thicker beds represent 12% of the beds in

amalgamated units. The linear trends for non-amalgamated and amalgamated beds intersect twice, at bed thicknesses of 30 cm and 70 cm. In this thickness range, there are more beds in amalgamated units than in non-amalgamated intervals. Beds 30-70 cm thick tend to occur more often in proximal sections PCDR, PRM1 and PRM2 and FP2, where amalgamated units abound.

Subfacies C2.1A consists of 838 structureless sandstone beds that may be massive or show poor to well developed normal grading. Half of the beds have mud clasts.

Beds of subfacies C2.1A that do not occur in amalgamated units were investigated to see if the beds with shale clasts have a different  $\beta$  values to those that lack clasts. Both beds with clasts and beds without clasts have plot as segmented lines (Figure B6d). The presence or lack of shale clasts does not significantly change the values of  $\beta$ . Beds 8-16 cm thick representing 28-38% of the population have a  $\beta$  of 1.1 to 1.2. Most of the beds thicker than 18 cm, representing about 40% of the population, have a  $\beta$  of 2.3 to -2.6.

There is a kink in the plot for beds >40 cm thick that is due to the presence of more beds with clasts that are ~60 cm thick compared with beds without clasts. Of the 20 beds that are thicker than 40 cm, 13 contain clasts. On a probability-log plot, beds with clasts plot as a segmented line (Figure B6c) and the variation in the slope of this line is due to the presence of thick beds with shale clasts that perhaps constitute a separate population. Most of these thick beds occur in the upper part of the sequence suggesting that temporal changes during the deposition of the sequence may have had a control on the deposition of thick beds with clasts.

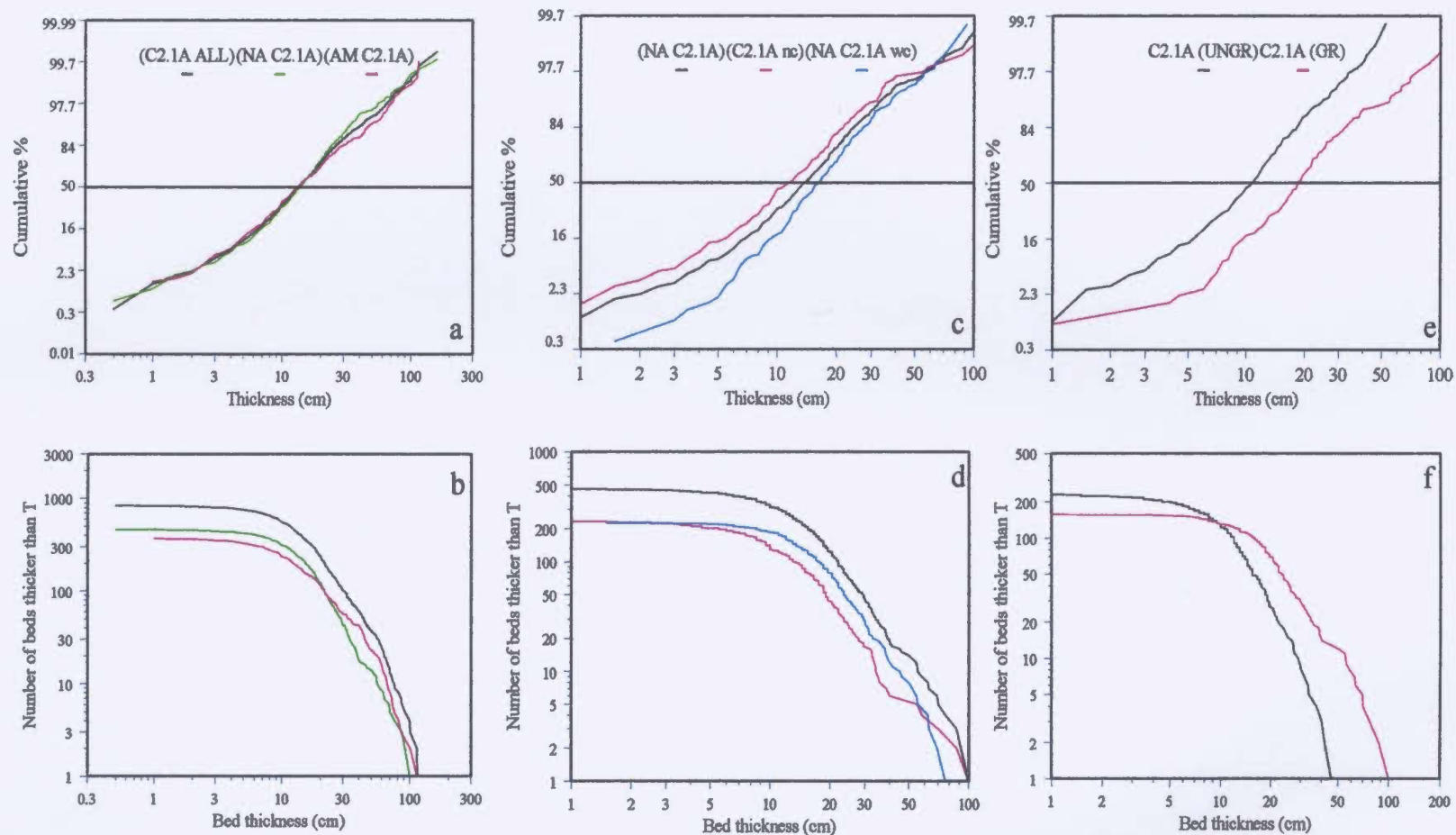


Figure B6. Comparison of beds of subfacies C2.1A that exhibit different characteristics. a,b: beds that occur in amalgamated units AM C2.1A and beds that occur in non- amalgamated units (NA C2.1A) plot more-or-less in the same place in the graph or have similar shape dealt with in the text.. c,d: beds with clasts (C2.1A wc) and beds without clasts (C2.1A nc) have similar slopes, but plot in different parts of the graph because beds with clasts are usually thicker. The cross over of the two lines is due to the presence of more beds that are > 60 cm thick and contain clasts. e,f: beds that are graded ( C2.1 GR) tend to be thicker and less abundant than ungraded beds (C2.1A UNGR).

Ungraded and graded beds of subfacies C2.1A were compared (Figure B6e,f). The  $\beta$  for both datasets is  $2.4 \pm 0.3$  for the beds 14–45 cm thick  $\sim 0.4 \pm 0.1$  for beds < 14 cm thick. The proportions represented in each segment are different, indicating that grading is better developed in thick beds (Table B3).

Other subfacies of facies C2.1 are beds that start with a structureless division followed by a division(s) that contain laminations ( $T_{ac}$ ,  $T_{ab}$ ,  $T_{abc}$ ). Only 100 such beds were observed, 11 of which occur in amalgamated units. Non-amalgamated beds of subfacies C2.1B, C2.1C and C2.1D were combined in a single dataset that consists of 89 beds and tested. The lognormal distribution best fits the bed thickness population of these subfacies (Figure B7). On the probability-log plot, the beds have three lognormal trends, one for beds 3–8 cm thick (22% of the beds), the second for beds 8–18 cm (25%) and the third for beds > 18 cm thick (53%). On the  $N>T$  versus  $T$  plot, two straight-line segments occur. One for beds less than  $\sim 18$  cm thick and has  $\beta = 0.44$ ; the other segment is for beds >  $\sim 18$  cm thick with a  $\beta = 2.4$ . The segmentation, at least for the thicker beds, is due to the presence of a high proportion (31 of 39 beds, or  $\sim 80\%$ ) of beds of subfacies C2.1B. Beds of subfacies C2.1C and C2.1D form thinner subpopulations.

Facies C2.2 consists of beds that are parallel laminated (subfacies C2.2A) or have a parallel laminated division in their lower part (subfacies C2.2B, C2.2C). Only 78 beds, 7 of which are amalgamated, were observed and are interpreted to have been deposited from waning turbidity currents. The lognormal distribution best fits the bed thickness data (Figure B8). There is a clear kink in the log-log and probability-log plots at a thickness of

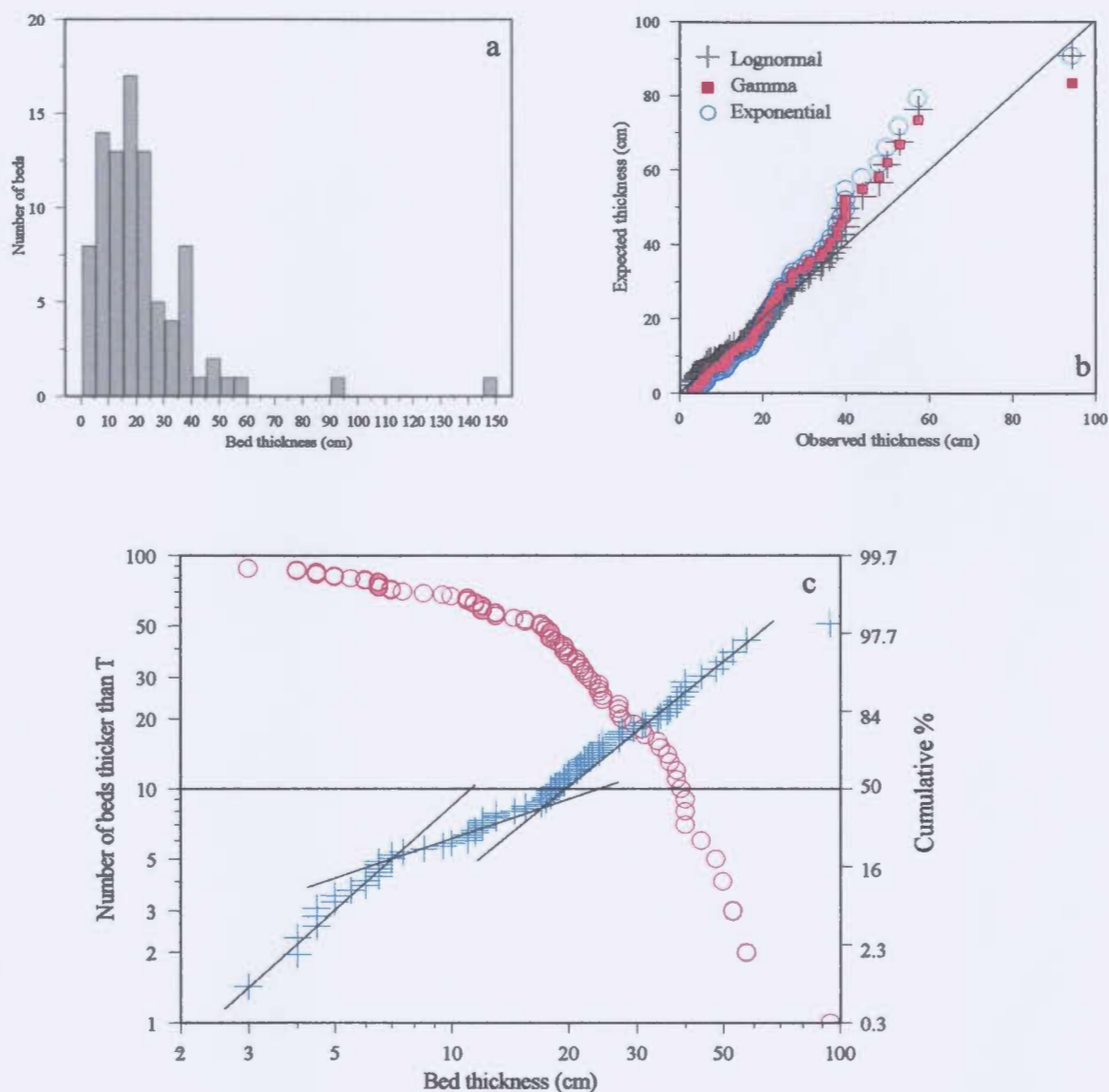


Figure B7. Subfacies C2.1B, C2.1C and C2.1D. The lognormal distribution best fits the data. c: Probability-log and log-log plot suggest three subpopulations, one for beds that are < 8 cm thick, one for beds 8- 20 cm thick and a third for beds that are >20 cm thick. Most of the thick beds belong to subfacies C2.1B.

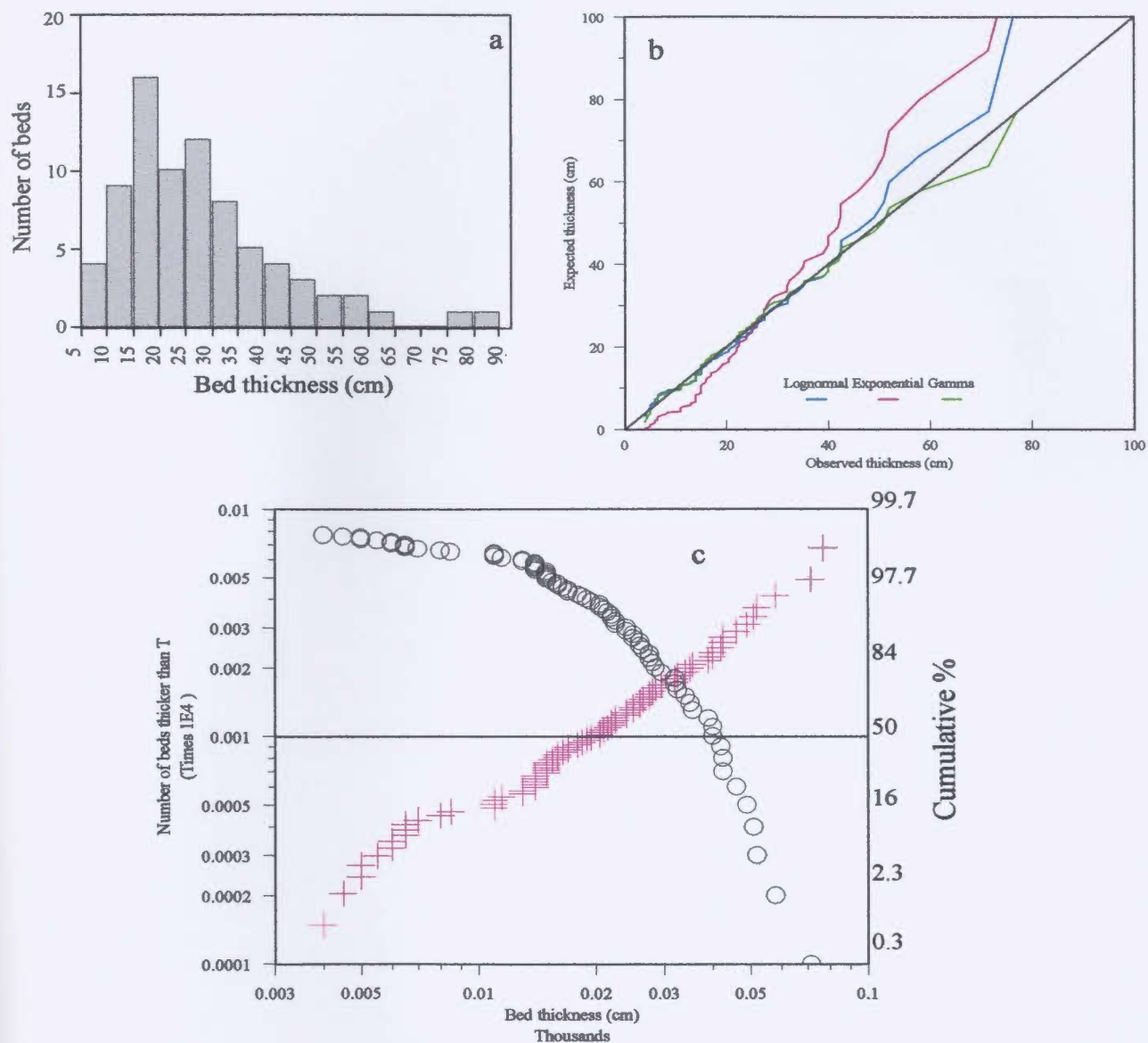


Figure B8. Facies C2.2. The lognormal distribution best fits the data (a,b). On the probability-log plot and the log-log plot, two populations are present, one for beds < 13 cm thick and the other for beds > 13 cm thick.

~13 cm. Eighteen beds are < 13 cm thick, four of which occur in amalgamated units and five of which belong to subfacies C2.2A. The remaining 65 beds are thicker than 13 cm and show a linear trend on the probability-log plot suggesting a lognormally distributed population. However, they do not have a well defined linear trend on the  $N>T$  versus  $T$  plot. The  $\beta$  for beds that are < 13 cm thick and those that are > 13 cm thick are presented in Table B3.

It is interpreted that the segmentation of the power-law plot, at least for the thinner beds is controlled by the facies type and degree of amalgamation. Beds of subfacies C2.2A display only parallel lamination suggesting steady flow during deposition. For beds thicker than 13 cm, no well defined linear trend argues against a power-law distribution.

Facies C2.3 is more common than facies C2.2. Thirty-five of the 386 beds occur in amalgamated units. The gamma distribution best fits the data for the thicker beds but thinner beds are better fitted by the lognormal distribution (Figure B9a,b). The gamma distribution is a better fit for the thicker beds but thinner beds are better fitted with the lognormal distribution. The probability-log plot shows three linear trends with slightly different slopes (Figure B9c): beds 1- 13 cm thick (51% of the beds), beds 13-20 cm-thick (19% of the beds), and beds > 20 cm thick (29% of the beds). This segmentation is less apparent for the  $N>T$  versus  $T$ . The relative proportion of each of the subfacies may account for this segmentation. Subfacies C2.3A forms most of the beds < 20 cm thick but less than 30% of beds that are thicker than 20 cm. All these subfacies occur in all of the



sections, but changing proportions may stem from sedimentological factors related to size of the flows and sediment concentration in these flows.

Megaturbidites (facies C2.4 and C2.5) are common and very distinctive in the thesis area (379 beds of facies C2.4 and 18 of facies C2.5). The lognormal distribution best fits the data (Figure B10). On the probability-log plot several linear trends are observed, each suggesting a separate lognormal subpopulation. These subpopulations are also apparent on the log-log plot as different near linear segments. These subpopulations might reflect the size of the flow from which the megaturbidites were deposited. Spatial factors such as bottom topography might also have influenced the thickness of these megaturbidites.

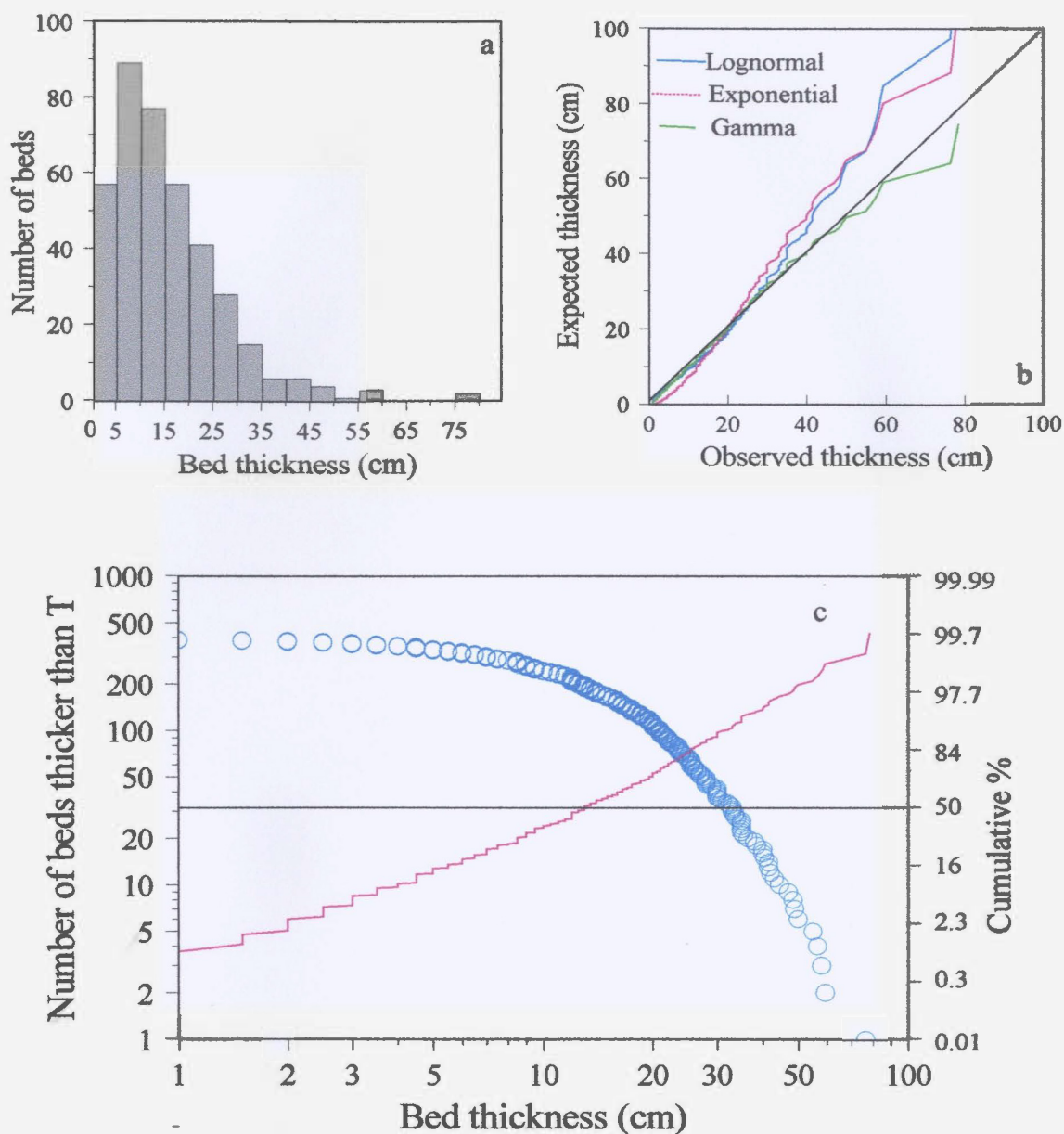


Figure B9. Facies C2.3. The gamma distributions best fit the data (a,b). The gamma distribution is a better fit for the thicker beds while the lognormal distribution is a better fit for the thinner beds. Linear trends stand out better on the probability-log plot than on the log-log plot. The linear trends reflect 3 subpopulations that are controlled by the proportions of subfacies.

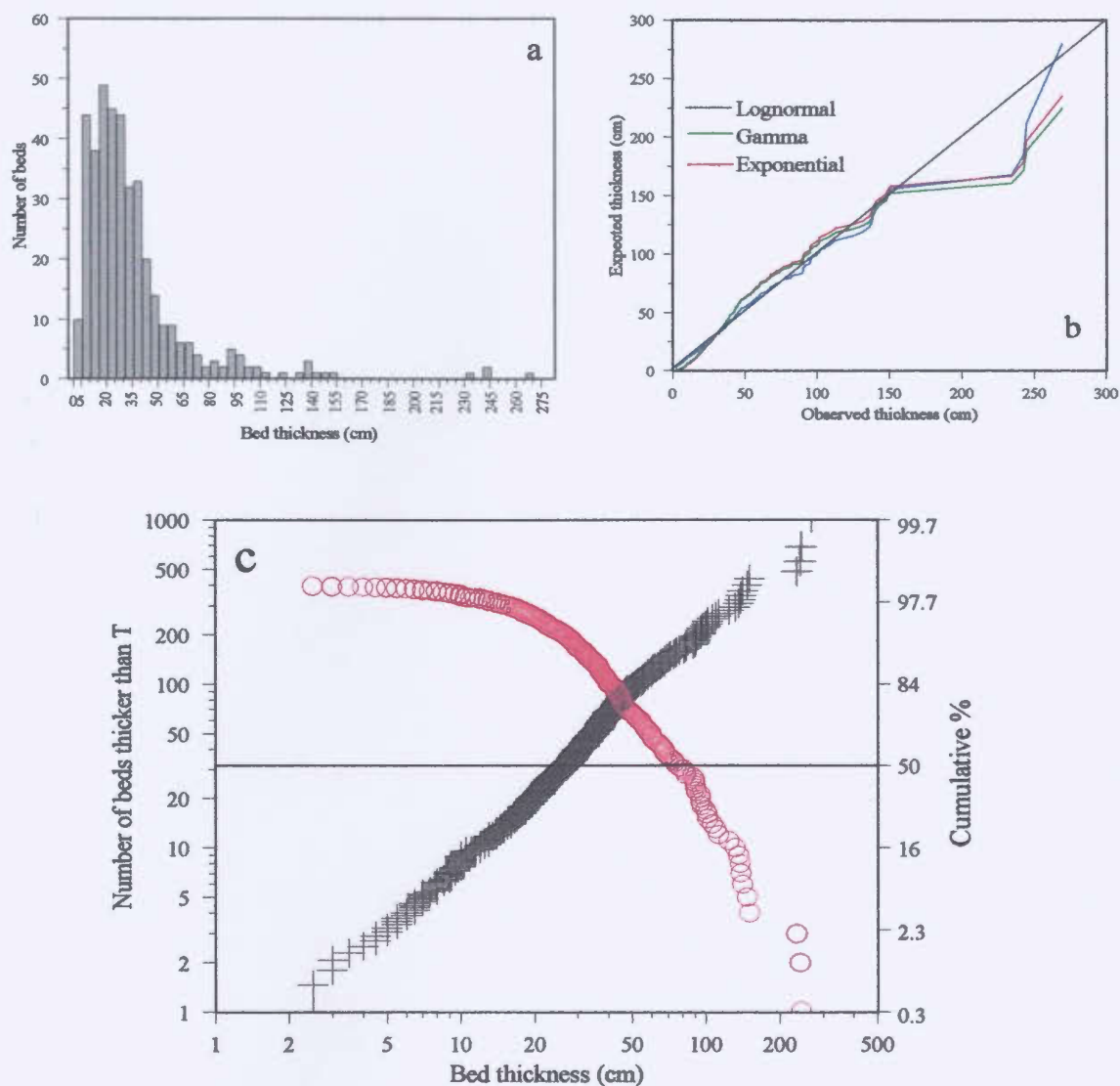


Figure B10. Megaturbidites of facies C2.4 and C2.5. The lognormal distribution best fits the data (a,b). There are several linear trends observed on both the probability-log plot and the log-log plot. These subpopulations reflect the size of the flows and various spatial and temporal factors that controlled the deposition of the megaturbidites.

Table B1. The probability density functions (pdf) and their parameters for the four distributions considered in the text. For the gamma distribution, if the shape parameter is an integer, then the gamma distribution is the Erlang distribution and if the shape parameter is equal to 1, then the gamma distribution is the exponential distribution.

Population	Probability density function (pdf)	Parameters
Lognormal	$f(x) = \frac{1}{x\sigma\sqrt{2\pi}} \times e^{-\frac{(\log x - \mu)^2}{2\sigma^2}}$	Scale = $\mu$ = mean log x, Shape ( $\sigma > 0$ ) = Standard deviation of log x.
Exponential	$f(x) = \frac{e^{(-x/b)}}{b}$ $f(x) = \lambda e^{(-\lambda x)}$	Scale = $b$ , the mean. or $\lambda = 1/b$ , ( $b > 0$ ). $\lambda$ is the hazard function.
Gamma	$f(x) = \frac{(x/b)^{c-1} e^{(-x/b)}}{b\Gamma(c)}$ $f(x) = \frac{e^{-\lambda x} (\lambda x)^{c-1} \lambda}{\Gamma(c)}$	Scale = $b = s^2/\bar{x}^2$ , $b > 0$ . Shape = $c = \bar{x}^2/s^2$ , $c > 0$ . $s^2$ = variance of x, $\bar{x}$ = mean of x $x$ = values. $\lambda = 1/b$ $\Gamma$ is the gamma function $(\Gamma(c) = \int_0^{\infty} e^{-u} u^{c-1} du)$ .

	Mean (cm)	Std (cm)	Minimum (cm)	Maximum (cm)	Tot. Tk (m)	1	5	10	15	20	25	30
<b>CLASS E</b>	14.8	25.4	0.5	510.0	1992.2	0.5	1.5	3.0	3.5	4.0	5.0	5.0
<b>CAPS</b>	102.0	82.9	13.0	490.0	384.5	15.4	24.9	29.9	35.7	40.0	45.3	48.0
<b>CLASS D</b>	4.1	5.2	0.5	95.0	487.6	0.5	0.5	0.5	1.0	1.0	1.0	1.0
D2.1	5.0	5.4	0.5	95.0	457.1	0.5	1.0	1.0	1.5	1.5	2.0	2.0
D2.2	5.6	4.8	0.5	25.0	11.3	0.5	0.5	1.0	1.0	1.0	1.5	2.0
D2.3	0.7	0.5	0.5	3.0	18.5	0.5	0.5	0.5	0.5	0.5	0.5	0.5
D2.1A	6.1	5.3	0.5	95.0	243.7	1.0	1.5	2.0	2.5	3.0	3.0	3.0
D2.1B	2.1	1.2	0.5	10.0	49.2	0.5	0.5	1.0	1.0	1.0	1.0	1.0
D2.1C	9.3	5.5	1.0	35.5	51.6	1.5	3.0	3.5	4.5	5.0	5.5	6.0
D2.1D	8.8	7.9	1.0	53.0	26.6	1.5	2.0	2.5	3.0	3.3	4.0	4.0
D2.1E	2.4	2.5	0.5	24.5	33.6	0.5	0.5	0.5	1.0	1.0	1.0	1.0
D2.1F	7.7	4.9	1.5	25.0	12.5	1.5	2.0	3.0	3.5	4.0	4.5	5.0
D2.1G	15.5	9.6	3.5	60.0	39.8	4.3	5.5	6.0	7.0	8.0	9.0	9.0
<b>CLASS C</b>	21.7	22.1	0.5	270.0	400.6	1.5	4.0	5.5	7.0	8.5	9.5	10.0
NA C	22.5	23.2	0.5	270.0	318.1	1.5	4.0	6.0	7.0	8.5	10.0	11.0
AM C	19.0	17.7	1.0	115.0	82.1	1.0	3.0	5.0	5.9	7.0	8.0	9.0
GRP C1	14.7	7.9	3.5	38.0	6.2	3.5	4.8	6.7	8.2	8.8	9.4	9.0
GRP C2	21.8	22.3	0.5	270.0	394.5	1.5	4.0	5.5	7.0	8.5	9.5	10.0
NA GRP C2	22.7	23.4	0.5	270.0	312.7	1.5	4.0	6.0	7.0	8.5	10.0	11.0
AM GRP C2	19.2	17.8	1.0	115.0	81.8	1.0	3.0	5.0	6.0	7.0	8.0	9.0
C2 1	19.5	16.5	0.5	160.0	173.8	1.2	3.5	5.5	6.5	7.5	8.5	10.0
NA C2 1	17.8	15.4	0.5	160.0	98.8	1.5	4.0	5.5	6.5	8.0	9.0	10.0
AM C2 1	19.5	17.9	1.0	115.0	75.0	1.0	3.0	5.0	6.0	7.5	8.5	9.0
C2.1A	17.0	14.2	0.5	160.0	79.1	1.3	3.5	5.5	7.0	8.5	9.0	10.0
C2.1A NC	14.9	15.4	0.5	160.0	35.5	0.7	2.5	4.0	5.4	6.5	7.5	8.0
C2.1A WC	19.2	12.6	1.5	91.5	43.6	3.1	6.5	7.9	9.0	11.0	11.5	12.0
C2.1A UN	12.2	7.9	1.0	52.0	28.2	1.2	2.5	4.0	5.5	6.0	7.0	7.0
C2.1A PG	18.8	11.5	0.5	91.5	14.3	0.5	5.8	9.4	9.8	11.2	13.0	14.0
C2.1A GR	23.2	19.2	0.5	160.0	36.6	2.6	7.0	8.5	9.5	11.5	13.0	14.0
C2.1BCD	22.1	20.2	3.0	150.0	19.7	3.0	4.5	5.5	6.5	7.0	10.5	11.0
C2.2	23.2	15.2	4.0	77.0	18.1	4.0	5.0	6.5	7.9	11.0	13.8	14.0
NA C2.2	24.3	15.3	4.5	77.0	17.2	4.5	5.8	6.6	10.5	13.4	14.0	15.0
C2.3	15.9	11.7	1.0	78.5	61.3	1.4	3.0	4.5	5.5	6.5	7.5	8.0
NA C2.3	15.8	11.0	1.0	76.5	55.4	1.3	3.0	4.1	5.5	7.0	8.0	9.0
C2.4	33.2	26.5	2.5	151.0	125.6	3.0	7.0	9.5	10.5	13.4	16.0	18.0
C2.5	78.0	95.5	4.5	270.0	14.0	4.5	4.5	6.8	13.0	17.2	18.8	19.0
<b>CLASS B</b>	22.6	20.0	2.0	165.0	58.7	3.2	7.0	8.5	10.0	11.0	12.0	13.0
GRP B1	41.1	29.4	10.5	85.0	2.5	10.5	10.5	10.5	10.9	13.5	16.1	19.0
B2.1A	38.5	32.9	2.0	166.0	22.0	2.0	5.7	10.3	14.9	17.1	18.8	19.0
GRP B2	21.3	19.2	2.0	166.0	56.2	3.2	7.0	8.5	10.0	11.0	12.0	13.0
B2 1	34.5	32.1	2.0	166.0	22.4	2.0	5.0	8.9	11.0	14.1	15.5	17.0
B2.2	16.7	9.0	3.5	102.5	34.8	3.6	7.0	8.5	9.5	11.0	11.1	12.0
NA B2.2	16.9	9.1	3.5	102.5	33.3	3.5	7.0	8.5	9.5	11.0	11.5	12.0
AM B2.2	14.0	6.6	4.5	29.0	1.5	4.5	4.5	5.1	6.9	8.3	9.5	10.0

Table B2. Statistical parameters of the facies and subfacies observed in the thesis area. The mean, standard deviation (s) and the 1, 5, 10, 15, 20, 25, 30, 40, 50, 60, 70, 75, 80, 85, 90, 95, 99 percentiles are also indicated.

Percentiles												
20	25	30	40	50	60	70	75	80	85	90	95	99
4.0	5.0	5.5	6.5	8.0	10.0	13.0	15.5	18.5	23.0	30.0	46.0	114.5
40.0	45.3	48.0	60.0	75.0	92.4	114.8	125.8	158.7	182.8	215.2	285.2	403.6
1.0	1.0	1.5	2.0	2.5	3.5	5.0	5.5	6.5	8.0	9.5	13.5	24.5
1.5	2.0	2.0	3.0	3.5	4.5	5.5	6.5	7.5	9.0	10.5	14.5	25.0
1.0	1.5	2.3	3.0	4.0	5.0	6.5	7.5	8.5	10.1	12.8	15.0	24.4
0.5	0.5	0.5	0.5	1.0	1.0	1.0	1.0	1.0	1.0	1.5	2.0	3.0
3.0	3.0	3.5	4.5	5.0	5.5	6.5	7.5	8.0	9.0	11.0	14.5	24.5
1.0	1.0	1.5	1.5	2.0	2.0	2.5	2.5	3.0	3.5	3.5	4.5	6.0
5.0	5.5	6.0	7.0	8.0	9.5	10.5	11.5	12.5	14.5	16.5	19.6	29.6
3.3	4.0	4.5	5.5	6.5	8.0	10.0	11.0	12.2	14.0	17.2	24.4	46.5
1.0	1.0	1.0	1.0	1.5	2.0	2.5	3.0	3.5	4.0	5.5	7.0	12.6
4.0	4.5	5.0	5.0	6.0	7.5	9.0	10.0	11.5	12.7	14.9	17.5	25.0
8.0	9.0	9.5	11.1	13.0	15.0	18.0	19.5	21.5	23.5	30.0	35.2	53.8
8.5	9.5	10.5	13.0	16.0	19.5	23.0	26.0	29.5	35.0	42.0	58.0	111.5
8.5	10.0	11.1	14.0	17.0	20.0	24.0	27.0	30.0	35.0	41.5	58.0	130.7
7.0	8.0	9.0	11.0	13.0	16.5	20.5	23.0	26.5	32.1	43.0	58.4	90.3
8.8	9.4	9.5	11.0	12.0	14.0	16.1	17.9	22.8	25.0	26.1	31.6	38.0
8.5	9.5	10.5	13.0	16.0	19.5	23.5	26.1	30.0	35.0	42.5	58.0	112.8
8.5	10.0	11.5	14.0	17.0	20.0	24.0	27.0	31.0	35.5	42.0	58.0	132.8
7.0	8.0	9.0	11.5	13.0	16.5	20.5	23.0	26.7	32.4	43.1	58.6	90.5
7.5	8.5	10.0	12.0	14.0	17.0	20.5	22.0	24.5	28.5	35.5	50.0	89.7
8.0	9.0	10.0	12.0	14.5	17.0	19.5	21.5	23.5	27.0	32.3	40.0	89.0
7.5	8.5	9.5	11.5	13.5	17.3	20.5	23.0	27.0	32.5	43.9	59.7	93.6
8.5	9.0	10.0	12.0	14.0	16.5	19.0	20.5	22.0	25.1	30.0	38.4	80.1
6.5	7.5	8.5	9.5	11.5	14.0	16.5	18.5	19.5	22.0	26.1	34.0	94.9
11.0	11.5	12.2	14.1	16.5	18.5	21.5	23.0	24.7	28.8	31.7	43.6	74.5
6.0	7.0	7.8	9.4	11.0	12.0	14.0	15.0	16.8	18.6	21.4	28.1	44.6
11.2	13.0	14.0	15.5	17.5	18.5	21.5	23.0	23.8	27.2	30.5	35.2	91.5
11.5	13.0	14.5	16.5	18.5	21.0	23.5	26.0	29.5	33.2	39.1	62.5	124.6
7.0	10.5	11.5	15.5	18.0	21.0	24.0	27.0	31.5	37.3	40.0	51.5	150.0
11.0	13.8	14.0	16.0	20.0	23.1	27.5	30.1	34.2	40.0	42.9	52.3	77.0
13.4	14.0	15.0	16.9	21.0	24.2	27.9	32.0	35.3	40.4	45.3	54.4	77.0
6.5	7.5	8.5	11.0	13.0	16.0	19.5	21.0	23.5	26.0	30.0	38.3	58.2
7.0	8.0	9.0	11.4	13.0	16.0	19.5	21.0	23.5	26.0	30.0	35.9	56.4
13.4	16.0	18.0	22.0	27.0	31.7	37.0	40.0	45.1	52.6	65.6	91.7	139.5
17.2	18.8	19.0	22.2	31.5	45.0	62.8	114.3	236.6	243.3	247.5	270.0	270.0
11.0	12.0	13.0	15.5	17.5	19.5	20.5	23.5	26.0	30.2	36.2	57.9	146.6
13.5	16.1	19.0	25.6	32.5	43.6	65.0	72.3	78.2	84.2	85.0	85.0	85.0
17.1	18.8	19.7	24.0	31.0	33.3	40.3	45.8	54.8	61.4	75.4	126.4	166.0
11.0	12.0	13.0	15.5	17.0	19.0	20.5	22.9	26.0	29.3	33.5	49.9	129.9
14.1	15.5	17.3	19.2	26.0	31.0	35.3	40.3	46.2	57.6	70.4	121.6	166.0
11.0	11.1	12.0	14.5	16.0	17.5	19.5	19.5	20.5	22.8	25.1	28.8	41.9
11.0	11.5	12.0	14.5	16.0	17.5	19.5	19.5	20.5	23.0	25.2	28.6	43.2
8.3	9.5	10.4	11.4	14.0	15.6	16.6	17.5	18.1	20.6	26.9	29.0	29.0

ean, standard deviation (Std(, minimum and maximum are in centimetres. The total thickness is in metres.

l.

Table B3. Power-law scaling parameter ( $\beta$ ) values for all facies classes (e.g., CLASS E), facies groups (e.g., C2), facies (e.g., C.2.3) and subfacies (e.g., *D2.1A*; *C2.1* shown in italics). The  $\beta$  value for subsets of certain facies classes, facies or subfacies was also calculated. Beds that occur in amalgamated units are indicated by AM preceding the facies class or facies (e.g., AM Class C); NA=non-amalgamated units. For subfacies *C2.1A*: beds with no clasts are abbreviated as *C2.1A (NC)*; beds with clasts as *C2.1A(WC)*; ungraded beds *C2.1A(UNR)*; and graded beds as *C2.1A (GR)*. Some cases have two  $\beta$  values because the power-law trend is best fitted with a line with more than one segment.

Facies	$\beta_1$	Min-tk. (cm)	Max-tk.	%	$-\beta_2$	Min-tk.	Max-tk.	%
<b>Class E</b>	0.9	4	~17	77	1.6	~17	200	22
<b>Class D</b>	0.6	0.5	4	61	1.5	4	12	32
D2.1	0.3	0.5	3	40	1.3	3	12	52
D2.2	0.2	0.5	2.5	62	1.1	2.5	10.5	18
D2.3					2.7	1	3	20
<i>D2.1A</i>	1.2	3	7	53	2.6	7	50	4
<i>D2.1B</i>	1.1	1	3	70	4.2	3	10	24
<i>D2.1C</i>	0.7	4	10	52	2.8	10	23	34
<i>D2.1D</i>	1.0	4	12	54	2.2	12	40	22
<i>D2.1E</i>	1.0	1	4	68	2.3	4	10	17
<i>D2.1F</i>	0.3	1.5	5	27				
<i>D2.1G</i>	1.2	8.5	16.5	45	2.4	16.5	32	28

Table B3. Continued

Facies	$\beta 1$	Min-tk (cm)	Max-tk	%	$\beta 2$	Min-tk	Max-tk	%
<b>CLASS C</b>					2.0	20	100	37
	3.0	100	270	1.4				
NA Class C	2.0	20	100	37	3.0	100	270	1.5
AM Class C	1.3	10	50	60	3.9	50	115	7
Gp. C1	1.7	8	25	79	6.0	25	38	19
Gp. C2	0.7	8	16.1	32	1.9	16.1	147.6	49
NA Gp.C2	0.6	8	14.5	25	1.8	14.5	138.9	57
AM Gp.C2	1.2	8	40	63	3.2	40	100	13
C2.1	1.0	8	20	48	2.1	20	85.3	30
NA C2.1	0.8	8	20	51	2.3	20	100	20
AM C2.1	1.2	8	40	65	3.2	40	100	12
<i>C2.1A</i>	0.9	8	16	25	2.5	15.7	91	43
<i>C2.1A(NC)</i>	1.1	8	13.5	31	2.3	13.5	87	42
<i>C2.1A(WC)</i>	1.2	10	18	38	2.6	17.6	63	43
<i>C2.1A (UNGR)</i>	0.5	1	14	70	2.7	14	30	27
<i>C2.1A(GR)</i>	0.3	1	14	29	2.1	14	46	63
<i>C2.1B,C,D</i>	0.4	3	20	57	2.4	20	150	43



Table B3. Continued

<b>Facies</b>	<b><math>\beta 1</math></b>	<b>Min-tk</b>	<b>Max-tk</b>	<b>%</b>	<b><math>-\beta 2</math></b>	<b>Min-tk</b>	<b>Max-tk</b>	<b>%</b>
C2.2	0.2	4	13	24	1.3	13	33	58
C2.3	1	8	20	45	3.2	20	78.5	29
NA C2.3	3.3	20	57.9	285	1.0	8	20	46
C2.4	1.9	25.3	371	51	0.5	10	25.3	35
B2.2	0.9	8	16	38	4.1	16	42	8

Table B4. Distribution parameters for facies classes (e.g., CLASS E), facies groups (e.g., C2), facies (e.g., C.2.3) and subfacies (e.g., *D2.1A*; *C2.1* shown in italics). Distribution parameters for subsets of subfacies C2.1A are also shown. For these subsets, beds that occur in amalgamated units are indicated by AM preceding the facies class or facies (e.g., AM Class C) while beds that do not occur in amalgamated units are indicated by NA. For subfacies *C2.1A*: beds with no clasts are abbreviated as *C2.1A (NC)*; beds with clasts as *C2.1A(WC)*; ungraded beds *C2.1A(UGR)*, and graded beds as *C2.1A (GR)*. For the exponential and gamma distributions the scale parameter  $\lambda$  was calculated instead of  $b$ . Note that  $\lambda=1/b$ .

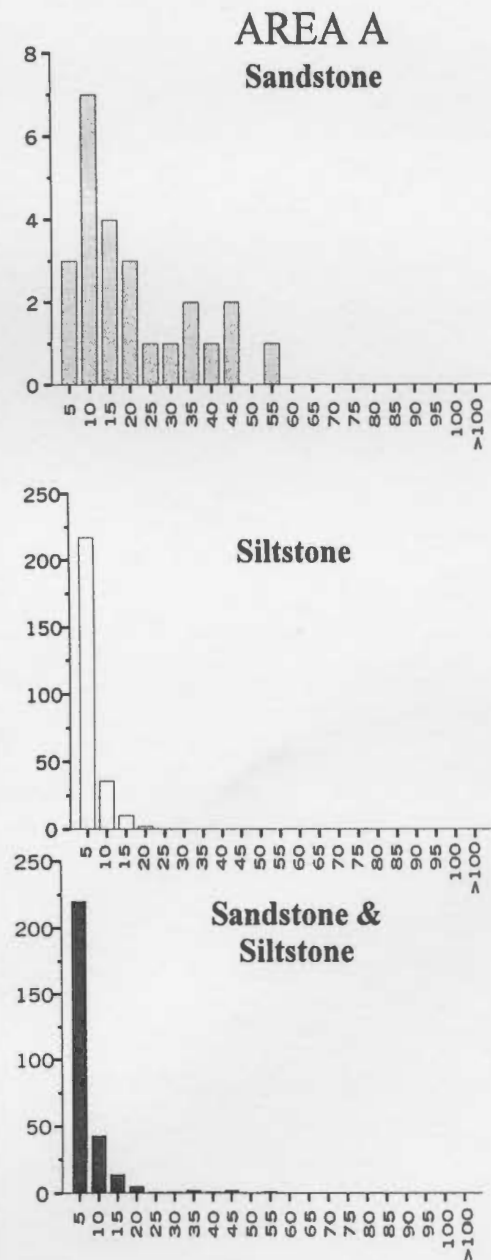
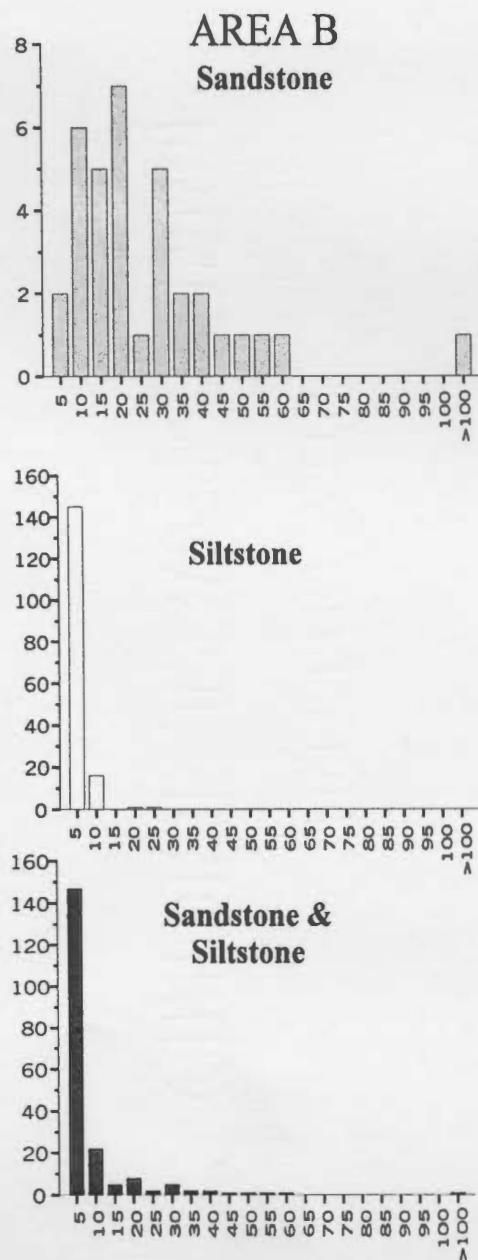
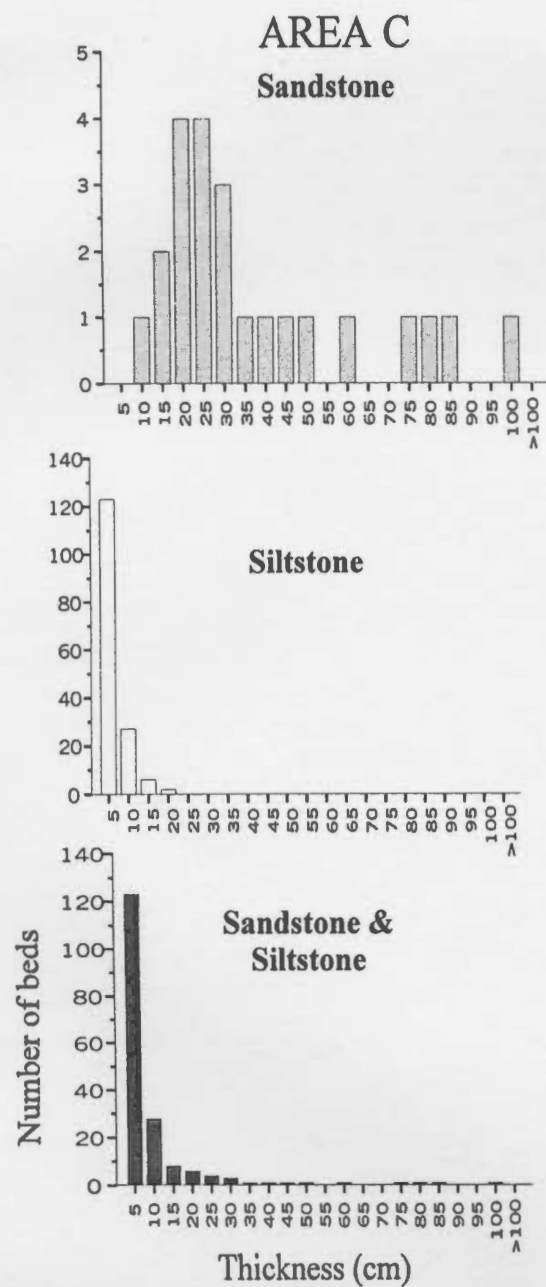
FACIES	# OF BEDS	EXPONE- NTAIL	GAMMA		LOGNORMAL	
		$\lambda$	Scale ( $\lambda$ )	Shape ( $c$ )	Scale ( $\mu$ )	Shape ( $\sigma$ )
<b>CLASS E</b>	13,479	0.07	0.02	0.34	0.93	0.44
E no Caps	13,077	0.08	0.83	0.07	0.9	0.41
Caps	402	0.01	0.01	1.51	1.9	0.32
<b>CLASS D</b>	11,248	0.25	0.15	0.62	0.42	0.43
D2.1	9,013	0.23	0.16	0.7	0.53	0.39
<i>D2.1A</i>	3,971	0.19	0.22	1.34	0.57	0.3
<i>D2.1B</i>	2,369	0.48	1.39	2.9	0.25	0.25
<i>D2.1C</i>	557	0.11	0.31	2.83	0.9	0.25
<i>D2.1D</i>	302	0.11	0.14	1.25	0.82	0.33
<i>D2.1E</i>	1395	0.42	0.39	0.93	0.23	0.35
<i>D2.1F</i>	161	0.13	0.32	2.45	0.81	0.27
<i>D2.1G</i>	257	0.06	0.17	2.61	1.11	0.25
D2.2	211	0.19	0.23	1.24	0.55	0.43
D2.3	2026	1.1	3.9	3.6	0.0	0.2

Table B4 Continued

FACIES	# OF BEDS	EXPONE..	GAMMA		LOGNORMAL	
			Scale ( $\lambda$ )	Shape( $c$ )	Scale ( $\mu$ )	Shape( $\sigma$ )
<b>CLASS C</b>	1842	0.04	0.05	0.97	1.2	0.36
NA Class C	1410	0.04	0.04	0.94	1.21	0.36
AM ClassC	431	0.05	0.06	1.16	1.13	0.37
Gp. C1	42	0.07	0.24	3.48	1.1	0.23
Gp.C2	1800	0.05	0.04	0.96	1.19	0.36
NA Gp.C2	1373	0.04	0.04	0.94	1.21	0.36
AM Gp.C2	427	0.05	0.06	1.16	1.13	0.37
C2.1	939	0.05	0.07	1.26	1.14	0.35
NA C2.1	554	0.06	0.08	1.34	1.14	0.33
AM C2.1	385	0.05	0.06	1.18	1.14	0.37
<i>C2.1A</i>	465	0.06	0.08	1.43	1.12	0.33
<i>C2.1A (NC)</i>	238	0.07	0.06	0.94	1.04	0.36
<i>C2.1A (WC)</i>	227	0.05	0.12	2.33	1.21	0.26
<i>C2.1A (UGR)</i>	231	0.08	0.19	2.35	1.00	0.30
<i>C2.1A(GR)</i>	158	0.04	0.06	1.46	1.26	0.31
<i>C2.1 BCD</i>	89	0.05	0.05	1.2	1.22	0.33
C2.2	78	0.04	0.1	2.33	1.27	0.3
C2.3	386	0.06	0.1	1.86	1.14	0.34
C2.4+C2.5	397	0.02	0.02	0.78	1.41	0.34
<b>CLASS B</b>	270	0.04	0.04	0.84	1.24	0.28
NA B2.2	197	0.06	0.21	3.45	1.18	0.19

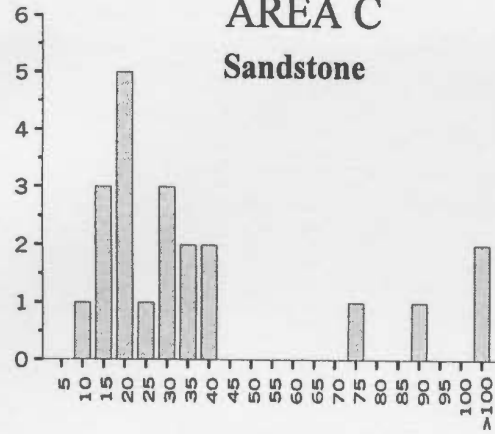
Figure B11. These are histograms for the sandstone, siltstone and a combined sandstone and siltstone beds for each some of the time-slices and sub-slices. Note that time-slice 5 is not included and part of time-slice 1 was combined with time-slice 2. The x-axis is the thickness in cm and the y-axis is the frequency.

# Time-slices 1 and 2

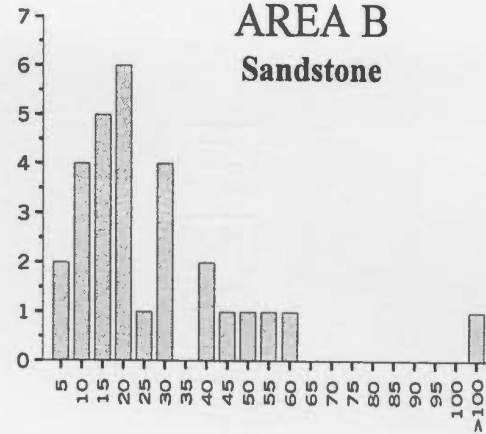


# Time-slices 3

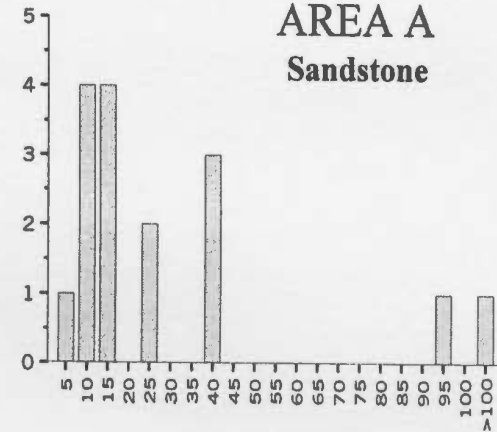
**AREA C**  
**Sandstone**



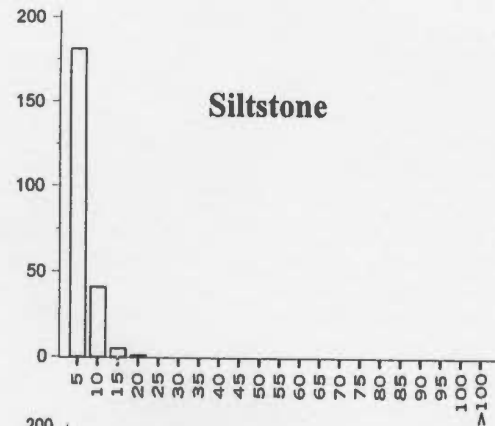
**AREA B**  
**Sandstone**



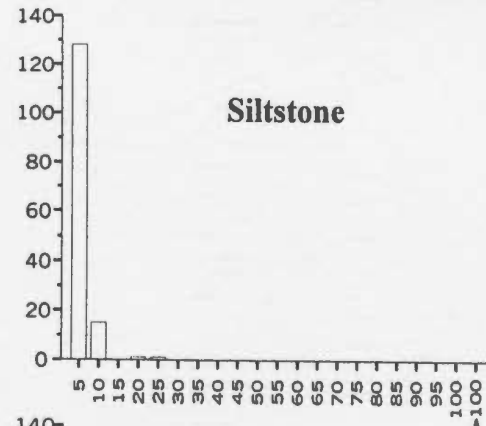
**AREA A**  
**Sandstone**



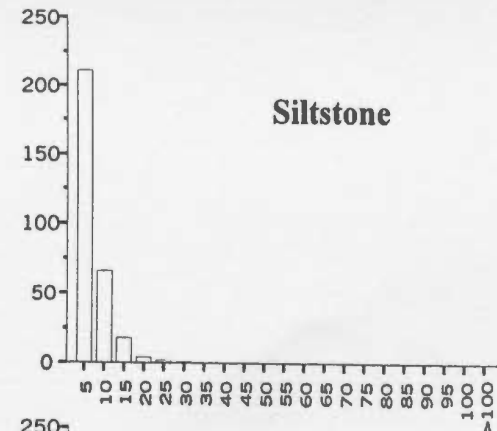
**Siltstone**



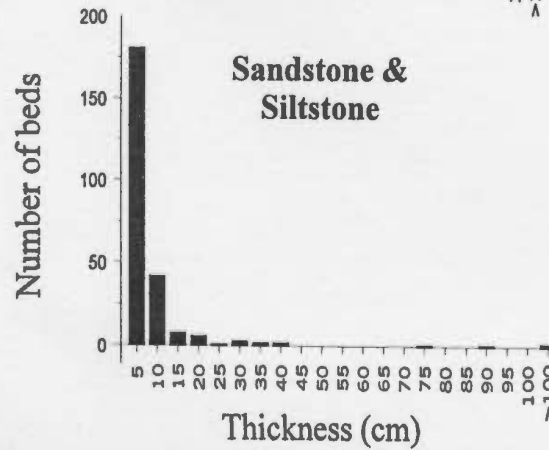
**Siltstone**



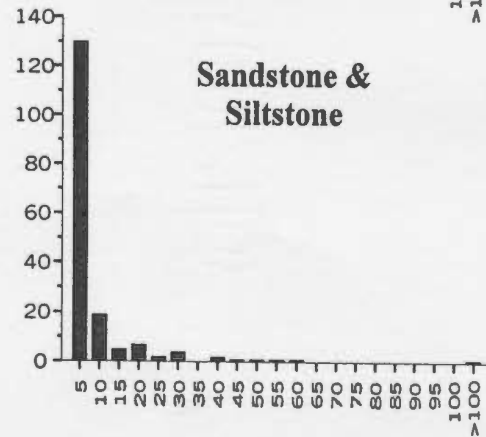
**Siltstone**



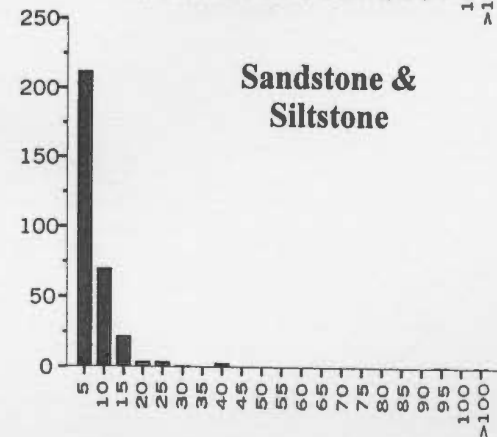
**Sandstone & Siltstone**



**Sandstone & Siltstone**

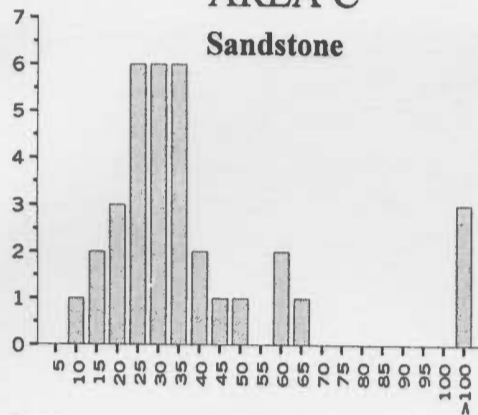


**Sandstone & Siltstone**

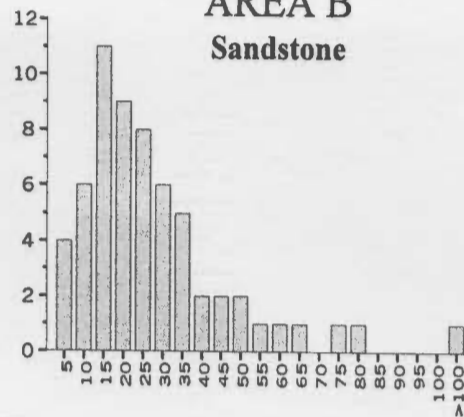


# Time-slices 4

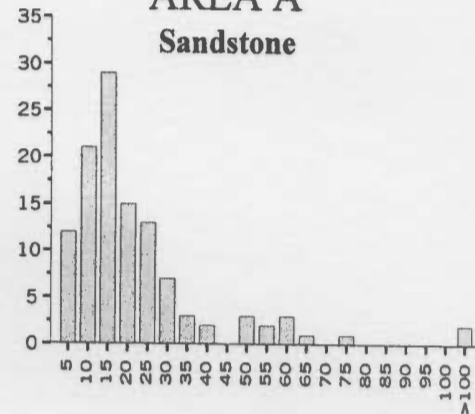
**AREA C**  
**Sandstone**



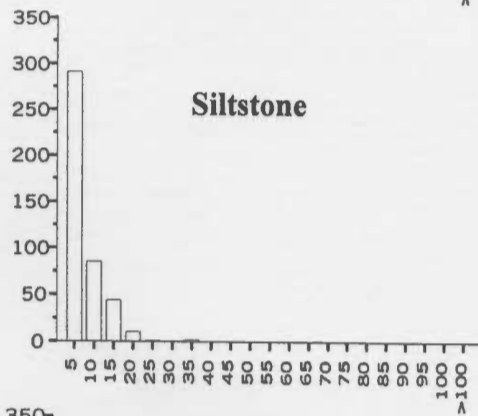
**AREA B**  
**Sandstone**



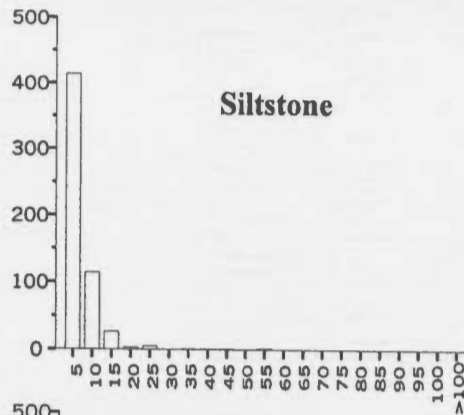
**AREA A**  
**Sandstone**



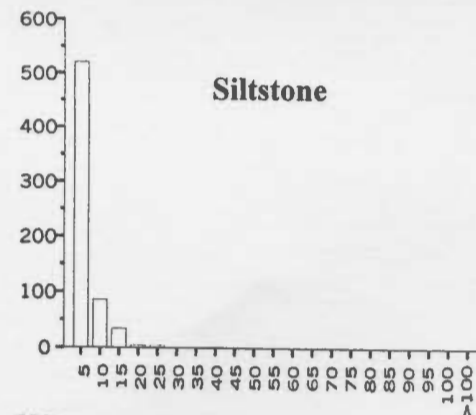
**Siltstone**



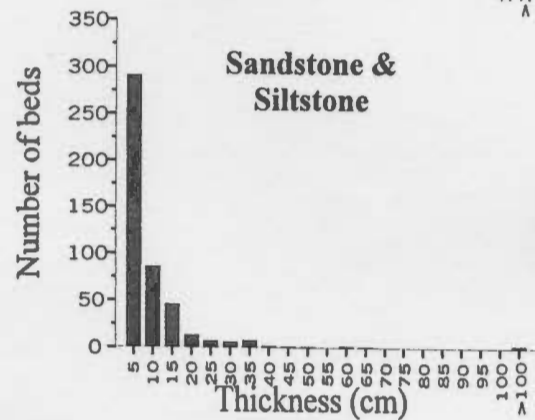
**Siltstone**



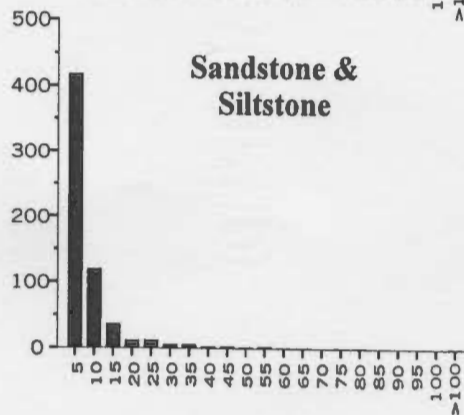
**Siltstone**



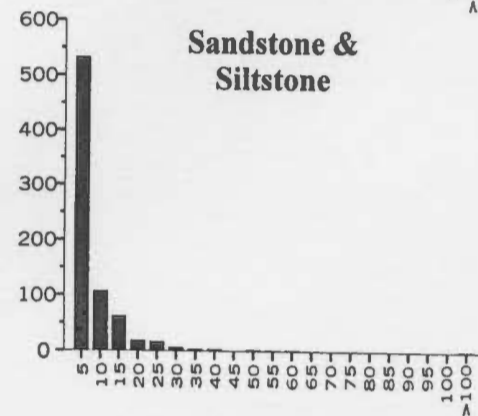
**Sandstone & Siltstone**



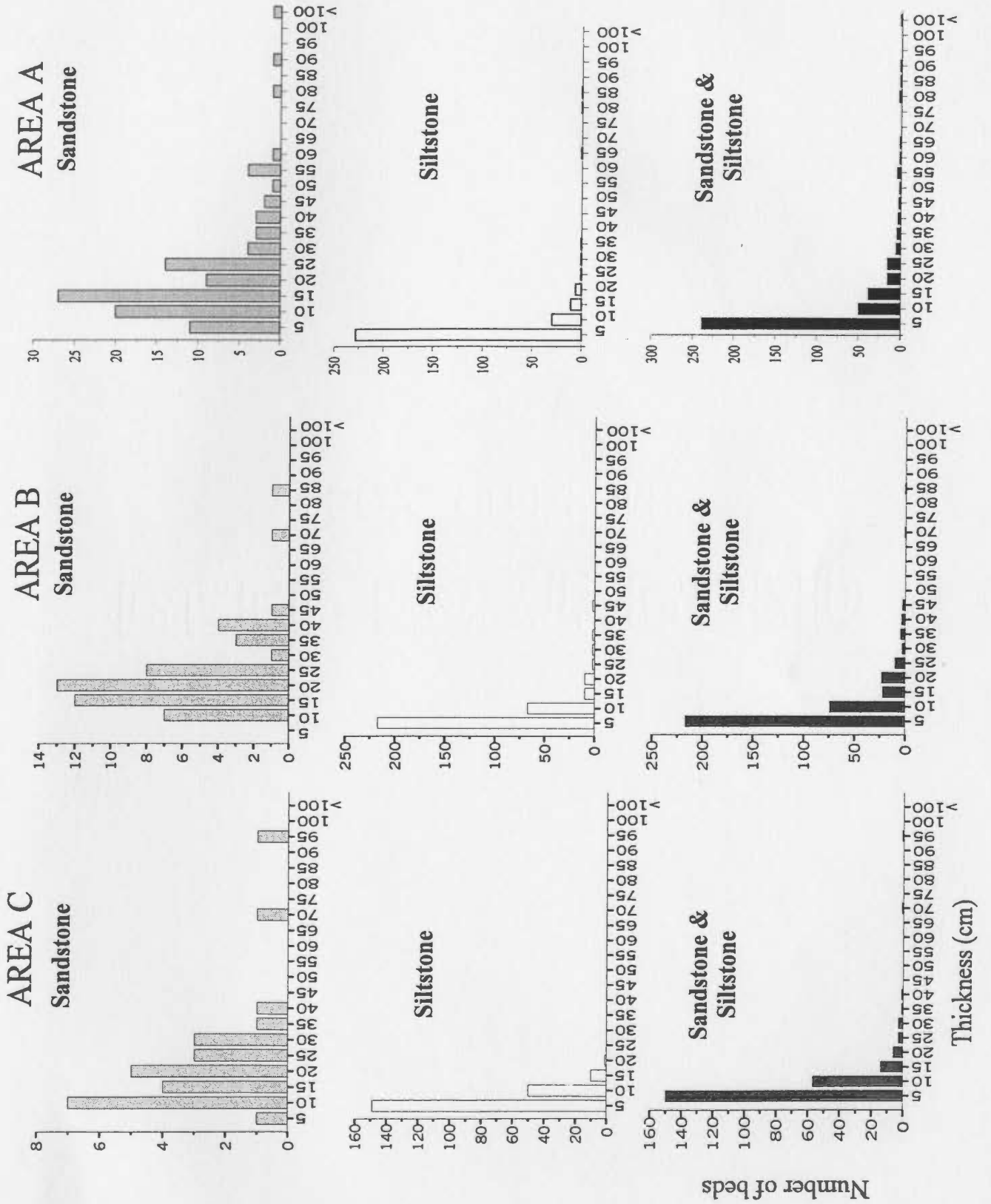
**Sandstone & Siltstone**



**Sandstone & Siltstone**

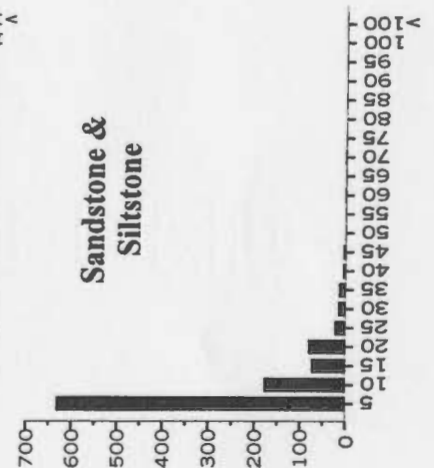
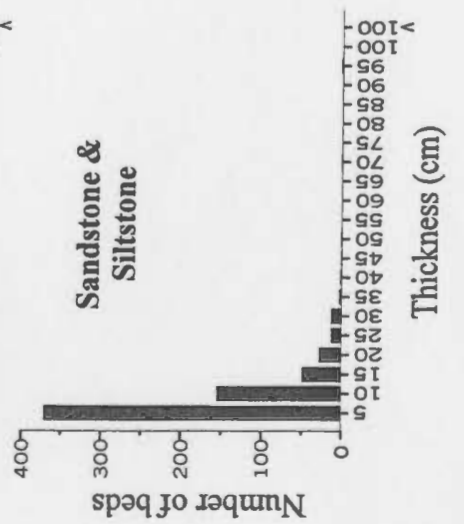
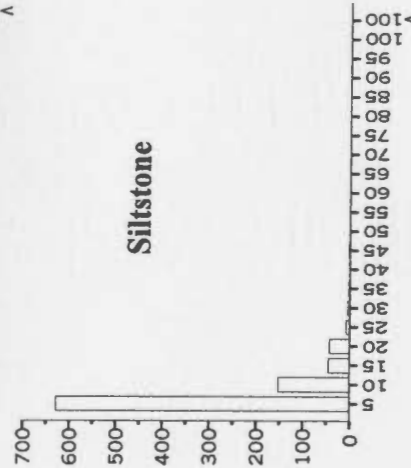
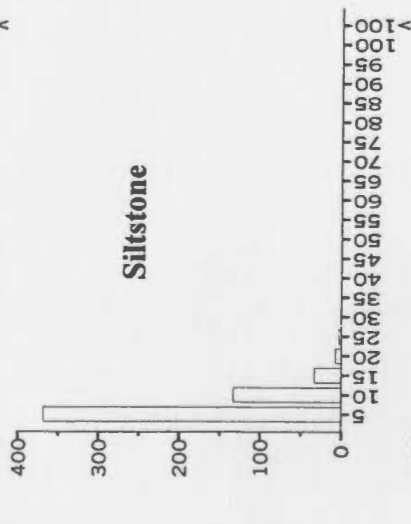
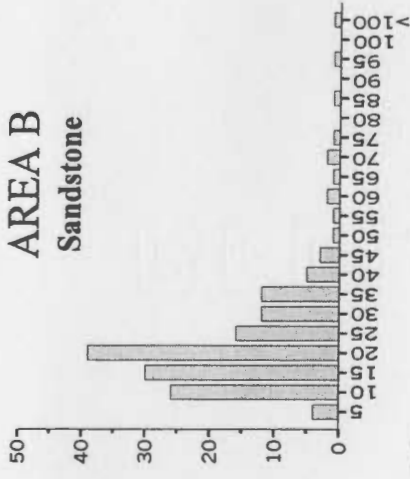
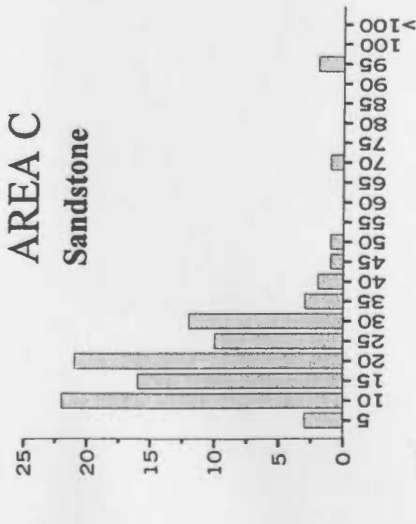


Sub-slice 6-1





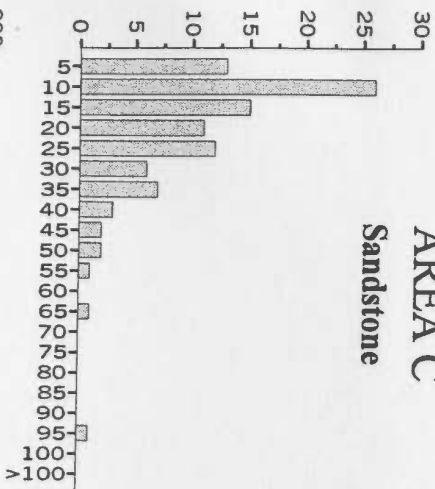
Sub-slice 6-2



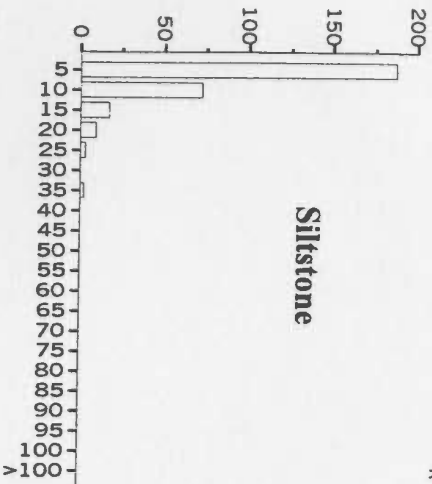
# Time-slices 7

## AREA C

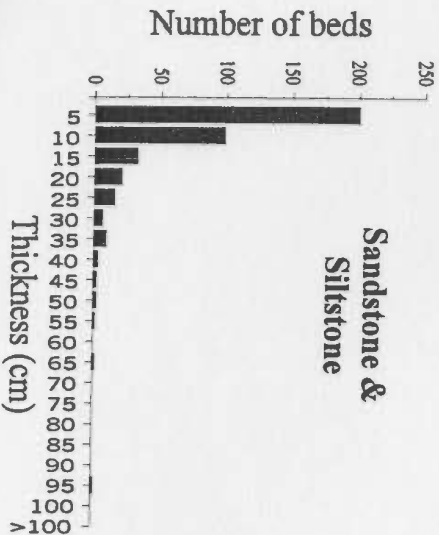
### Sandstone



### Siltstone

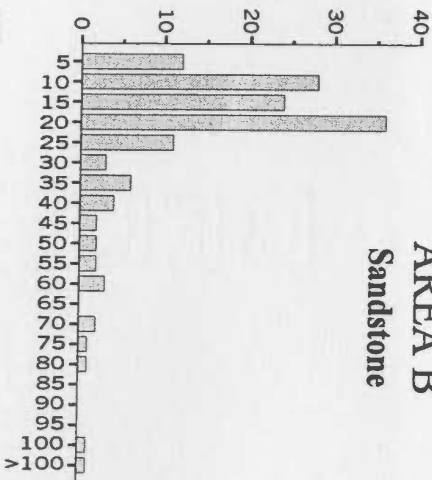


### Sandstone & Siltstone

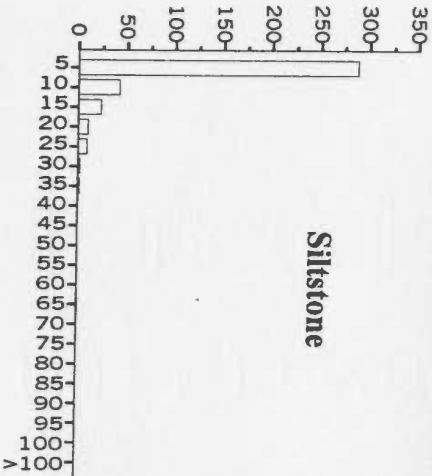


## AREA B

### Sandstone



### Siltstone



### Sandstone & Siltstone

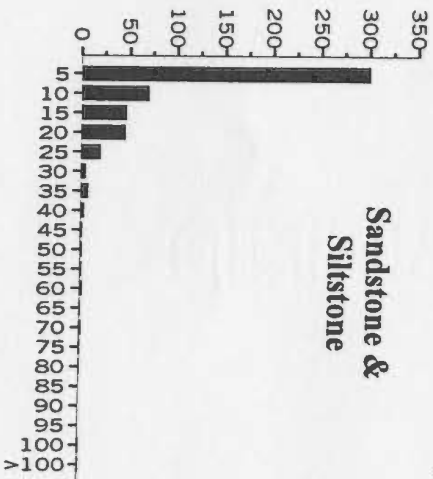
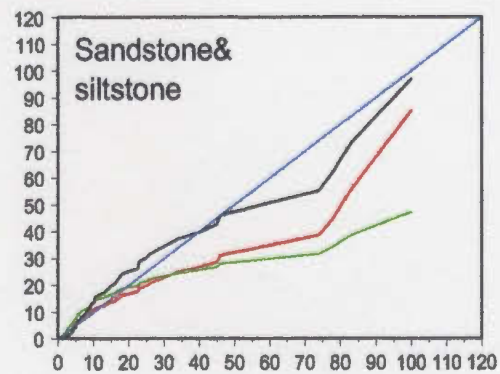
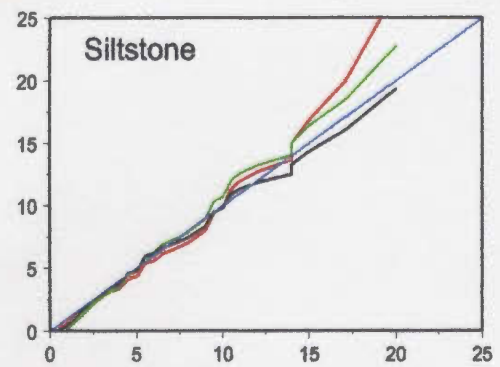
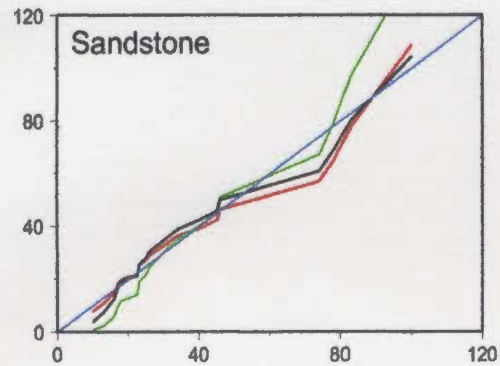


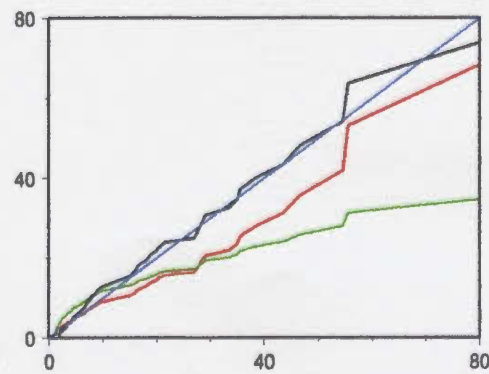
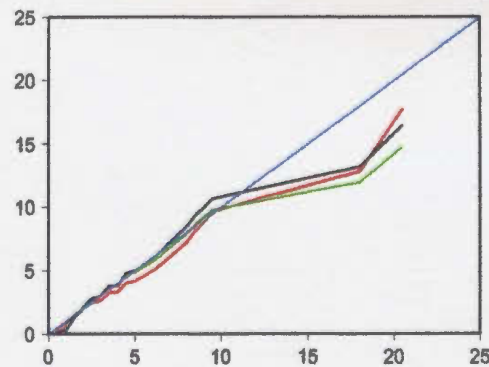
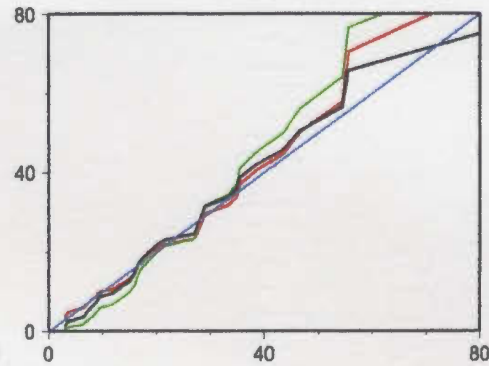
Figure B12. These are q-q plots for the sandstone, siltstone and a combined sandstone and siltstone beds for each some of the time-slices and sub-slices. Note that time-slice 5 is not included and part of time-slice 1 was combined with time-slice 2. The x-axis is the actual bed thickness in cm while the y-axis is the expected bed thickness. Red is for the lognormal distribution, green is for the exponential distribution and black is for the gamma distribution.

# Time-slices 1&2

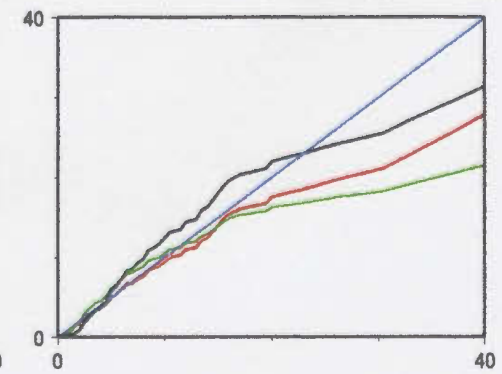
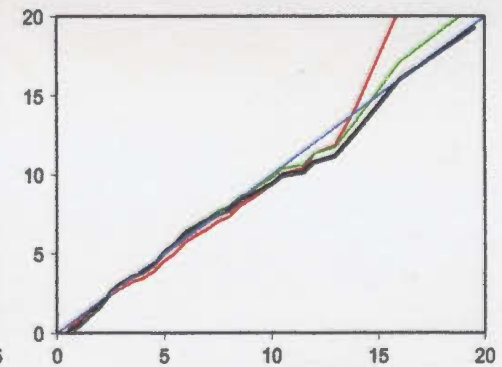
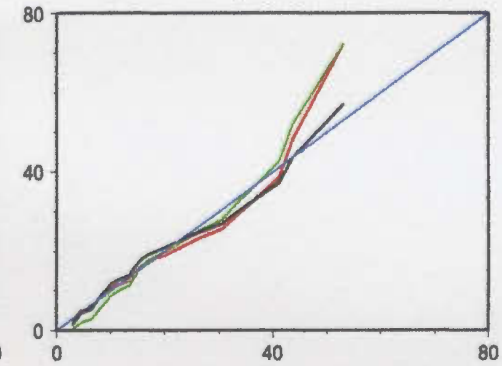
## AREA C (PF)



## AREA B (SH-SYE)

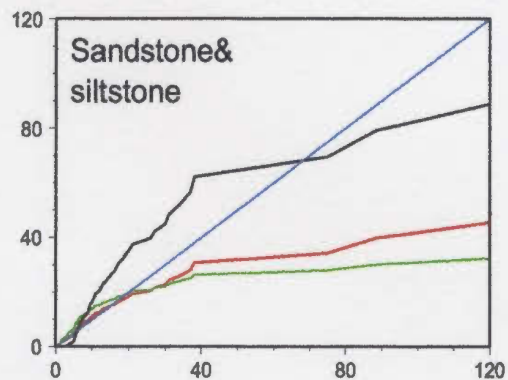
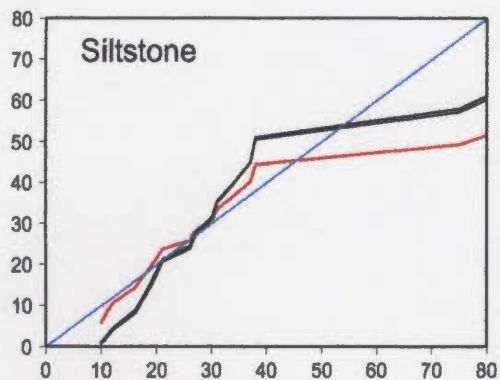
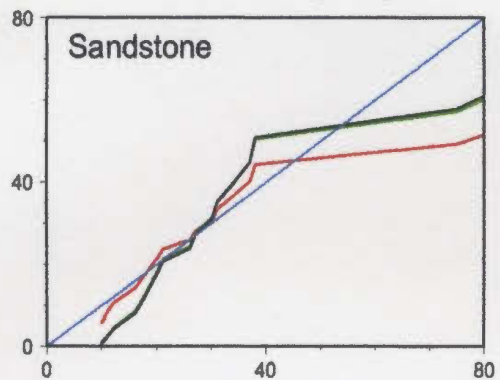


## AREA A (RE-PCDR)

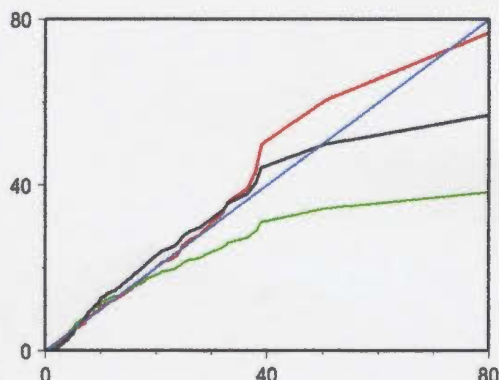
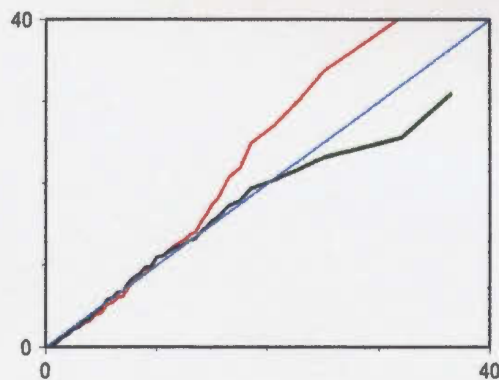
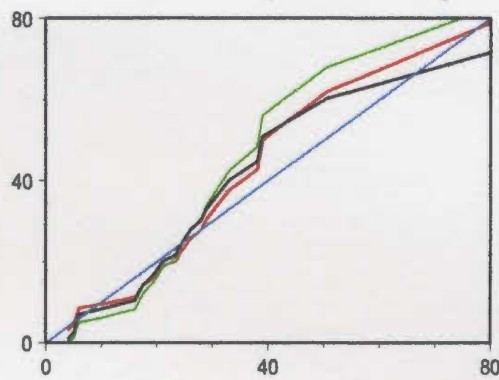


# Time-slice 3

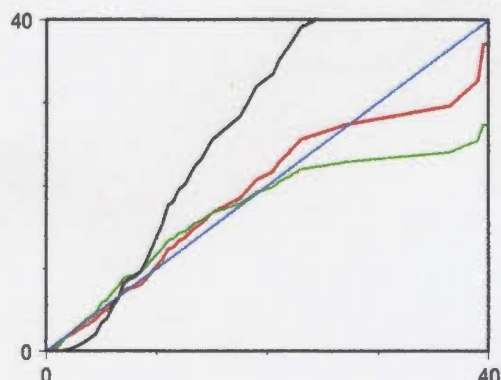
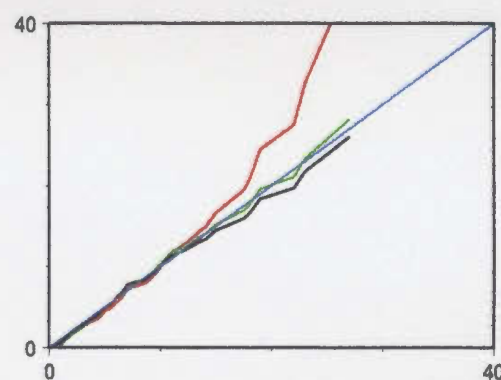
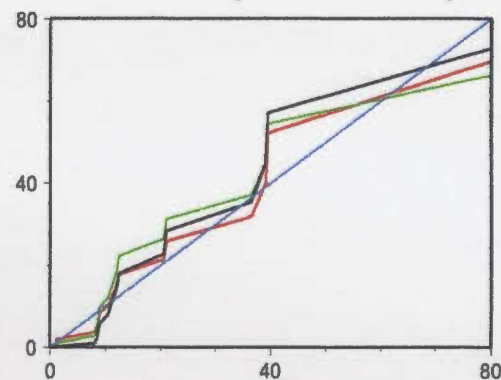
## AREA C (PF)



## AREA B (SH-SYE)

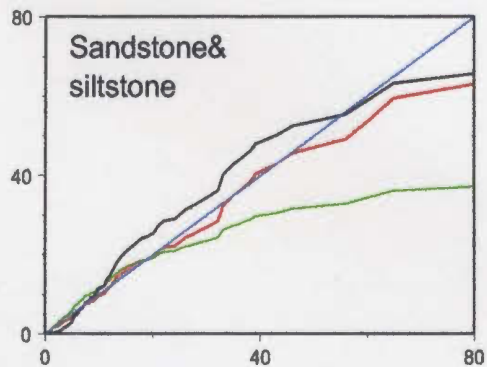
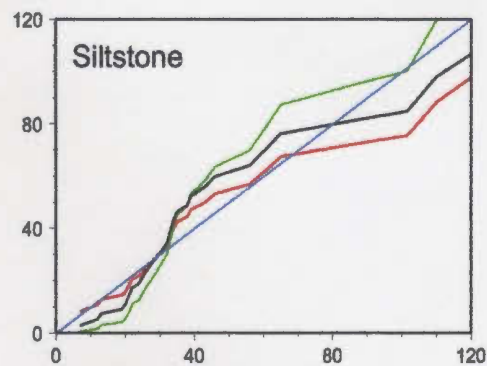
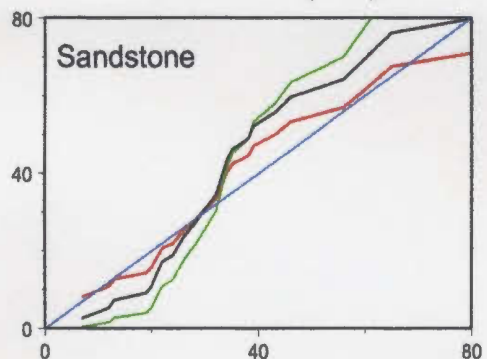


## AREA A (RE-PCDR)

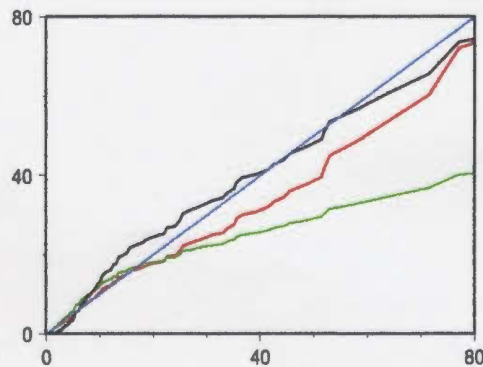
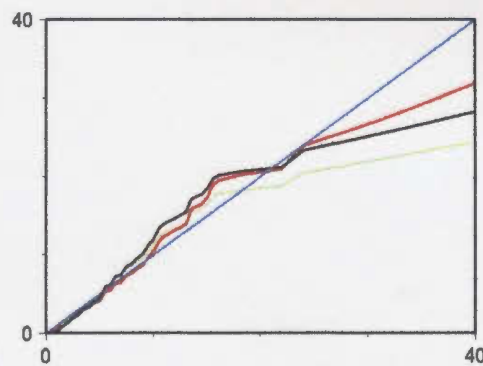
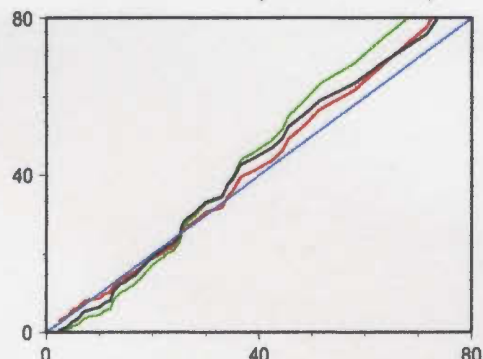


# Time-slice 4

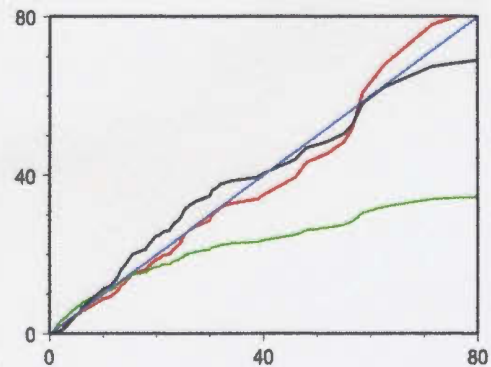
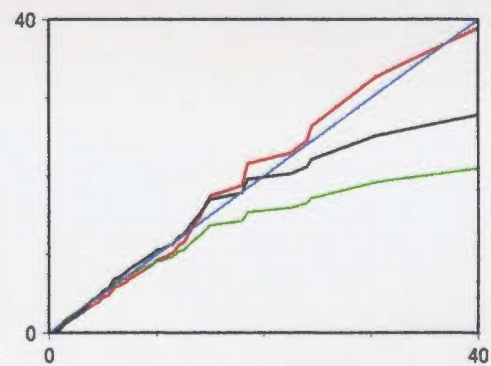
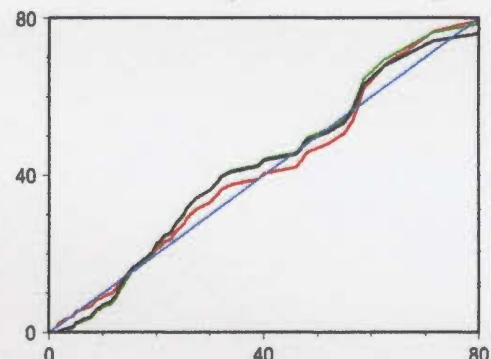
## AREA C (PF)



## AREA B (SH-SYE)



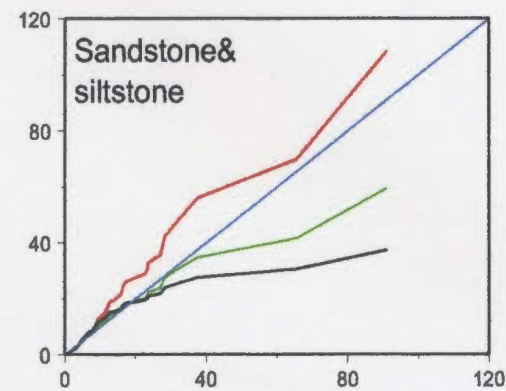
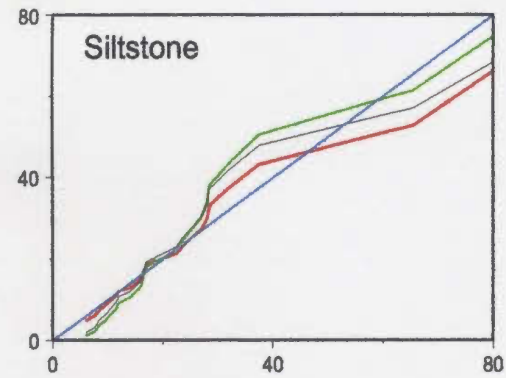
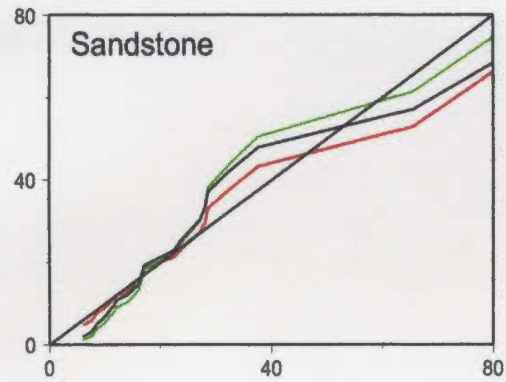
## AREA A (RE-PCDR)



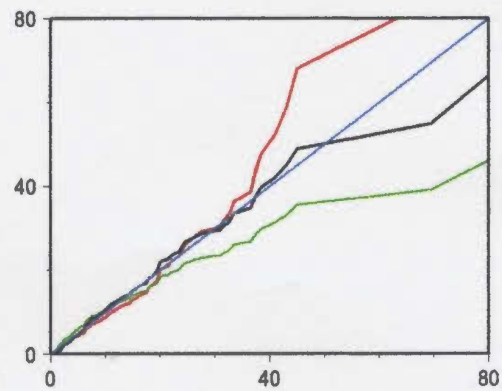
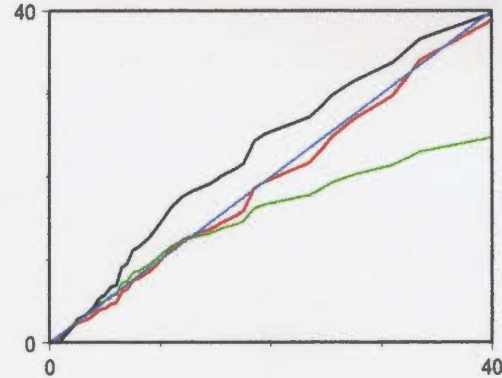
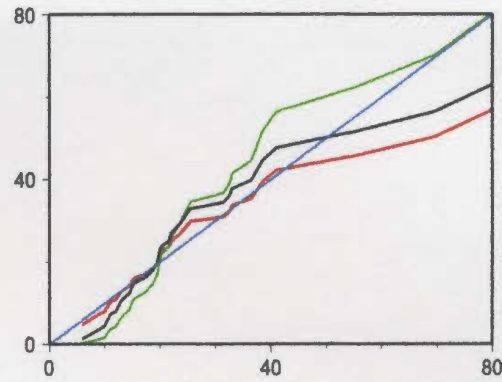


# Sub-slice 6-1

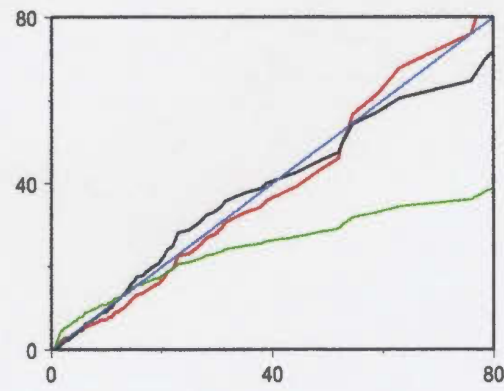
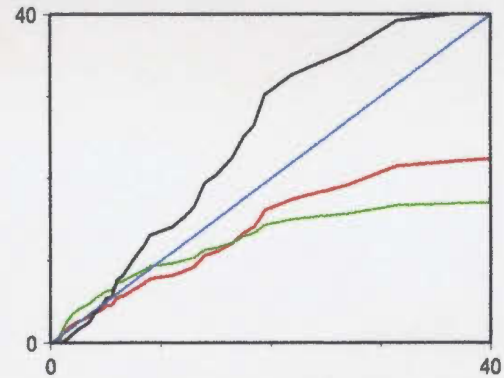
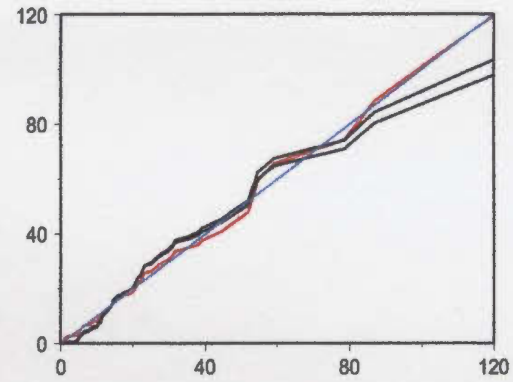
## AREA C (PF)



## AREA B (SH-SYE)



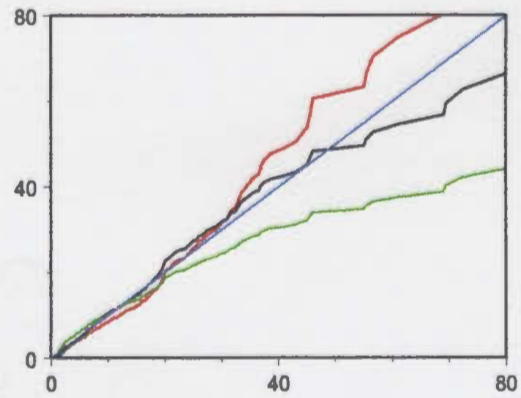
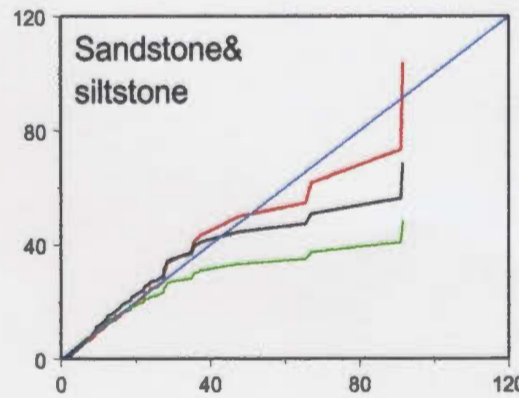
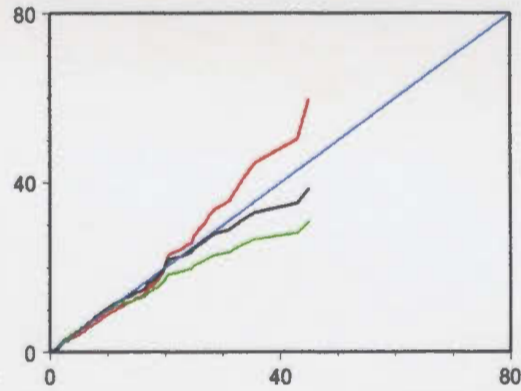
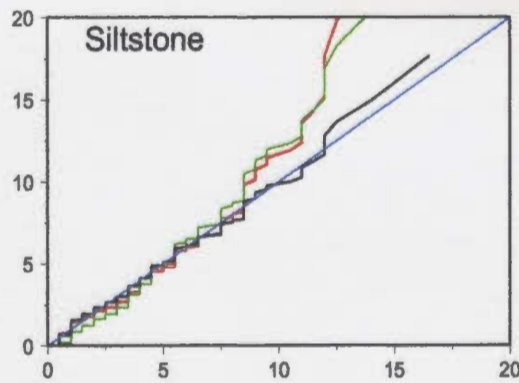
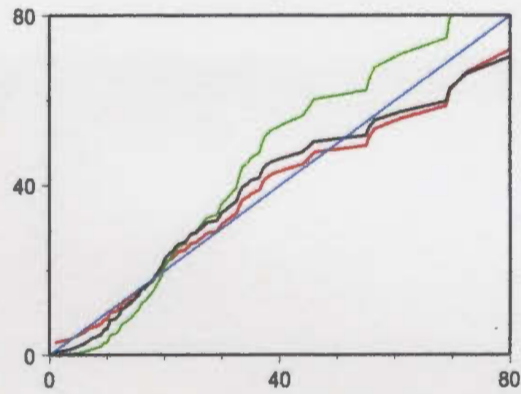
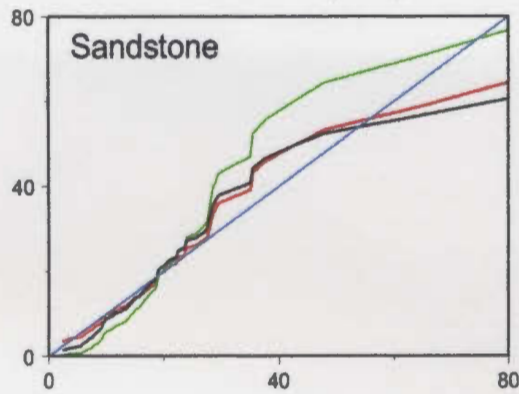
## AREA A (RE-PCDR)



# Sub-slice 6-2

## AREA C (PF)

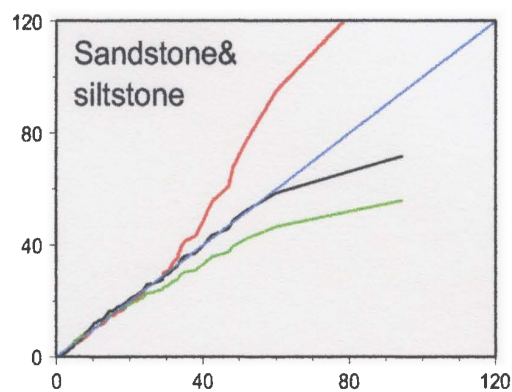
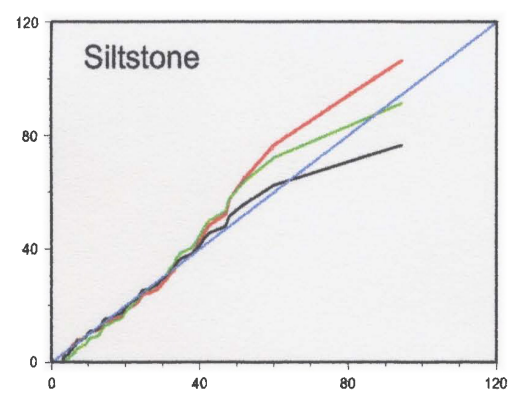
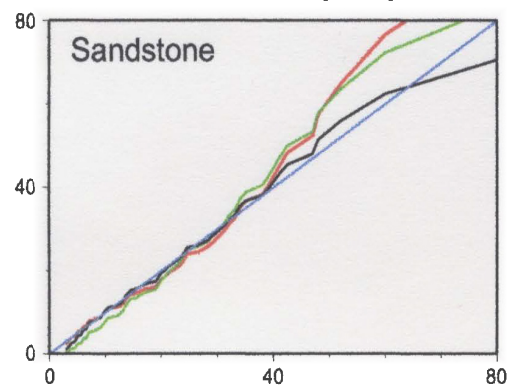
## AREA B (SH-SYE)



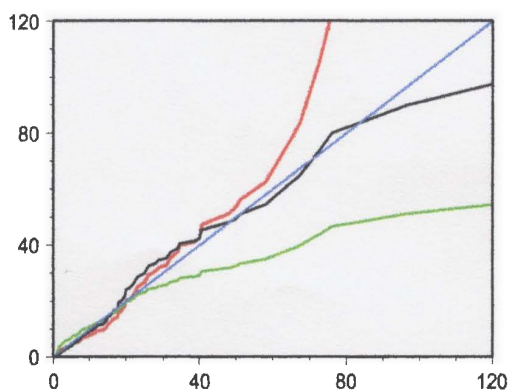
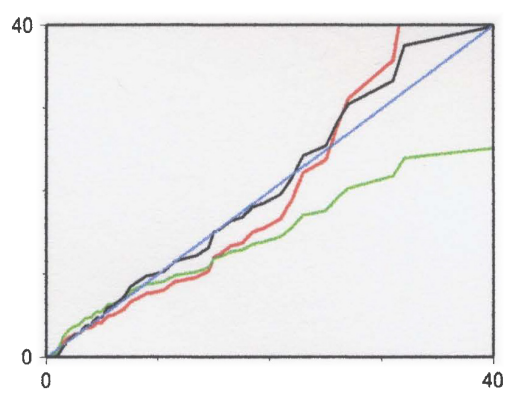
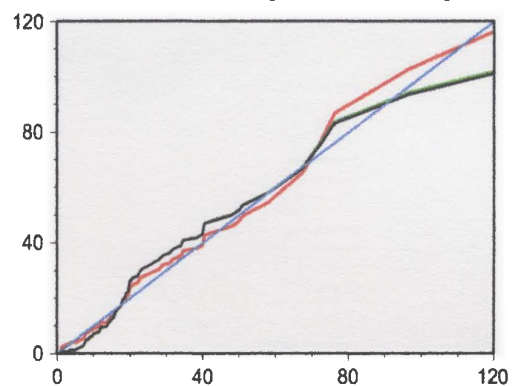


# Time-slice 7

## AREA C (PF)



## AREA B (SH-SYE)



## **APPENDIX C**

Appendix C are 7 tables (CD-T1 through CD-T7) that are saved on a CD-ROM disk. These tables include that data presented in Chapter 5. The tables are saved in Portable Digital Format (pdf) which may be viewed using Adobe Acrobat software. This program is available at the Adobe website ([WWW. Adobe.com](http://WWW.Adobe.com)).

**UMI<sup>®</sup>**

**Dissertation**

**NQ84077**

**2002  
CD 1 of 1**

**Awadallah, Sherif Abdel Monem**

**"Architecture and depositional history of the  
lower Cloridorme Formation, Gaspe  
Peninsula, Quebec, Canada"**

Reproduced with permission of Copyright Owner. Further reproduction prohibited without permission, or in accordance with the U.S. Copyright Act of 1976 or other applicable Copyright Law.

Reproduced with permission of Copyright Owner. Further reproduction prohibited without permission, or in accordance with the U.S. Copyright Act of 1976 or other applicable Copyright Law.

Q805014923B2168431  
VERBATIM  
DataLifePlus CD-R



